University of Alberta
Department of Civil Engineering

Structural Engineering Report No. 91

An Investigation of Reinforced Concrete Block Masonry Columns

by

G.R. Sturgeon

J. Longworth

and

J. Warwaruk

September, 1980

THE UNIVERSITY OF ALBERTA

AN INVESTIGATION OF REINFORCED CONCRETE BLOCK MASONRY COLUMNS

by

G.R. Sturgeon[1], J. Longworth[2], and J. Warwaruk[3]

September 1980

DEPARTMENT OF CIVIL ENGINEERING

EDMONTON, ALBERTA

---

[1]Former Graduate Student, Dept. of Civil Engineering, University of Alberta, Edmonton, Canada.
[2]Professor of Civil Engineering, University of Alberta, Edmonton, Canada, T6G 2G7.
[3]Professor of Civil Engineering, University of Alberta, Edmonton, Canada, T6G 2G7.

Acknowledgements

This investigation was made possible through funds from the Natural Sciences and Engineering Research Council of Canada and the Alberta Masonry Institute. Testing facilities were provided by the Department of Civil Engineering at the University of Alberta. The concrete blocks and the ready-mix concrete used in the fabrication of the test specimens were donated by Edcon Block Products and Consolidated Concrete Products.

This report was originally prepared as a Master of Science thesis under the joint supervision of Profs. J. Longworth and J. Warwaruk at the University of Alberta.

Abstract

Previous investigations, available design methods, and code requirements for plain and reinforced concrete block masonry columns are reviewed.

The experimental study investigates the behavior of reinforced concrete block masonry columns subject to axial concentric compression, and combined bending and axial compression. A total of forty-three concentrically loaded columns, sixteen eccentrically loaded columns, and forty-seven prisms were manufactured and tested to failure. Fabrication and test variables included percentage and grade of vertical reinforcement, grout compressive strength and slump, lateral tie details, and eccentricity of load. The behavior of the test specimens was observed by measurements of load, vertical and lateral strain, and lateral deflections.

On the basis of a study of the assumptions of inelastic design of reinforced concrete columns, and on the basis of data gathered from tests conducted herein, theories and empirical equations for the prediction of masonry column and prism behavior are developed. Consideration is given to masonry failure mode, ultimate strength, vertical and lateral failure strains, cracking stresses, and elastic modulus as a function of the fabrication and test variables.

Table of Contents

List of Tables

List of Figures

List of Plates

List of Symbols

Dimensions and Section Properties

A = cross-sectional area

a = depth of the equivalent rectangular stress block

A_c = core area of block unit

A_g = gross cross-sectional area of column perpendicular to the applied load

A_n = net area of cross-section

A_{shell} = masonry shell area

A_s = cross-sectional area of longitudinal reinforcing steel

A'_s = cross-sectional area of longitudinal compression steel

A_{st} = transformed area of tension steel in terms of equivalent masonry area

A'_{st} = transformed area of compression steel in terms of equivalent masonry area

b = width of a masonry cross-section

c = depth to the neutral axis

d = depth to tension steel from extreme compression fiber

d' = depth to compression steel from extreme compression fiber

d'' = distance from tension steel to plastic centroid of the cross-section

e = eccentricity of the applied load with respect to the centroid of the effective masonry cross-section
= eccentricity of the applied load with respect to the plastic centroid of the cross-section

e' = eccentricity of the applied load measured from mid-depth of the masonry cross-section for working stress analysis
= eccentricity of the applied load measured from

tension steel for ultimate strength analysis

e_k = kern eccentricity

I = moment of inertia

I_n = moment of inertia of the masonry net cross-section about the centroidal axis

t = thickness of masonry cross-section

T_b = block unit height

T_j = masonry (mortar) joint thickness

Z = the distance from the compression face to the centroid of the effective masonry section

Material Properties

E = elastic modulus

E_b = elastic modulus of the concrete block unit

E_c = elastic modulus of column or prism grout or concrete

E_j = elastic modulus of the mortar joint

E_m = elastic modulus of masonry

E_s = elastic modulus of steel reinforcement

E_{shell} = masonry shell elastic modulus

G = shear modulus

ν = Poisson's ratio

Forces and Moments

M = applied moment

P = applied load

P_{crack} = load at which cracks in the masonry become visible to an observer

P_{linear} = load to which the masonry load-strain curve is approximately linearly elastic

P_s = load carried by vertical reinforcement

P_{shell} = load carried by the block shell at column failure

Pu_b = ultimate load of block unit

Pu_c = ultimate load for a tied column

Pu_m = ultimate load of masonry prism

Pmp_c = plain column ultimate load

S = column strength

Stresses and Strains

ε = strain

ε_s = strain in tension steel at ultimate conditions

ε_s' = strain in compression steel at ultimate conditions

ε_u = ultimate concrete compression strain

ε_y = strain at first yield in tension steel

f_b' = ultimate brick or concrete block unit compressive strength

f_c' = standard concrete cylinder compressive strength

f_m = allowable stress in masonry

f_m' = ultimate uniaxial masonry prism compressive strength

f_{max} = maximum stress at outer fiber

f_{min} = minimum stress at outer fiber

f_{mpc}' = plain column net area compressive strength

f_{mpg}' = plain prism gross area compressive strength

f_{mpn}' = plain prism net area compressive strength

f_{pc}' = stripped shell prism core compressive strength

f_s = tension steel service stress
= yield strength of longitudinal tension steel for

ultimate strength analysis

f'_s = compression steel service stress
= yield strength of longitudinal compression steel for ultimate strength analysis

f_t = masonry flexural tensile stress

f_u = ultimate strength of steel

f_y = yield stress of longitudinal reinforcement

f'_y = yield stress of compression reinforcement

Miscellaneous

C_e = eccentricity coefficient

C_s = slenderness coefficient

Δ = column lateral deflection

K = ratio of masonry compressive strength to brick unit compressive strength

ρ_n = ratio of area of vertical reinforcement to masonry net cross-sectional area

ρ = ratio of longitudinal steel area to column cross-sectional area

ρ' = lateral steel ratio in terms of gross area

η = ratio of steel elastic modulus to masonry elastic modulus

r = correlation coefficient

σ = standard deviation

W = unit weight of concrete
= air dry concrete block density

1. INTRODUCTION

1.1 General Remarks

Reinforced masonry columns are common structural elements which are used to support compressive vertical loads as well as provide lateral support to masonry walls.

A limited number of studies have been carried out for the purpose of developing strength design procedures for brick masonry columns, and even fewer studies have explored concrete block masonry columns. Although it has been proposed that reinforced brick masonry columns may be designed using the Ultimate Strength Design Method for concrete, the lack of information has necessitated most masonry building codes to retain service load design equations. As more information is gained, better predictions of strength and behavior can be made. These may evolve into design procedures which more closely reflect material properties and structural element strength and behavior.

The designer must be able to predict with confidence, material properties and structural behavior before load factors and performance factors may be assessed for use in a Limit States Design procedure. Economy of design would result because of a better understanding of the material.

Detailing of reinforcement, grout strength, and core-block shell interaction are important factors affecting the strength and behavior of reinforced concrete block masonry columns. Present codes for reinforced masonry

parallel codes for reinforced concrete in the detailing of reinforcement. However, there is some question whether detailing of reinforcement for concrete columns is strictly applicable to certain types of masonry columns. The question of whether reinforced concrete ultimate strength equations for concentrically and eccentrically loaded columns are applicable to reinforced concrete block masonry columns has not been answered, nor are the effects of the contribution of a masonry shell to the column at all understood. Research is needed to confirm, extend, or adapt existing theory and procedures.

The Second Progress Report of the Canadian Masonry Research Council (1977) considers studies and tests of structural design topics leading to safer and more economical design in masonry to be of high to very high priority.

1.2 Object and Scope

The objectives of this study are:

1. To briefly review and present our current understanding of the behavior of reinforced concrete block masonry columns.
2. To examine the effect of concrete core strength and slump on the strength and behavior of concentrically loaded reinforced concrete block masonry columns.
3. To determine the effects of vertical and lateral reinforcement detailing on the strength and behavior of

concentrically loaded reinforced concrete block masonry columns.

4. To examine the behavior of eccentrically loaded reinforced concrete block masonry columns.
5. To determine behavioral and strength relationships between small-scale prism test data, and full-scale column test data.
6. To develop or extend existing analyses for predicting the strength of reinforced concrete block masonry columns subject to axial compression or combined bending and axial compression.

2. REVIEW OF PREVIOUS INVESTIGATIONS, STRENGTH ANALYSIS, AND CODE DESIGN PROCEDURE

2.1 Introduction

This chapter provides a review of previous concrete column and masonry column studies, and briefly describes what is known about the behavior and strength of plain and reinforced brick columns, concrete block columns, and concrete columns subjected to concentric and eccentric axial loads. In addition, the available design theories for plain and reinforced concrete and concrete block masonry columns are presented, and the design criteria for concrete block masonry columns as specified by CSA-S304-1977,[40] the current Canadian masonry design code, are examined.

2.2 Review of Previous Investigations

2.2.1 Brick Masonry Columns

Previous to 1900, attempts were made to establish a relationship between the compressive strength of hollow and solid, plain brick piers, and the compressive strength of the brick unit. Variables considered were column height, cross-sectional area, and mortar type. Tests as early as 1882 are reported, and by 1886, the strength of a brick column was considered to be inversely proportional to its height to thickness ratio. Variations in column height, cross-sectional area, and mortar type produced ratios of masonry strength to brick strength between 6.1% and 60.9%.[1]

By 1906, it had been established that column strength increased considerably with age and also increased with higher mortar strengths.

The first investigation into the effects of horizontal reinforcement in brickwork piers was made at Cornell University in 1900.[1] Further tests were conducted at the Bureau of Standards in Pittsburg in 1915.[1] Both studies showed that through the placement of wire netting or mesh in every joint, the compressive strength of brick piers could be substantially increased.

Researchers at the University of Illinois,[1] in 1908, were the first to study the effects of workmanship and mortar type on the compressive strength and elastic modulus of brick columns. Generally, it was found that both these properties decreased with decreased brick unit strength, decreased with decreasing mortar strength, and decreased with poorly laid mortar.

In 1916, researchers at the Swedish Technical Institute[1] studied eccentrically loaded brick piers, and results indicated an accompanying strength decrease.

In 1930, Shank and Foster[2] attempted to duplicate in the laboratory, the eccentric loading conditions encountered in plain brick pilasters under actual service conditions. The tests showed that pilaster strength under eccentric load is less than that under uniform concentric load, and that the relation between these strengths depends on the column stiffness and the column's ability to absorb the load.

However, no design expressions were derived from these tests.

Lyse,[1] in 1933, was the first to investigate the effect of vertical reinforcement in brick piers. In this study, thirty-three columns, all 10 feet in height and all with a 12-1/2 inch square cross-section, were tested in vertical compression. Three brick types, and five mortar types were used. Vertical and lateral reinforcement percentages ranged between 0 and 2%, and 0 and 0.8%, respectively.

As did his predecessors, Lyse found that, in general, the stronger the mortar or brick used, the stronger the column, and that workmanship of the mason affected column strength to a non-quantifiable degree. Furthermore, an increased thickness of mortar joint was observed to decrease column strength. Lyse concluded that the strength of a reinforced brick column, having what is termed, "sufficient" lateral reinforcement to prevent buckling of the vertical bars, is a function of the effective strength of the brick plus the yield strength of the longitudinal reinforcement. The former is affected by brick type, mortar type, workmanship, height to thickness ratio of the column, thickness of the mortar joint, and curing time. The strength is therefore:

$$S = A(Kf'_b + \rho f_s) \quad \ldots\ldots\ldots\ldots\ldots\ldots \quad 2.1$$

where

S = column strength

A = column area

ρ = ratio of longitudinal steel area to column cross-sectional area

f'_b = ultimate brick strength

K = effectiveness ratio of brick masonry = ratio of masonry strength to brick unit strength

f_s = yield point of longitudinal steel

Lyse recommended that K be determined experimentally by testing small brick prisms constructed of similar materials and under similar conditions to the columns in the actual structure.

Withey,[3] in 1934, conducted concentric compression tests on thirty-two reinforced brick columns, 6 feet in height, and 12-1/2 inches square in cross-section. The percentages of longitudinal reinforcement, and hooped, lateral joint reinforcement were varied from 0 to 4% and 0 to 1.5%, respectively. As well, two mortar types and two brick types were employed. Results suggested that column strength varied directly with the plain masonry strength and the percentage of vertical steel reinforcement, and could be further increased with the use of lateral joint reinforcement. These observations are expressed in the following equation presented by Withey for use in the calculation of the maximum load carried by reinforced brick columns:

$$\frac{P}{A} = f_b(1 - \rho) + \rho f_s + K\rho' f'_s \quad \ldots\ldots\ldots\ldots \quad 2.2$$

where

P = maximum load

A = gross area of cross-section

f_b = unit stress for plain brick column

ρ = longitudinal steel ratio in terms of gross area

ρ' = lateral steel ratio in terms of gross area

f_s = yield point of longitudinal steel

f_s' = yield point of lateral hoop reinforcement

K = constant assumed to depend on the ratio of gross area to core area, and possibly on brick type

Davey and Thomas[4] (1950), carried out concentric and eccentric compression tests on plain brick piers. Variables considered were mortar type, brick type, cross-sectional area, and column height; the latter being varied from 1 ft. to 12 ft. in order to study slenderness effects. Eccentricities ranged from t/12 to t/3. Results showed that the effects of slenderness are not independent of the eccentricity of loading. Concentric and eccentric compression tests were also conducted on reinforced brick columns, 9 feet in height, and with varied cross-sections. Percentages of vertical reinforcement were small, ranging from only 0.1 to 0.2%. Unfortunately, a failure theory or design method was not developed by Davey and Thomas for either the plain or the reinforced brick columns.

Anderson and Hoffman[5] (1967) proposed an ultimate strength design procedure for reinforced brick masonry columns based on the American Concrete Institute USD method

(ACI 318-63) for reinforced concrete columns. Moreover, exploratory tests were conducted on eccentrically loaded, reinforced brick masonry columns each having a length of 10 ft.-2 inches, and a 12 by 16 in. cross-section. Eccentricities varied between 0 and 34% of the column depth. Ultimate loads calculated by the USD method for short reinforced concrete columns compared very favourably with the ultimate test loads; the latter varied between 0.97 and 1.11 of the former. Anderson and Hoffman concluded that the ACI USD method for reinforced concrete columns could be applicable for reinforced brick masonry columns provided more reliable data could be obtained concerning the shape of the compression stress-strain curve for brick masonry, the ultimate strain of the masonry, and the effect of different percentages of vertical reinforcement on the behavior of the masonry.

In 1969, Brettle[6] proposed a rapid, computer aided ultimate strength design procedure for proportioning reinforced brickwork piers subjected to compression and biaxial bending. A comparison with the test results of Davey and Thomas indicated that the experimental failure loads for unreinforced brick columns were, on the average, 30% higher than those computed using the proposed theory, but for reinforced columns, were only 4% lower.

2.2.2 Concrete Block Masonry Columns

In 1931, Shank and Foster[7] studied the behavior of

plain concrete block pilasters when subjected to eccentric loads. These tests were similar to those previously conducted on plain brick piers. Program variables included block type, cross-sectional area, and pilaster height. It was found that the ultimate compressive strength of the masonry was about half of that of the unit. Furthermore, pier strengths were inversely proportional to block absorption and in direct relationship with moduli of elasticity.

The first tests of reinforced concrete block masonry columns were conducted by Feeg,[8] in 1978, at the University of Alberta. Specifically, this program was undertaken to determine the effects of reinforcement detailing on the strength and behavior of these columns under compressive loads. The load was applied concentrically to the columns through pinned ends. Short columns were studied so that slenderness effects could be neglected.

All columns were 64 inches high and all had a nominal 16 inch square cross-section. Of the thirty-seven columns tested, thirty-four were constructed with 8 x 8 x 16 in., lightweight, plain corner block (2 oval core, 59% net area), with an average unit net area strength of 2470 psi. The column cross-section consisted of two such units laid in running bond. The remaining three columns employed 16 inch single core, lightweight, autoclaved pilaster units (16 x 16 x 8 in., 39% net area, 2450 psi net area). These columns consisted of a single unit laid in stacked bond. Face shell

bedding was used throughout, and a joint thickness of 3/8 inch was maintained. All columns were constructed with type S mortar having volume proportions of 1:1/2:4 (C:L:S), and an average 28 day compressive strength determined from tests on standard mortar cubes of 1860 psi when cured under wet burlap, and 650 psi when cured under laboratory conditions. Columns were filled with a grout having volume proportions of 1:3:2 (C:S:A), and an average compressive strength of 2680 psi determined from tests on standard moist cured cylinders.

All vertical reinforcement was placed coincident with a core centroid. Block unit shape restricted the placement of all tie reinforcement to the joints between courses; consequently, an 8 inch vertical spacing was maintained.

Variables investigated in this study were:

1. Tie diameter and tie location within the column cross-section. Tie diameters of 0.1483 in., 0.1875 in., and 0.25 in. were used. Ties were positioned either in the mortar joint between the outer face shells of the units, or in direct contact with the vertical reinforcement.
2. The amount of vertical reinforcement. Reinforcement areas varied between 0.7 and 1.3% of the total column cross-sectional area.
3. Vertical reinforcement distribution. Columns with identical percentages of vertical reinforcement, but employing differing bar sizes, were compared.
4. Grade of vertical reinforcement. Grade 40 and Grade 60 (ksi) steels were used.

All columns exhibited elastic behavior to about 75% of their ultimate load. The average elastic modulus was found to be about 800 times the masonry prism strength. The

average ultimate strain was observed to increase with the addition of grout, and increased tie diameter, but showed no definite trends with varied percentages of vertical reinforcement.

Increasing tie diameter resulted in increased column strength, accompanied with a decreased amount of vertical cracking at failure. No significant difference in strength was observed between columns having ties in contact with the vertical reinforcement and those which did not. However, it was considered that the former provided greater restraint against buckling of the vertical reinforcement. The column strength, for a given percentage of vertical reinforcement, decreased with increasing bar diameter. This was expected, since it is generally known that stresses developed in masonry surrounding rebar increase with increased bar diameter and larger differences in Poisson's ratio between the two materials. The ability of the vertical reinforcement to reach yield depended on the strength developed by the masonry.

It was further observed that failure to remove mortar droppings from the interior base of a column through clean-out holes considerably lowers column strength, and that the use of a high slump grout in columns constructed with pilaster units results in excessive shrinkage and interface cracking between the block and fill which is detrimental to their strength and behavior.

Unfortunately, equations predicting ultimate load or

deformations were not presented by Feeg.

2.2.3 Reinforced Concrete Columns

In contrast with reinforced masonry columns, a comparatively large number of studies have been directed at establishing ultimate strength design criteria and behavioral aspects of reinforced concrete columns subjected to both concentric and eccentric loadings. Consequently, many aspects of column design and reinforcement detailing in CSA-S304, "Masonry Design and Construction for Buildings", are taken directly, or adapted from CAN3-A23.3, "Code for the Design of Concrete Structures for Buildings", or from the older working stress design codes. Because every structural engineer is familiar with ultimate strength and working stress design procedures and the behavior of reinforced concrete columns, only a very brief survey of previous studies to trace the development of USD procedures related to short reinforced columns, will be presented.

Ultimate strength concepts in concrete are not recent developments. They can be shown to date back to Thullies' flexural theory of 1897, and Ritter's parabolic stress distribution in 1899. Nevertheless, at the turn of the century, Coignet's and Tedesco's straight line theory gained rapid acceptance, since it was accurate enough for design purposes and commanded mathematical simplicity. The first Joint Committee on Standard Specifications for Concrete and Reinforced Concrete adopted the straight line theory in

1909.

Beam tests by Lyse and Slater,[9] and their subsequent safety factor study, and McMillan's report[10] on creep stress in columns in the early 1920's, re-emphasized the actual inelastic behavior of concrete and questioned the use of allowable stress design. In 1930, these reports led to an extensive investigation of reinforced concrete columns by Lyse and Slater at Lehigh University, and Richart at the University of Illinois, in cooperation with the American Concrete Institute.[11,12,13,14,15] Particular attention was given to column size, concrete strength, grade and amount of longitudinal and spiral reinforcement, rate of load application, and shrinkage and creep under sustained loads. This study developed the first rational equations for the strength of concentrically loaded, short, reinforced concrete columns. The failure load of tied columns was determined to be the sum of the strengths of the concrete core and shell, plus the yield point strength of the vertical reinforcement. The failure load of spirally reinforced columns was composed of the concrete core strength, the yield point strength of the vertical bars, and a contribution by the spiral reinforcement.

During the late 1930's, Whitney[16,17,18] proposed and extended the use of a rectangular compressive stress block for ultimate flexural strength computations, to replace the approximately parabolic stress distribution actually exhibited by concrete. This afforded the designer with a

simple, yet accurate method in which basic static equilibrium is used to predict failure loads of members when subjected to flexure alone, such as in a beam, or in combination with direct load, as in an eccentrically loaded column. This concept forms the basis for state-of-the-art ultimate strength design of reinforced concrete beams and columns, since it is applicable to the entire range of concrete and steel strengths used in practice.

Subsequent inelastic flexural studies by Jensen[19] (1943), and Hognestad[20] (1951), primarily assisted Whitney's stress block concept by lending further credibility to the constants selected by Whitney which defined the rectangular "dimensions" of the stress block. Both experimental and analytical investigations continued to support the use of the equivalent rectangular stress block.[11,12,13,14,15,19,20,21,22,23,24] Based on these studies, the ASCE-ACI Joint Committee,[25] in 1955, presented recommendations and formulas for the design of reinforced concrete structures by Whitney's ultimate strength theory. This concept became widely used in design practice with its appearance in the 1956 ACI Building Code.

Hognestad *et al*[26] (1961) derived design strength equations for members subjected to flexure alone, or in combination with axial load, for a variety of cross-sections based on the rectangular stress block. These equations are currently used in design.

Ultimate strength interaction diagrams for axial

compression and bending about one axis for reinforced concrete columns have been well established by Hognestad *et al*[20] (1951) and Pfrang *et al*[27] (1964).

The investigation and design of rectangular sections subjected to axial compression and biaxial bending has been given particular attention by Bresler[28] (1960), and Parme[29] (1966).

2.2.4 Deformations of Concrete Block and Concrete Block Masonry

Elements and materials in a building are not inert. All materials will expand and contract with temperature changes. All materials change dimensions with applied stress. Some materials flow plastically under sustained loads, and some move with changes in moisture content.

The five basic deformational characteristics of concrete block and concrete block masonry are, or are defined by:

1. shrinkage
2. coefficient of thermal expansion
3. elastic modulus
4. shear modulus
5. creep

Because this report is concerned with the performance of concrete block columns under short term loading, only a brief review of our current understanding of elastic modulus of concrete block masonry will be presented. Important data

are lacking for the modulus of elasticity of concrete block and concrete block masonry; it has only been defined by relating it to material strength and/or block density. These relationships are strictly empirical, and are irrelevant from a theoretical standpoint.

2.2.4.1 The Block Unit

Richart, Moorman and Woodworth[30] (1932) have reported an approximate relationship between elastic modulus and block strength of:

$$E_b = 1000\, f'_b \quad \ldots\ldots\ldots\ldots\ldots\ldots \quad 2.3$$

where

f'_b = block compressive strength, psi

Pauw[31] (1960) showed that for cast-in-place concretes:

$$E_c = 33\, W^{3/2}\sqrt{f'_c} \quad \ldots\ldots\ldots\ldots\ldots\ldots \quad 2.4$$

where

W = unit weight of concrete, lb./cu. ft.

f'_c = compressive strength of concrete, psi

Presently, this is the equation accepted by ACI 318-77, "Building Code Requirements for Reinforced Concrete".

Tests carried out by Holm[32] (1976) on 8 x 8 x 16 in., 2 core block, have permitted derivation of an equivalent formula for the elastic modulus of block concrete:

$$E_b = 22\, W^{3/2}\sqrt{f'_b} \quad \ldots\ldots\ldots\ldots\ldots\ldots \quad 2.5$$

where

E_b = block elastic modulus, psi

W = air dry block density, lb./cu. ft.

f'_b = block compressive strength, psi

Unfortunately, Holm provides no statistical data which assess the reliability of this equation, nor experimental results permitting such calculations.

However, Sturgeon[33] (1978) placed Holm's equation over data reported by Richart *et al*[30], and showed that the equation provides somewhat low estimates of elastic modulus. This suggests that the appropriate constant in Eq. 2.5 lies between 22 and 33. One expects a value less than 33 (for cast-in-place concrete) because of the high void content of machine moulded, zero slump concrete. Sturgeon[33] (1978) suggests:

$$E_b = 25\, W^{3/2} \sqrt{f'_b} \quad \ldots\ldots\ldots\ldots\ldots\ldots \quad 2.6$$

2.2.4.2 Concrete Block Masonry

The modulus of elasticity of masonry is affected by the moduli of both the block and mortar. Sahlin[34] (1971) derived the following theoretical equation:

$$E_m = \frac{1}{\frac{1-\delta}{E_j} + \frac{\delta}{E_b}} \quad \ldots\ldots\ldots\ldots\ldots\ldots \quad 2.7$$

where

E_m = elastic modulus of the masonry

E_j= the elastic modulus of the joint, (mortar)

E_b= the elastic modulus of the block unit

and

$$\delta = \frac{T_b}{T_b + T_j} \quad \ldots\ldots\ldots\ldots\ldots\ldots \quad 2.8$$

where

T_b= the block height

T_j= the joint thickness

Work by Turkstra *et al*[35] (1975) consisted of reviewing masonry prism and wall test data previously presented by Read and Clements[36] (1972) and Richart *et al*[30] (1932), and establishing a regression equation to predict the initial tangent modulus. It was found to correlate best with masonry strength alone. This relationship was based on net area, and found to be:

$$E_m = 731{,}000 + 440.0\, f'_m \quad \ldots\ldots\ldots\ldots\ldots\ldots \quad 2.9$$

where

f'_m= ultimate uniaxial masonry compressive strength, psi

Dispersion of data about this line is considerable.

The Building Research Station[37] (1972) reported an approximate relationship of:

$$E_m = 850\, f'_m \quad \ldots\ldots\ldots\ldots\ldots\ldots \quad 2.10$$

The same relationship was reported by Fattal and Cattaneo[38]

(1977). Hatzinikolas, Longworth, and Warwaruk[39] (1978) recommended:

$$E_m = 750\ f'_m \quad \ldots\ldots\ldots\ldots\ldots\ldots \quad 2.11$$

based on their wall tests. Feeg *et al*[8] (1979), in his study of reinforced block columns, suggested:

$$E_m = 800\ f'_m \quad \ldots\ldots\ldots\ldots\ldots\ldots \quad 2.12$$

CSA Standard S304-1977[40] recommends:

$$E_m = 1000\ f'_m \leq 3.0 \times 10^6 \text{ psi} \quad \ldots\ldots\ldots\ldots \quad 2.13$$

Research clearly indicates that the Canadian Masonry Code over-estimates E_m, in general, by some 15 to 25 percent.

Equation 2.7 indicates that modulus of elasticity will decrease with increasing joint thickness and will increase with the compressive strength of the mortar. As well, it has been shown that full mortar bedding will increase the elastic modulus from 0 to 15 percent over face-shell bedding, other factors being equal.

It is well accepted that, due to the linear nature of the stress-strain curves of concrete masonry in the lower to middle range, the initial tangent modulus is well representative of the elastic modulus at working stresses.

2.3 Strength Analysis Procedures

2.3.1 General

In Canada, masonry is presently designed by working stress analysis. However, it is anticipated that a limit states code will be introduced shortly. Masonry columns must have sufficient structural capacity to resist safely and effectively, certain specified service loads which act upon them. These loads may be considered individually, or in combination, and include dead loads, live loads, wind and earthquake effects, and loads resulting from contraction or expansion of materials due to temperature changes, shrinkage, creep and differential movement. As with columns of other materials, the net effect is to subject the member to end moments, lateral loads and concentric or eccentric axial loads. A masonry column is thus designed such that the stresses resulting from these applied service loads, and based on elastic theory, do not exceed the allowable stresses specified by the Code. These allowable values are some fraction of the ultimate compressive strength of the masonry, which may be established by prism tests or from the independent unit and mortar strengths.

The decision to use plain or reinforced masonry must be based on several considerations, which include:

1. the magnitude of the loads and necessary resistance;
2. masonry cracking due to moisture and temperature variations, and;
3. ductility.

Reinforcement has a favourable effect on each of these.

2.3.2 Elastic Analysis of Eccentrically Loaded Plain Masonry Columns

In working stress or straight line analysis, where all stresses are in the elastic range, five assumptions are made for plain masonry:

1. Plane sections before bending remain plane after bending.
2. Stress is proportional to strain, which in turn, is proportional to the distance from the neutral axis.
3. Masonry provides no tensile resistance.
4. Elastic modulus is constant in the member.
5. Masonry elements (block and grout) form a homogeneous material.

The stress distribution in a plain masonry column subjected to an eccentric load is shown in Fig. 2.1 for various combinations of load and moment. In order to construct these distributions, the stress-strain relation and the tensile and compressive strengths of the masonry must be known. Failure in the masonry occurs when, at the extreme fiber, either the compressive or tensile strength is attained. The distribution of Fig 2.1(d) shows that the modulus of rupture of the masonry has been exceeded over part of the cross-section, thus creating cracking in this region. Since this condition will clearly not satisfy serviceability requirements for plain masonry, it will not be considered in the following analysis.

Basic mechanics can be used to obtain the stresses at the extreme fibers of a cross-section, with the

superposition of stresses created by axial and flexural loads:

$$f = \frac{P}{A_n} \pm \frac{Mt}{2I_n} \quad \ldots\ldots\ldots\ldots\ldots\ldots \quad 2.14$$

where

f = outer fiber stresses

P = applied load

A_n = net area of masonry cross-section (A_n=A for solid rectangular sections)

M = applied moment

t = thickness of masonry cross-section

I_n = moment of inertia of the net cross-section about the centroidal axis (I_n=I for solid rectangular sections)

In the case where flexural stresses result from the eccentricity of the applied load, M = Pe, where:

e = eccentricity of the applied load measured from mid-depth of the section

Since masonry is assumed to carry no tensile stresses, Eq. 2.14 is valid only when the eccentricity of the applied load does not exceed the kern eccentricity. For an eccentricity equal to the kern eccentricity, the stress at the most distant fiber is zero. With a larger eccentricity, tensile stresses will develop.

For rectangular solid sections with width b, and thickness t, the kern eccentricity may be calculated using Eq. 2.14:

$$0 = \frac{P}{A} - \frac{Pet}{2I}$$

$$e_k = \frac{2I}{At} = \frac{2\,\frac{bt^3}{12}}{(bt)t} = \frac{t}{6}$$

Equation 2.14 may be expressed in the simpler form of:

$$f_{max} = \frac{P}{A} + \frac{Pet}{2\,\frac{bt^3}{12}} = \frac{P}{bt} + \frac{6Pe}{bt^2} = \frac{P}{A}\left[1 + \frac{6e}{t}\right] \quad \ldots\ldots \quad 2.15$$

$$f_{min} = \frac{P}{A}\left[1 - \frac{6e}{t}\right] \quad \ldots\ldots\ldots\ldots\ldots\ldots \quad 2.16$$

where

f_{max} = maximum stress at the outer fiber (compression fiber)

f_{min} = minimum stress at the outer fiber (tension fiber)

The stress distribution for a member subjected to an axial load with an eccentricity greater than e_k is shown in Fig. 2.2. Consider a column of width b, and thickness t. Force equilibrium requires:

$$P = \frac{1}{2} f_{max}\, xb = \frac{1}{2} f_{max}\, x\left(\frac{A}{t}\right)$$

$$x = \frac{2Pt}{Af_{max}} \quad \ldots\ldots\ldots\ldots\ldots\ldots \quad 2.17$$

Moment equilibrium about point O requires:

$$P(e + x - t/2) = \frac{2}{3} x(1/2) f_{max} xb = \frac{2}{3} x(1/2) f_{max} x\left(\frac{A}{t}\right) \quad \ldots\ldots \quad 2.18$$

Substitution of Eq. 2.17 into Eq. 2.18 gives:

$$P\left(e + \frac{2Pt}{Af_{max}} - \frac{t}{2}\right) = \frac{1}{3} \cdot \frac{4P^2t^2}{A^2f_{max}^2} \cdot \frac{A}{t} f_{max}$$

$$e + \frac{2Pt}{Af_{max}} - \frac{t}{2} = \frac{4}{3} \cdot \frac{Pt}{Af_{max}}$$

$$-\left(e - \frac{t}{2}\right) = \frac{2}{3} \cdot \frac{Pt}{Af_{max}}$$

$$f_{max} = \frac{P}{A}\left[\frac{-(2/3)t}{e - (t/2)}\right] \quad \ldots\ldots\ldots\ldots\ldots\ldots \quad 2.19$$

Equation 2.19 defines the maximum stress for a solid rectangular section with no tensile stress considerations, under an axial load P, with eccentricity exceeding e_k. It must be re-emphasized that Eqs. 2.14 and 2.19 apply to uncracked, plain masonry sections.

2.3.3 Elastic Analysis of Eccentrically Loaded Reinforced Masonry Columns

2.3.3.1 General

The benefits of placing reinforcement in masonry columns have been previously considered. The same assumptions of elastic analysis for plain columns apply to reinforced columns. However, reinforcement is present to resist any flexural tensile forces in the column. Tension may or may not exist, depending on the magnitude of the eccentricity of load. Thus, in analyzing reinforced columns by the elastic theory, two cases must be considered: firstly, when the applied moment (or eccentricity) is sufficiently small, and compression exists over the whole

section; and secondly, when the eccentricity is large, and tensile stress exists over a portion of the section which is then assumed to be cracked.

The elastic theory approach employs transformed section theory, in which the steel of area A_s is transformed into an equivalent masonry area $E_s A_s / E_m$, and the "all masonry" section is analyzed by conventional methods, assuming the section to be homogeneous.

2.3.3.2 Compression Over Entire Section

The masonry stresses in a short column with uniaxial bending due to a load P acting at an eccentricity e from the centroid of the transformed section are given by:

$$f = \frac{P}{A} \pm \frac{Pey}{I} \quad \ldots\ldots\ldots\ldots\ldots\ldots \quad 2.20$$

where

y = distance from the centroid of the transformed section to the fiber under consideration

A = area of the transformed section

I = moment of inertia of the transformed section about the centroidal axis

In order to calculate e, I, and A, the position of the centroidal axis must be found by taking moments about a convenient point on the cross-section. The centroidal axis for a symmetrically reinforced section is at mid-depth.

2.3.3.3 Tension Over Part of the Section

The stress and strain diagrams for a reinforced column

subjected to a sufficiently large moment to cause cracking are shown in Fig. 2.3.

The position of the neutral axis may be calculated from internal moment and force considerations:

$$n = E_s/E_m$$

$$f'_s = \frac{kd - d'}{kd} \cdot nf_m \quad \ldots\ldots\ldots\ldots\ldots\ldots \quad 2.21$$

$$f_s = \frac{1 - k}{k} \cdot nf_m \quad \ldots\ldots\ldots\ldots\ldots\ldots \quad 2.22$$

Summing forces:

$$P = \frac{1}{2} f_m bkd + f'_s A'_{st} - f_s A_{st} \quad \ldots\ldots\ldots \quad 2.23$$

Summing moments about the section mid-depth:

$$Pe' = \frac{1}{2} f_m bkd\left(\frac{h}{2} - \frac{kd}{3}\right) + f'_s A'_{st}\left(\frac{h}{2} - d'\right) + f_s A_{st}\left(\frac{h}{2} - d'\right) \quad \ldots\ldots \quad 2.24$$

Substitution of Eqs. 2.21 and 2.22 into Eq. 2.24 results in a cubic equation which may be solved to obtain the neutral axis depth kd. By means of back-substitution of kd into Eqs. 2.21, 2.22, and 2.23, the values of f_m, f_s, and f'_s are found.

The flexural properties of the cracked section can now be calculated, and the stresses may then be checked by applying Eq. 2.20. Thus:

$$A = kbd + A_{st} + A'_{st}$$

and

$$Z = GB = \frac{(kd)^2 b/2 + A_{st}(d) + A_{st}'(d')}{A}$$

where

Z = the distance from the compression face to the centroid of the effective section

$$I = \frac{b(kd)^3}{12} + bkd(Z - \frac{kd}{2})^2 + A_{st}(Z - d)^2 + A_{st}'(Z - d')^2$$

The true eccentricity with respect to the centroid of the effective section is:

$$e = e' - \frac{h}{2} + Z$$

2.3.4 Ultimate Strength Analysis

2.3.4.1 General

The principles of reinforced concrete ultimate strength design have been, and currently are being used by designers to evaluate failure loads for masonry columns. Of course, a prime concern of this report is to investigate the validity of this assumption since, to date, experimental evidence has neither confirmed nor denied the use of this practice. The following discussion of ultimate strength analysis of reinforced concrete is restricted to rectangular, tied columns, which are those most commonly encountered in masonry structures.

The following general assumptions are made in ultimate strength design:

1. At ultimate strength, a concrete stress of intensity

0.85 times the compressive strength of a standard moist cured cylinder is assumed to act over the width of the member, and from the region of maximum compressive strain to a depth $\beta_1 c$. The distance c is the depth to the neutral axis from the region of maximum compressive strain, and β_1 is taken as 0.85 for concrete cylinder strengths below 4.0 ksi, and is reduced linearly at a rate of 0.05 for each 1.0 ksi in excess of 4.0 ksi, with a lower limit of 0.65. This basically defines Whitney's rectangular stress block.

2. Tensile strength of the concrete is assumed to be zero.

3. A linear strain distribution is present in the concrete, even at ultimate load.

4. The maximum strain at the compression face of the member is, for the most part, independent of compressive strength, and is conservatively assumed equal to 0.003. Average ε_u values of 0.0034 to 0.0038 have been reported in tests.[20,21,22]

5. Strain hardening of reinforcement steel above yield stress is neglected. Consequently, for steel strains above yield point strain, the reinforcement stress is considered equal to yield point stress.

2.3.4.2 Concentrically Loaded Short Columns

It is assumed that the entire column cross-section is stressed to an intensity of 0.85 of the concrete cylinder strength, and uniformly strained to 0.003 in./in. Furthermore, it is assumed that sufficient lateral ties are provided to enable the vertical reinforcement to yield before buckling. The ultimate strength as determined by Lyse *et al*[11,12,13], and Richart *et al*[14,15], is given by:

$$P_o = 0.85f'_c (A_g - A_s) + f_y A_s \quad \ldots\ldots\ldots \quad 2.25$$

where

P_o = ultimate load for a tied column

A_g = gross cross-sectional area of column perpendicular to the applied load

f_c = standard concrete cylinder strength

A_s = cross-sectional area of longitudinal reinforcement

f_y = yield stress of longitudinal reinforcement

It seems reasonable to consider that the compressive strength of the concrete in a column is 0.85 times that in a standard cylinder, since there is a difference in size and shape between a column and a test cylinder, and since bleeding and segregation within the concrete is more pronounced in the column than in the cylinder.

2.3.4.3 Eccentrically Loaded Short Columns--Combined Bending and Axial Load

For reinforced concrete sections resisting flexural and axial loads, there are five possible failure modes:

1. A balanced condition where, at the ultimate load, the tension reinforcement reaches yielding simultaneously with the concrete failing at the compression edge.
2. Failure by excessive concrete compressive strains before the tension steel reaches yielding.
3. A failure initiated by yielding of the tension steel at the yield point with a subsequent shift of the neutral axis, leading to excessive concrete strains.
4. Compression failure of the concrete with tension steel stresses in excess of yield point. Since the effect of strain hardening is not considered, this case is associated with failure mode 3.
5. Rupture of the tension steel following tension crack formation in the concrete. This is a brittle failure mode which only occurs with small percentages of reinforcement and is therefore not important in practical considerations.

1. Balanced Failure

This loading condition produces a compressive strain of $\varepsilon_u = 0.003$ in the extreme concrete fiber simultaneous with the strain ε_y at the first yield in the tension steel.

Referring to Fig. 2.4, considering equilibrium conditions, and assuming yield in the compression reinforcement:

$$\frac{c}{d} = \frac{0.003}{0.003 + f_y/E_s}$$

$$c = \frac{0.003d}{0.003 + (f_y/29 \times 10^6)} = \frac{87{,}000d}{f_y + 87{,}000}$$

$$a = \beta_1 c$$

$$P_u = C_c + C_s - T$$

$$P_u = 0.85f'_c ab + A'_s(f_y - 0.85f'_c) - A_s f_y \quad \ldots . \quad 2.26$$

The eccentricity e is measured from the plastic centroid whose location is defined by:

$$d'' = \frac{0.85f'_c bh\left(\frac{d - d'}{2}\right) + A'_s f'_y (d - d')}{0.85f'_c bh + A'_s f'_y + A_s f_y}$$

Note that for symmetrical sections, the plastic centroid and mid-depth coincide.

$$P_u e = C_c\left(d - \frac{a}{2} - d''\right) + C_s(d - d' - d'') + Td''$$

$$P_u e = M = 0.85f'_c ab\left(d - \frac{a}{2} - d''\right) + A'_s(f_y - 0.85f'_c) \cdot (d - d' - d'') + A_s f_y d'' \quad . . \quad 2.27$$

For symmetrical sections, Eqs. 2.26 and 2.27 may be simplified to:

$$P_u = 0.85f'_c ab - 0.85f'_c A'_s$$

$$P_u = 0.85f'_c(ab - A'_s) \quad \ldots\ldots\ldots\ldots\ldots\ldots \quad 2.28$$

and

$$P_u e = 0.425f'_c ab(h - a) + A'_s(2f_y - 0.85f'_c)\left(\frac{h}{2} - d'\right)$$

$$P_u e = 0.425f'_c ab(h - a) + A'_s(f_y - 0.425f'_c)(h - 2d')$$

$$\ldots\ldots \quad 2.29$$

2. Compression Failure

Section capacity is controlled by compression of the concrete when the ultimate eccentric load P_u is greater than the balanced load P_b, or when the eccentricity e is less than the balanced eccentricity e_b. In this case, the strain in the vertical tension reinforcement is smaller than the yield point strain. Consequently the tensile force will be some value less than that based on yield stress, and may, in fact, be a compressive force.

From the linear strain distribution of Fig. 2.4:

$$\frac{c}{d} = \frac{\varepsilon_u}{\varepsilon_u + \varepsilon_s} \qquad \varepsilon_s = \frac{(d - c)}{c} \cdot \varepsilon_u$$

$$f_s = E_s\frac{(d - c)}{c} \cdot 0.003 \quad \ldots\ldots \quad 2.30$$

$$\frac{c}{\varepsilon_u} = \frac{c - d'}{\varepsilon'_s} \qquad \varepsilon'_s = \frac{(c - d')}{c}0.003$$

$$f'_s = E_s\frac{(c - d')}{c}0.003 \quad \ldots\ldots\ldots \quad 2.31$$

If $a = \beta_1 c < h$, then Eqs. 2.30 and 2.31, in conjunction with

$$P_u = 0.85f'_c ab + A'_s(f'_s - 0.85f'_c) - A_s f_s \quad \ldots \quad 2.32$$

and

$$P_u e = 0.85f'_c ab\left(\frac{h - a}{2}\right) + A'_s(f'_s - 0.85f'_c)\left(\frac{h}{2} - d'\right) + A_s f_s\left(\frac{h}{2} - d'\right) \quad \ldots \quad 2.33$$

apply for symmetrical sections.

If $a = \beta_1 c > h$, then Eqs. 2.32 and 2.33 become:

$$P_u = 0.85f'_c bh + A'_s(f'_s - 0.85f'_c) + A_s(f_s - 0.85f'_c) \quad \ldots \quad 2.34$$

$$P_u e = A'_s(f'_s - 0.85f'_c)\left(\frac{h}{2} - d'\right) + A_s f_s\left(\frac{h}{2} - d'\right) \quad \ldots \quad 2.35$$

Solving these equations requires the difficult cubic equation solution. A method of successive approximations is suggested, which considers the actual strain variation as the unknown, and applies the principles of statics:

1. Assume a value for c in Eqs. 2.30 and 2.31, and calculate f_s and f'_s.
2. Solve for P_u in Eq. 2.33.
3. Resolve for c in Eq. 2.32.
4. Continue until the assumed and resolved values of c are sufficiently close.

3. Tension Failure

Tension in the steel controls the capacity of the section if $P_u < P_b$, or $e > e_b$. In this case, the ultimate tensile steel strain will be greater than the yield point strain. Assuming that the strain in the compression steel is larger than yield strain, and considering strain variation, and force and moment equilibrium, one obtains, with some simplification:

$$P_u = 0.85f'_c bd \left\{ \rho'(m-1) - \rho m + \left(1 - \frac{e'}{d}\right) + \sqrt{\left(1 - \frac{e'}{d}\right)^2 + 2\left[\frac{e'}{d}(\rho m - \rho' m + \rho') + \rho'(m-1)\left(1 - \frac{d'}{d}\right)\right]} \right\} \quad \ldots\ldots \quad 2.36$$

where

$$m = \frac{f_y}{0.85f'_c} \quad ; \quad \rho = \frac{A_s}{bd} \quad ; \quad \rho' = \frac{A'_s}{bd}$$

and when $\rho = \rho'$, then:

$$P_u = 0.85f'_c bd \left\{ -\rho + 1 - \frac{e'}{d} + \sqrt{\left(1 - \frac{e'}{d}\right)^2 + 2\rho\left[(m-1)\left(1 - \frac{d'}{d}\right) + \frac{e'}{d}\right]} \right\} \quad \ldots\ldots \quad 2.37$$

As for the case of compression failure, a solution may be achieved by a successive approximation procedure, in which the strain variation is assumed and the principles of statics are applied.

2.4 CSA-S304-1977 Building Code Requirements and Design Procedures for Plain and Reinforced Concrete Block Masonry Columns

In this section, the design and construction requirements for plain and reinforced concrete block masonry columns will be examined, as specified in the CSA Standard S304-1977, "Masonry Design and Construction for Buildings".

In the previous section, the capacity of plain and reinforced masonry columns was presented using engineering analysis based on the elastic working stress design procedure. In actual practice, however, account for variations in material dimensions and performance, workmanship, etc. must be considered in conjunction with purely theoretical analyses. It is the purpose of the CSA-S304-1977 Code to define these transitions between theory and practice through the provision of adequate safety factors.

In the CSA-S304 Code, the capacity of plain and reinforced masonry columns is based on allowable stresses. The allowable masonry stress f_m, is a function of the masonry compressive strength f'_m ; the latter being established either by actual prism tests (Art. 4.3.2), or by individual unit and mortar tests (Art. 4.3.3), and both methods require subsequent field control tests (Arts. 4.4.1 and 4.4.2). The maximum allowable stresses for plain concrete block and reinforced concrete block masonry are presented in Table 5 and Table 7, respectively, of the

Standard.

Depending on the magnitude of the virtual eccentricity e, of the applied load in relation to the column thickness t, two design procedures are specified by the Code. The eccentricity of the load is measured from the centroid of the member (Art. 4.6.5.6), and for rectangular columns, the effective thickness in the direction of the principal axis is taken as the actual thickness, except where raked joints are used, in which case the latter is reduced by the depth of the raking (Art. 4.6.4). It is important to note that e, the virtual eccentricity, is the sum of the eccentricity of the vertical load and the value calculated by dividing the member end moment by the axial load.

Case 1. $e \leq t/3$

1. For plain masonry columns, and reinforced masonry columns without tied reinforcement, and subject to uniaxial bending, the vertical load capacity is given in Arts. 4.6.7.1 and 4.6.7.3 as:

$$P = C_e C_s f_m A_n \quad \ldots\ldots\ldots\ldots\ldots\ldots \quad 2.38$$

2. For reinforced masonry columns with tied reinforcement under uniaxial bending, the permissible vertical load is given in Art. 4.6.7.5 as:

$$P = C_e C_s (f_m + 0.80\rho_n f_s) A_n \quad \ldots\ldots\ldots\ldots \quad 2.39$$

where, for Eqs. 2.38 and 2.39:

P = allowable vertical load

C_e = eccentricity coefficient defined in Art. 4.6.5.7

$C_e = 1.0$ for $e \leq t/20$

$$C_e = \frac{1.3}{1 + \frac{6e}{t}} + \frac{1}{2}\left(\frac{e}{t} - \frac{1}{20}\right)\left(1 - \frac{e_1}{e_2}\right) \quad \text{for } \frac{t}{20} < e \leq \frac{t}{6}$$

$$C_e = 1.95\left(\frac{1}{2} - \frac{e}{t}\right) + \frac{1}{2}\left(\frac{e}{t} - \frac{1}{20}\right)\left(1 - \frac{e_1}{e_2}\right) \quad \text{for } \frac{t}{6} < e \leq \frac{t}{3}$$

with

e_1 = the smaller virtual end eccentricity

e_2 = the larger virtual end eccentricity

Alternatively, the value of C_e may be taken from Table 9 of the Standard.

C_s = slenderness coefficient defined by Art. 4.6.2

$$C_s = 1.2 - \frac{h/t}{300} \quad 5.75 + \left(1.5 + \frac{e_1}{e_2}\right)^2 \leq 1.0$$

with

h = effective column height (Art. 4.6.3)

t = effective thickness (Art. 4.6.4)

Note that $\left(\frac{h}{t}\right) \leq 5\left(4 - \frac{e_1}{e_2}\right)$ (Art. 4.6.1)

C_s may be taken from Table 8 of the Standard

f_m = allowable masonry compressive stress
= $0.20f'_m$ for concrete block masonry columns (Tables 5 and 7 of the Standard)

A_n = net cross-sectional area

ρ_n = ratio of area of vertical reinforcement to masonry net cross-sectional area

= A_s/A_n

f_s = allowable compressive stress in reinforcement
f_s must not exceed $0.40f_y$ or 24000 psi (Art. 4.5.2)

Case 2. e > t/3

1. Where the maximum virtual eccentricity exceeds t/3, the allowable flexural tensile stress f_t, normal to the bed joints, must not be exceeded for plain masonry columns. The limits of f_t are given in Table 5 of the Standard. f_t is calculated using a linear stress distribution (Art. 4.6.7.1).

2. For reinforced masonry columns with or without tied reinforcement, and where e exceeds t/3 or a value which will produce tension in the reinforcement, the allowable load is determined on the basis of a transformed section and linear stress distribution. As well, the load must be modified for slenderness, using the C_s coefficient (Arts. 4.6.7.3 and 4.6.7.5).

3. For columns without lateral ties, compression reinforcement is neglected (Art. 4.6.7.3).

4. The maximum permissible compressive stress in the masonry is governed by flexure in this case, hence:

   $f_m = 0.28f'_m$ for concrete masonry columns
   (Table 7 of the Standard)

5. From Article 4.5.2, the allowable tensile and compressive stresses in the reinforcement must not exceed 18000 to 24000 psi, depending on grade.

6. The elastic modulus of the steel E_s is assumed as 29×10^6 psi (Art 4.5.3), and for the masonry, $E_m = 1000f'_m$ (Table 7 of the Standard).

Article 5.9 of the Standard specifies block type and lateral support spacings for masonry columns. Vertical and lateral reinforcement details are outlined in Arts. 4.6.8.3, 4.8.4.21, and 4.11.

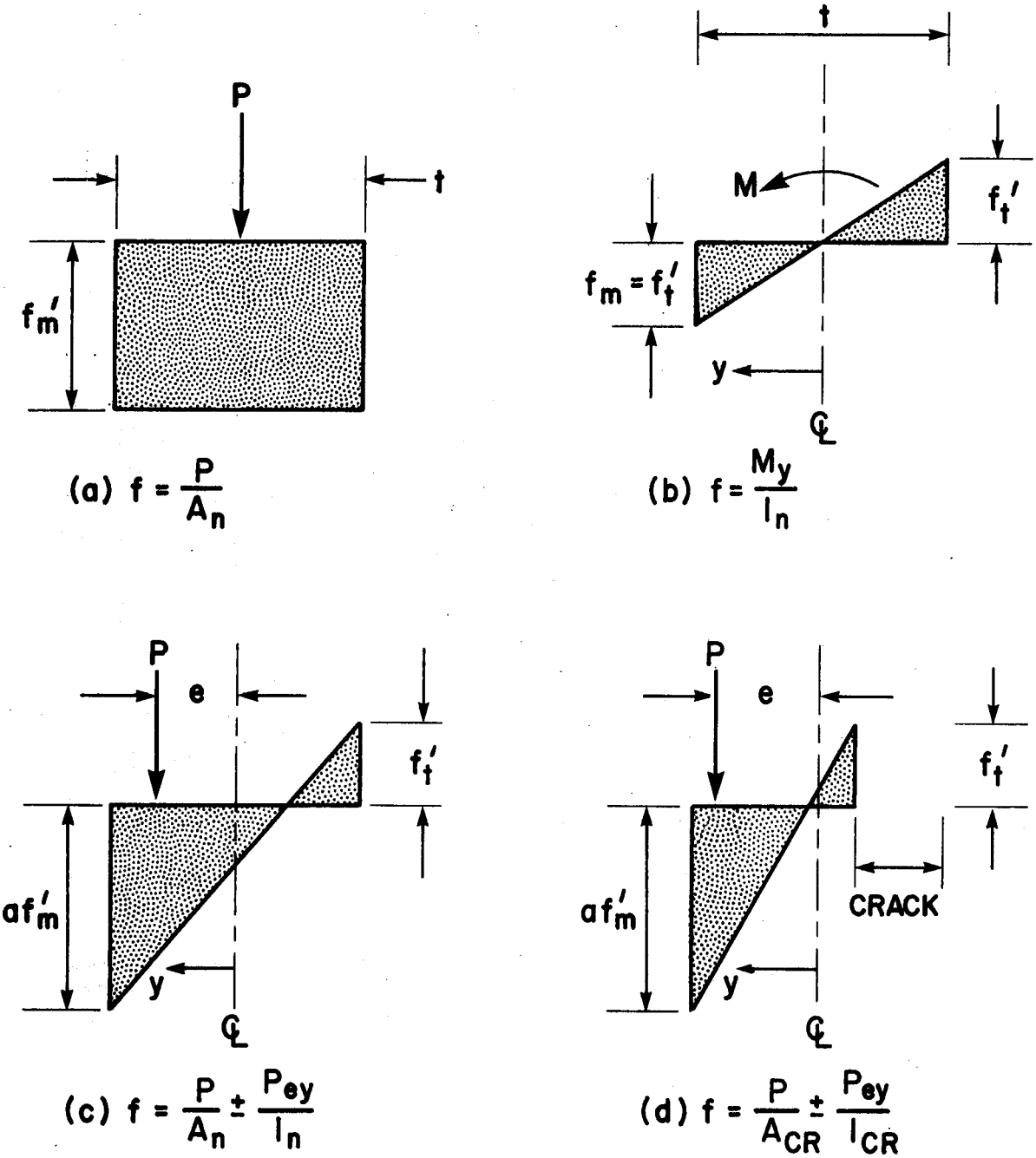

FIGURE 2.1 Stress Distributions in Masonry at Failure for Various Load-Moment Combinations

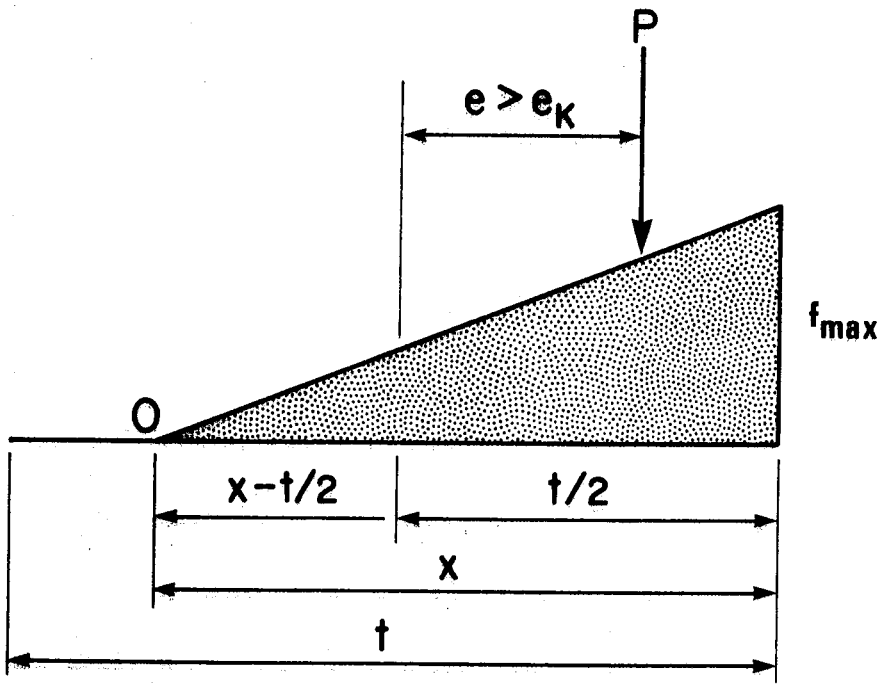

FIGURE 2.2 Stress Distribution for Plain Masonry with Solid Cross-section, Zero Tensile Strength, and Having Eccentricity of Load Greater than the Kern Eccentricity

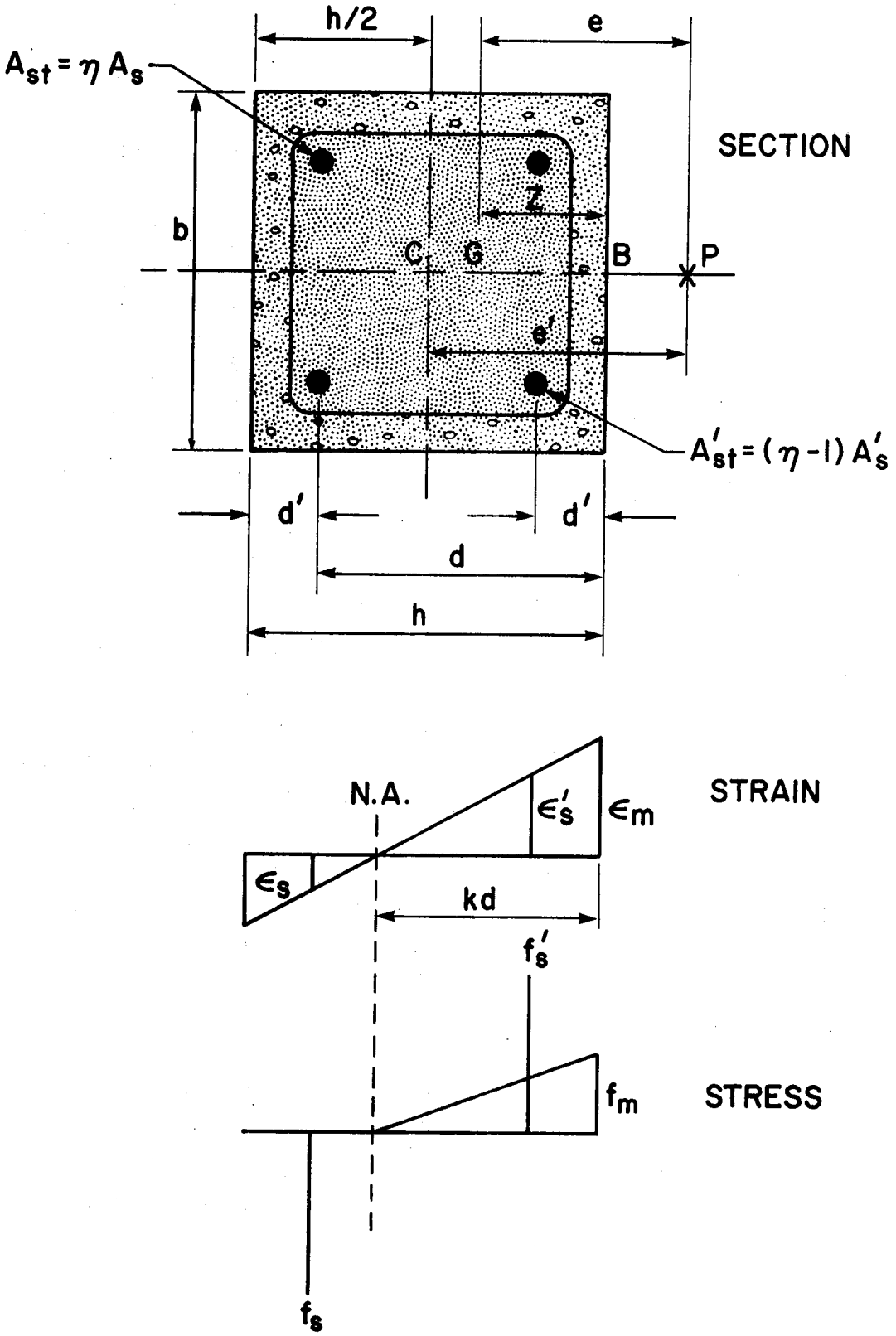

FIGURE 2.3 Cracked Reinforced Masonry Column with Eccentric Loading

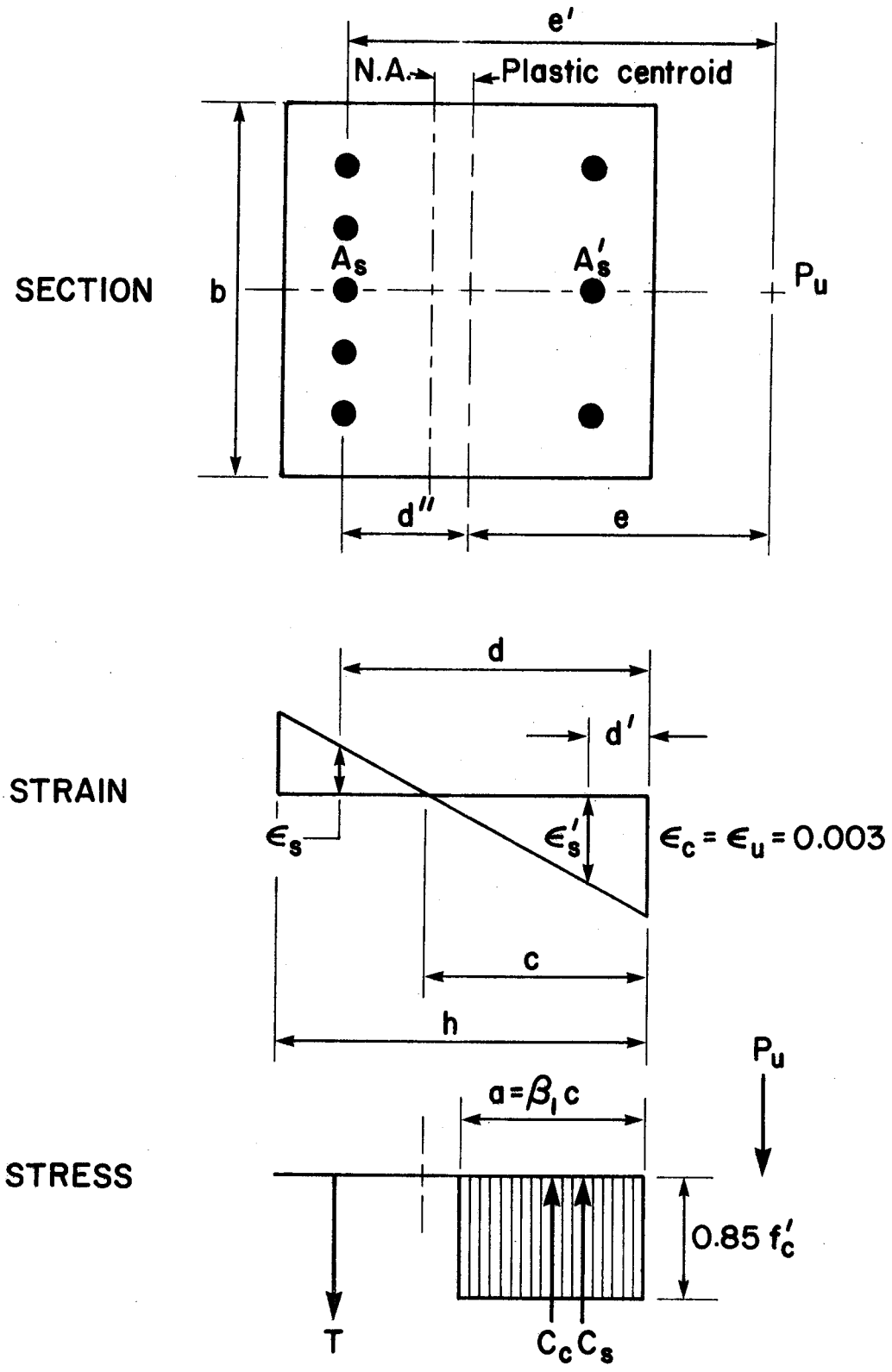

FIGURE 2.4 Stresses and Strains in Reinforced Concrete Sections for Ultimate Conditions

3. EXPERIMENTAL PROGRAM

3.1 Materials

All materials used for the construction of the test specimens are readily available on the Edmonton commercial market, and are representative of those used in masonry construction in the area.

3.1.1 Concrete Block Units

All columns and prisms were constructed with lightweight, autoclaved, 16 in. single core blocks. The unit nominal dimensions are shown in Fig. 3.1. Physical properties, based on three test repetitions in accordance with ASTM C140, are listed in Table 3.1. Gross area measurements for ten block samples are recorded in Table 3.2.

3.1.2 Mortar

The mortar used in all columns and prisms was type S, proportioned in accordance with the specifications of CSA-S304-1977. Type I portland cement, type S hydrated lime, and masonry sand were proportioned 1:1/2:4 by volume. The sieve analysis of the sand, as shown in Table 3.3 and plotted in Fig. 3.2, conformed to the requirements of ASTM C144. Moisture content was determined by ASTM C566, and found to be 5.9%.

From each mortar batch, six 2 x 2 x 2 in. cubes were

cast in accordance with ASTM C109. Of these, four cubes were cured in saturated lime water, and the remaining two were stored in the laboratory under the same conditions as their companion columns and prisms. All cubes were tested at 28 days. Because the columns were constructed with a horizontal line spanning as many as twelve columns, and each batch permitted laying of approximately fifty blocks, the mortar strength varied at different elevations in the columns. Retempering was permitted, but mortar older than 3-1/2 hours was not used.

3.1.3 Grout and Concrete

Five mix designs with varying compressive strength and slump were used in the test program. Mix proportions, design strength, slump and designation for these mixes are given in Table 3.4.

Concrete mixes 5C and 4C were obtained from local ready-mix suppliers. The remaining mixes, 3C, 3G, and 2C were batched in the laboratory. Mixes 5C and 4C represented strengths in excess of the block unit strength, and mixes 3C, 3G, and 2C provided strengths below block unit strength. Type I normal portland cement, CSA Type 10, was used in all five mixes.

The aggregate used in laboratory batching was obtained from a local supplier and stored in overhead bins in the laboratory until required. Results of moisture content, specific gravity, and absorption analyses, in accordance

with ASTM C566 and ASTM C127, for the laboratory concrete sand, 3/8, and 3/4 inch aggregates, appear in Table 3.5. Sieve analyses for these aggregates, as well as for the 3/8 - 3/4 inch blend employed in mix 3C, are given in Tables 3.6 through 3.9, and are plotted in Figs. 3.2 and 3.3. Although these aggregates did not conform to ASTM C33, deviations were small, and they were considered satisfactory for the experimental program. Sieve analyses for those aggregates used in the ready-mix were not available, but assurances were made that these satisfied ASTM C33 requirements.

Laboratory concretes were mixed in a rotary type, upright, flat bottom mixer of nine cubic foot capacity. All batches were about seven cubic feet in volume. Generally, this permitted filling a single column, or 2-1/2 prisms, with some material remaining for control specimens. Mixing time for each batch was about ten minutes to ensure uniformity. Because the moisture content in the aggregates varied from mix to mix, the slump was maintained constant rather than the amount of water added.

With each batch of concrete for Series A columns, generally two standard cylinders, and two 4 x 4 x 7-5/8 in. block moulded prisms were cast. Of these, one cylinder and one prism were moist cured; the remaining cylinder and prism were cured in the laboratory under conditions identical to those of the test specimens. For the remaining series, only the cylinders were cast and both were moist cured.

The ready-mix concretes were ordered in sufficient

volume to permit grouting of all the desired columns from one load. Consequently, ten standard cylinders and ten 4 x 4 x 7-5/8 in. block moulded specimens were cast and considered representative of each mix design. For Series A, seven specimens of each were moist cured, and the remaining three were laboratory cured. For the other series, all control specimens were standard moist cured cylinders. Block moulded prisms and air cured cylinders were eliminated subsequent to Series A tests since moist cured cylinders were found to be better representative of the concrete strengths within the columns.

All control specimens were tested at the same age as the corresponding column or prism.

3.1.4 Reinforcement

Vertical reinforcement of Imperial sizes and strengths was not readily available at the time of construction. As a substitute, deformed metric bars #20M - 300MPa yield, #20M - 400MPa yield, and #25M - 400MPa yield were used as vertical reinforcement for the columns. All ties were bent from 1/4 in. diameter, plain bars.

Tension tests were conducted to determine reinforcement yield and ultimate strengths. The bars exhibited a well defined yield point and yield plateau. Table 3.10 reports the yield and ultimate strengths of each bar type. Each value is the average of at least five tests. Coefficients of variation were all below 3 percent. The idealized

stress-strain relationships are shown in Fig. 3.4.

3.2 Test Specimens

A detailed description of the column and prism specimens and their methods of fabrication are presented in this section.

3.2.1 Columns

3.2.1.1 General

Fifty-nine, nine block high, short columns were constructed using the 16 in. single core pilaster units described in Section 3.1.1. Full mortar bedding was used and a joint thickness of 3/8 inch was maintained. Nominal column dimensions were thus, 72 inches by 16 inches square. Figure 3.5(a) illustrates schematically the dimensions of these columns.

Variables considered in the materials or method of fabrication were: 1) percent and grade of vertical reinforcement, 2) grout compressive strength and slump, and 3) lateral tie details.

The following sections will provide more detailed information concerning these variables, and how they were incorporated into fabrication.

3.2.1.2 Details of Reinforcement

The columns were designed to have three percentages of longitudinal steel; 0.76, 1.3, and 2.6 based on the gross

cross-sectional area of the column. A 0.76% was achieved by using four #20M bars at the four column corners; 1.3% was similarly obtained using four #25M bars; and for 2.6%, an additional four #25M bars were placed with the latter, two on each opposing side. The reinforcement percentages selected in the test program provided a good range within those permitted by CSA-S304-1977, (0.5 to 4.0%). Unreinforced, grouted columns were considered to contain 0% reinforcement; consequently, the program effectively examined four reinforcement percentages.

Where longitudinal steel was required, ties were wired directly to the steel, and all reinforcement was then placed in the column as a unit. Several columns were constructed without vertical reinforcement, but with grout and lateral ties. In these cases, the horizontal reinforcement was placed within the mortar joint of the cross-section. According to CSA-S304, either location is acceptable. An 8 inch vertical spacing was maintained for all tie reinforcement, with an exception at the ends for those columns containing vertical reinforcement. An additional lateral tie was placed 3 inches from the column top and bottom to assist in the prevention of local crushing failures.

All lateral ties were fabricated from 1/4 inch diameter plain steel. This diameter was selected on the basis of observations and recommendations by Feeg[8] (1978). Ties were cut from 20 ft. lengths supplied by the fabricator. All ties

were bent cold, using a jig and lever arm. This process permitted tight dimensional control with uniform tie sizing. Five tie types were used in the program; dimensions are shown in Fig. 3.6. Type A and Type D ties were used with the #20M bars; Type B and Type E were used in conjunction with the #25M bars and Type C, which were somewhat larger, were placed in those columns with lateral, but no vertical reinforcement. Type C ties required straightening for ease of placement in the 3/8 inch mortar joints, which necessitated small tack welds at the tie hook. Plates 3.1 and 3.2 show the three basic styles of lateral ties used in the study.

The configuration of vertical reinforcement for the varying percentages, spacing, and clearances are also illustrated in Fig. 3.6. Longitudinal reinforcement spacing and clearance, and tie bend diameters, hooks, spacing and clearance, all conform to the ACI-318-77, CAN3-A23.1, CAN3-A23.3, and CSA-S304-1977 Standards. The concrete Standards, however, recommend that at least a #3 deformed bar be used as lateral reinforcement for vertical bars of #7 and #8 sizes. Fig. 3.6 also shows the locations of tie SR-4 electrical resistance strain gauges used in testing.

Plates 3.3 through 3.7 illustrate the construction of a typical reinforcement cage. Eighty inch lengths of vertical reinforcement were cut from the 40 ft. lengths supplied by the fabricator. The eight inches in excess of column height, as will be shown later, afforded a means of transport for

the column once it had been constructed. Before wiring the cages, all SR-4 electrical resistance strain gauges were mounted on the reinforcing steel and waterproofed.

Two reinforcement bars were first placed on the saw horses as shown in Plate 3.3. As illustrated in Plate 3.4 , lateral ties were introduced over these bars, and oriented such that all tie hooks subtended one vertical bar. This would tend to create a line of structural weakness along this bar. This scheme is probably representative of construction methods, and constitutes the conservative, least favourable condition. After the two lower bars were positioned, all bar ends were inserted into wooden templates to maintain bar spacing, and the lateral ties were positioned for wiring. Interior and exterior views of a typical connection are shown in Plate 3.5 and Plate 3.6, respectively. Plate 3.7 is a photograph of the completed cage.

3.2.1.3 Column Fabrication

All columns and prisms were constructed by an experienced mason providing good workmanship. All lower course blocks for columns which were to be grouted had a 4 x 4 inch clean-out hole cut in one face using a rotary concrete saw blade. Surface irregularities on the bottom of these blocks were chiselled to provide a flat surface for column construction. Any blocks with flaws, such as large chips or cracks, were rejected.

For all columns, the first course was centered on a 1/2 in. x 15-5/8 in. square, fir plywood template which had been placed on a polyethylene sheet covering the structural floor. These templates had pre-drilled clearance holes to assist centering of the reinforcement cages after the column shell had been constructed. Templates, with proper hole sizing and spacing, were available for each of the three percentages of vertical reinforcement examined in the study. Columns with no vertical reinforcement were placed on solid templates to provide equal elevation and permit more rapid construction. No mortar joint was placed between the template and the first course. All templates were oiled to facilitate easy separation from the concrete following cure. These construction techniques are shown in Plates 3.8 and 3.9.

For those columns of Series B, in which the blocks were stripped from the concrete core, all blocks used in their construction were first notched at one corner, then lined with paper towels. The paper towels acted as a porous separator which permitted water to be absorbed by the block from the core, and at the same time, prevented a bond at the interface. Later, by hammering the notch with a chisel, sufficient tensile forces were introduced which split the block, and allowed its removal without distress to the core.

The mason kept the inner column face in alignment using a horizontal line and level. In this fashion, as many as twelve columns were constructed simultaneously.

A description of mortar type was provided in Section 3.1.2. The mortar was retempered several times during a 3-1/2 hr. period, after which time, remaining mortar was discarded.

No particular attention was paid to the orientation of the blocks as they were laid, except that the smooth block surface with the wide face shell was placed up, hence the block face shells tapered (narrowed) downward. The mortar joints on both exterior and interior faces were cut flush, with the former being tooled to provide concave joints. Mortar droppings were removed from the bottom through the clean-out hole after erecting the column shell. The mortar was then permitted to cure for approximately a week before grouting.

In the interim, 1/4 in. diameter holes were drilled through the bed joint between the fifth and sixth courses to accommodate electrical connections for the SR-4 strain gauges mounted on the reinforcement cages. As the cages were lowered into the columns by an overhead crane, these electrical wires were pulled through the holes and secured to prevent them from being drawn inward during grouting. The cages were centered by positioning the ends of the bars in the pre-drilled holes in the templates at the column bases. For those columns containing 2.6% vertical reinforcement, the additional four lengths of vertical reinforcement not wired into the cage were dropped separately into their respective holes, and were then tack welded to the cage top

using two steel bars spanning the cage sides. This can be seen in Plate 3.11. Following placement of the reinforcement cages, the column bottom was vacuumed to remove fallen block particles.

For those columns containing lateral, but no vertical reinforcement, the horizontal ties were pushed into the mortar bed as the column shell was being constructed. This technique is common construction practice and does not permit the mortar to fully envelop the reinforcement.

As indicated in Section 3.1.3, concrete was either ready-mixed or batched in the laboratory. In both cases, the column grouting procedure was identical. A four sided box with dimensions 14 x 14 x 12 inches, constructed of 1/2 in. plywood, was placed over the column to be grouted, and was sufficiently secured by the 8 in. extensions of the vertical reinforcement. All clean-out holes were closed by clamping planks across them. Concrete was lifted in a "concrete buggy" above the columns using the overhead crane. The concrete was released and passed through a plywood funnel which rested on planks above the column, through the plywood box, and into the column. The columns were grouted in one lift. The concrete was then vibrated with a one inch diameter vibrator. Neither grouting nor vibration caused damage to the column shell. These procedures are shown in Plates 3.10 and 3.11.

For those columns of Series B, in which the external column shells were stripped, metal banding was placed around

the lower four courses to prevent splitting during grouting.

Following vibration, the columns were trowelled smooth, then air cured in the laboratory environment maintained at about 70 deg. F and 40% relative humidity.

3.2.2 Prisms

Forty-seven, four block high prisms were built using the 16 in. single core pilaster units described in Section 3.1.1. Five of these prisms were ungrouted, and forty-two were grouted with the design mixes described in Section 3.1.3. Eight of the grouted prisms were subsequently stripped to permit testing of the cores alone. All prisms contained neither vertical or lateral reinforcement. Figure 3.5(b) illustrates schematically the dimensions of these prisms. Their h/t ratio of 2 fulfills the requirements of CSA-S304-1977 for prism specimens.

The fabrication and cure of these control specimens followed closely those procedures outlined for column construction in the previous section.

3.3 Program of Study

3.3.1 Columns

The following characteristics are peculiar to all columns tested, and since each can affect the strength and behavior of masonry, they are considered to be controlled variables in this study.

1. A 15-5/8 inch square cross-section, employing

autoclaved, lightweight, single core pilaster units of equal strength.

2. Type S mortar with full bedding, and 3/8 inch joints.
3. Concentric or eccentric vertical load applied through pinned ends.
4. A height of 72 inches, corresponding to a height/thickness ratio of 4.5.
5. Fiberboard end capping.
6. Longitudinal reinforcement flush with the column ends.
7. Vertically reinforced columns tied with 1/4 in. diameter, plain steel at 8 in. centers, and in contact with the longitudinal reinforcement.

In order to eliminate the effects of slenderness, S304-1977 specifies that the column height to thickness ratio must not exceed 5.0. In the present study, 4.5 was selected, since this corresponded to a nine course high specimen, and provided a block face at midheight to facilitate the mounting of SR-4 electrical resistance strain gauges.

High lateral constraint at the bearing plates of the testing machine due to plaster or sulfur capping have been observed to restrict lateral expansion of masonry specimens, and produce shear or diagonal tension failure. A reduction in this lateral restraint creates a tensile failure which is typically the mode responsible for failure of masonry under compression. Previous studies[41,42,43] have shown that a fiberboard capping effectively reduces this bearing plate restraint and more closely models masonry service conditions than does high strength, stiff compounds. The use of fiberboard capping is known to reduce individual block

compressive strength by about 10 percent as compared to plaster capping.

Earlier tests at Lehigh and Illinois[11,14] (1931) showed that concrete columns with longitudinal steel flush with their ends developed higher strength than columns with capitals or spliced reinforcement.

The fifty-nine columns in this study were divided into six series, with each series examining a particular variable of concrete block masonry column design. A description of these series follows.

1. **Series A**

Variables considered in this series were:

1. effect of percentage and grade of vertical reinforcement on column behavior; and
2. effect of concrete compressive strength on column behavior.

Two longitudinal reinforcement steel grades, 300MPa and 400MPa yield, as described in Section 3.1.4, were employed. Henceforth, these will be referred to as Grade 40 (ksi) and 60 (ksi) steels, respectively. Four percentages of longitudinal reinforcement were used: 0, 0.76, 1.3, and 2.6 percent.

Low slump concrete (4 to 6 inches), with 28 day compressive strengths of 1.5, 2.5, 4.0, and 5.0 ksi were selected for this series. These correspond to mix designs 2C, 3C, 4C, and 5C in Section 3.1.3.

The variables and their effects on column strength and behavior were investigated using the column details

described in Table 3.11. A total of twenty-four columns were tested under axial, concentric compression.

2. Series B

This series consisted of three columns identical to those constructed in Series A, with 0.76%, Grade 60 longitudinal reinforcement and concrete compressive strengths of 2.5, 4.0, and 5.0 ksi (mix designs 3C, 4C, and 5C), but with stripped shells. These columns were to assist in determining the relationship between concrete strengths provided by standard cylinder or block moulded prism tests, and the actual strength of the column core. Ultimately, by comparison with companion Series A columns, these were to assist in the evaluation of the individual contributions of the column core and shell to the ultimate strength of the masonry column.

These columns were tested under axial, concentric compression. Details of these columns are provided in Table 3.12.

3. Series C

Series C columns modelled those columns of Series A which were grouted with mix design 3C, (a 2.5 ksi, 4 in. slump concrete). These columns, however, were grouted with mix design 3G, (a 2.5 ksi, 9 in. slump grout). Thus, the effect of slump on the behavior and strength of masonry columns could be evaluated by comparison of A and C series specimens. The details of these six columns are presented in Table 3.13. All columns were tested under axial, concentric

compression.

4. Series D

The Series D study was initiated after the completion of Series A column tests. Statistically, more meaningful data would be acquired if several column tests of Series A were duplicated. Those columns of Series A containing Grade 60 steel, with 0.76, 1.3, and 2.6 percent longitudinal reinforcement, and mix designs 5C and 3C, were selected for duplication. As well, another ungrouted column shell was tested. The details of these seven columns are listed in Table 3.14.

5. Series E

The behavior and strength of reinforced masonry columns subjected to combined bending and axial load were examined in Series E. Variables considered in this study were concrete strength, and grade and percentage of longitudinal reinforcement.

Identical columns were axially loaded under eccentricities of 0, t/12, t/6, and t/3. These test results were to provide data for the construction of interaction diagrams in the region of $e < e_b$ or $P > P_b$ to assist in the evaluation of theoretical modelling. Previous research has shown that for eccentricities greater than t/3, particular attention must be paid to the design of the loading plate or column cap to achieve the desired compression-flexure failure at midheight, and prevent local crushing failure at the top of the specimen. To avoid these difficulties,

eccentricities less than t/3 were selected in this study.

Although different loading plates were used for Series A and Series E columns, concentric compression test results of identical Series A columns were considered to be representative of a Series E column with a zero eccentricity. Minor dimensional differences between the two plate types would only slightly alter height/thickness ratios of the columns, but would not alter the strength and behavioral characteristics. Loading plate details are discussed in Section 3.5.

Series E column details are presented in Table 3.15.

6. Series F

Series F consisted of six columns of identical construction to those of Series A, except that 135 deg. bends plus 4 in. extensions were used as hooks on the lateral ties (Type D and E ties of Section 3.2.1.2), rather than 90 deg. bends plus 2-1/2 in. extensions (Type A and B ties of Section 3.2.1.2).

The effect of tie anchorage on the behavior and ultimate load of the columns was assessed by comparing the test results for Series F with results for similar columns of Series A and D.

Column details are given in Table 3.16. All were tested under axial, concentric compression.

3.3.2 Prisms

The following characteristics are common to all prisms

tested, and are considered to be controlled variables in the study.

1. Nominal 16 in. square, single core pilaster units.
2. Type S mortar with full bedding and 3/8 in. joints.
3. Concentric vertical load applied through a flat, fixed bottom end, with swivel platen at the upper end.
4. Height/thickness ratio of 2.
5. Fiberboard end capping.

Companion prisms were built at the time of construction of a given column series. Thus, the only variable which these prisms monitored was concrete mix design. Details of these prisms appear in Table 3.17.

As mentioned in Section 3.2.2, the shells of eight prisms; two in the CP3.- series, three in the DP5.- series, and three in the DP3.- series, were stripped to permit separate testing of the concrete core.

3.4 Instrumentation

3.4.1 Mortar Cubes

Vertical and lateral strains for a number of 2 x 2 x 2 in. mortar specimens were measured by 1-inch concrete strain gauges attached to the cube face. Although lateral restraint by the loading head on a specimen of this size would significantly reduce lateral deformations, it was felt that this restraint was representative of the actual interaction between a concrete block and the mortar in a joint.

3.4.2 Concrete Cylinders and Block Moulded Prisms

Vertical strains for the block moulded prisms were taken as the average of the readings from two 1 in. concrete strain gauges mounted on opposing block faces. Lateral strain measurements were provided by a single strain gauge mounted at midheight.

Vertical deformation measurements for the concrete cylinders were obtained by means of a dial gauge with 0.0001 inch increments, supported by two concentric aluminum rings clamped to the cylinders. Lateral strains were approximated by a 1-inch strain gauge attached to the circumferential face of the cylinder at midheight.

3.4.3 Concrete Masonry Blocks

Deformations in the unit masonry block were monitored in the same fashion as those of the concrete block moulded prisms.

3.4.4 Columns

Lateral deflections of the columns were measured at midheight of every second course using linear variable differential transducers (LVDT's) capable of reading 0.0001 in. These transducers were fixed on an independent support and attached to the column with thin wires about three feet in length. This length effectively eliminated apparent transverse deflections resulting from vertical deformations of the column and fiberboard cap.

Strains on the east and west column face were monitored using LVDT's spanning a 32-inch gauge length centered at column midheight. Special pin supports were manufactured which provided rotational freedom for the LVDT's in the direction of column bending. These supports are shown in Plate 3.12. Vertical and lateral strains in the block face of the column were measured at column midheight using 1-inch concrete strain gauges. Strains in the reinforcing steel were measured by means of 1/2 inch steel strain gauges. On the vertical reinforcement, these were placed at column midheight, and for the lateral reinforcement, a gauge was fixed on the inside face of the tie located immediately below column midheight, as shown in Fig. 3.6.

For columns under eccentric load, additional LVDT's monitoring 16 in. gauge lengths centered at column midheight, were attached to the column face at positions corresponding to the interior placement of the longitudinal steel corner bars.

Schematic diagrams illustrating instrumentation for each column type are shown in Fig. 3.7. Plate 3.13 illustrates typically, the instrumentation of these columns.

3.4.5 Prisms

Strains on the east and west prism face were recorded using LVDT's monitoring 24-inch gauge lengths centered at prism midheight. As well, a number of specimens had 1 in. concrete strain gauges attached to measure vertical and

lateral block strains. Schematic diagrams illustrating instrumentation are shown in Fig. 3.7. Plate 3.14 shows prism instrumentation prior to testing.

3.4.6 Data Collection and Processing

Vertical load, horizontal deflections, and strains were monitored and recorded automatically using the NOVA 210/E digital computer. After completion of each test, these data were transferred to the AMDAHL 470 computer for subsequent processing.

3.5 Test Procedure

3.5.1 Columns

The cages of longitudinally reinforced columns were made about 8 inches longer than the columns to facilitate transport. Reinforcement bars were welded across diametrically opposing bars to provide a hook for the overhead crane. Those columns and prisms containing no reinforcement but with grout only, had a U-hook embedded in their top surface at the time of grouting. Those columns consisting of shells only were transported by bar clamps and forklift. Transport details are shown in Plates 3.15, 3.16, and 3.17.

Columns and prisms to be tested with stripped shells had these shells removed only a few days before testing to permit gauge mounting. Shell removal is shown in Plate 3.18.

Before placing a column in the testing machine, the 1/2 in. long vertical steel projections on the column bottom, and the 8 in. projections on the top were cut off with an oxy-acetylene torch. The bar ends were ground flush with the concrete surface using a disc grinder, and the surfaces were then brushed clean.

The column was then positioned in the testing machine using the bar clamp device and forklift shown in Plate 3.17. All concentrically loaded columns were oriented such that tie hooks were situated in the north-west corner. For eccentrically loaded columns, the column was rotated 90 degrees so that hooks were in the north-east corner in a potential tension zone.

A 1/2 inch by 15-5/8 inch square natural Tentest fiberboard capping was used on the column bottom. Because of concrete shrinkage, the column top was somewhat dished, hence a plaster cap was first cast, followed immediately by a fiberboard cap. A small preload, on the order of 10 kips, was applied to seat the fiberboard in the plaster, and maintain the column in plumb.

Vertical load was applied by the head of a 1.4 million lb. capacity hydraulic testing machine. As mentioned earlier, different loading plates were used for eccentrically and concentrically loaded columns. Those for the latter are shown in Plates 3.19 and 3.20. The lower support consisted of a 2 in. thick, 15-3/4 in. square steel plate, supported by a semi-circular rocker positioned in a

cylindrical groove. Pin action was provided in the east-west direction. At the column top, the swivel head of the testing machine doubled as the pin and loading plate.

For eccentrically loaded columns, load was applied through a 10 in. deep and 15-3/4 in. square steel channel section, with 3/4 in. side plates and a 3 in. base. By welding small C sections to the side plates, threaded rods could be positioned and tightened to bear the plates against the block course, and assist in the prevention of local crushing failures. A 2 in. diameter cold rolled steel bar resting between two 2 in. thick, 4 in. wide steel plates with cylindrical grooves was placed on top of the channel section in contact with the machine platen. The same type of plate was provided at the column bottom. Pin action was provided in the east-west direction. This device is shown in Plate 3.21. By moving the roller assembly to predetermined positions on the channel, and securing it with bolts threaded into the roller, plates and channel, the desired eccentricities could be got.

Following vertical alignment of the column, transducers were positioned, and all electrical connections were made.

A preload of about 75 kips was applied to all columns, with the exception of the ungrouted, unreinforced specimens, for which a preload of only 25 kips was applied. This load was reduced to 5 kips, strain gauges were balanced, and initial readings were taken. Subsequent readings were recorded at convenient load increments. To prevent damage to

the instrumentation, the LVDT's were normally removed just prior to column failure.

3.5.2 Prisms

As indicated in Section 3.3.2, concentric vertical load was applied through a flat, fixed bottom end, and a swivel platen upper end, with fiberboard caps. Prisms were positioned, and load was applied using the same procedure as for the column specimens.

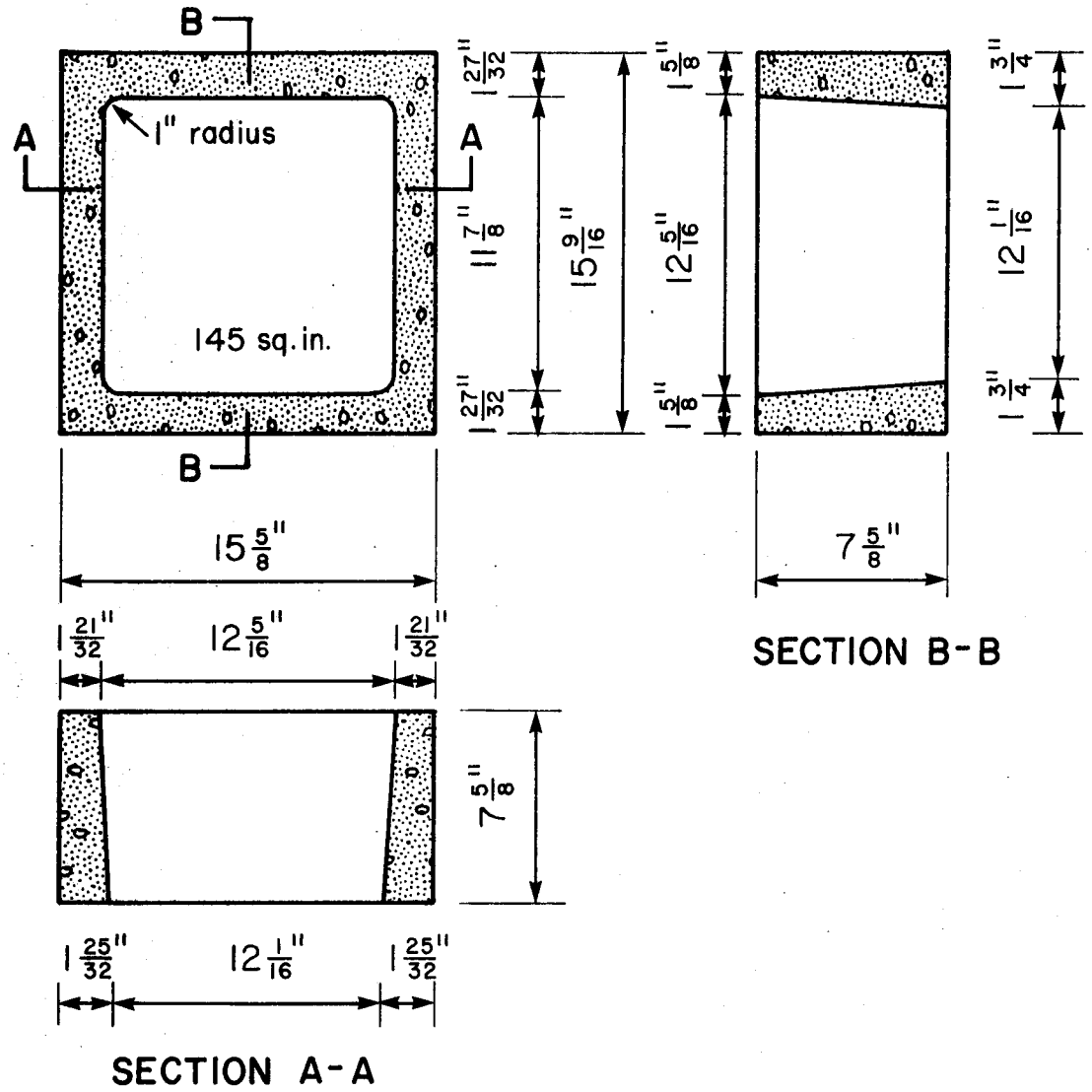

FIGURE 3.1 Dimensions of Single Core Pilaster Concrete Block Units Used in the Study

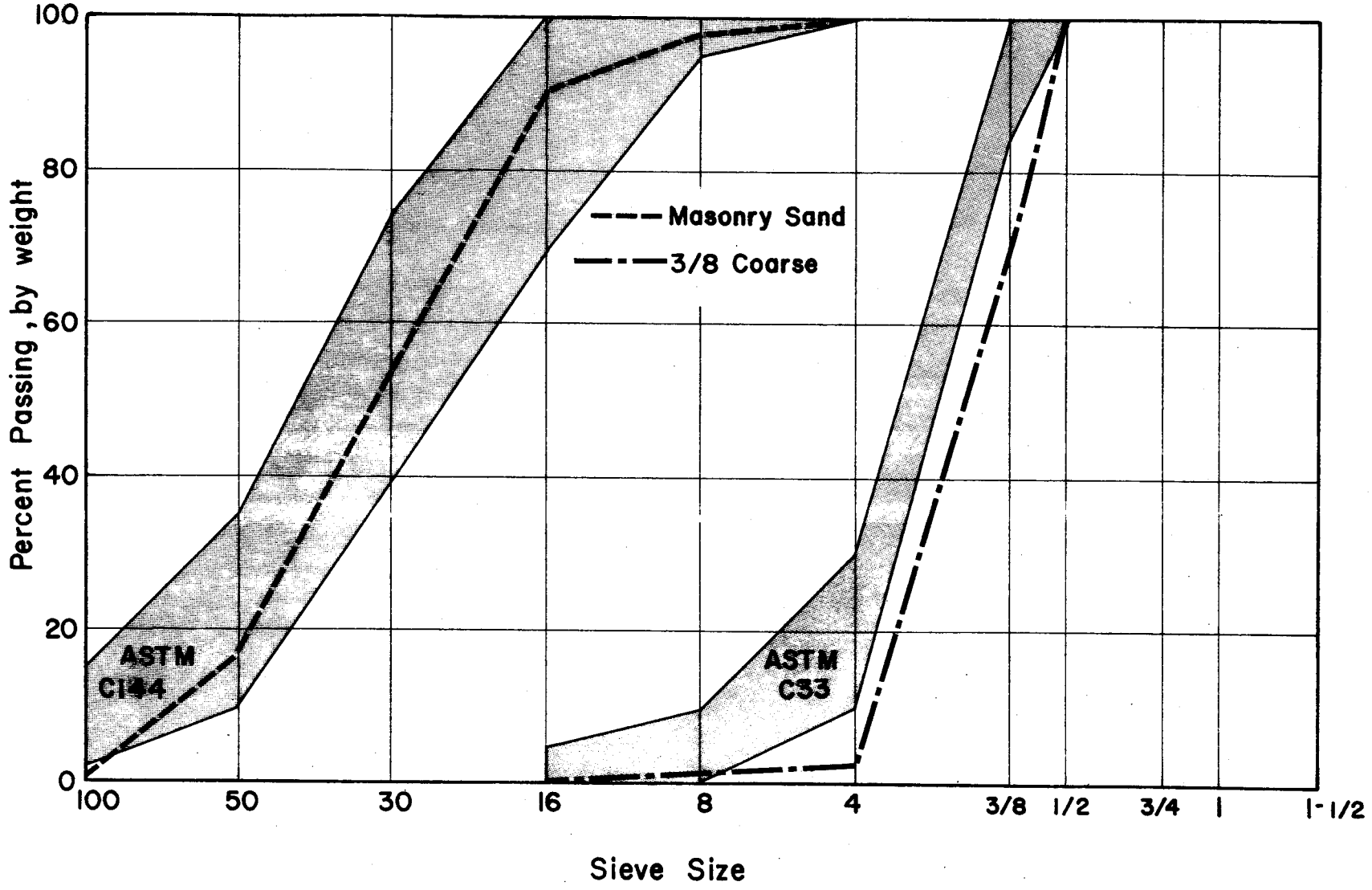

FIGURE 3.2 Sieve Analysis and ASTM Requirements for Masonry Sand and 3/8-in. Laboratory Aggregate

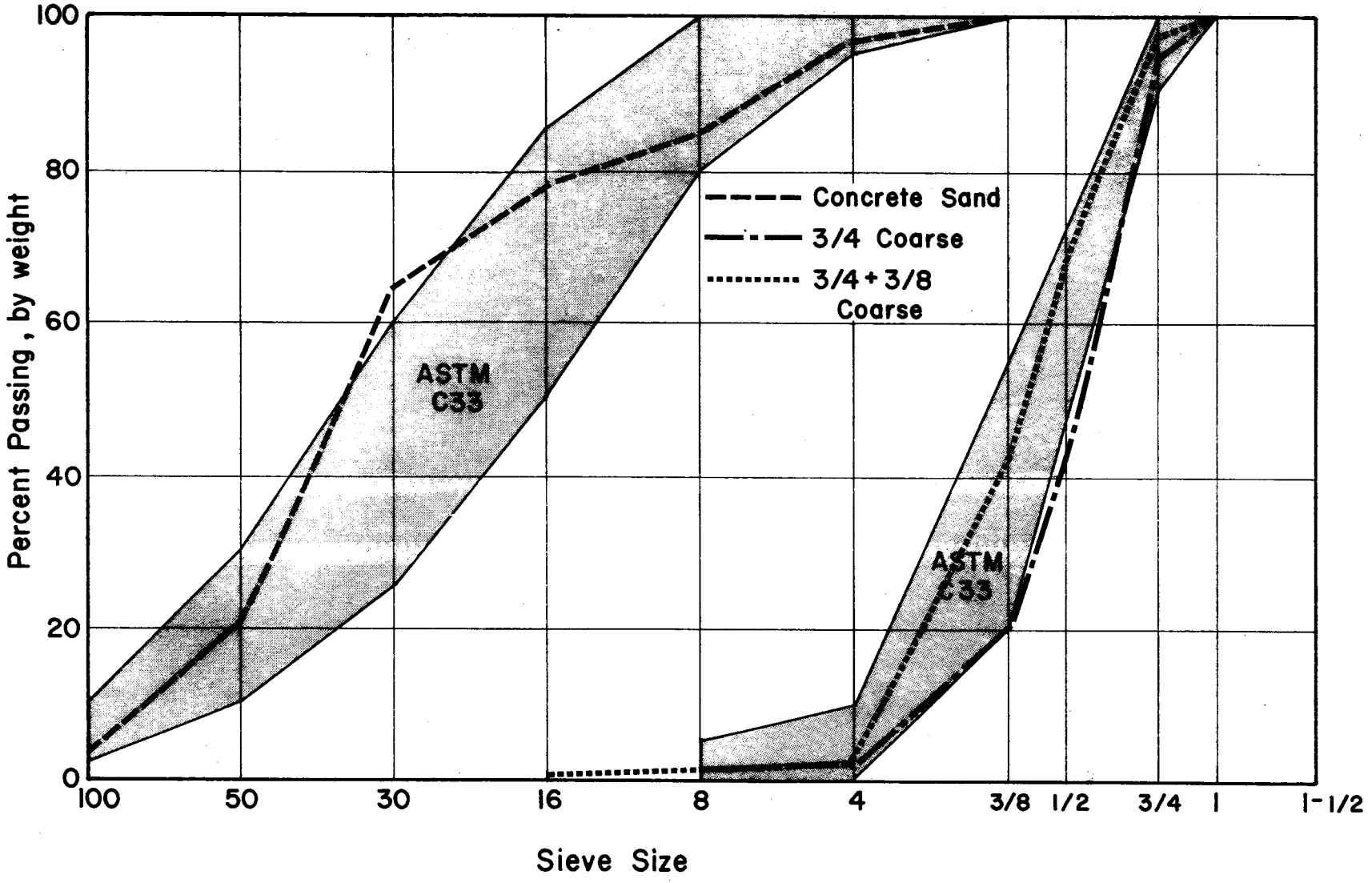

FIGURE 3.3 Sieve Analysis and ASTM Requirements for Concrete Sand, and 3/4-in. and 3/4-3/8-in. Blend Laboratory Aggregates

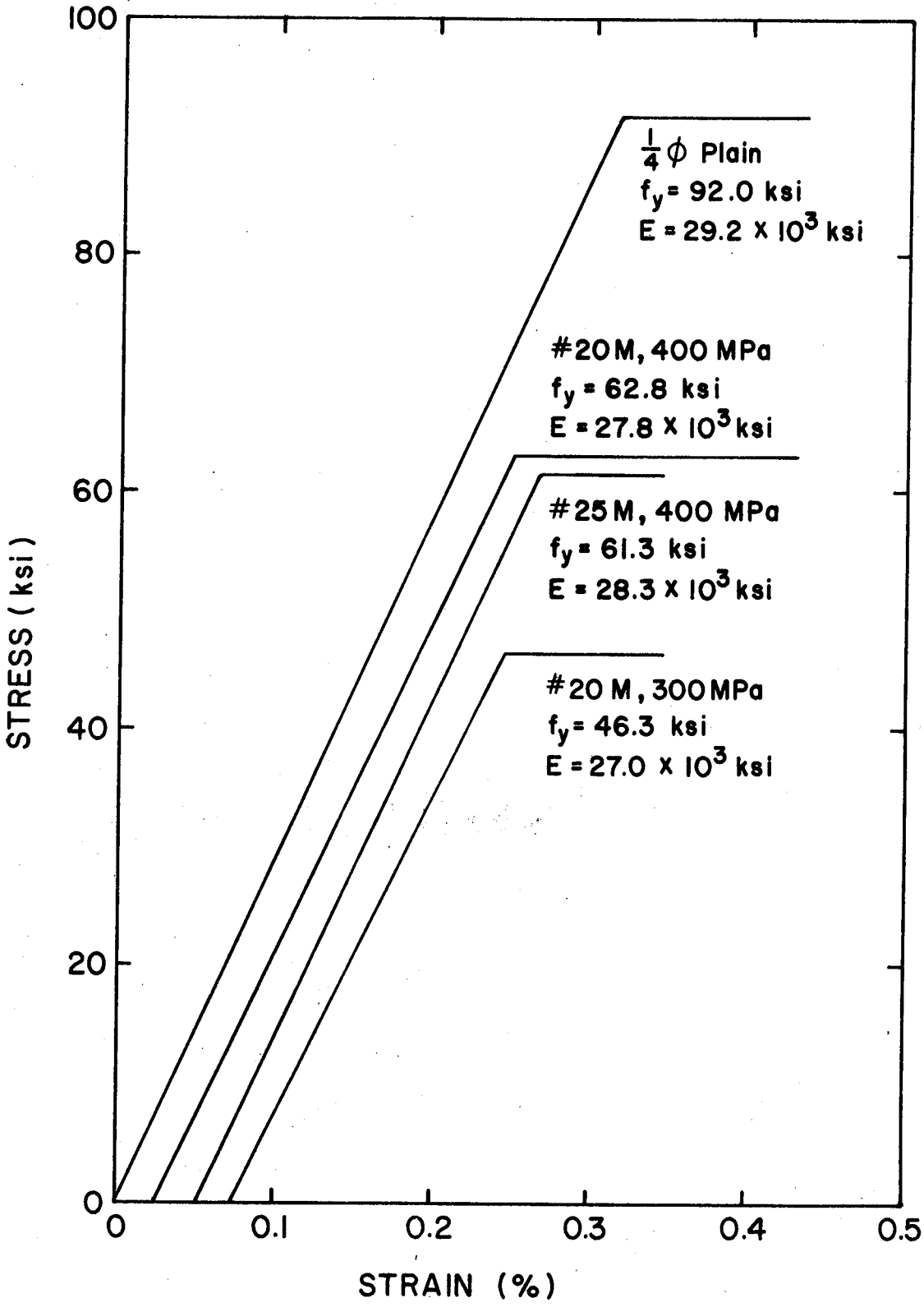

FIGURE 3.4 Idealized Stress-Strain Relations for Reinforcing Steel

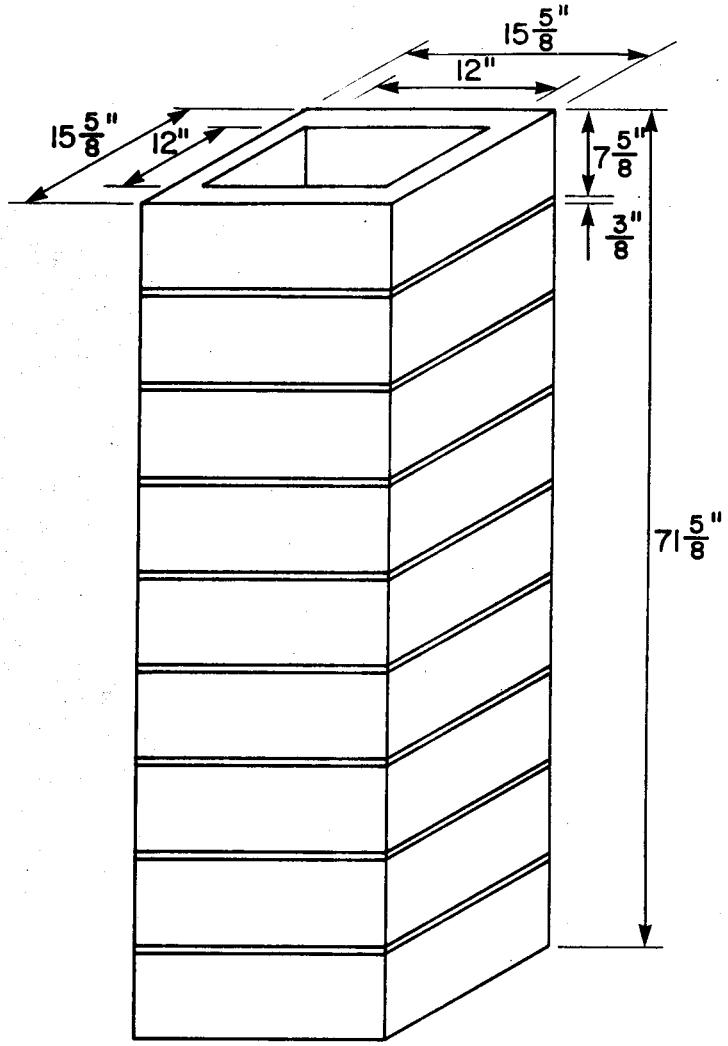

FIGURE 3.5(a) Column Specimen Dimensions

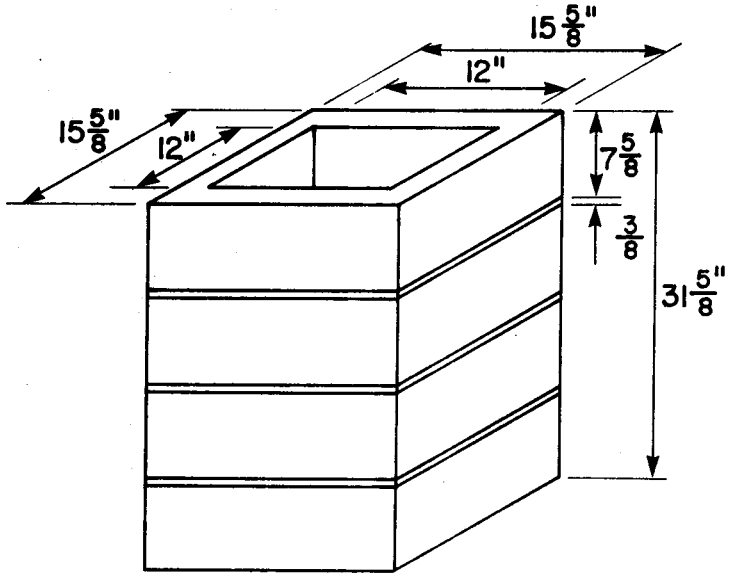

FIGURE 3.5(b) Prism Specimen Dimensions

TYPE A TIES

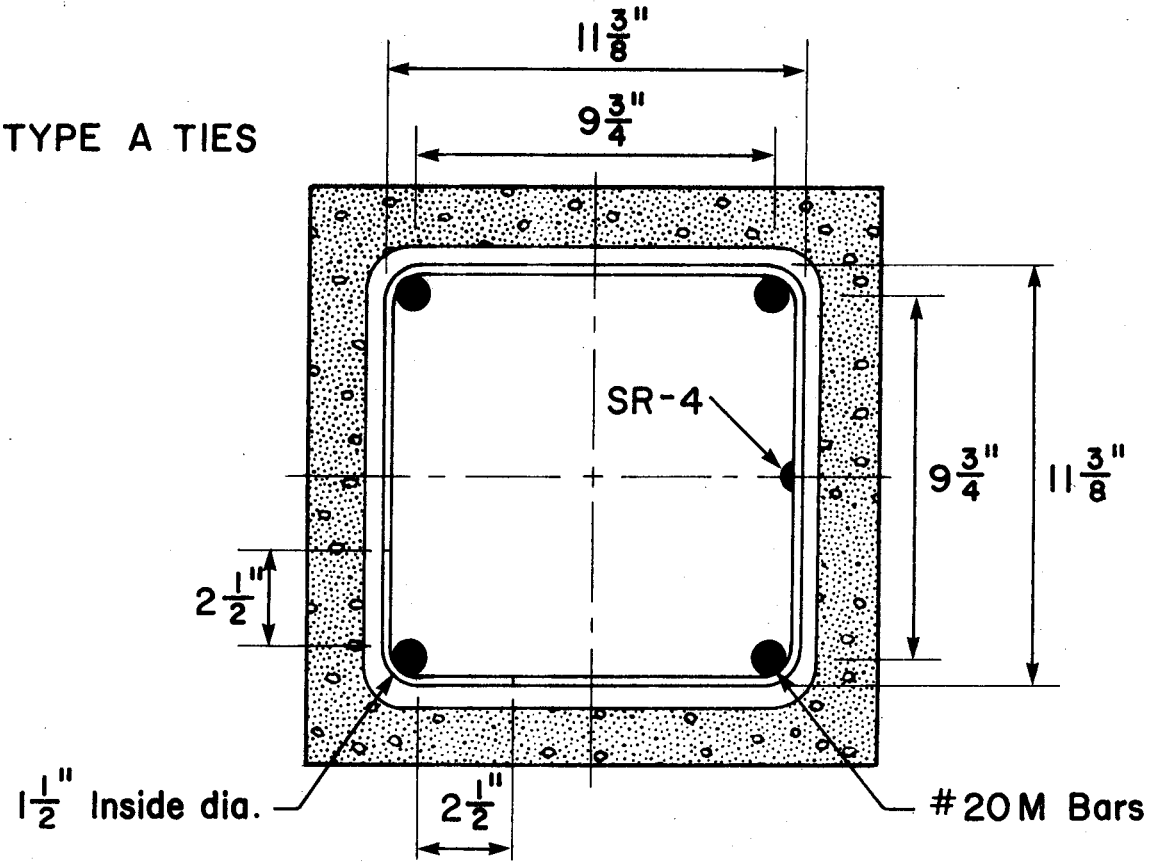

TYPE B TIES

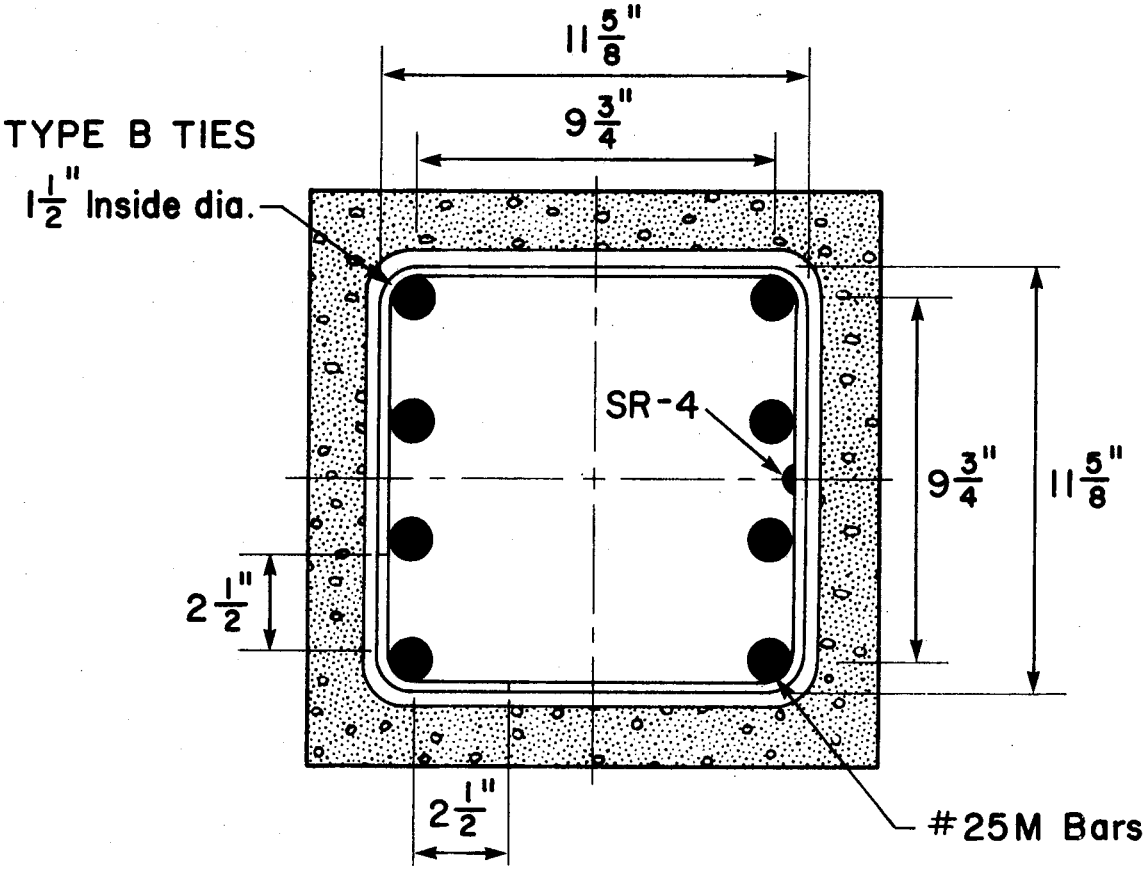

TYPE C TIES

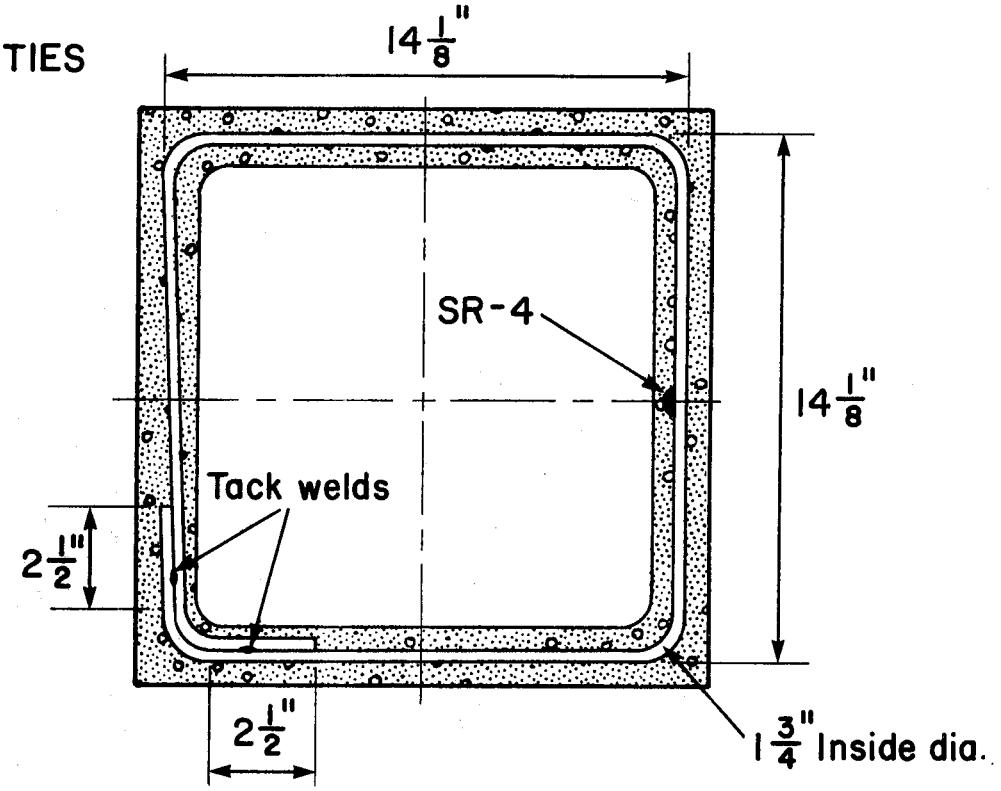

TYPE D TIES

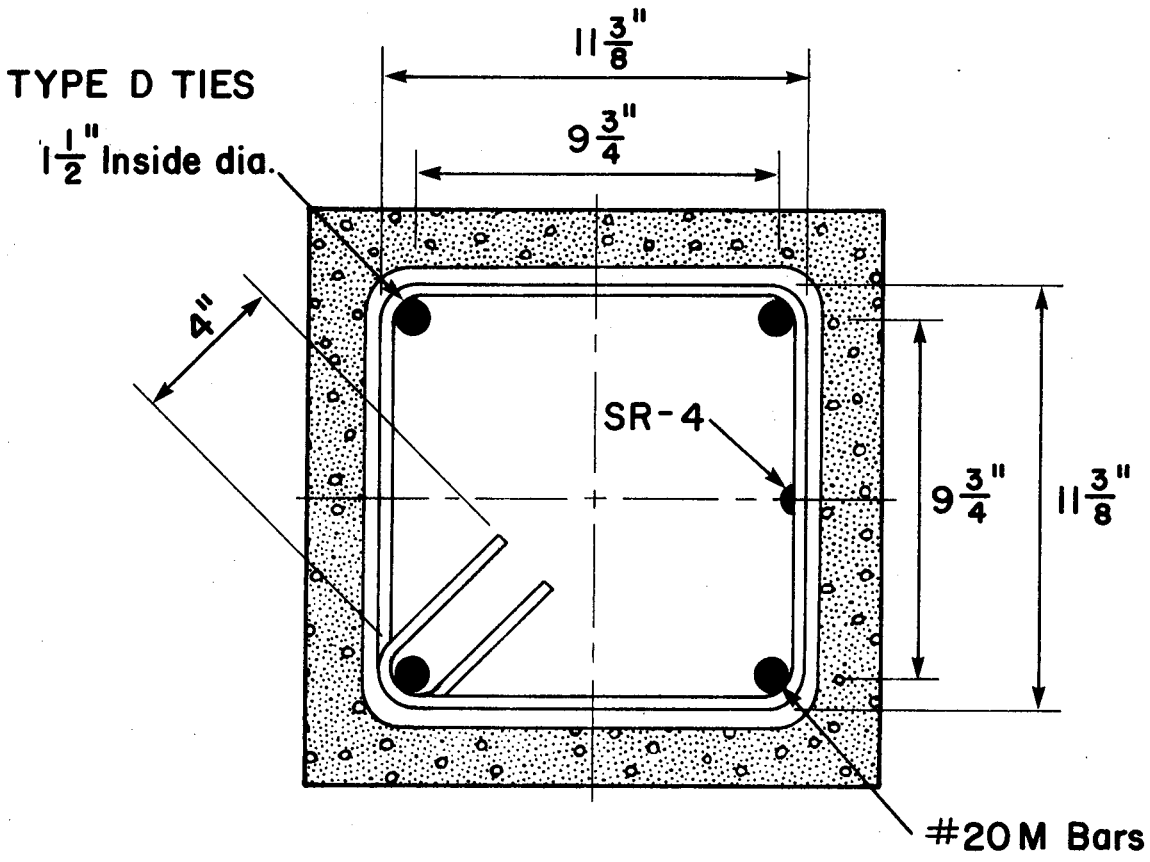

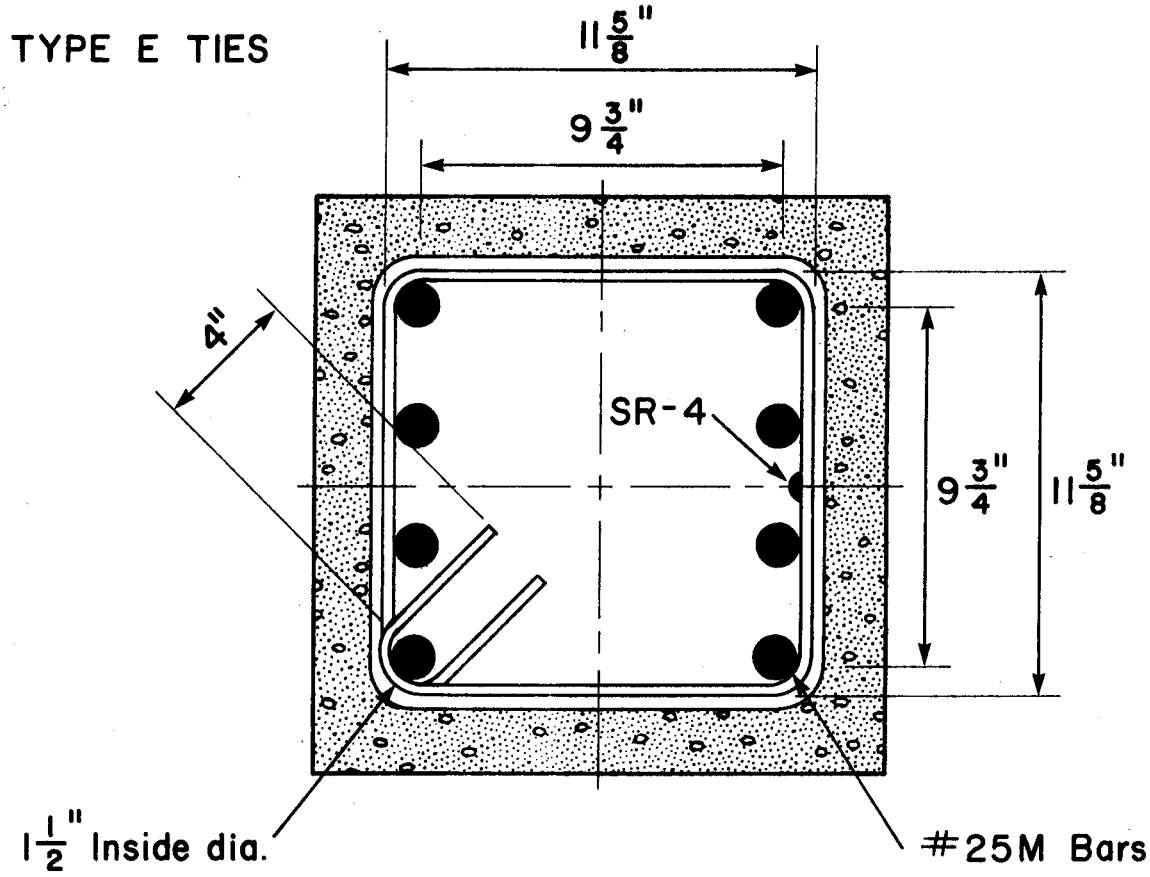

FIGURE 3.6 Tie Type, Dimensions, Spacings and Clearances of Column Cross-sections

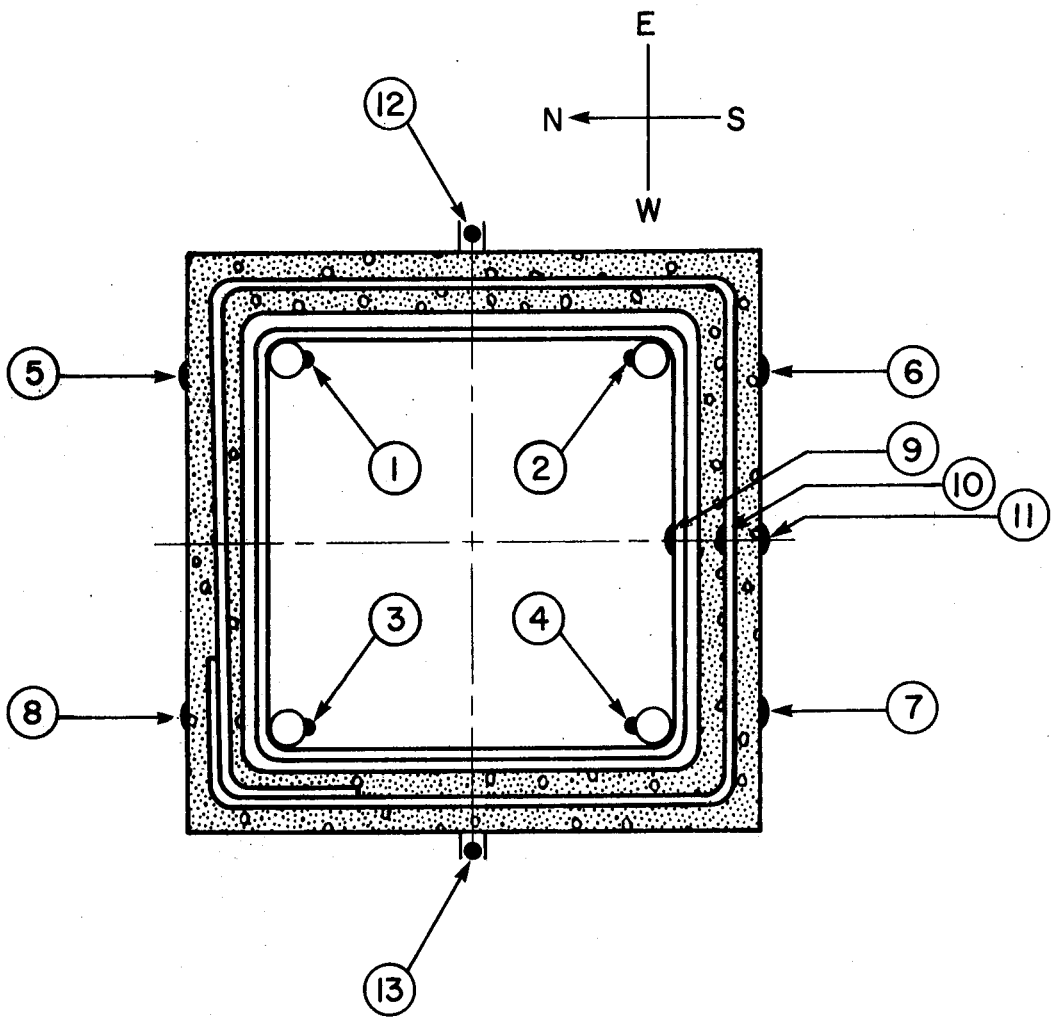

1-4: Vertical SR-4 Steel Strain Gauges--1/2 in.
5-8: Vertical Concrete Strain Gauges--1 in.
9-10: Lateral SR-4 Steel Strain Gauges--1/2 in.
11: Lateral Concrete Strain Gauge--1in.
12-14: Vertical LVDT---32 in. Gauge Length

Instrumentation

A Columns Contain 1,4,5,7,9,11,12,13
B Columns Contain 1,2,3,4,5,6,7,8,9,11,12,13
C Columns Contain 5,7,11,12,13
D Columns Contain 5,7,10,11,12,13

FIGURE 3.7(a) Concentrically Loaded Column Instrumentation

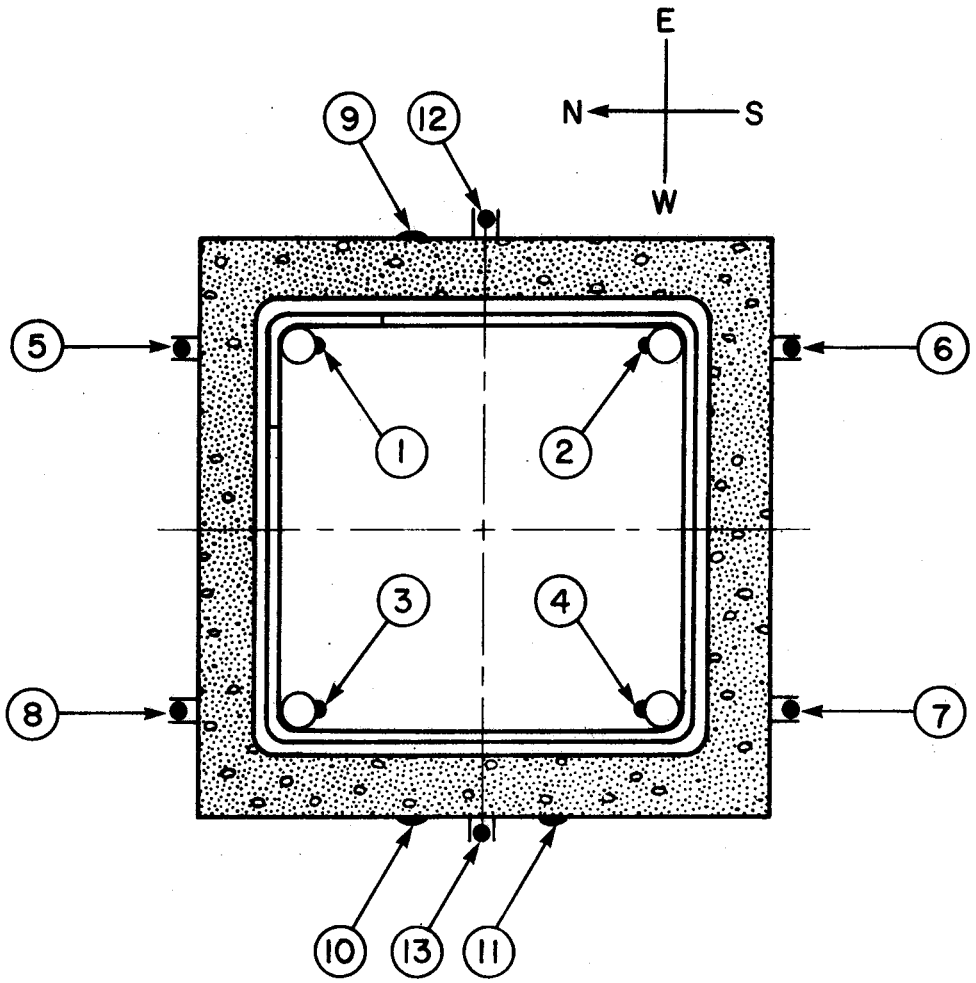

1-4: Vertical SR-4 Steel Strain Gauges--1/2 in.
5-8: Vertical LVDT--16 in. Gauge Length
9-10: Vertical Concrete Strain Gauges--1 in.
11: Lateral Concrete Strain Gauge--1 in.
12-13: Vertical LVDT--32 in. Gauge Length for Columns
--24 in. Gauge Length for Prisms

Instrumentation

E Columns Contain All of the Above
Prisms Contain 10,11,12,13

FIGURE 3.7(b) Eccentrically Loaded Column, and Prism Instrumentation

Table 3.1: Physical Properties of Concrete Block Units

Pilaster Unit 16in. Single Core	Nominal Dimensions			Actual Dimensions		Net Area	Absorption		Moisture Content	Density
	Width (in.)	Height (in.)	Length (in.)	Width (in.)	Length (in.)	(%)	(lb./ft.^{3})	(%)	(%)	(lb./ft.^{3})
1	15 5/8	7 5/8	15 5/8	15 17/32	15 17/32	39.3	15.5	16.6	33.5	93.3
2	15 5/8	7 5/8	15 5/8	15 9/16	15 17/32	39.4	15.7	16.6	29.0	94.5
3	15 5/8	7 5/8	15 5/8	15 17/32	15 9/16	39.3	14.2	15.6	9.9	90.9
					Avg.	39.3	15.1	16.3	24.1	92.9

Table 3.2 : Dimensions, Gross Area and Net Area of Concrete Block Units

Block No.	Length (in.)	Width (in.)	Gross Area (in^2)	Net Area (in^2)
P1	15 9/16	15 9/16	242.2	95.2
P2	15 35/64	15 9/16	241.9	95.1
P3	15 35/64	15 9/16	241.9	95.1
P4	15 17/37	15 19/32	242.2	95.2
P5	15 9/16	15 9/16	242.2	95.2
P6	15 9/16	15 19/32	242.7	95.4
P7	15 9/16	15 19/32	242.7	95.4
P8	15 9/16	15 9/16	242.2	95.2
P9	15 9/16	15 19/32	242.7	95.4
P10	15 9/16	15 9/16	242.2	95.2
Average	15.55	15.57	242.1	95.2
σ	0.014	0.022	0.4	0.2
C.V. %	0.09	0.14	0.18	0.18

Table 3.3 : Sieve Analysis of Masonry Sand

Sample Size = 110.66 g.

Sieve No.	Sample Wt. Retained (g)	% Retained	Cumulative % Retained	% Passing
4	0	0	0	100
8	2.38	2.2	2.2	97.8
16	7.82	7.1	9.2	90.8
30	40.62	36.7	45.9	54.1
50	41.26	37.3	83.2	16.8
100	17.44	15.8	99.0	1.0
pan	1.14	1.0	-	-
Total	110.66	100.0	239.5	
Fineness Modulus 2.40				

Table 3.4 : Concrete and Grout Mix Design

Mix Designation	28 Day Design Strength (ksi)	Slump (in)	Mix Proportions by Weight (Kg/m^3)	Air Entrainment
5C	5.0	6	C:415 S:730 1/2A:500 3/4A:540 H_2O:151	No
4C	4.0	5	C:340 S:715 3/4A:1080 H_2O:160	Yes (to give 5 ± 1% air content)
3C	2.5	4	C:310 S:895 3/8A:510 3/4A:650 H_2O:230	No
3G	2.5	9 1/2	C:395 S:985 3/8A:750 H_2O:255	No
2C	1.5	4	C:215 S:875 3/4A:1065 H_2O:215	No

Table 3.5 : Moisture Content, Specific Gravity, and Absorption of Laboratory Aggregates

Max. Size Aggregate	Moisture Content (%)	Specific Gravity (Bulk)	Absorption (%)
3/4	0.2	2.53	1.4
3/8	0.4	2.47	1.7
Concrete Sand	2.4	-	-

Table 3.6 : Sieve Analysis for 3/4 in. Laboratory Aggregate

Sample Size = 19.35 lbs.

Sieve No.	Sample Wt. Retained (lb)	% Retained	Cumulative % Retained	% Passing
1	0	0	0	100
3/4	1.15	5.9	5.9	94.1
1/2	10.40	53.7	59.6	40.4
3/8	4.05	20.9	80.5	19.5
4	3.40	17.6	98.1	1.9
8	0.10	0.5	98.6	1.4
pan	0.25	1.3	-	-

Table 3.7 : Sieve Analysis for 3/8 in. Laboratory Aggregate

Sample Size = 2164.6 g.

Sieve No.	Sample Wt. Retained (g)	% Retained	Cumulative % Retained	% Passing
1/2	0	0	0	100
3/8	668.9	30.9	30.9	69.1
4	1437.9	66.4	97.3	2.7
8	45.4	2.1	99.4	0.6
16	1.8	0.1	99.5	0.5
pan	14.8	0.7	-	-

Table 3.8 : Sieve Analysis for 3/4-3/8 Laboratory Aggregate Blend for Mix 3C

Sample Size = 30.00 lbs.

Sieve No.	Sample Wt. Retained (lb)	% Retained	Cumulative % Retained	% Passing
1	0	0	0	100
3/4	0.99	3.3	3.3	96.7
1/2	9.01	30.3	33.3	66.7
3/8	7.60	25.3	58.6	41.4
4	11.72	39.1	97.7	2.3
8	0.28	0.9	98.6	1.4
pan	0.40	1.3	-	-

Table 3.9 : Sieve Analysis for Laboratory Concrete Sand

Sample Size = 591.8g.

Sieve No.	Sample Wt. Retained (g)	% Retained	Cumulative % Retained	% Passing
4	19.1	3.23	3.23	96.77
8	72.6	12.27	15.50	84.50
16	40.9	6.91	22.41	77.59
30	78.2	13.21	35.62	64.38
50	262.2	44.31	79.93	20.07
100	100.2	16.93	96.86	3.14
pan	18.6	3.14	-	-
Total	591.8	100	254	
Finess Modulus	2.54			

Table 3.10 : Mechanical Properties of Steel Reinforcement

Bar Type	No. of Tests	Yield Strength (ksi) f_y	Ultimate Strength (ksi) f_u	Elastic Modulus (ksi) E	First Yield Strain ε_y
1/4 Ø, plain	5	92.0	99.7	29.2×10^3	3.15×10^{-3}
#20,300MPa	5	46.3	76.5	27.0×10^3	1.71×10^{-3}
#20,400MPa	8	62.8	104.0	27.8×10^3	2.26×10^{-3}
#25,400MPa	11	61.3	100.2	28.3×10^3	2.17×10^{-3}

Table 3.11: Series A Column Details

Column Mark	28 Day Concrete Strength (ksi)	Concrete Mix Design	Longitudinal Reinforcement				Instrumentation Refers to Fig. 3.7	Tie Type
			Grade (ksi)	Percent (ρ)	Area (A_s) (in^2)	Detail		
A1	1.5	2C	N/A	0[x]	0	N/A	C	N/A
A2.1	2.5	3C	"	"	"	"	"	"
A2.2	2.5	3C	"	"	"	"	"	"
A3	4.0	4C	"	"	"	"	"	"
A4.1	5.0	5C	"	"	"	"	"	"
A4.2	5.0	5C	"	"	"	"	"	"
A5	1.5	2C	40	0.76	1.86	4-#20M	A	A
A6	2.5	3C	"	"	"	"	"	"
A7	4.0	4C	"	"	"	"	"	"
A8	5.0	5C	"	"	"	"	"	"
A9	1.5	2C	60	0.76	1.86	4-#20M	A	A
A10	2.5	3C	"	"	"	"	"	"
A11	4.0	4C	"	"	"	"	"	"
A12	5.0	5C	"	"	"	"	"	"
A13	2.5	3C	N/A	0†	0	N/A	D	C
A14	2.5	3C	60	1.3	3.1	4-#25M	A	B
A15	2.5	3C	60	2.6	6.2	8-#25M	B	B
A16	5.0	5C	N/A	0†	0	N/A	D	C
A17	5.0	5C	60	1.3	3.1	4-#25M	A	B
A18	5.0	5C	60	2.6	6.2	8-#25M	B	B
A19	N/A	N/A	N/A	0[x]	0	N/A	C	N/A

x - no ties
† - ties within mortar bed

Table 3.12: Series B Column Details

Column Mark	28 Day Concrete Strength (ksi)	Concrete Mix Design	Longitudinal Reinforcement				Instrumentation Refers to Fig. 3.7	Tie Type
			Grade (ksi)	Percent (ρ)	Area (A_s) (in^2)	Detail		
B1	2.5	3C	60	0.76	1.86	4-#20M	A	A
B2	4.0	4C	"	"	"	"	"	"
B3	5.0	5C	"	"	"	"	"	"

Table 3.13: Series C Column Details

Column Mark	28 Day Concrete Strength (ksi)	Concrete Mix Design	Longitudinal Reinforcement				Instrument-ation refers to Fig. 3.7	Tie Type
			Grade (ksi)	Percent (ρ)	Area (A_s) (in^2)	Detail		
C1	2.5	3G	N/A	0[x]	N/A	N/A		N/A
C2	2.5	3G	40	0.76	1.86	4-#20M	A	A
C3	2.5	3G	60	0.76	1.86	4-#20M	A	A
C4	2.5	3G	N/A	0[†]	N/A	N/A	D	C
C5	2.5	3G	60	1.3	3.1	4-#25M	A	B
C6	2.5	3G	60	2.6	6.2	8-#25M	B	B

x - no ties
† - ties within mortar bed

Table 3.14: Series D Column Details

Column Mark	28 Day Concrete Strength (ksi)	Concrete Mix Design	Longitudinal Reinforcement				Instrument-ation refers to Fig. 3.7	Tie Type
			Grade (ksi)	Percent (ρ)	Area (A_s) (in^2)	Detail		
D12	5.0	5C	60	0.76	1.86	4-#20M	A	A
D17	5.0	5C	60	1.3	3.1	4-#25M	A	B
D18	5.0	5C	60	2.6	6.2	8-#25M	B	B
D10	2.5	3C	60	0.76	1.86	4-#20M	A	A
D14	"	"	"	1.3	3.1	4-#25M	A	B
D15	"	"	"	2.6	6.2	8-#25M	B	B
A19.1	N/A	N/A	N/A	N/A	N/A	N/A	C	N/A

Table 3.15: Series E Column Details

Column Mark	28 Day Concrete Strength (ksi)	Concrete Mix Design	Longitudinal Reinforcement				Eccentricity	Instrumentation refers to Fig. 3.7	Tie Type
			Grade (ksi)	Percent (ρ)	Area (A_s) (in^2)	Detail			
E1.1	2.5	3C	40	0.76	1.86	4-#20M	+/6	E	A
E1.2	"	"	"	"	"	"	+/12	"	"
E1.3	"	"	"	"	"	"	+/3	"	"
E1.4	"	"	"	"	"	"	+/3	"	"
E3.1	5.0	5C	40	0.76	1.86	4-#20M	+/12	E	A
E3.2	"	"	"	"	"	"	+/6	"	"
E3.3	"	"	"	"	"	"	+/3	"	"
E3.4	"	"	"	"	"	"	+/3	"	"
E4.1	5.0	5C	60	1.3	3.1	4-#25M	+/12	E	B
E4.2	"	"	"	"	"	"	+/6	"	"
E4.3	"	"	"	"	"	"	+/3	"	"
E4.4	"	"	"	"	"	"	+/3	"	"
E5.1	5.0	5C	60	0.76	1.86	4-#20M	+/12	E	A
E5.2	"	"	"	"	"	"	+/6	"	"
E5.3	"	"	"	"	"	"	+/3	"	"
E5.4	"	"	"	"	"	"	+/3	"	"

Table 3.16: Series F Column Details

Column Mark	28 Day Concrete Strength (ksi)	Concrete Mix Design	Longitudinal Reinforcement				Instrument-ation refers to Fig. 3.7	Tie Type
			Grade (ksi)	Percent (ρ)	Area (A_s) (in^2)	Detail		
F8	5.0	5C	40	0.76	1.86	4-#20M	A	D
F17	"	"	60	1.3	3.1	4-#25M	A	E
F18	"	"	60	2.6	6.2	8-#25M	B	E
F6	2.5	3C	40	0.76	1.86	4-#20M	A	A
F14	"	"	60	1.3	3.1	4-#25M	A	E
F15	"	"	60	2.6	6.2	8-#25M	B	E

Table 3.17 : Prism Specimens

Prism Designation	Number of Prisms	Grout Mix Design	Companion Column Series	Stripped Shells
AP0.1 to AP0.5	5	Ungrouted	A	x
AP2.1 to AP2.5	5	2C	A	x
AP3.1 to AP3.5	5	3C	A	x
AP4.1 to AP4.5	5	4C	A	x
AP5.1 to AP5.5	5	5C	A	x
CP3.1 to CP3.2 Cores	2	3G	C	✓
CP3.3 to CP3.5	3	3G	C	x
DP3.1 to DP3.3 Cores	3	3C	D,E,F	✓
DP3.4 to DP3.6	3	3C	D,E,F	x
DP5.1 to DP5.3 Cores	3	5C	D,E,F	✓
DP5.4 to DP5.6.	3	5C	D,E,F	x
EP5.1 to EP5.5	5	5C	E	x

Designation is as follows:

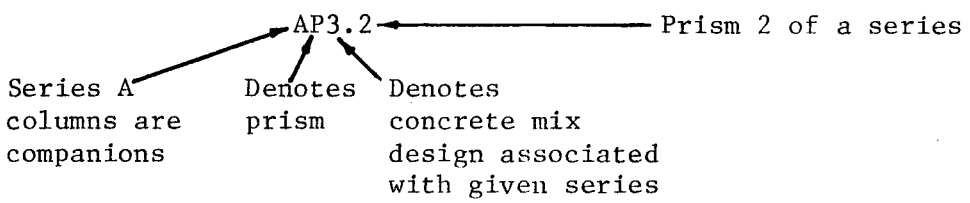

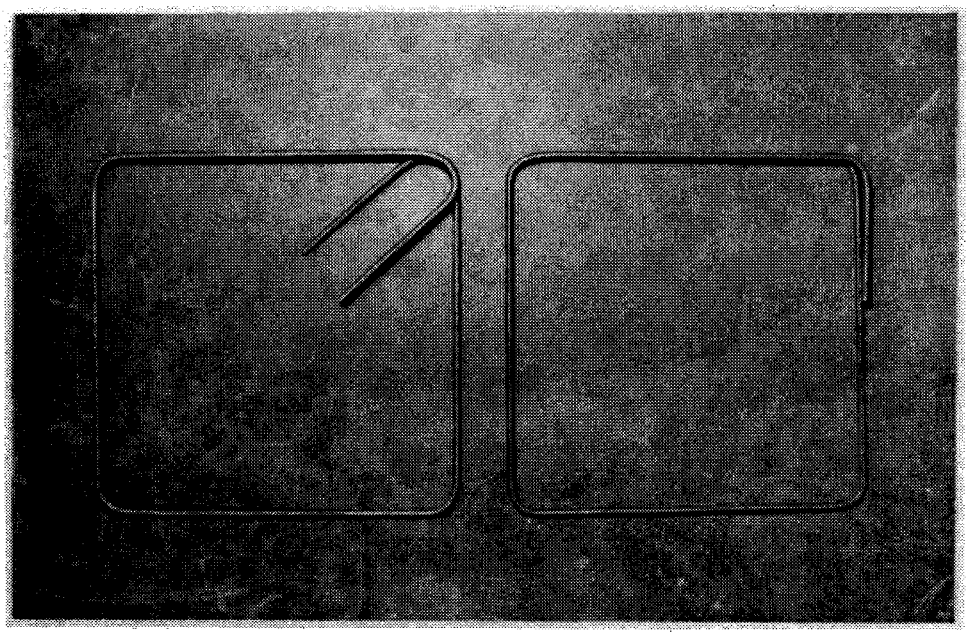

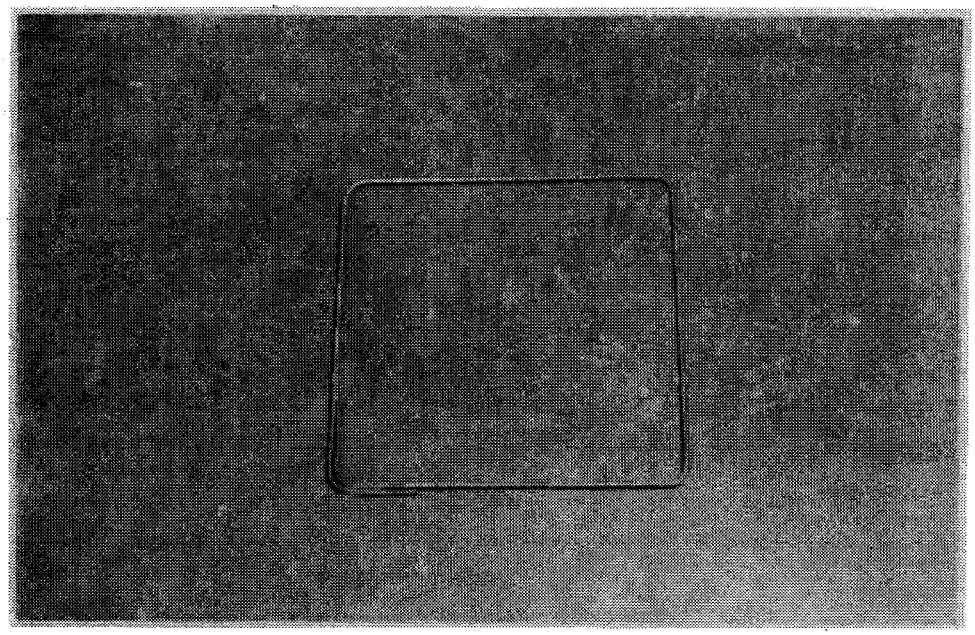

PLATE 3.1 and PLATE 3.2
The Three Styles of Lateral Ties
Used in the Study

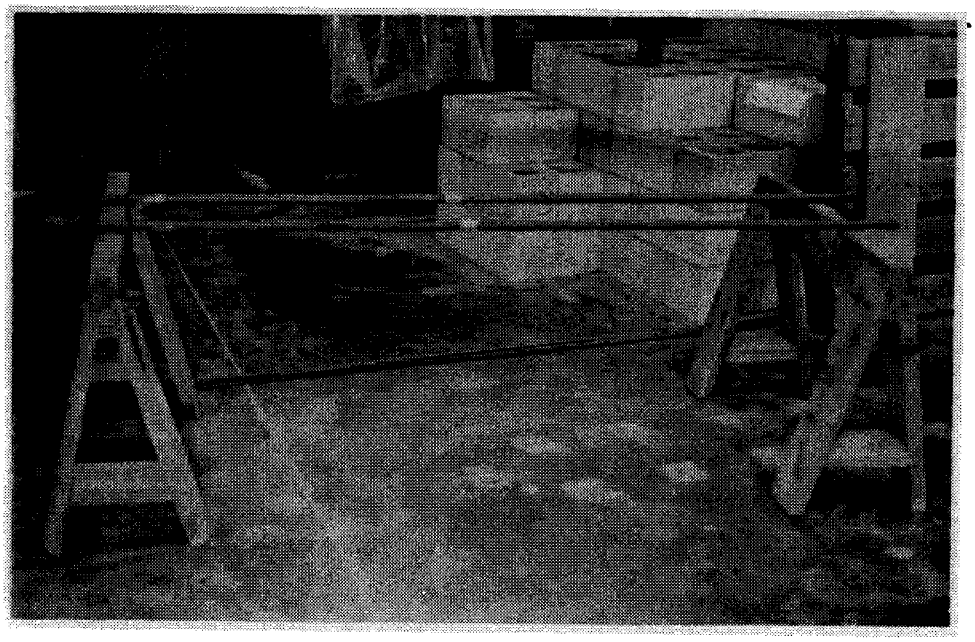

PLATE 3.3
Cage Construction--Placement of Reinforcement on the Saw Horses

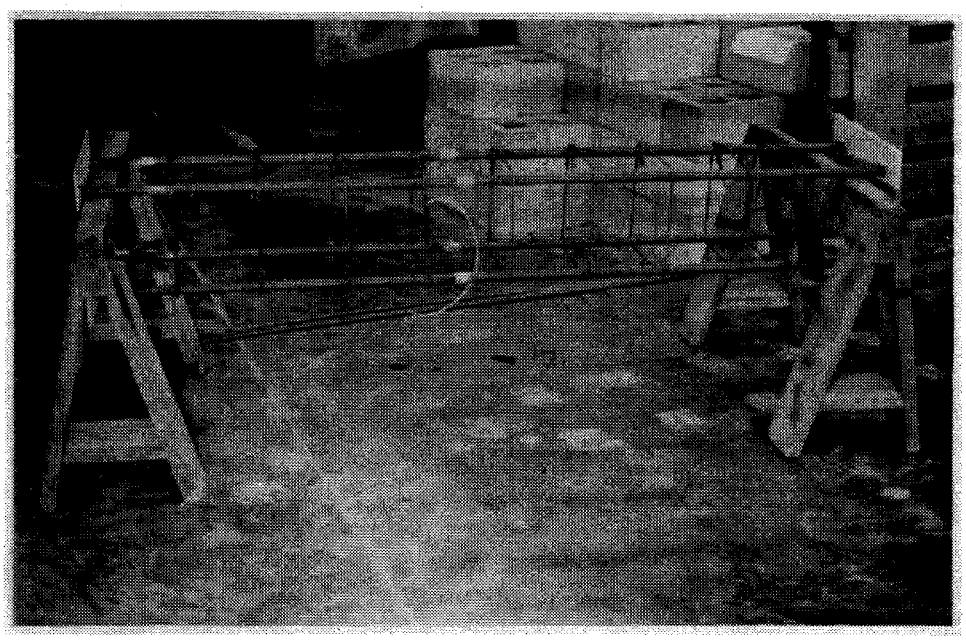

PLATE 3.4
Cage Construction--Lateral Ties are Positioned to Sebtend one Vertical Bar

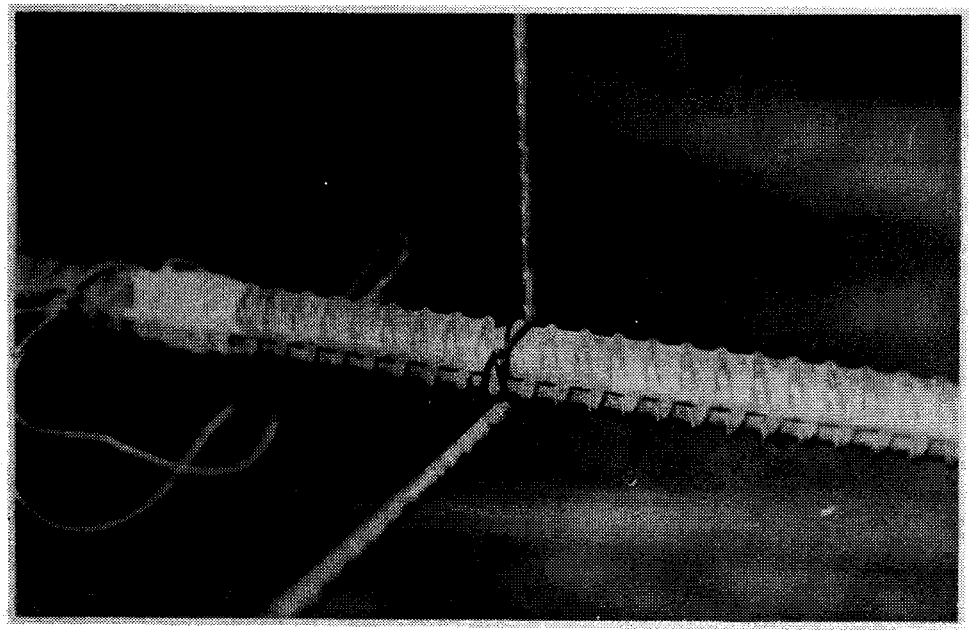

PLATE 3.5
Cage Construction--Interior View
of Tie-Vertical Reinforcement
"Connection"

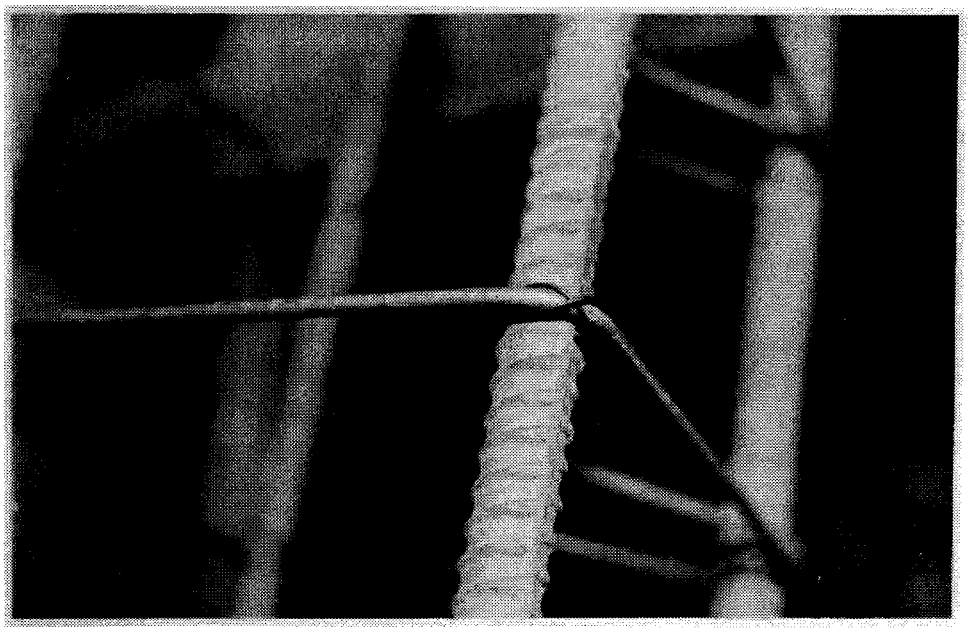

PLATE 3.6
Cage Construction--Exterior View
of Tie-Vertical Reinforcement
"Connection"

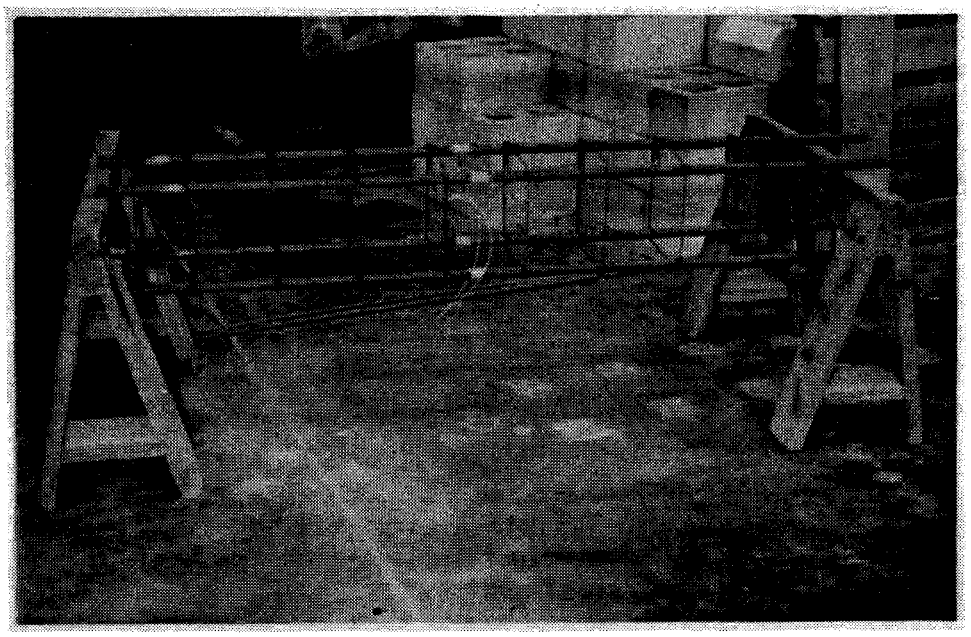

PLATE 3.7
Cage Construction--The Completed Reinforcement Cage

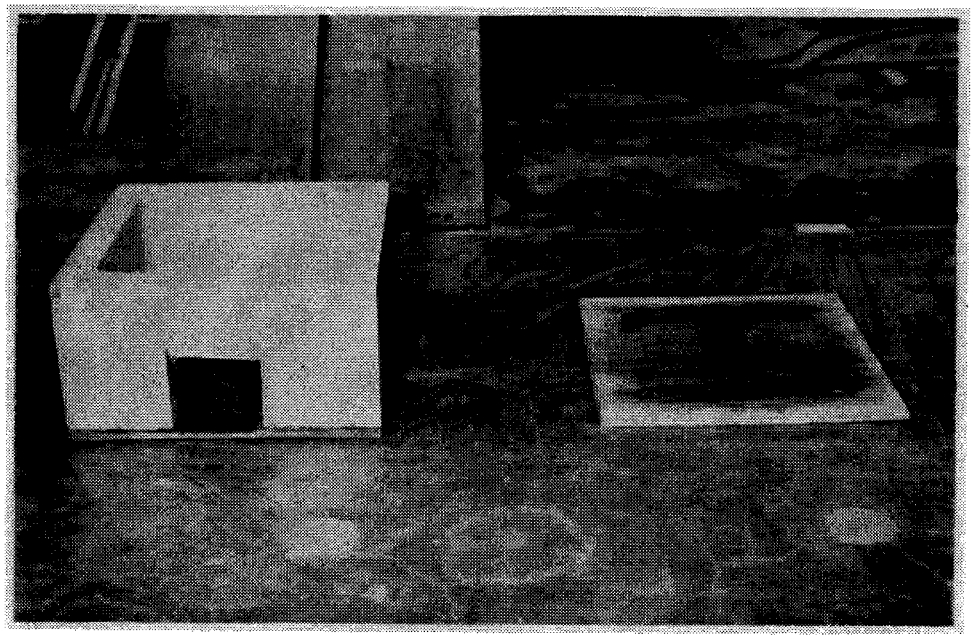

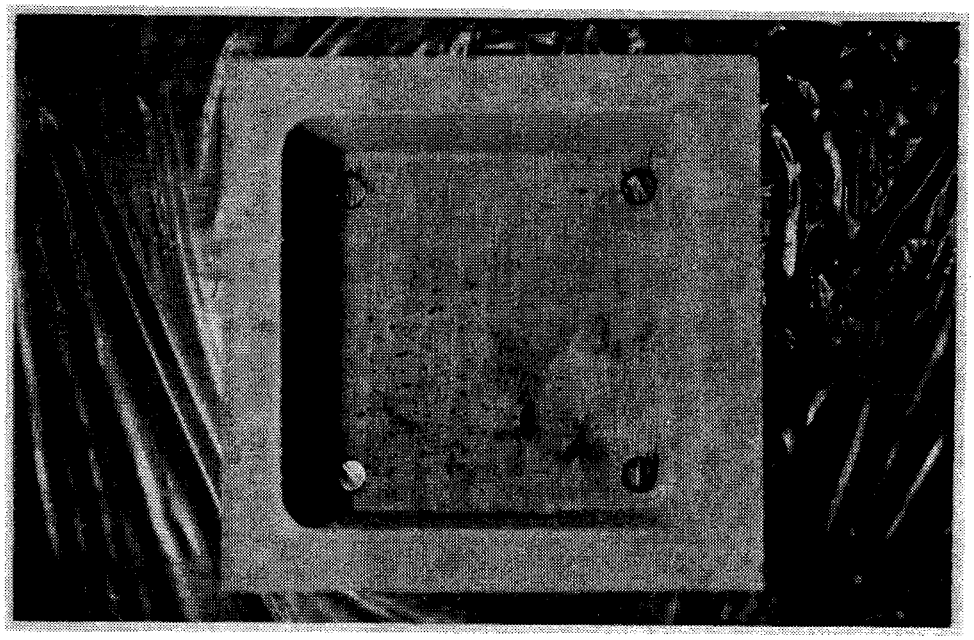

PLATE 3.8 and PLATE 3.9
Column Lower Course Block, Showing Clean-out Hole, and Pre-drilled Plywood Template

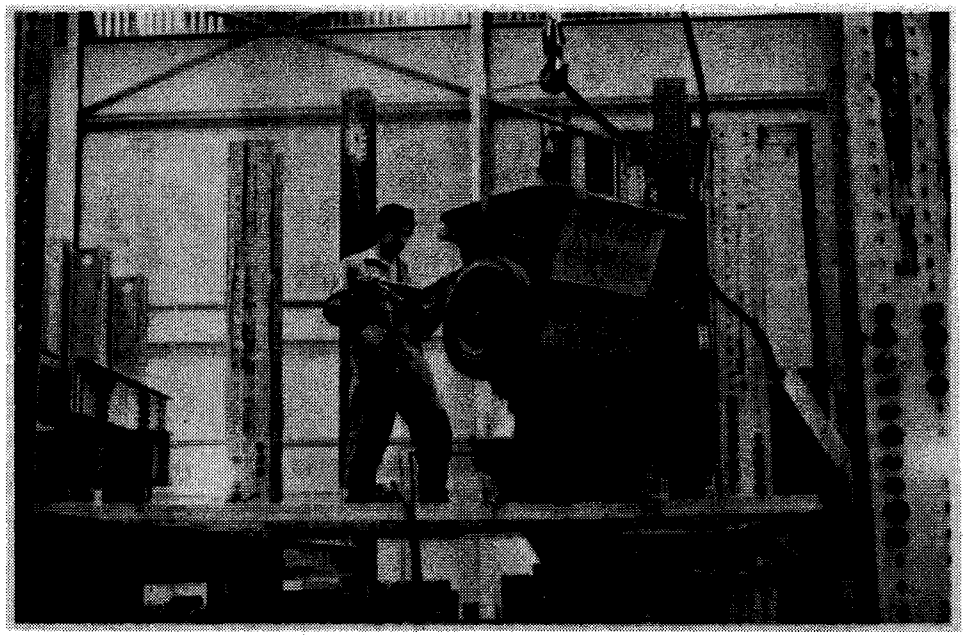

PLATE 3.10
The Column Grouting Operation
Showing Buggy, Funnel, and Box

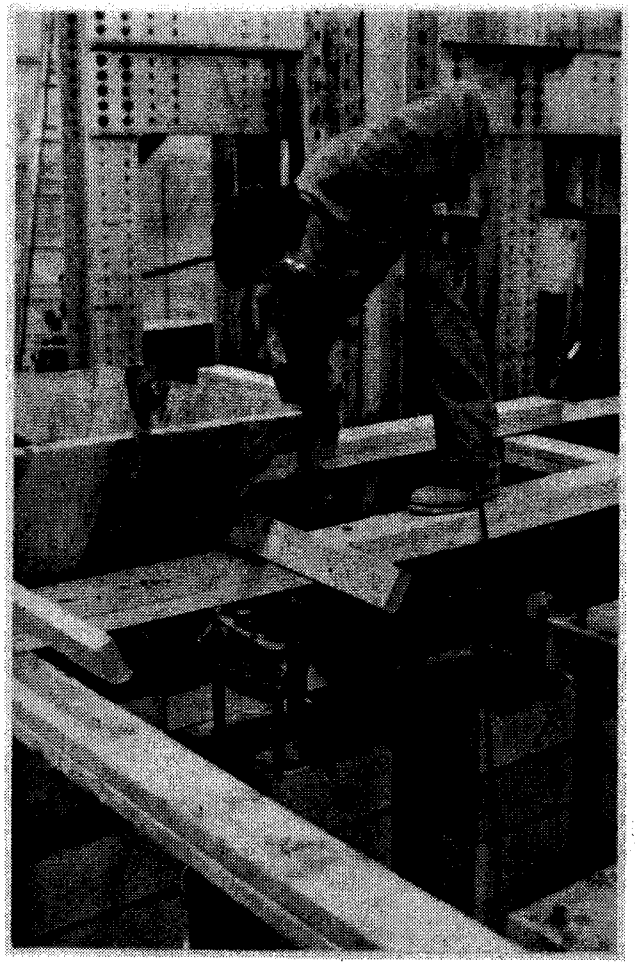

PLATE 3.11
The Concrete Vibration Operation

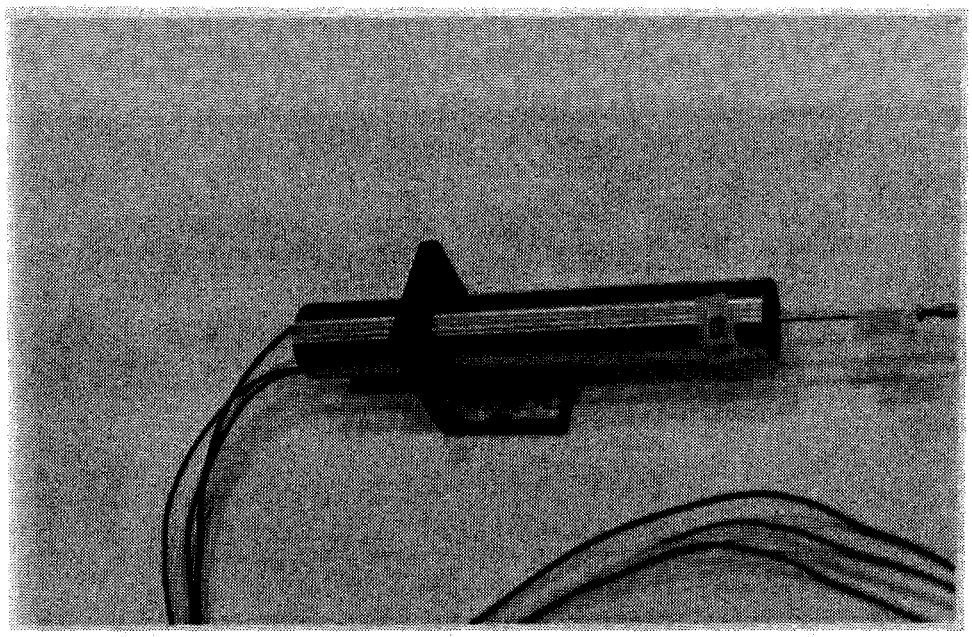

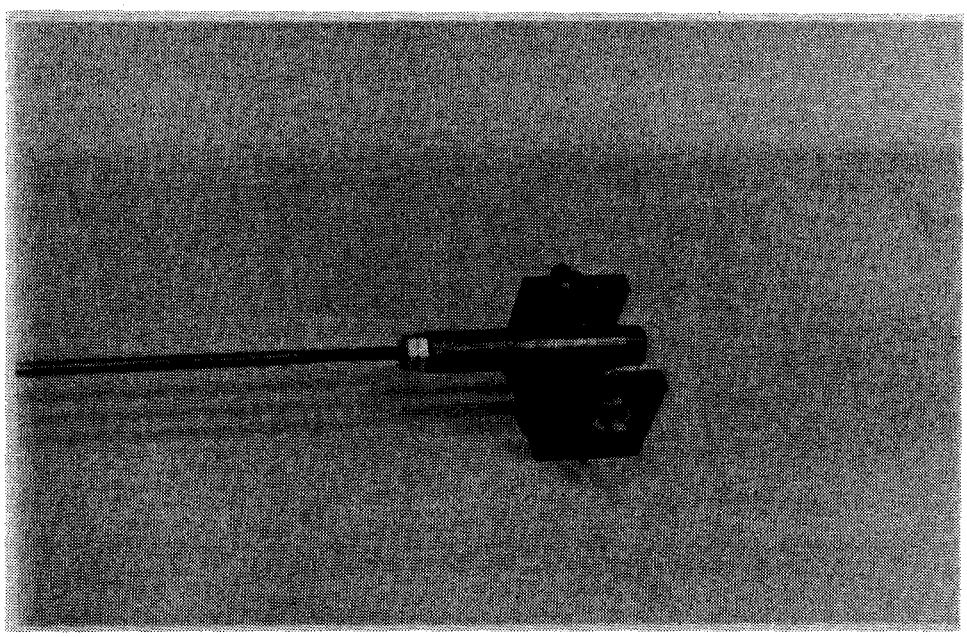

PLATE 3.12(a) and PLATE 3.12(b)
Pin Supports Provided Rotational Freedom for the LVDT's Placed on the Column Faces

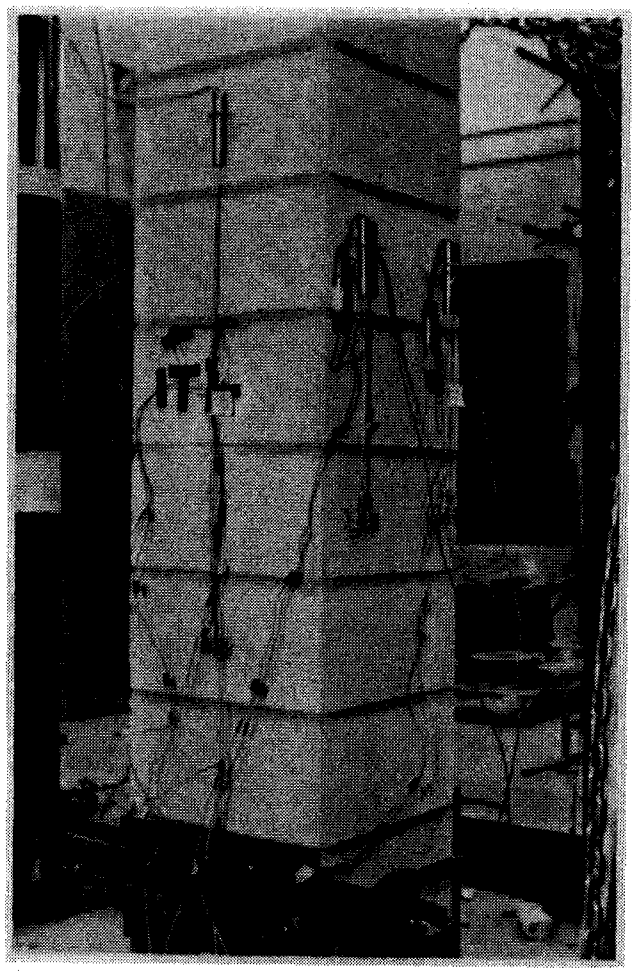

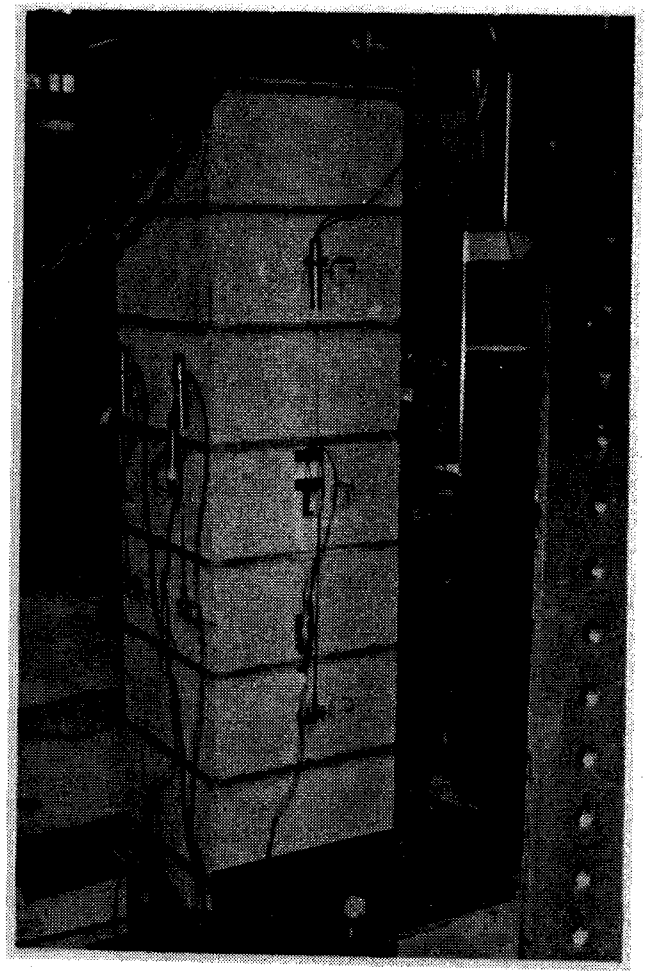

PLATE 3.13(a) and PLATE 3.13(b)
Typical Column Instrumentation

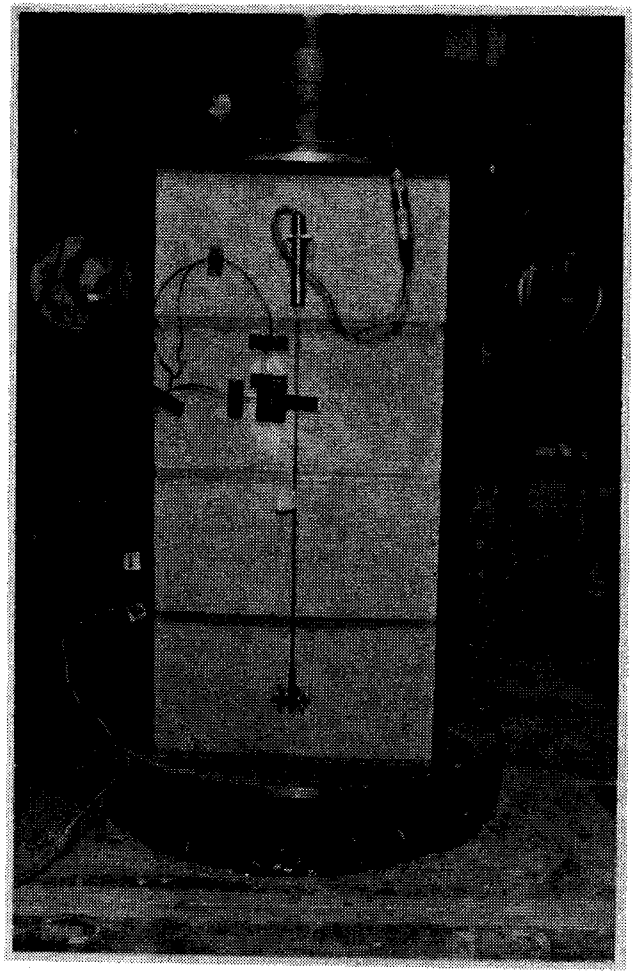

PLATE 3.14
Typical Prism Instrumentation

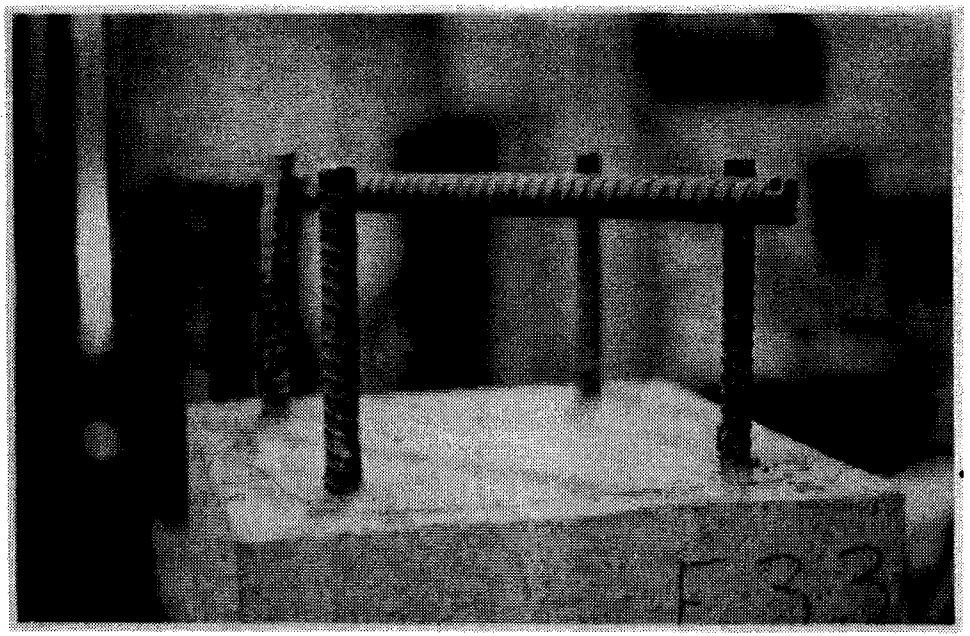

PLATE 3.15
Reinforcement Welded Across Opposing Bars Provided a Hook for Column Transport by Overhead Crane

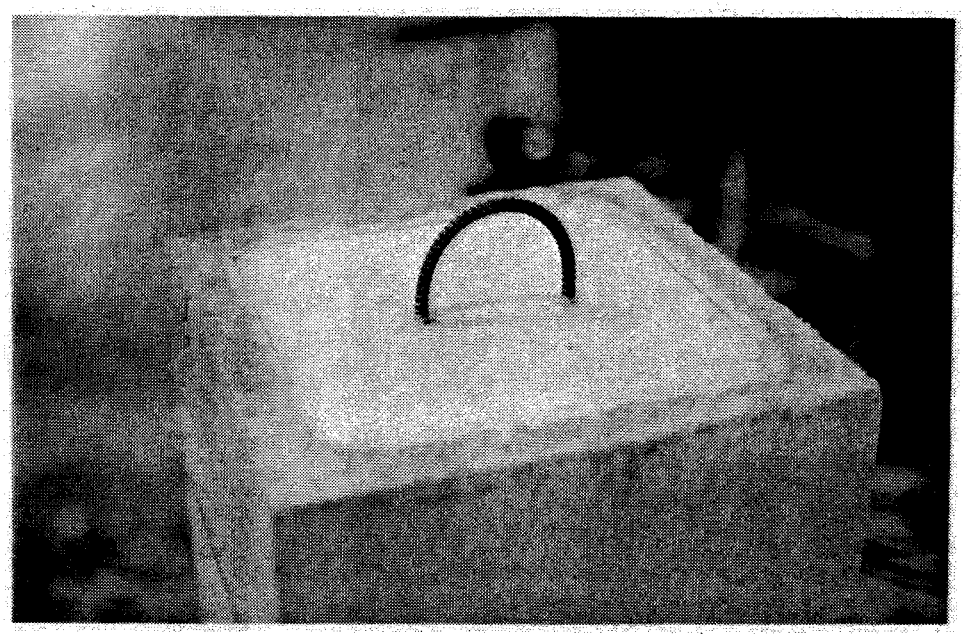

PLATE 3.16
U-hook for Transport of
Unreinforced Grouted Columns

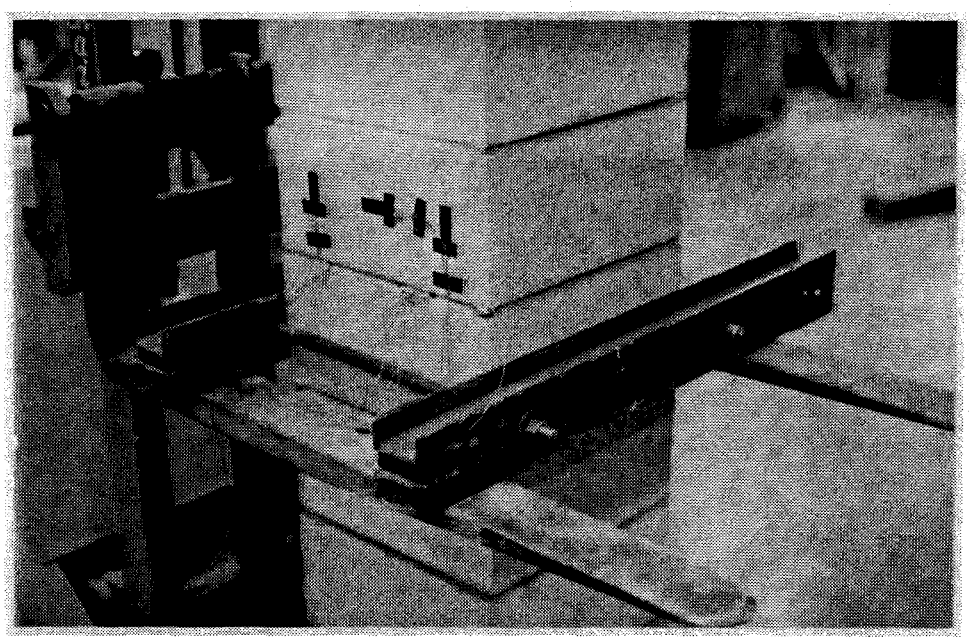

PLATE 3.17
Transport of Ungrouted Columns
by Clamp and Forklift

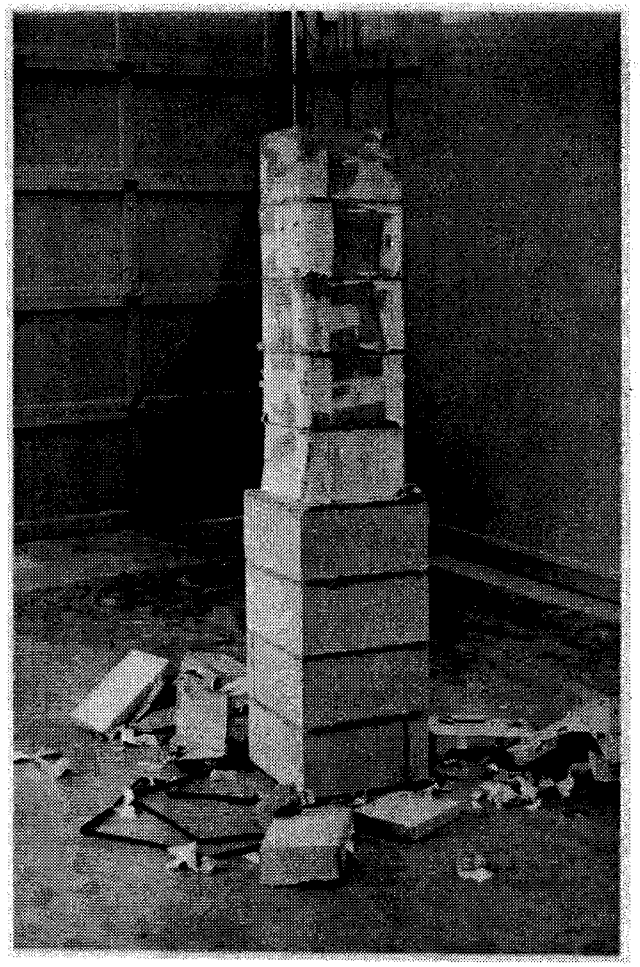

PLATE 3.18
Removing Shells from Stripped Columns

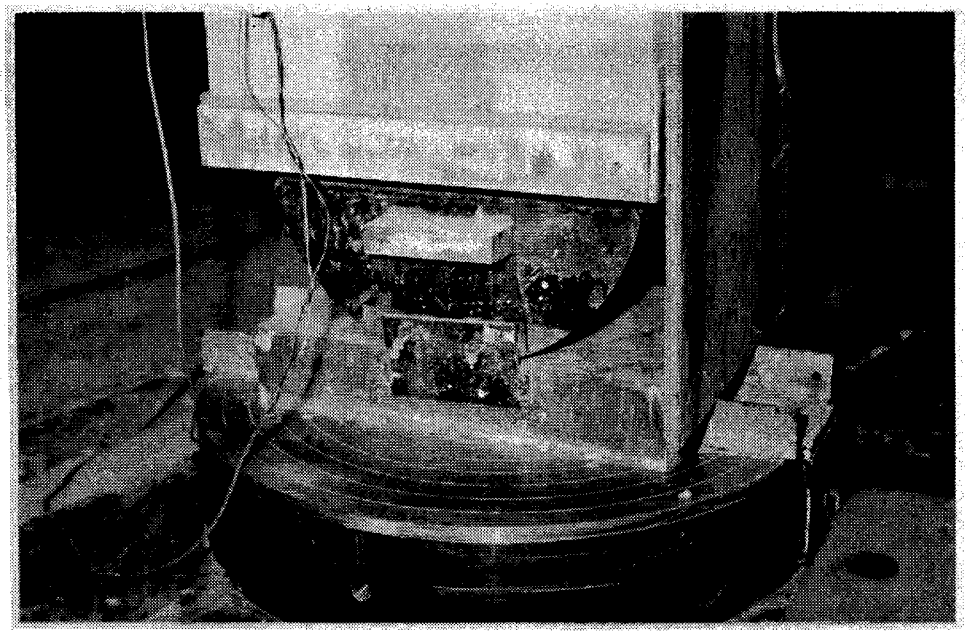

PLATE 3.19
Lower Loading Plate for Concentrically Loaded Columns

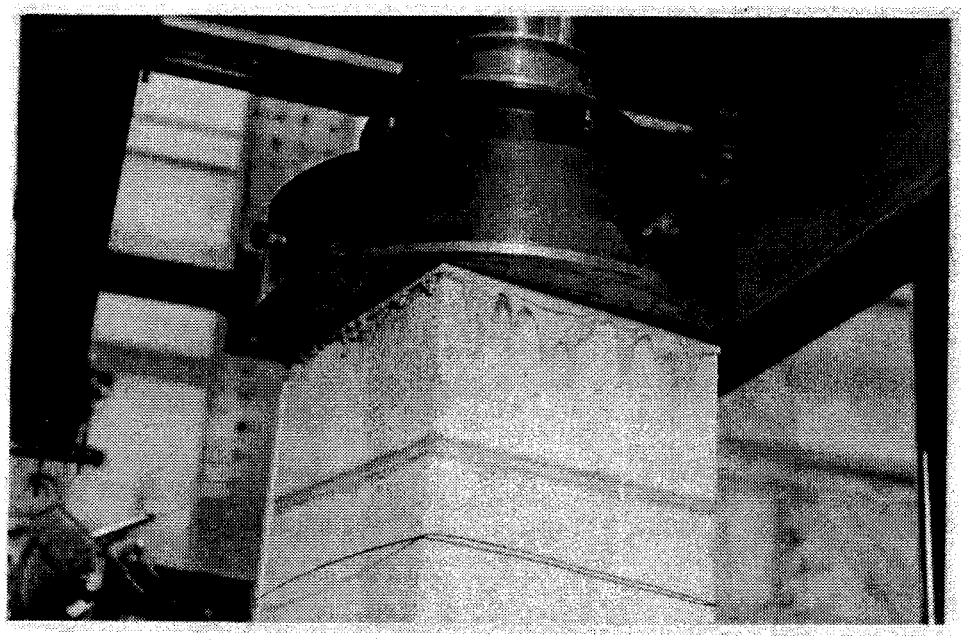

PLATE 3.20
Machine Swivel Upper Platen
Doubled as Pin and Loading Plate
for Concentrically Loaded Columns

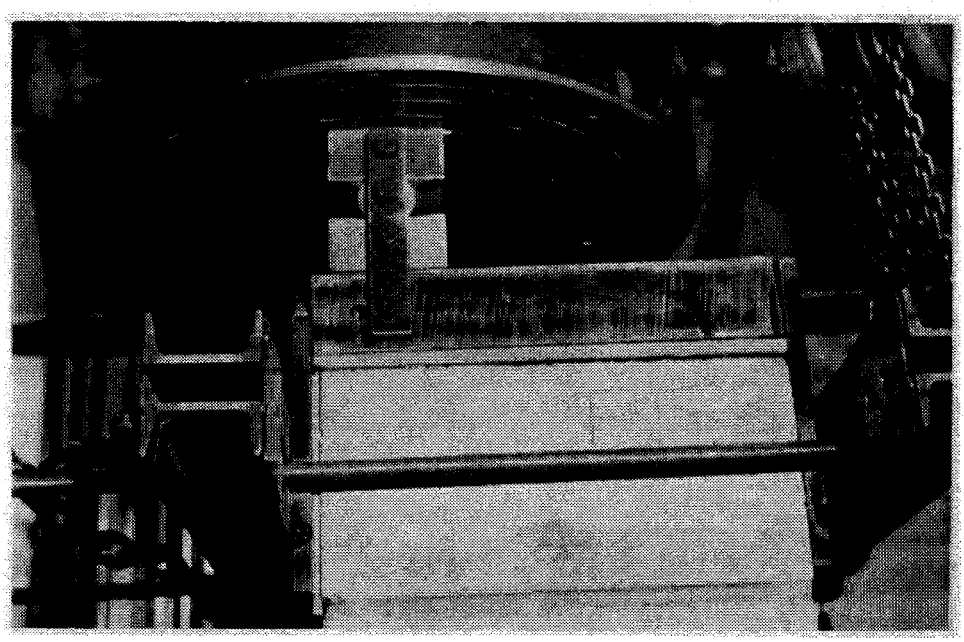

PLATE 3.21
Column Eccentric Loading Plates

4. MATERIAL PROPERTIES, PRISM RESULTS AND DISCUSSION

4.1 Introduction

In this chapter, the properties of the individual materials which constitute a masonry assemblage are examined experimentally. The properties of the masonry prisms constructed with these materials are then studied from a theoretical and experimental base. Their behavior is predicted through the formulation of theoretical and empirical relations which are developed herein, or were presented in previous investigations, and which make use of the individual component properties.

4.2 Properties of Masonry Units

4.2.1 Compressive Strength

The standard masonry block compressive strength test consists of capping the ends of a single masonry unit with a suitable material to ensure a uniform load distribution, placing the unit with service orientation in a standard compression testing machine, and applying load. Unfortunately, this simple test is influenced by a number of factors which can significantly affect the compressive strengths of blocks composed even of the same type of material. Moreover, it is known that the test does not adequately represent block strength in a masonry assemblage.

Masonry units are normally tested between steel platens which are much stiffer than the units and restrict the

lateral expansion at the unit ends. This confinement tends to increase block compressive strength by producing shear or diagonal tensile failure in the block, rather than the normal vertical tensile splitting failure. Since this restraint is confined primarily to the block ends, an increase in block height reduces the effect at midheight and lowers the compressive strength.

The capping material of the block can also affect strength by either increasing or reducing the frictional restraint of the steel plates for a given block height.

Other factors which affect block strength are aspect ratio, curing conditions including moisture content, test age, loading rates, load control at failure, and the number of test replicates. These factors are discussed in detail by Maurenbrecher.[42,43]

In addition, the stress state of a block unit in a masonry assemblage differs from the uniaxial compressive state imposed by the standard compression test. The elastic modulus of the concrete block is usually greater than that of the mortar and, consequently, free lateral deformation of the mortar is greater than that of the block. However, in a plain masonry shell, free lateral expansion of the mortar in the joint is confined by the block due to friction and bond resistance. As a result, tensile stresses are introduced into the block and tensile failure can occur before unit compressive strength is reached. This phenomenon is examined in some detail by Hatzinikolas *et al*.[39] Drysdale *et al*,[44,45]

in a study of grouted block masonry prisms, suggests that at high stresses in the grout core, inelastic lateral deformations produce bilateral tensile stresses in the masonry shell as it attempts to confine the grout. When combined with the vertical compressive stress, these stresses cause a premature splitting failure of the blocks under a state of biaxial compression-tension stress. Consequently, although one may be able to determine the compressive strength of a given type of block unit with some certainty using the standard test and a suitable number of test replicates, this strength, under the influence of other factors, may never be reached in a masonry assemblage. For these reasons, researchers in the past have had some difficulty in relating masonry strength to block unit strength.

In this study, the compressive strength of the pilaster units was based on ten test repetitions in accordance with ASTM C140. These strengths are recorded in Table 4.1. All units were capped with high strength plaster cast on a glass plate. These are the same blocks for which gross and net area measurements were reported earlier in Table 3.2. For samples P1 to P5, the maximum and minimum observed net area failure stresses were 3370 and 3060 psi, respectively, with a mean of 3150 psi, and a coefficient of variation of 4.0 percent. Net area failure stresses for blocks P6 to P10 were somewhat greater, having a mean of 3700 psi, with maximum and minimum values of 3990 and 3370 psi, and a coefficient

of variation of 7.0 percent.

Block samples P1 to P5 were tested shortly after delivery, and samples P6 to P10 were tested about four months later with the column and prism specimens. The latter are therefore considered to be more representative of the block strength in the column. Comparison of these samples suggests that the autoclaving process does not cure blocks to a 28 day compressive strength, as is commonly assumed, and that significant strength increases can be expected if blocks are used in construction shortly after their manufacture.

4.2.2 Elastic Modulus

The elastic modulus of masonry units has been shown to vary with aggregate type (density), type of cure, aspect ratio and cement type. To date, only empirical relationships such as those presented in Section 2.2.4 have been used to predict elastic modulus. Any accurate estimate of this important engineering property is precluded by the extreme data scatter about these regression lines.

Compressive and lateral strains were measured on block samples P6 to P10, and Fig. 4.1 presents their average stress-strain relationship. Table 4.1 reports a mean elastic modulus of 1.56×10^6 psi with a coefficient of variation of 5.4 percent, a Poisson's ratio of 0.16, and an average strain at failure of 0.0022 in./in.

Applying Eq. 2.6, and using 93 lb./cu. ft. for the unit

weight, and 3700 psi for the strength, the elastic modulus for the concrete block pilaster units of this study is:

$$E_b = 25\, W^{3/2} \sqrt{f'_b} = 25\, (93)^{3/2} \sqrt{3700}$$

$$= 1.36 \times 10^6 \text{ psi}$$

This value is in good agreement with the observed data.

Eq. 2.3 provides a gross over-estimation of unit elastic modulus:

$$E_b = 1000 f'_b = (1000)(3700) = 3.7 \times 10^6 \text{ psi}$$

4.3 Properties of Mortar

At present, ASTM C109 requires that the compressive strength of mortar be determined from vertical compression tests of 2 x 2 x 2 in. cubes which have been cured in saturated lime water for a 28 day period. Understandably, this mode of cure seldom reflects actual construction practice. Often, due to suction of water from the mortar into the blocks, or excessive evaporation during summer construction, an insufficient amount of water remains within the mortar to complete hydration. The resulting mortar strength is much lower than that indicated by standard cubes. Alternatively, the volume of water removed by suction from the mortar to the surrounding blocks may be sufficient only to reduce the elevated water/cement ratio needed for workablility and thereby produce a stronger mortar than that indicated by the standard mortar specimens.

In this study, fifty 2 x 2 x 2 in. cubes were tested in compression to obtain 28 day strengths. Of these, thirty-five were cured in saturated lime water and fifteen were stored in the laboratory under conditions similar to those of their companion prisms and columns. For a number of these cubes, vertical and lateral strain measurements were also recorded as a function of load. A complete set of cube results is given in Table 4.2. The mean compressive strength of lime cured cubes was 1780 psi with a coefficient of variation of 13.9 percent, and for the lab cured cubes, the mean compressive strength was somewhat lower, at 1640 psi, with a coefficient of variation of 16.5 percent.

The load-deformation characteristics of a number of these cubes are shown in Figs. 4.2 and 4.3. A straight line passing through the average stress-strain data yields an elastic modulus of 1.5×10^6 psi for saturated lime water cubes, and 1.7×10^6 psi for laboratory cubes. Although the initial tangent modulus is slightly higher for the latter, it is seen from Fig. 4.3 that this modulus is representative only to approximately 0.40 f'_{mort}, whereas for lime cured specimens, the stress-strain relationship is linear to about 0.65 f'_{mort}. In either case, data are scattered and only "ball park" values can be obtained since the coefficient of variation of the elastic modulus for both cube types is 50 percent. Similarly, mean Poisson's ratios of 0.11 and 0.17 for lime and lab cubes, respectively, show large variations.

In this study, differences between lime and lab cured

specimens are insignificant, and either set of values may be considered as a reasonable representation of the mortar existing in the column and prism specimens.

Both Eqs. 2.3 and 2.4 have been applied in previous investigations to fit test data for modulus of elasticity versus mortar strength. Since in this study the density of the mortar is not known, only Eq. 2.3 may be used:

$$E_{mort} = 1000 f'_{mort}$$

$$= 1000(1780) = 1.8 \times 10^6 \text{ psi}$$

This value is in good agreement with experimental measurements.

4.4 Properties of Concrete and Grout

Mix designs for the concretes and grout used in this investigation were presented earlier in Table 3.4. Because of the large number of columns and prisms tested, certain series were necessarily fabricated in different time periods. Initially, all columns and prisms of Series A and B were constructed and tested, followed by Series E, and then those of Series C, D, and F were completed.

Before grouting the columns, a mix design program was undertaken to ensure that those mixes presented in Table 3.4 yielded the desired 28 day standard moist cured cylinder compressive strengths. For the test columns, favourable strengths were obtained for Series A, B, and E specimens. However, for the remaining series, cement supplied by a

different manufacturer was employed in these mixes and this resulted in significant strength increases. Because of the large number of specimens and variables examined in this program, the intended comparisons could still be made, and the elevated core strengths in Series C, D, and F specimens were in no way detrimental to the study.

As noted earlier, for the Series A and B columns and prisms, moist cured and lab cured standard cylinders and moist cured and lab cured block moulded prisms were cast as control samples. Since moist cured cylinders were later found to be best representative of the concrete existing in the pilaster cores, the other three types were discontinued for the subsequent series.

Values of concrete strength, ultimate strain, elastic modulus, and Poisson's ratio for each concrete are presented in Table 4.3. Average stress-strain curves for these concretes obtained from moist cured cylinder tests are shown in Fig. 4.4.

Elastic moduli of the moist cured cylinders for all series varied between 2.0×10^6 psi and 3.7×10^6 psi, with higher values tending to be associated with higher compressive strength. Variations in ultimate strains were small and showed no definite trends with concrete strength.

4.5 Prism Investigation

4.5.1 General

Prisms are small-scale masonry assemblages used for predicting full-scale masonry properties such as compressive strength, elastic modulus, shear strength, shear modulus, cracking stresses, shrinkage, creep and temperature deformations, and failure modes. Clearly, prism behavior should reflect that of the masonry used in the actual construction, and this necessarily requires that prisms should be fabricated with similar materials, joint thicknesses, workmanship, core and bond patterns, and curing conditions; and moreover, prisms should be tested in a manner which simulates actual service conditions of the full-scale masonry. Reports by Maurenbrecher[42,43] explain in some detail how such factors as height/thickness ratio, capping, bond pattern, thickness, curing conditions, moisture content, age, loading rates and control, and the number of test replicates can affect observed prism strength and behavior under direct compression.

Details of the prism investigation reported herein have already been given in Sections 3.2.2 and 3.3.2. The failure load and corresponding stress, masonry and block elastic moduli, Poisson's ratio, cracking load, maximum vertical and lateral strains, and failure type for each of these prisms are reported in Table 4.4. The stresses and moduli of the tested prisms given in this table were calculated on the basis of the net area A_n for the plain specimens, on the

basis of the gross area A_g for the grouted specimens, and on the basis of the core area A_c for the stripped shell core specimens.

4.5.2 Prism Failure Mode

All of the plain masonry prisms displayed sudden, complete, and explosive failures. Advance "warning" cracks were noted in only one of the five prisms. A photograph of a typical failed specimen is shown in Plate 4.1.

Grouted prism failures were characterized by two typical modes. Type A failure may be described as a simultaneous splitting of the block shell and crushing of the prism core. In the majority of these cases, failure was gradual and shell cracking was noted in advance of prism ultimate load. Vertical splitting of the prisms tended to originate at block face centers in the upper or lower course. This indicated that the fiberboard cap was effective in reducing the confining effect of the platens. Type B failure was observed in a small number of specimens, and was characterized by gradual splitting, with subsequent separation from the prism core, and spalling of the block shell before core crushing. Shell cracking was normally observed at loads before shell spalling. All prism cores, irrespective of failure mode, showed a typical conical shear failure similar to that observed in standard concrete test cylinders. The prisms shown in Plates 4.2 and 4.3 are typical of failure modes A and B, respectively. Table 4.4

indicates failure type for each prism tested.

Failure mode, in general, showed no associative patterns with grout strengths. One might normally assume, for instance, that Type B failure would be peculiar to those prisms with the lower strength concrete cores, where bond at the block-core interface would be considered relatively weak because of lower cement contents. Yet those prisms of Series E, with grout cylinder strengths averaging 5090 psi, were most exemplary of Type B failure. Ultimate load for four of these prisms could actually only be attributed to core strength since the entire shell had separated and popped off at an earlier loading stage.

4.5.3 Compressive Strength of Prisms

The compressive strength of plain masonry is a function of block unit strength, mortar strength, grout strength, joint thickness, workmanship and testing conditions, slenderness, and capping material. In this study, only the grout strength is considered to affect the strength and behavior of the masonry prisms since a degree of uniformity was maintained for other factors.

For the grouted prisms which displayed failure Type A, and therefore for the majority of prisms tested, compressive strength is clearly a summation of the load carried by the prism core and the load carried by the masonry shell. For those prisms which exhibited Type B failure, although their loading history previous to shell spalling is affected by

both the prism core and the masonry shell, ultimate load is represented only by the load contribution of the concrete core.

The question arises as to how one determines the individual contribution of each element in terms of its known material properties in order that general design equations might be developed. Previous research has demonstrated that at failure, block shells of grouted masonry assemblages contribute only a fraction of that load carried by an identical plain masonry specimen. High bilateral tensile stresses imposed on the shell as it attempts to confine the lateral deformations of the grout core, in combination with the vertical compressive stresses, can cause premature failure and thus prevent the axial strength of the outer shell from being fully developed. Furthermore, research has shown that the load contribution of the concrete in a reinforced concrete column is $0.85f'_cA_c$, where f'_c is the concrete compressive strength determined from tests of standard cylinders. The factor 0.85 primarily accounts for the differences in quality existing between the concrete in standard cylinder and the concrete in the column due to segregation and bleeding. If a similar approach is taken in this program, this reduction factor, in addition, must account for apparent strength differences caused by material capping and water loss from the core due to block absorption. Since all standard cylinders were sulphur capped, and all prisms were capped with fiberboard which is

known to comparatively reduce platen end restraint, one might expect the reduction factor to be somewhat less than 0.85. However, absorption of core moisture by the block should decrease the water/cement ratio, thereby increasing concrete strength, and thus should serve to increase this empirical constant.

Figure 4.5 shows the values of the stripped shell prism core strengths, f'_{pc}, as a function of their standard concrete cylinder strengths, f'_c. Although data are scattered, results indicate that the ratio of f'_{pc}/f'_c is independent of concrete strength. This ratio varied between 0.60 and 0.84, and averaged about 0.74, with a coefficient of variation of 11.8 percent. If those prisms of Series EP5P- which clearly failed in Type B mode are included, then the mean ratio becomes 0.75 with a coefficient of variation of 10.1 percent. That core strength is best represented by standard moist cured concrete cylinders is not surprising. Although the absorption of water by the block shell is known to change the water/cement ratio of the concrete, and thus its strength, it is reasoned that in these prisms with a relatively large 12 inch square core, only the periphery is affected. The blocks function more as a barrier to evaporation and tend to contain water in the prism. This was observed in several specimens in which after failure, the concrete was quite moist although it had been cured 28 days. This would imply that there was sufficient water to complete hydration in the core.

Figure 4.6 shows the values of grouted prism strength in terms of the compressive strength of the grout calculated from standard concrete cylinder strengths. Also indicated are the net area and gross area compressive strengths of the plain masonry prisms, f'_{mp_n} and f'_{mp_g}, respectively. Clearly, large increases in prism strength are achieved with increasing grout strength, and an approximately linear function relates the two. Using linear regression analysis, the strength of the grouted prisms can be related to grout strengths indicated by standard cylinder strengths as:

$$f'_m = 0.43f'_c + 570 \quad \text{(psi, gross area)} \quad . \quad . \quad . \quad . \quad . \quad . \quad . \quad 4.1$$

$$r = \text{correlation coefficient} = 0.90$$

Expressing this relation in terms of force:

$$A_g f'_m = 0.43A_g f'_c + 570A_g$$

$$= 0.43(A_g/A_c)A_c f'_c + 570(A_g/A_{shell})A_{shell}$$

$$= 0.43(242.1/146.9)A_c f'_c + 570(242.1/95.2)A_{shell}$$

$$Pu_m = 0.71f'_c A_c + 1450A_{shell} \quad \text{(psi)} \quad . \quad . \quad . \quad . \quad . \quad . \quad . \quad . \quad 4.2$$

The first term of Eq. 4.2, $0.71f'_cA_c$, defines the contribution of the concrete core to the ultimate load of the prism in terms of core area and core standard cylinder strength. The y intercept of Eq. 4.2 effectively defines the contribution of the masonry shell to the prism ultimate load in terms of shell area. The assumption that the y intercept

of this regression equation adequately represents the contribution of the prism shell at failure is given credence if one examines the failure loads for those prism series containing stripped cores and exhibiting Type A failure. If the mean failure loads of the cores, 460 kips and 710 kips for Series CP3P- and DP5P-, respectively, are subtracted from their corresponding grouted mean prism strengths of 630 kips and 830 kips, then shell contribution is found to be 170 kips and 120 kips, with an average of 145 kips. This compares favourably with that value provided by Eq. 4.2, which is (1450)(95.2) = 138 kips.

Although not strictly correct, since only one block strength was examined in this study, the second term of Eq. 4.2 may be changed to a function of plain prism strength as follows:

$$Pu_b = 352.7 \text{ kips}$$

$$f'_b = 3700 \text{ psi}$$

$$f'_{mp_n} = 2080 \text{ psi}$$

$$Pu_m = 0.71 f'_c A_c + (1450/3700) A_{shell} f'_b$$

$$Pu_m = 0.71 f'_c A_c + 0.39 f'_b A_{shell}$$

$$Pu_m = 0.71 f'_c A_c + 0.4 f'_b A_{shell} \quad \ldots\ldots\ldots\ldots \quad 4.3(a)$$

$$Pu_m = 0.71 f'_c A_c + 0.7 f'_{mp_n} A_{shell} \quad \ldots\ldots\ldots\ldots \quad 4.3(b)$$

The empirical constant of 0.71 is in good agreement with 0.74 evaluated using the stripped shell prism core failure stresses plotted in Fig. 4.5. It is worth noting that the regression analysis used in the derivation of Eq. 4.3 included those prisms of Series E and C known to have no shell contribution at failure load. If these prisms are eliminated from the analysis, Eq. 4.4 is derived:

$$Pu_m = 0.75f'_c A_c + 0.35f'_b A_{shell} \quad \ldots\ldots\ldots\ldots \quad 4.4(a)$$

$$r = 0.92$$

$$Pu_m = 0.75f'_c A_c + 0.62f'_{mp_n} A_{shell} \quad \ldots\ldots\ldots\ldots \quad 4.4(b)$$

which provides less variation, and better agreement between the two methods.

These tests therefore showed large increases in prism strength associated with grout strength increases, and indicated that the prism core reached full strength development whereas the masonry shell reached only about 60 percent of its full development. It must be re-emphasized that these empirical equations have been obtained using one block size and only one block strength.

Since these tests have shown that the designer is not guaranteed that sufficient bond will exist between the shell and the core to ensure shell contribution at ultimate load, even with elevated concrete core strengths, it is recommended that a conservative approach be adopted until the relationship is better understood, and that the second

term in Eq. 4.4, which is of secondary importance for pilaster units with dimensions tested herein, be neglected for ultimate strength calculations.

Similar tests were conducted by Drysdale[44] on three course high, grouted prisms fabricated with single core masonry units. Each prism had a gross area of 39.4 sq. in., a net area of 24.5 sq. in., and a height/thickness ratio of 4.2. Results of these tests for type S mortar are reproduced and plotted in Fig. 4.7. For these data, the companion relation to Eq. 4.4 is:

$$Pu_m = 0.33f'_c A_c + 1.0f'_{mp_n} A_{shell} \quad \ldots\ldots\ldots\ldots \quad 4.5$$

$$r = 0.83$$

Comparison of Eqs. 4.4 and 4.5 shows that they are nowhere equal and that the relationship between strength contributions of grout and shell at failure is complex, and depends upon prism gross area, net area and the ratio of (net area/gross area) as well as block strength and ungrouted prism strength. Tests by Drysdale showed that little increase in prism strength was achieved with large increases in grout strength. He suggested that the masonry shell strength was not permitted to fully develop because of lateral expansion of the grout which leads to a premature tensile splitting failure of the prism shell. Although this author does not dispute the theory in general, it is felt that results presented by Drysdale do not effectively lead one to this conclusion. It is argued that in tests conducted

by Drysdale, the prism shell was in fact fully developed, as indicated by the second term of the regression Eq. 4.5 (this is better shown in Fig. 4.7 where f'_{mp_g} is seen to lie on the regression equation), and that lateral expansion of the grout caused excessive cracking and failure subsequent to full shell development. In fact, it is the grout strength which was not permitted to reach full development. The excessively low coefficient of 0.33 for the concrete strength term in Eq. 4.5 supports this conclusion, as does the observation that the grout core was usually intact when removed from the failure zone. Lateral grout strains were not sufficient to cause premature shell failure in the majority of the specimens tested.

The tests conducted in this program are perhaps more demonstrative of the failure mechanism proposed by Drysdale. In this case, Eq. 4.4 shows that the prism core strength, rather than that of the block shell, was fully developed. It is suggested that by virtue of a smaller (net area/gross area) ratio for these pilaster units, lateral displacements in the grout core were sufficient to induce significant tensile strains and stresses in the shell and cause premature failure. Those prisms exhibiting Type B failure were exemplary of the more radical form of this behavior.

In addition, tests reported herein clearly indicate that it is not sufficient to use a grout or concrete strength equal to the net area plain masonry strength in order to achieve this strength over the gross area of a

grouted prism. Although one does not achieve this strength derived from a direct superposition by $f_{mp_n} A_{shell} + f'_c A_c$, the present study does indicate, however, that the concept of strength superposition permitted by CSA-S304 is valid for the masonry units tested. This concept permits the compressive strength of hollow units filled with grout or concrete to be based on the strength of the ungrouted masonry assemblage provided that the grout or concrete strength is at least equal to that of the units. Figure 4.6 shows that a concrete cylinder compressive strength of about 3500 psi is required to produce a grouted prism strength equal to the mean net area strength of the plain masonry prisms. This requirement is 200 psi less than masonry unit strength.

Tests by Drysdale[44] indicated that the strength superposition concept was not valid even for grout strengths well in excess of unit strength. This observation led to the recommendation that it would be more appropriate to match the deformational characteristics of the grout to those of the block rather than matching strengths. The discrepancies in the observations between these two test programs further serve to indicate the complex relationship existing between grout strength, block strength, A_n, A_g, and A_n/A_g.

4.5.4 Modulus of Elasticity of Masonry Prisms

The modulus of elasticity of masonry is an important property affecting strength calculations and deflection

calculations. Because masonry is a composite material, the determination of elastic modulus is a difficult task since it is dependent upon the moduli of the block unit, the mortar, and the grout. A brief review of our current understanding of this property has already been presented in Section 2.2.4.

The vertical stress-strain relationship for plain and grouted prisms of Series A are plotted in Fig. 4.8. It can be seen that, for grout strengths less than block unit strength, the grouted prisms have less axial stiffness (based on gross area) than do plain prisms (based on net area). For grout strengths in excess of block strength, the reverse is true. In addition, an increased grout strength produces a higher elastic modulus, as one might expect. The mean initial tangent modulus for each prism series is reported in Table 4.4.

Tests by Drysdale[44] showed that elastic moduli exhibited by grouted prisms (based on gross area) were all substantially less than those of plain prisms (based on net area) even for grout strengths above block unit strength. These relationships follow closely those observed for compressive strength. If however, for both programs, the elastic moduli of the plain prisms are expressed in terms of gross area, the elastic moduli of the grouted prisms are all in excess of the plain prisms and clearly indicate that grout provides a favourable service load contribution, though not to the extent one might initially anticipate.

Figure 4.9 shows the variation of prism elastic modulus as a function of prism compressive strength. The moduli of the plain prisms of Series APOP- are represented in terms of their net area. Prism elastic modulus is seen to increase in direct proportion with prism compressive strength. Using a linear regression analysis, these may be related by:

$$E_m = 432 f'_m + 677{,}000 \quad \text{(psi)} \quad \ldots\ldots\ldots\ldots \quad 4.6$$

$$r = 0.86$$

This relation is in close agreement with that found by Turkstra in Eq. 2.9, and shows less variation.

Although the application of this empirical equation may be adequate for design purposes, it clearly has little theoretical basis. It implies that a prism with no compressive strength will have an elastic modulus of 6.77×10^6 psi. Such a discrepancy questions the entire concept of relating elastic modulus to masonry compressive strength. Moreover, if the prism failure mechanism presented earlier is reviewed, it is realized that the factors affecting these properties are entirely different since they occur at the extremes of the loading history.

It can be shown that the gross area elastic modulus of a composite material such as masonry, with a block shell and grout core, is given by:

$$E_m = \frac{E_c A_c + E_{shell} A_{shell}}{A_g} \quad \ldots\ldots\ldots\ldots \quad 4.7$$

where

E_m= elastic modulus of the grouted prism

E_c= elastic modulus of the grout core

A_c= core area

E_{shell}= masonry shell elastic modulus

A_{shell}= masonry shell area

A_g= prism gross area

The elastic modulus of the shell may be taken as 1.66×10^6 psi, which is the value found experimentally for Series APOP-, or it may be calculated using Eq. 2.7:

$$E_m = \frac{1}{\frac{1 - \delta}{E_j} + \frac{\delta}{E_b}}$$

$$E_b = 1.56 \times 10^6 \text{ psi}$$

$$E_j = 1.5 \times 10^6 \text{ psi}$$

$$\delta = 7.625/8 = 0.953$$

$$E_m = \frac{1}{\frac{1 - 0.953}{1.5 \times 10^6} + \frac{0.953}{1.56 \times 10^6}} = 1.56 \times 10^6 \text{ psi}$$

Experimental and theoretical shell moduli are in good agreement. Subsequent calculations will make use of the experimental value.

Table 4.5 presents calculated values of prism elastic moduli obtained from Eq. 4.7 with the mean elastic moduli measured from the standard moist cured cylinder tests substituted for E_c. In all cases, experimental elastic

modulus is grossly over-estimated. This, perhaps, implies that the standard moist cured cylinders are not an adequate representation of the core elastic modulus. This has already been shown to be true for compressive strengths, since a coefficient of 0.75 was required as a conversion.

Fig. 4.10 plots the different average stress-strain relationships obtained for the cores of the stripped shell series. When these moduli are compared with their corresponding standard cylinder moduli, it is discovered that the former averages only 0.56 of the latter. The actual ratios are 0.65, 0.48, and 0.54 for Series CP3P-, DP3P-, and DP5P-, respectively. With the assumption that this relationship is applicable to the remaining core strengths, then Eq. 4.7 may be written as:

$$E_m = \frac{0.56E_cA_c + E_{shell}A_{shell}}{A_g} \quad \ldots\ldots\ldots\ldots \quad 4.8$$

Elastic moduli calculated for the prism series using Eq. 4.8 are also given in Table 4.5, and these values show excellent agreement with the average experimental moduli.

Figure 4.11 illustrates the relationship between moduli predicted by Eqs. 4.7 and 4.8, and those measured experimentally. If each equation were a perfect predictor, then each observed modulus would equal the "theoretical" modulus; a number of such points plotted would define a line of slope one. Such a line is shown in Fig. 4.11. Points not on this line represent an inaccuracy in prediction.

Returning to Fig. 4.9, it is shown that the CSA-S304 formula, Eq. 2.13, significantly over-estimates masonry elastic modulus for prism strengths in excess of 2000 psi.

The information gained through this elastic modulus study may provide a key to the failure mechanism presented in the previous section. Figure 4.12 shows the elastic moduli values determined from standard cylinder compressive tests plotted against their respective strengths. Also shown are these same values modified by the 0.56 factor, which converts the cylinder moduli to the more accurate representation of the core moduli. It was found earlier that in order to obtain a grouted gross area prism compressive strength equal to that of a plain net area prism strength, a substantially higher grout strength than plain prism strength was needed. In Fig. 4.12, a horizontal line representing the mean of the plain prism elastic moduli is shown intersecting the core elastic modulus curve. Dropping a perpendicular to the x axis indicates that a cylinder strength of about 3200 psi is needed to achieve this elastic modulus. This strength is remarkably close to that shown to be required using the compressive strength method, in Fig. 4.6. This serves to reinforce the theory presented by Drysdale that it may be more appropriate to match the deformational characteristics of the grout to those of the block rather than matching the strengths as is suggested by the masonry code.

The shape of the prism vertical stress-strain curves

are shown for a number of core strengths in Fig. 4.8. The curves display nearly linear behavior over most of their range. For each prism, Table 4.4 contains the percentage of the compressive strength of the prism over which the stress-strain curve is approximately linear. Considering that the code does not permit axial column stresses to exceed $0.20f'_m$, present design practice places masonry behavior well within the elastic range of the material. Figure 4.13 plots these percentages against core strength and visibly shows that no linear association can be made between core strength and linearity percentages. In general, these prisms displayed linear elastic behavior to a stress of $0.55f'_m$, with large variations.

When reviewing the values of prism block elastic modulus presented in Table 4.4, an important observation is made. It is noted that each block elastic modulus is usually significantly greater than its corresponding masonry elastic modulus. When these values are plotted, a more striking observation is made. Figure 4.14 shows the relation between prism block elastic modulus and prism core elastic modulus calculated from strains measured during the standard concrete cylinder tests. Block strains were measured using a one inch SR-4 strain gauge placed at block midheight on the third course. Although data are scattered, it appears from this figure that during elastic loading of the masonry, block strains are essentially independent of core elastic modulus. Yet it has already been shown that masonry strains

are not independent of core elastic modulus (Fig. 4.9 and Eq. 4.8 show this). These observations seem to imply that, by and large, strains in the mortar joint account for an appreciable portion of masonry strain even for grouted prisms for which it has been generally acknowledged that the grout provides continuity and thus a reduction in the significance of mortar joint strain. Unfortunately, mortar joint strains were not monitored, and a verification of this assertion is not possible.

4.5.5 Prism Lateral Strains

The load-lateral strain curves for a number of prisms, each considered to be representative of its respective series, are plotted in Fig. 4.15. All plots were made to the same scale to permit easy comparisons. These curves clearly indicate that for loads less than the mean failure load of the plain prisms, lateral tensile strains in the grouted prisms were significantly smaller than those for the plain prisms, and in addition, these strains decreased with increasing grout strength. However, for higher loads, all grouted prisms exhibited larger tension strains than the lateral failure strains of the plain prisms. Moreover, these larger lateral strains are observed at progressively lower loads as the grout strength of the prism decreases. These observations suggest that at these higher load levels, large lateral tensile strains resulting from the inelastic deformations of the grout core are introduced into the

surrounding block shell as it attempts to confine the core, and cause the premature splitting failure of the block.

A rather striking observation was made from a study of the prism load-lateral strain curves. Ten of the twenty-two prisms monitoring lateral deformations showed lateral compressive strains up to stresses as high as $0.70f'_m$, even though the face upon which the gauges were placed was in vertical compression. Recorded for each prism in Table 4.4, are values of the maximum load for which these compressive strains were observed (designated by -P), and the ratio of $-P/Pu_m$. This behavior showed no associative patterns with grout strength. No suitable explanation for the phenomenon has been found. The possibility of defective gauges can be over-ruled by virtue of the number of prisms which displayed this behavior, and the argument that the gauge was merely seating itself seems unreasonable since the loads for which this behavior was noted were unusually high, and since gauges applied with similar workmanship to the plain prisms and core specimens provided linear elastic measurements from initial loading.

4.5.6 Prism Cracking Loads

The loads at which prism shell cracks were first visible to an observer are plotted against prism core cylinder compressive strength in Fig. 4.16. It is acknowledged that shell microcracking would have commenced well in advance of these visible cracks. However, visible

cracking may be interpreted as a measure of engineering serviceability. Because of the nature of the cracking definition, these observations are somewhat subjective and one should expect large variations in the reported data.

The cracking loads of all grouted prisms were greater than the mean ultimate load of the plain prisms. This seems reasonable since the stresses in the masonry shell of the grouted prism would be significantly less than those of a plain prism at the same load by virtue of load sharing with the prism core. Since the loading conditions of this study assured that uniform axial strains were imposed in both the masonry shell and the grouted core, the compression load was shared between these in proportion to their axial stiffness. In addition, this observation is in keeping with those made earlier which showed that the lateral tensile strains in grouted prisms were less than those of a plain prism for this load level.

Figure 4.16 clearly illustrates that cracking load is directly proportional to prism core strength. The prism cracking load may be related to the grout strength using the following linear regression equation:

$$P_{crack} = 61.5f'_c + 190 \quad \text{(kips)} \quad \ldots\ldots\ldots\ldots \quad 4.9$$

$$r = 0.73$$

The observation that an increased core strength results in a higher cracking load is consistent with the failure mechanism proposed earlier. Since higher strength grout is

associated with greater lateral stiffness, relatively smaller tensile strains and stresses will be imposed on the masonry shell for a given load and tensile cracking will occur during a later stage.

The relationship between the ratio of prism cracking load/prism ultimate load, and prism grout compressive strength is shown in Fig. 4.17. For each prism the P_{crack}/P_{u_m} ratio is in excess of the ratio of P_{linear}/P_{u_m}, which indicates that shell cracking occurs in the inelastic stage of loading. Consequently, any attempt to predict cracking load based on an elastic analysis is not strictly correct. The ratio of P_{crack}/P_{u_m} decreases with increasing grout strength, and may be roughly approximated by:

$$P_{crack} = -0.045f'_c + 1.0 \quad \text{(where } f'_c \text{ is in ksi)} \qquad 4.10$$

The cracking load of the shell, as is the compressive strength, is clearly dependent upon block strength and core strength, and it must therefore be recognized that Eqs. 4.9 and 4.10 will likely only strictly apply to blocks with dimensions and strengths similar to those used in this study.

4.5.7 Ultimate Prism Masonry Strain

Figure 4.18 shows the ultimate masonry strains measured over a 24-inch gauge length for all the prisms tested in the program. Compressive strains at failure were between 0.001

and 0.002 in./in., and clearly, no direct relation exists between ultimate strain and prism core compressive strength. Prism concrete block face strains were normally about 10 to 20 percent less than prism masonry strains at ultimate load. Yet block elastic modulus and mortar elastic modulus were almost identical when measured independently, and thus one might expect masonry and block strains to be similar at failure. One must remember, however, that linearity of the stress-strain curve for mortar cubes is only about $0.65f'_{mort}$ = 1200 psi, whereas that for the block is about 2500 psi. These stress levels indicate that large, inelastic deformations occur in the mortar joint in advance of inelastic block deformations, and hence the former accounts for an appreciable portion of masonry ultimate strain.

4.5.8 Effect of Grout Slump

Plate 4.4 is a photograph of the top surface of a Series CP3P- prism, grouted with a 9 in. slump, 4290 psi grout (mix 3G). Extensive shrinkage cracking between the grout fill and the pilaster unit is clearly visible. These cracks were measured with a steel scale and found to be about 1.5 mm. in width. Their depth of penetration could not easily be determined, but it is known that this depth exceeded 1.5 inches.

Plate 4.5 shows the top surface of a prism from the DP3P- series, grouted with a 3880 psi, 4 in. slump concrete (mix 3C). Shrinkage cracking at the block-core interface is

not nearly as extensive as that shown in Plate 4.4. These cracks measured only about 0.5 mm. in width, and were estimated to have extended to a depth of about 0.5 inches. Cracking in this prism was typical of all prisms filled with 4 in. slump concrete, regardless of strength. There was no cracking on the lower surface of any of the prisms.

These interface shrinkage cracks are the result of segregation and bleeding which create a high water/cement ratio in the concrete occupying the upper region of the prism core. The depth to which these cracks penetrate the core is not known, and this leads one to question the nature of the bond between the block and fill when high slump concretes are used for sections with a large area, such as those used in the present study. Feeg[8] reported that these cracks were detrimental to the structural performance of columns which are constructed with these pilaster units.

Tests conducted herein, however, have shown that extensive cracking in no way affects the structural performance of a masonry prism in direct compression. The compressive strengths, elastic moduli, and cracking loads for prisms in Series CP3P- were in every respect comparable to, and in good agreement with, expected values based on the performance of the other series. In all likelihood, this cracking is a localized phenomenon, and is restricted to a depth of only a few inches.

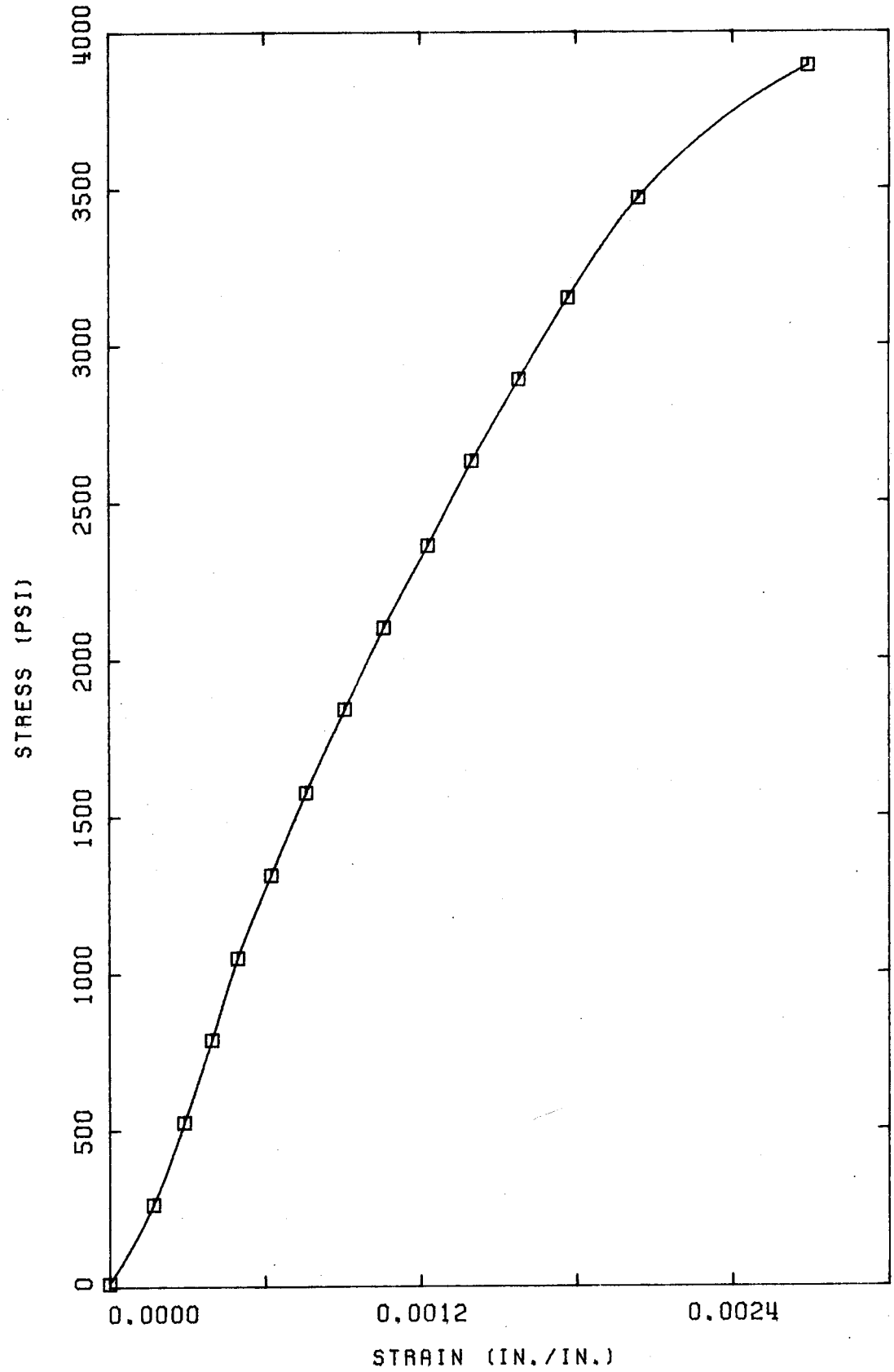

FIG. 4.1: PILASTER UNIT STRESS-STRAIN RELATIONSHIP

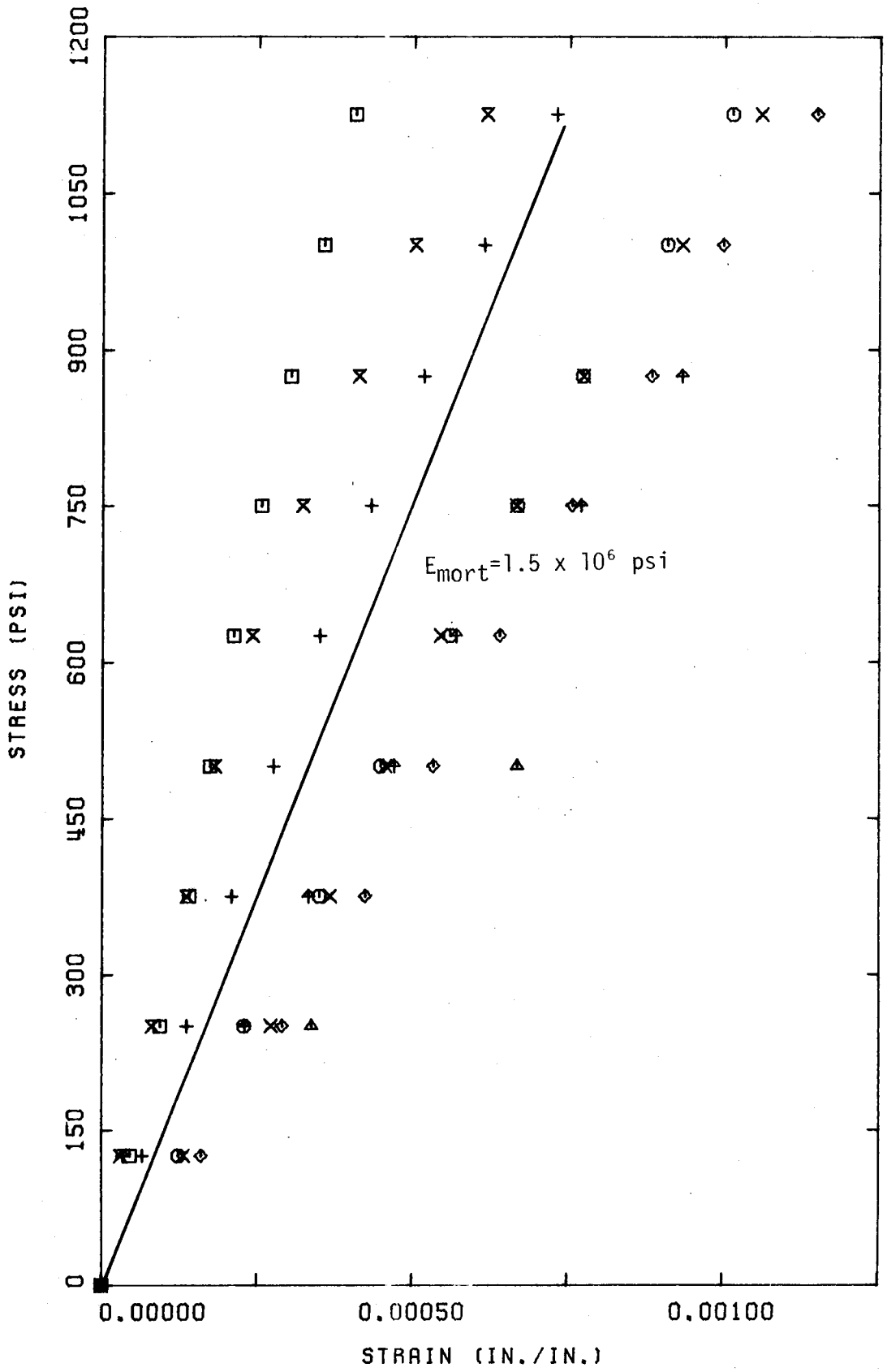

FIG. 4.2: LIME CURED MORTAR CUBES

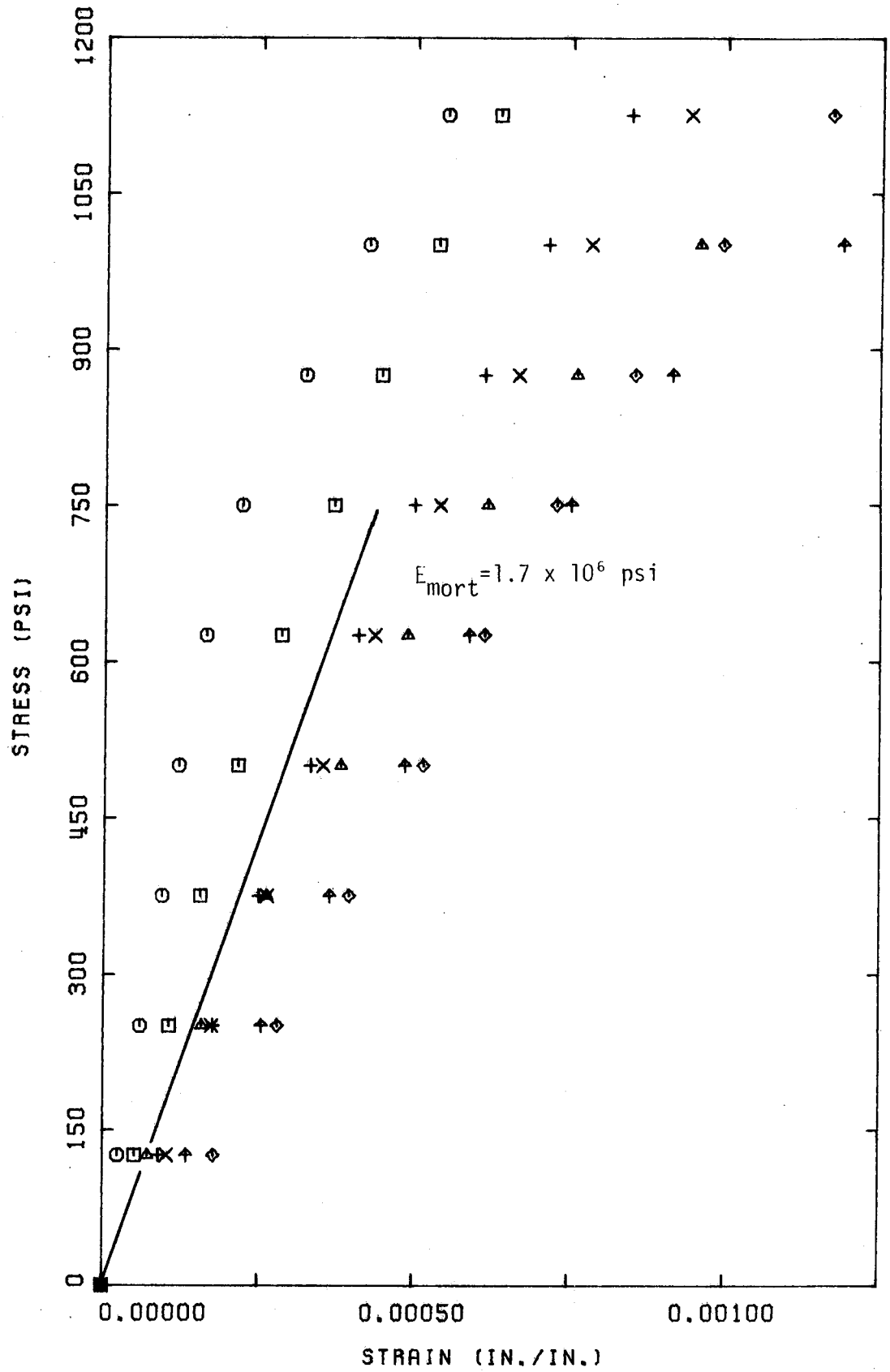

FIG. 4.3: LAB CURED MORTAR CUBES

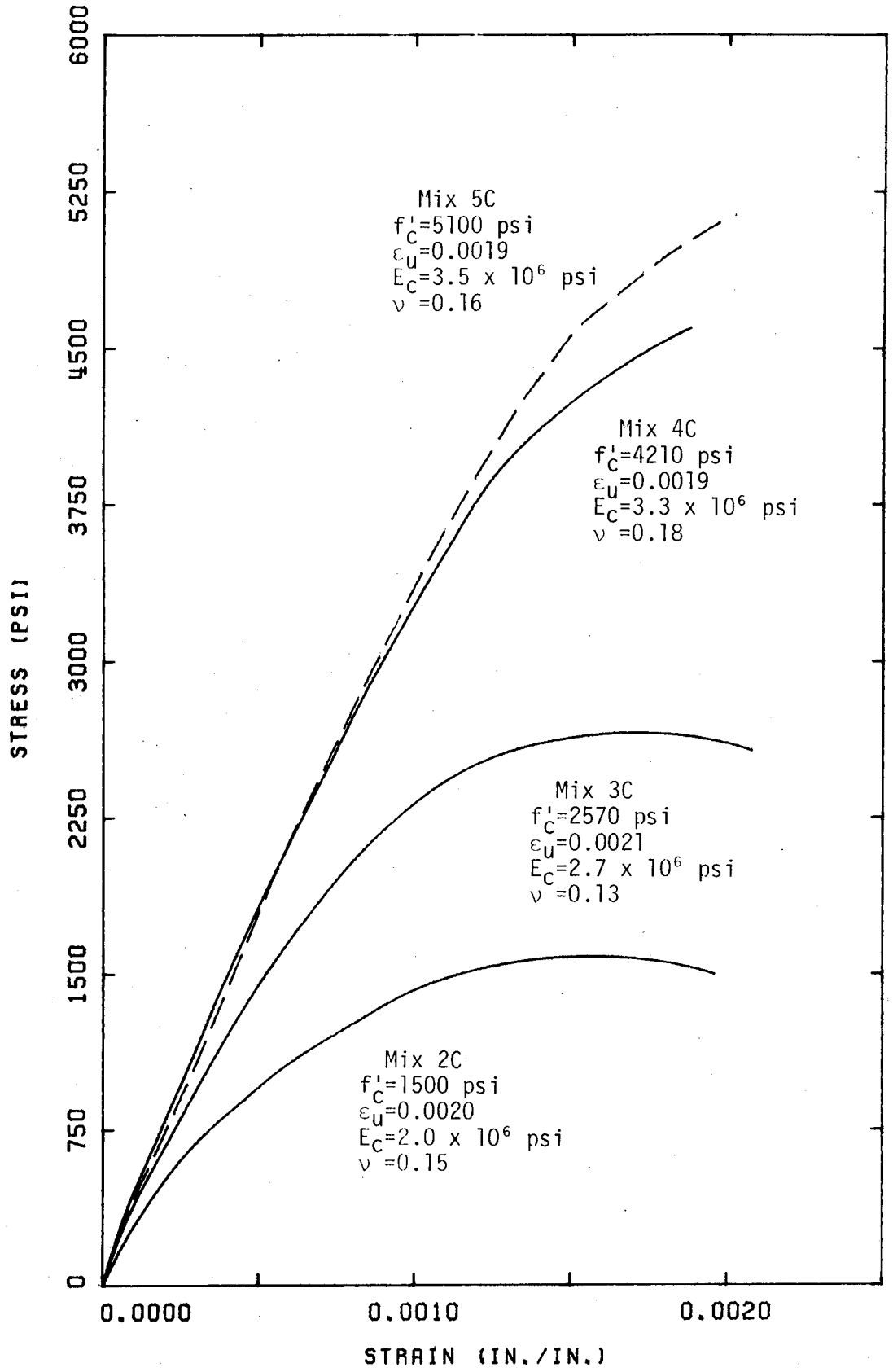

FIG. 4.4(a): SERIES "A" MOIST CURED CONCRETE CYLINDERS

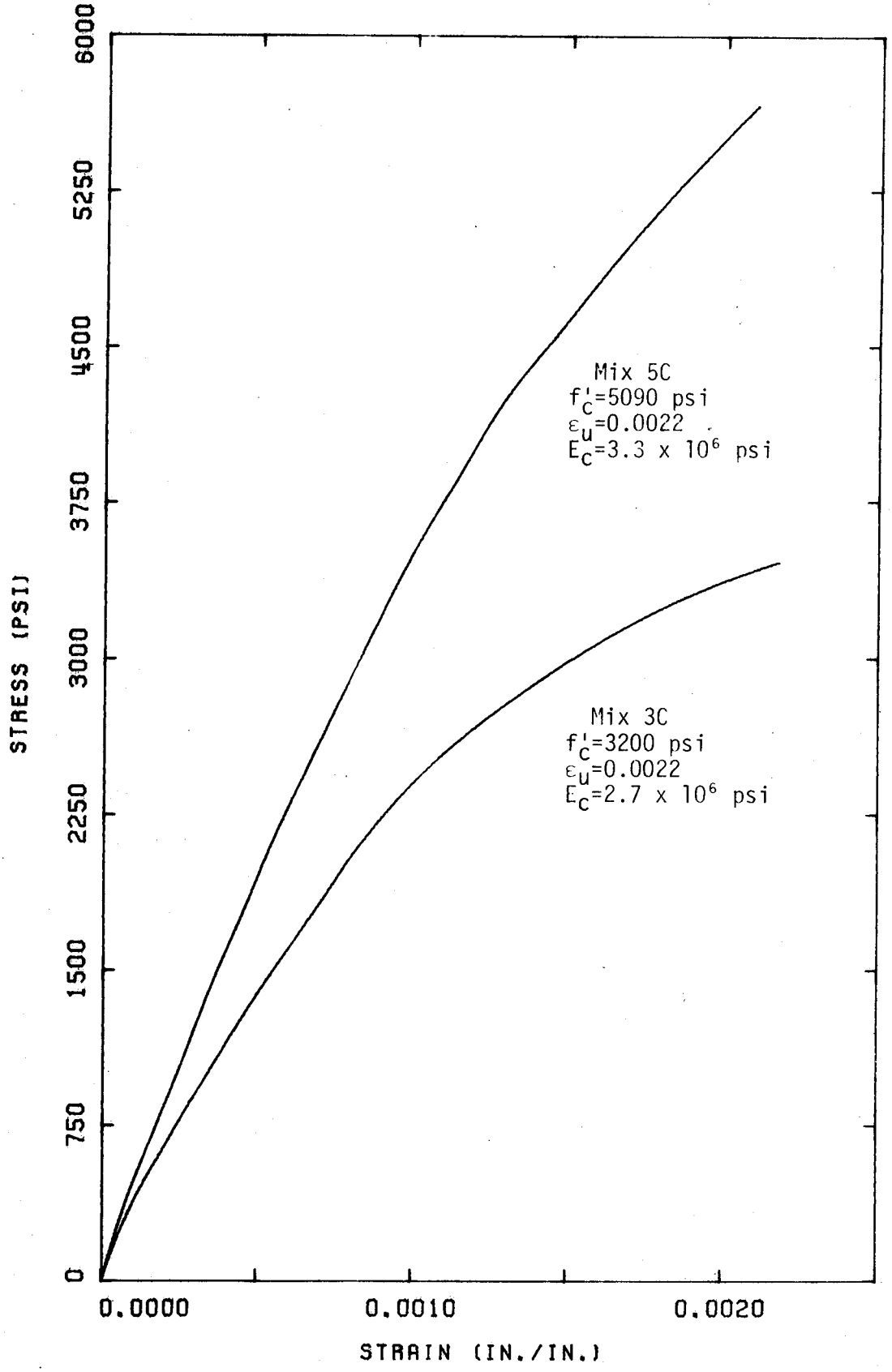

FIG. 4.4(b): SERIES "E" MOIST CURED CONCRETE CYLINDERS

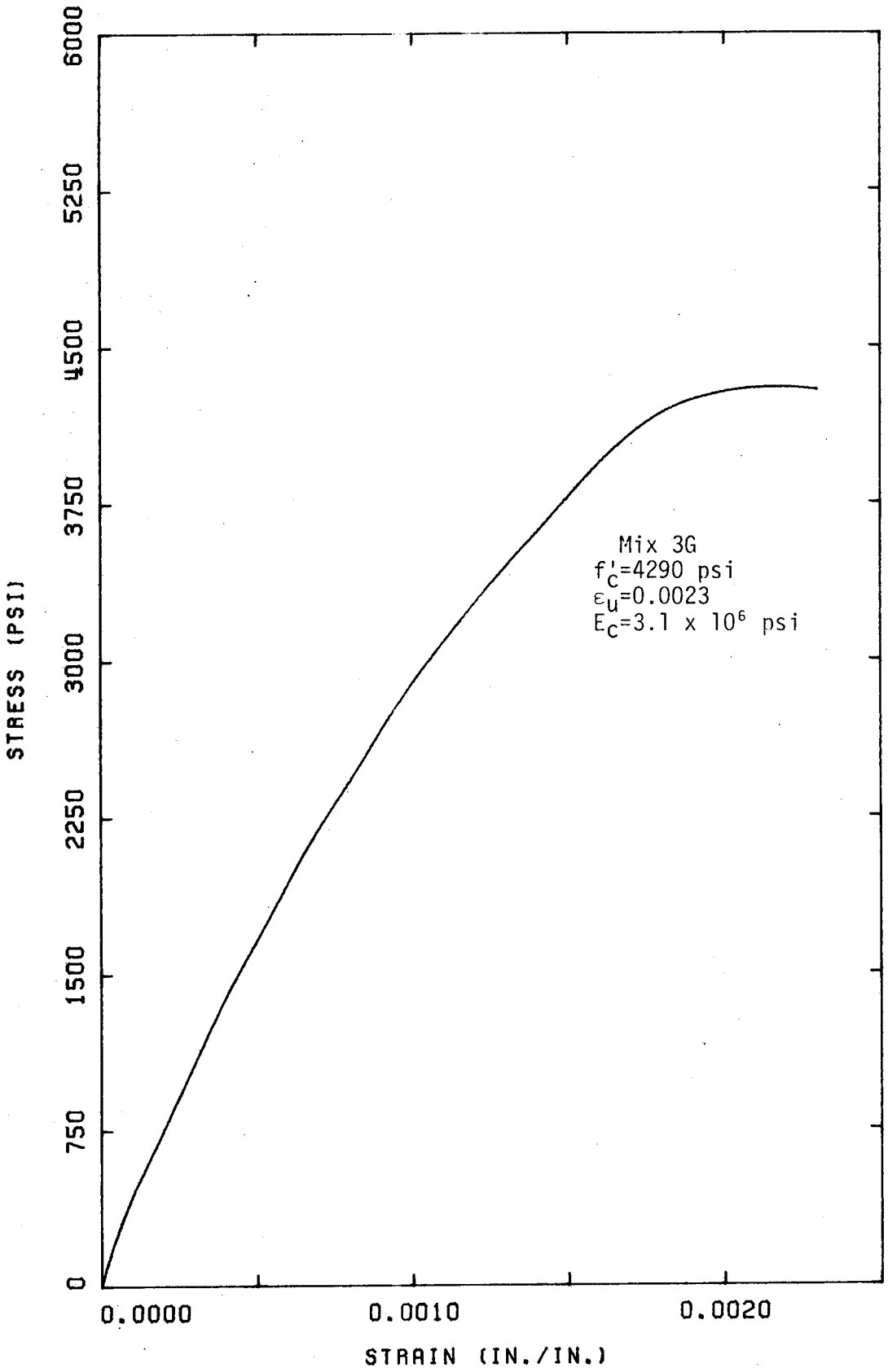

FIG. 4.4(c): SERIES "C" MOIST CURED CONCRETE CYLINDERS

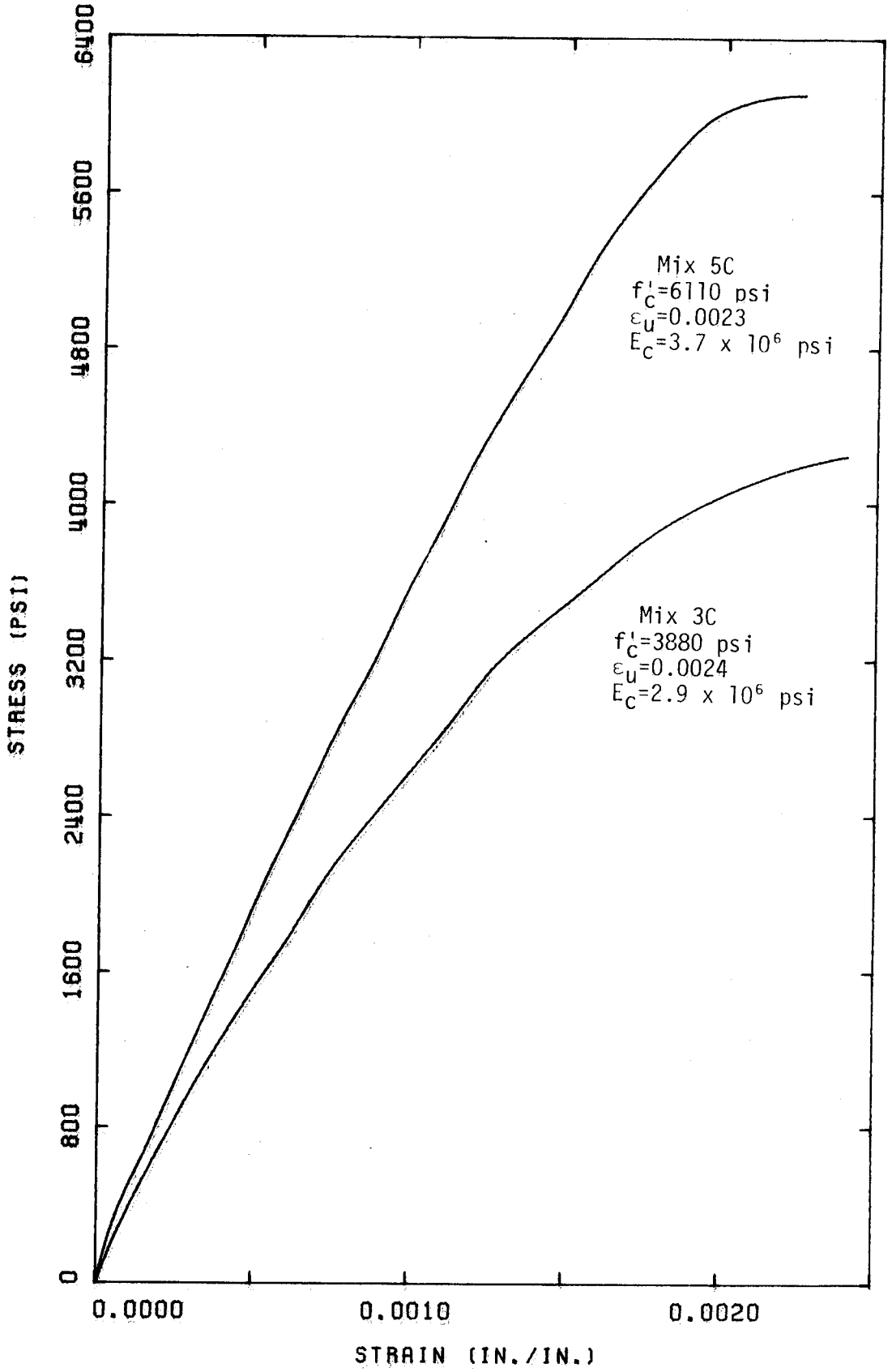

FIG. 4.4(d): SERIES "D" AND "F" MOIST CURED CYLINDERS

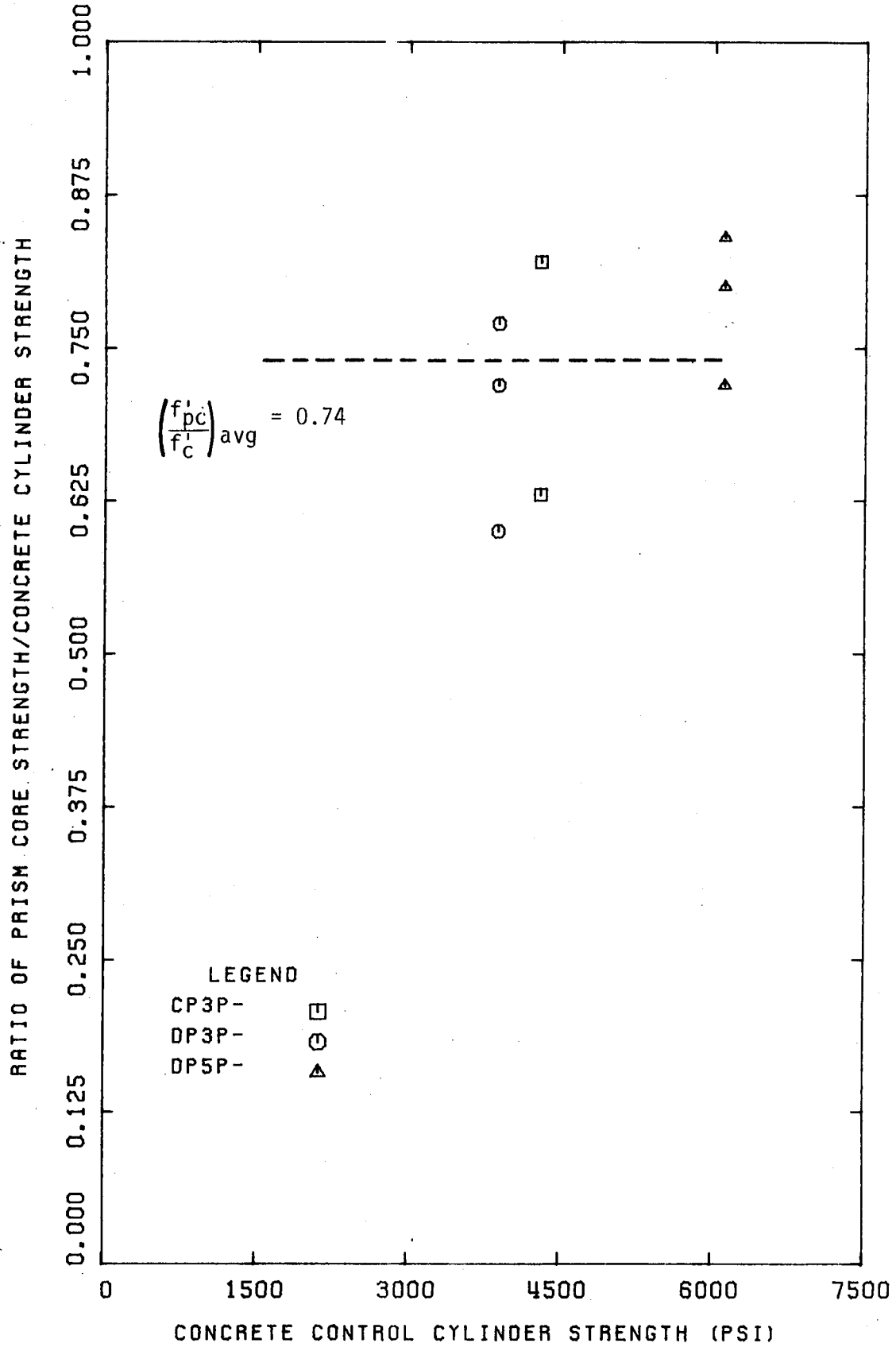

FIG. 4.5: PRISM CORE STRENGTH VS. CYLINDER STRENGTH

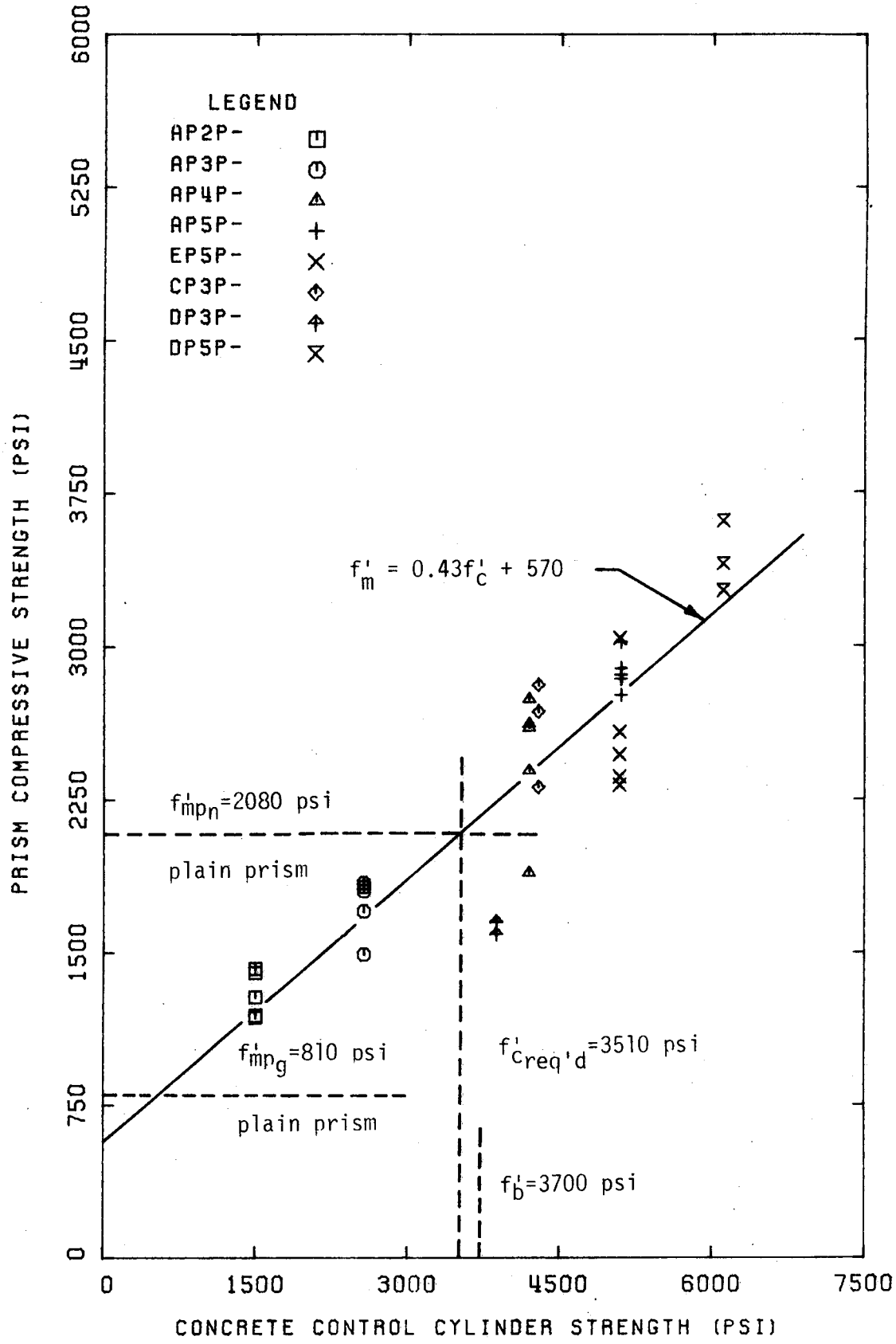

FIG. 4.6: PRISM STRENGTH VS. CONCRETE CYLINDER STRENGTH

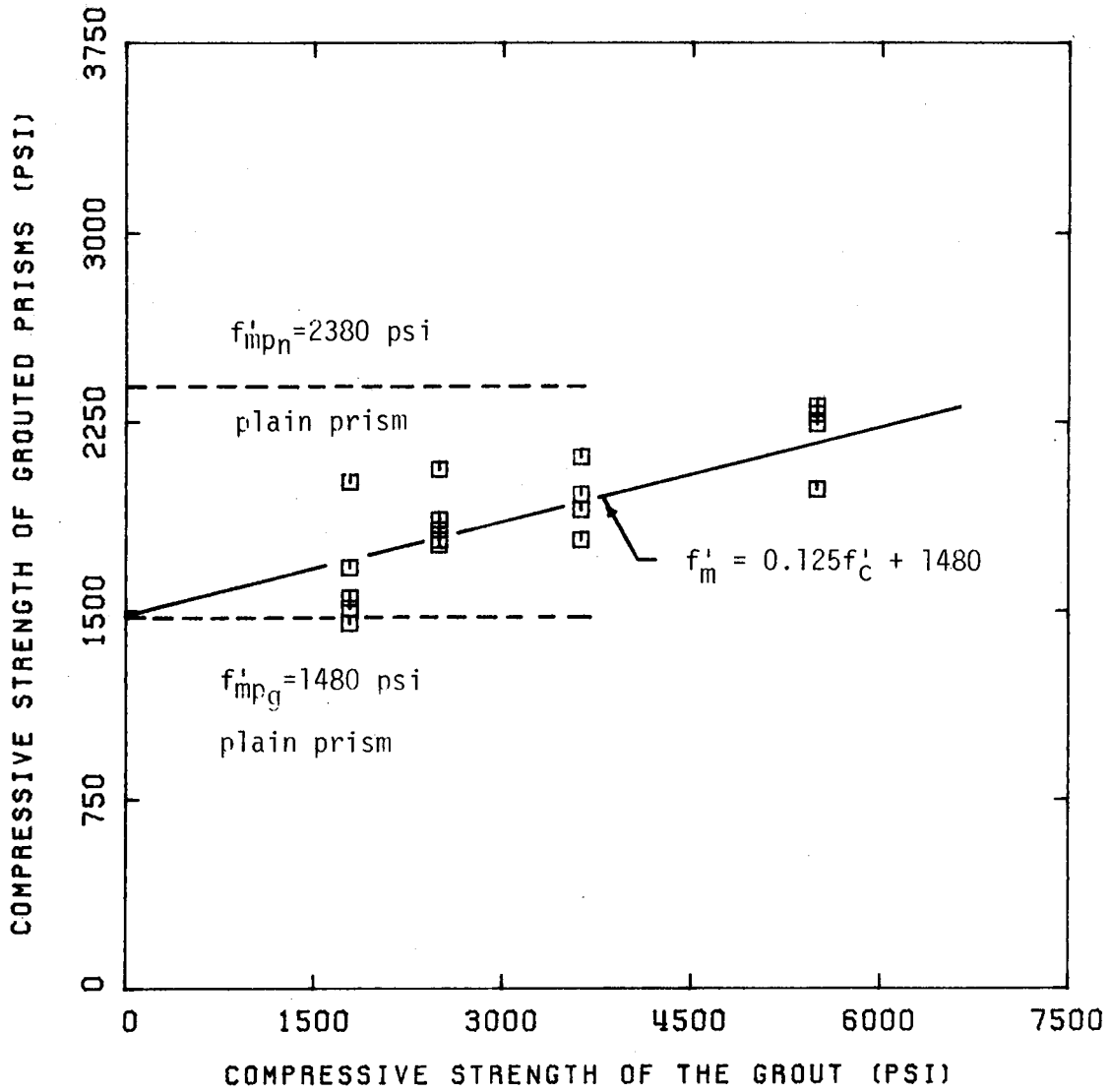

FIG. 4.7: DRYSDALE PRISM STRENGTH VS. GROUT STRENGTH

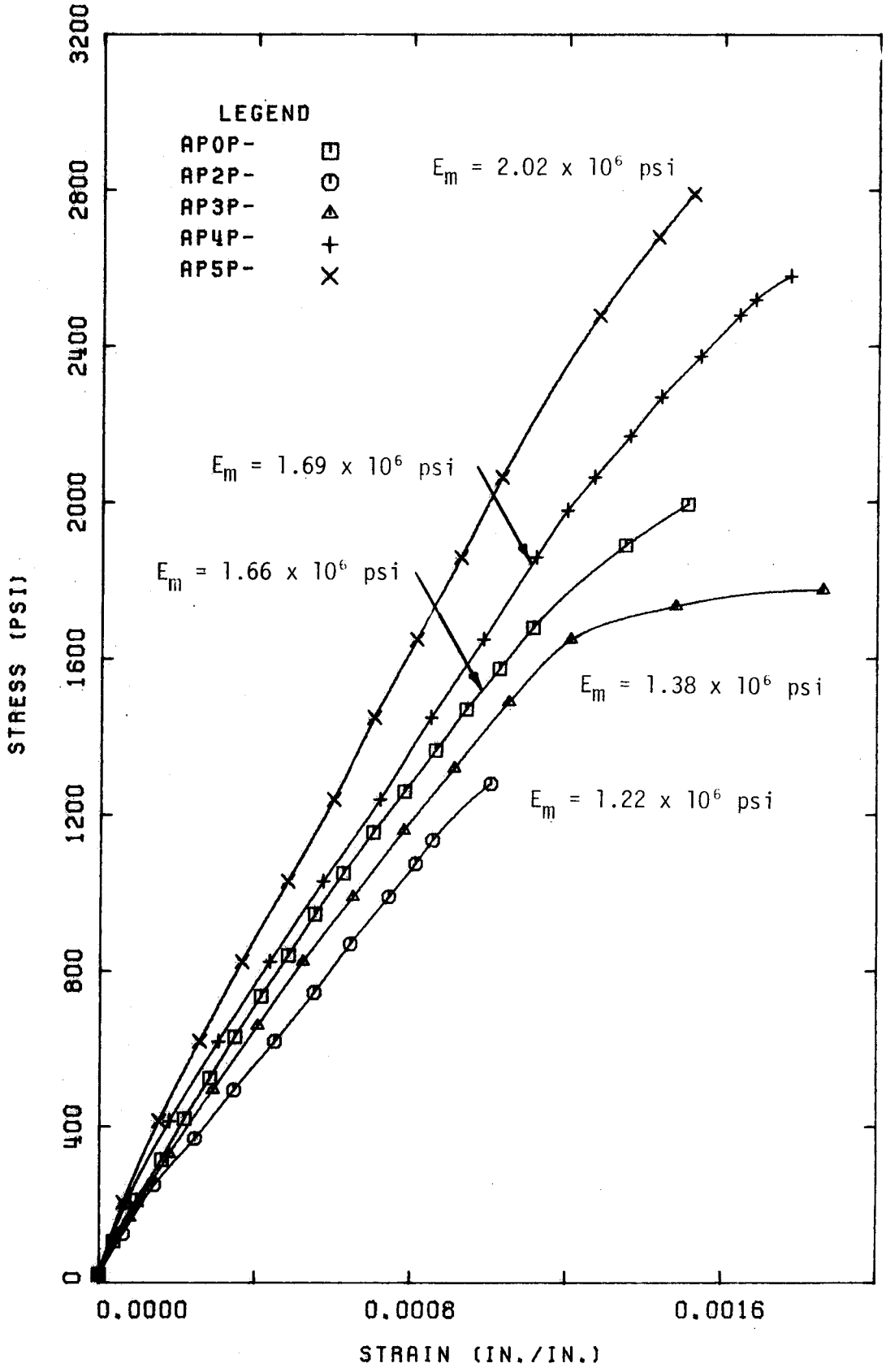

FIG. 4.8: PRISM STRESS-STRAIN RELATIONSHIPS

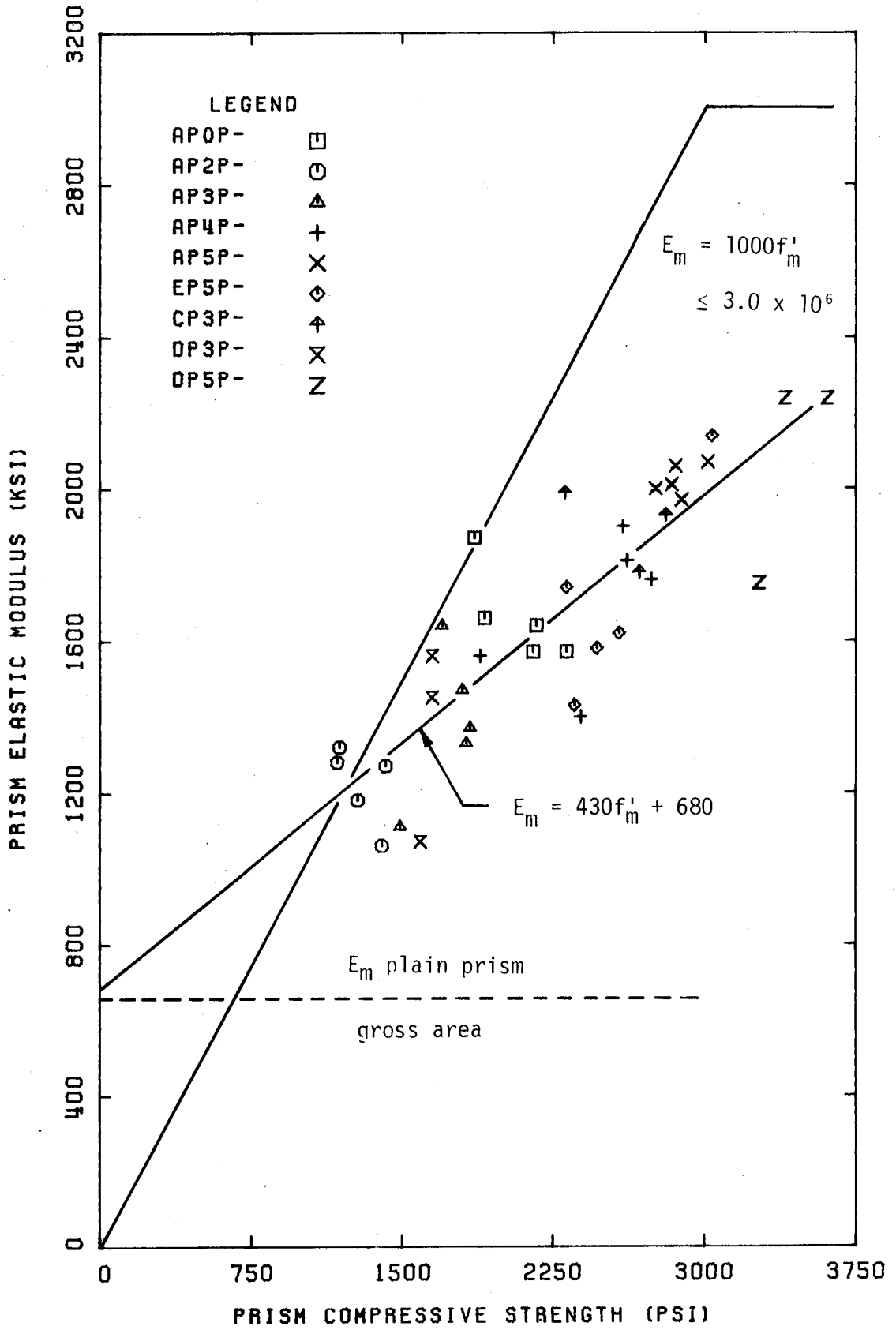

FIG. 4.9: PRISM ELASTIC MODULUS VS. COMPRESSIVE STRENGTH

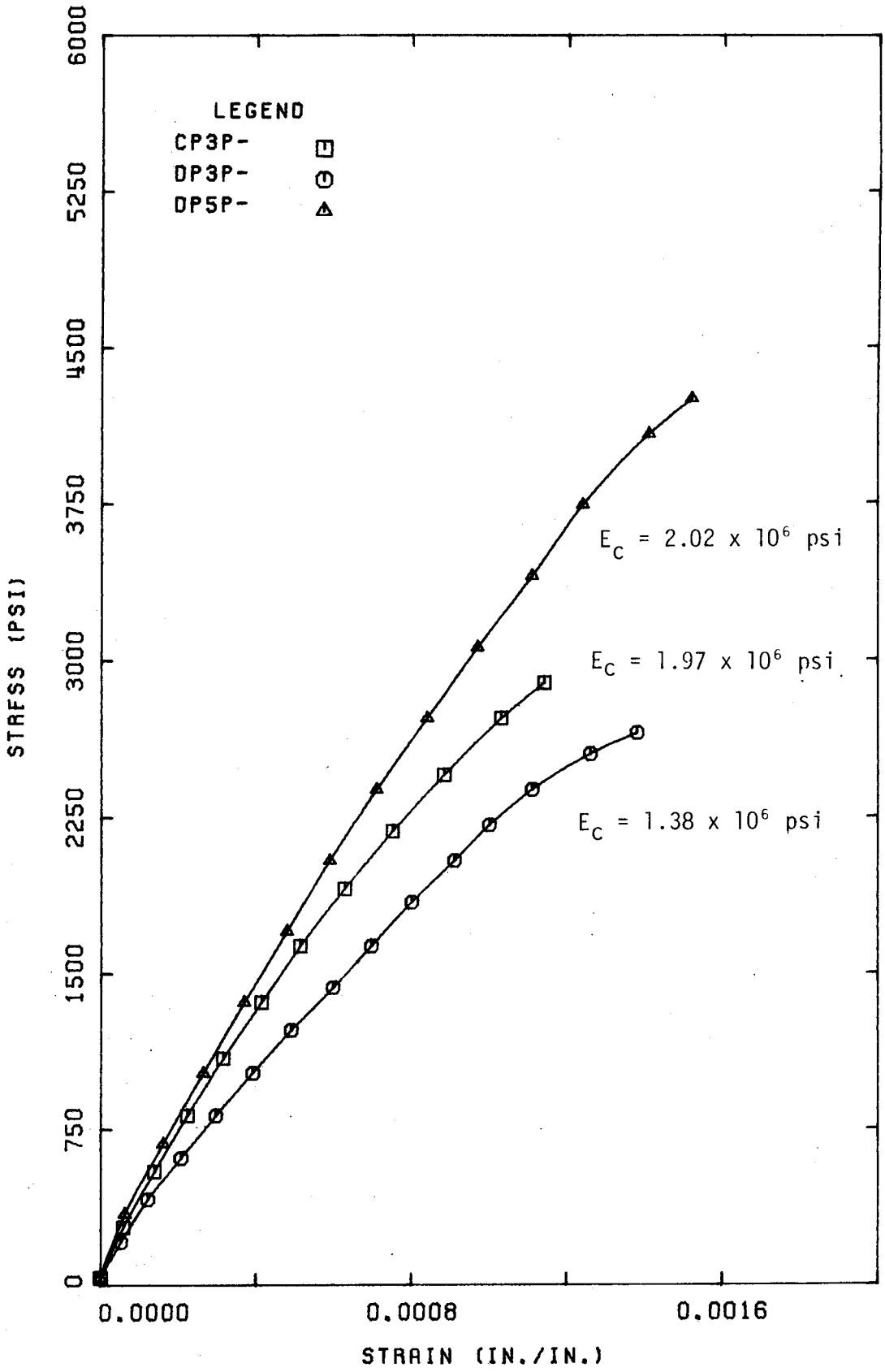

FIG. 4.10: PRISM CORE STRESS-STRAIN RELATIONSHIPS

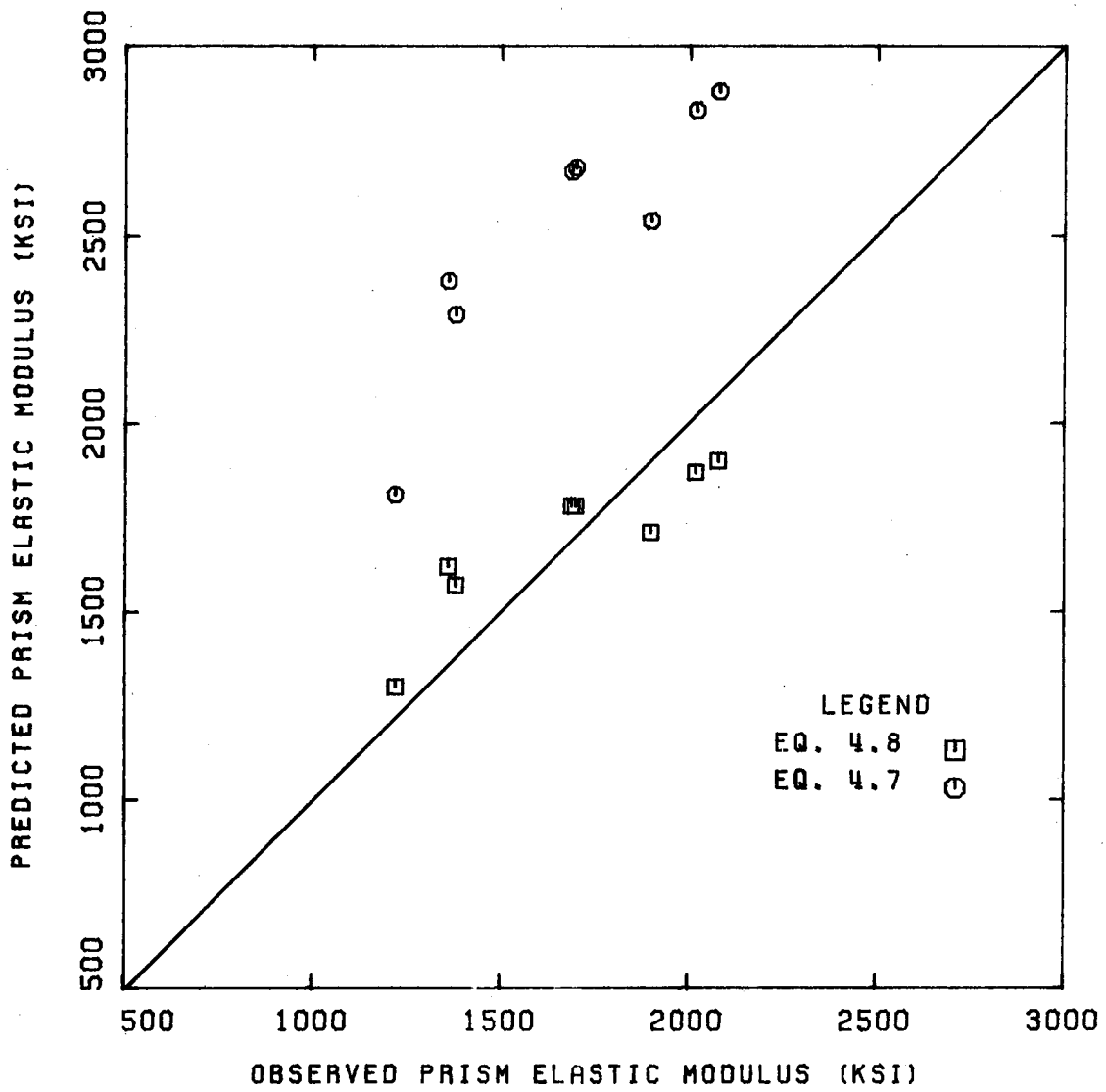

FIG. 4.11: PREDICTED VS. OBSERVED PRISM E_m

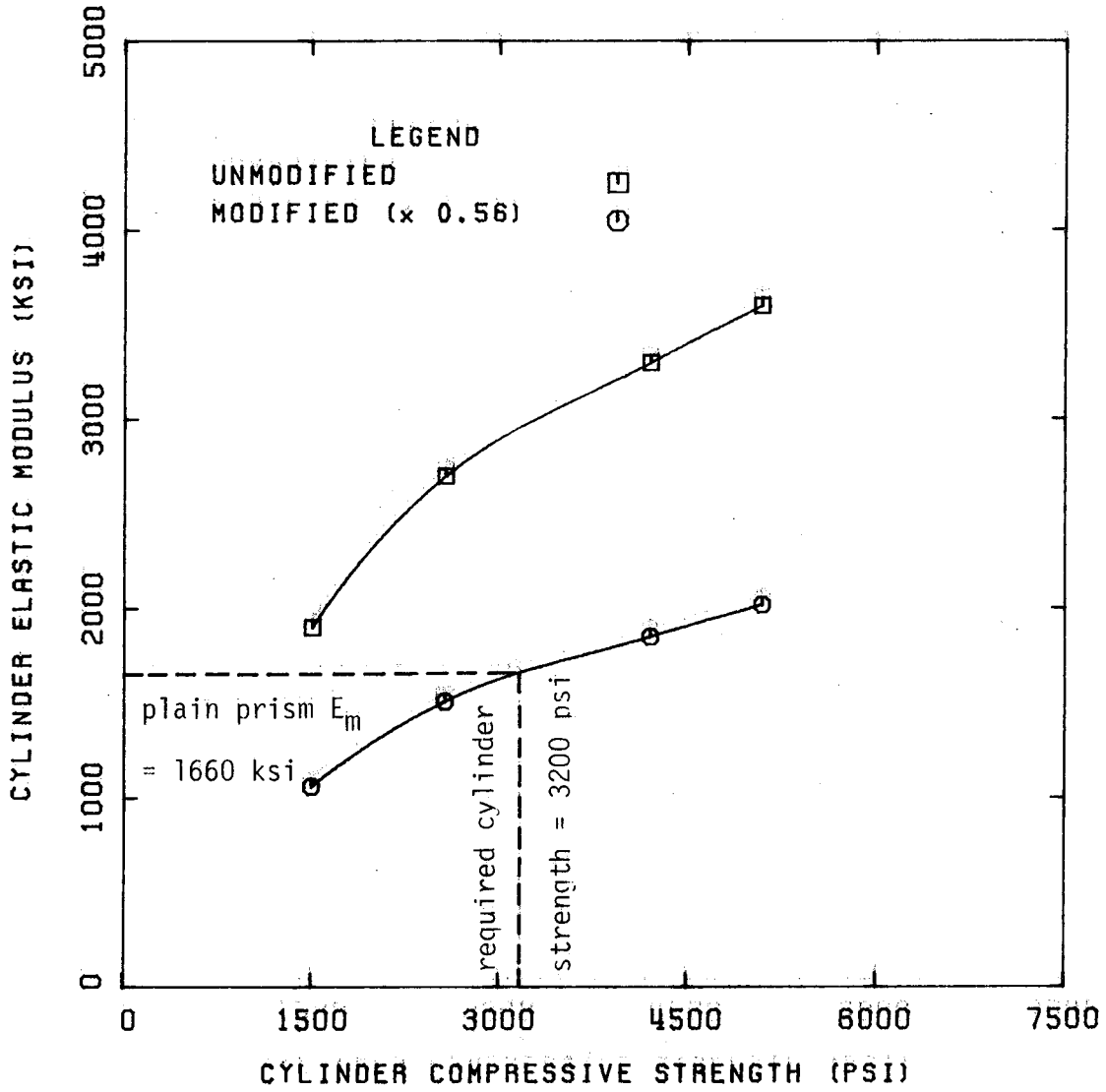

FIG. 4.12: CYLINDER ELASTIC MODULUS VS. CYLINDER STRENGTH

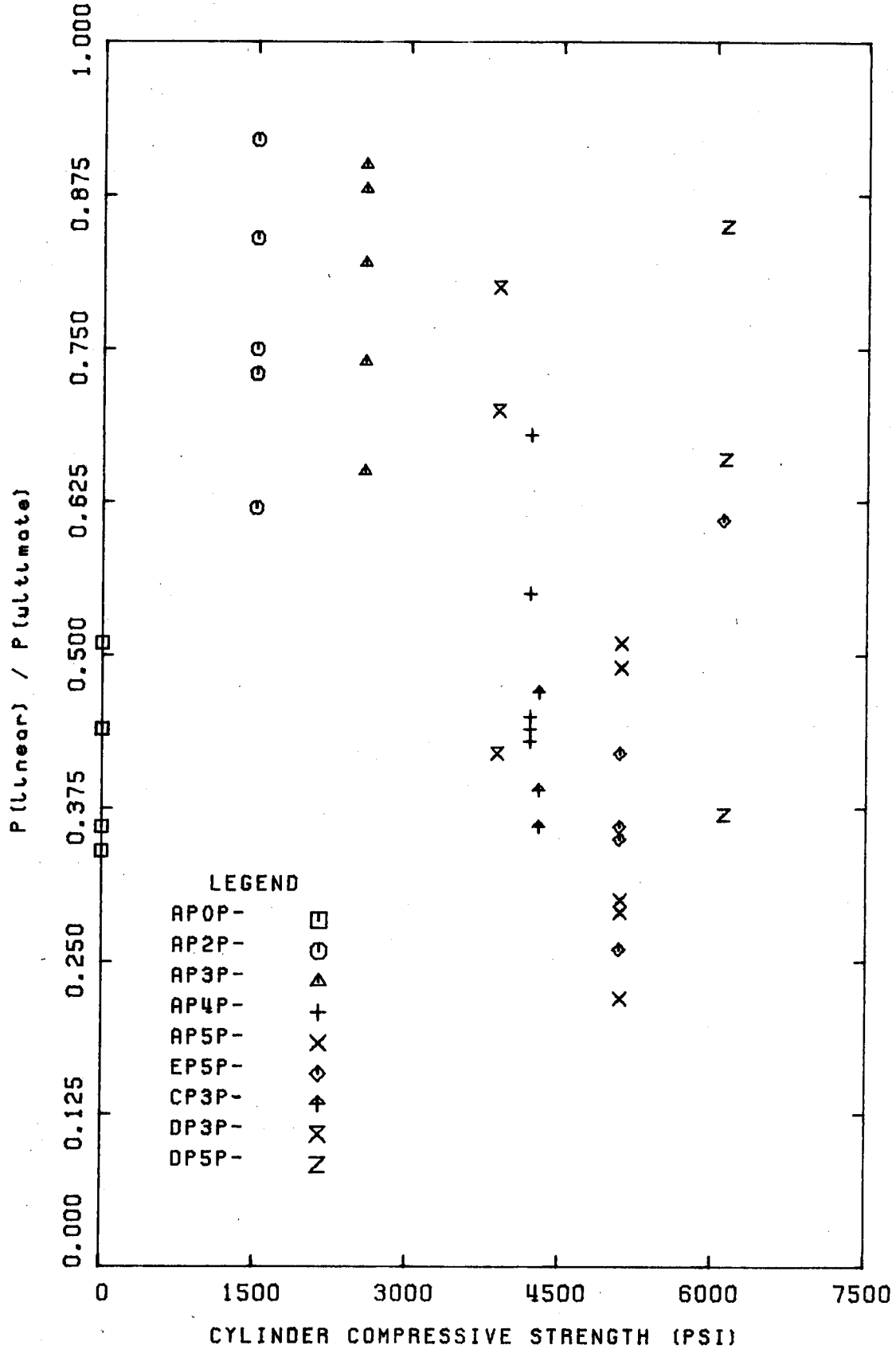

FIG. 4.13: PRISM P(Linear) VS. P(ultimate)

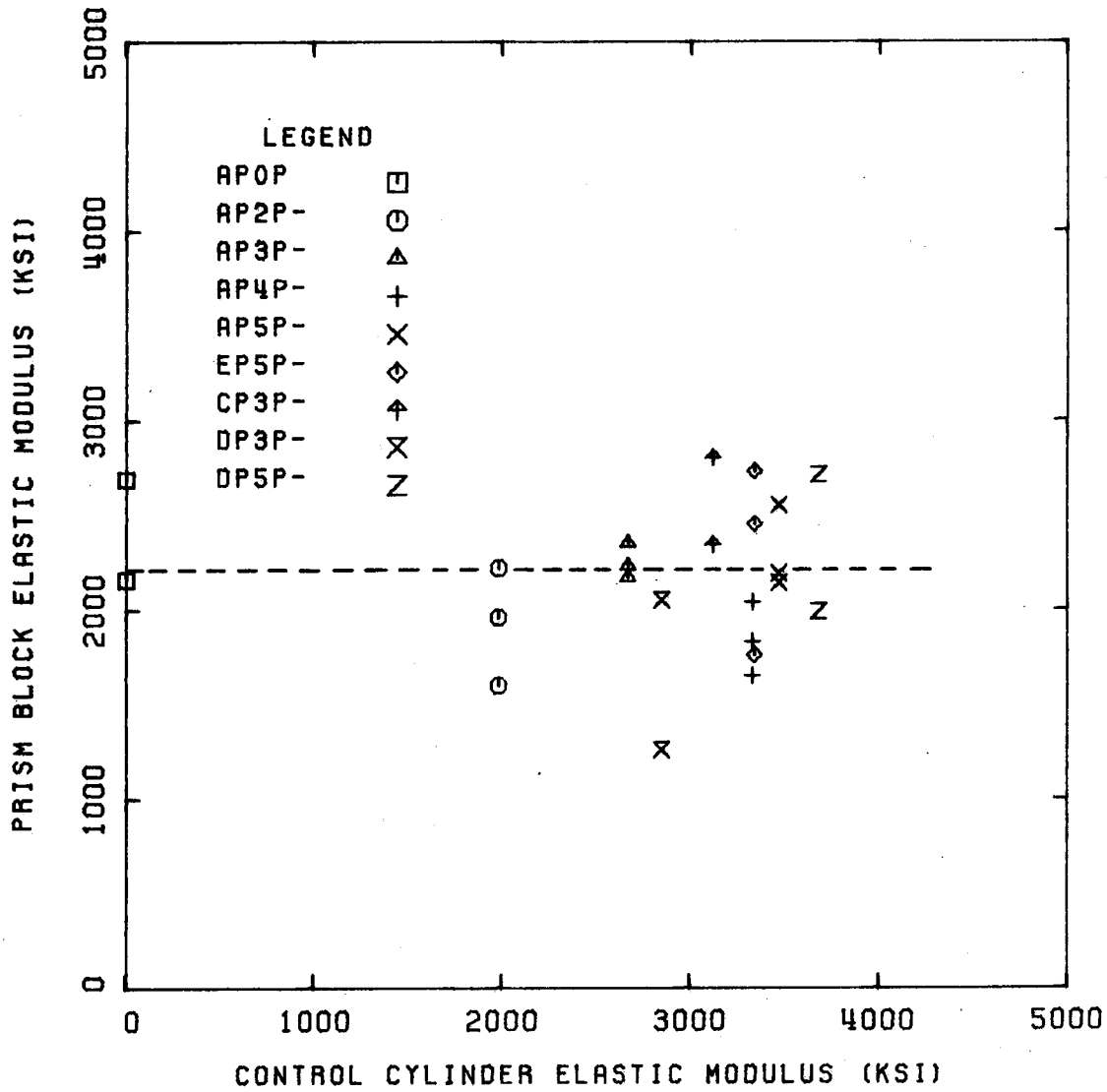

FIG. 4.14: CONTROL CYLINDER E VS. PRISM BLOCK E

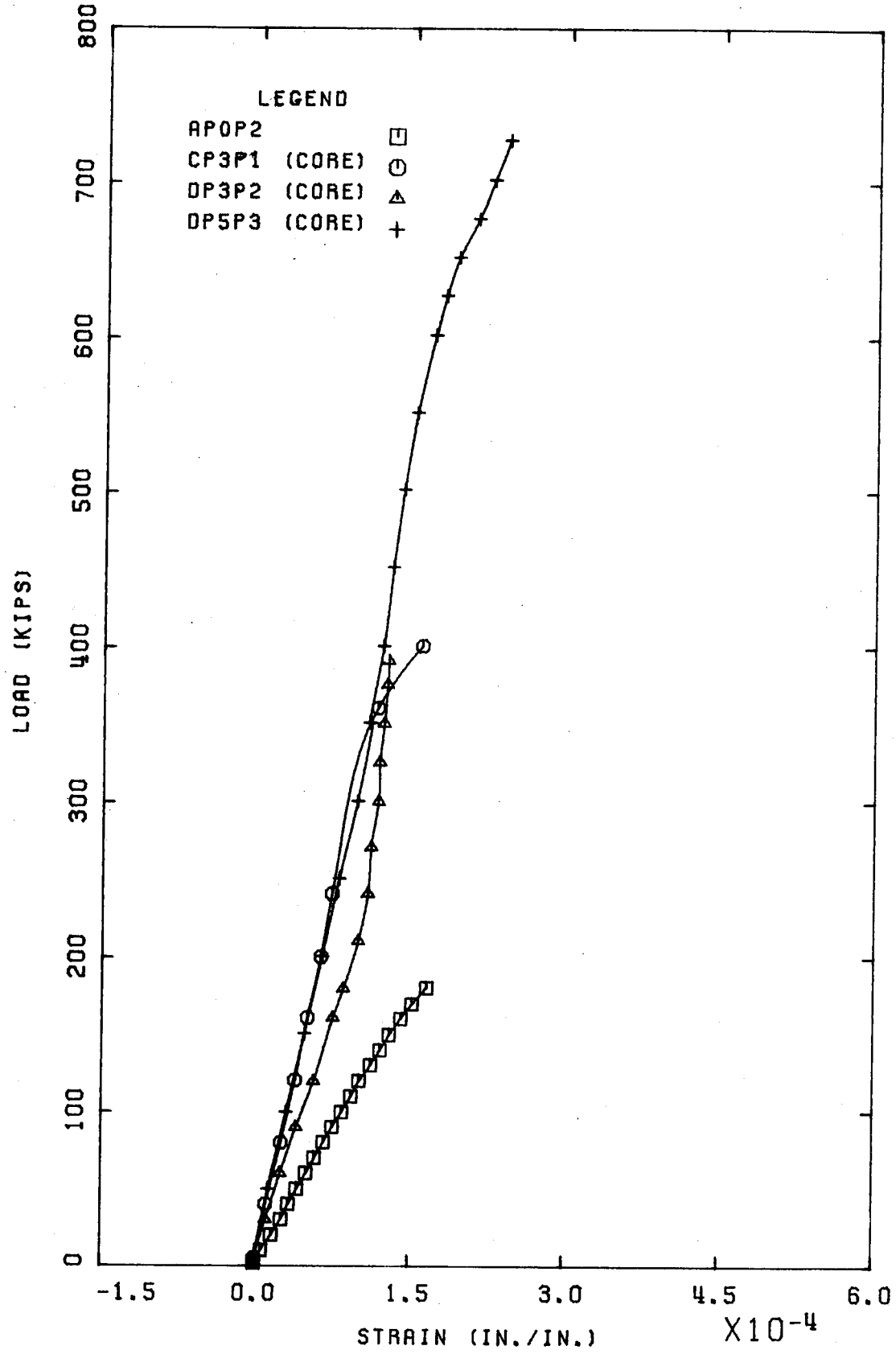

FIG. 4.15(a): LOAD VS. PRISM BLOCK FACE LATERAL STRAIN

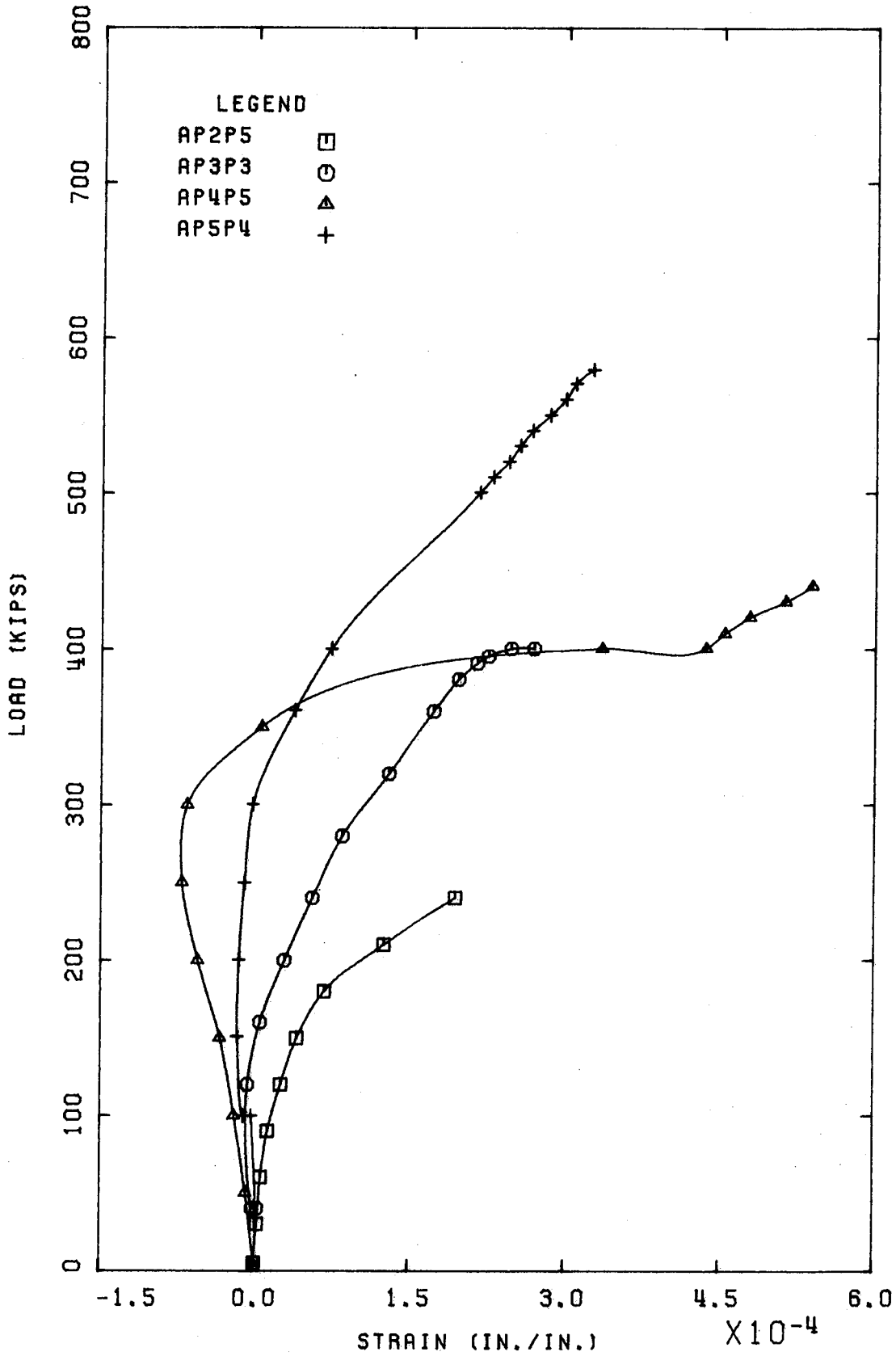

FIG. 4.15(b): LOAD VS. PRISM BLOCK FACE LATERAL STRAIN

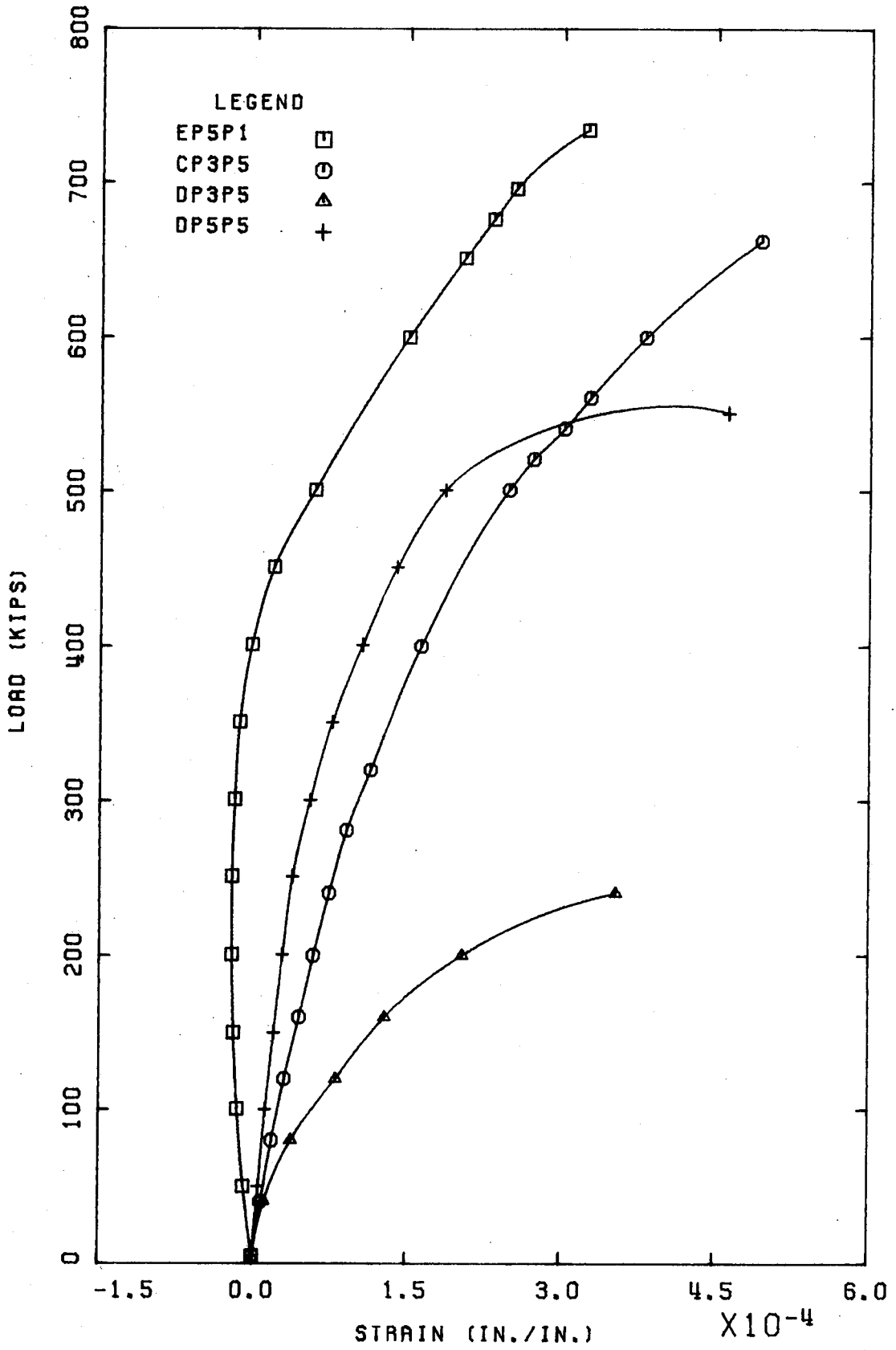

FIG. 4.15(a): LOAD VS. PRISM BLOCK FACE LATERAL STRAIN

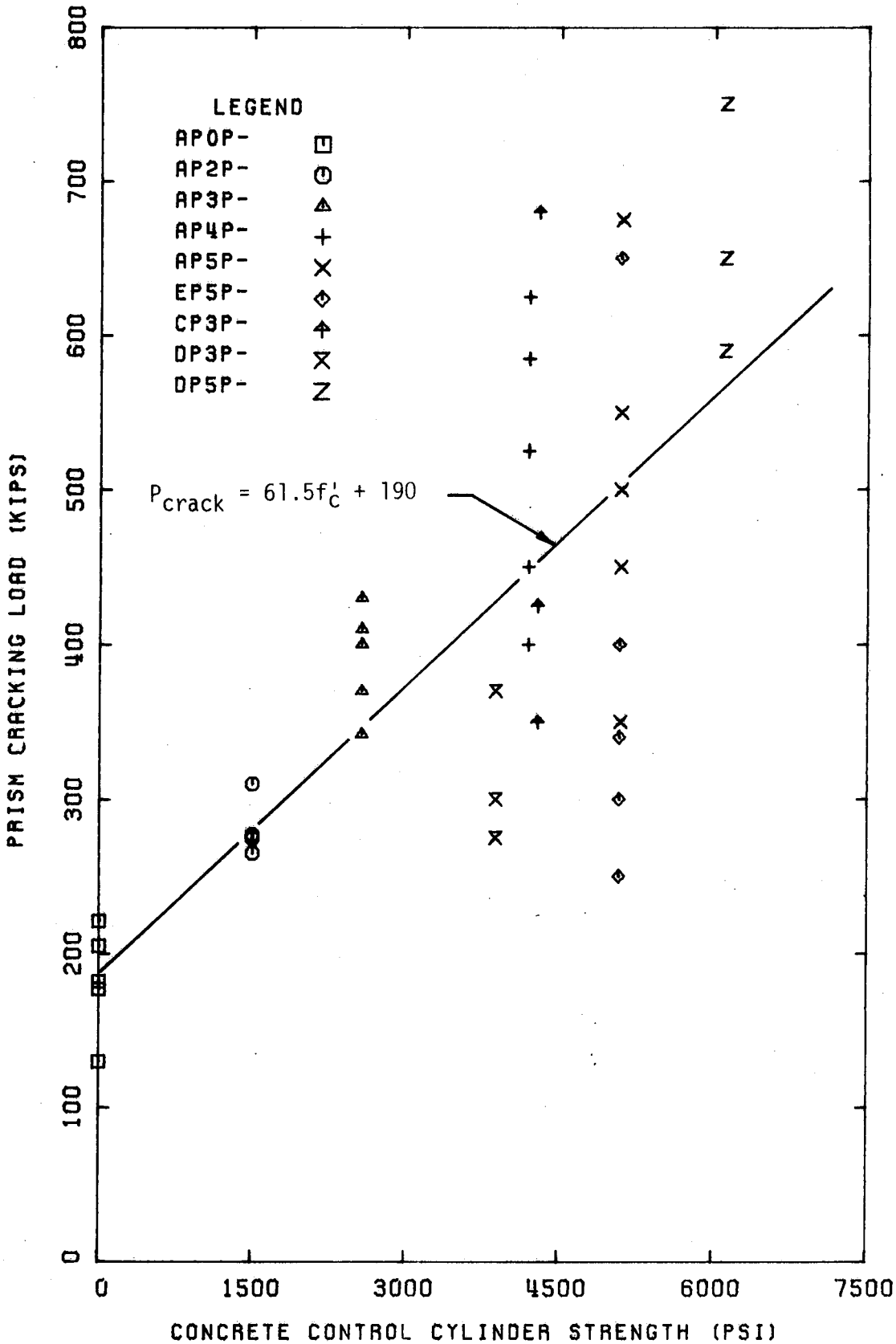

FIG. 4.16: PRISM CRACKING LOAD VS. CYLINDER STRENGTH

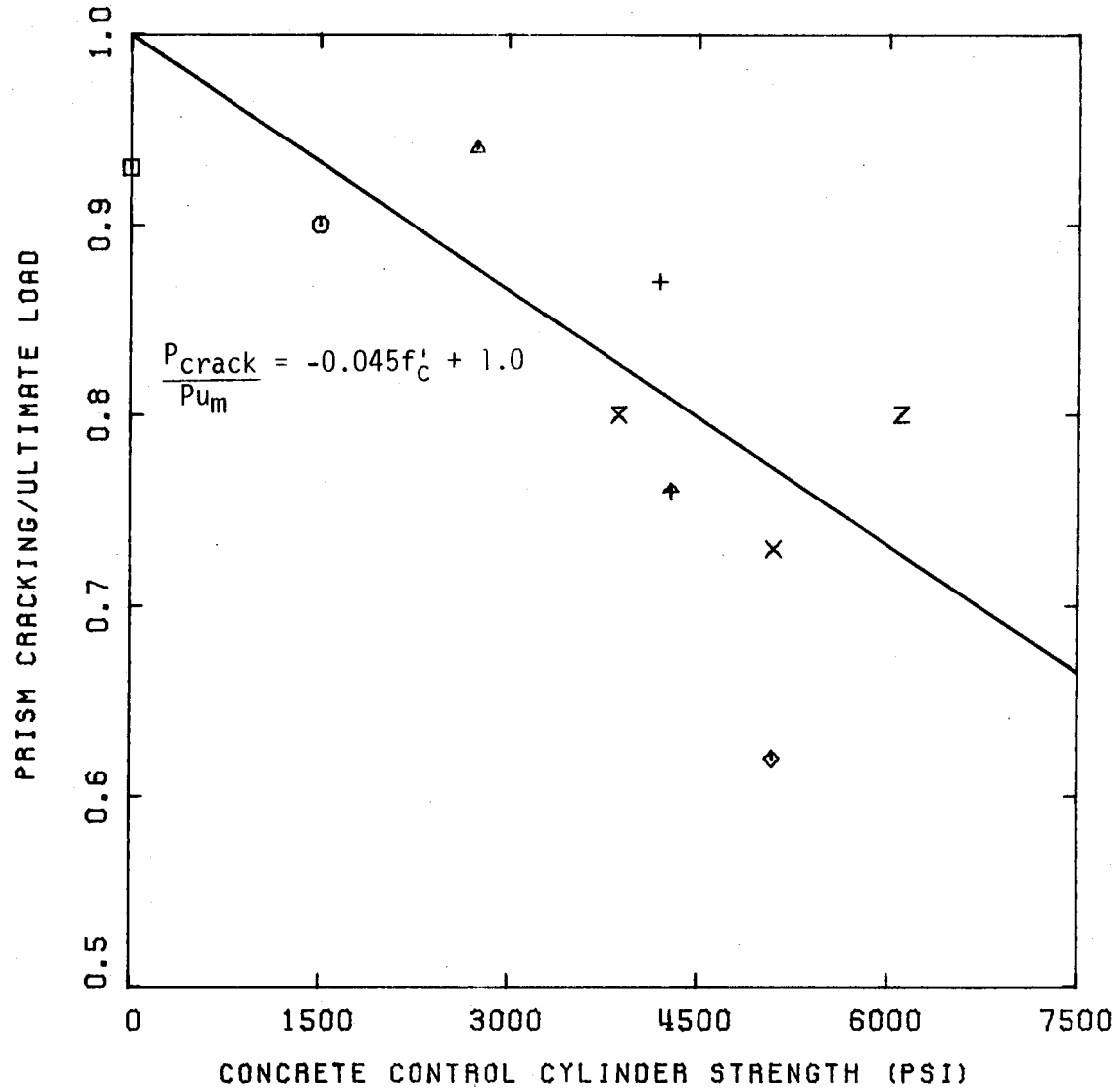

FIG. 4.17: PRISM CRACK/ULTIMATE LOAD VS. CYLINDER STRENGTH

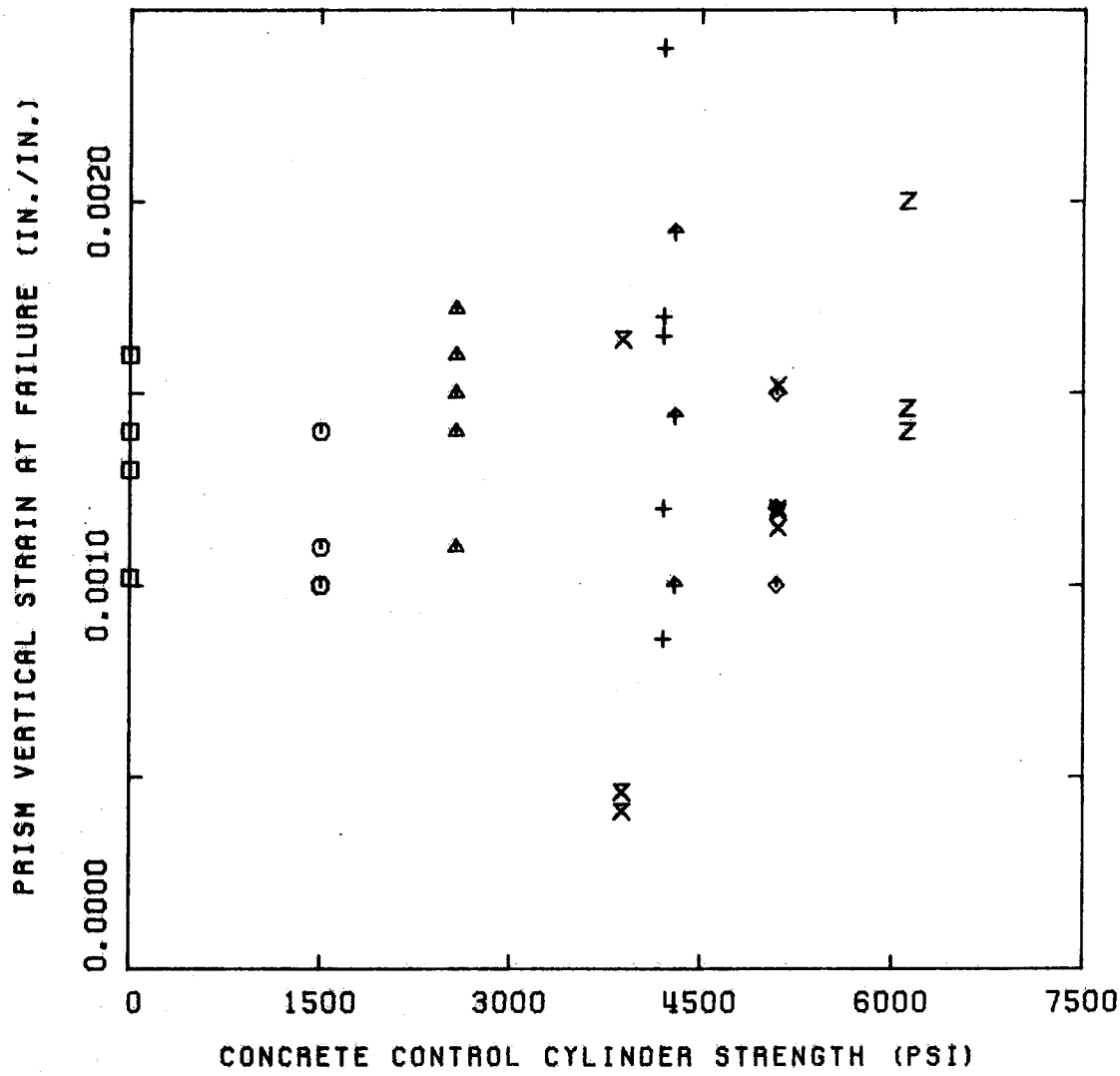

FIG. 4.18: PRISM VERTICAL STRAIN AT FAILURE

Table 4.1 : Strength, Elastic Modulus,Ultimate Strain and Poisson's Ratio of Pilaster Units

Block No.	Failure Load (K)	f'_b (gross) (ksi)	f'_b (net) (ksi)	E_b (psi) (net area)	E_ν (psi) (net area)	Poisson's Ratio ν	Vertical Strain at Failure ε_u	Lateral Strain at Failure ε_{u_ν}
P1	292.8	1210	3080	-	-	-	-	-
P2	291.0	1200	3060	-	-	-	-	-
P3	320.1	1320	3370	-	-	-	-	-
P4	299.7	1240	3150	-	-	-	-	-
P5	294.9	1220	3100	-	-	-	-	-
Average	299.7	1238	3150	-	-	-	-	-
C.V.		4.0%						
P6	380.0	1570	3990	1.63×10^6	8.31×10^6	0.20	0.0027	0.00057
P7	320.4	1320	3370	1.49×10^6	1.08×10^7	0.14	0.0017	0.00042
P8	362.4	1500	3810	1.67×10^6	1.37×10^7	0.16	0.0018	0.00024
P9	367.2	1520	3860	1.51×10^6	1.38×10^7	0.11	0.0019	0.00026
P10	333.5	1380	3500	1.50×10^6	8.25×10^7	0.18	0.0028	0.00068
Average	352.7	1460	3700	1.56×10^6	1.1×10^7	0.16	0.0022	0.00043
C.V.		7.0%		5.4%	22.1%	22.1%	24.1%	44.2%

Table 4.2 : Compressive Strength and Elastic Modulus of 2x2x2 in. Mortar Cubes

No.	Cure	Failure Stress (psi)	E_{mort} (psi)	ν
1	SL	2250	1.17×10^6	0.04
2	SL	2175	3.08×10^6	-
3	SL	1600	0.75×10^6	0.11
4	SL	1830	1.78×10^6	-
5	SL	2150	1.05×10^6	0.11
6	SL	2200	1.06×10^6	-
7	SL	1725	1.07×10^6	0.16
8	SL	1700	1.94×10^6	-
9	SL	1575	-	
10	SL	1775	-	
11	SL	1250	-	
12	SL	1400	-	
13	SL	1800	-	
14	SL	1725	-	
15	SL	1300	-	
16	SL	1375	-	
17	SL	1850	-	
18	SL	2075	-	
19	SL	1750	-	
20	SL	1825	-	
21	SL	1725	-	
22	SL	2175	-	
23	SL	1825	-	
24	SL	1825	-	
25	SL	1850	-	
26	SL	1800	-	
27	SL	2000	-	
28	SL	1750	-	
29	SL	1850	-	
30	SL	1775	-	
31	SL	1550	-	
32	SL	1525	-	
33	SL	1600	-	
34	SL	1775	-	
35	SL	1950	-	
	Avg	1780	1.5×10^6	0.11
	C.V.	13.9%	50%	47%

No.	Cure	Failure Stress (psi)	E_{mort} (psi)	ν
36	L	1975	2.12×10^6	0.23
37	L	1700	3.45×10^6	-
38	L	1530	1.24×10^6	0.10
39	L	1550	1.49×10^6	-
40	L	1625	1.38×10^6	-
41	L	1875	1.12×10^6	-
42	L	1200	1.10×10^6	0.18
43	L	1150	-	
44	L	1700	-	
45	L	1675	-	
46	L	2250	-	
47	L	1700	-	
48	L	1500	-	
49	L	1575	-	
50	L	1600	-	
	Avg	1640	1.7×10^6	0.17
	C.V.	16.5%	50%	39%

SL = Saturated Lime Cured Specimens

L = Laboratory Cured Specimens

Table 4.3: Strengths and Deformational Characteristics of Program Concretes

(a) Series A and B Concretes

No.	f_c' (psi)	ε_u (in./in.)	E_c (psi)	ν
Mix Design 5C				
Moist Cured Cylinders Series A and B				
1	5000	0.00185	3.49×10^6	0.12
2	4950	0.00186	3.45×10^6	0.20
3	5130	0.00197	3.46×10^6	0.14
4	4950	-	-	-
5	5010	-	-	-
6	5540	-	-	-
Average	5100	0.0019	3.5×10^6	0.16
C.V.	4.5%	3.5%	0.6%	29%
σ-ε displays linearity to 0.75 f_c'				
Lab Cured Cylinders Series A and B				
1	4440	0.00222	3.18×10^6	0.14
2	4740	0.00217	3.26×10^6	0.16
3	4460	0.00206	-	-
Average	4550	0.0022	3.2×10^6	0.15
C.V.	3.7%	3.8%	-	-
σ-ε displays linearity to 0.5 f_c'				
Moist Cured Block Moulded Prisms Series A and B				
1	6070	0.00179	3.71×10^6	0.16
2	6160	0.00178	3.93×10^6	0.24
3	6350	0.00185	4.17×10^6	-
4	6250	-	-	-
5	5450	-	-	-
6	6530	-	-	-
7	7190	-	-	-
Average	6290	0.0018	3.95×10^6	0.20
C.V.	8.3%	2.1%	5.8%	29%
σ-ε displays linearity to 0.9 f_c'				
Lab Cured Block Moulded Prisms Series A and B				
1	4720	0.00146	3.18×10^6	0.17
2	5880	0.00219	3.29×10^6	0.16
3	5750	0.00208	3.76×10^6	-
Average	5450	0.0019	3.4×10^6	0.16
C.V.	11.7%	20.6%	9.0%	-
σ-ε displays linearity to 0.6 f_c'				

(a) Continued Series A and B Concretes

Mix Design 4C				
Moist Cured Cylinders Series A and B				
No.	f_c' (psi)	ε_u (in./in.)	E_c (psi)	ν
1	4280	0.00182	3.24×10^6	-
2	4150	-	-	-
3	3840	-	-	-
4	4330	0.00184	3.35×10^6	0.19
5	4270	0.00200	3.36×10^6	0.19
6	4380	0.00186	3.38×10^6	0.14
Average	4210	0.0019	3.3×10^6	0.18
C.V.	4.7%	4.3%	1.9%	16.9%
σ-ε displays linearity to 0.6 f_c'				
Lab Cured Cylinders Series A and B				
1	2760	0.00233	2.28×10^6	0.13
2	2740	0.00215	2.27×10^6	0.17
3	2920	0.00222	2.46×10^6	0.14
Average	2800	0.0022	2.3×10^6	0.15
C.V.	3.6%	4.1%	4.6%	14.5%
σ-ε displays linearity to 0.5 f_c'				
Moist Cured Block Moulded Prisms Series A and B				
1	5960	-	-	-
2	6890	0.00185	4.06×10^6	0.22
3	6700	0.00201	3.75×10^6	0.08
4	6530	0.00221	4.22×10^6	-
5	5540	-	-	-
6	6020	-	-	-
7	6780	-	-	-
8	6970	-	-	-
Average	6420	0.0020	4.0×10^6	0.15
C.V.	8.1%	8.9%	6.0%	-
σ-ε displays linearity to 0.8 f_c'				
Lab Cured Block Moulded Prisms Series A and B				
1	4820	0.00204	2.6×10^6	0.15
2	4900	0.00228	2.73×10^6	0.18
3	4930	0.00172	2.63×10^6	-
Average	4880	0.0020	2.7×10^6	0.17
C.V.	1.2%	14.0%	2.6%	-
σ-ε displays linearity to 0.6 f_c'				

(a) Continued Series A and B Concrete

Mix Design 3C				
Moist Cured Cylinders Series A and B				
No.	f_c' (psi)	ε_u (in./in.)	E_c (psi)	ν
1	2580	0.00217	2.63×10^6	0.16
2	-	-	-	-
3	2490	-	-	-
4	-	-	-	-
5	2490	-	2.85×10^6	-
6	2670	0.00203	2.68×10^6	0.12
7	2690	0.00204	2.70×10^6	0.13
8	2670	-	2.52×10^6	-
9	2410	-	2.63×10^6	-
Average	2570	0.0021	2.7×10^6	0.13
C.V.	4.3%	3.7%	4.1%	14.5%
σ-ε displays linearity to 0.65 f_c'				
Moist Cured Block Moulded Prisms Series A and B				
1	4290	0.00184	3.36×10^6	0.15
2	3940	-	-	-
3	3220	-	-	-
4	3260	-	-	-
5	3720	0.00170	2.88×10^6	0.07
6	4780	0.00275	4.20×10^6	-
7	3810	-	-	-
8	3470	-	-	-
9	3990	-	-	-
Average	3830	0.0021	3.5×10^6	0.11
C.V.	3.1%	27%	19.2%	-
σ-ε displays linearity to 0.65 f_c'				
Lab Cured Block Moulded Prisms Series A and B				
1	4420	0.00227	3.19×10^6	-
2	3410	-	-	-
3	2680	-	-	-
4	3040	-	-	-
5	2990	0.00206	2.83×10^6	0.14
6	3870	0.00215	2.81×10^6	0.13
7	3090	-	-	-
8	2960	-	-	-
9	3110	-	-	-
Average	3290	0.0022	2.9×10^6	0.14
C.V.	16.4%	4.9%	7.3%	-
σ-ε displays linearity to 0.55 f_c'				

(a) Continued Series A and B Concretes

Mix Design 2C				
Moist Cured Cylinders Series A and B				
No.	f_c' (psi)	ε_u (in./in.)	E_c (psi)	ν
1	1560	0.00170	2.05×10^6	0.15
2	1520	0.00217	-	-
3	1400	-	1.91×10^6	-
4	1610	-	-	-
5	1400	0.00200	-	-
Average	1500	0.0020	2.0×10^6	0.15
C.V.	6.3%	12%	5.0%	-
σ-ε displays linearity to 0.5 f_c'				
Lab Cured Cylinders Series A and B				
1	1290	-	-	-
2	1380	0.00250	1.27×10^6	0.08
3	1430	0.00344	1.22×10^6	-
4	1200	0.00181	1.50×10^6	0.18
Average	1330	0.0026	1.3×10^6	0.13
C.V.	7.6%	31%	11.2%	-
σ-ε displays linearity to 0.5 f_c'				
Moist Cured Block Moulded Prisms Series A and B				
1	2390	0.00225	2.04×10^6	-
2	2380	-	-	-
3	2500	-	-	-
4	2500	-	-	-
5	2210	0.00194	2.52×10^6	0.13
Average	2400	0.0021	2.3×10^6	0.13
C.V.	5.0%	-	-	-
σ-ε displays linearity to 0.65 f_c'				
Lab Cured Block Moulded Specimens Series A and B				
1	2180	0.00215	2.00×10^6	0.14
2	2210	0.00178	2.55×10^6	-
3	2310	-	-	-
4	2270	-	-	-
5	2090	0.00232	2.55×10^6	0.16
Average	2210	0.0021	2.4×10^6	0.15
C.V.	3.8%	13.1%	13.4%	-
σ-ε displays linearity to 0.5 f_c'				

(b) Series E Concretes

Mix Design 5C			
Moist Cured Cylinders Series E			
No.	f_c' (psi)	ε_u (in./in.)	E_c (psi)
1	5410	0.00239	2.84×10^6
2	5230	0.00211	3.70×10^6
3	5230	0.00209	3.74×10^6
4	4650	0.00200	3.81×10^6
5	4920	0.00254	2.63×10^6
Average	5090	0.0022	3.3×10^6
C.V.	5.9%	10.2%	16.8%
σ-ε displays linearity to 0.75 f_c'			

Mix Design 3C			
Moist Cured Cylinders Series E			
1	3040	0.00194	2.63×10^6
2	2920	0.00192	2.70×10^6
3	3570	0.00268	2.59×10^6
4	2970	-	-
5	3480	0.00219	2.72×10^6
Average	3200	0.0022	2.7×10^6
C.V.	9.5%	16.2%	2.3%
σ-ε displays linearity to 0.45 f_c'			

(c) Series C Concrete

Mix Design 3G			
Moist Cured Cylinders Series C			
1	4210	0.00231	3.0×10^6
2	4510	-	-
3	4000	0.00228	3.16×10^6
4	3980	-	-
5	4420	0.00243	3.12×10^6
6	4370	-	-
7	4100	0.00217	3.10×10^6
8	4350	-	-
9	4530	0.00233	3.22×10^6
10	4630	-	-
11	4050	-	-
Average	4290	0.0023	3.1×10^6
C.V.	5.4%	4.1%	2.6%
σ-ε displays linearity to 0.45 f_c'			

(d) Series D and F Concretes

Mix Design 5C Moist Cured Cylinders Series D and F			
No.	f_c' (psi)	ε_u (in/in)	E_c (psi)
1	5800	0.00211	3.80×10^6
2	6380	0.00238	3.70×10^6
3	6330	0.00228	3.56×10^6
4	6230	0.00219	3.80×10^6
5	5800	0.00231	3.56×10^6
Average	6110	0.0023	3.7×10^6
C.V.	4.7%	4.7%	3.3%
σ-ε displays linearity to 0.55 f_c'			

Mix Design 3C Moist Cured Cylinders Series D and F			
1	3710	0.00233	2.86×10^6
2	3640	-	-
3	3960	0.00233	2.92×10^6
4	4460	0.00237	3.0×10^6
5	4210	-	-
6	4030	0.00247	2.79×10^6
7	3880	0.00244	2.74×10^6
8	4030	0.00233	2.81×10^6
9	3820	-	-
10	3590	-	-
11	3610	-	-
12	3660	-	-
Average	3880	0.0024	2.9×10^6
C.V.	6.9%	2.6%	3.3%
σ-c displays linearity to 0.45 f_c'			

Table 4.4: Test Results for Axially Loaded Prisms and Cores

Prism	Concrete Core f_c' (psi)	Prism Area (in^2)	Failure Load Pu_m(K)	Failure Stress f'_m (psi)	Masonry Elastic Modulus E_m(psi)	Block Elastic Modulus E_b(psi)	Lateral Elastic Modulus E_ν(psi)	Poisson's Ratio ν	f_{linear} for σ-ε (psi)	$\frac{f_{linear}}{f'_m}$	P_{crack} (K)	$\frac{P_{crack}}{Pu_m}$	Vertical Masonry Failure Strain ε'_m	Vertical Block Failure Strain ε'_b	Lateral Block Failure Strain ε'_{bl}	-P (K)	$\frac{-P}{Pu_m}$	Failure Mode
AP0.1	0	95.2	204.8	2150	$1.57x10^6$	$2.16x10^6$	$1.22x10^7$	0.13	950	0.44	204	1.0	0.0016	0.0010	0.00018	-	-	-
.2	"	"	182.1	1910	$1.66x10^6$	$2.16x10^6$	$1.23x10^7$	0.13	840	0.44	182	1.0	0.0013	0.0009	0.00017	-	-	-
.3	"	"	206.9	2170	$1.64x10^6$	-	-	-	740	0.34	130	0.63	0.0014	-	-	-	-	-
.4	"	"	176.6	1860	$1.87x10^6$	$2.69x10^6$	$3.17x10^7$	0.09	950	0.51	176	1.0	0.0010	0.0007	0.00009	-	-	-
.5	"	"	220.9	2320	$1.57x10^6$	-	-	-	840	0.36	220	1.0	0.0016	-		-	-	-
Average	-	-	198.3	2080	$1.66x10^6$	$2.34x10^6$	$1.87x10^7$	0.12	860	0.42	182.9	0.93	0.0014	0.0009	0.00015	-	-	-
C.V.	-	-	9.3%	9.3%	7.4%	13.1%	60%	19.8%	10.3%	16.4%	18.9%	17.9%	18.0%	16.3%	33.6%	-	-	-
AP2.1	1500	242.1	340.0	1400	$1.06x10^6$	-	-	-	860	0.62	265	0.78	0.0014	-	-	-	-	A
.2	"	"	289.0	1190	$1.32x10^6$	$2.22x10^6$	$2.67x10^6$	NC	870	0.73	275	0.96	0.0011	-	0.00006	-	-	B
.3	"	"	343.0	1420	$1.27x10^6$	$1.60x10^6$	$3.48x10^7$	NC	1070	0.75	275	0.80	0.0010	-	0.00023	120	0.35	A
.4	"	"	310.0	1280	$1.18x10^6$	-	-	-	1180	0.92	310	1.0	0.0010	-	-	-	-	A
.5	"	"	285.0	1180	$1.28x10^6$	$1.96x10^6$	$1.02x10^7$	0.19	990	0.84	275	0.96	0.0010	-	0.00008	-	-	A
Average	-	-	313.4	1290	$1.22x10^6$	$1.93x10^6$	$1.59x10^7$	0.19	990	0.77	280	0.90	0.0011	-	0.00012	120	0.35	-
C.V.	-	-	8.7%	8.7%	8.5%	16.1%	106%	-	13.7%	14.8%	6.2%	11.3%	15.7%	-	75%	-	-	-
AP3.1	2570	242.1	438.8	1820	$1.33x10^6$	-	-	-	1490	0.82	370	0.84	0.0011	-	-	-		A
.2	"	"	358.0	1490	$1.11x10^6$	-	-	-	1340	0.90	340	0.96	0.0016	-	-	-		B
.3	"	"	434.6	1800	$1.47x10^6$	$2.23x10^6$	$6.2x10^6$	0.24	1170	0.65	400	0.92	0.0014	0.0013	0.00010	100	0.25	A
.4	"	"	410.0	1700	$1.64x10^6$	$2.17x10^6$	$4.75x10^6$	0.35	1500	0.88	410	1.0	0.0017	0.0008	0.00038	100	0.25	A
.5	"	"	446.0	1840	$1.37x10^6$	$2.35x10^6$	$3.19x10^6$	0.74	1360	0.74	430	0.96	0.0015	0.0016	0.00048	280	0.63	A
Average	-	-	417.5	1730	$1.38x10^6$	$2.25x10^6$	$4.71x10^6$	0.44	1370	0.80	390	0.94	0.0015	0.0012	0.00032	160	0.38	
C.V.	-	-	8.6%	8.6%	14.0%	4.1%	31.9%	60%	9.8%	13.0%	9.1%	6.5%	15.8%	32.8%	61.6%	-	-	
AP4.1	4210	242.1	635.0	2620	$1.81x10^6$	$1.83x10^6$	$2.47x10^7$	0.07	1440	0.55	625	0.98	0.0017	0.0026	0.00028	450	0.71	A
.2	"	"	665.2	2740	$1.76x10^6$	-	-	-	1230	0.45	585	0.88	0.0017	-	-	-	-	A
.3	"	"	579.0	2390	$1.40x10^6$	$1.65x10^6$	$2.52x10^7$	0.06	1020	0.43	525	0.91	0.0009	0.0010	0.00037	300	0.66	A
.4	"	"	630.0	2600	$1.90x10^6$	-	-	-	1760	0.68	450	0.71	0.0012	-	-	-	-	A
.5	"	"	458.0	1890	$1.56x10^6$	$2.04x10^6$	$1.37x10^7$	0.11	830	0.44	400	0.88	0.0024	0.0013	0.00061	-	-	A
Average	-	-	593.4	2450	$1.69x10^6$	$1.84x10^6$	$2.12x10^7$	0.08	1260	0.51	520	0.87	0.0016	0.0016	0.00042	375	0.69	
C.V.	-	-	13.8%	13.7%	12.0%	10.6%	30.7%	33.1%	28.9%	20.9%	18.0%	11.4%	36.2%	52.1%	40.6%	-	-	

Table 4.4 Continued

Prism	Concrete Core f_c' (psi)	Prism Area (in^2)	Failure Load Pu_m (K)	Failure Stress f'_m (psi)	Masonry Elastic Modulus E_m (psi)	Block Elastic Modulus E_b (psi)	Lateral Elastic Modulus E_ν (psi)	Poisson's Ratio ν	f_{linear} for σ-ε (psi)	$\frac{f_{linear}}{f'_m}$	P_{crack} (K)	$\frac{P_{crack}}{Pu_m}$	Vertical Masonry Failure Strain ε_m'	Vertical Block Failure Strain ε_b'	Lateral Block Failure Strain ε_{bl}'	-P (K)	$\frac{-P}{Pu_m}$	Failure Mode
AP5.1	5100	242.1	700.0	2890	1.97×10^6	2.55×10^6	2.02×10^7	0.10	840	0.29	500	0.72	0.0012	-	-	-	-	A
.2	"	"	693.0	2860	2.06×10^6	-	-	-	620	0.22	350	0.51	0.0012	-	-	-	-	A
.3	"	"	668.0	2760	2.0×10^6	2.14×10^6	2.76×10^7	0.07	830	0.30	450	0.67	0.0012	0.0019	0.00072	300	0.45	A
.4	"	"	730.0	3020	2.07×10^6	2.19×10^6	4.0×10^7	0.05	1470	0.49	550	0.75	-	-	-	300	0.41	A
.5	"	"	687.0	2840	2.01×10^6	-	-	-	1440	0.51	675	0.98	0.0015	-	-	-	-	A
Average	-	-	695.6	2880	2.02×10^6	2.29×10^6	2.93×10^7	0.07	1040	0.36	505	0.73	0.0013	0.0019	0.00072	300	0.43	-
C.V.	-	-	3.3%	3.3%	2.1%	9.8%	34%	34%	37.4%	36%	23.8%	23.3%	11.8%	-	-	-	-	-
EP5.1	5090	242.1	736.0	3040	2.14×10^6	2.73×10^6	4.69×10^7	0.05	1850	0.61	650	0.88	0.0015	0.0019	0.00028	400	0.55	A
.2	"	"	561.0	2320	1.74×10^6	1.76×10^6	-	N.C.	840	0.36	340	0.61	0.0012	0.0011	0.00054	-	-	B
.3	"	"	572.0	2360	1.43×10^6	2.45×10^6	9.34×10^7	0.02	830	0.35	300	0.52	0.0010	0.0020	0.00029	-	-	B
.4	"	"	624.1	2580	1.63×10^6	-	-	-	670	0.26	250	0.40	-	-	-	-	-	B
.5	"	"	597.4	2470	1.58×10^6	-	-	-	1040	0.42	400	0.67	-	-	-	-	-	B
Average	-	-	618.1	2550	1.70×10^6	2.31×10^6	7.0×10^7	0.04	1050	0.40	390	0.62	0.0012	0.0017	0.00037	400	0.55	-
C.V.	-	-	11.4%	11.4%	15.8%	21.6%	-	-	44.8%	32.6%	40.3%	29.1%	20.4%	29.6%	39.8%	-	-	-
CP3.1Core	4290	146.9	400.0	2720	2.02×10^6	-	1.38×10^7	0.15	1360	0.50	300	0.75	0.0015	-	0.00016	-	-	-
.2Core	"	"	518.0	3520	2.02×10^6	-	1.22×10^7	0.16	1090	0.31	500	0.97	0.0015	-	0.00016	-	-	-
Average	-	-	460.0	3120	2.02×10^6	-	1.30×10^7	0.16	1230	0.41	400	0.86	0.0015	-	0.0016	-	-	-
C.V.	-	-	-	-	-	-	-	-	-	-	-	-	-	-	-	-	-	-
CP3.3	4290	242.1	560.1	2310	1.99×10^6	2.34×10^6	7.72×10^6	0.26	830	0.36	350	0.63	0.0010	-	0.00012	-	-	B
.4	"	"	649.7	2680	1.78×10^6	N.C.	N.C.	-	1050	0.39	425	0.65	0.0014	0.0018	0.00030	-	-	A
.5	"	"	679.4	2810	1.93×10^6	2.80×10^6	1.29×10^6	0.15	1320	0.47	680	1.0	0.0019	-	-	-	-	A
Average	-	-	629.7	2600	1.90×10^6	2.57×10^6	4.51×10^6	0.21	1070	0.41	485	0.76	0.0014	0.0018	0.00021	-	-	-
C.V.	-	-	9.9%	9.9%	5.7%	-	-	-	23%	14.0%	35.7%	27.4%	31.5%	-	-	-	-	-
DP3.1Core	3880	146.9	410.0	2790	1.15×10^6	-	6.74×10^6	0.17	1700	0.61	325	0.79	0.0019	-	-	-	-	-
.2Core	"	"	436.0	2970	1.49×10^6	-	8.70×10^6	0.17	1420	0.48	425	0.97	0.0015	-	0.00013	-	-	-
.3Core	"	"	341.0	2320	1.51×10^6	-	7.69×10^6	0.20	1280	0.55	341	1.0	0.0011	-	-	-	-	-
Average	-	-	395.7	2690	1.38×10^6	-	7.71×10^6	0.18	1470	0.55	365	0.92	0.0015	-	0.00013	-	-	-
C.V.	-	-	12.4%	12.4%	14.7%	-	12.7%	9.6%	14.6%	11.9%	14.8%	12.3%	26.7%	-	-	-	-	-

Table 4.4 Continued

Prism	Concrete Core f_c' (psi)	Prism Area (in^2)	Failure Load (P_{um}) (K)	Failure Stress f_m'(psi)	Masonry Elastic Modulus E_m(psi)	Block Elastic Modulus E_b(psi)	Lateral Elastic Modulus E_ν(psi)	Poisson's Ratio ν	f_{linear} for σ-ε (psi)	$\frac{f_{linear}}{f'_m}$	P_{crack} (K)	$\frac{P_{crack}}{Pu_m}$	Vertical Masonry Failure Strain ε'_m	Vertical Block Failure Strain ε'_b	Lateral Block Failure Strain ε'_{bl}	-P (K)	$\frac{-P}{Pu_m}$	Failure Mode
DP3.4	3880	242.1	384.0	1590	$1.07x10^6$	$1.26x10^6$	$2.7x10^7$	0.04	680	0.42	275	0.72	0.0016	0.0010	0.00053	200	0.52	A
.5	"	"	400.5	1650	$1.45x10^6$	$2.05x10^6$	$3.62x10^6$	0.04	1160	0.70	300	0.75	0.0004	.0.0006	-	-	-	A
.6	"	"	400.0	1650	$1.56x10^6$	-	-	-	1320	0.80	370	0.93	0.0005	-	-	-	-	A
Average	-	-	394.8	1630	$1.36x10^6$	$1.66x10^6$	$1.53x10^7$	0.22	1050	0.64	315	0.80	0.0008	0.0008	0.00053	200	0.52	-
C.V.	-	-	24%	2.1%	18.9%	-	-	-	31.6%	30.8%	15.6%	14.2%	80%	-	-	-	-	-
DP5.1Core	6110	146.9	649.0	4420	$1.91x10^6$	-	$1.32x10^7$	0.14	2740	0.62	650	1.0	0.0016	-	-	-	-	-
.2Core	"	"	721.0	4910	$1.90x10^6$	-	$1.48x10^7$	0.13	2410	0.49	721	1.0	0.0017	-	0.00018	-	-	-
.3Core	"	"	761.0	5180	$2.10x10^6$	-	$1.41x10^7$	0.15	3060	0.59	760	1.0	0.0019	-	0.00024	-	-	-
Average	-	-	710.3	4840	$1.97x10^6$	-	$1.40x10^7$	0.14	2740	0.57	710	1.0	0.0017	-	0.00021	-	-	-
C.V.	-	-	8.0%	8.0%	5.7%	-	5.7%	7.1%	11.9%	12.0%	7.9%	0%	8.8%	-	-	-	-	-
DP5.4	6110	242.1	822.0	3400	$2.24x10^6$	$2.71x10^6$	$6.06x10^6$	0.37	2890	0.85	750	0.91	0.0014	-	0	-	-	A
.5	"	"	875.0	3610	$2.24x10^6$	$1.99x10^6$	$2.63x10^7$	0.08	1840	0.51	650	0.75	0.0015	-	0.00044	-	-	A
.6	"	"	792.0	3270	$1.75x10^6$	-	-	-	2150	0.66	590	0.75	0.0020	-	0	-	-	A
Average	-	-	830.0	3430	$2.08x10^6$	$2.35x10^6$	$1.62x10^7$	0.23	2295	0.67	665	0.80	0.0016	-	0.00044	-	-	-
C.V.	-	-	5.1%	5.1%	13.6%	-	-	-	23.5%	25.3%	12.2%	11.5%	19.7%	-	-	-	-	-

N.C. = Not Calculable - Erratic Results

C.V. = Coefficient of Variation

Table 4.5: Observed and Predicted Grouted Prism Elastic Moduli

Prism Series	Observed E_m (psi)	Predicted E_m (Eq. 4.7) (psi)	Predicted E_m (Eq. 4.8) (psi)
AP2P-	1.22×10^6	1.81×10^6	1.30×10^6
AP3P-	1.38×10^6	2.29×10^6	1.57×10^6
AP4P-	1.69×10^6	2.67×10^6	1.78×10^6
AP5P-	2.02×10^6	2.83×10^6	1.87×10^6
EP5P-	1.70×10^6	2.68×10^6	1.78×10^6
CP3P-	1.90×10^6	2.54×10^6	1.71×10^6
DP3P-	1.36×10^6	2.38×10^6	1.62×10^6
DP5P-	2.08×10^6	2.88×10^6	1.90×10^6

PLATE 4.1
Typical Ungrouted Prism Failure

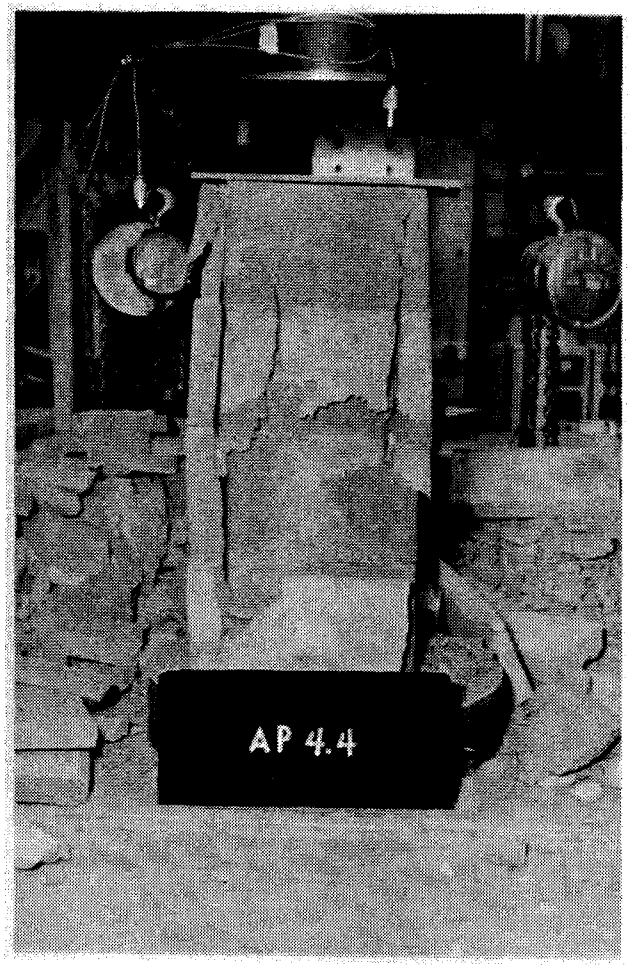

PLATE 4.2
Type A Prism Failure

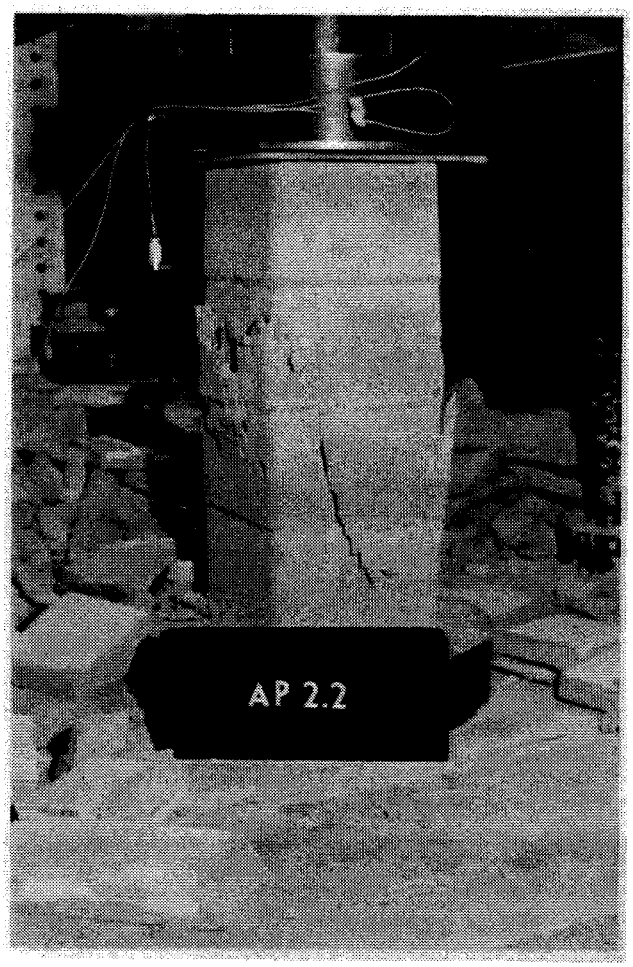

PLATE 4.3
Type B Prism Failure

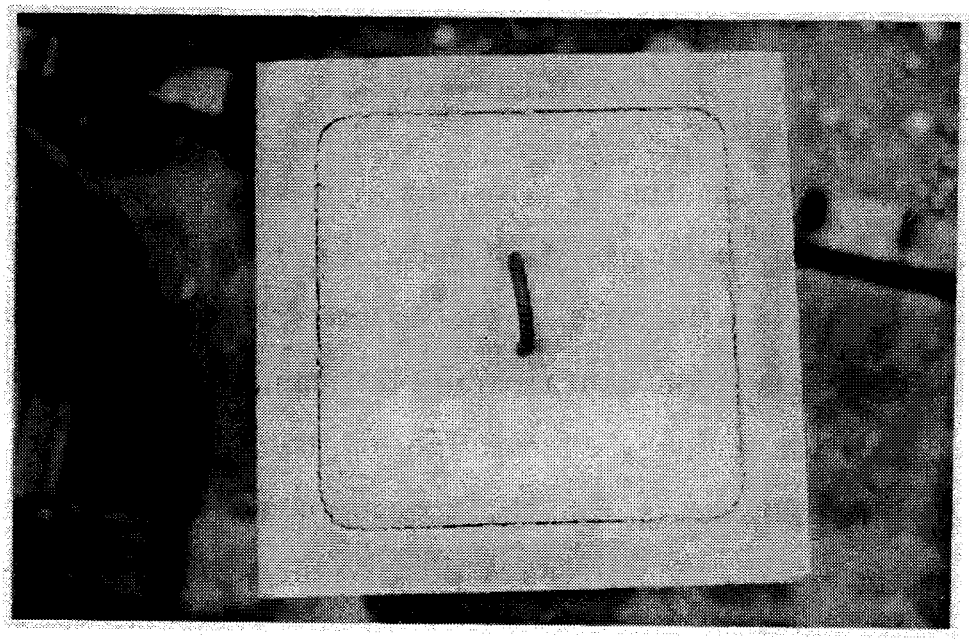

PLATE 4.4
Shrinkage Cracking in Prisms
Containing High Slump Grout

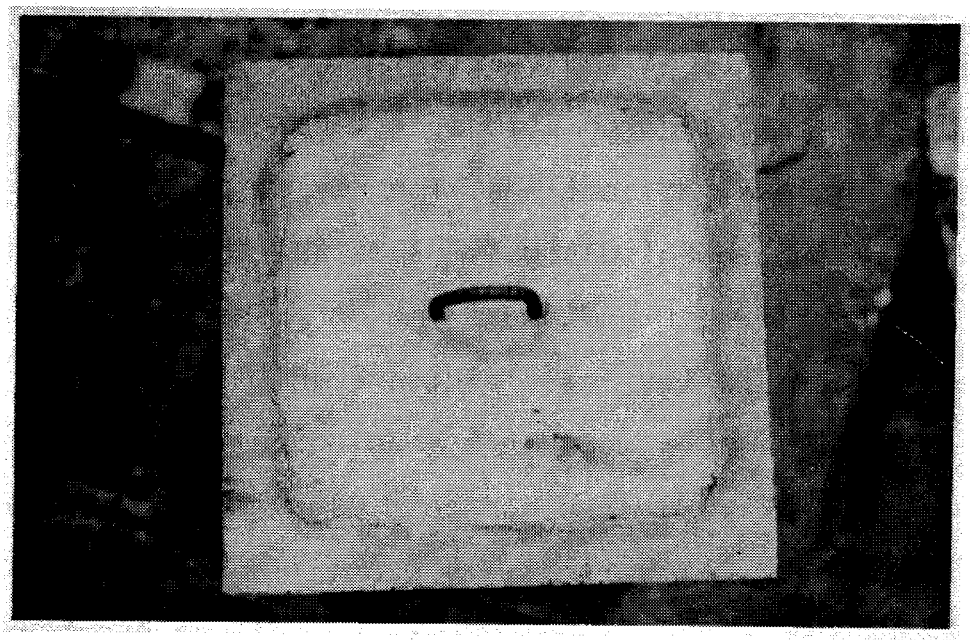

PLATE 4.5
Shrinkage Cracking in Prisms
Containing Low Slump Concrete

5. COLUMN TEST RESULTS AND DISCUSSION

5.1 Introduction

Details of the column investigation reported herein have already been given in Sections 3.2.1 and 3.3.1. The discussion of the fifty-nine columns tested is presented in two sections, one containing test results for the forty-three axially loaded specimens, and the other containing results for the specimens subjected to eccentric loading. Table 5.1 gives a description of the concentrically loaded columns, their failure loads, cracking loads, elastic moduli, strains at failure, failure modes, and data used to construct all graphs presented in this chapter. Similar data are reported in Table 5.2 for the eccentrically loaded columns. Appendix A contains typical column load-strain curves for lateral and vertical block deformations, masonry and steel axial deformations, lateral tie strains, and column lateral deflections. The review of the test results and the subsequent discussions establish the effect of concrete strength and slump, masonry shell strength, grade and percent of vertical reinforcement, lateral tie details, and the effect of eccentric loading on the strength and behavior of reinforced concrete block masonry columns. The effects of these factors are quantified using theoretical and rational empirical analyses. An effort has been made to avoid generalizations, to present data fully, and report only the important relations indicated by these tests.

5.2 Concentrically Loaded Columns

5.2.1 Failure Mode--General Remarks

The concentrically loaded columns were observed to fail in one of the following three modes:

1. Type A; overall vertical splitting and crushing of the block shell and the concrete core,
2. Type B; simultaneous splitting of the masonry shell, crushing of the concrete core, and buckling of the vertical reinforcement between tie spacing,
3. Type C; same as B, but with lateral tie hook pulling, and buckling of the vertical reinforcement over two or more courses.

Type A failure was characteristic of all plain or grouted columns containing no vertical reinforcement. This included those columns with lateral reinforcement only. Plain column failures were similar to those of their companion prisms. The two plain columns tested displayed sudden, complete, and explosive failures. "Warning" cracks were noted only just prior to column collapse. Vertical cracking was initiated at the block face centers at the top of the specimen and propagated down several courses just prior to failure. Plate 5.1 illustrates typical block center face cracking in the failed specimen.

The failure of grouted columns containing no lateral reinforcement was similar to failure Type A described earlier for their companion prisms. In this mode, vertical splitting of the shell originated at block face centers in the upper courses well in advance of column collapse. Subsequent loading elongated and widened these cracks until overall splitting of the shell and crushing of the concrete

core occurred. The columns shown in Plates 5.2, 5.3, and 5.4 are exemplary of this failure type. Removal of the shell from the failure zone revealed that the failure plane of the column core was conical, and formed an angle of about 30 deg. with the axis of the column as illustrated in Plate 5.5. A fewer number of these grouted columns failed by simultaneous overall vertical splitting of the masonry shell and concrete core. This is shown in Plate 5.6(a) and 5.6(b). In general, columns containing high strength concrete cores failed explosively, and those with low strength concretes settled gradually under the load.

Grouted columns containing lateral reinforcement in the mortar joints displayed a slightly different behavior. Vertical cracking prior to failure was originated in the upper courses at the column corners rather than at block centers. This is clearly shown in Plate 5.7. In addition, the lateral ties tended to confine the block shell and prevent explosive spalling of the shell at failure.

In general, for all grouted, unreinforced columns tested, the shell-core interface bonding in the failure zone had been completely broken, and the masonry shell could be easily removed in order to view the concrete core. Distress to the shell was observed throughout most of the column height whereas cracking and crushing of the core was confined primarily to the immediate conical failure zone as shown in Plate 5.5.

Failure Type B for reinforced columns constructed with

lateral ties having 90 deg. hooks and 2-1/2 in. extensions was peculiar only to those columns with 0.76% vertical reinforcement. These column failures were characterized by simultaneous splitting of the shell, crushing of the core, and buckling of the vertical reinforcement between tie spacing. The columns shown in Plates 5.8, 5.9, 5.10, and 5.11 are illustrative of this failure type. Note that in these failures, the tie hooks did not pull. They provided adequate support for the vertical reinforcement, and prevented buckling from occurring over more than one course.

In contrast to this behavior, Plates 5.12 to 5.20 clearly indicate that these ties did not adequately restrain buckling for the higher percentages of vertical reinforcement and thus Type C failure was precipitated. In some cases, the tie hooks were pulled to form an included angle of about 120 deg., as shown in Plate 5.13, and in extreme cases, such as those illustrated in Plates 5.15, 5.16, and 5.20, a number of tie hooks pulled, allowing bars to buckle over as many as five courses. This resulted in rather explosive failures for these columns regardless of concrete core strengths, since extensive buckling of the vertical bars popped off large sections of the masonry shell.

Series F columns were constructed with lateral ties using 135 deg. hooks and 4 in. extensions. All columns of Series F displayed Type B failures. Plates 5.21, 5.22, and 5.23 show that these ties did not pull even for the higher

percentages of longitudinal reinforcement, and restricted buckling to the lateral tie spacing. Because of this confinement, failure was not as sudden and distress to the core and shell was not as extensive in the failure zones as for those columns with Type C failure.

It is of interest to note that even for those columns exhibiting Type B failure, the lateral ties, although they did not pull, showed extensive outward bowing upon post-failure investigation. This behavior suggests that column ties are subjected to both axial and flexural stresses.

In the case of all reinforced columns, cracking originated at the column corners in the upper courses in advance of column failure and extended down vertically as loading continued. That the cracking of vertically reinforced masonry columns originated in the column corners adjacent to the longitudinal reinforcement is not surprising. As load increases, the vertical reinforcement expands laterally more than the surrounding concrete due to the differences in stiffness and in Poisson's ratio between the steel and masonry, thus creating localized lateral tensile stresses in the masonry shell. These stresses are relieved when shell cracking occurs.

The columns of Series A grouted with the 5100 psi, 4 in. slump concrete of mix 5C, in comparison with all other column series and mixes, showed a far superior bond between the concrete core and masonry shell. The distress to the

column core and shell for these columns was essentially confined to the immediate failure zone where the ties pulled and the vertical bars buckled. The bond between core and block adjacent to a failure zone is shown in Plate 5.13. In addition, the spalling failure plane for these columns often occurred within the blocks themselves, and was thus not necessarily a result of bond failure between the core and shell. These observations, as do those of the companion prisms, indicate that increased bond strength is not necessarily associated with increased concrete strength.

Furthermore, it was observed that 4-inch slump concretes can be satisfactorily placed in pilaster units of these dimensions when sufficient vibration is provided. Examination of the Series B stripped shell columns and examination of columns following failure revealed excellent concrete penetration between the vertical reinforcement and the block shell. The 9-inch slump grout used in Series C columns showed no superiority in workability over the grouts used in the other series.

An observation made early in the test program is worth noting. Failure generally occurred within the upper half of the column. In order to establish whether or not this was the result of end conditions, six columns were selected at random and tested in an inverted position. Five of these six columns failed in their lower half. It was thus concluded that the failure zone was located in the column upper region because of weaker concrete in the upper core, caused by

bleeding and segregation during pouring and vibration.

In view of the observations reported herein, the following tie details are suggested for masonry columns:

1. For concrete block masonry columns constructed with 16 x 16 x 8 in. pilaster units, the use of 1/4 in. diameter plain steel for fabrication of lateral ties should be avoided when possible. These ties do not adequately contain core expansion. They do not adequately support the longitudinal reinforcement and thus permit large lateral deformations which lead to extensive shell splitting and explosive failures. ACI Standard 318-77 for reinforced concrete columns states that longitudinal bars #10 or smaller must be enclosed by deformed lateral ties at least #3 in size. It is recommended that this requirement be adopted by the masonry code for columns constructed of pilaster units similar to those used in this study until further tests are conducted.

2. If it is necessary to use 1/4 in. diameter plain bars, it is recommended that 135 deg. bends plus a minimum of 4 in. extensions be employed. Alternatively, if 90 deg. bends plus 2-1/2 in. extensions are used, the overlapping extensions should be tack welded to prevent pulling. In addition, it is suggested that in order to reduce distress to the column shell, mortar joint lateral reinforcement should be provided to assist those ties in contact with the vertical reinforcement in confining lateral expansion of the core and maintaining concrete core and shell integrity.

3. As will be shown later, those columns which failed by mode B in Series F reached only slightly higher axial strains than those exhibiting Type C failure. Only one of the columns tested reached yield point stress in the vertical reinforcement. This would suggest that vertical tie spacing of 8 in., although acceptable to both the Canadian concrete and masonry codes, is not sufficient to prevent buckling of the vertical reinforcement before yield is attained, and it is recommended that this spacing be decreased for masonry columns constructed with units which permit a reduced spacing. (Columns constructed with 8 x 8 x 16 in. plain corner blocks do not permit a decreased spacing).

4. Since the positioning of lateral tie hooks along one vertical reinforcement bar creates a line of structural weakness in the column, it is suggested that tie hooks should subtend a different corner bar, on a rotational basis, with each successive tie.

5.2.2 Column Ultimate Strength

5.2.2.1 General

In order to rationally predict the ultimate strength of a concrete block masonry column, an attempt must be made to account for the portion of the strength of a column contributed by each of its elements. A well-established method of expressing the strength of a masonry column may be adopted from reinforced concrete design. The strength of a concentrically loaded, tied reinforced concrete column is considered to be made up of two elements; (1) the ultimate strength of the net concrete core area, expressed in terms of standard control cylinder strength and, (2) the load required to stress the compressive reinforcement to its yield point. However, tied reinforced concrete block masonry columns are somewhat different in that the load contribution of the block shell must also be considered. Moreover, the strength contribution of the core area as a function of control cylinder strength has not been established for concrete block masonry columns, nor has it been shown that vertical reinforcement in these columns reaches yield stress at failure. It is well known that the strength of the concrete in a column with a height/thickness ratio of five is less than that in a 6 in. by 12 in. standard control cylinder. The results of tests conducted on concrete columns at Lehigh University and the University of Illinois in the 1930's, showed the strength of plain columns to be 75 to 85 percent of that of companion cylinders. Current Canadian and

American concrete codes have adopted a ratio of 0.85. However, concrete column tests should not necessarily be considered representative of concrete block column cores since curing conditions within masonry columns are different than those of reinforced concrete columns. A further difficulty in predicting block column ultimate strength lies in the knowledge that the load contribution of the block shell of a grouted masonry column is somewhat lower than the failure load of an identical plain masonry shell. As was shown in the prism investigation, the load contribution of the shell in terms of ungrouted masonry is a complex relationship dependent upon block strength, grout strength, block net area, block gross area, and the ratio of block net area/gross area. In addition, experimental results of masonry wall tests suggest that shell strengths are also affected by the percent of vertical reinforcement, and the distribution of this vertical reinforcement.[39] Accurate prediction of a masonry column ultimate load is clearly a more complex task than that for a reinforced concrete column because of the addition and the uncertain behavior of the block shell.

Figure 5.1 shows the values of column failure loads as a function of concrete control cylinder strength for all concentrically loaded columns tested in the program. These values are plotted without regard to percentage of vertical reinforcement, and consequently these data are somewhat scattered. The point to be made is the superior performance

of Series A columns in comparison with identical Series D columns, and in comparison with Series F columns which were constructed with higher strength concrete and improved lateral ties. Strength differences between these series are even more striking when loads carried by vertical reinforcement, calculated from measured strains at failure, are subtracted from column ultimate loads to compute the loads carried by the shell and core alone. Loads carried by the column shell and core at failure are plotted as a function of control cylinder strength in Fig. 5.2. These strength differences can only be attributed to variations in materials used for Series A columns, and those for columns of Series C, D, and F. In particular, these differences must be attributed to cement variations since blocks, vertical and lateral reinforcing steel, aggregates, mortar mixes, and controlled curing conditions were similar for all columns. Although the concretes of Series C, D, and F achieved higher control cylinder strengths than did their companion concretes of Series A using the same mix and cement type, their performance in the masonry columns was somewhat inferior. This suggests not only that cement types produced by different manufacturers can severely affect the strength and performance of concrete with identical mixes, but more importantly, that the concrete strengths obtained from control cylinder tests are not necessarily representative of how this concrete will perform in the actual structure. Thus, the whole concept of applying one factor, 0.85, as the

ratio of column strength/standard cylinder strength is somewhat shaded. The value of 0.7 assigned to the undercapacity factor for tied reinforced concrete columns by the Canadian and American concrete codes is clearly warranted. It is interesting to note that no noticeable effects on prism strengths existed for the companion prism series constructed with concretes of the same mix, and using identical cements.

In view of these results, direct comparisons of Series C columns to Series A columns in order to determine the effects of concrete slump, and direct comparisons of Series F columns to Series A columns to establish tie detailing effects, are not rational. The effects of these variables may be estimated, however, through comparisons between Series C, D, and F columns.

5.2.2.2 Strength of Plain Columns

The ultimate strengths of the Series A grouted columns fabricated with no lateral reinforcement are plotted as a function of their control cylinder strengths in Fig. 5.3. It is evident that column strength increases are in direct order with increasing concrete strength, and an approximately linear function relates the two. Using linear regression analysis, the ultimate strength of these plain masonry columns may be approximated by:

$$Pu_c = 0.125f'_c + 153 \quad \text{(Kips)} \quad \ldots\ldots\ldots \quad 5.1$$

$$r = 0.98$$

This equation may be expressed in terms of core and shell areas:

$$Pu_c = \frac{125A_c f'_c}{146.9} + \frac{153}{95.2} A_{shell} \quad \text{(Kips)}$$

$$Pu_c = 0.85f'_c A_c + 1.60A_{shell} \quad \text{(Kips)} \quad \ldots\ldots \quad 5.2$$

The first term of Eq. 5.2 establishes the contribution of the concrete core to the ultimate strength of the masonry column in terms of net core area and its concrete control cylinder strength. These test results are in remarkable agreement with the accepted empirical relationship which is universally applied to plain and reinforced concrete columns. The y intercept of Eq. 5.2 is theoretically equal to zero for a plain concrete column since the equation must be representative of column strength when the concrete core is considered to have zero compressive strength. However, with a masonry column, this term defines the load contribution of the block shell to column ultimate strength. It can be shown that the regression intercept value of 153 kips is a reasonable estimate of shell strength if one compares the failure loads for stripped shell Series B columns with companion Series A columns. If the failure loads of the cores, 676 kips, 602 kips, and 301 kips for columns B1, B2, and B3, respectively, are subtracted from their corresponding masonry column strengths of 791 kips,

701 kips, and 454 kips for columns A12, A11, and A10, then the shell contribution is found to be 115 kips, 99 kips, and 153 kips, with an average of 122 kips. The 153 kip value provided by Eq. 5.2 compares favourably with this, and it is also in good agreement with the 138 kip load attributed to prism shell strength derived earlier in the thesis.

The shell strength term of Eq. 5.2 may be converted to a function of experimental net area plain column strength, f'_{mp_c}, as follows:

$$P_{mp_c} = \frac{125 + 163}{2} = 144 \text{ kips}$$

$$f'_{mp_c} = \frac{144}{95.2} = 1.51 \text{ ksi}$$

$$Pu_c = 0.85f'_c A_c + \left[\frac{1.60A_{shell}}{1.51}\right] f'_{mp_c}$$

conservatively;

$$Pu_c = 0.85f'_c A_c + 1.0f'_{mp_c} A_{shell} \quad \ldots\ldots\ldots \quad 5.3(a)$$

Alternatively, Eq. 5.2 may be converted to a function of plain prism strength f'_{mp_n}:

$$Pu_c = 0.85f'_c A_c + 0.7f'_{mp_n} A_{shell} \quad \ldots\ldots\ldots \quad 5.3(b)$$

Comparison of Eq. 5.3(b) with Eq. 4.4(b), which was similarly derived for grouted prisms, shows that grouted prism strengths were, by and large, somewhat lower than grouted column strengths by virtue of both a decreased core and a decreased shell contribution. On the average, grouted prism strengths attained only about 85 percent of their

corresponding column strengths for all concrete strengths employed in the program. Since the prism height/thickness ratio was considerably lower than that for the columns, and since the columns were pin ended, the opposite should be expected. It is definitely known that lateral end restraint of the test specimen by the loading platens serves to increase compressive strength for smaller height/thickness ratios. Furthermore, prism height/thickness was equal to that of the standard concrete control cylinder and thus prism core strengths should display a more direct relation with cylinder strengths than do column core strengths. No suitable explanation for these observations can be presented. Accordingly, tests conducted herein indicate that grouted prisms provide a conservative measure of the compressive strength of grouted columns constructed with similar materials and with no slenderness considerations.

5.2.2.3 Effect of Lateral Joint Reinforcement

Figure 5.4 shows the strengths of grouted columns containing lateral reinforcement plotted with the strengths of grouted columns having no lateral ties. The additional confinement afforded by these ties served to increase the strength of the core and shell by 159 kips (or 21%) for Series A- mix 5C columns, 37 kips (or 8%) for Series A- mix 3C columns, and 100 kips (or 28%) for Series C- mix 3G columns. Feeg[8] reported an average increase of 15.9 percent in ultimate masonry strength for columns containing 0.25

inch diameter lateral ties over columns with no ties. It is therefore evident that an empirical equation used to predict the ultimate strength of grouted columns with no lateral reinforcement, such as Eq. 5.3(b), should provide conservative strength estimates for columns containing lateral ties in the mortar joints.

5.2.2.4 Effect of Steel Grade

Figure 5.5 shows, as ordinates, the total loads carried by the columns of Series A containing 0.76% vertical reinforcement, Grade 40 and Grade 60 steel, and as abscissas, the strengths of their control cylinders. The strengths of the reinforced columns increased linearly with the increase in strength of the control cylinders. The dotted curve represents the grouted, plain column strengths, and falls directly over the regression line for Grade 60 reinforcement. Since the rate of increase in strength of the reinforced columns is nearly equal to that of the plain grouted columns, it would appear that the increase in the strength of the concrete was just as effective in a reinforced column as it was for an unreinforced grouted column. It was shown in the previous section that for a plain grouted column, the core strength was 85 percent of its cylinder strength regardless of the strength of the concrete. Therefore, the increase in strength of the reinforced column would be equal to the net area of its concrete times 85 percent of the increase in strength of its

control cylinder, regardless of the grade of longitudinal reinforcement. Furthermore, the reinforced column strengths are seen to be only slightly higher than those of the grouted plain columns. These observations would imply that although the steel was effective in contributing axial load resistance to the column, it effectively reduced the load contribution of the masonry shell by nearly an identical amount. This observation is more clearly shown in Fig. 5.6 which plots the shell and core strength of these reinforced columns as a function of control cylinder strengths. These strengths were determined by subtracting the load contribution of the reinforcement steel, based on the steel strain measurements recorded during testing, from the ultimate column strength. Shell and core strengths for these columns are all below the regression equation which defines grouted plain column strengths. Linear regression shows that the shell contribution has decreased to only about 75 kips. This represents a shell strength decrease of 153 - 75 = 78 kips. Average load carried by the steel for these eight columns is 76 kips, and thus, the offsetting effect is seen. This behavior seems reasonable since it has been shown in masonry wall investigations that differences in Poisson's ratio and stiffness between the reinforcement steel, and the grout core and the masonry shell can induce lateral tensile stresses in the shell which effectively reduce the compressive strength of the shell at failure. This theory is also in accord with the shell cracking patterns observed

during the compressive tests of the reinforced columns. Figures 5.5 and 5.6 also show that the strengths for those columns fabricated with Grade 40 steel are consistently higher than those with Grade 60 steel. This suggests that the deformational characteristics of the Grade 40 steel are more compatible with the masonry shell and concrete core than are the Grade 60 steels. Unfortunately, the effects of steel grades were not examined in this study for the higher percentages of longitudinal reinforcement. However, it is not unreasonable to assume that a similar behavior would develop.

Series C columns also showed a strength increase for Grade 40 steel. Column C2 failed 96 kips higher than Grade 60 column C3.

These test results indicate that the principle of direct superposition cannot be applied in order to establish the compressive strength of a reinforced column. That is, summation of those loads supported by the core and shell of a plain grouted column, as represented by Eq. 5.3, and the added strength provided by lateral ties, together with the load supported by the vertical reinforcement, over-estimates the load capacity of a reinforced block masonry column.

5.2.2.5 Effect of Percentage of Vertical Reinforcement

In Figs. 5.7(a) and 5.7(b), the maximum loads carried by reinforced columns have been plotted as ordinates and the percentage of vertical reinforcement as abscissas. Columns

with no longitudinal reinforcement in Fig. 5.7(a) are represented by plain grouted columns containing lateral reinforcement. The strengths of plain grouted columns with no lateral reinforcement are indicated by the dashed lines at the figure margin. All column strengths plotted in this figure are those associated with Grade 60 steel. Columns without vertical reinforcement were not constructed for Series D and F, hence, in Fig. 5.7(b), the curves for these series are discontinuous at 0.76%. In addition, the failure loads representing 0.76% vertical reinforcement for Series F columns are for those columns fabricated with Grade 40 steel.

The most striking feature of these curves is the pronounced decrease in column strength associated with 0.76% longitudinal reinforcement. No series shows exception to this behavior. However, if one considers only those reinforced columns containing #25M bars, and thus only 0%, 1.3%, and 2.6% longitudinal reinforcements, it can be seen in Fig. 5.7(a) that the loads associated with these three percentages approximate a straight line, and that the straight lines representing the relation between column strength and the percentage of reinforcement for a given concrete strength are very nearly parallel. It may thus be assumed that the strength added to a reinforced column due to a given increase in concrete strength was the same for all the percentages of longitudinal reinforcement used, provided the percentages were formed from combinations of

bars of the same size. The variation from this generalization by the 0.76% reinforced columns fabricated with #20M bars cannot, unfortunately, be attributed either to an actual anomaly caused by this percentage of reinforcement, or to a strength decrease caused by smaller bar diameters, since an insufficient number of columns were tested. Nevertheless, one might have expected the opposite behavior since bars of larger diameter should introduce larger radial displacements into the surrounding concrete due to differences in stiffness and lateral expansion between the two materials, and prevent the shell from reaching higher strengths.

The curves representing the relation between column strength and the percentage of vertical reinforcement in Figs. 5.7(a) and 5.7(b) do not increase directly with the increased load carried by the vertical reinforcement by virtue of increased areas. This behavior necessarily leads to the conclusion that an increasing percentage of reinforcement decreases the load carried by the masonry shell plus the concrete core. This is better illustrated in Figs. 5.8(a) and 5.8(b), in which a shell and core strength decrease is clearly associated with a reinforcement percentage increase. Since past investigations of reinforced concrete columns have shown that the increase in core strength of reinforced columns is equal to the net area of its concrete times 85 percent of the increase in strength of its control cylinders regardless of the percentage of

reinforcement, it must be logically assumed that core plus shell strength decreases in masonry columns associated with increased percentages of reinforcement must be primarily attributed to shell strength decreases. These decreases are apparently "subtracted" from the increased shell strength which results from the confinement provided by lateral ties, since the majority of reinforced column (shell + core) strengths in Fig. 5.8(a) are greater than the load carried by their corresponding plain grouted column strength.

Adjustment for decreased (core + shell) strength resulting from the physical displacement of concrete as reinforcement percentages increase has been made for the failure loads plotted in Figs. 5.9(a) and 5.9(b), and it is apparent that this adjustment is not sufficient to account for the observed strength decreases in (core + shell) strength. Adjusted strengths were obtained by the addition of $0.85f'_c A_s$ to the shell and core strengths reported in Figs. 5.8(a) and 5.8(b).

In summary, it is proposed that the addition of lateral reinforcement in a masonry column primarily serves to increase the shell load carrying capability by affording a core confinement which results in a net (core + shell) strength increase. The introduction of longitudinal reinforcement increases the lateral expansion of the column core under compressive loading and reduces the effectiveness of the lateral ties. The strength of the masonry shell decreases with greater core lateral deformation, and hence

with increasing percentages of vertical reinforcement. However, load contribution by the steel exceeds this decrease, and the net effect is to increase the ultimate load of the column. For the percentages of vertical reinforcement tested herein (0 to 2.6%), shell strength did not decrease below that provided by the shell of a plain, grouted masonry column. It is evident that Eq. 5.3(b) provides an adequate estimate of column (shell + core) strength for reinforced masonry columns fabricated with the reinforcement percentages permitted by the masonry code. This failure mechanism implies that reinforced masonry columns constructed with stiff lateral ties, achieved by means of increased elastic modulus, increased area, or effective hook embedment should outperform like columns with less stiff ties. Test results reported by Feeg[8] showed that the increase in ultimate masonry strength for tied columns over columns with no ties averaged 7.4%, 12.6%, and 15.9% for tie diameters of 0.1483, 0.1875, and 0.25 inches, respectively. Thus, one might reasonably expect the columns of Series F, fabricated with longer tie hook development lengths, to fail at higher loads than those of otherwise similar Series D columns.

The load carried by the masonry shell may be calculated from the experimental column ultimate strengths using the following equation:

$$P_{shell} = Pu_c - 0.85f'_c(A_c - A_s) - \varepsilon_s E_s A_s \quad \ldots \quad 5.4$$

where

P_{shell} = shell load at column failure

Pu_c = column ultimate load

A_c = column core area = 146.9 in.^{2}

A_s = longitudinal steel area

ε_s = longitudinal steel strain at column failure

ε_y = longitudinal steel yield point strain

E_s = elastic modulus of longitudinal steel

It is important to recognize when applying this equation that accidental variations in column strength have thus been included in the portion attributed to the masonry shell. Results of these computations for Series A columns are presented in Table 5.1 and in Fig. 5.10. This figure plots shell strength as a function of vertical reinforcement percentage for Series A columns with mix 5C and mix 3C concretes. In general, decreasing shell strength associated with increasing longitudinal percentages is shown, as is the decreased shell strength anomaly for 0.76% reinforcement. In Fig. 5.11 shell strengths have been plotted as ordinates, and control cylinder strengths as abscissas. It is evident that there are minor shell strength increases with column core strength. Percentage of vertical reinforcement is undoubtedly the most influencial factor affecting shell strength.

5.2.2.6 Contribution of Vertical Reinforcement

It has been well established that the strength added by

the longitudinal reinforcement to concentrically loaded, short, concrete columns is equal to the product of the longitudinal steel area and its yield stress, regardless of the percentage or grade of reinforcement. The stress-strain relation, yield stress, and yield strain for the steel grades used in this study were presented earlier in Fig. 3.4 and Table 3.10. Figure 5.12 presents the ultimate masonry strain for each column tested in this program, with the exception of Series F specimens. Each value is the average of the failure strains measured by the SR-4 electrical resistance strain gauges attached to the longitudinal steel bars, and the masonry failure strains recorded by the 32-inch gauge LVDT's located on the east and west column faces. Compressive strains at failure were between 0.001 and 0.002 in./in. with excessive variation.

The important observation to be made is that yield strain in the longitudinal reinforcement was reached in only one column. Figure 5.13 presents mean failure strain data as a function of concrete control cylinder strength. Figure 5.14 presents mean failure strain data in relation to percentage of vertical reinforcement. It is evident from these figures that no direct relation exists between column ultimate strain and cylinder compressive strength or percent of vertical reinforcement. In fact, ultimate strain appears to be a constant independent of these factors, with a mean value of about 0.00142 and a coefficient of variation of 20 percent. Accordingly, the contribution of vertical

reinforcement to the ultimate strength of masonry columns may be generally expressed as:

$$P_s = 0.00142\, E_s A_s$$

$$P_s = \frac{E_s A_s}{700} \qquad \text{. . . . . 5.5}$$

It is of interest to note that previous investigations[20] have shown that for a column subjected to vertical compression, increasing strains exist from the bottom towards the top of a vertically cast column due to differences in concrete quality. Since all failures occurred in the upper half of these columns, and since strain readings were monitored at column midheight, it might be argued that these strains are somewhat lower than those which occurred in the actual failure region, and that yield strains were in fact reached in the vertical reinforcement. Thus, Eq. 5.5 may provide a conservative estimate of the vertical reinforcement contribution. It is recommended for future column studies that additional gauges be placed at the column upper quarter point.

5.2.2.7 Effect of Tie Embedment

The effect of superior tie development on the failure mode of Series F columns was presented earlier, in Section 5.2.1. The effects of tie embedment will be established through comparisons of Series F columns, which were constructed with Type D and E ties, and identical Series D columns which used Type A and B ties. It can be seen from

Figs. 5.7(b) and 5.8(b) that Series F tie detailing was directly responsible for column ultimate strength increases of 145 to 250 kips, representing increases of 29 to 38 percent over Series D column strengths. Mean ultimate strength increase was 200 kips, equivalent to a 35 percent increase. Similar increases are recorded for core and shell strengths.

In addition, slightly higher ultimate strains were measured for Series F columns. Average ultimate strain for these columns was 0.00162 in./in. with a coefficient of variation of 8.9 percent, whereas for Series D, these values were 0.00151 in./in. and 27 percent, respectively. It has previously been stated that mean failure strain for all columns tested, excluding Series F, was 0.00142 in./in. This indicates that the load contribution for steel reinforcement expressed by Eq. 5.5 may be conservative for columns having lateral ties with sufficient embedment.

5.2.2.8 Effect of Concrete Slump

Excessive block-core interface shrinkage cracking similar to that reported earlier for the Series C prisms, was observed on the top surface of all Series C columns. The effects of increased concrete slump on the column compressive strength and the (core + shell) strength are best shown in Figs. 5.15(a) and 5.15(b), respectively, which plot these strengths as a function of concrete control cylinder strengths. Test results indicate that Series C

columns complete an approximately linear strength relationship with Series D columns grouted with mix designs 5C and 3C and fabricated with identical lateral reinforcement. This would imply that a high slump has no detrimental effects upon column ultimate strength or (core + shell) strength. These observations are in keeping with those reported earlier for Series C prisms.

Mean ultimate strain for these columns was 0.0013 in./in. with a coefficient of variation of 15.8 percent. This value is only slightly less than the mean strain equal to 0.00142 in./in. reported for all columns, and because of the large variations in these figures, Series C columns cannot rationally be classified as having less ductility on the average.

5.2.2.9 Ultimate Strength Equation

A synthesis of these test results permits the formulation of the following equation which can be used to predict the ultimate strength of a concentrically loaded, short, reinforced concrete block masonry column fabricated with materials, dimensions, and workmanship similar to those used in this study:

$$Pu_C = 0.85f'_c(A_c - A_s) + E_s A_s/700 \quad \ldots\ldots\ldots \quad 5.6$$

Equation 5.6 is considered to provide a conservative strength estimate for columns fabricated with stiff, well developed lateral ties, columns with no vertical

reinforcement, columns with Grade 40 longitudinal steel, and columns filled with high strength grouts. It is recommended that the undercapacity factor used for reinforced concrete columns, $\phi = 0.7$, also be applied to reinforced concrete block masonry columns. Also, it is recommended that the load contribution of the shell not be considered analytically since the portion of the load taken by the shell appears to be quite variable, and to be dependent upon the bonding characteristics of the concrete rather than the concrete strength, as shown by the columns of Series A- mix 5C. Until this interaction is better understood, a conservative approach should be taken.

Alternatively, column ultimate strength may be conservatively predicted by the addition of the steel term in Eq. 5.6 to the failure loads of experimental prisms constructed with the same materials used in the column. This method is thought to give more accurate values than Eq. 5.6 in most cases, since it should provide a better estimate of the shell contribution.

The experimental column ultimate strengths are plotted against the predicted column strengths for these two methods in Figs. 5.16 and 5.17. Points which lie below the diagonal in these figures represent predicted column strengths in excess of experimental strengths. Both methods show the desired central tendency about the diagonal. The correlation coefficient for experimental and predicted strengths for both these methods is 0.70.

Both procedures provide a safe column design after the undercapacity factor of 0.70 has been applied to the predicted strengths. This is shown in Figs. 5.18 and 5.19.

5.2.3 Modulus of Elasticity of Masonry Columns

The mean values of initial tangent modulus for the vertical steel, masonry, and block face are recorded for each column in Table 5.1. From a review of these data, it is apparent that column axial stiffness increases significantly with increasing core strength, and increasing percentages of vertical reinforcement. These trends are shown for the Series A- mix 5C and mix 3C columns in Figs. 5.20 and 5.21, respectively. Moreover, the majority of these columns showed only minor variations between masonry face and longitudinal steel deformations throughout the column loading history for all strengths and percentages of vertical reinforcement. This indicates that there was a uniform strain distribution across the column cross-section, and that there was no slippage between the concrete shell, core, and longitudinal steel.

Figure 5.22 shows the variation of column elastic modulus as a function of prism compressive strength. Column elastic modulus has been calculated from the average masonry strains measured by the LVDT's, and the SR-4 strain gauges attached to the longitudinal reinforcement at column midheight. It is seen that the CSA-S304 formula, Eq. 2.13, significantly over-estimates column elastic modulus for

prism strengths exceeding 2000 psi. A similar observation was noted earlier for prisms in Section 4.5.4, Fig. 4.9. A more conservative estimate of column elastic modulus is provided by $E_m = 750f'_m$. This curve is also drawn in Fig. 5.22, and is in good agreement with empirical formulas derived from previous research.[8,37,38,39]

It can be shown that the gross area elastic modulus of a composite material such as masonry, with a block shell and grout core containing vertical reinforcement steel, is given by:

$$E_m = \frac{E_c(A_c - A_s) + E_{shell}A_{shell} + E_sA_s}{A_g} \quad \ldots \quad 5.7$$

where

E_m = elastic modulus of the column

E_c = elastic modulus of the concrete core

A_c = core area

E_s = longitudinal steel elastic modulus

A_s = area of vertical reinforcement

E_{shell} = masonry shell elastic modulus

A_{shell} = masonry shell area

A_g = column gross area

It was stated earlier, in Section 4.5.4, that the elastic modulus measured from standard moist cured concrete control cylinders is not an adequate representation of the core elastic modulus of a masonry prism specimen. In fact, it was determined that use of the cylinder elastic modulus in Eq. 4.7 over-estimated experimental prism modulus of

elasticity, and stripped core specimens indicated that the prism core modulus was only about half of that of a standard cylinder. Use of cylinder elastic modulus in Eq. 5.7 also over-estimates column elastic modulus. This would imply that a similar relationship to that between prism core and cylinder moduli exists between column core and cylinder moduli. Since there were no plain, grouted, stripped shell columns tested which would have permitted a direct comparison between column core and test cylinder, it was necessary to determine this empirical constant by using Eq. 5.7, and solving for a value of kE_c. Both E_{shell} and E_s have been well established, with small variation. The former may be taken from the experimental results of the five plain prisms and the two plain columns tested, and has a mean value of 1.63×10^6 psi and a coefficient of variation of 7.0 percent. Reinforcement steel moduli were presented in Table 3.10, and Fig. 3.4, and show variations less than 3.0 percent. It may then be assumed that variations between experimental moduli, and those given by Eq. 5.7, primarily rest in the value kE_c. The value of the elastic modulus conversion factor k has been calculated for each column using Eq. 5.7 and these are presented in Table 5.1, and plotted as a function of concrete control cylinder strength in Fig. 5.23. There appears to be no direct relationship between these parameters, and the best estimate that can be provided is the mean value, $k = 0.79$, with a coefficient of variation of 20 percent. Because of this large variation,

primarily attributed to Series A- mix 5C, and Series C- mix 3G columns, the conversion factor may be taken as 0.8. Thus, test results in this program indicate that the elastic modulus of a concrete block masonry column may be approximated by:

$$E_m = \frac{0.8E_c(A_c - A_s) + E_{shell}A_{shell} + E_sA_s}{A_g} \quad . . \quad 5.8$$

Figure 5.24 illustrates the relationship and variability between column moduli calculated using Eq. 5.8, and those measured experimentally.

That the elastic modulus conversion factor for column cores is greater than that for prism cores seems reasonable in one respect, since the ratio of core strength/cylinder strength is also greater for columns. However, no acceptable explanation can be suggested for column core strengths and elastic moduli being larger than those for prisms.

The shapes of the vertical load-strain curves for a number of concentrically loaded columns tested in this program are presented in Appendix A. The curves display nearly linear behavior over most of their range, and there is a general trend for higher ratios of P_{linear}/P_{u_c} to be associated with higher concrete core strengths, larger percentages of vertical reinforcement, and more favourable tie development detailing. Table 5.1 contains for each column, the percentage of the ultimate load over which the load-strain curve is approximately linear. Figure 5.25 plots these percentages against control cylinder strength.

Eliminating those percentages of Series A- mix 5C columns, which are comparatively high, and thus the exception rather than the rule, these columns display linear elastic behavior to a mean load of $0.42Pu_c$, but have a coefficient of variation of 33 percent. However, all columns displayed linear load-strain behavior prior to a load of $0.25Pu_c$. Because the masonry code does not permit axial column stresses to exceed $0.20f'_m$, present design practice places column behavior within the elastic range of these members. Since the addition of longitudinal reinforcement should logically increase these percentages because of its linear behavior until yield, it is surprising that prism linear percentages were somewhat higher than those for the columns.

The column block elastic moduli are presented in Table 5.1. As with those of the prisms, it is noted that each block elastic modulus is significantly greater than its corresponding masonry elastic modulus, and since there is little variation in these moduli with core strength and percentage of vertical reinforcement, it may be concluded that strains in the mortar joint account for an appreciable portion of the masonry strain, and that the continuity provided by the concrete core and by the vertical reinforcement does not effectively reduce the significance of mortar joint strains.

5.2.4 Column Lateral Strains

Typical column load-lateral strain curves plotted from

strain measurements on the steel lateral ties and the concrete block faces are presented in Appendix A. These curves display nearly linear behavior up to column failure load and since this was not observed for the companion prisms, the conclusion must be drawn that the confinement provided by the lateral ties was responsible for this. Lateral stress-strain moduli and Poisson's ratios are tabulated in Table 5.1. Lateral strains at failure varied between 0.00010 and 0.00268 in./in. for the steel, and between 0.00011 and 0.0039 in./in. for the block faces, and both showed large variations.

As previously noted for all columns tested, the steel lateral ties in the column failure zone displayed large bending deformations resulting from lateral stresses from the expanding concrete core. Considering that the SR-4 tie gauges were located on the inside tie surface, compressive strains due to lateral bending in these ties would superimpose on the tie axial tensile deformations. Accordingly, it is not surprising that the steel lateral elastic modulus based on measurements from this gauge was greater than its corresponding block face lateral elastic modulus for twenty-three of the thirty-two columns in which these strains were monitored. In fact, compressive lateral tie steel strains were sometimes recorded. Thus, the constraining effect of the tie is largely dependent on its bending stiffness, and is clearly not a function of axial stiffness alone.

Values of Poisson's ratio are plotted in Fig. 5.26. These values were calculated on the basis of lateral strains measured on the block face, since these are considered to be more representative of the actual transverse strains in the column. Computed values of Poisson's ratio were between 0.04 and 0.50 with a mean of 0.21 and with a large variation. Elastic modulus of concrete block masonry has been established in CSA-S304 as:

$$E_m = 1000f'_m \leq 3.0 \times 10^6 \text{ psi}$$

The shear modulus, G, is theoretically related to elastic modulus, E, and Poisson's ratio, ν, by:

$$G = \frac{E}{2(1 + \nu)}$$

Substituting the mean Poisson's ratio obtained from the column tests reported herein, and the code elastic modulus equation into this theoretical relation yields:

$$G = \frac{1000f'_m}{2(1.21)} = 413f'_m$$

$$G = \frac{3.0 \times 10^6}{2(1.21)} = 1.24 \times 10^6 \text{ psi}$$

These calculated values compare remarkably well with the shear modulus specified in CSA-S304:

$$G = 400f'_m \leq 1.20 \times 10^6 \text{ psi}$$

and indicate that this specification is based primarily on that for elastic modulus, which has in itself, not been

accurately defined. An indication of the variability in the determination of G is thus provided since Poisson's ratio in these tests showed a coeffient of variation of 54 percent.

5.2.5 Column Cracking Loads

The loads at which column shell cracks were first observed are plotted as a function of concrete control cylinder strength in Fig. 5.27. As with prism cracking, the column cracking load is seen to be directly proportional to core strength and the two may be related by the following linear regression equation:

$$P_{crack} = 75.3f'_c + 186 \quad \text{(Kips)} \quad \ldots\ldots\ldots \quad 5.9$$

$$r = 0.74$$

Comparison of Eq. 5.9 with the prism cracking linear regression Eq. 4.9 shows that columns cracked at a higher load for a given core strength. This increase must therefore be attributed to the additional confinement of the core provided by the steel lateral ties. It is interesting that both Eqs. 4.9 and 5.9 indicate that the cracking load of a plain ungrouted specimen is approximately 190 kips, yet column failure load was below this value. This might suggest that the placement of lateral ties in the plain columns would increase failure load to some value above 190 kips. Unfortunately, no columns were constructed for such a comparison.

It is seen that Series F columns with superior tie

detailing cracked at significantly higher loads than their companion Series D columns. Series C columns cracked at somewhat lower loads than did the columns of the other series.

A plot was constructed with column cracking loads as the ordinates, and percent vertical reinforcement as the abscissas, but data were scattered and did not permit the derivation of an equation to relate the two. The relationship between the ratio of column cracking load/ultimate load, and concrete control cylinder strength is shown in Fig. 5.28, and it would appear that Eq. 4.10 derived for prism cracking/ultimate load adequately describes the relationship for columns as well.

Since shell cracking load is dependent upon block strength, core strength, and tie stiffness, it must be emphasized that Eqs. 5.9 and 4.10 will likely only apply to columns fabricated with similar materials to those employed in this program. Shell cracking load should be expected to increase with increased core strength, increased block strength, increased shell thickness, and increased tie stiffness and hook development.

5.2.6 Column Lateral Deflections

The deflected shapes of a number of columns, interpreted by lateral displacements recorded by LVDT's attached to the column face, are presented in Appendix A. Lateral deflections for the concentrically loaded columns

were small, and perhaps these measurements indicate more the lateral expansion of the column, rather than the lateral deflection. Most plots do not show symmetrical bending about column midheight, but rather show increased deflections in the upper column region where failure normally occurred and where lateral deformations due to the expanding concrete core were the largest. The majority of these columns showed single curvature bending.

5.3 Eccentrically Loaded Columns

5.3.1 Ultimate Strain

It is generally known that considerably larger concrete strains are developed in bending before failure than in concentric compression. Apparently the outer fibers are able to yield and transfer stress to the less strained fibers closer to the neutral axis of the section.

The ultimate compressive masonry strain for each of the sixteen eccentrically loaded columns tested is reported in Table 5.2. Since transducers were normally removed just prior to column failure, the last strain increments could not be observed. For these columns, ultimate strains were obtained by extrapolation of strain to the known ultimate load using the column load-strain curves. The average failure strain was 0.002 in./in. on the compression face, with a coefficient of variation of 14.2 percent. Mean ultimate strain for the concentrically loaded columns was on the order of 0.0015 in./in. The eccentric strain value is

somewhat below the mean experimental concrete failure strain of 0.0038 in./in. obtained from the eccentric load tests of tied reinforced concrete columns conducted by Hognestad[20] (1951), and below the conservative value of 0.003 in./in. accepted by ACI-318-77 for concrete subjected to flexure. However, the ultimate strain measurements reported herein are difficult to interpret since these were gauged along 32-inch lengths centered on column midheight, and it was observed that all columns failed in the upper half. All concrete columns tested by Hognestad failed in compression in the upper half as well. This may be attributed to bleeding, resulting in an increased water/cement ratio in the column upper region, and to better compaction in the lower part of the column. Hognestad, however, measured strains at a number of column elevations, and noticed that a general trend of increasing strains exists from the bottom towards the top of a column shaft which has been vertically cast. The mean ultimate strain of 0.0038 in./in. reported by Hognestad was based on those strains measured by SR-4 gauges with 6-inch gauge lengths attached to the compression face in the column failure region, and thus, the discrepancy between the ultimate concrete strains reported in these studies should not be surprising. In fact, strains at or below column midheight in the Hognestad study were between about 0.0015 and 0.002 in./in., and thus in this respect, a favourable agreement with the masonry column strains is reached. Variations should be expected since the test values

are sensitive to loading rate, gauge lengths, and gauge location with respect to compression cracks. Accordingly, it might be logically assumed that ultimate flexural strains in the masonry column failure region were also on the order of 0.003 in./in. This permits the adoption of the principles of reinforced concrete column design to predict the ultimate strength of a masonry column constructed with pilaster units similar to those used in this study.

5.3.2 Strain Distribution

Figures 5.29 and 5.30 show typical strain distributions across a masonry column cross-section as a function of load. Distributions for several columns are presented in Appendix A. The outer measurements were provided by the 32-inch gauge length east and west LVDT's. The inner measurements are the average readings from the east and west SR-4 strain gauges mounted on the vertical reinforcement bars. Deviations can be expected due to inherent inaccuracies in the measurements of the gauges and due to uncertainties in the actual location of the gauges on the reinforcement bars. There is good agreement between the reinforcement strains and the surface masonry strains, and no patterns can be seen for the deviations from linearity, indicating that these deviations are of a non-systematic nature. Thus, it may be assumed that the hypothesis of linear strain distributions is valid for masonry columns subjected to combined bending and axial load.

5.3.3 Reinforcement and Shell Slip

Since deformed longitudinal reinforcement bars were used, it is reasonable to assume that, in general, there was no slippage between the column concrete core and the reinforcing steel. In addition, strains recorded by the 16-inch gauge length LVDT's attached to the masonry shell adjacent to the vertical steel are in excellent agreement with the strains measured by gauges mounted on the reinforcement, and indicate that the shell, core, and reinforcement act as a unit until failure. Typical load-strain curves for these LVDT's and SR-4 gauges are shown in Fig. 5.31, for column E5P2. The curves for a number of other columns are provided in Appendix A.

5.3.4 General Behavior and Failure Mode

The only failure type observed for specimens tested in this program was compression failure, that is, crushing of the concrete and buckling of the vertical reinforcement before yielding in the tension steel. Column behavior within this failure type was essentially a function of eccentricity of load.

Type 1 failure was peculiar to columns with load eccentricities of t/12 and t/6, regardless of concrete strength, and grade or percentage of vertical reinforcement. This mode was characterized by an explosive removal of the column block shell on the compression face, with subsequent crushing of the concrete core and buckling of the

compression longitudinal steel. Vertical shell cracking did not normally appear until shortly before column failure, and was initiated in the column upper corners. Distress to the shell on the compression face was along the entire column length, although the actual failure zone in the concrete core was generally confined to two or three courses in the middle to upper region of the column. Since tie hooks were positioned in the potential tension face of these columns, the ties did not pull, and reinforcement buckling was restricted to spaces between ties only. The bond between the concrete core and the tension face blocks was completely broken through much of the column height, as was the bond between mortar and block for those joints located between courses in the failure zone. Plates 5.24 , 5.25, and 5.26 show typical Type 1 column failures. Thus, the mode of failure for these eccentrically loaded columns was found to be very similar to the failure of columns with adequate tie development and subjected to concentric compression. The loading apparatus adequately confined the top and bottom column courses, and prevented local crushing failures in these regions.

However, local crushing problems were encountered with those columns loaded with an eccentricity of t/3. Local crushing was characteristic of failure Type 2. These columns crushed either in the bottom or the top course even though the loading plates were designed to confine these courses. Upper and lower course failures are shown in Plates 5.27,

5.28 and 5.29, and Plates 5.30 and 5.31, respectively. Distress to the shell and core was normally confined only to these courses and such failures are clearly not a good representation of the idealized behavior which places the failure zone at column midheight. The loading plates for the larger eccentricities did not provide an adequate transfer of load to the tension face of the column. Lateral column deflections and the deforming fiberboard permitted the loading plate on the tension side of the column to separate from the top surface. As loading increased, and deflections and fiberboard deformations increased, the actual bearing surface between the loading plate and the column decreased, and this produced high stresses in a concentrated area of the column which precipitated local crushing failure. Although this was not the intended or desired behavior for these experimental columns, these observations indicated that transfer of load to a column by use of a simple bearing plate which rests on the column surface is a poor detail. This practice can cause local crushing failure of the column even though analysis has indicated the column to be of sufficient capacity. For tests subsequent to E4P3 and E1P3, wood was positioned beneath the bottom loading plate on the tension side after a load of 150 kips had been applied to the column. The wood prevented larger rotations and thereby reduced the stress concentrations. Although failure mode was still Type 2, significant strength increases resulted for companion E4P4 and E1P4 columns. Hence the remaining columns

with t/3 eccentricities were tested in this fashion.

In order to test reinforced concrete block masonry columns under load eccentricities equal to or greater than t/3, an improved loading system must be developed to prevent local crushing failures. Such an apparatus might be similar to that used for the eccentric load tests of reinforced concrete columns conducted by Hognestad.[20] Columns for these tests were fabricated with vertical reinforcement bars which extended into concrete capitals above and below the column shaft. Additional reinforcement was provided in the capitals and welded to the longitudinal bars to prevent tension, diagonal tension or bond failure in the capitals. Auxiliary reinforcement, similar to the device used in this study to confine the upper and lower column courses, was attached to the capitals to provide additional confinement. The capitals provided an effective means in which to transfer the eccentric load and its moment to the prismatic shaft of the columns. This testing arrangement is shown in Fig. 5.32.

5.3.5 Ultimate Load

The masonry columns in this study have been shown to conform to the basic assumptions used in reinforced concrete column Ultimate Strength Design, namely, ultimate strains on the order of 0.003 in./in. in the failure zone, a linear strain distribution, and absence of slip between the longitudinal reinforcement and the concrete core. Thus, the suitability of application of the ACI-318-77 Ultimate

Strength Design procedure for reinforced concrete columns to reinforced block masonry columns will be examined. The ultimate loads for the columns tested are given in Table 5.2.

The USD, reinforced concrete column design procedure was applied to the masonry columns for three different conditions. Case 1 assumed that the masonry shell compressive strength was equal to that of the concrete core, and thus the masonry column was considered to be identical to a reinforced concrete column having column core strength over the gross section. Case 2 assumed that the column shell strength was equal to the 153 kip (1.6 ksi) shell strength determined from the regression Eq. 5.2. The factor β_1 for this case was taken as 0.85 for both the shell and the core in the E1P- series, and conservatively chosen as 0.80 for the E3P-, E4P-, and E5P- series. Case 3 neglected any contribution by the masonry shell, and the masonry column was analysed as though it were a reinforced concrete column with strength and dimensions equal to those of the masonry core. The results of these analyses are presented in Table 5.2. The ratios of P_{test}/P_{calc} were calculated for each column and averaged for each case. Case 1 analysis grossly over-estimates the experimental failure loads for these columns regardless of core strength, and grade or percentage of reinforcement. The mean P_{test}/P_{calc} ratio is 0.60, with a coefficient of variation of 12.7 percent. This scheme is clearly an inadequate representation of column behavior.

Case 2 provides only somewhat better results, yielding a P_{test}/P_{calc} ratio of 0.81, with a coefficient of variation of 9.2 percent. The ratios between test and calculated ultimate load values for Case 3 analysis are in very favourable agreement. The mean ratio for all columns tested is 1.0, with a coefficient of variation of 10.7 percent. This ratio necessarily implies that the masonry shell of these columns provided an insignificant load contribution at failure. Moreover, since the experimental and predicted strength ratios averaged 0.96, 0.98, and 0.97 for Series E3P-, E4P-, and E5P-, respectively, it is evident that shell contribution may be relatively independent of percent or grade of longitudinal reinforcement. The increased ratio of 1.12 for the lower strength core E1P- columns may suggest that the shell provides some load contribution for the lower strength concretes. Because of the limited number of tests conducted in this study, only these general observations can be made.

Case 3 analysis, in addition to providing a favourable estimate of column ultimate load, also permitted reasonable estimates for the location of the neutral axis in the section at failure. The observed positions of the neutral axis for the experimental columns were measured from the strain gradient curves. Since the theoretical positions of the neutral axis are calculated for the ultimate loads, and the observed values are for strain readings at normally about 90 percent of ultimate load, the direction of travel

of the neutral axis shown by the gradients is indicated by the arrows in Table 5.2. These values are measured distances from the core edge, and not the shell edge, in order to make comparisons with the Case 3 analysis. The experimental values are all slightly in excess of those determined analytically. This is reasonable however, since experimental strains were measured at column midheight, and not in the failure region itself.

The mode of failure of all test columns agreed very well with theoretical prediction. Case 3 ACI USD procedure indicated that all column failure loads were in excess of the balanced load, which should create compression failures in the columns.

The experimental column failure loads are plotted against their failure moment to produce the column interaction diagram in Fig. 5.33. The effects of lateral deflection have been accounted for in the bending moment by the addition of a P-Δ term based on the deflection at column midheight obtained from measurements taken during testing. Consequently, the experimental values are slightly offset from their corresponding eccentricity. The experimental failure loads for the concentric columns are taken from test results of Series A- mix 5C columns, which were grouted with concrete having a 5100 psi control cylinder strength. The solid lines represent the theoretical interaction curves derived from the Case 3 ultimate strength design procedure. These lines are shown only for compression failures, and are

discontinuous at the balanced failure condition. The dotted lines extending from loads corresponding to an eccentricity of t/12, for which the masonry shell apparently provides an insignificant strength contribution, to the concentric loads, for which it is assumed that the shell provides a contribution of 153 kips at failure, are merely linear approximations to account for the transition between these behaviors. It can be seen that Case 3 analysis generally affords a conservative, yet accurate estimate of column failure load and moment. As may be expected, the ultimate load decreases for increasing eccentricity, and for small eccentricities, large variations in ultimate loads result from variations in concrete strength. As well, changes in As' have a significant effect on ultimate load for columns failing in compression. It must be emphasized that Case 3 analysis would likely only be applicable to masonry columns fabricated with pilaster units similar to those used in this study, and more importantly, to units with similar net/gross area ratios.

5.3.6 Shape of the Stress-Strain Curve

The load strain curves for the eccentrically loaded columns presented in Appendix A show that the stress-strain relations on both the compression and tension side of the columns are nearly linear up to failure. As with the concentrically loaded columns, the concrete block strains are, in general, less for a given load than are the masonry

face strains. In fact, for all eccentricities considered, the vertical block strains on the tension face of these columns have the same order of magnitude as the lateral column strains. This indicates that the bond between the blocks and the mortar on the tension face is broken early in the loading history, and thus significant tensile stresses are not introduced into these blocks.

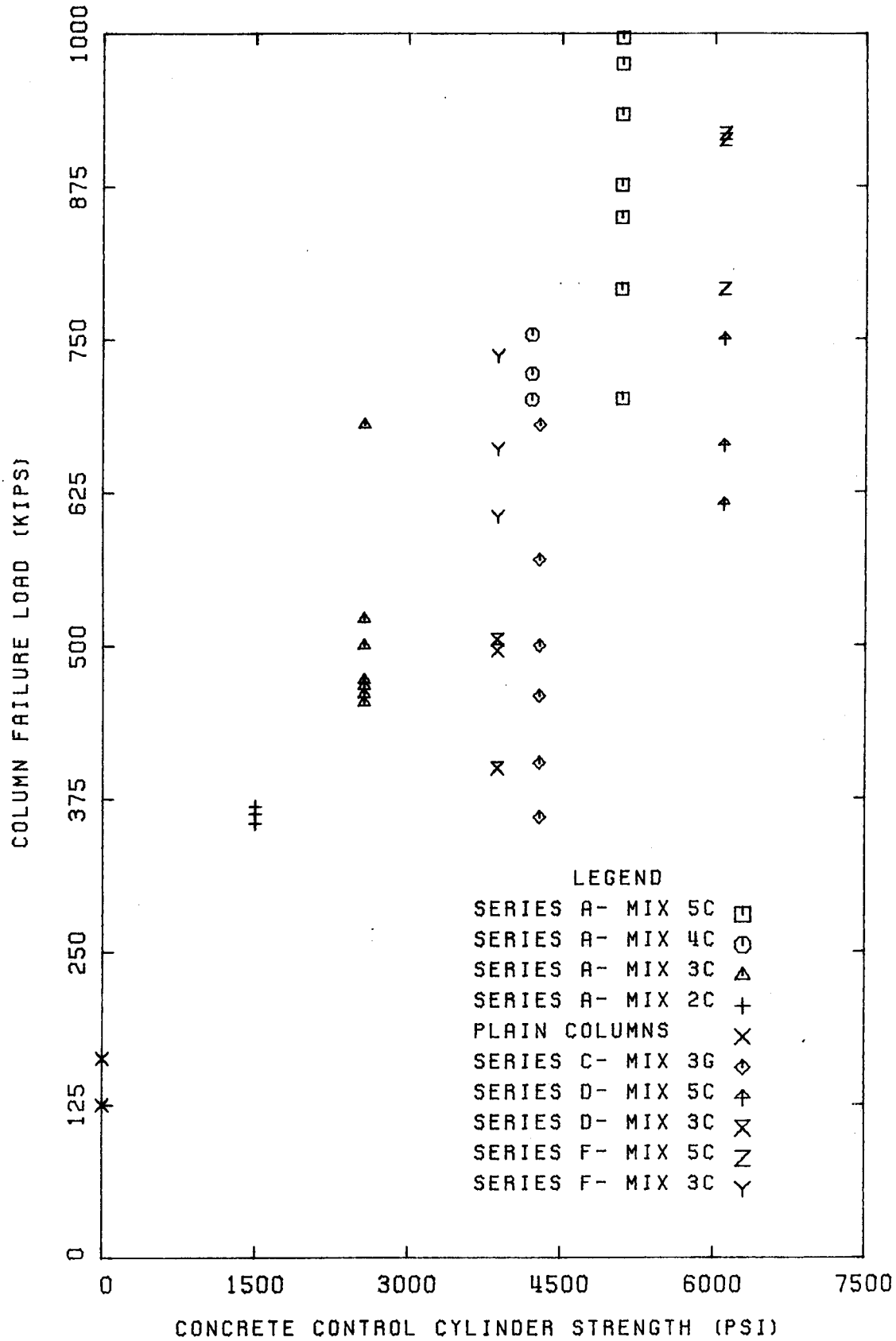

FIG. 5.1: COLUMN FAILURE LOAD VS. CYLINDER STRENGTH

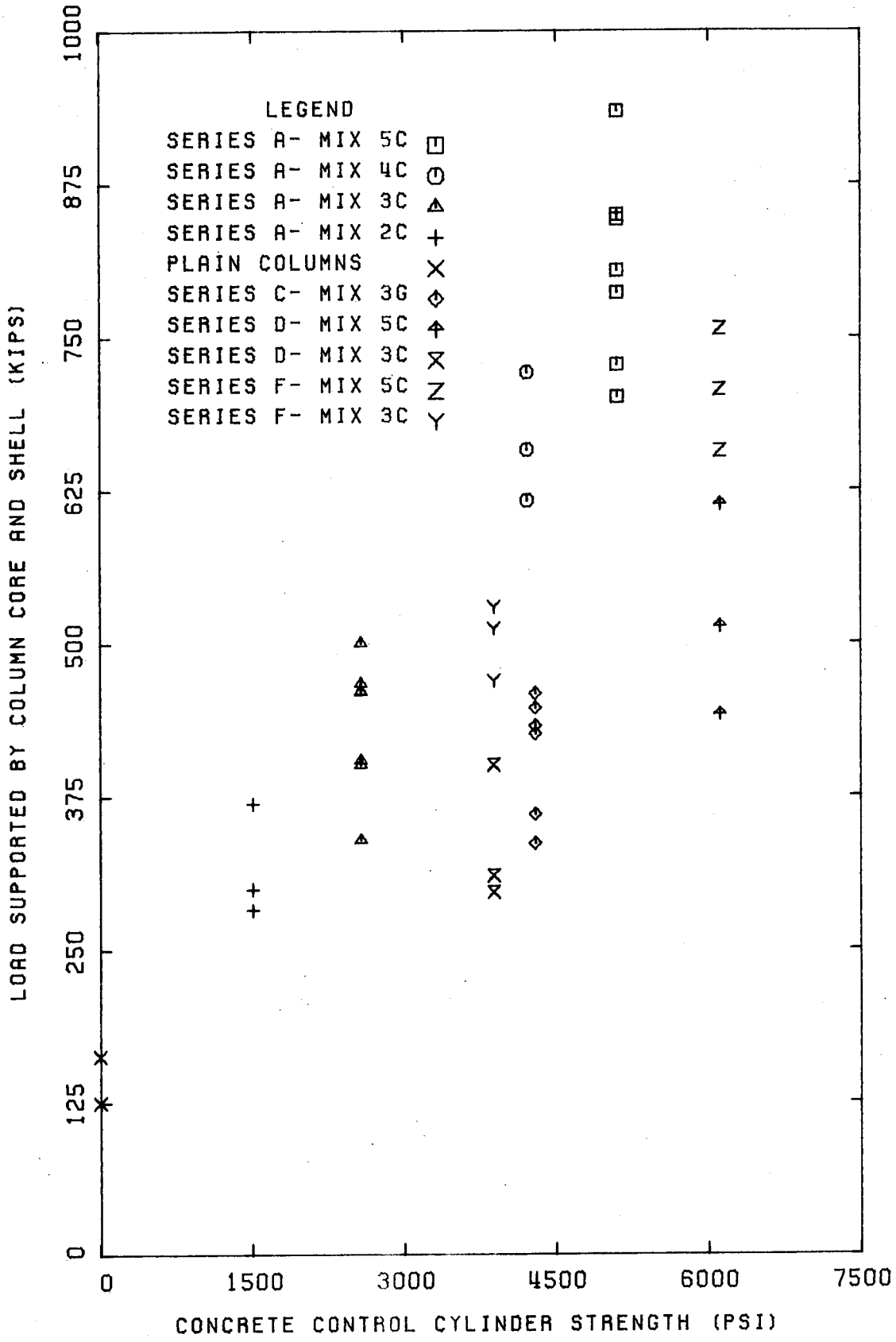

FIG. 5.2: COLUMN CORE AND SHELL LOAD AT FAILURE

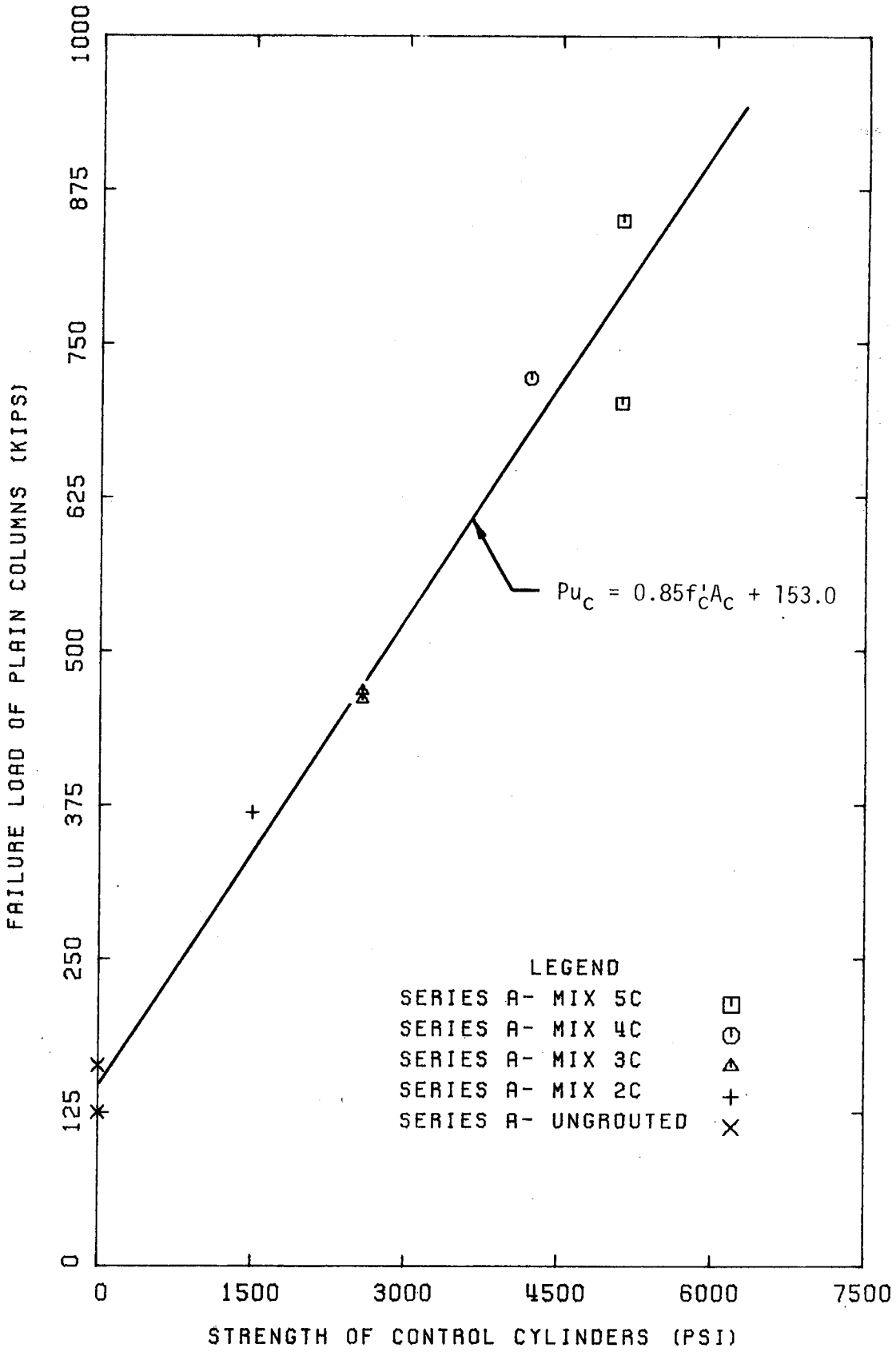

FIG. 5.3: PLAIN COLUMN FAILURE LOAD VS CYLINDER STRENGTH

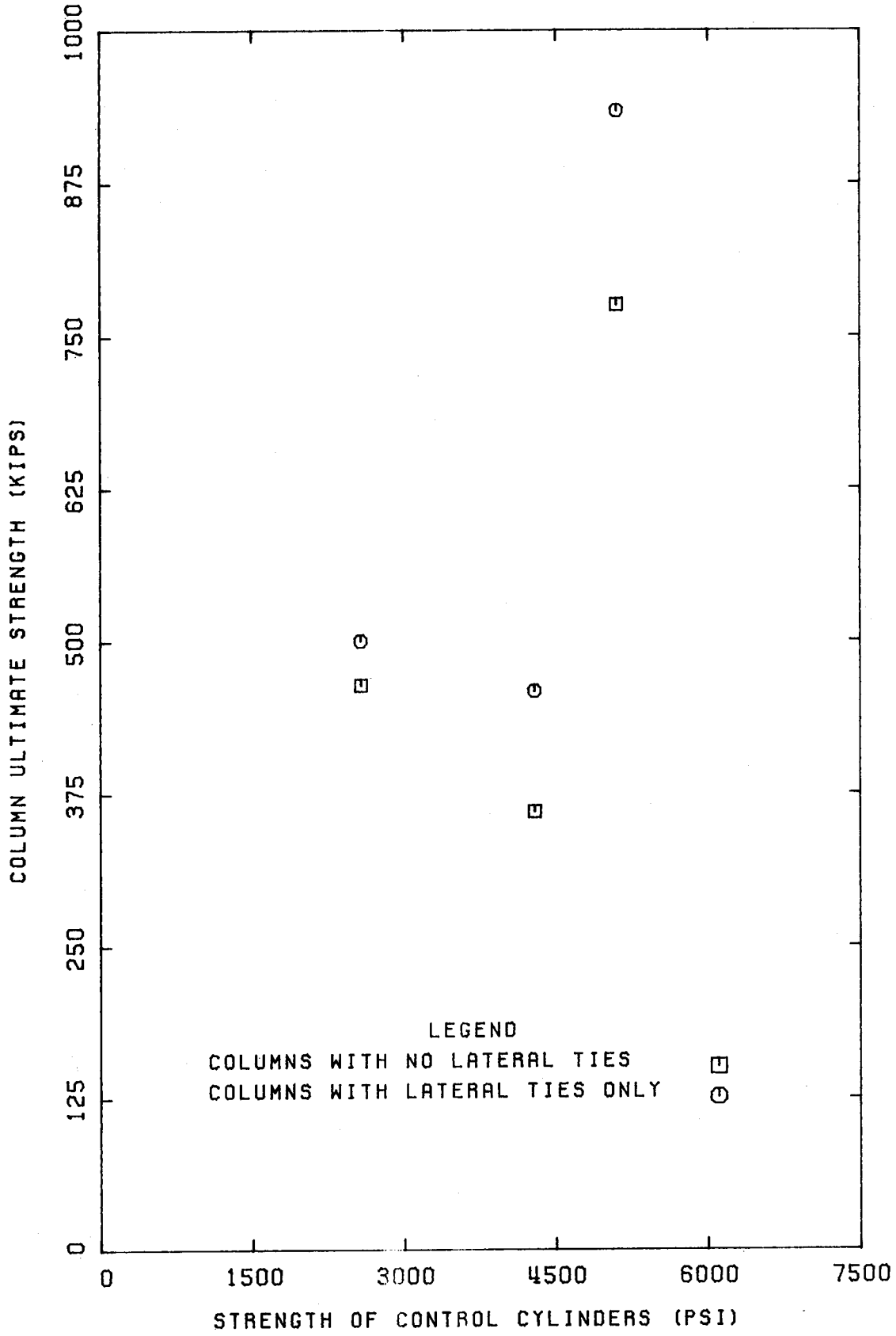

FIG. 5.4: EFFECT OF LATERAL TIES ON COLUMN STRENGTH

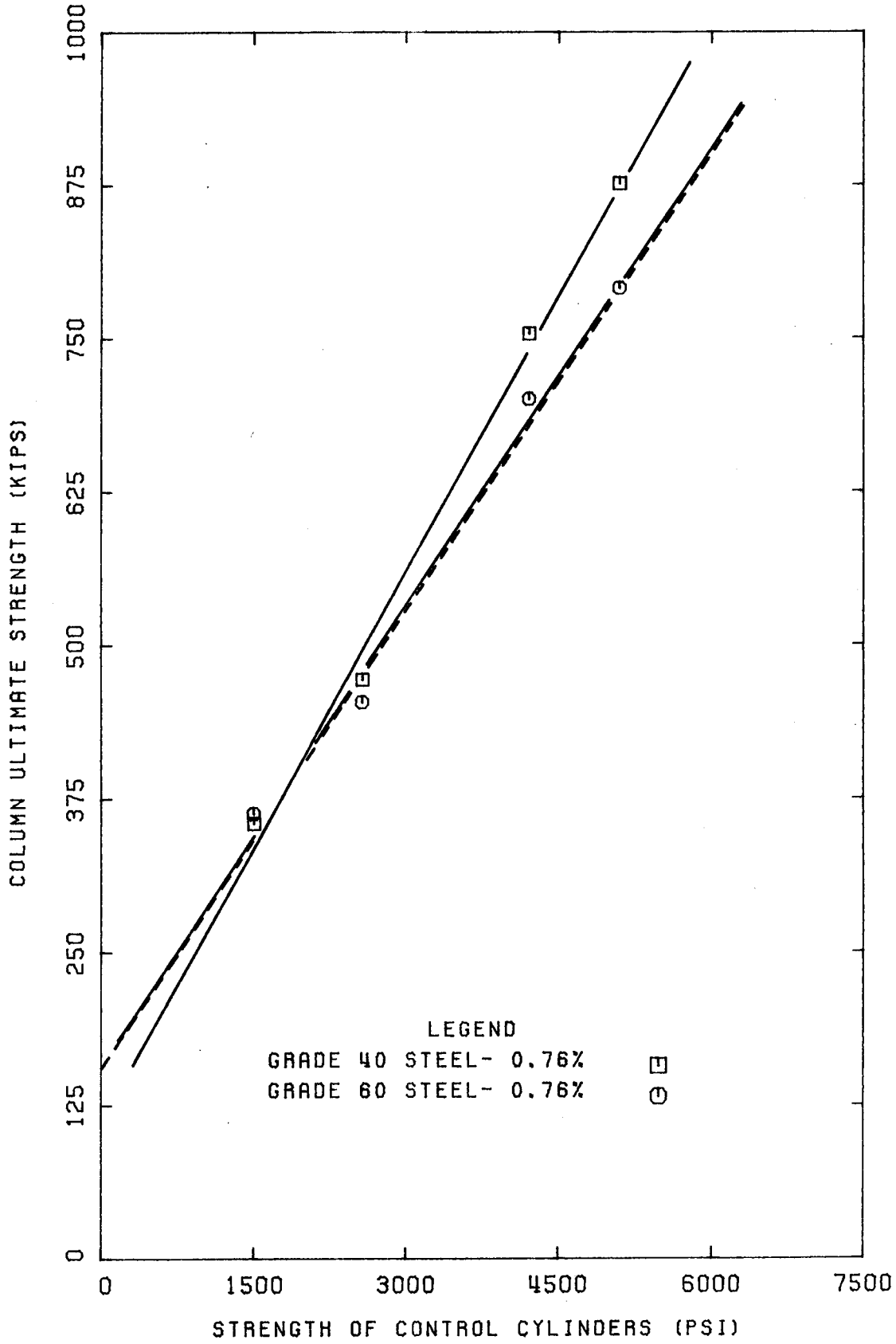

FIG. 5.5: EFFECT OF STEEL GRADE ON COLUMN STRENGTH

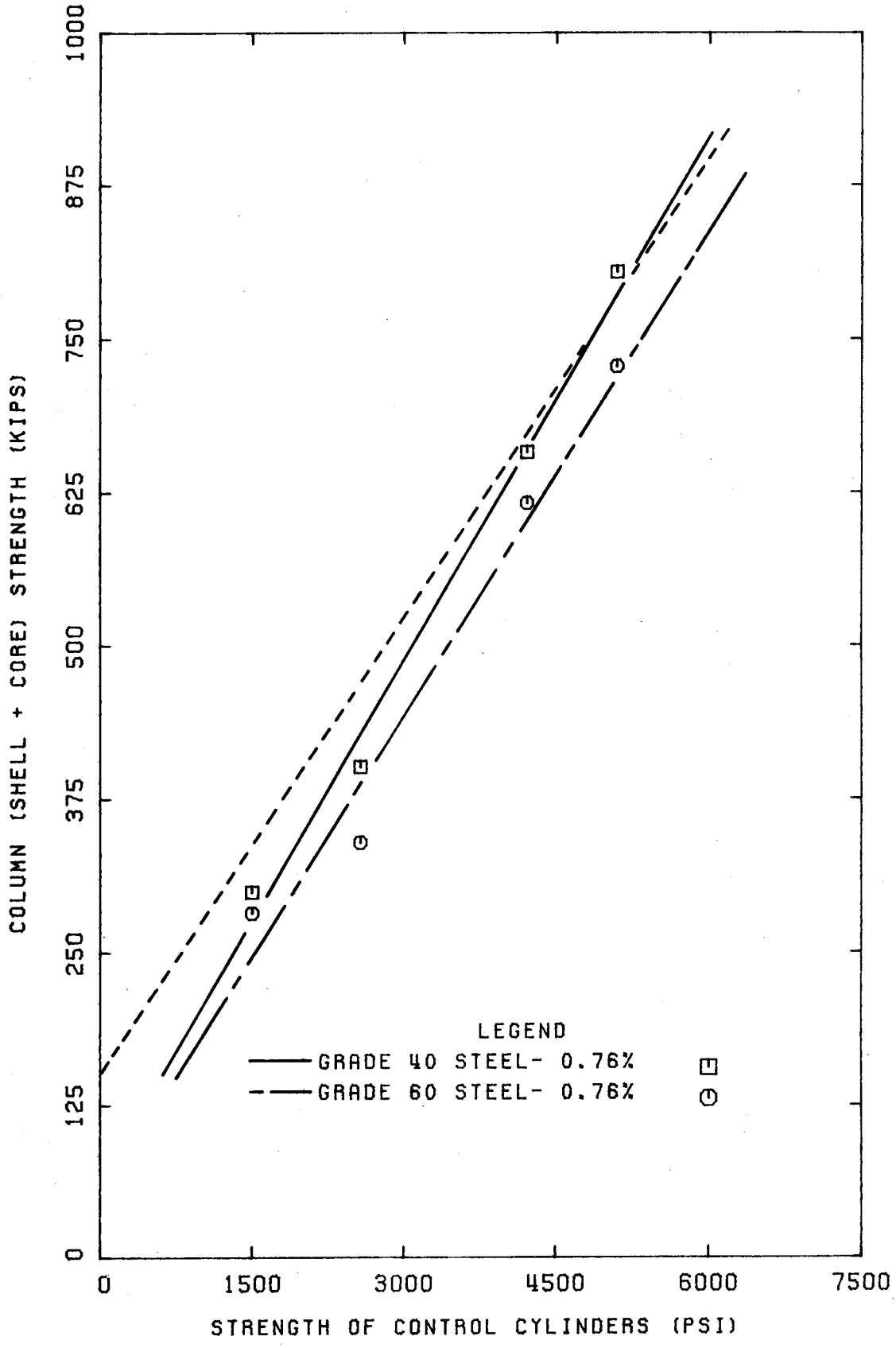

FIG. 5.6: EFFECT OF STEEL GRADE ON SHELL AND CORE STRENGTH

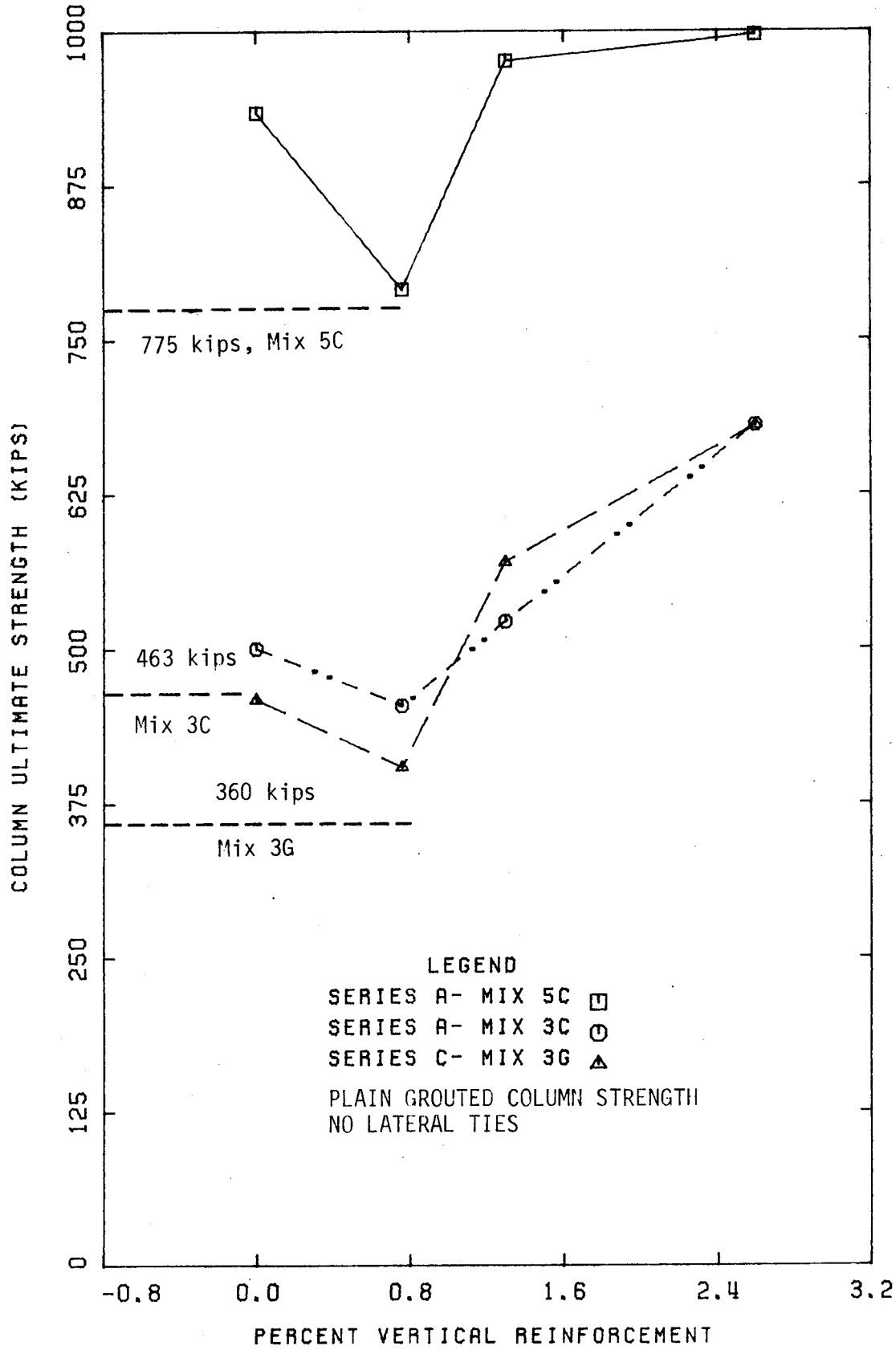

FIG. 5.7(a): COLUMN STRENGTH VS. % VERTICAL REBAR

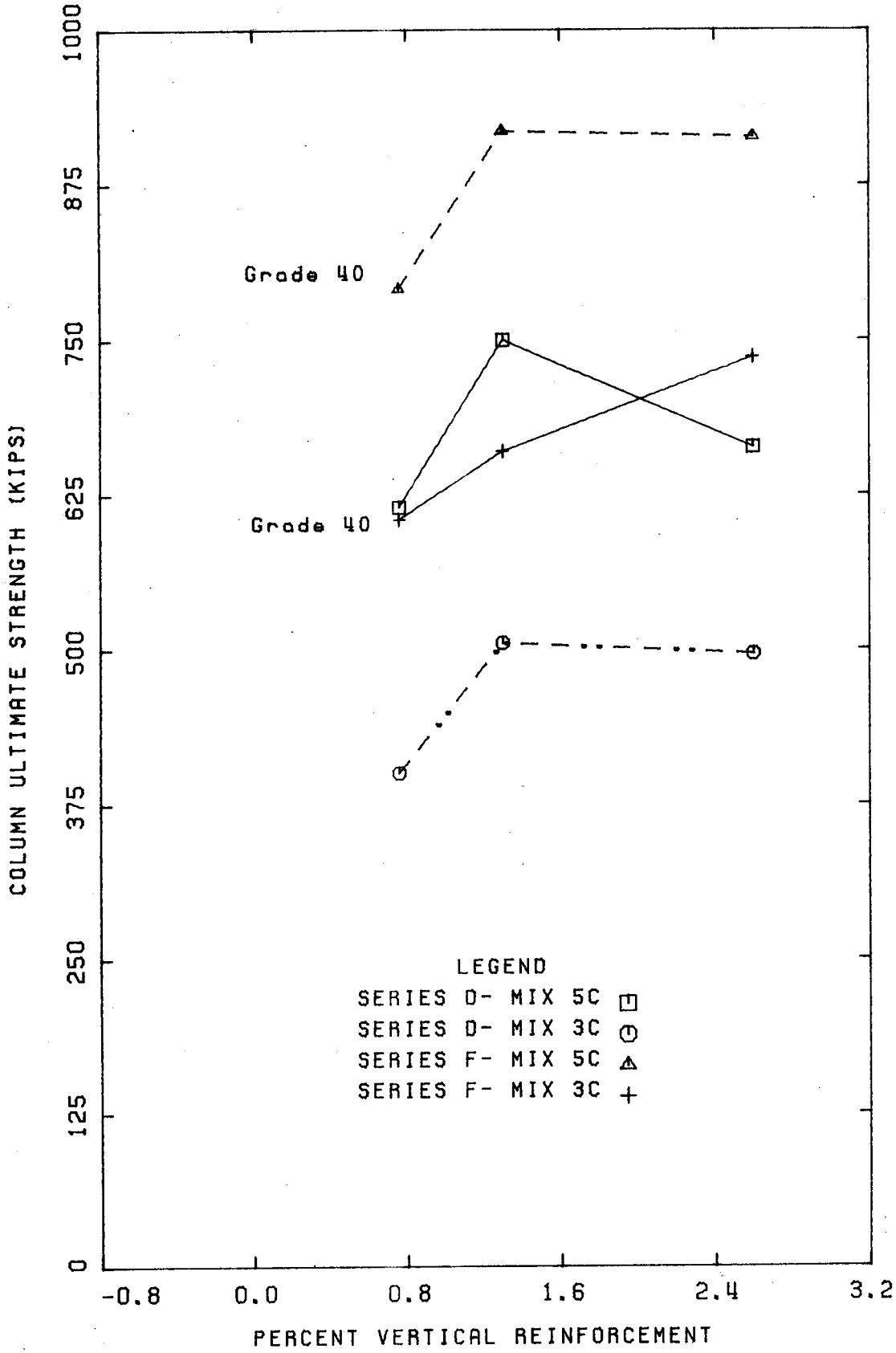

FIG. 5.7(b): COLUMN STRENGTH VS. % VERTICAL REBAR

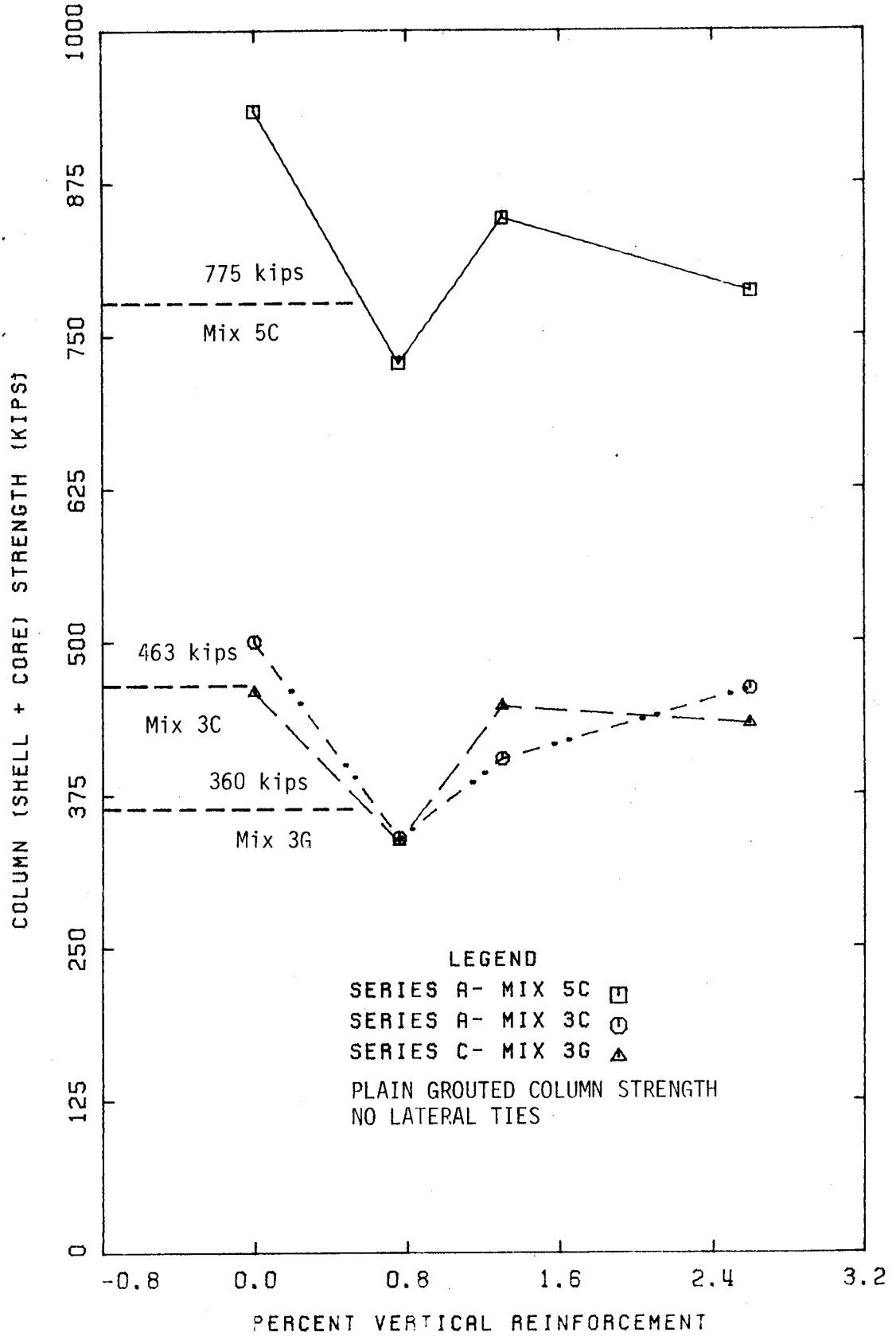

FIG. 5.8(a): (SHELL + CORE) STRENGTH VS. % VERTICAL REBAR

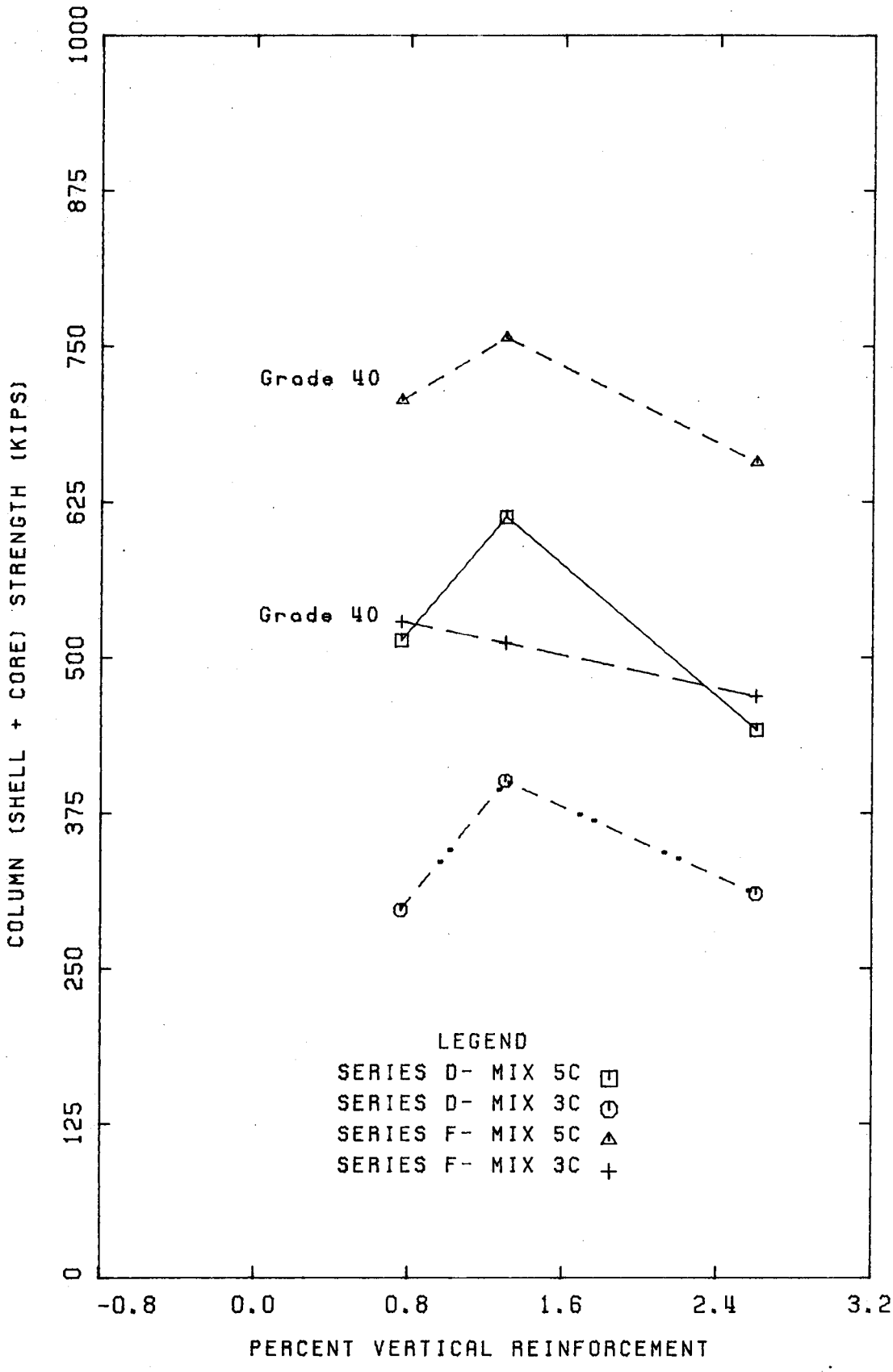

FIG. 5.8(b): (SHELL + CORE) STRENGTH VS. % VERTICAL REBAR

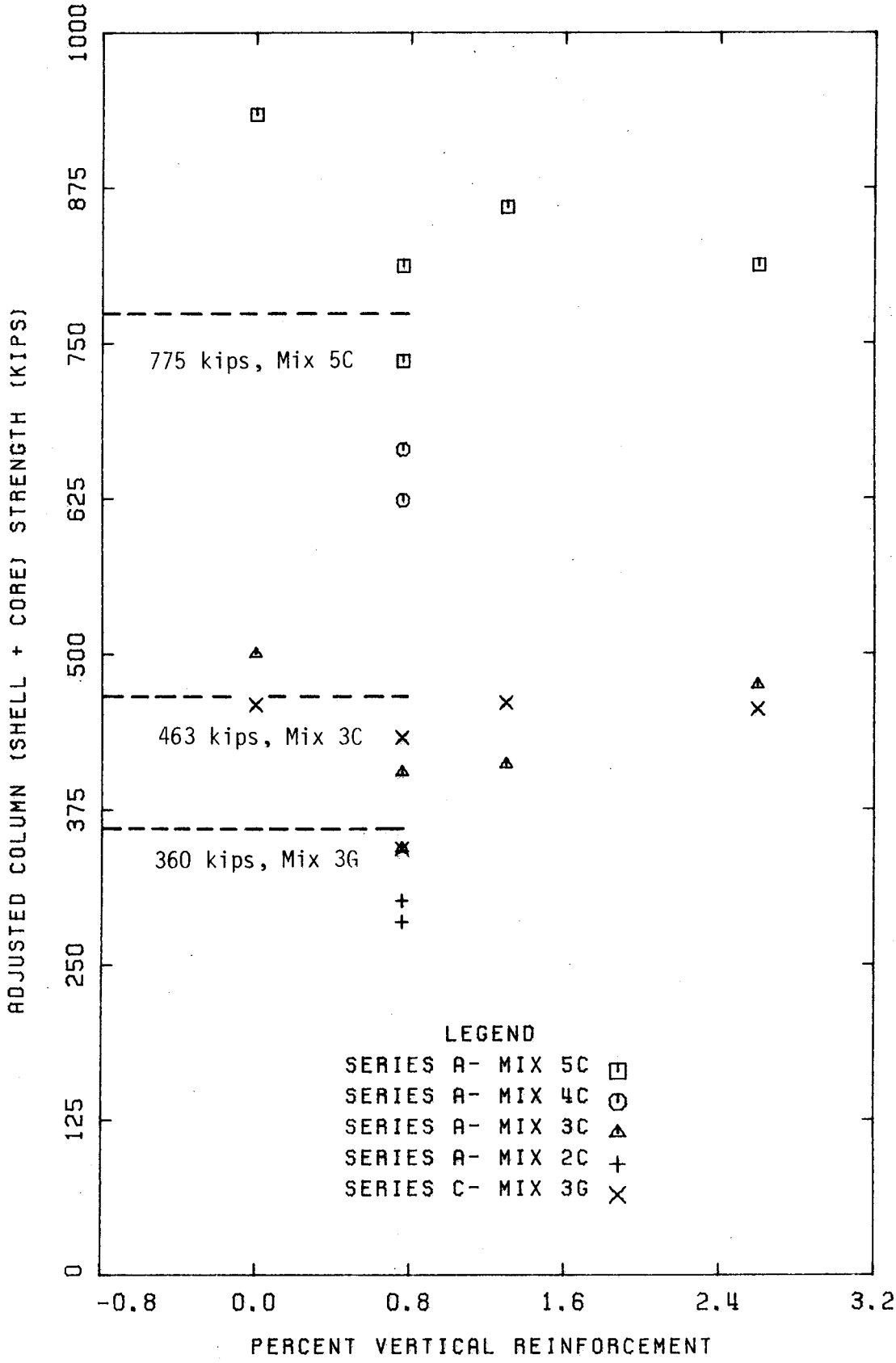

FIG. 5.9(a): ADJUSTED (SHELL + CORE) STRENGTH

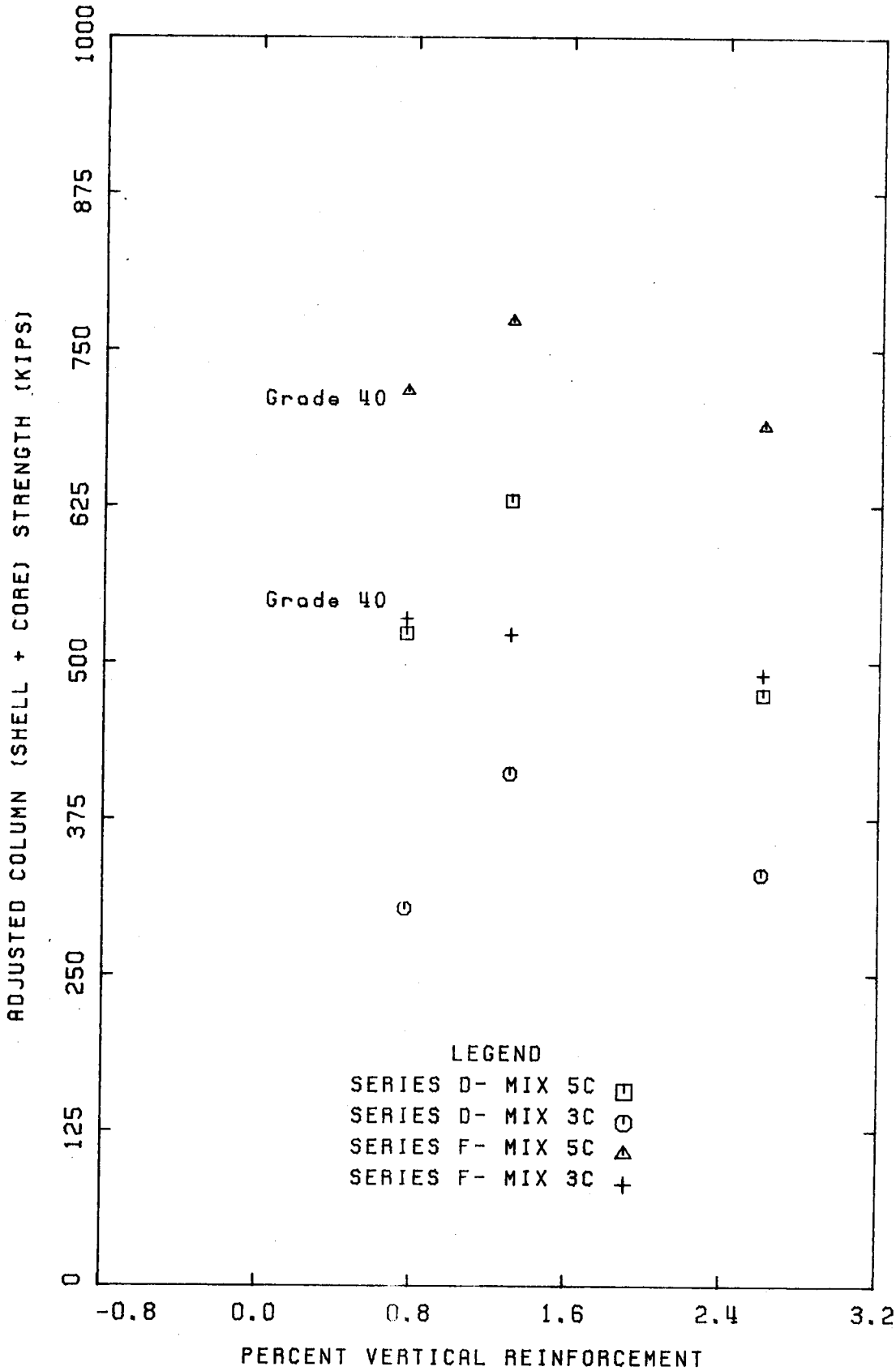

FIG. 5.9(b): ADJUSTED (SHELL + CORE) STRENGTH

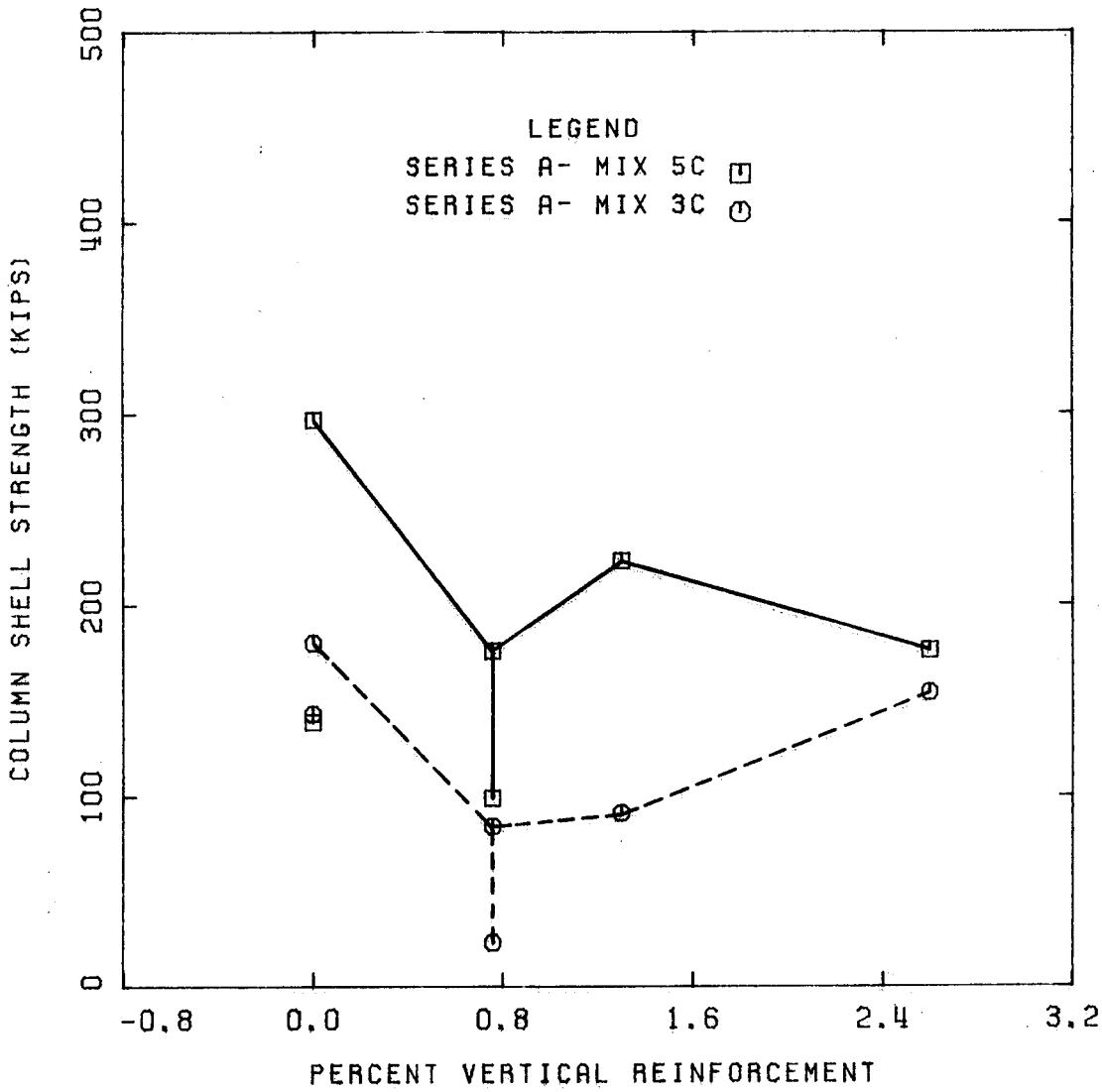

FIG. 5.10: SHELL STRENGTH VS. % VERTICAL REBAR

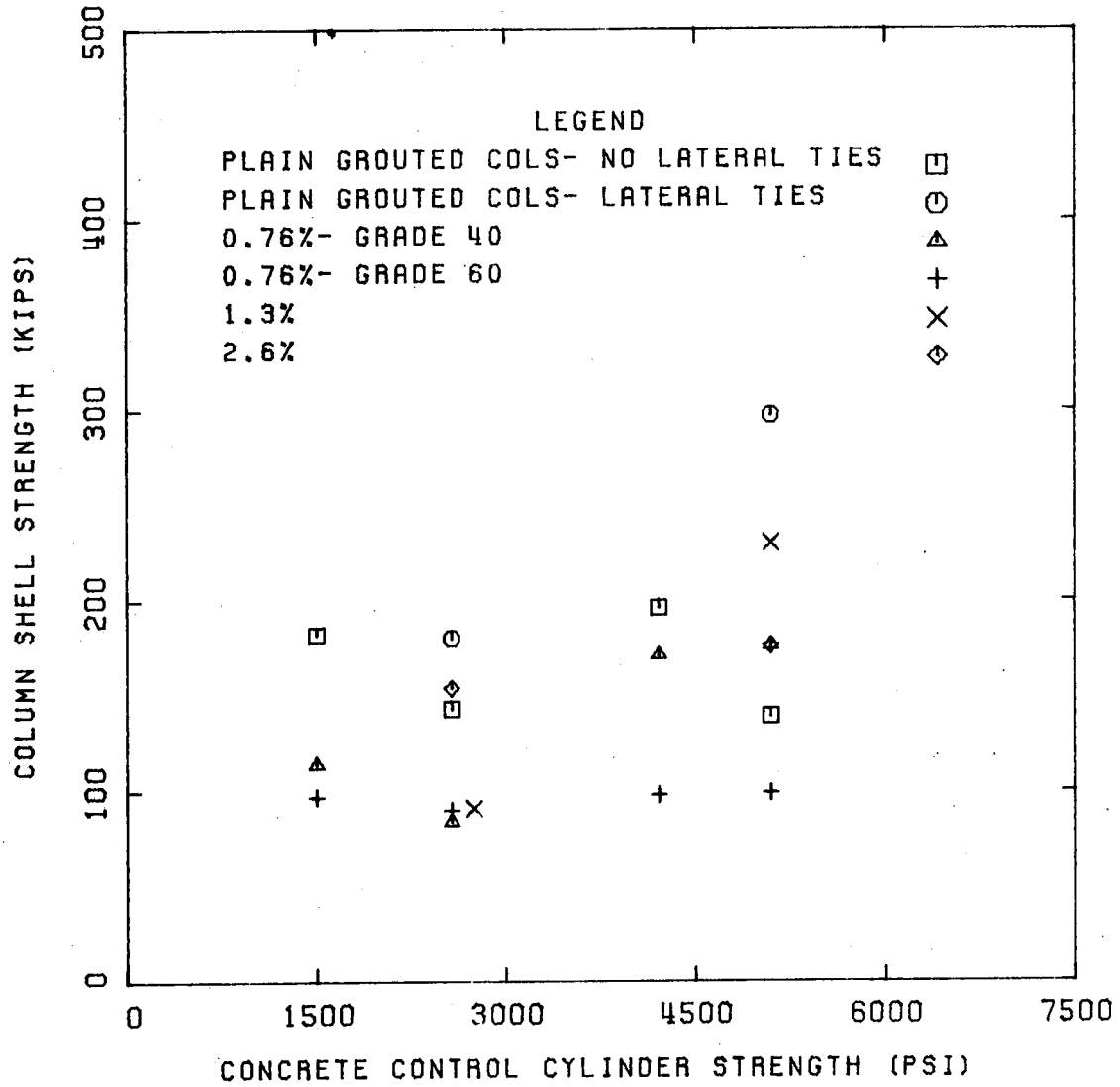

FIG. 5.11: SHELL STRENGTH VS. CONTROL CYLINDER STRENGTH

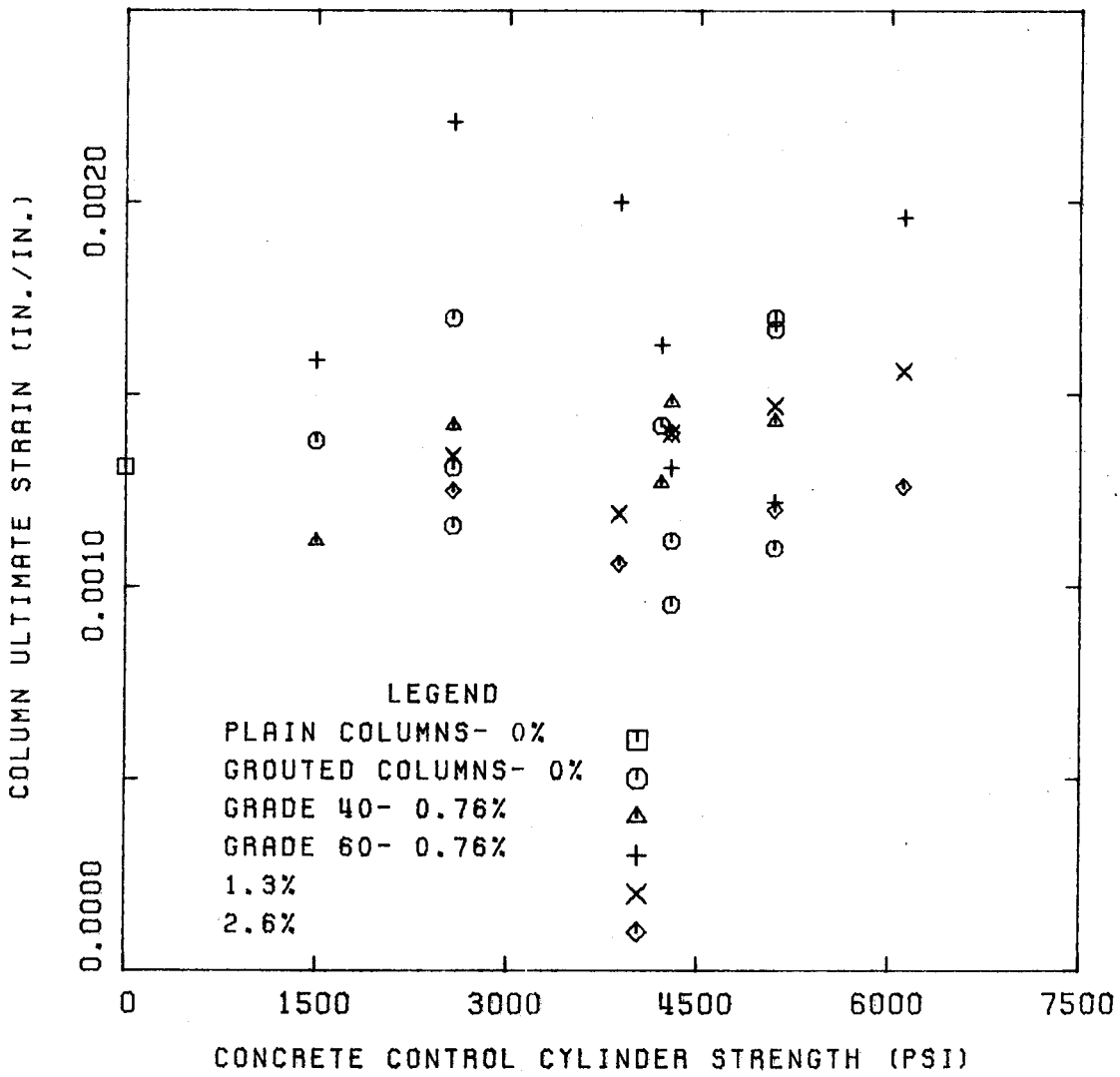

FIG. 5.12: COLUMN ULTIMATE STRAIN VS. CYLINDER STRENGTH

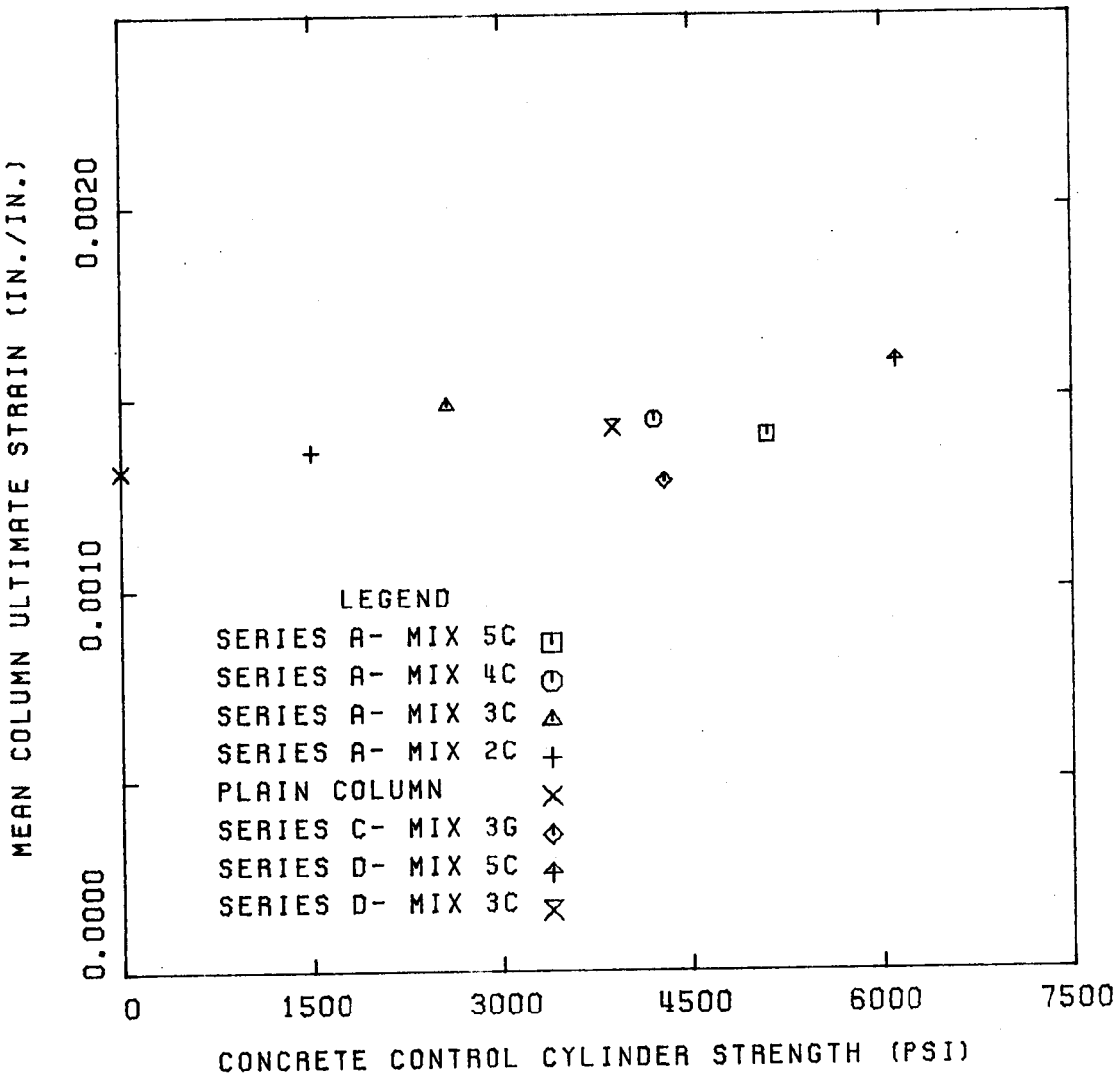

FIG. 5.13: MEAN ULTIMATE STRAIN VS. CYLINDER STRENGTH

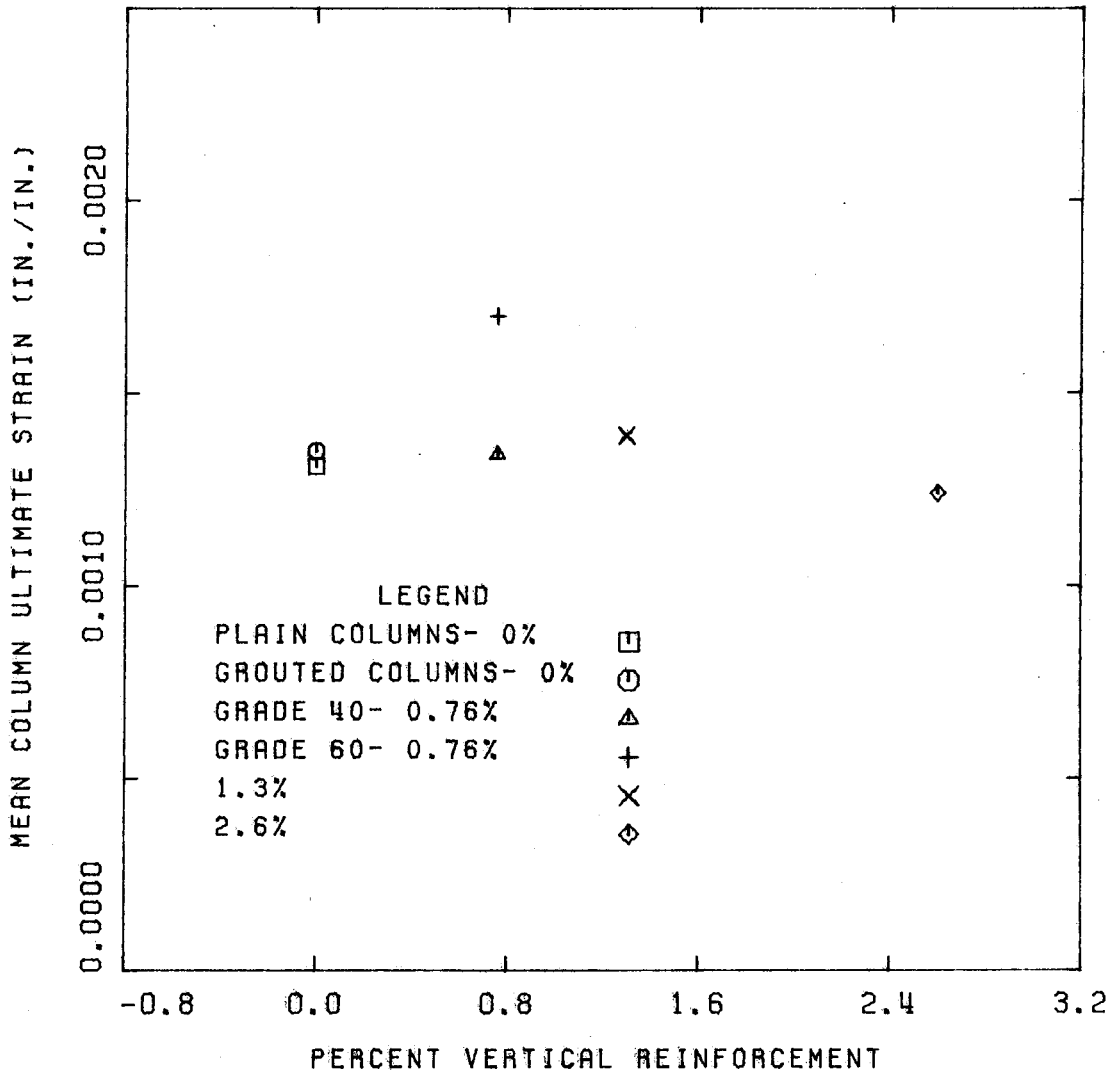

FIG. 5.14: MEAN ULTIMATE STRAIN VS. % VERTICAL REBAR

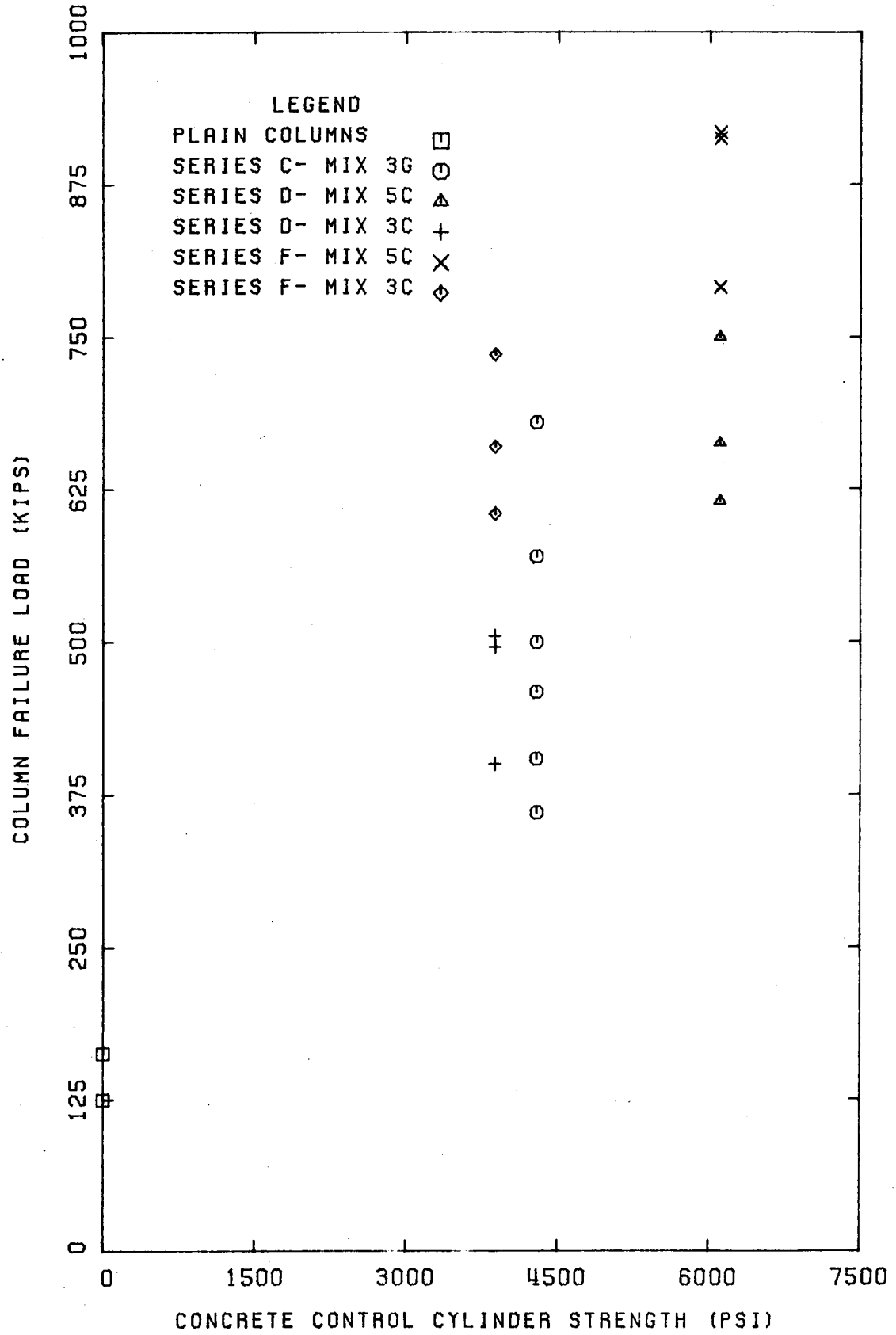

FIG. 5.15(a): COLUMN FAILURE LOAD VS. CYLINDER STRENGTH

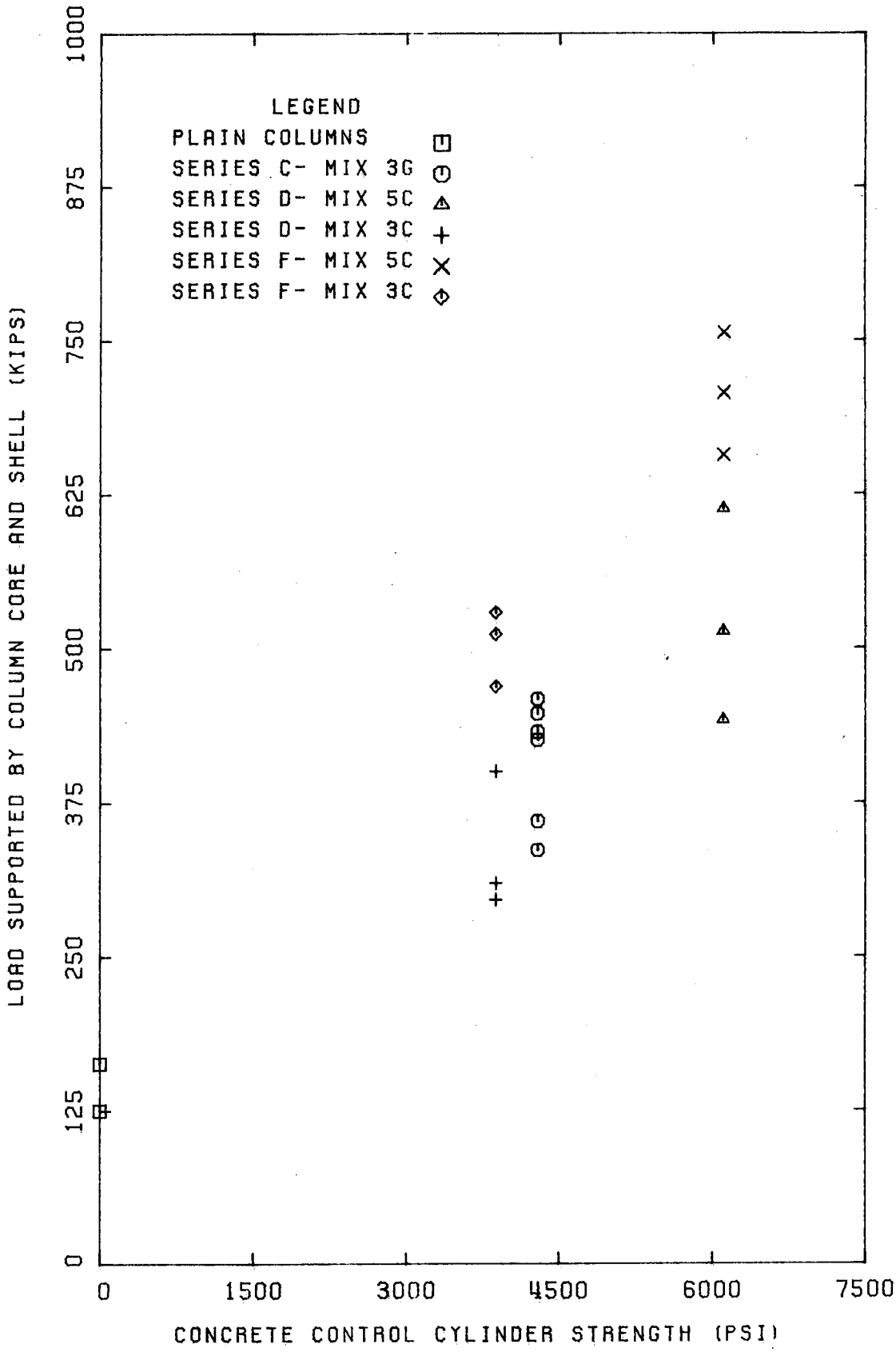

FIG. 5.15(b): (CORE + SHELL) LOAD VS. CYLINDER STRENGTH

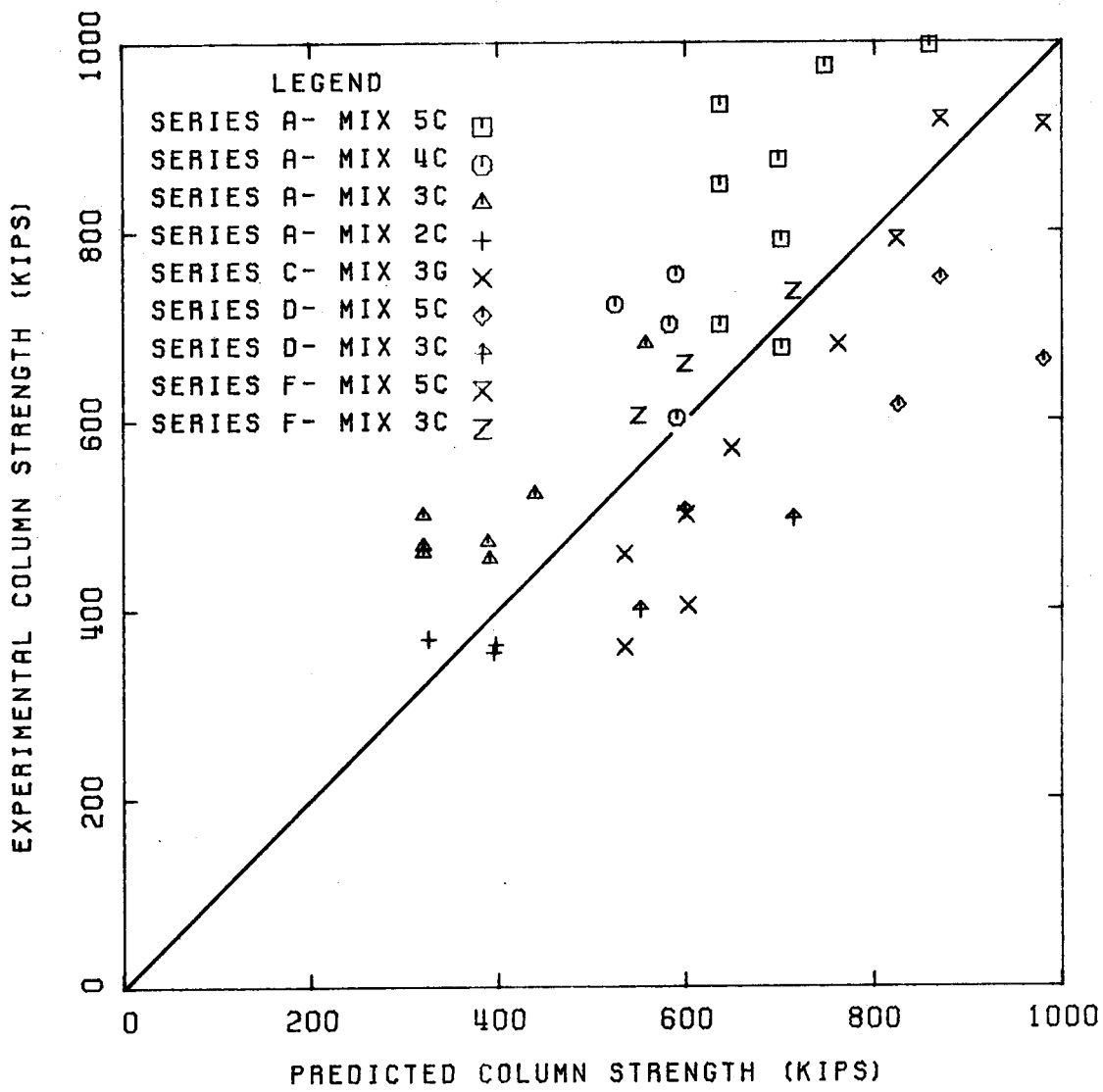

FIG. 5.16: PREDICTED COLUMN STRENGTH (EQ. 5.6)

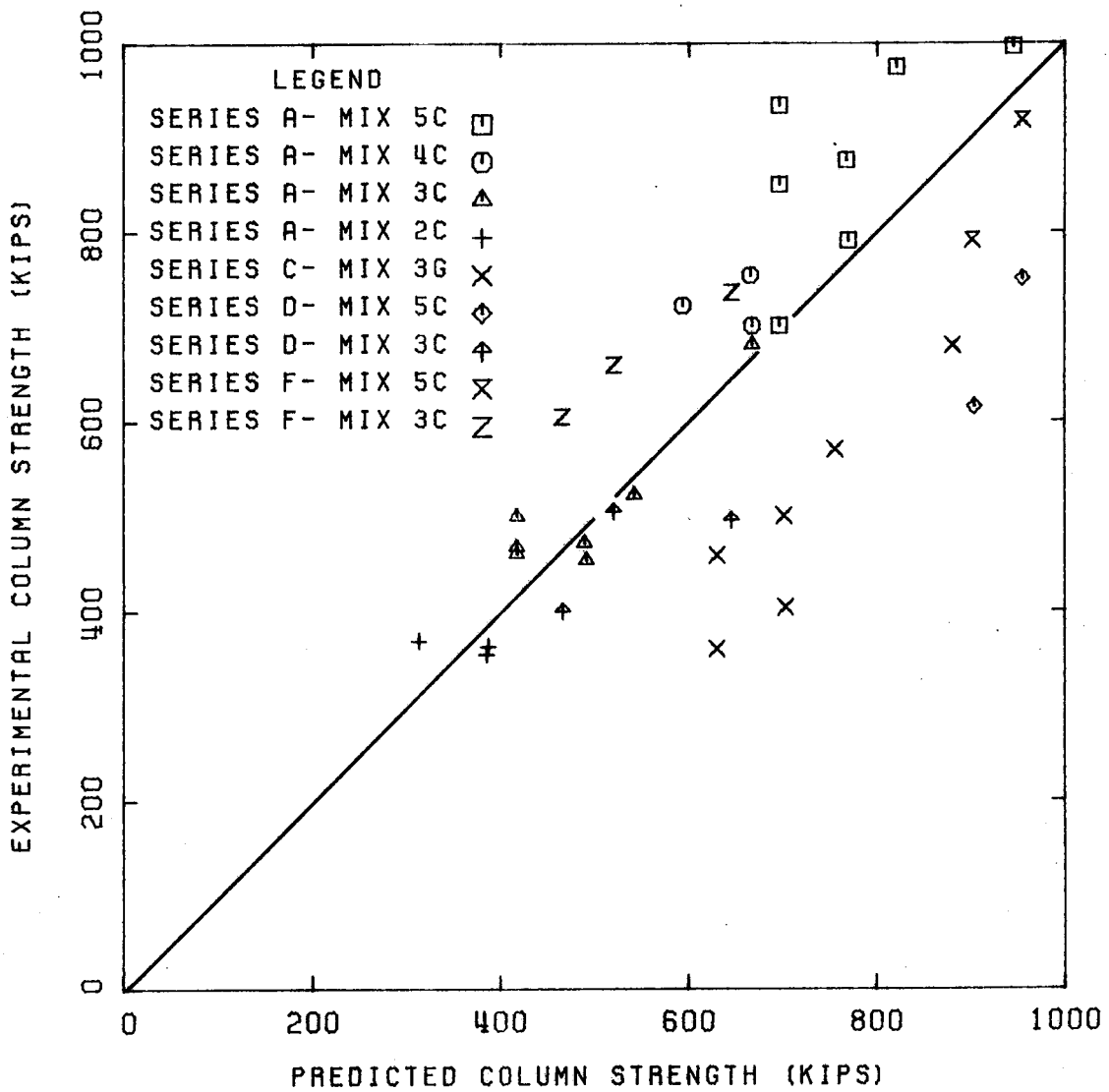

FIG. 5.17: PREDICTED COLUMN STRENGTH (PRISM METHOD)

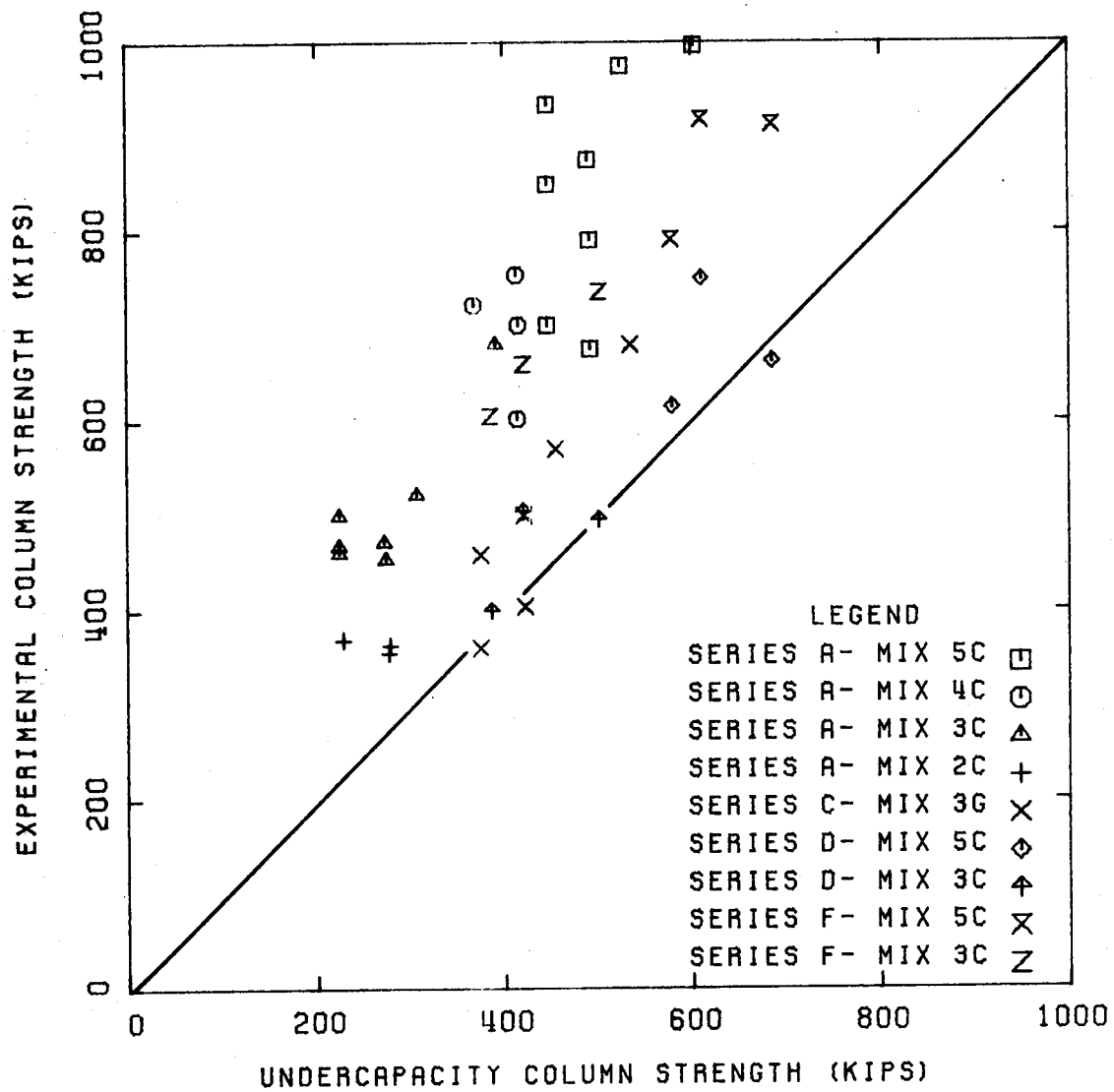

FIG. 5.18: UNDERCAPACITY COLUMN STRENGTH (EQ. 5.6)

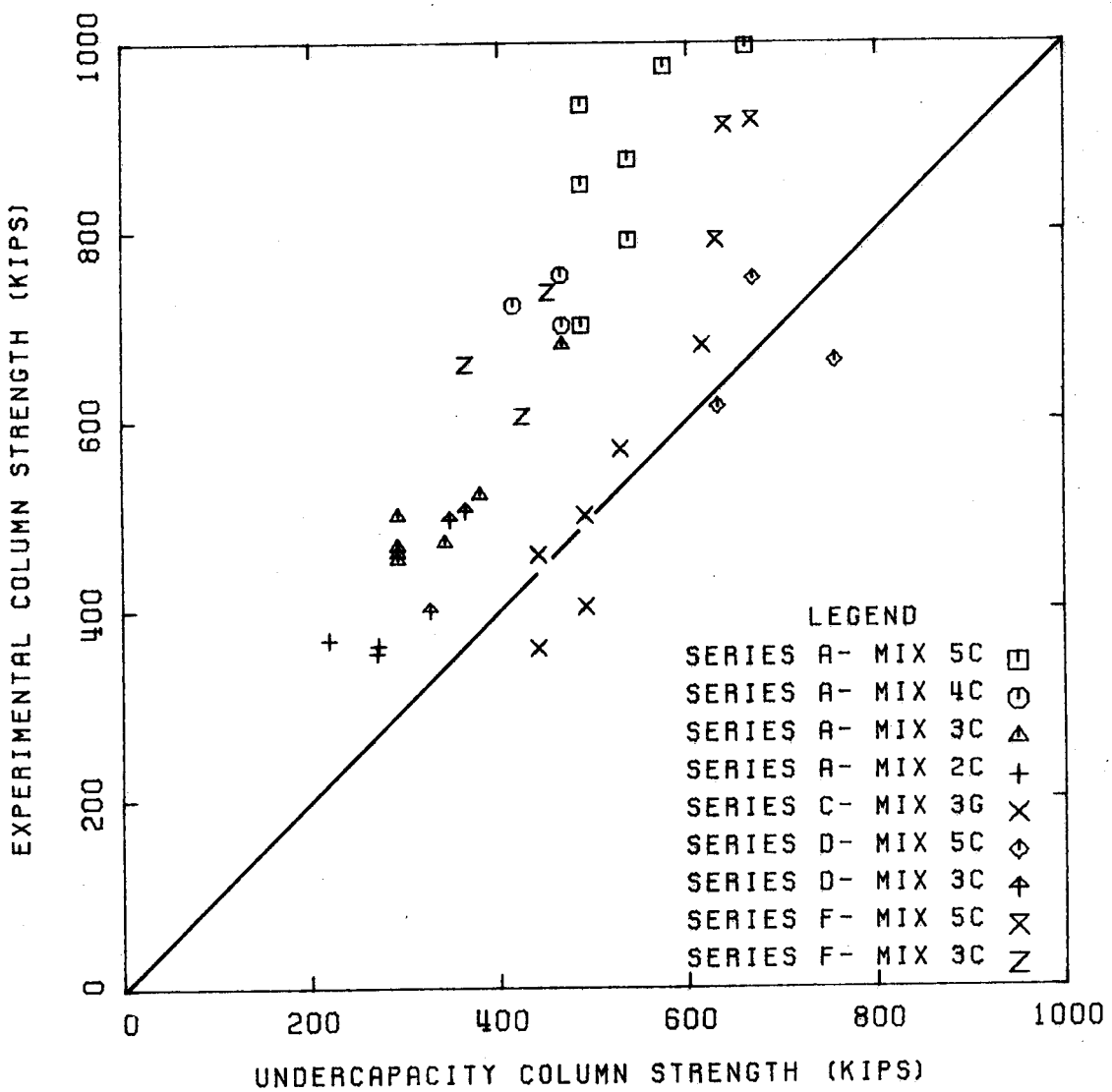

FIG. 5.19: UNDERCAPACITY COLUMN STRENGTH (PRISM METHOD)

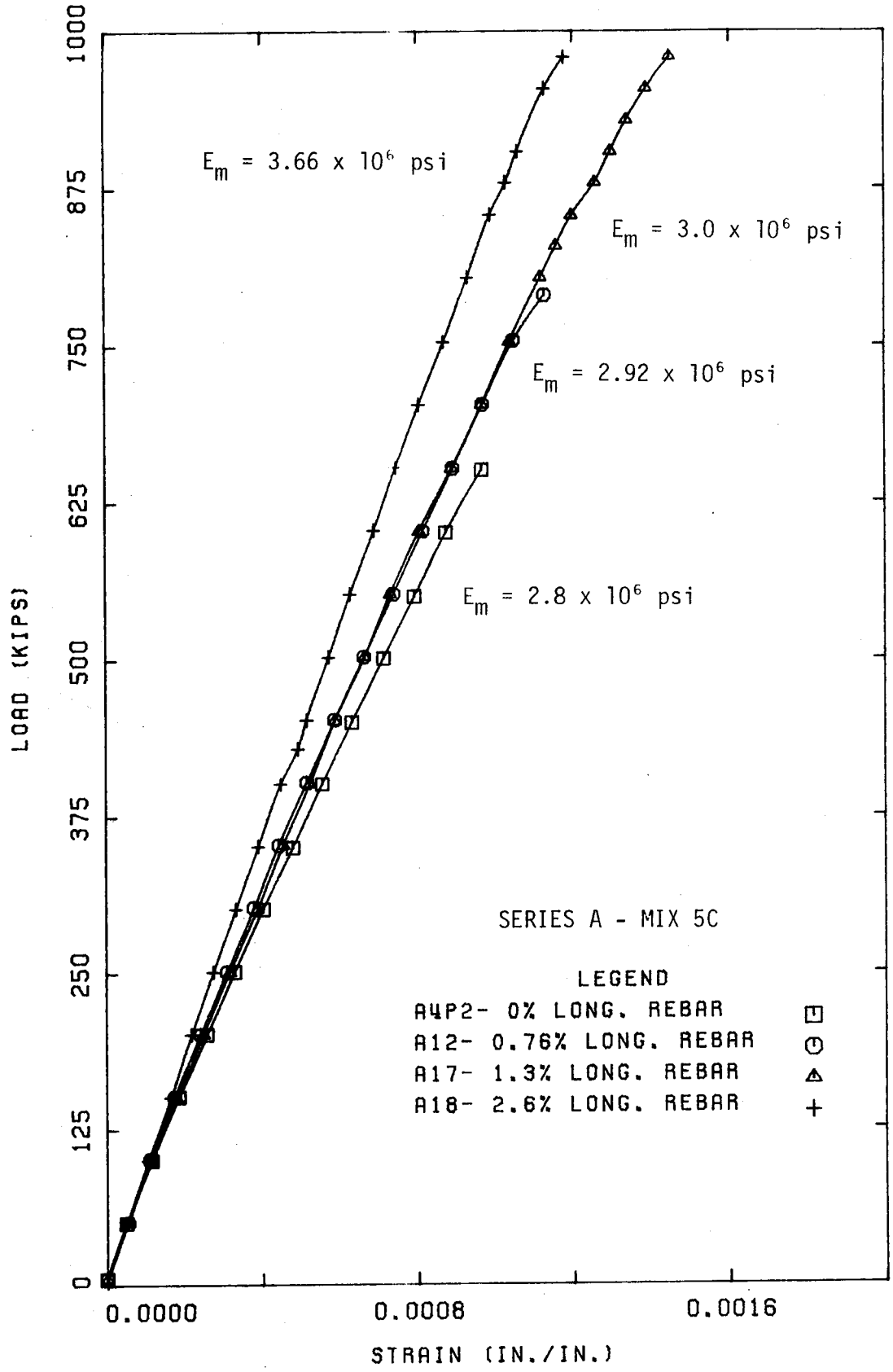

FIG. 5.20: COLUMN ELASTIC MODULI

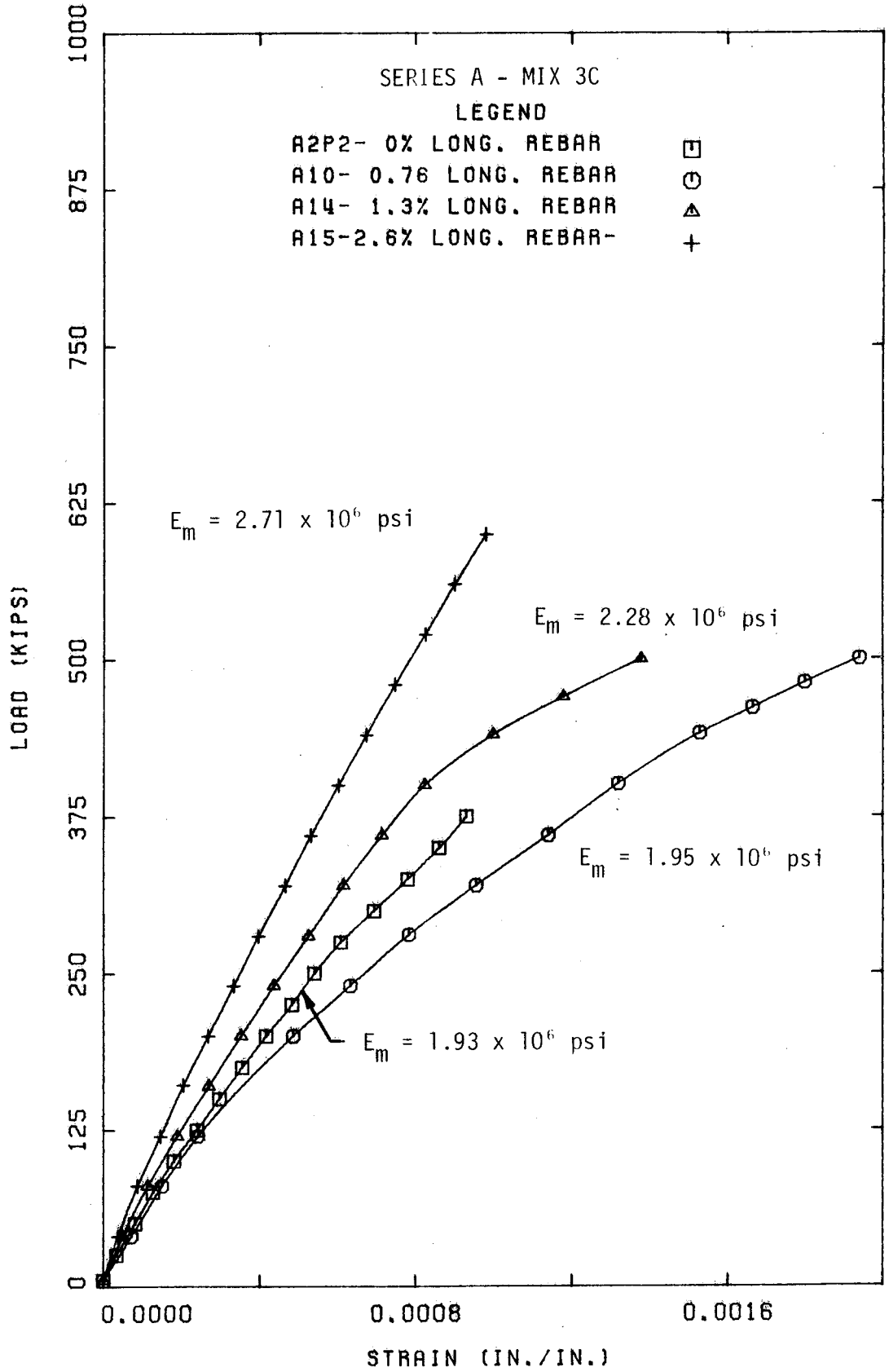

FIG. 5.21: COLUMN ELASTIC MODULI

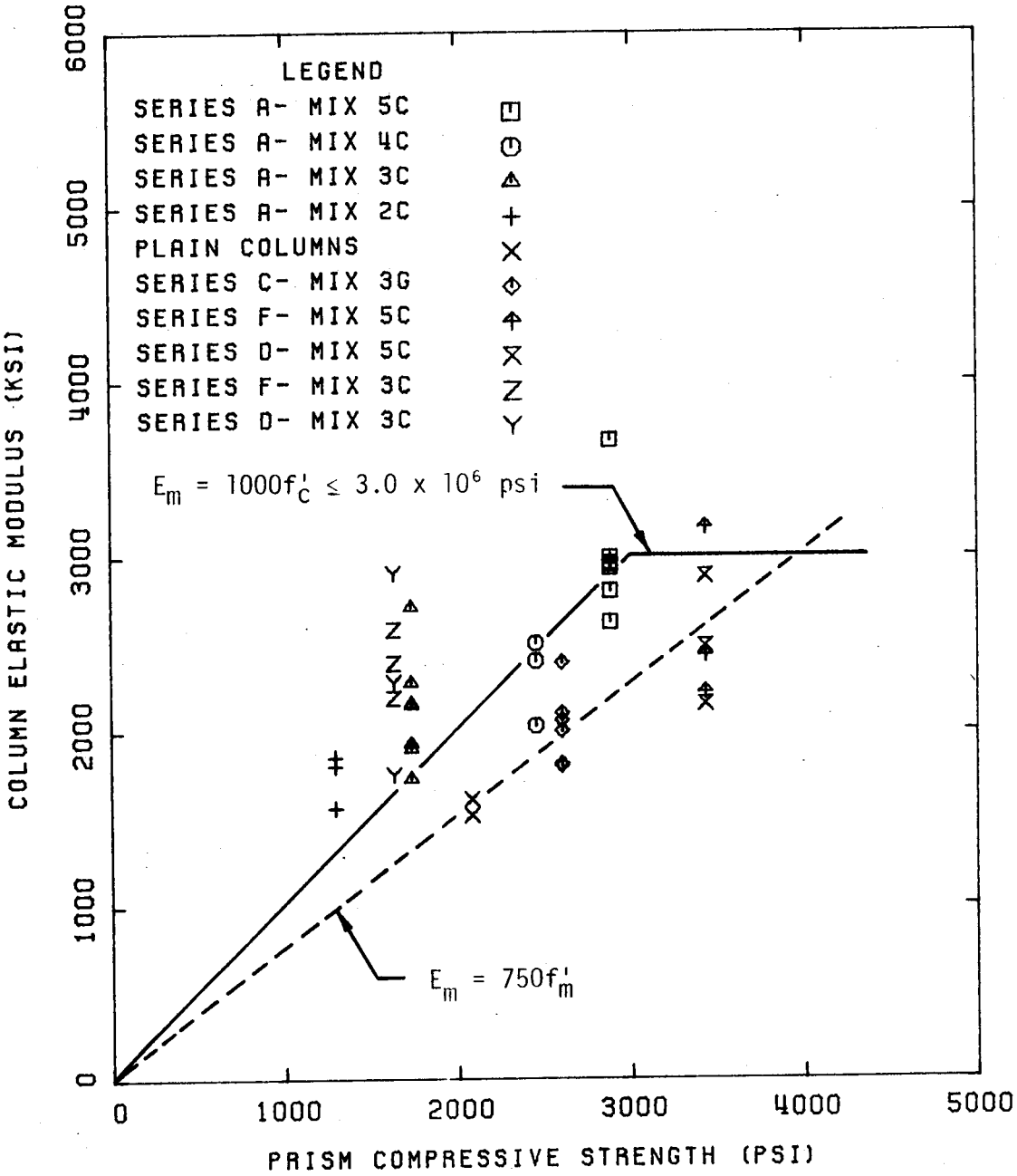

FIG. 5.22: COLUMN ELASTIC MODULUS VS. PRISM STRENGTH

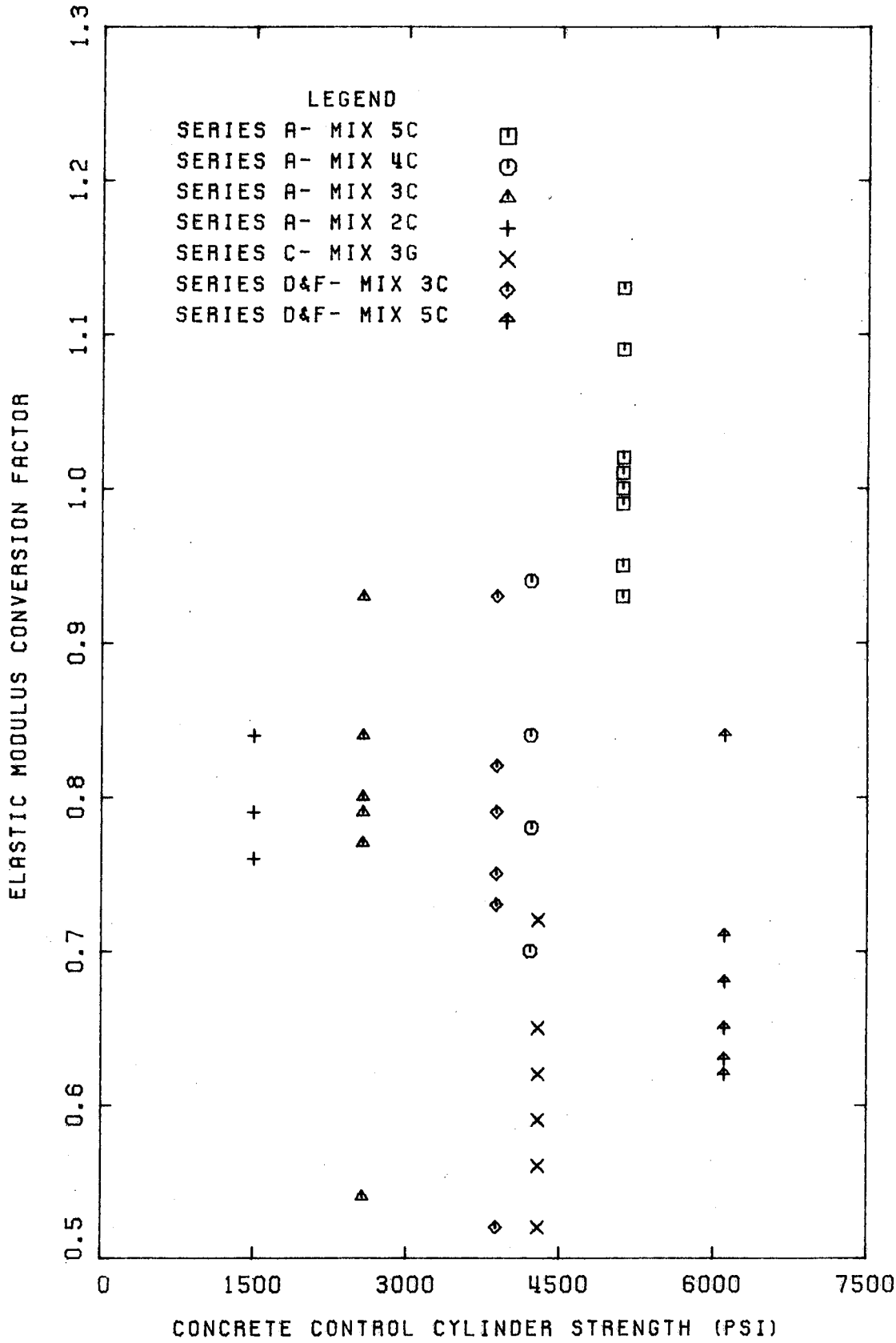

FIG. 23: ELASTIC MODULUS CONVERSION FACTORS

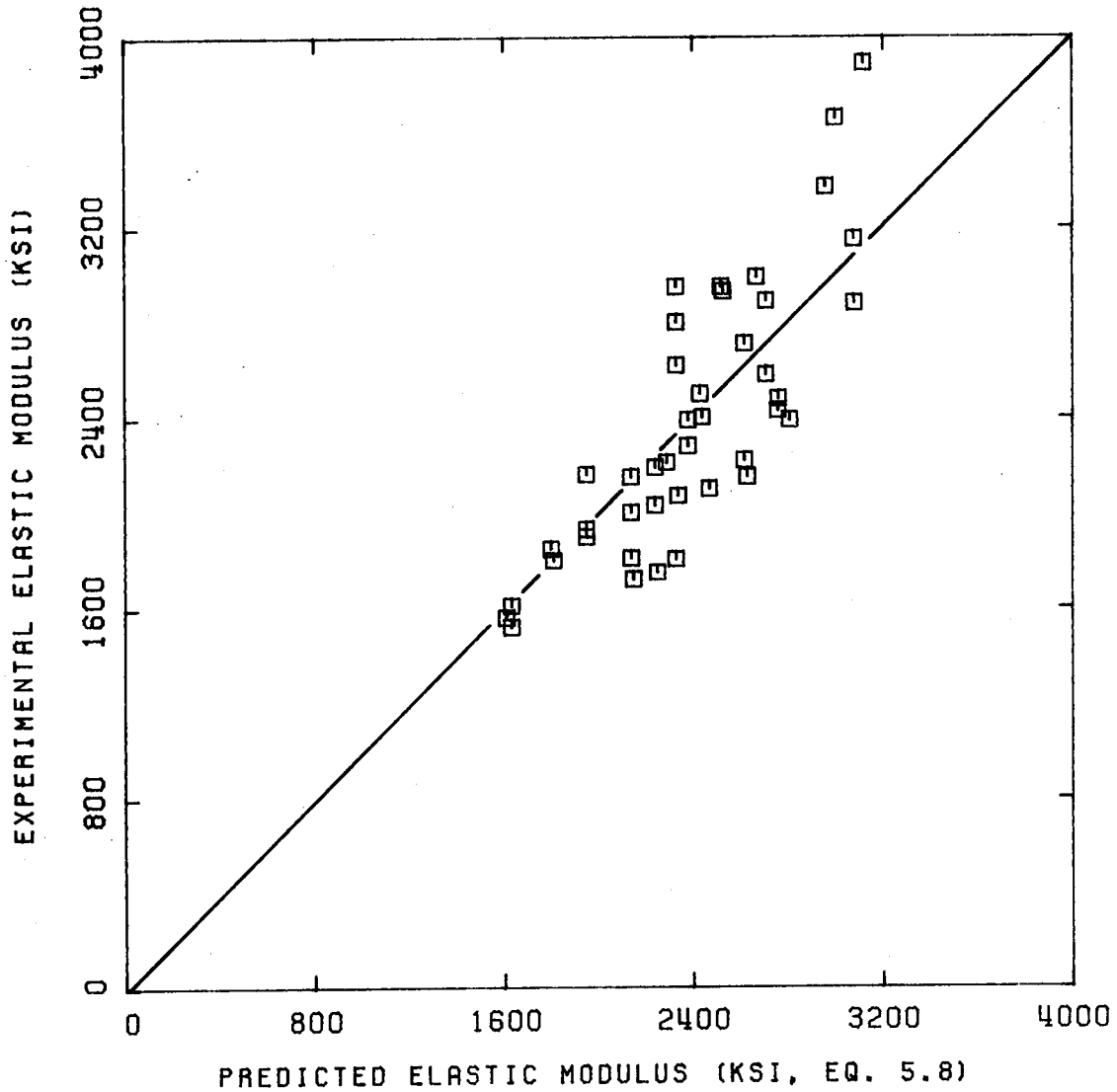

FIG. 5.24: PREDICTED COLUMN ELASTIC MODULUS

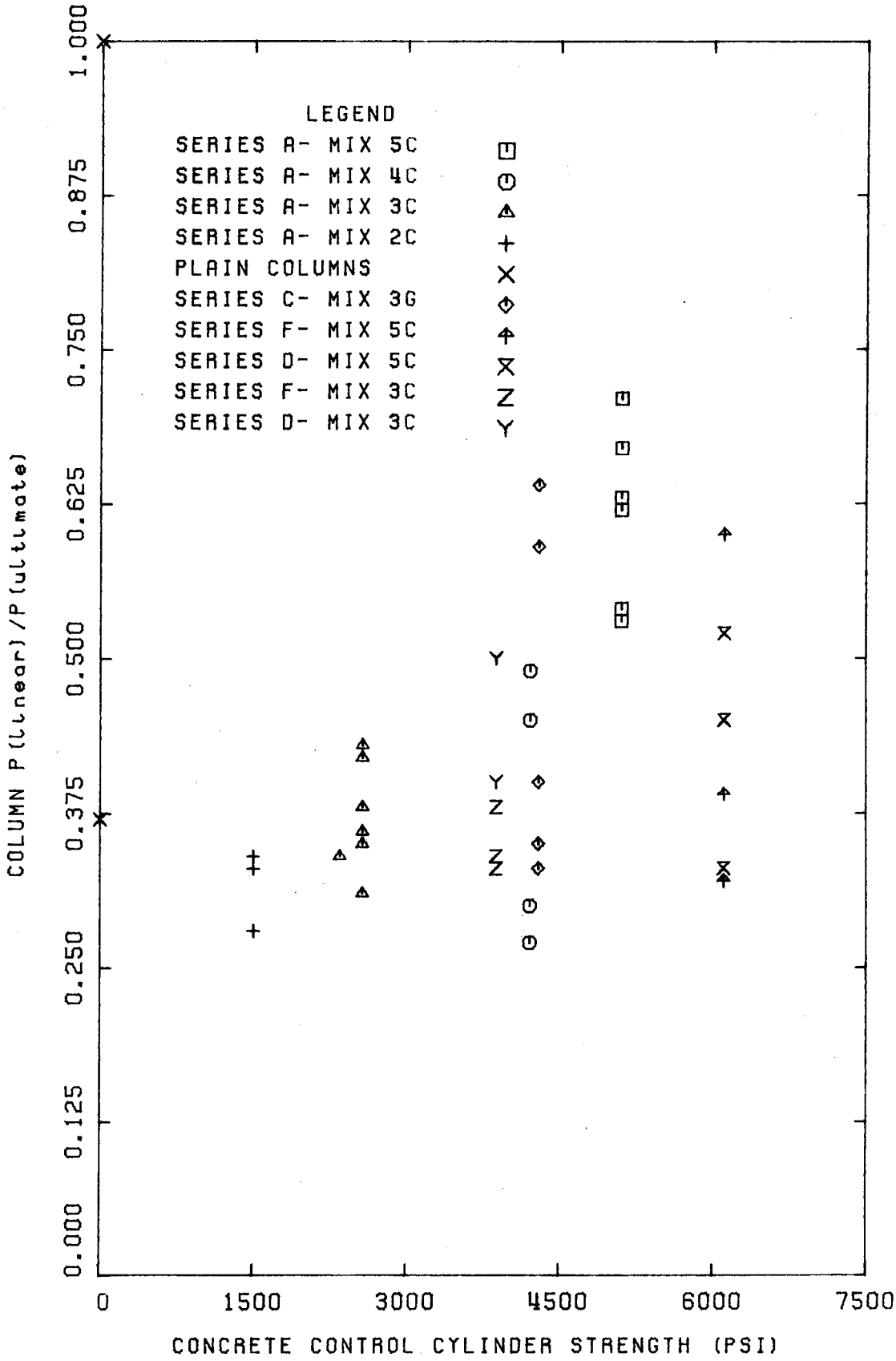

FIG. 5.25: P(linear)/P(ultimate) VS. CYLINDER STRENGTH

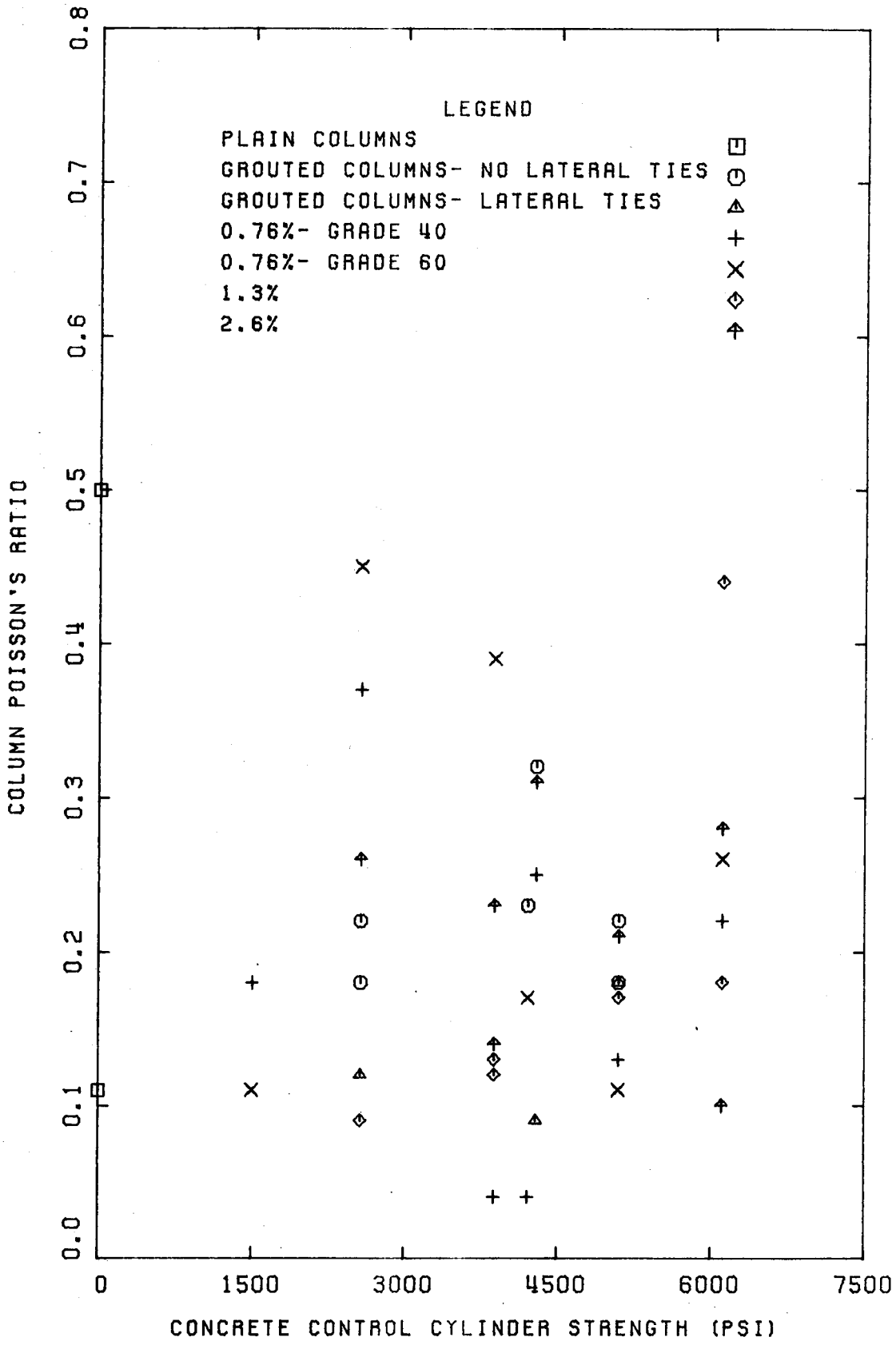

FIG. 5.26: COLUMN POISSON'S RATIO VS. CYLINDER STRENGTH

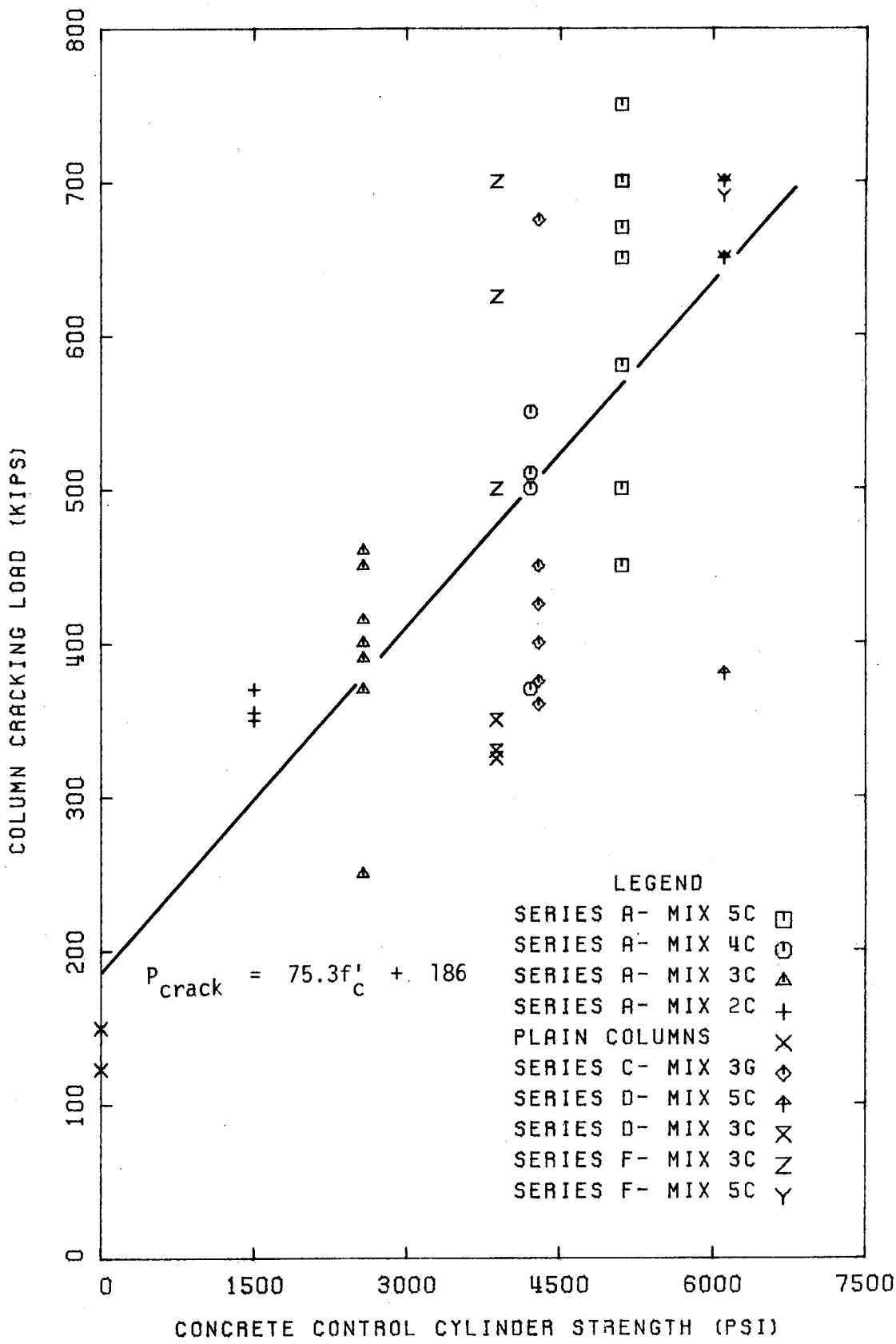

FIG. 5.27: COLUMN CRACKING LOAD VS. CYLINDER STRENGTH

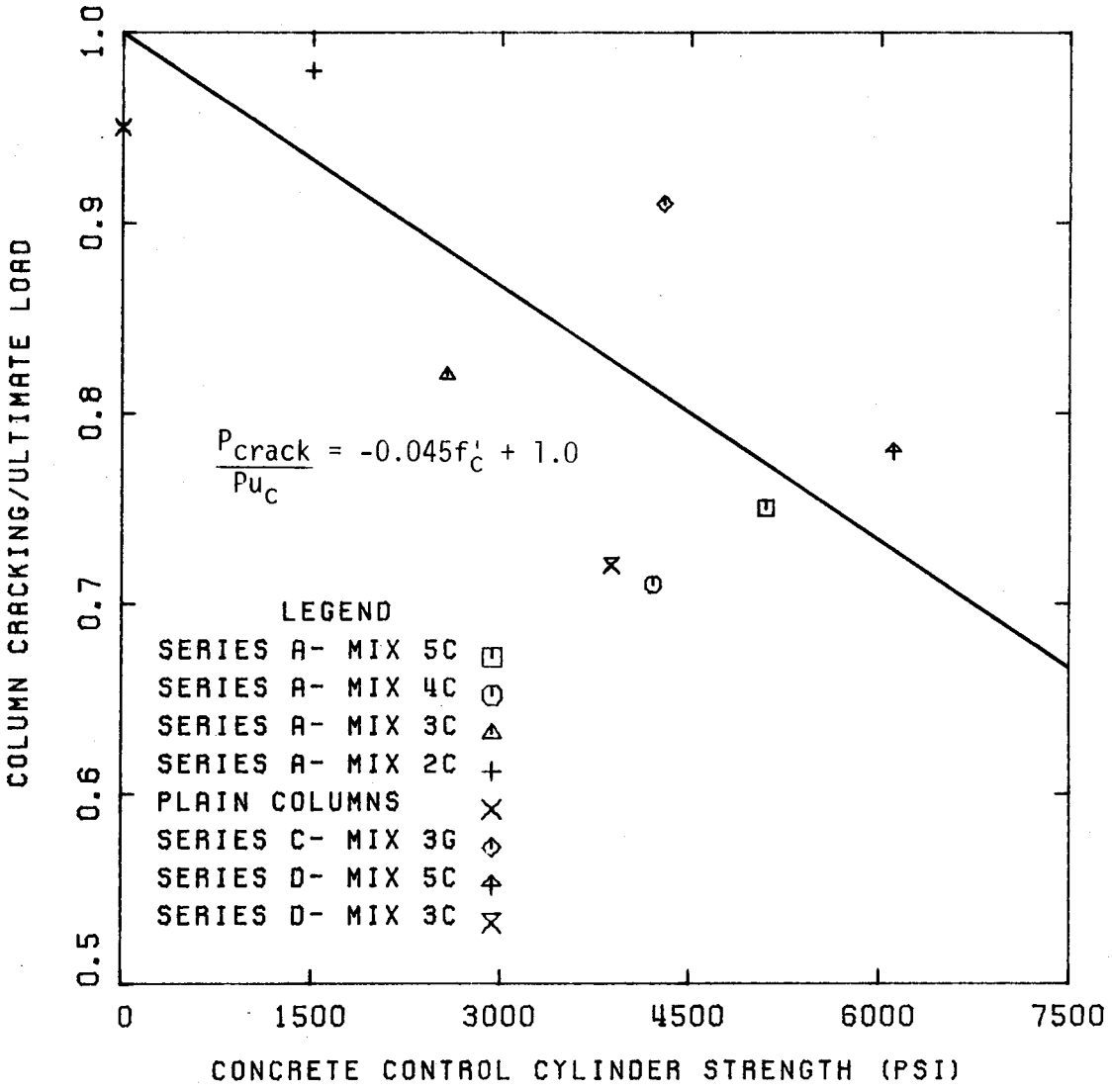

FIG. 5.28: COLUMN CRACKING/ULTIMATE LOAD

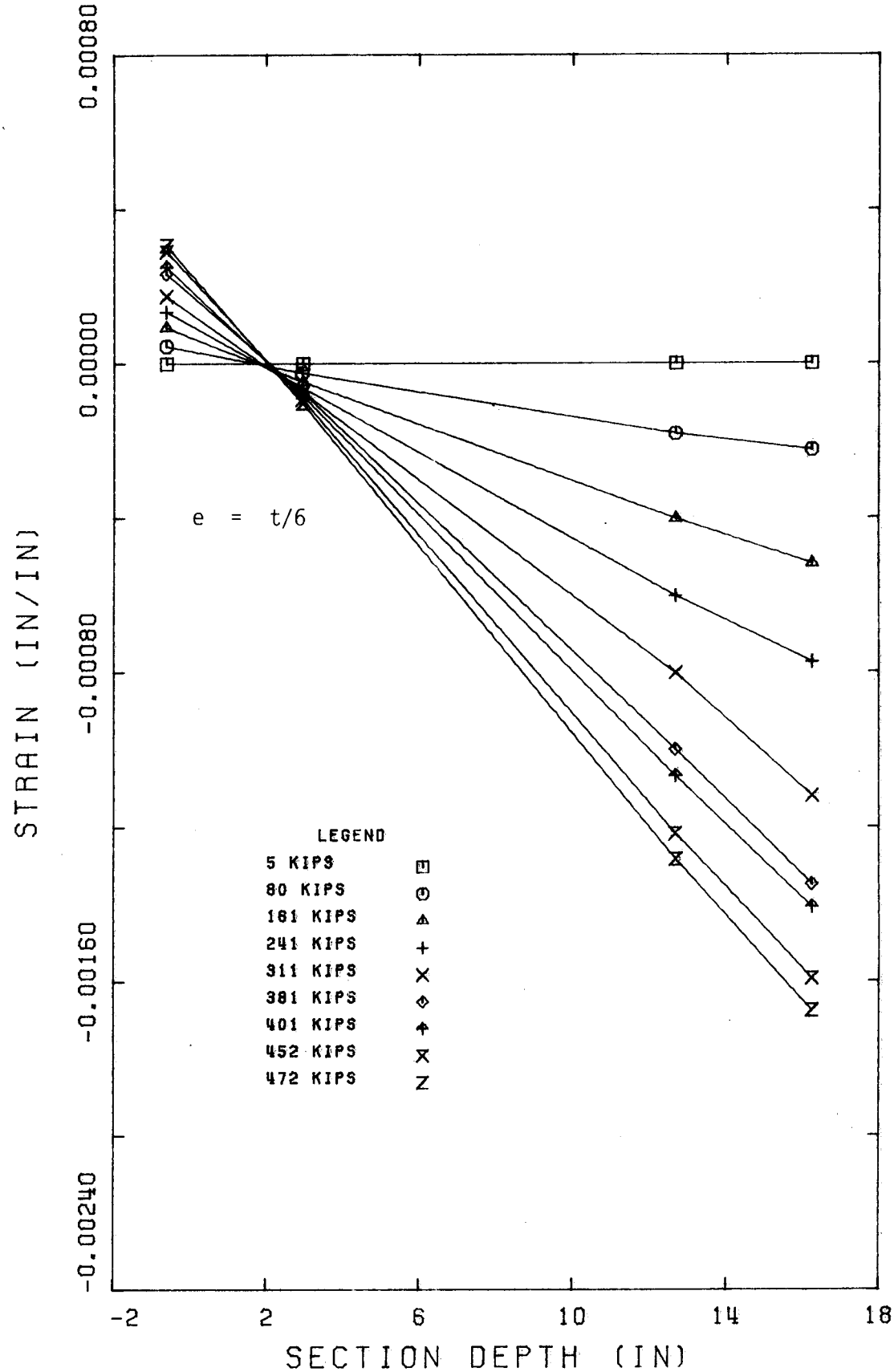

FIG. 5.29: STRAIN ACROSS COLUMN CROSS-SECTION, e = t/6
COLUMN: E4P2

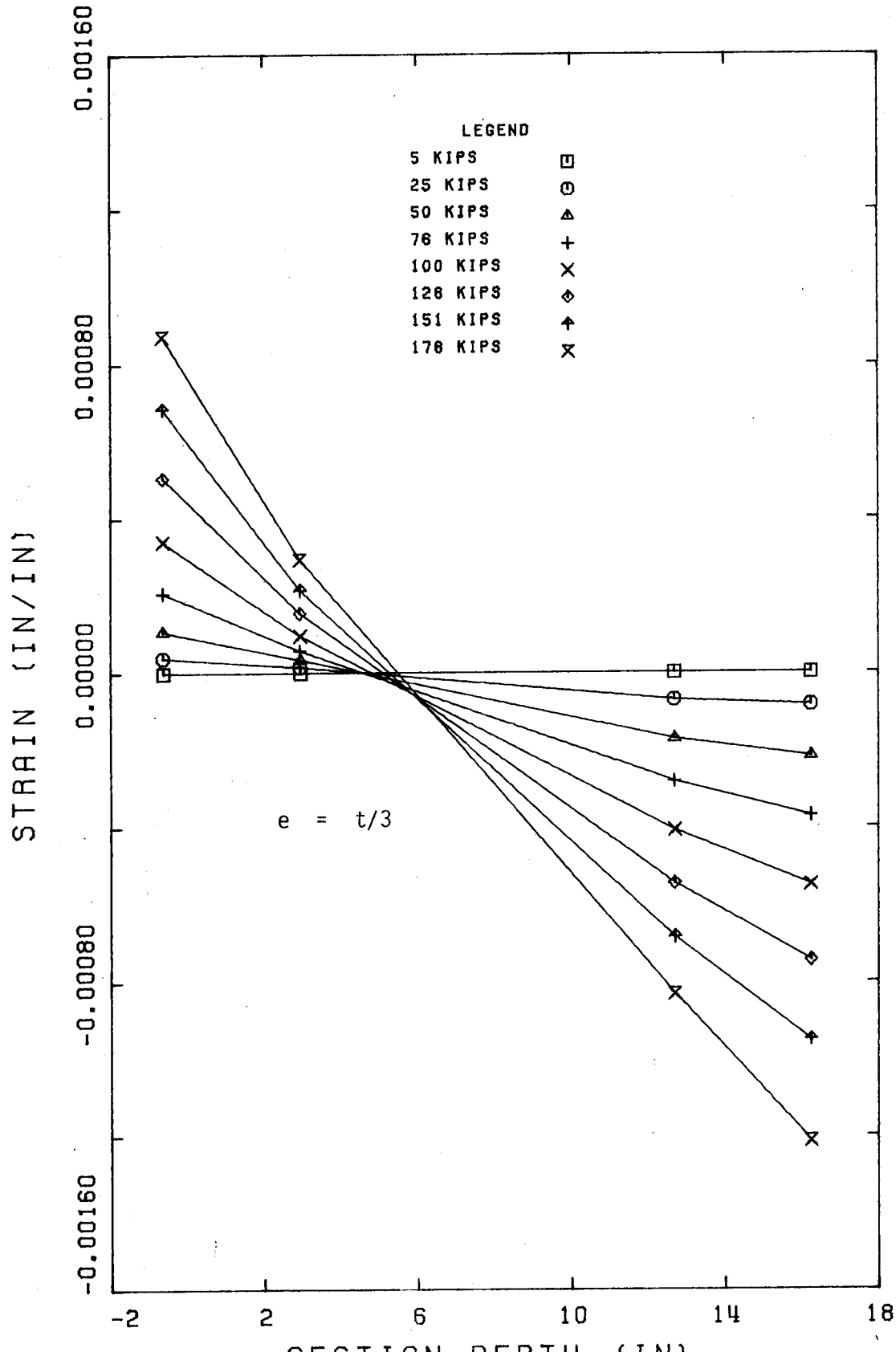

FIG. 5.30: STRAIN ACROSS COLUMN CROSS-SECTION, e = t/3

COLUMN: E5P3

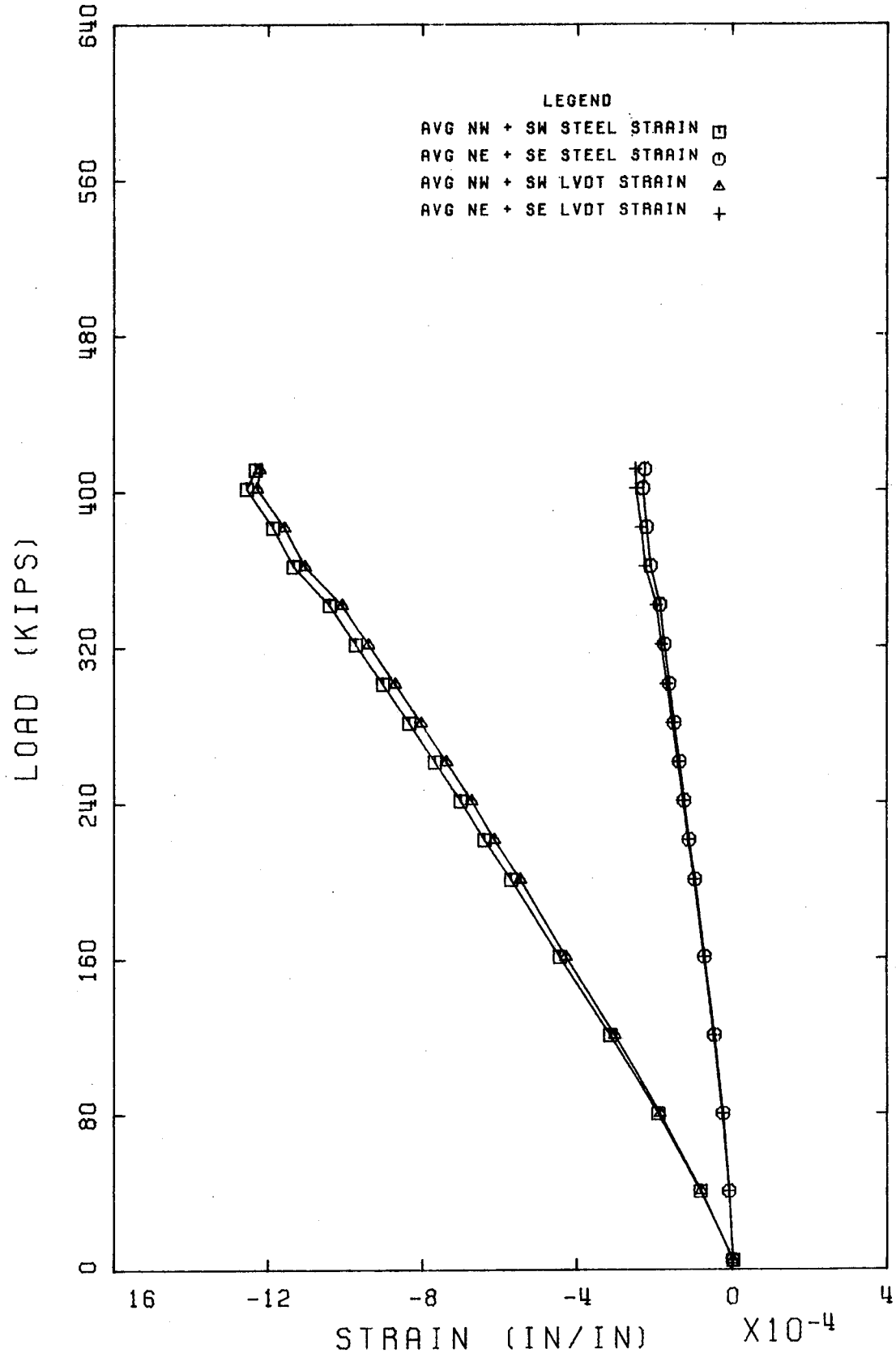

FIG. 5.31: AVERAGE SR-4 STEEL STRAINS AND LVDT STRAINS
COLUMN: E5P2

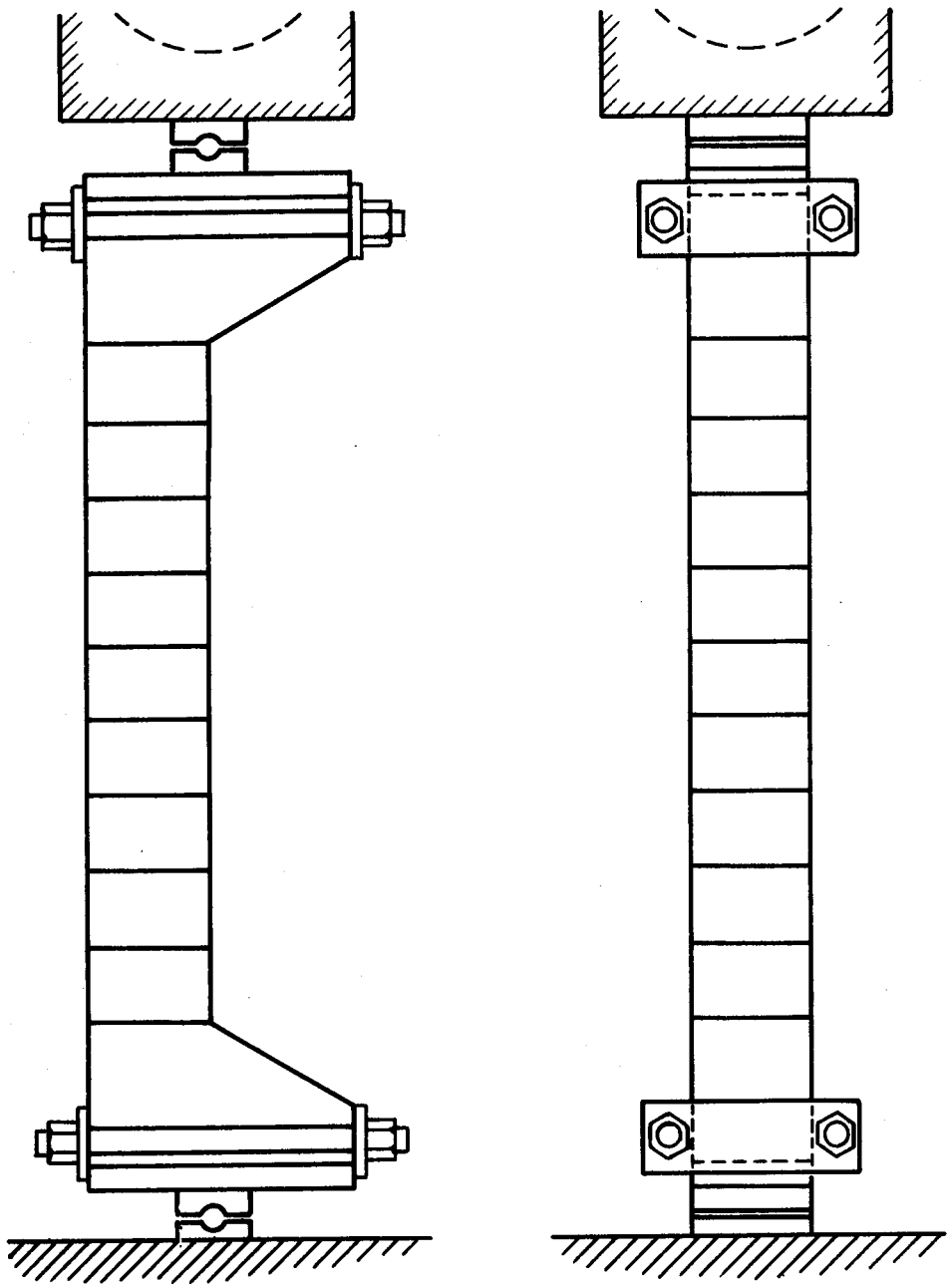

FIGURE 5.32 Proposed Testing Arrangement

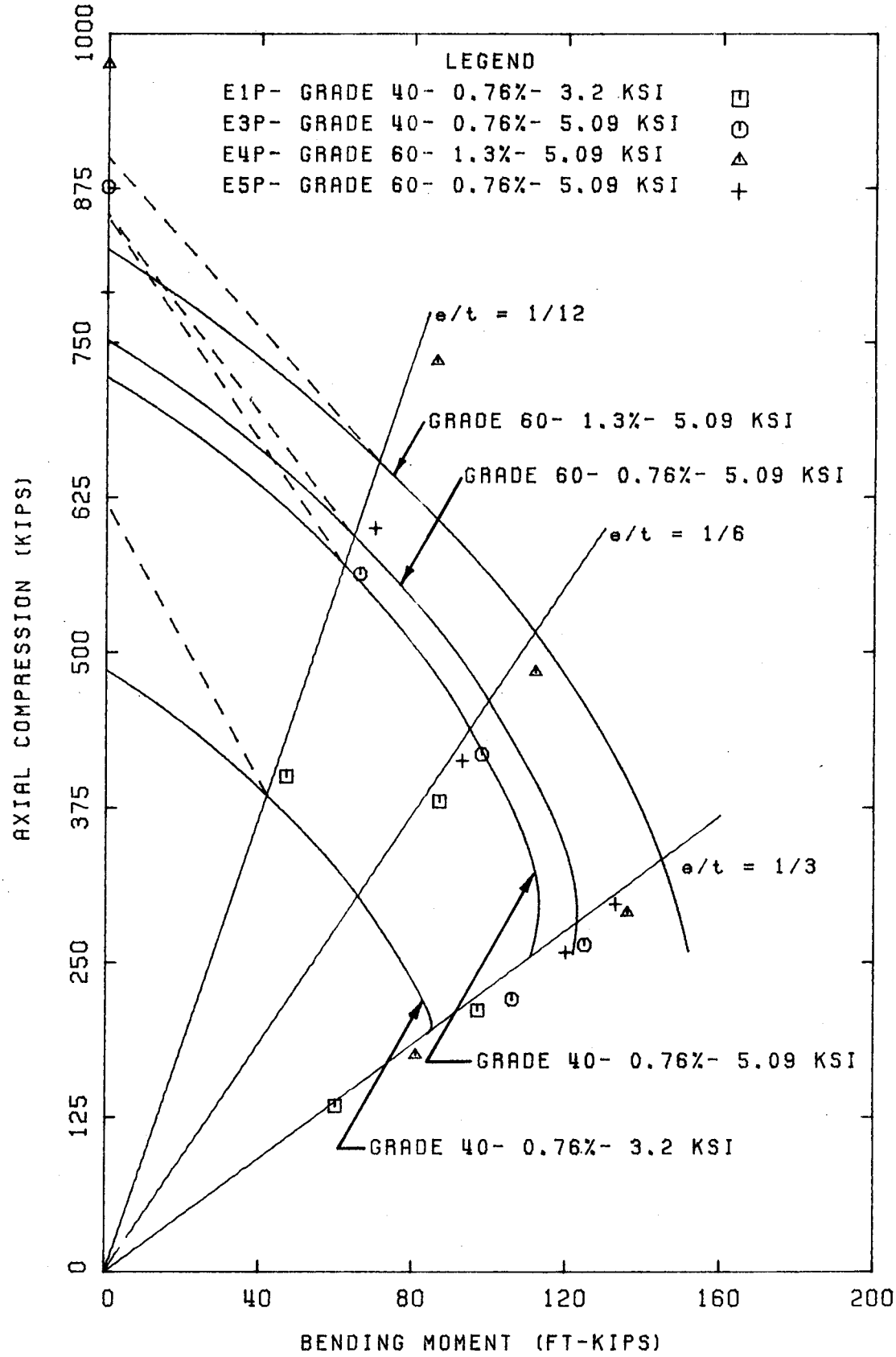

FIG. 5.33: MASONRY COLUMN INTERACTION DIAGRAM

Table 5.1 Column Test Results

Series A - Mix 5C

Col no.	Steel Area	Steel Grade	Concrete Strength	Column Test	Failure Location	Failure Mode	Failure Load	% of Pu_c at which LVDT's Removed	Ultimate Strain						Load Taken by Steel	Load Taken by Core & Shell
									Lateral Steel	Lateral Concrete	Concrete Block	Vertical Steel	Masonry LVDT's	Avg of Steel & LVDT		
	A_s (in^2)	(ksi)	f'_c (psi)				Pu_c (kips)	(%)	(in/in)	(in/in)	ε_b (in/in)	ε_s (in/in)	ε_{m1} (in/in)	ε_m (in/in)	$\varepsilon_m E_s A_s$ (kips)	(kips)
A4.1	0	--	5100	UP	TOP	A	701	73	-------	0.00020	0.00089	-------	0.00110	0.00110	---	701
A4.2	0	--	"	INV	BOT	A	850	77	-------	0.00016	0.00150	-------	0.00170	0.00170	---	850
A8	1.86	40	"	UP	TOP	B	876	100	0.00018	0.00016	0.00145	0.00140	0.00145	0.00143	72	804
A12	1.86	60	"	UP	TOP	B	791	100	0.00012	0.00015	0.00112	0.00114	0.00130	0.00122	63	728
A16	0*	--	"	UP	TOP	A	934	80	0.00043	0.00033	0.00133	-------	0.00167	0.00167	---	934
A17	3.1	60	"	UP	TOP	C	975	87	0.00028	0.00023	0.00130	0.00145	0.00149	0.00147	129	846
A18	6.2	60	"	UP	TOP	C	997	100	-------	0.00021	0.00100	0.00118	0.00122	0.00120	211	786
B3	1.86	60	"	UP	TOP	B	676	100	0.00017	0.00025	0.00105	0.00118	0.00120	0.00119	62	614
Avg.																807
C.V.																9.8%

Series A - Mix 4C

A3	0	--	4210	UP	TOP	A	722	100	-------	0.00036	0.00102	-------	0.00142	0.00142	---	722
A7	1.86	40	"	INV	BOT	B	754	100	0.00068	0.00015	0.00115	0.00126	0.00128	0.00127	64	658
A11	1.86	60	"	UP	CENT	B	701	---	0.00047	0.00080	0.00159	0.00163	-------	0.00163	84	616
B2	1.86	60	"	UP	TOP	C	602	92	0.00010	0.00043	0.00092	0.00134	0.00142	0.00138	71	530
Avg.																665
C.V.																8.0%

Series A - Mix 3C

A2.1	0	--	2570	UP	TOP	A	468	96	-------	0.00017	0.00110	-------	0.00131	0.00131	---	468
A2.2	0	--	"	INV	BOT	A	461	100	-------	0.00033	0.00127	-------	0.00116	0.00116	---	461
A6	1.86	40	"	UP	TOP	B	472	100	0.00012	0.00075	0.00115	0.00147	0.00136	0.00142	71	401
A10	1.86	60	"	UP	TOP	B	454	100	0.00038	0.00036	0.00130	0.00225	0.00217	0.00221	114	340
A13	0*	--	"	UP	TOP	A	500	94	0.00011	0.00390	0.00135	-------	0.00170	0.00170	---	500
A14	3.1	60	"	UP	TOP	C	522	96	0.00010	0.00011	0.00100	0.00124	0.00143	0.00134	118	405
A15	6.2	60	"	INV	TOP	C	681	100	0.00014	0.00038	0.00100	0.00125	0.00127	0.00126	219	461
B1†	1.86	60	"	INV	BOT	C	301	100	0.00016	0.00015	0.00113	0.00180	0.00217	0.00199	103	198
Avg.																434
C.V.																12.5%

Series A - Mix 2C

A1	0	--	1500	INV	BOT	A	369	81	-------	0.00031	0.00118	-------	0.00138	0.00138	---	369
A5	1.86	40	"	UP	TOP	C	355	100	0.00013	0.00036	0.00090	0.00110	0.00114	0.00112	36	299
A9	1.86	60	"	UP	TOP	C	363	96	0.00032	0.00012	0.00088	0.00151	0.00159	0.00156	81	282
Avg.																317
C.V.																14.5%

Plain Columns

A19	0	--	0	UP	---	-	163	92	-------	0.00011	0.00091	-------	0.00131	0.00131	-------	-------
A19.1	0	--	0	UP	---	-	125	44	-------	0.00026	0.00100	-------	-------	-------	-------	-------

Series C - Mix 3G

C1	0	--	4290	UP	TOP	A	360	100	-------	0.00031	0.00074	-------	0.00095	0.00095	---	360
C2	1.86	40	"	UP	TOP	B	500	92	-------	0.00018	0.00095	0.00148	0.00148	0.00148	74	426
C3	1.86	60	"	UP	TOP	C	404	93	-------	0.00012	0.00070	0.00131	0.00131	0.00131	68	337
C4	0*	--	"	UP	TOP	A	459	100	0.00060	------	0.00101	-------	0.00112	0.00112	---	459
C5	3.1	60	"	UP	TOP	B	570	97	0.00050	0.00031	0.00154	0.00138	0.00141	0.00140	123	447
C6	6.2	60	"	UP	TOP	C	680	99	0.00018	0.00034	0.00105	0.00147	0.00135	0.00141	247	433
Avg.																410
C.V.																12.1%

Series D & F - Mix 5C

D12	1.86	60	6110	UP	CENT	B	615	65	0.00268	0.00070	0.00167	0.00208	0.00184	0.00196	102	514
D17	3.1	60	"	UP	CENT	C	750	100	0.00021	0.00016	0.00136	0.00168	0.00146	0.00157	137	613
D18	6.2	60	"	UP	TOP	C	663	84	0.00020	0.00054	0.00092	0.00130	0.00121	0.00126	221	442
F8	1.86	40	"	UP	TOP	B	791	94	-------	-------	-------	-------	0.00167	0.00167	84	707
F17	3.1	60	"	UP	TOP	B	918	92	0.00230	-------	0.00140	0.00198	0.00170	0.00184	161	757
F18	6.2	60	"	UP	TOP	B	913	95	0.00110	0.00028	0.00123	0.00144	0.00147	0.00146	256	657
Avg.																523 707
C.V.																16.4% 7.0%

Series D & F - Mix 3C

D10	1.86	60	3880	UP	TOP	C	400	82	0.00091	-------	0.00105	0.00210	0.00190	0.0020	104	297
D14	3.1	60	"	UP	TOP	C	505	89	0.00009	0.00026	0.00113	0.00133	0.00105	0.00119	104	401
D15	6.2	60	"	UP	TOP	C	496	66	0.00008	-------	0.00134	0.00106	0.00106	0.00106	186	310
F6	1.86	40	"	UP	TOP	B	605	95	0.00018	0.00031	0.00158	0.00144	0.00157	0.00151	76	529
F14	3.1	60	"	UP	TOP	B	660	95	0.00036	0.00030	0.00129	0.00174	0.00164	0.00169	148	512
F15	6.2	60	"	UP	CENT	B	736	95	-------	0.00046	0.00157	0.00151	0.00152	0.00152	267	469
Avg.																336 503

Col no.	Adjusted Shell & Core Strength	Load Taken by Shell	Steel f_s/f_y at Failure	Predicted Pu_c		% Linearity of σ-ε Curve	Experimental Elastic Modulus					Predicted Elastic Modulus	Lateral Concrete Block Elastic Modulus	Poisson's Ratio	Cracking Load	$\frac{P_{crack}}{Pu_c}$
				Eq. 5.6	Prism Method		Concrete Block	Vertical Steel	Masonry LVDT's	Avg E_s & E_m	Elastic Modulus Conversion Factor					
	(kips)	(kips)	(%)	(kips)	(kips)	(%)	E_b (psi)	E_s (psi)	E_{ml} (psi)	E_m (psi)	K	(psi)	E_{bh} (psi)	$\nu = E_m/E_{bh}$	(kips)	
A4.1	701	65	--	637	696	71	3.38×10^6	--------	2.95×10^6	2.95×10^6	1.09	2.33×10^6	1.86×10^7	0.18	450	0.64
A4.2	850	213	--	637	696	53	3.10×10^6	--------	2.80×10^6	2.80×10^6	1.01	2.33×10^6	1.44×10^7	0.22	580	0.68
A8	812	176	83	699	767	63	3.17×10^6	2.99×10^6	2.91×10^6	2.95×10^6	1.00	2.52×10^6	2.26×10^7	0.13	750	0.86
A12	736	99	54	702	769	63	2.95×10^6	3.02×10^6	2.83×10^6	2.93×10^6	0.99	2.53×10^6	2.57×10^7	0.11	700	0.89
A16	934	297	--	637	696	54	3.08×10^6	--------	2.62×10^6	2.62×10^6	0.93	2.33×10^6	1.74×10^7	0.18	670	0.72
A17	860	223	68	748	821	62	3.33×10^6	3.03×10^6	2.94×10^6	2.99×10^6	0.95	2.67×10^6	1.73×10^7	0.17	700	0.72
A18	813	176	55	860	946	71	4.09×10^6	3.76×10^6	3.56×10^6	3.66×10^6	1.13	3.00×10^6	1.78×10^7	0.21	500	0.50
B3	622	---	53	702	---	67	4.24×10^6	3.91×10^6	3.87×10^6	3.89×10^6	1.02	3.12×10^6	2.37×10^7	0.16	650	0.96
Avg.	815	178									1.02			0.17	625	0.75
C.V.	9.6%	44%									6.6%			22%	16.9%	20%
A3	722	196	--	525	593	27	3.29×10^6	--------	2.03×10^6	2.03×10^6	0.70	2.24×10^6	9.0×10^7	0.23	370	0.51
A7	665	171	74	590	665	30	2.94×10^6	2.54×10^6	2.47×10^6	2.50×10^6	0.84	2.43×10^6	5.66×10^7	0.04	500	0.66
A11	624	98	72	593	667	49	2.85×10^6	2.28×10^6	2.52×10^6	2.40×10^6	0.78	2.44×10^6	1.45×10^7	0.17	510	0.73
B2	---	---	61	591	---	45	--------	3.52×10^6	3.21×10^6	3.37×10^6	0.94	2.96×10^6	1.38×10^7	0.24	550	0.92
Avg.	670	155									0.82			0.17	483	0.71
C.V.	7.3%	33%									12.4%			54%	16.2%	24%
A2.1	468	147	--	320	417	43	3.25×10^6	--------	2.16×10^6	2.16×10^6	0.93	1.95×10^6	9.73×10^6	0.22	250	0.53
A2.2	461	140	--	320	417	43	2.87×10^6	--------	1.93×10^6	1.93×10^6	0.79	1.95×10^6	1.09×10^7	0.18	370	0.81
A6	405	84	83	389	489	34	2.79×10^6	2.30×10^6	2.0×10^6	2.15×10^6	0.80	2.14×10^6	5.82×10^6	0.37	415	0.88
A10	344	23	100	391	491	35	2.36×10^6	1.50×10^6	1.95×10^6	1.72×10^6	0.54	2.15×10^6	3.85×10^7	0.45	460	1.00
A13	500	180	---	320	417	35	2.40×10^6	--------	1.90×10^6	1.90×10^6	0.77	1.95×10^6	1.54×10^7	0.12	400	0.80
A14	411	91	66	439	542	31	2.78×10^6	2.21×10^6	2.35×10^6	2.21×10^6	0.80	2.29×10^6	2.55×10^7	0.09	450	0.86
A15	475	154	57	558	667	36	3.44×10^6	2.56×10^6	2.86×10^6	2.71×10^6	0.84	2.62×10^6	1.03×10^7	0.26	390	0.85
B1	---	---	80	---	---	--	--------	--------	--------	--------	----	--------	--------	----	---	1.00
Avg.	438	117									0.78			0.24	391	0.84
C.V.	12.3%	46%									15.2%			54%	17.8%	17.5%

A1	369	182	--	325	313	33	1.88×10^{6}	--------	1.56×10^{6}	1.56×10^{6}	0.76	1.61×10^{6}	--------	----	370	100
A5	357	114	66	395	385	34	2.59×10^{6}	1.83×10^{6}	1.88×10^{6}	1.85×10^{6}	0.84	1.80×10^{6}	1.05×10^{7}	0.18	355	99
A9	365	97	70	397	387	28	2.38×10^{6}	1.73×10^{6}	1.87×10^{6}	1.80×10^{6}	0.79	1.81×10^{6}	1.60×10^{7}	0.11	350	96
Avg.	364	131									0.80			0.15	358	98
C.V.	1.7%	34%									5.0%			---	2.9%	2.1%
A19	---	163	--	---	---	37	1.93×10^{6}	--------	1.52×10^{6}	1.52×10^{6}	----	1.63×10^{6}	1.37×10^{7}	0.11	150	92
A19.1	---	125	--	---	---	100	1.61×10^{6}	--------	1.61×10^{6}	1.61×10^{6}	----	1.63×10^{6}	3.17×10^{7}	0.50	122	98
Avg.	---	144									----			0.31	136	95
C.V.	---	---									----			----	---	--
C1	360	---	---	535	630	33	3.18×10^{6}	--------	1.81×10^{6}	1.81×10^{6}	0.62	2.14×10^{6}	5.66×10^{6}	0.32	360	100
C2	433	---	86	601	701	64	2.69×10^{6}	1.64×10^{6}	1.97×10^{6}	1.81×10^{6}	0.52	2.33×10^{6}	7.26×10^{7}	0.25	400	80
C3	344	---	58	603	703	40	3.79×10^{6}	2.10×10^{6}	2.03×10^{6}	2.07×10^{6}	0.65	2.34×10^{6}	1.11×10^{7}	0.19	375	93
C4	459	---	--	535	630	35	3.18×10^{6}	--------	2.0×10^{6}	2.0×10^{6}	0.72	2.14×10^{6}	2.18×10^{7}	0.09	450	100
C5	458	---	64	650	755	35	2.51×10^{6}	2.20×10^{6}	1.99×10^{6}	2.10×10^{6}	0.59	2.47×10^{6}	1.86×10^{7}	0.11	425	75
C6	455	---	68	763	880	59	3.33×10^{6}	--------	2.39×10^{6}	2.39×10^{6}	0.56	2.81×10^{6}	7.65×10^{6}	0.31	675	99
Avg.	418										0.61			0.21	448	91
C.V.	12.5%										11.5%			46%	26%	12.1%
D12	524	---	92	827	903	52	2.67×10^{6}	1.90×10^{6}	2.40×10^{6}	2.15×10^{6}	0.63	2.63×10^{6}	8.28×10^{6}	0.26	380	62
D17	629	---	78	872	955	33	2.34×10^{6}	2.44×10^{6}	2.52×10^{6}	2.48×10^{6}	0.68	2.76×10^{6}	1.36×10^{7}	0.18	700	97
D18	474	---	60	981	1080	45	3.50×10^{6}	2.77×10^{6}	2.98×10^{6}	2.88×10^{6}	0.71	3.08×10^{6}	1.04×10^{7}	0.28	650	84
F8	717	---	--	825	901	32	2.78×10^{6}	2.03×10^{6}	2.41×10^{6}	2.22×10^{6}	0.62	2.62×10^{6}	1.0×10^{7}	0.22	700	88
F17	773	---	91	872	955	39	3.0×10^{6}	2.24×10^{6}	2.62×10^{6}	2.43×10^{6}	0.65	2.76×10^{6}	5.47×10^{6}	0.44	650	71
F18	689	---	66	981	1080	60	4.22×10^{6}	3.26×10^{6}	3.05×10^{6}	3.16×10^{6}	0.84	3.08×10^{6}	3.31×10^{7}	0.10	700	77
Avg.	542										0.69			0.25	577	81
	726														683	79
C.V.	14.6%										11.8%			46%	30%	21.8%
	5.9%														4.2%	10.9%

D10	303	---	93	552	466	50	--------	1.61×10^{6}	1.88×10^{6}	1.75×10^{6}	0.52	2.25×10^{6}	4.42×10^{6}	0.39	325	82
D14	411	---	61	600	520	40	2.66×10^{6}	2.11×10^{6}	2.45×10^{6}	2.28×10^{6}	0.75	2.38×10^{6}	1.90×10^{7}	0.12	350	69
D15	330	---	49	715	645	50	3.58×10^{6}	2.88×10^{6}	2.91×10^{6}	2.90×10^{6}	0.93	2.71×10^{6}	2.05×10^{7}	0.14	330	66
F6	535	---	84	550	465	33	3.24×10^{6}	2.12×10^{6}	2.26×10^{6}	2.19×10^{6}	0.79	2.24×10^{6}	5.6×10^{7}	0.04	500	83
F14	523	---	80	600	520	38	3.55×10^{6}	2.34×10^{6}	2.44×10^{6}	2.39×10^{6}	0.82	2.38×10^{6}	1.83×10^{7}	0.13	625	95
F15	489	---	70	715	645	34	3.70×10^{6}	2.50×10^{6}	2.66×10^{6}	2.58×10^{6}	0.73	2.71×10^{6}	1.13×10^{7}	0.23	700	95
Avg.	348										0.76			0.18	335	72
	516														608	91
C.V.	16.2%										17.8%			67%	3.9%	11.8%
	4.6%														16.6%	7.6%

* Plain Column - no lateral ties
† Premature failure due to broken lower course
Note: In the case of LVDT's removed prior to failure, failure strains are based on extrapolation of load-strain curve to known failure load.

Table 5.2: Eccentric Column Test Results

Col. no.	% Vertical Rebar	Steel Area	Steel Grade	Eccentricity of Load		Concrete Strength	Failure Mode	Failure Load	Failure Moment	Column Midheight Deflection at Failure	Failure Moment + P-Δ	Neutral Axis at Failure		Compression Failure Strain	Cracking Load
												Based on Gross X-section	Based on Core X-section		
		A_s (in^2)			(in.)	f_c' (psi)		Pu_c (K)	M (K-ft)	Δ (in.)	M_c (K-ft)	(in.)	(in.)	ϵ_{ml} (in/in)	P_{crack} (K)
E1P2	0.76	1.86	40	+/12	1.3	3200	1	400	43	0.10	47	21.4↓	1 9.6↓	0.0017	400
E1P1	"	"	"	+/6	2.6	"	1	380	82	0.15	87	14.6	12.8	0.0020	326
E1P3	"	"	"	+/3	5.2	"	2	134*	58	0.15	60	10.4↓	8.6↓	------	100
E1P4	"	"	"	+/3	5.2	"	2	211	92	0.28	97	9.6↓	7.8↓	0.0017	208
E3P1	0.76	1.86	40	+/12	1.3	5090	1	563	61	0.11	66	15.75	14.0	0.0024	563
E3P2	"	"	"	+/6	2.6	"	1	418	91	0.20	98	15.1 ↓	13.3↓	0.0020	280
E3P3	"	"	"	+/3	5.2	"	2	220	96	0.58	106	8.8	7.0	0.0018	208
E3P4	"	"	"	+/3	5.2	"	2	264	115	0.45	125	9.4	7.6	0.0024	210
E4P1	1.3	3.1	60	+/12	1.3	5090	1	735	80	0.10	86	22.8↓	21.0↓	0.0023	521
E4P2	"	"	"	+/6	2.6	"	1	484	105	0.17	112	13.5	11.7	0.0017	250
E4P3	"	"	"	+/3	5.2	"	2	175*	76	0.37	81	9.6	7.8	0.0011	175
E4P4	"	"		+/3	5.2	"	2	290	126	0.41	136	9.6	7.8	0.0022	200
E5P1	0.76	1.86	60	+/12	1.3	5090	1	600	65	0.10	70	----	----	0.0022	600
E5P2	"	"	"	+/6	2.6	"	1	413	90	0.11	93	14.6	12.8	0.0017	413
E5P3	"	"	"	+/3	5.2	"	2	297	129	0.20	133	10.1↓	8.3↓	------	175
E5P4	"	"	"	+/3	5.2	"	2	258	112	0.36	120	----	----	0.0020	200
Average C.V.														0.0020 14.2%	

Table 5.2 continued

Col no.	$\frac{P_{crack}}{Pu_c}$	Case 1 USD Analysis				Case 2 USD Analysis				Case 3 USD Analysis			
		Ultimate Load	Neutral Axis Based on Gross Area	Failure Moment	$\frac{P_{test}}{P_{calc}}$	Ultimate Load	Neutral Axis Based on Gross Area	Failure Moment	$\frac{P_{test}}{P_{calc}}$	Ultimate Load	Neutral Axis Based on Gross Area	Failure Moment	$\frac{P_{test}}{P_{calc}}$
		P (K)	(in)	M (K-ft)		P (K)	(in)	M (K-ft)		P (K)	(in)	M (K-ft)	
E1P2	1.0	620	15.6	67	0.65	506	15.0	55	0.79	385	11.97	42	1.04
E1P1	0.86	504	12.75	109	0.75	405	12.3	88	0.93	303	9.63	66	1.25
E1P3	0.75	320	8.65	139	----	257	8.7	112	----	195	6.98	85	----
E1P4	0.99	320	8.65	139	0.66	257	8.7	112	0.82	195	6.98	85	1.08
	Avg.	P_b=289		M_b=140	0.69	P_b=230		M_b=114	0.85	P_b=192		M_b=84	1.12
E3P1	1.0	948	16.45	103	0.59	695	15.35	75	0.81	570	12.35	62	0.99
E3P2	0.67	770	13.38	167	0.54	546	12.4	118	0.77	438	9.67	95	0.95
E3P3	0.94	465	8.45	202	0.47	324	8.4	141	0.68	255	6.10	111	0.86
E3P4	0.80	465	8.45	202	0.57	324	8.4	141	0.81	255	6.10	111	1.04
	Avg.	P_b=433		M_b=200	0.54	P_b=306		M_b=142	0.77	P_b=287		M_b=133	0.96
E4P1	0.71	1030	16.69	116	0.71	777	15.75	84	0.95	654	12.88	71	1.12
E4P2	0.51	835	13.55	181	0.58	620	12.8	134	0.78	516	10.25	112	0.94
E4P3	1.0	525	9.06	228	----	385	9.0	167	----	334	7.28	145	----
E4P4	0.69	525	9.06	228	0.55	385	9.0	167	0.75	334	7.28	145	0.87
	Avg.	P_b=391		M_b=236	0.61	P_b=257		M_b=173	0.83	P_b=259		M_b=152	0.98
E5P1	1.0	972	16.56	105	0.62	719	15.5	78	0.83	595	12.56	64	1.01
E5P2	1.0	786	13.38	170	0.53	568	12.5	123	0.73	460	9.8	100	0.90
E5P3	0.59	475	8.5	206	0.63	333	8.4	146	0.89	283	6.6	123	1.05
E5P4	0.78	475	8.5	206	0.54	333	8.4	146	0.77	283	6.6	123	0.91
	Avg.	P_b=388		M_b=207	0.58	P_b=255		M_b=143	0.81	P_b=257		M_b=122	0.97
Avg. C.V.					0.60 12.7%				0.81 9.2%				1.0 10.7%

* Premature Column Failure

P_b=Balanced Load

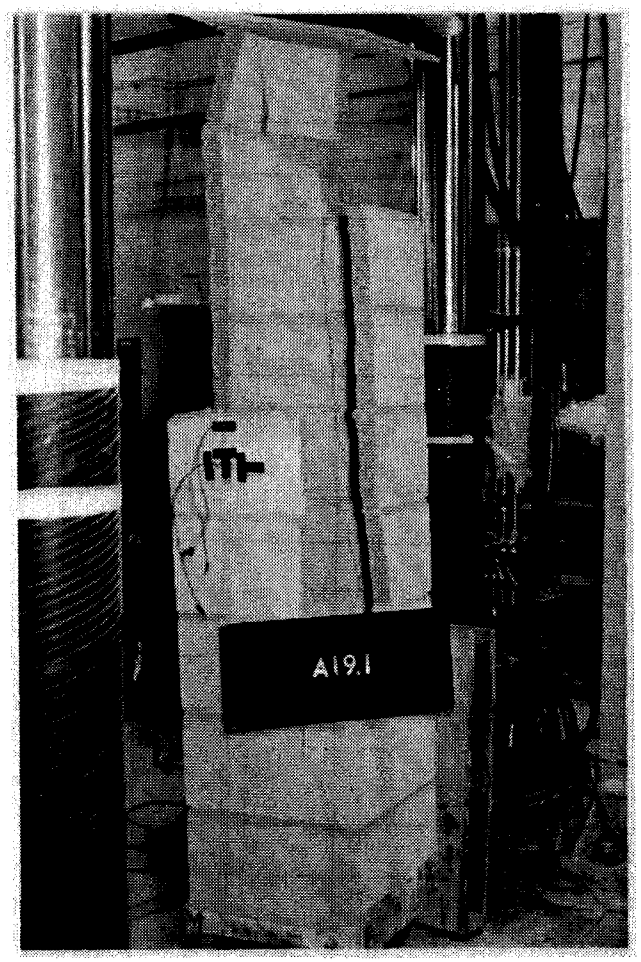

PLATE 5.1
Ungrouted Column Failure Showing
Block Center Face Cracking

PLATE 5.2

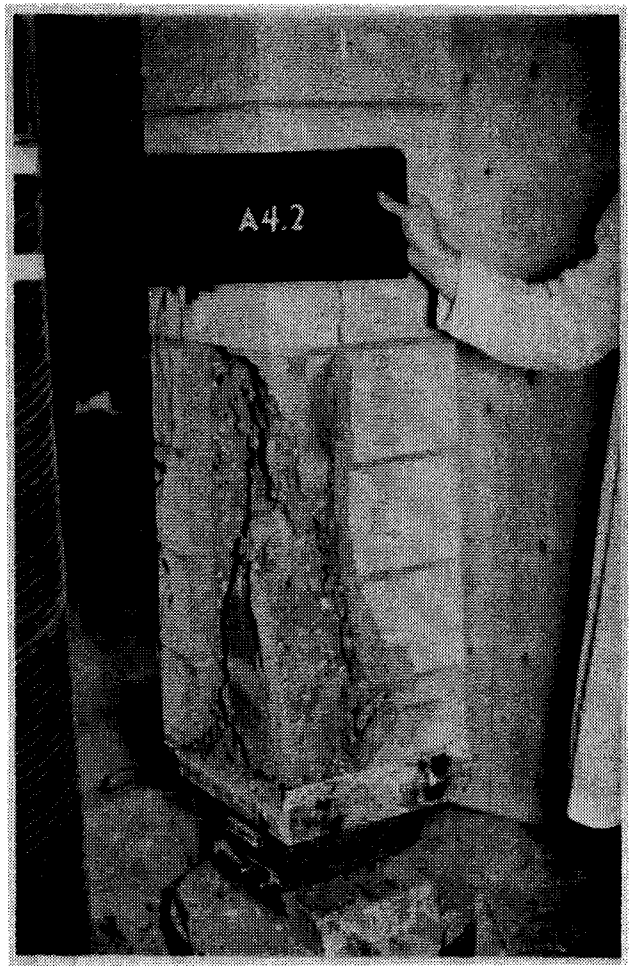

PLATES 5.2, 5.3, and 5.4
Simultaneous Shell Splitting and Core Crushing Associated with Grouted Column Type A Failure

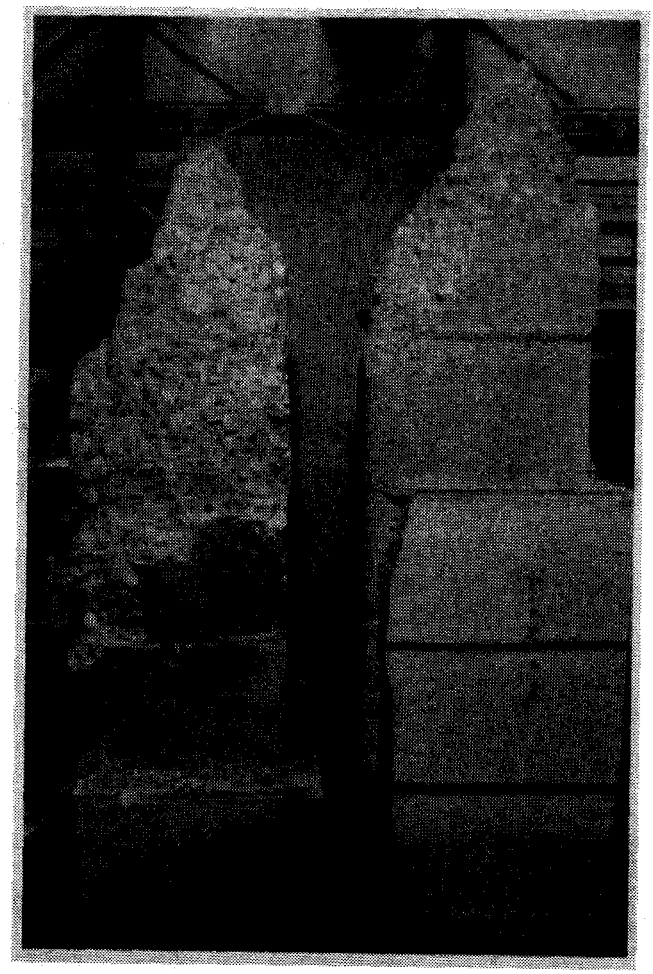

PLATE 5.5
Conical Failure Plane in Grouted Columns

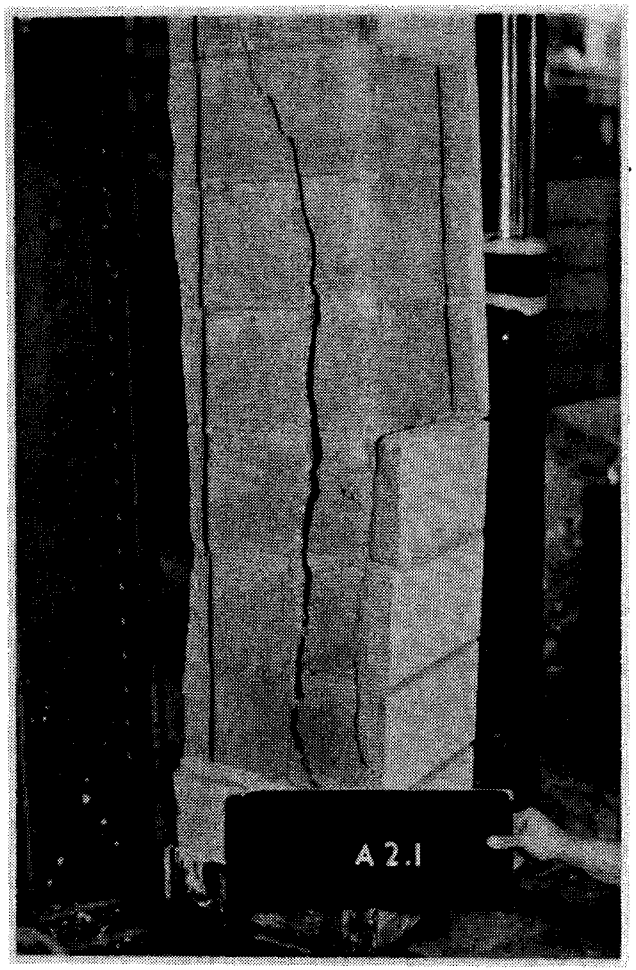

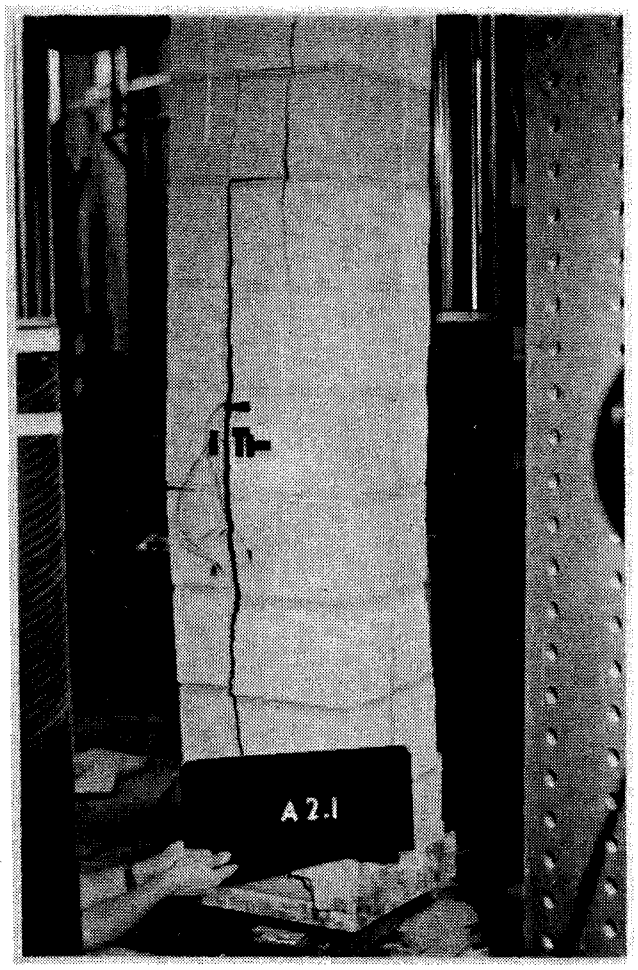

PLATE 5.6(a) and PLATE 5.6(b)
Simultaneous Vertical Splitting of the Masonry Shell and Concrete Core in Grouted Columns

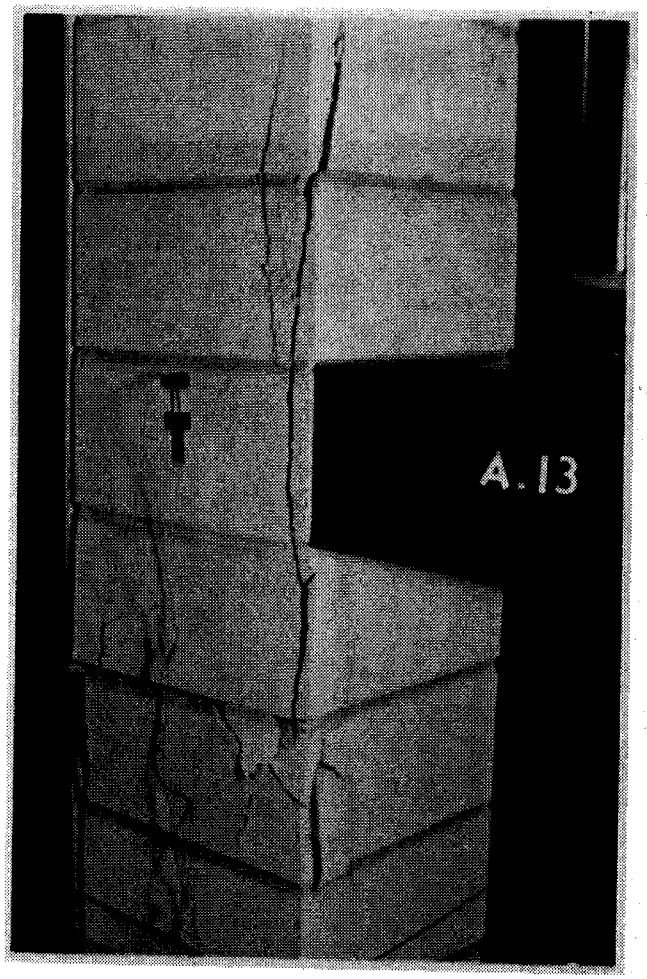

PLATE 5.7
Failure of Grouted Column
Containing Lateral Reinforcement

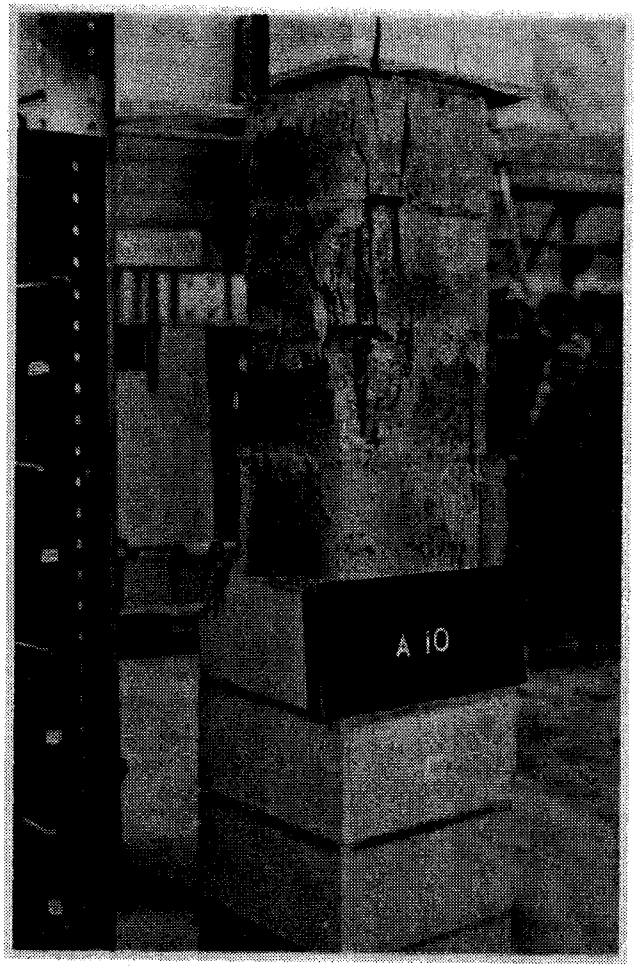

PLATE 5.8

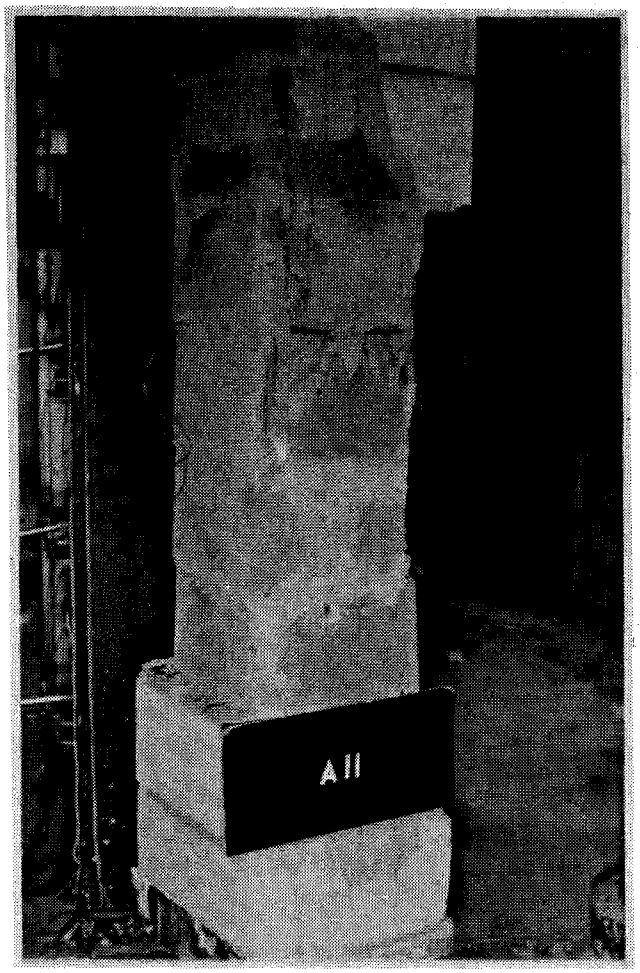

PLATE 5.9

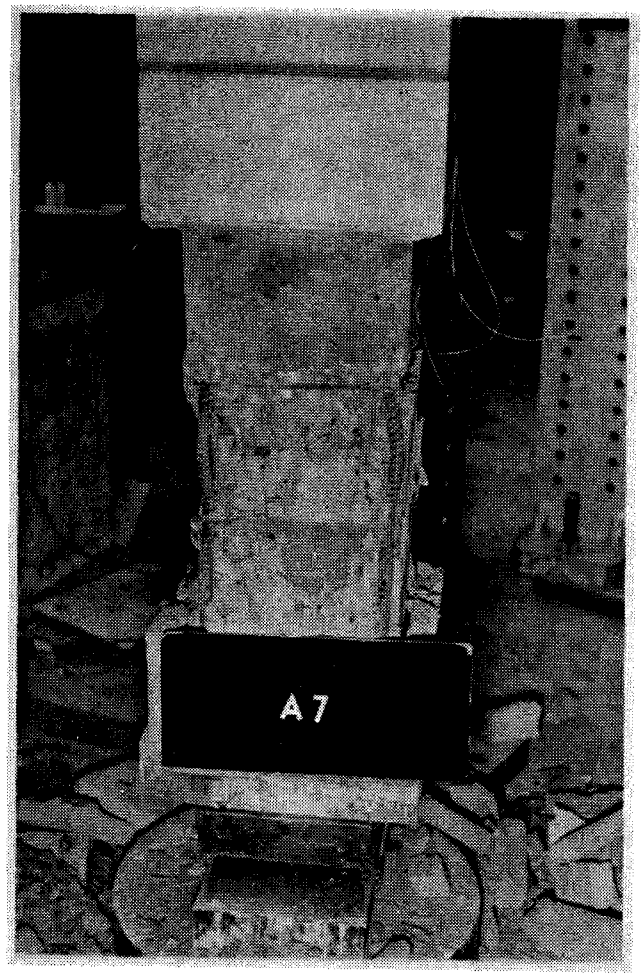

PLATE 5.10

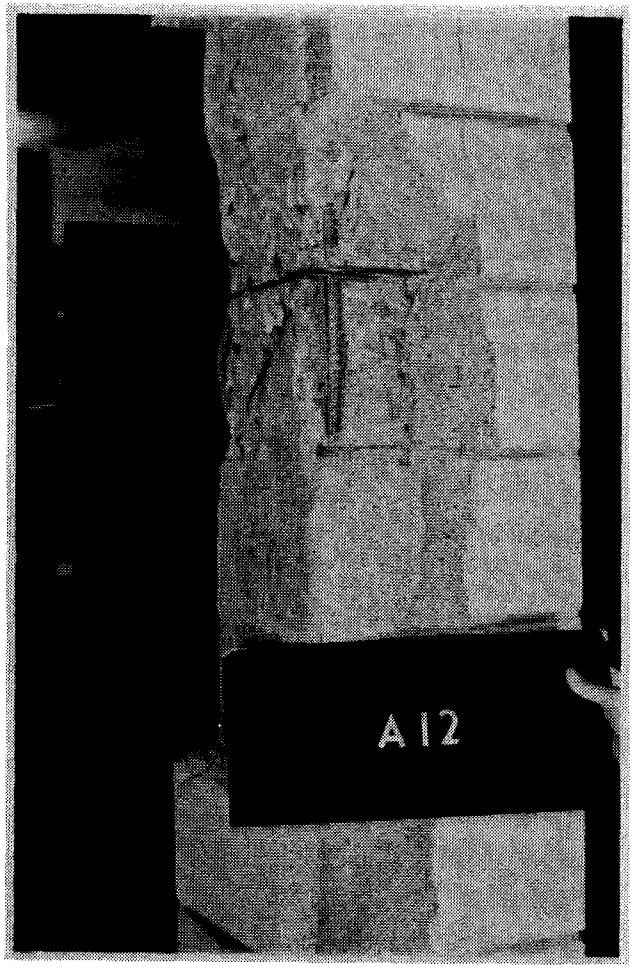

PLATES 5.8, 5.9, 5.10, and 5.11
Type B Failures of Columns Fabricated with Lateral Ties Having 90 deg. Hooks, Showing Reinforcement Buckling Between Tie Spacings

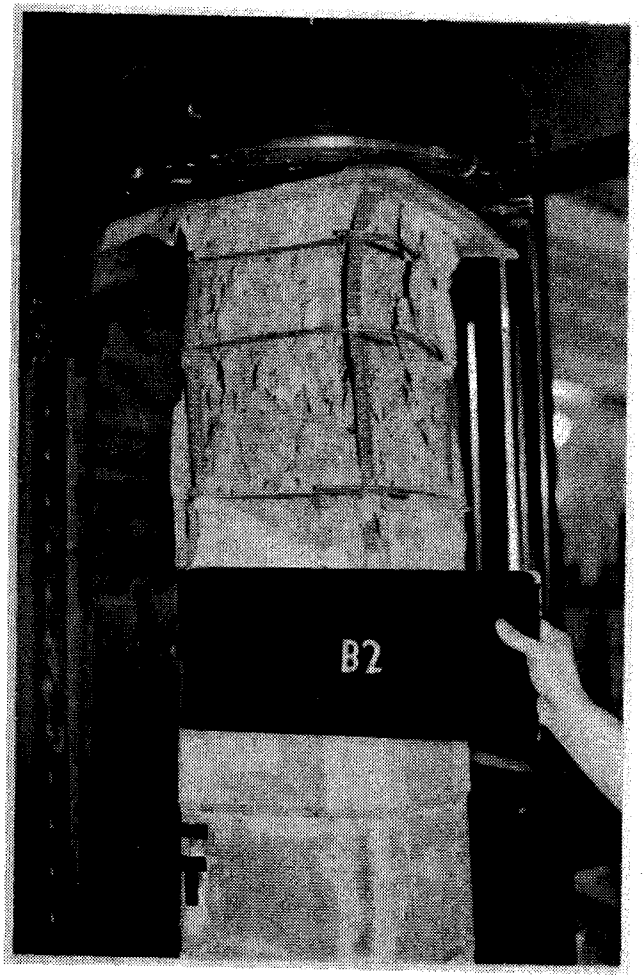

PLATE 5.12

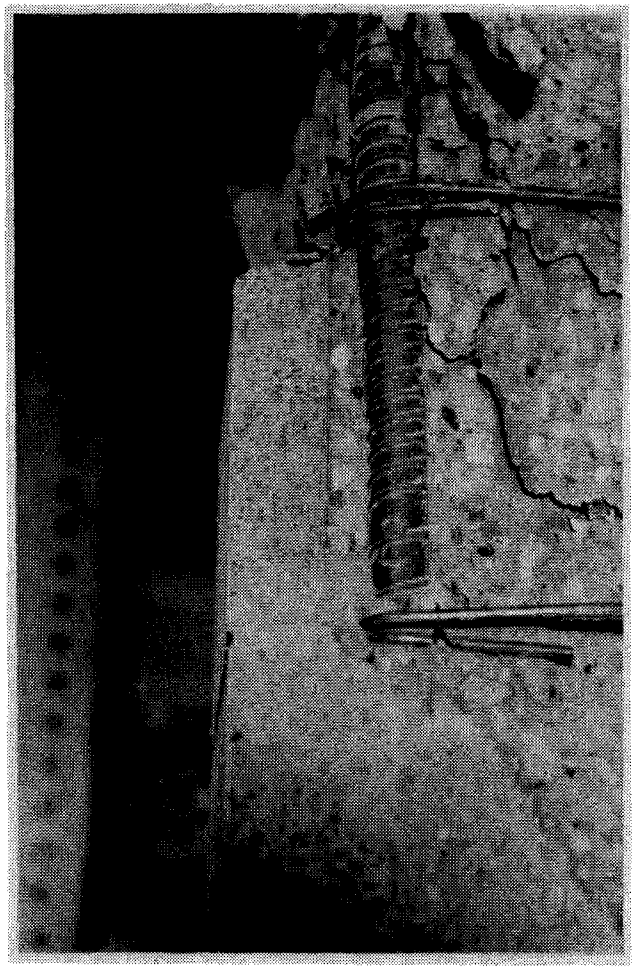

PLATE 5.13

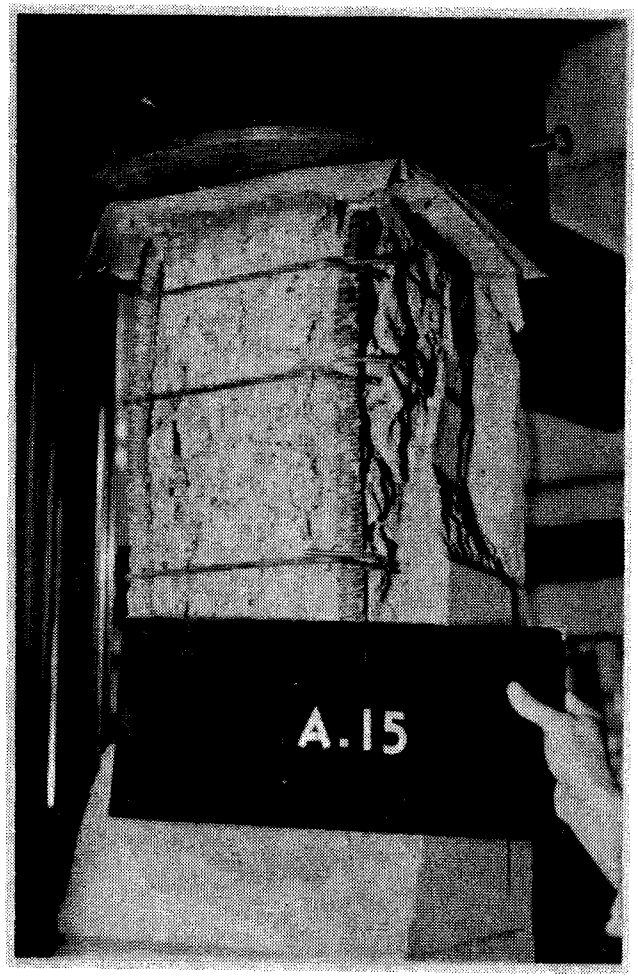

PLATE 5.14

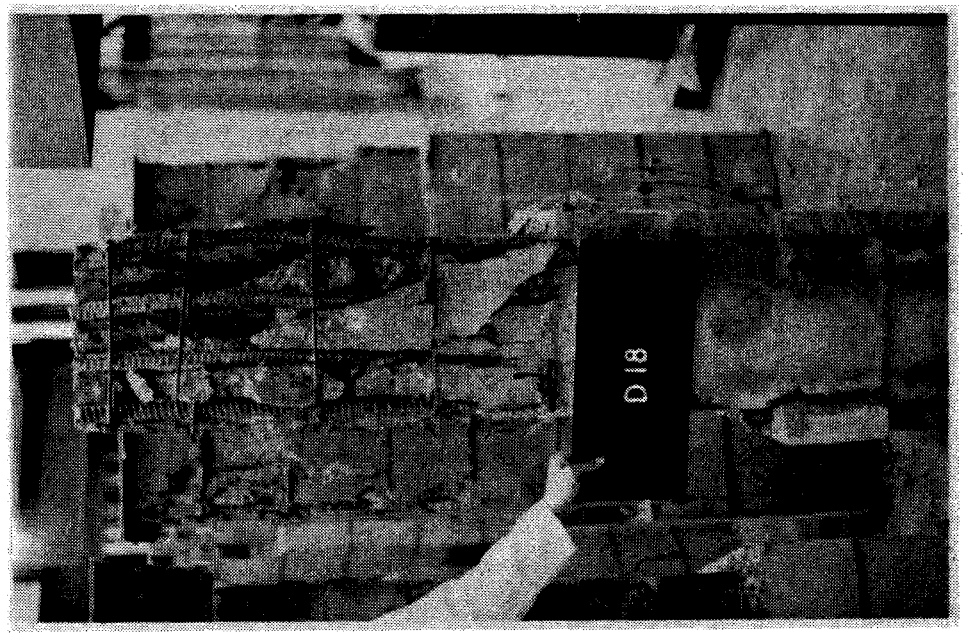

PLATE 5.16

PLATE 5.15

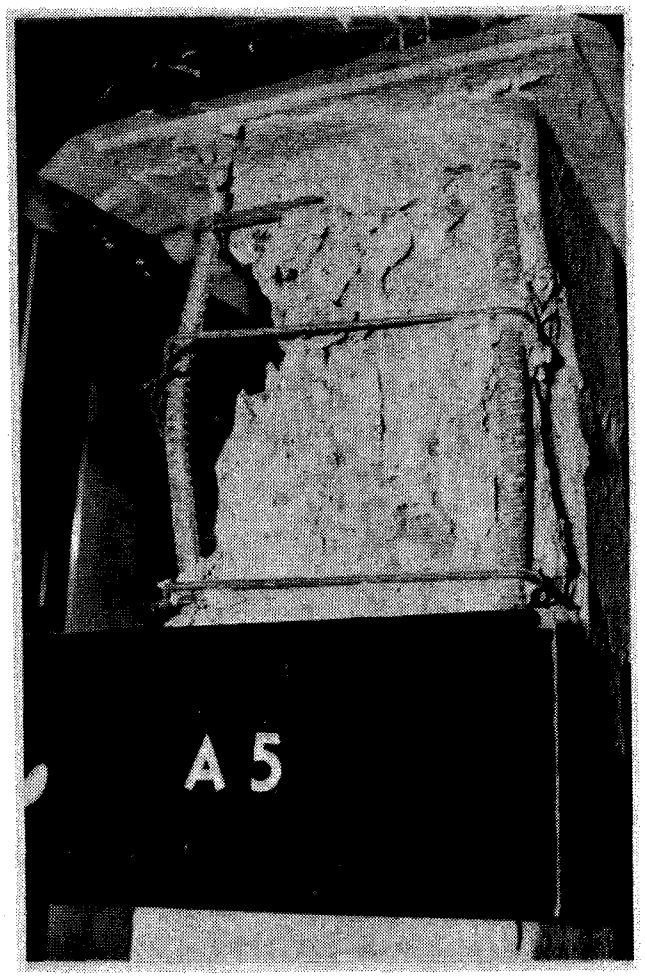

PLATE 5.17

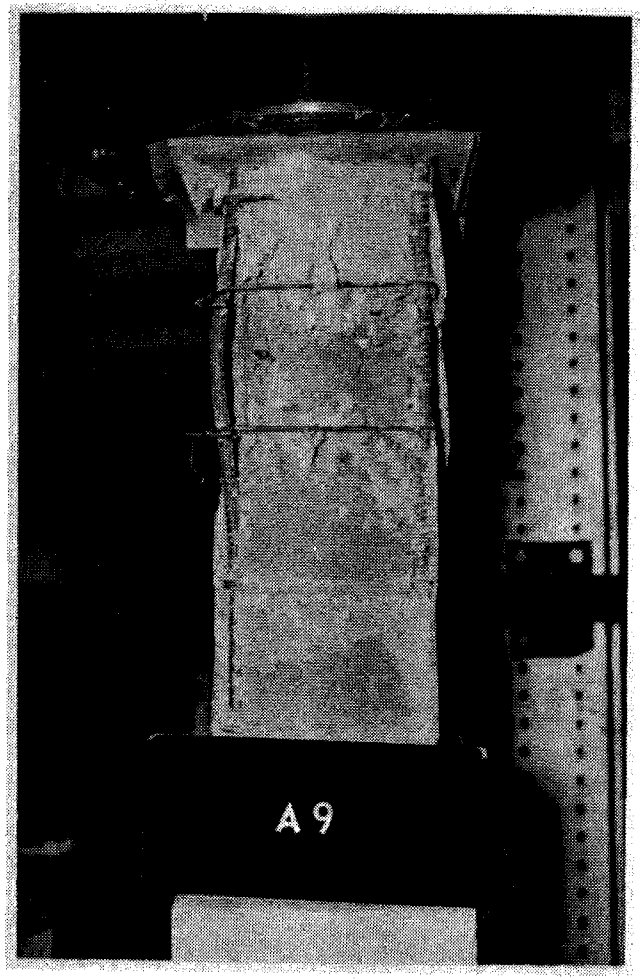

PLATE 5.18

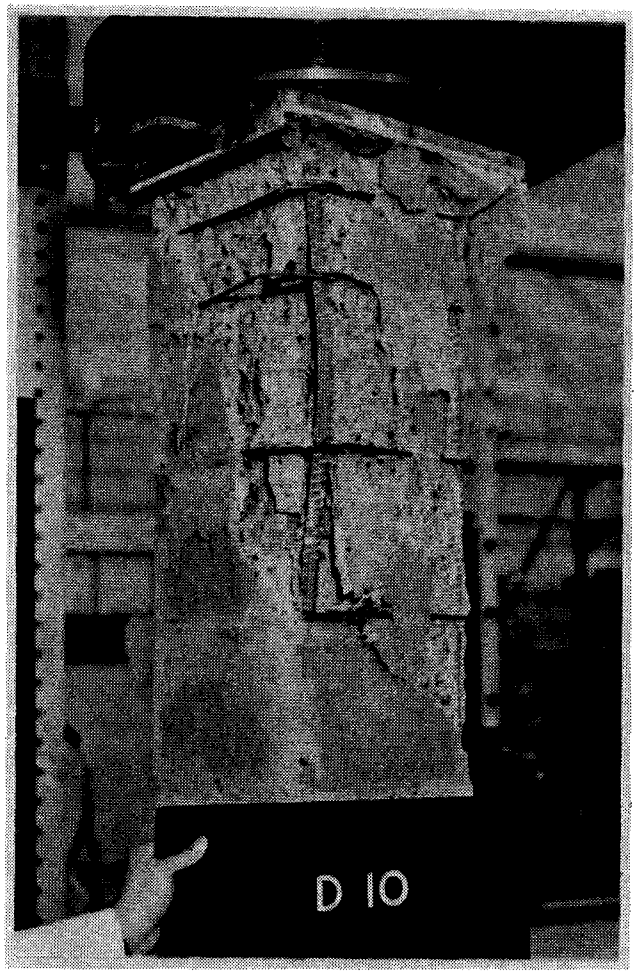

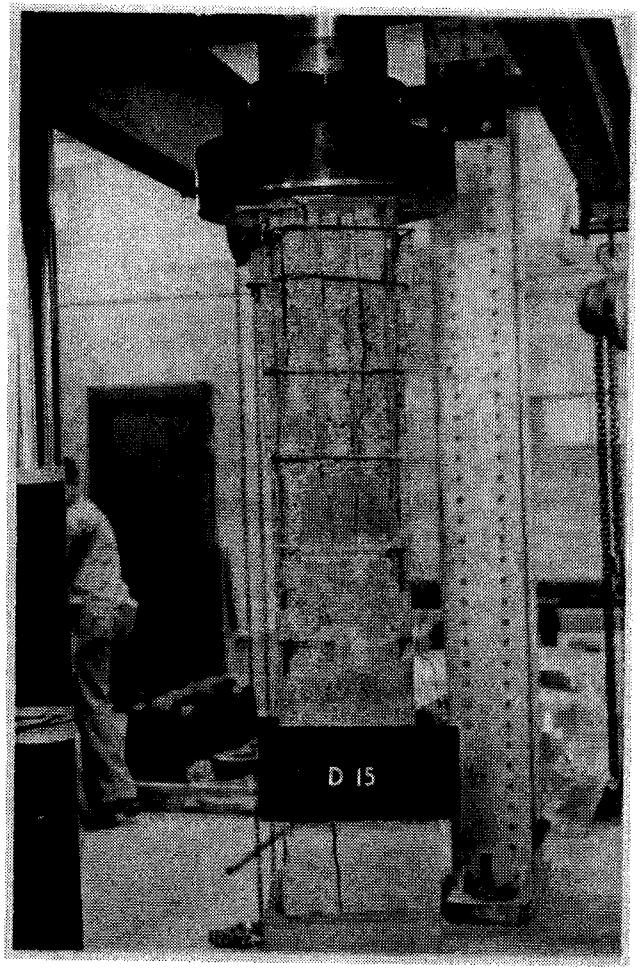

PLATES 5.12 to 5.20
Type C Failures of Columns Constructed with Lateral Ties Having 90 deg. Hooks, Showing Tie Pulling and Reinforcement Buckling Over Several Courses

PLATE 5.21

PLATE 5.22

PLATES 5.21, 5.22, and 5.23
Type B Failures of Columns Laterally Reinforced with Ties Having 135 deg. Hooks, Showing Reinforcement Buckling Between Tie Spacings

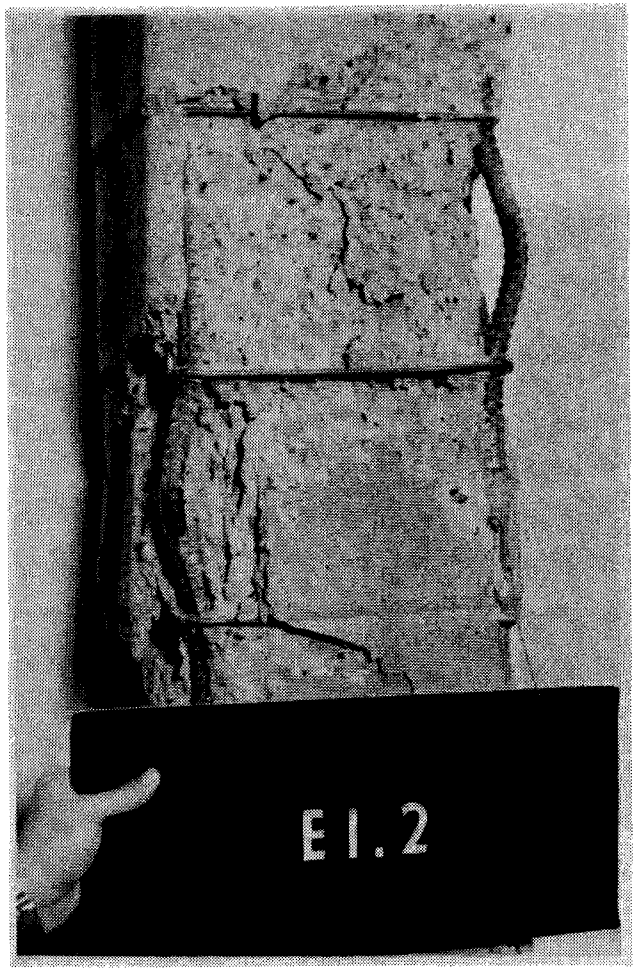

PLATE 5.24

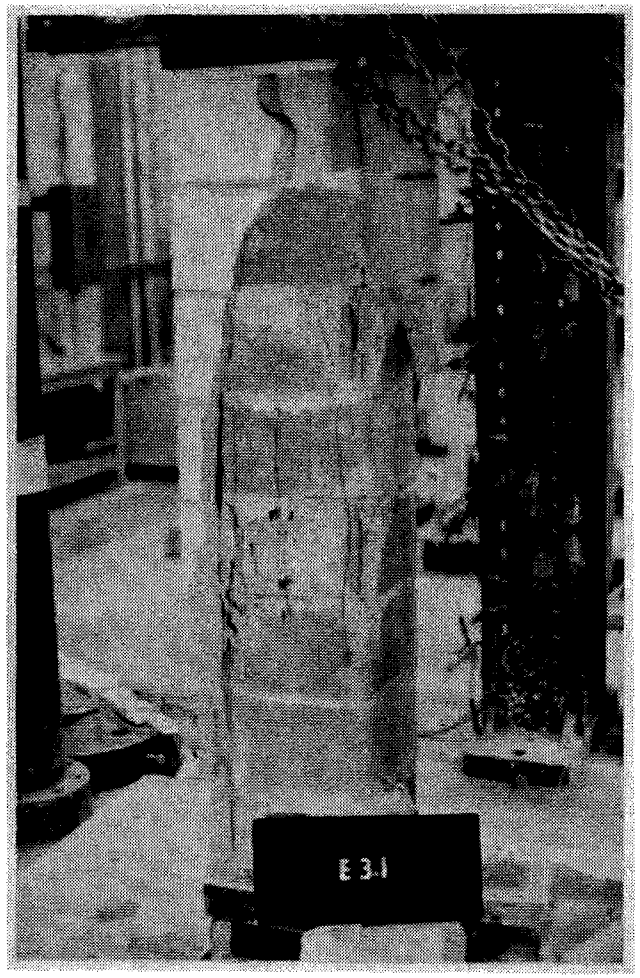

PLATE 5.25

PLATES 5.24, 5.25, and 5.26
Type 1 Eccentrically Loaded Column Failures

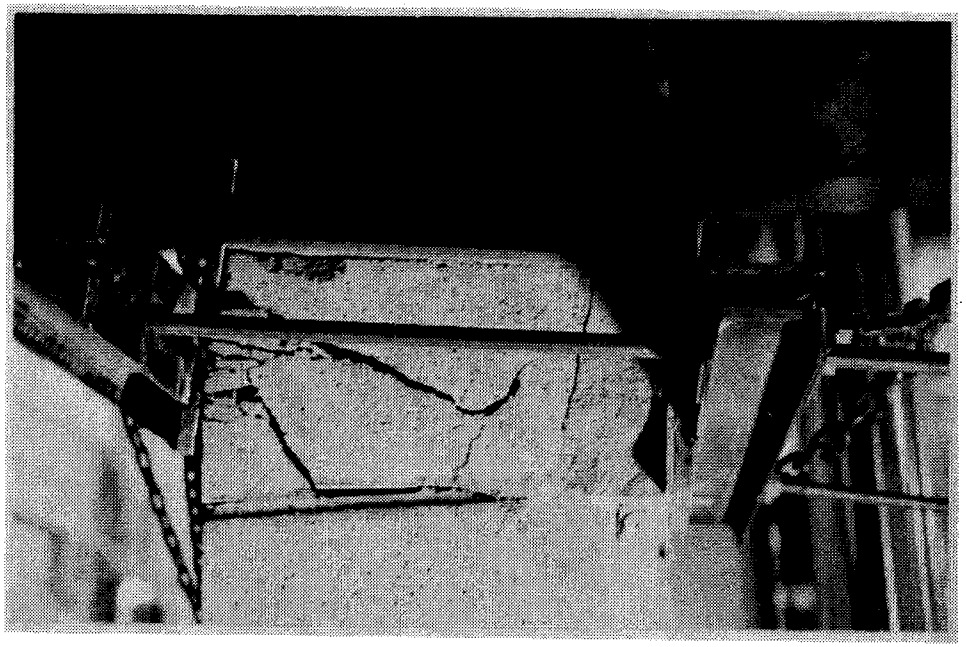

PLATE 5.27

PLATE 5.28

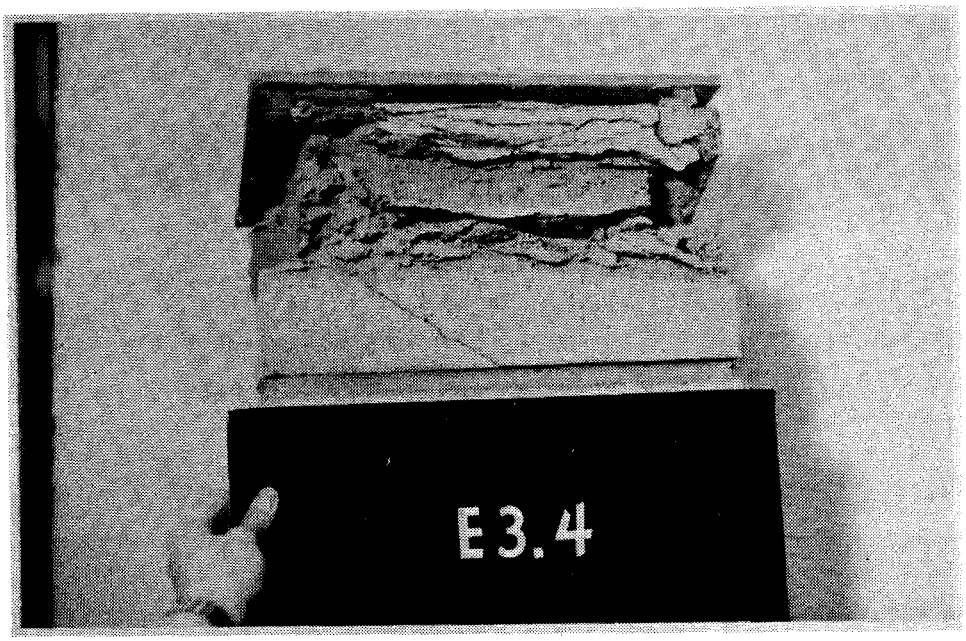

PLATES 5.27, 5.28, and 5.29
Type 2 Eccentrically Loaded Column Failures
in the Upper Course

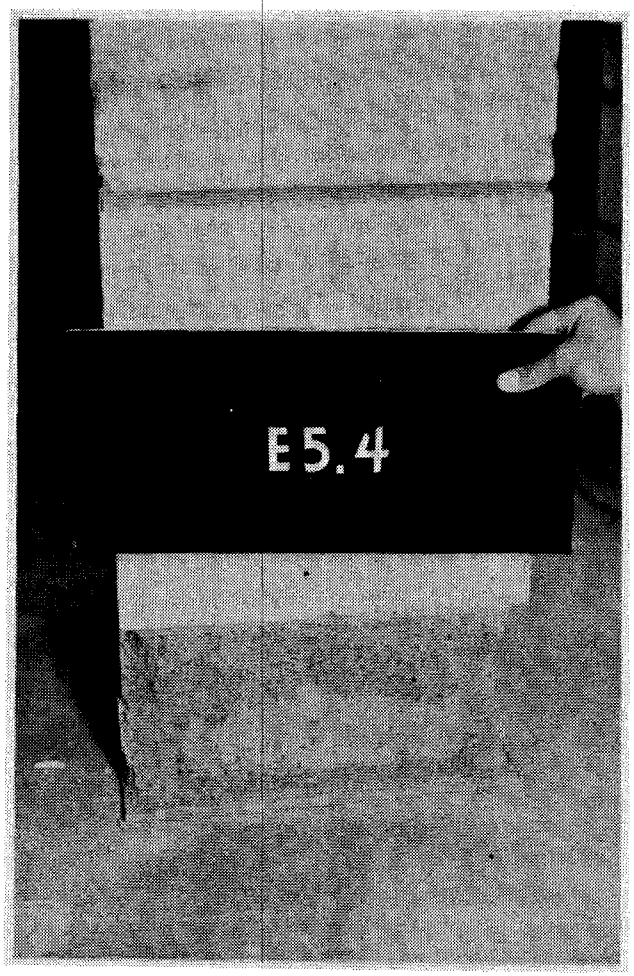

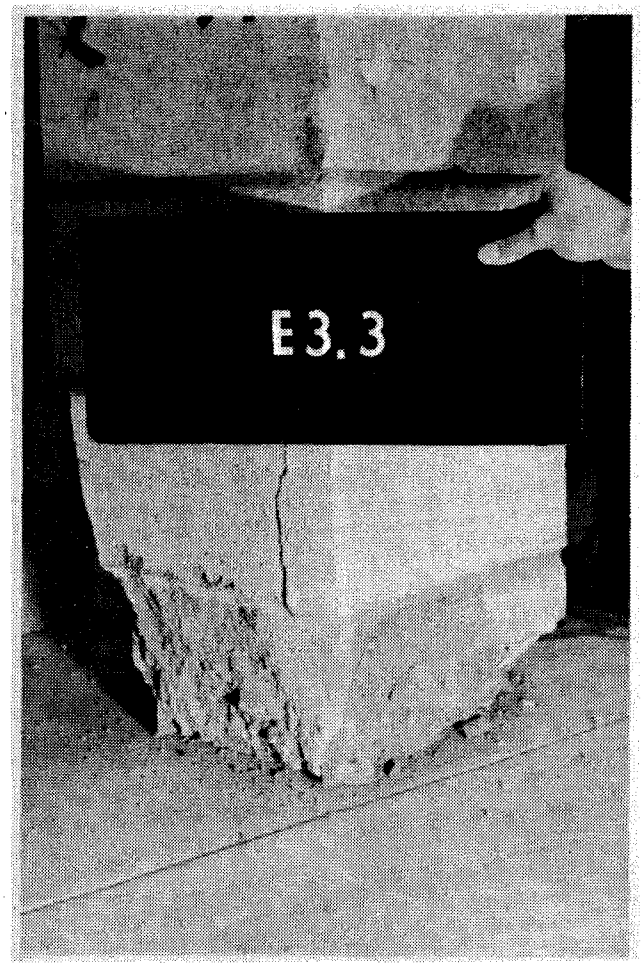

PLATES 5.30 and 5.31
Type 2 Eccentrically Loaded Column Failures
in the Lower Course

6. SUMMARY, CONCLUSIONS, AND RECOMMENDATIONS

6.1 Summary

The object of the study reported herein was to investigate the behavior of reinforced concrete block masonry columns subject to axial concentric compression, and combined bending and axial load. Nominal 8 x 16 x 16 in. single core pilaster units were used in the fabrication of the test columns. All columns were 72 inches in height, and all were loaded through pinned ends.

A total of forty-three concentrically loaded columns were manufactured and tested to failure. These columns were divided into five series. Series A and D columns were tested in order to establish the effect of percentage and grade of vertical reinforcement and the effect of concrete core compressive strength on column strength and behavior. Series B columns were identical to those constructed in Series A, but were tested with stripped shells. Series F columns were fabricated with lateral ties having superior hook detailing to those of Series A. Series C specimens were grouted with high slump concrete in order to determine the effect of increased workability and increased core shrinkage on the strength of reinforced block columns having large core areas. Concrete qualities for the concentrically loaded columns were varied from about 1500 psi to 6000 psi, and the percentage of vertical reinforcement was varied from 0 to 2.6 percent. Grade 40 and Grade 60 steels were used, and

4-inch and 9-inch slump concretes were cast in the column cores. Sixteen eccentrically loaded columns were constructed and tested to failure. Two concrete strengths, two percentages of vertical reinforcement, and two grades of vertical steel were used in the fabrication of these specimens; namely, 3200 psi and 5090 psi, 0.76 and 1.3 percent, and Grade 40 and Grade 60, respectively. The eccentricity of loading varied from 0 to 1/3 times the lateral dimension of the columns. The general behavior of the test columns was observed by measurements of load, strain, and deflections.

Forty-seven, four block high prisms were built using the 16 in. square single core pilaster units. These specimens were grouted with concrete strengths which varied from 1500 psi to 6000 psi, and were tested to failure under concentric compression in order to determine the nature of the shell-core interaction, and to establish a strength and behavioral relationship between small-scale control specimens and full-scale columns.

A study of the basic assumptions of inelastic design of reinforced concrete columns was made. On the basis of this study, and on the basis of data gathered from the present tests, theories and equations for the prediction of masonry column and prism strengths and material properties were extended and developed.

6.2 Conclusions

The results and discussions which have been presented in this report lead to the following conclusions:

1. Compression failures of grouted prisms are characterized by either simultaneous splitting of the block shell and crushing of the prism core, or by splitting and spalling of the block shell before core crushing. Failure mode shows no associative patterns with grout strength, and appears to be more a function of bond strength between the shell and the core.
2. The core strengths of grouted prisms and columns constructed with pilaster units having dimensions comparable to those used in this study are best represented by the strengths obtained from compression tests on standard moist cured concrete cylinders.
3. At failure, block shells of grouted masonry assemblages contribute some fraction of that load carried by an otherwise identical plain masonry specimen. The combination of the vertical compressive stresses and the bilateral tensile stresses imposed on the shell by the lateral expansion of the concrete core can cause premature failure and prevent the shell from reaching full development. The percent of full development attained by the shell is believed to be dependent upon prism gross area, net area, and the ratio of net area/gross area, as well as block strength and ungrouted prism strength.

4. The superposition concept of grout strength and block strength permitted by CSA-S304 is not valid. It may be more appropriate to match the deformational characteristics of grout to those of the block rather than matching the strengths as is suggested by the masonry code.
5. Low slump concretes are easily accommodated by pilaster units having dimensions comparable to those used in this study when adequate vibration is provided.
6. High slump concretes cast in columns and prisms built with pilaster units having large core areas produce extensive shrinkage cracking in the upper region of the core. The depth of penetration of these cracks, however, is considered to be only a few inches, and tests show that they do not have a detrimental effect on the structural performance of masonry subjected to concentric compression.
7. Failures occur in the upper regions of both concentrically and eccentrically loaded masonry columns since bleeding and segregation during pouring and vibration produce a weaker concrete in the upper core.
8. Cement types produced by different manufacturers can severely affect the strength and performance of concrete with identical mixes.
9. The average strength of the core of a plain masonry column under concentric loading is approximately 85 percent of the concrete strength indicated by standard

control cylinders, and the strength contributed by its masonry shell is approximately equal to that of a plain, ungrouted masonry column.

10. Grouted prisms provide an adequate estimate of the compressive strength of grouted columns constructed with similar materials and with no slenderness considerations.
11. The addition of lateral reinforcement to a plain, grouted masonry column increases the strength of the block shell, and prevents explosive spalling of the shell at failure.
12. Column lateral ties fabricated from 1/4 in. diameter plain bars, and having hooks formed with 90 deg. bends and 2-1/2 in. extensions do not provide adequate development length or stiffness to confine the column core and the vertical reinforcement, and thus permit premature failure. Columns fabricated with tie hooks having adequate embedment to prevent pulling show favourable strength and ductility increases and higher cracking loads, and display less sudden and less destructive failures.
13. Increasing percentages of longitudinal reinforcement decreases the load carried by the column block shell. However, load contribution by the steel exceeds this decrease, and the net effect is to increase column ultimate load.
14. Vertical reinforcement is not fully developed in a

reinforced concrete block masonry column tested to failure under concentric compression.

15. Tests indicate that the strength of a concentrically loaded, short, reinforced concrete block masonry column constructed with pilaster units is equal to the summation of 85 percent of the concrete control cylinder strength times the net area of the concrete core, plus 0.0014 times the product of the steel area and the elastic modulus of the vertical reinforcement, plus the compressive strength of a plain ungrouted column fabricated with similar block and mortar materials and strengths.
16. The properties of masonry columns can be predicted from the properties of the constituent materials, namely, the blocks, mortar, concrete and steel reinforcement.
17. The elastic modulus based on strain measurements taken during compressive tests of standard moist cured cylinders over-estimates prism core elastic modulus by about 80 percent, and column core elastic modulus by about 25 percent.
18. The stress-strain curves of concentrically loaded reinforced masonry columns, and plain columns and prisms approximate linearity to about 50 percent of the failure stress.
19. The CSA-S304 masonry elastic modulus specification over-estimates the elastic modulus of reinforced columns and plain columns and prisms having core strengths, as

indicated by tests of standard concrete control cylinders, in excess of 2000 psi. A more conservative estimate of column elastic modulus is provided by 750 to 800 times prism compressive strength.

20. The cracking load of masonry is dependent upon block strength and core strength and is directly proportional to core strength. Cracking load decreases with increasing percentages of vertical reinforcement.
21. The hypothesis of linear strain distributions is valid for masonry columns subjected to combined bending and axial load.
22. Masonry columns tested under load eccentricities greater than 1/3 the section depth require reinforced concrete column capitals to provide suitable load and moment transfer and to prevent local crushing failures in the column shaft.
23. The ACI-318-77 Ultimate Strength Design procedure for eccentrically loaded reinforced concrete columns is applicable to reinforced block masonry columns. This procedure provides reasonable estimates of column strength and accurately predicts column failure mode. However, it is necessary to neglect any contribution of the block shell in the analysis.

6.3 Recommendations

Considering the state-of-the-art of concrete block column design, the following recommendations are made:

1. It is recommended that the elastic modulus permitted by

CSA-S304 be reduced to 750 f'_m.

2. It is recommended that a further study of concentrically loaded columns be undertaken to more accurately define the effects of the percentage of vertical reinforcement on strength as a function of the bar size used to provide a given percentage. In addition, it is recommended that a variety of column cross-sections and block strengths be employed in order to establish the load contribution of the concrete shell with respect to these variables. These tests would provide additional statistical data to assist in the evaluation of performance factors for Limit States Design of masonry columns.
3. It is suggested that further studies be conducted to increase our understanding of masonry column tie detailing. Variables to be considered include tie bar sizes, tie placement, tie vertical spacing, and hook development lengths.
4. It is recommended that tests on eccentrically loaded masonry columns be initiated. Studies in all areas of eccentrically loaded block masonry columns are required before ultimate strength design can be economically applied to these members.

REFERENCES

1. Lyse, I.: "Tests of Reinforced Brick Columns." Journal Am. Ceramic Soc., Nov., 1933.

2. Shank, J.R., and Foster H.D.: "Strength of Brick and Tile Pilasters Under Varied Eccentric Loading." Ohio State University Engineering Experimental Station, Bulletin No. 57, 1930.

3. Withey, M.O.: "Tests on Reinforced Brick Masonry Columns." Proceedings, A.S.T.M., Vol. 34, Part II, 1934, p. 387.

4. Davey, N., and Thomas, F.G.: "The Structural Use of Brickwork." Struct. Build. Paper No. 24, Inst. Civ. Eng., Feb., 1950, pp. 13-66.

5. Anderson, D.E., and Hoffman, E.S.: "Design of Brick Masonry Columns." International Conference on Masonry Structural Systems, University of Texas, Austin, 1967.

6. Brettle, H.J.: "Ultimate Strength Design of Reinforced Brickwork Piers in Compression and Biaxial Bending." UNICIV Report No. R49, The School of Civil Engineering, University of New South Wales, Australia, June, 1969.

7. Shank, J.R., and Foster, H.D.: "Strength of Concrete Block Pilasters Under Varied Eccentric Loading." Ohio State University Engineering Experimental Station, Bulletin No. 60, 1931.

8. Feeg, C., Longworth, J., and Warwaruk, J.: "Effects of Reinforcement Detailing for Concrete Masonry Columns." MSc. Thesis, Civil Engineering Department, University of Alberta, 1979.

9. Slater, W.A., and Lyse, I.: "Compressive Strength in Flexure as Determined from Tests in Reinforced Beams." Journal of the American Concrete Institute, Proceedings, Vol. 26, 1930, pp. 831-874.

10. McMillan, F.R.: "A Study of Column Test Data." Journal of the American Concrete Institute, Proceedings, Vol. 17, 1921, pp. 150-171.

11. Slater, W.A., and Lyse, I.: "Column Tests at Lehigh University." Journal of the American Concrete Institute, Proceedings; Vol. 27, Feb., 1931, pp. 677-730; March, 1931, pp. 791-835; Vol. 28, Nov., 1931, pp. 159-166.

12. Lyse, I., and Kreidler, C.L.: "Column Tests at Lehigh University." Journal of the American Concrete Institute,

Proceedings, Vol. 28, Jan., 1932, pp. 317-346.

13. Lyse, I.: "Column Tests at Lehigh University." Journal of the American Concrete Institute, Proceedings, Vol. 29, June, 1933, pp. 433-442.

14. Richart, F.E., and Staehle, G.C.: "Column Tests at the University of Illinois." Journal of the American Concrete Institute, Proceedings; Vol. 27, Feb., 1931, pp. 731-760; March, 1931, pp. 761-790; Vol. 28, Nov., 1931, pp. 167-175; Jan., 1932, pp. 279-315.

15. Richart, F.E., and Brown, R.L.: "An Investigation of Reinforced Concrete Columns." Engineering Experiment Station Bulletin No. 267, University of Illinois, Urbana, 1934, 91 pp.

16. Whitney, C.S.: "Design of Reinforced Concrete Members Under Flexure and Combined Flexure and Direct Compression." Journal of the American Concrete Institute, Proceedings, Vol. 33, March, pp. 483-498.

17. Whitney, C.S.: "Eccentrically Loaded Reinforced Concrete Columns." Concrete and Constructional Engineering, Vol. 33, No. 11, Nov., 1938, pp. 549-561.

18. Whitney, C.S.: "Plastic Theory in Reinforced Concrete Design." Proceedings, ASCE, Dec., 1940; Transactions, ASCE, Vol. 107, 1942, pp. 251-326.

19. Jensen, V.P.: "The Plastic Ratio of Concrete and Its Effects on the Ultimate Strength of Beams." Journal of the American Concrete Institute, Vol. 14, No. 6, June, 1943.

20. Hognestad, E.: "A Study of Combined Bending and Axial Load in Reinforced Concrete Members." Engineering Experiment Station Bulletin No. 399, University of Illinois, Urbana, Nov., 1951, 128 pp.

21. Billet, D.F., and Appleton, J.H.: "Flexural Strength of Prestressed Concrete Beams." Journal of the American Concrete Institute, Proceedings, Vol. 50, June, 1954, pp. 837-854.

22. Hognestad, E., Hanson, N.W., and McHenry, D.: "Concrete Stress Distribution in Ultimate Strength Design." Journal of the American Concrete Institute, Proceedings, Vol. 52, Dec., 1955, pp. 455-479.

23. Kriz, L.B.: "Ultimate Strength Criteria for Reinforced Concrete." Proceedings, ASCE, EM3, July, 1959, pp. 95-110.

24. Hognestad, E.: "Confirmation of Inelastic Stress Distribution in Concrete." Proceedings, ASCE, ST2, Mar., 1957, pp. 1-17.

25. "Report of ASCE-ACI Joint Committee on Ultimate Strength Design." Proceedings, ASCE, Vol. 81, Paper No. 809, Oct., 1955, 68 pp.

26. Mattock, A.H., Kriz, L.B., and Hognestad, E.: "Rectangular Concrete Stress Distribution in Ultimate Strength Design." Journal of the American Concrete Institute, Proceedings, Vol. 57, No. 8, Feb., 1961, pp. 875-928.

27. Pfrang, E.O., Siess, C.P., and Sozen, M.A.: "Load-Moment-Curvature Characteristics of Reinforced Concrete Cross-Sections." Journal of the American Concrete Institute, Proceedings, Vol. 61, July, 1964, pp. 763-778.

28. Bresler, B.: "Design Criteria for Reinforced Columns Under Axial Load and Biaxial Bending." Journal of the American Concrete Institute, Proceedings, Vol. 57, Nov., 1960, pp. 481-490.

29. Parme, A.L., Nieves, J.M., and Gouwens, A.: "Capacity of Reinforced Rectangular Columns Subject to Biaxial Bending." Journal of the American Concrete Institute, Proceedings, Vol. 63, Sept., 1966, pp. 911-923.

30. Richart, F.E., Woodworth, P.M., and Moorman, R.B.: "Strength and Stability of Concrete Masonry Walls." Engineering Experiment Station Bulletin No. 251, University of Illinois, Urbana, July, 1932.

31. Pauw, Adrian.: "Static Modulus of Elasticity of Concrete as Affected by Density." Journal of the American Concrete Institute, Proceedings, Vol. 32, No. 6, Dec., 1960, pp. 679-687.

32. Holm, T.A.: "Block Concrete is a Structural Material." Journal of Testing and Evaluation, Vol. 4, July, 1976, pp. 293-299.

33. Sturgeon, G.R.: "Deformations of Concrete Block and Concrete Block Masonry." Bach. Eng. Thesis, Carleton University, Ottawa, Ontario, March, 1978.

34. Sahlin, Sven.: "Structural Masonry." Prentice-Hall, Inc., N.J., 1971.

35. Eskenazi, A., Ojinaga, J., and Turkstra, C.J.: "Some Mechanical Properties of Brick and Block Masonry Interim Report." Structural Masonry Series No. 75-1, McGill

University, Dec., 1975.

36. Read, J.B., and Clements, S.W.: "The Strength of Concrete Block Walls. Phase II: Under Uniaxial Loading." Technical Report 42.473, Cement and Concrete Association, London, 1972, pp. 17.

37. Roberts, J.J.: "A Survey of Literature Relating to the Properties and Use of Concrete Blocks." Technical Report 42.467, Cement and Concrete Association, 1972.

38. Fattal, S.G., Cattaneo, L.E.: "Structural Performance of Masonry Walls Under Compression and Flexure." N.B.S. Building Science Series 73, National Bureau of Standards, Washington D.C., 1977.

39. Hatzinikolas, M., Longworth, J., and Warwaruk, J.: "Concrete Masonry Walls." Structural Engineering Report #70, Civil Engineering Department, University of Alberta, Sept., 1978.

40. CSA-S304-1977 Standard: "Masonry Design and Construction for Buildings." Canadian Standards Association, Ontario, Canada, May, 1977.

41. Self, M.W.: "Structural Properties of Load-Bearing Concrete Masonry." Masonry: Past and Present, ASTM STP 589, 1975, pp. 233-254.

42. Maurenbrecher, A.H.P.: "Use of the Prism Test to Determine Compressive Strength of Masonry." North American Masonry Conference, University of Colorado, Aug., 1978.

43. Maurenbrecher, A.H.P.: "Effect of Test Procedures on Compressive Strength of Masonry Prisms." Second Canadian Masonry Symposium, Carleton University, Ottawa, Ontario, June, 1980.

44. Drysdale, R.G., Hamid, A.A., Heidebrecht, A.C.: "Effect of Grouting on the Strength Characteristics of Concrete Block Masonry." North American Masonry Conference, University of Colorado, Aug., 1978.

45. Drysdale, R.G., Hamid, A.A.: "Behavior of Concrete Block Masonry Under Axial Compression." Journal of the American Concrete Institute, June, 1979.

APPENDIX A

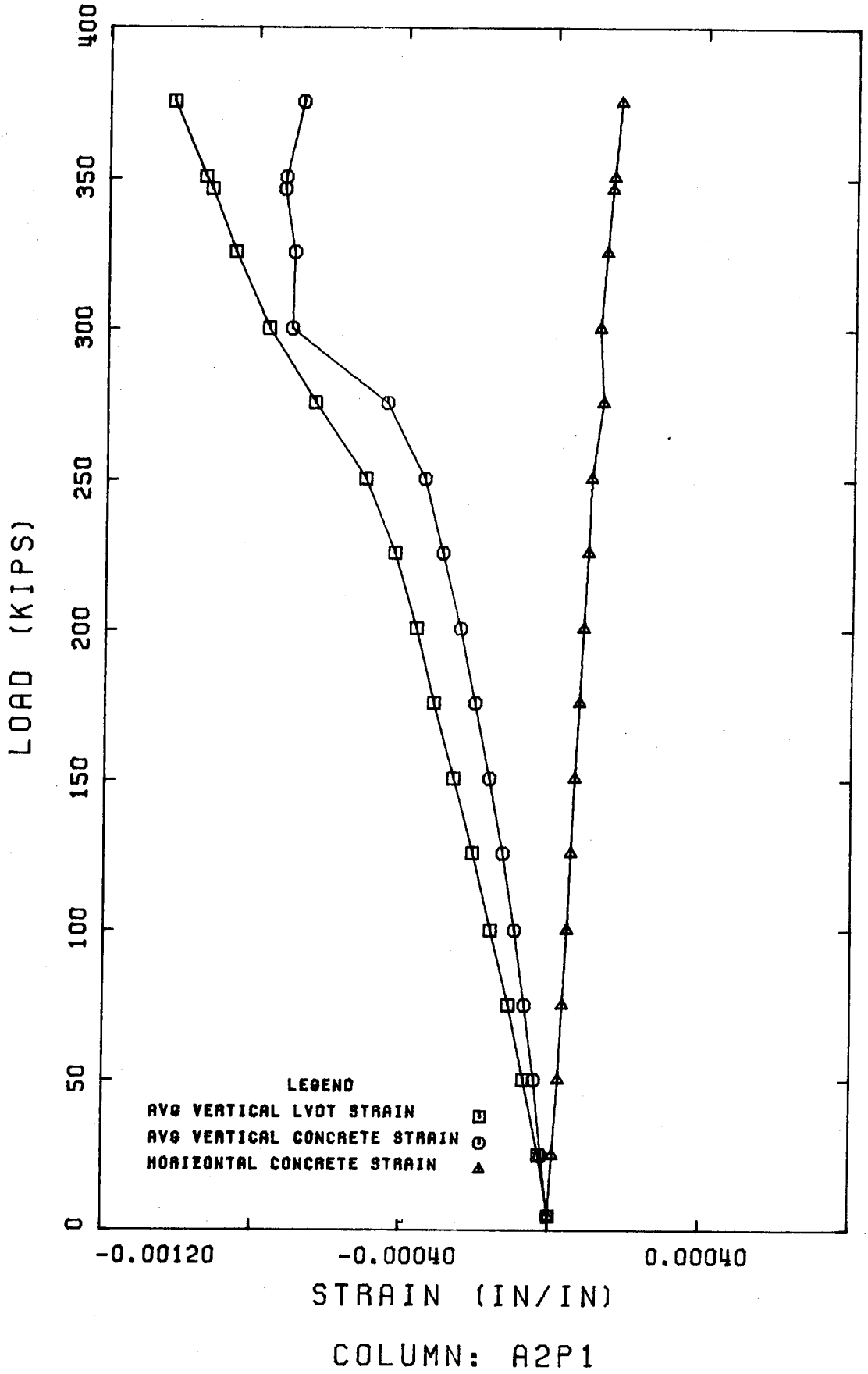
LOAD (KIPS)
0
50
100
150
200
250
300
350
400
-0.00120
-0.00040
0.00040
STRAIN (IN/IN)
LEGEND
AVG VERTICAL LVDT STRAIN
AVG VERTICAL CONCRETE STRAIN
HORIZONTAL CONCRETE STRAIN
COLUMN: A2P1

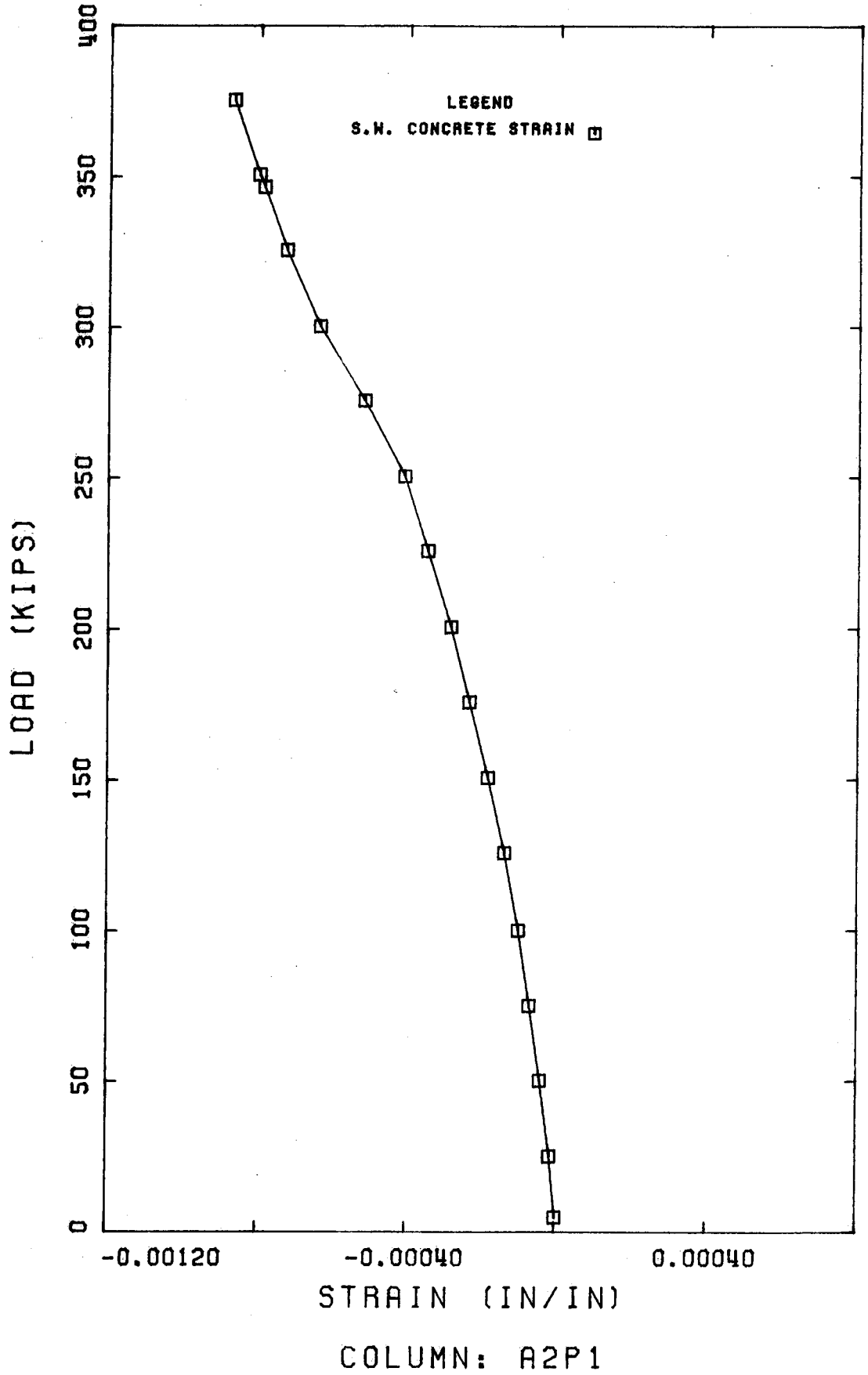
LEGEND
S.W. CONCRETE STRAIN
LOAD (KIPS)
0
50
100
150
200
250
300
350
400
-0.00120
-0.00040
0.00040
STRAIN (IN/IN)

COLUMN: A2P1

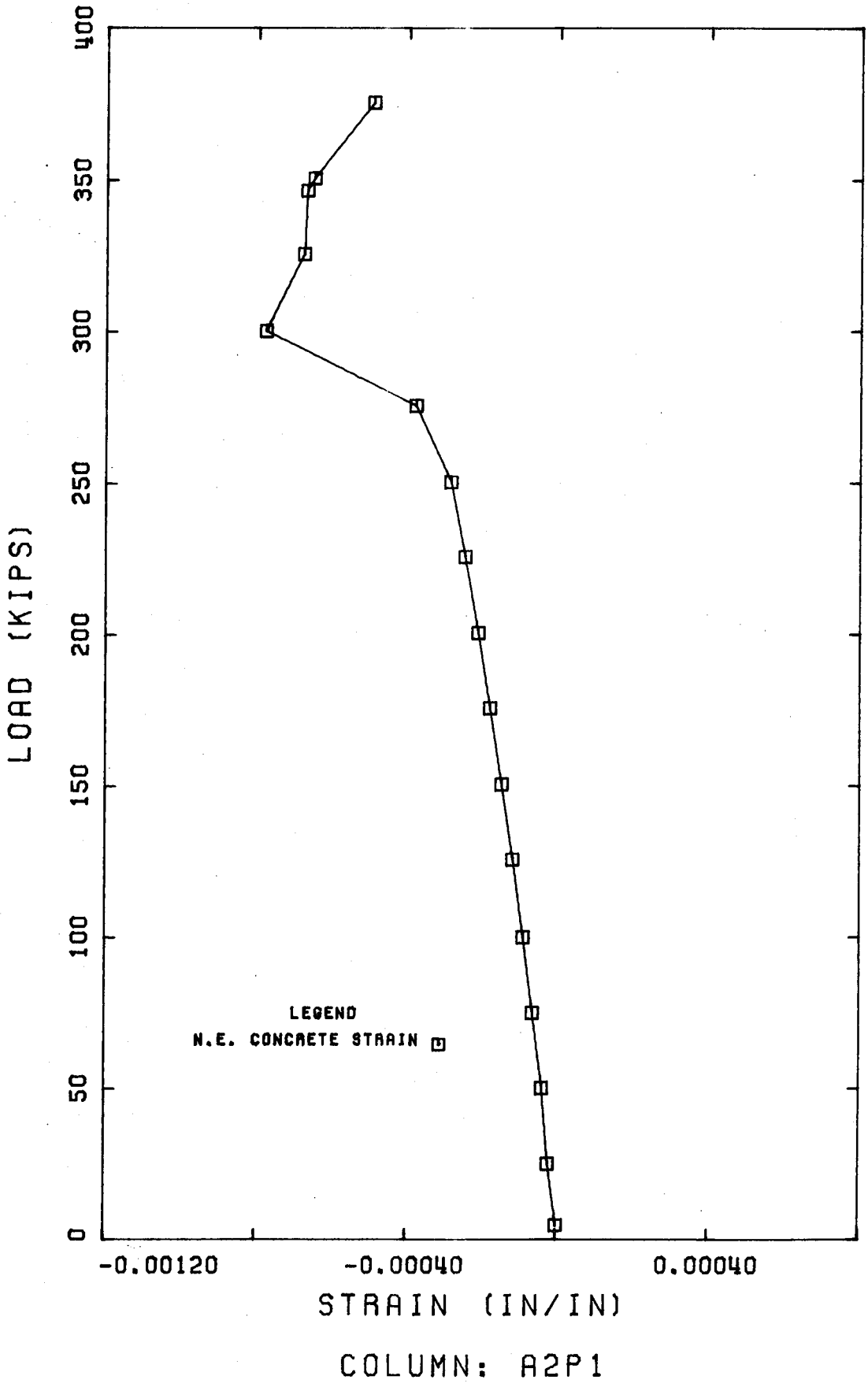
LOAD (KIPS)
0
50
100
150
200
250
300
350
400
-0.00120
-0.00040
0.00040
STRAIN (IN/IN)
LEGEND
N.E. CONCRETE STRAIN
COLUMN: A2P1

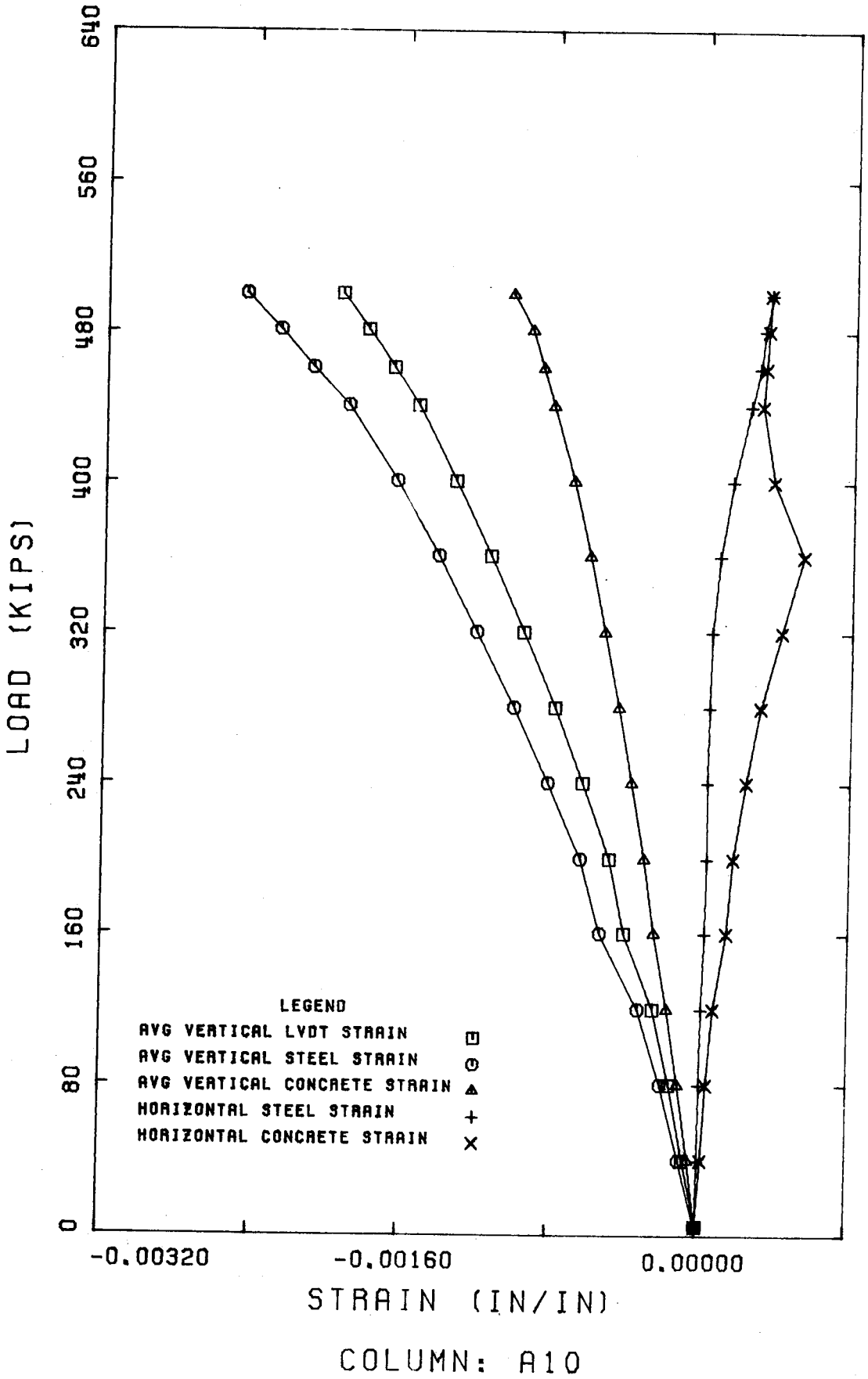
LOAD (KIPS)
640
560
480
400
320
240
160
80
0
-0.00320
-0.00160
0.00000
STRAIN (IN/IN)
LEGEND
AVG VERTICAL LVDT STRAIN
AVG VERTICAL STEEL STRAIN
AVG VERTICAL CONCRETE STRAIN
HORIZONTAL STEEL STRAIN
HORIZONTAL CONCRETE STRAIN

COLUMN: A10

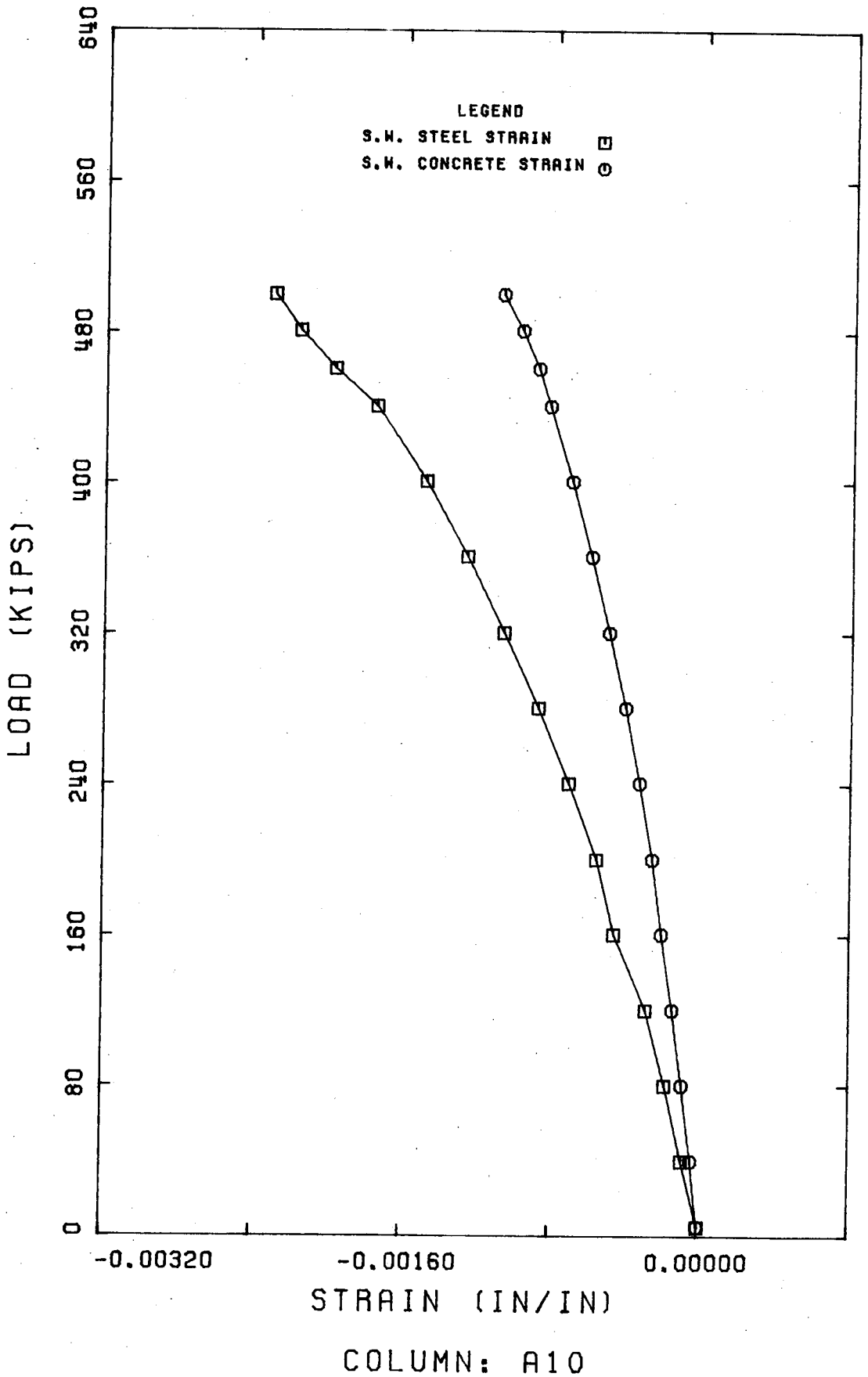
LEGEND
S.W. STEEL STRAIN
S.W. CONCRETE STRAIN
LOAD (KIPS)
0
80
160
240
320
400
480
560
640
-0.00320
-0.00160
0.00000
STRAIN (IN/IN)

COLUMN: A10

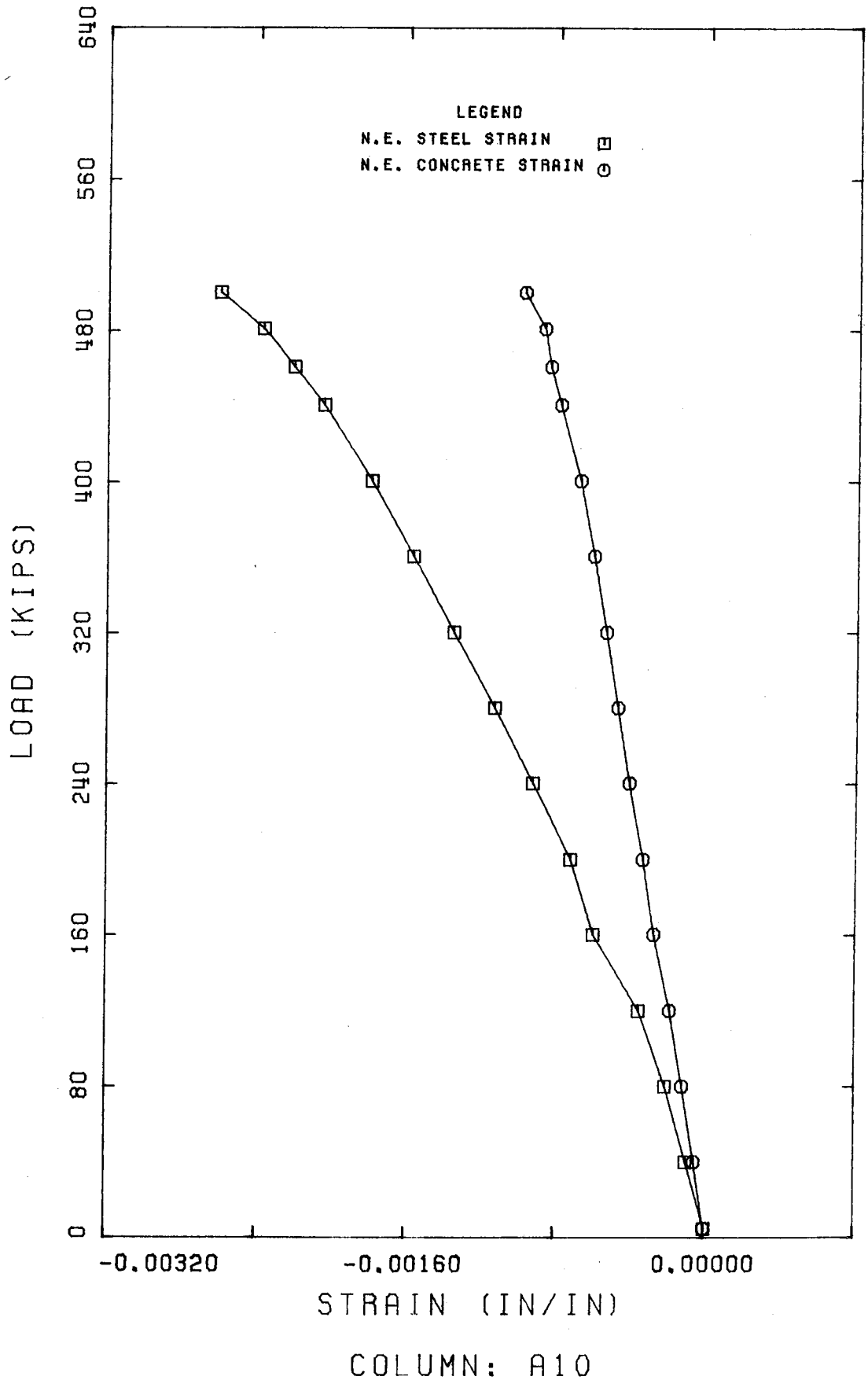
LEGEND
N.E. STEEL STRAIN
N.E. CONCRETE STRAIN
LOAD (KIPS)
0
80
160
240
320
400
480
560
640
-0.00320
-0.00160
0.00000
STRAIN (IN/IN)

COLUMN: A10

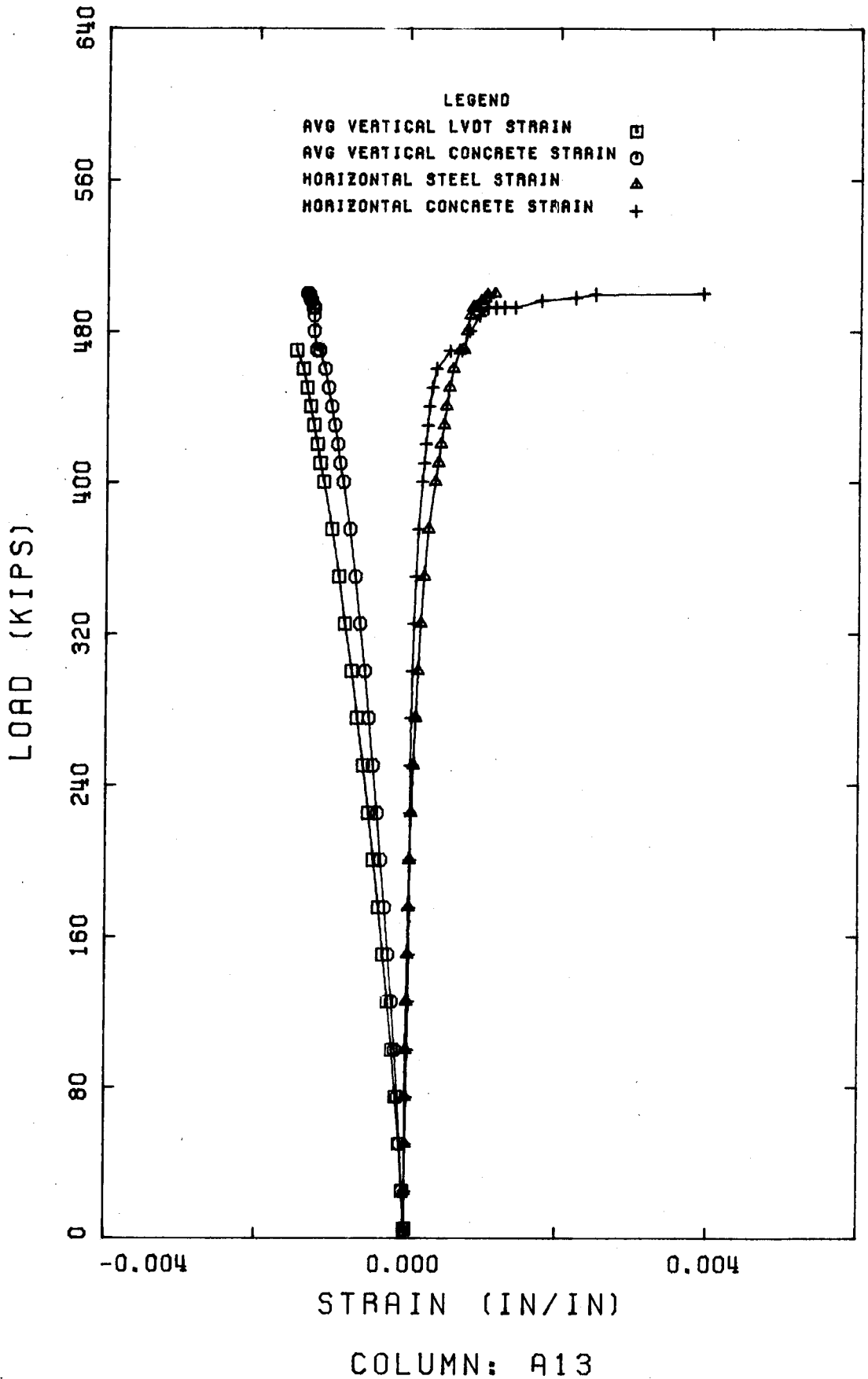
LEGEND
AVG VERTICAL LVDT STRAIN
AVG VERTICAL CONCRETE STRAIN
HORIZONTAL STEEL STRAIN
HORIZONTAL CONCRETE STRAIN
LOAD (KIPS)
0
80
160
240
320
400
480
560
640
-0.004
0.000
0.004
STRAIN (IN/IN)

COLUMN: A13

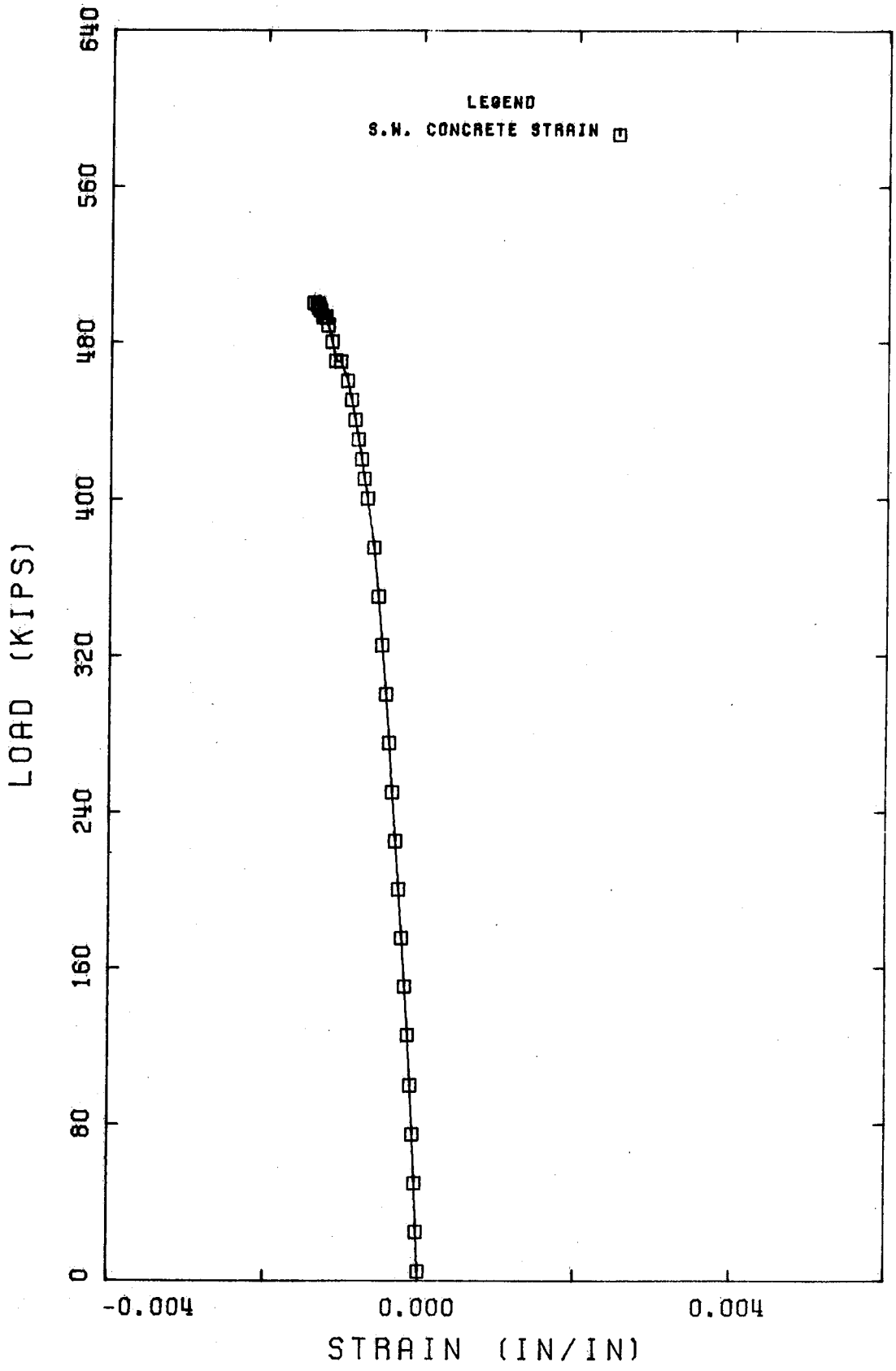
LEGEND
S.W. CONCRETE STRAIN
LOAD (KIPS)
640
560
480
400
320
240
160
80
0
-0.004
0.000
0.004
STRAIN (IN/IN)

COLUMN: A13

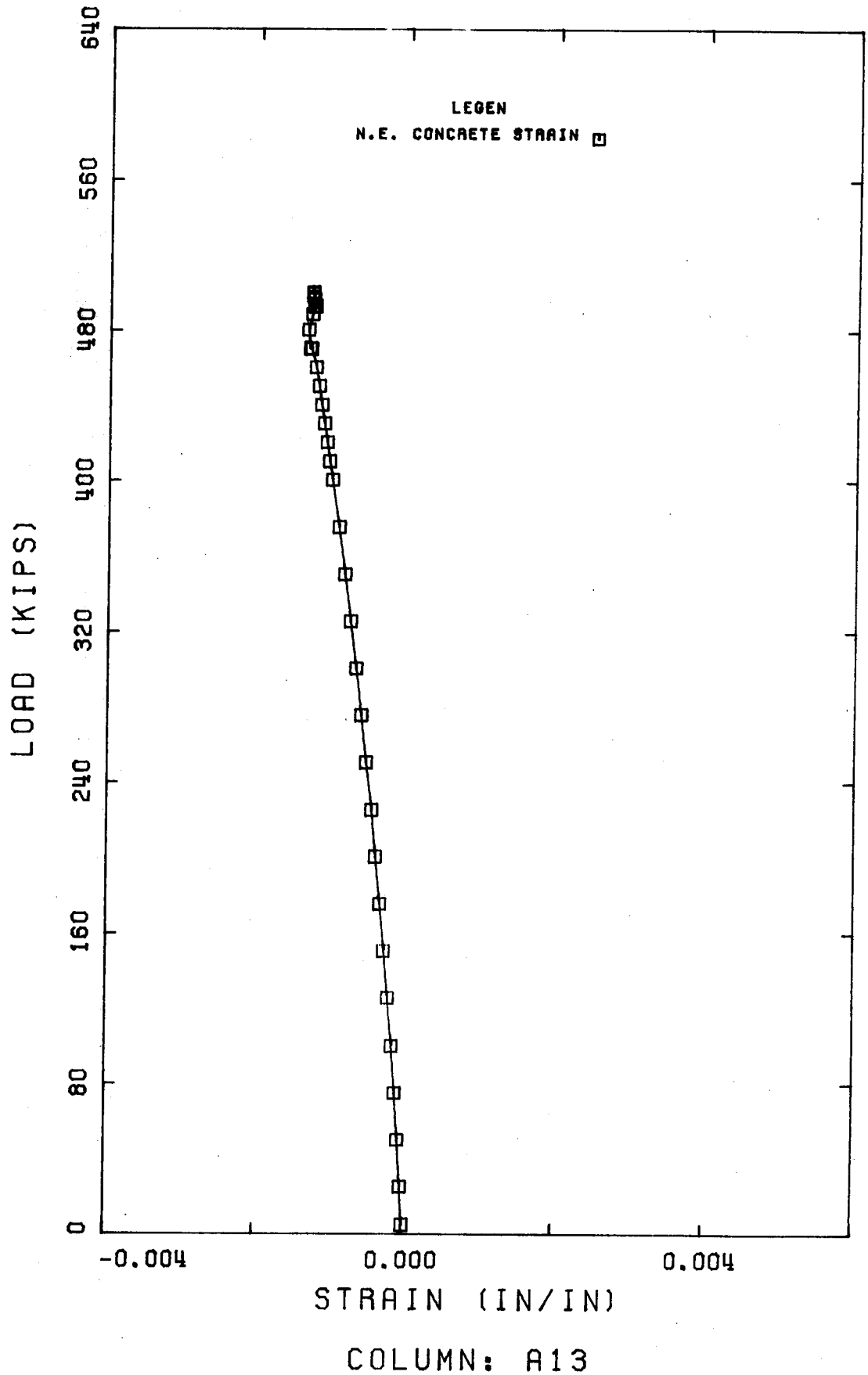
LEGEN
N.E. CONCRETE STRAIN
LOAD (KIPS)
0
80
160
240
320
400
480
560
640
-0.004
0.000
0.004
STRAIN (IN/IN)

COLUMN: A13

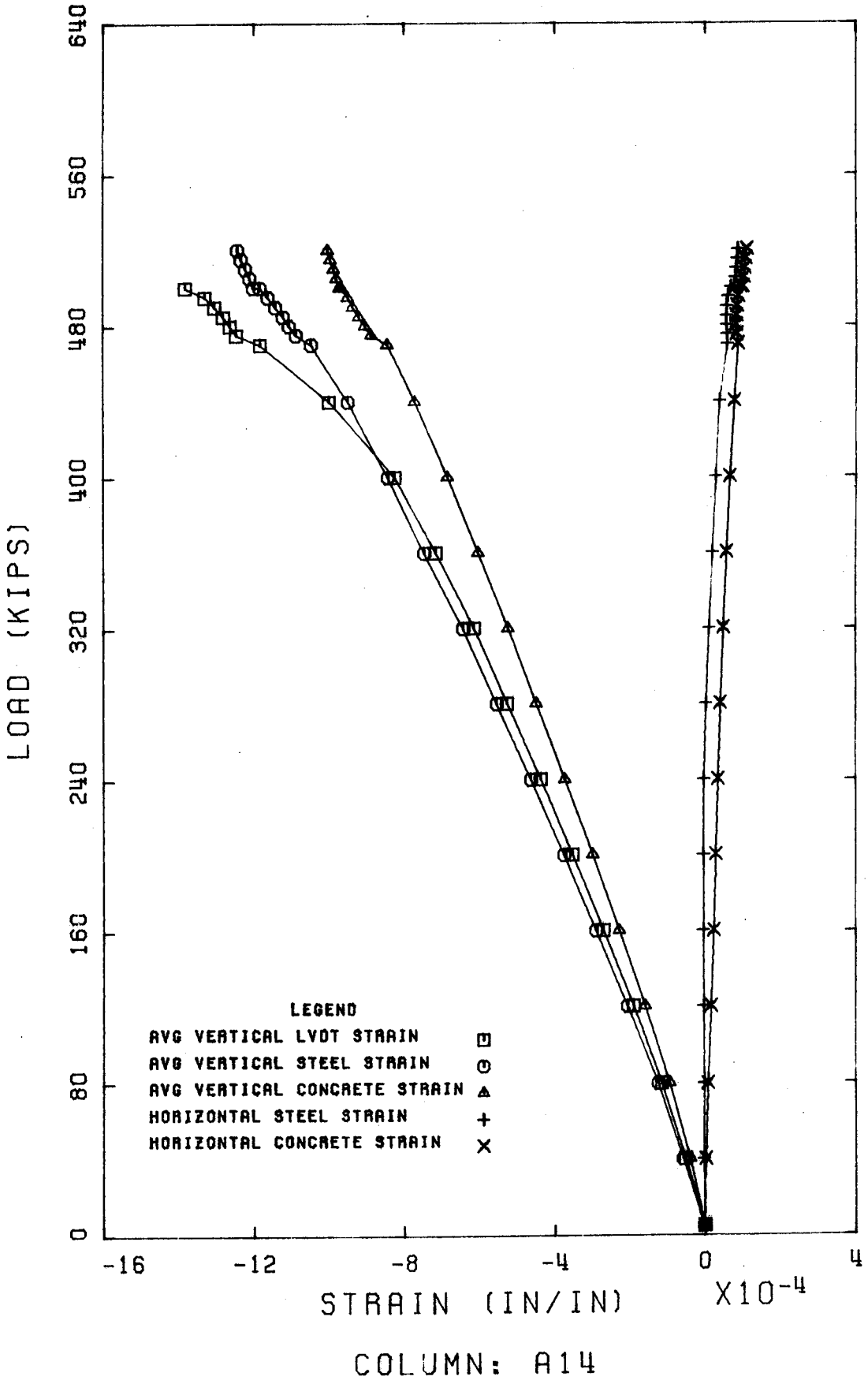
LOAD (KIPS)
640
560
480
400
320
240
160
80
0
-16
-12
-8
-4
0
4
STRAIN (IN/IN)
X10-4
LEGEND
AVG VERTICAL LVDT STRAIN
AVG VERTICAL STEEL STRAIN
AVG VERTICAL CONCRETE STRAIN
HORIZONTAL STEEL STRAIN
HORIZONTAL CONCRETE STRAIN

COLUMN: A14

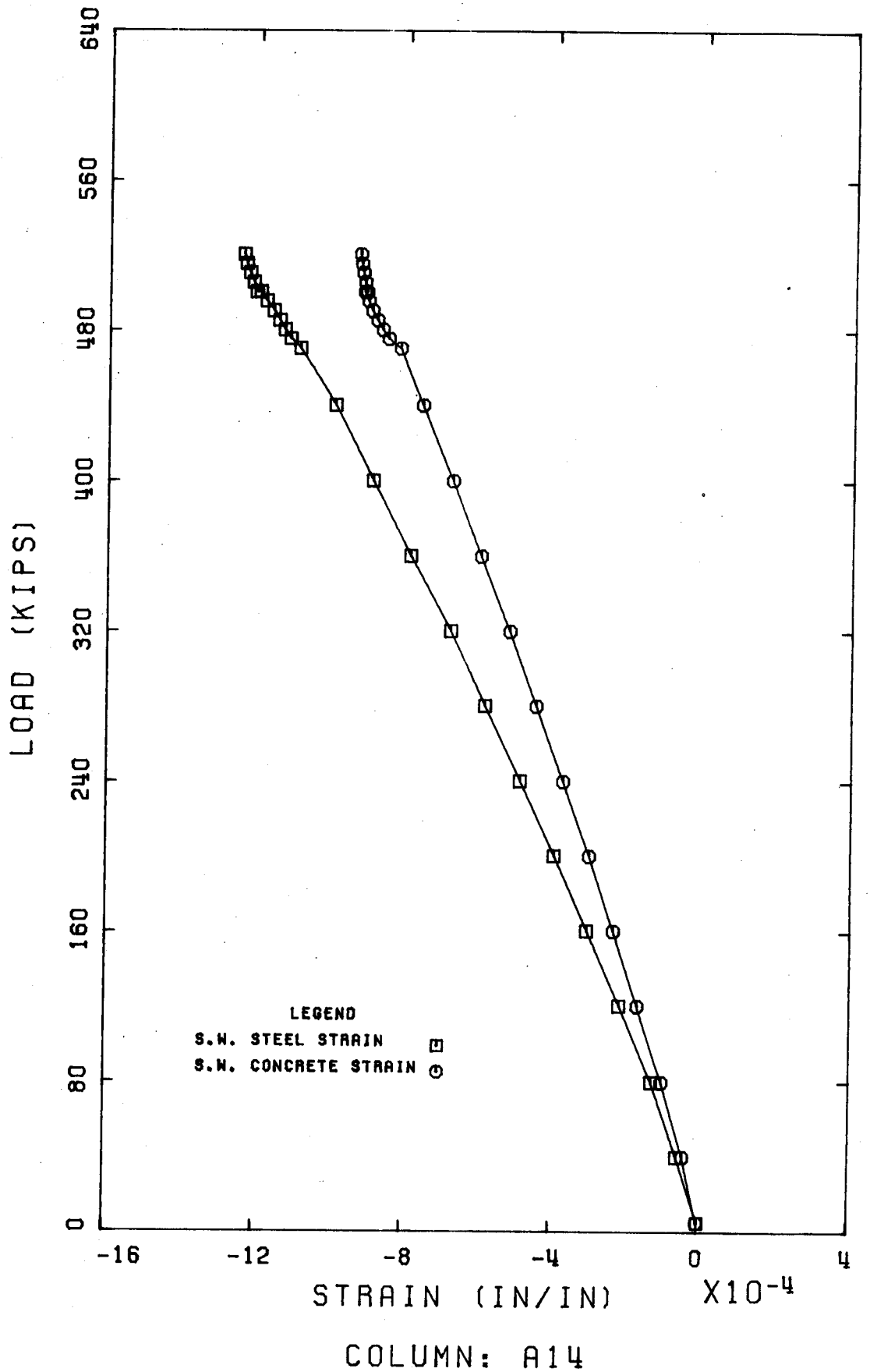
LOAD (KIPS)
640
560
480
400
320
240
160
80
0
-16
-12
-8
-4
0
4
STRAIN (IN/IN)
X10-4
LEGEND
S.W. STEEL STRAIN
S.W. CONCRETE STRAIN

COLUMN: A14

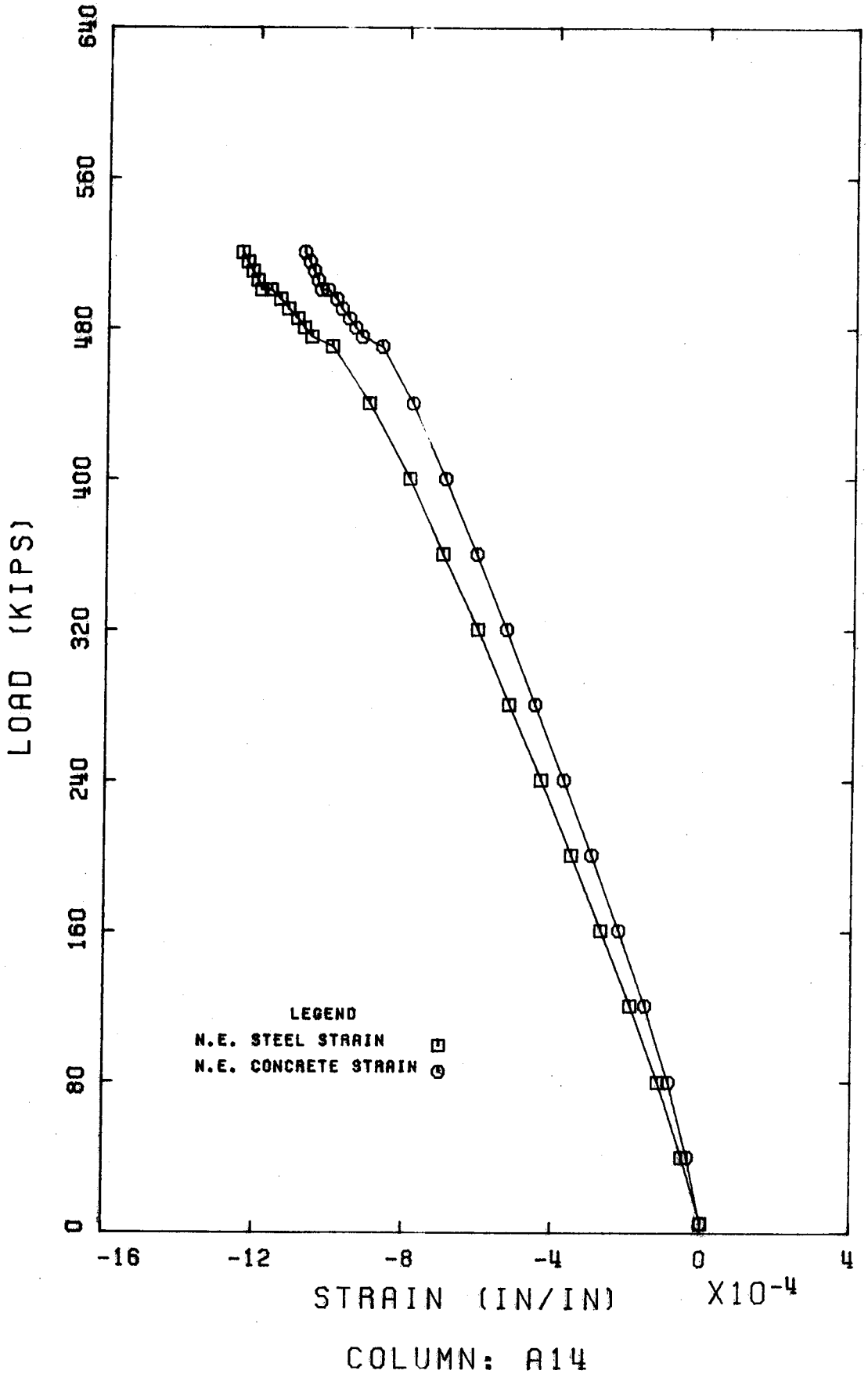
640
560
480
400
320
240
160
80
0
LOAD (KIPS)
-16
-12
-8
-4
0
4
STRAIN (IN/IN)
X10-4
LEGEND
N.E. STEEL STRAIN
N.E. CONCRETE STRAIN
COLUMN: A14

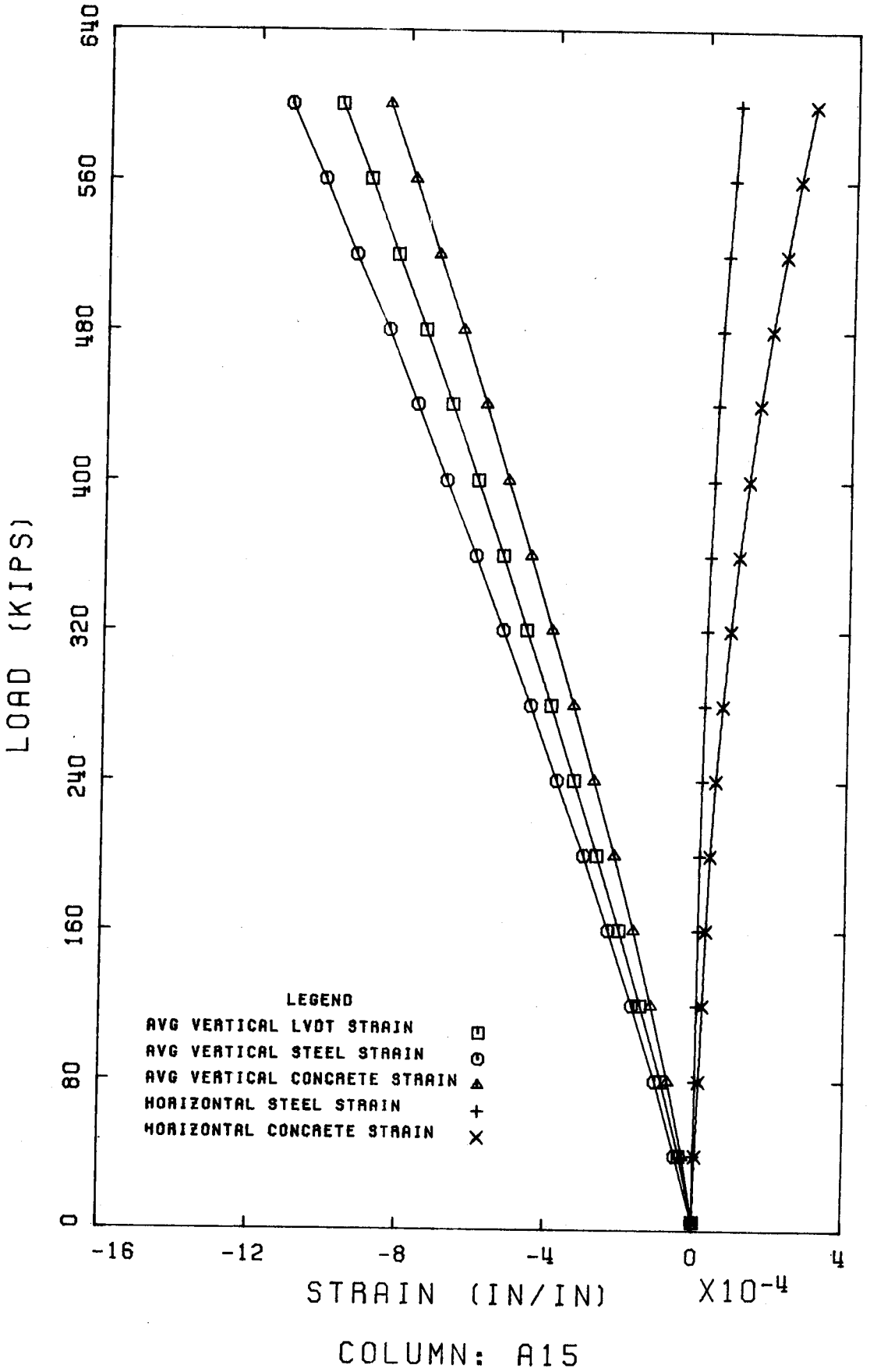
LOAD (KIPS)
0
80
160
240
320
400
480
560
640
-16
-12
-8
-4
0
4
STRAIN (IN/IN) X10-4
LEGEND
AVG VERTICAL LVDT STRAIN
AVG VERTICAL STEEL STRAIN
AVG VERTICAL CONCRETE STRAIN
HORIZONTAL STEEL STRAIN
HORIZONTAL CONCRETE STRAIN

COLUMN: A15

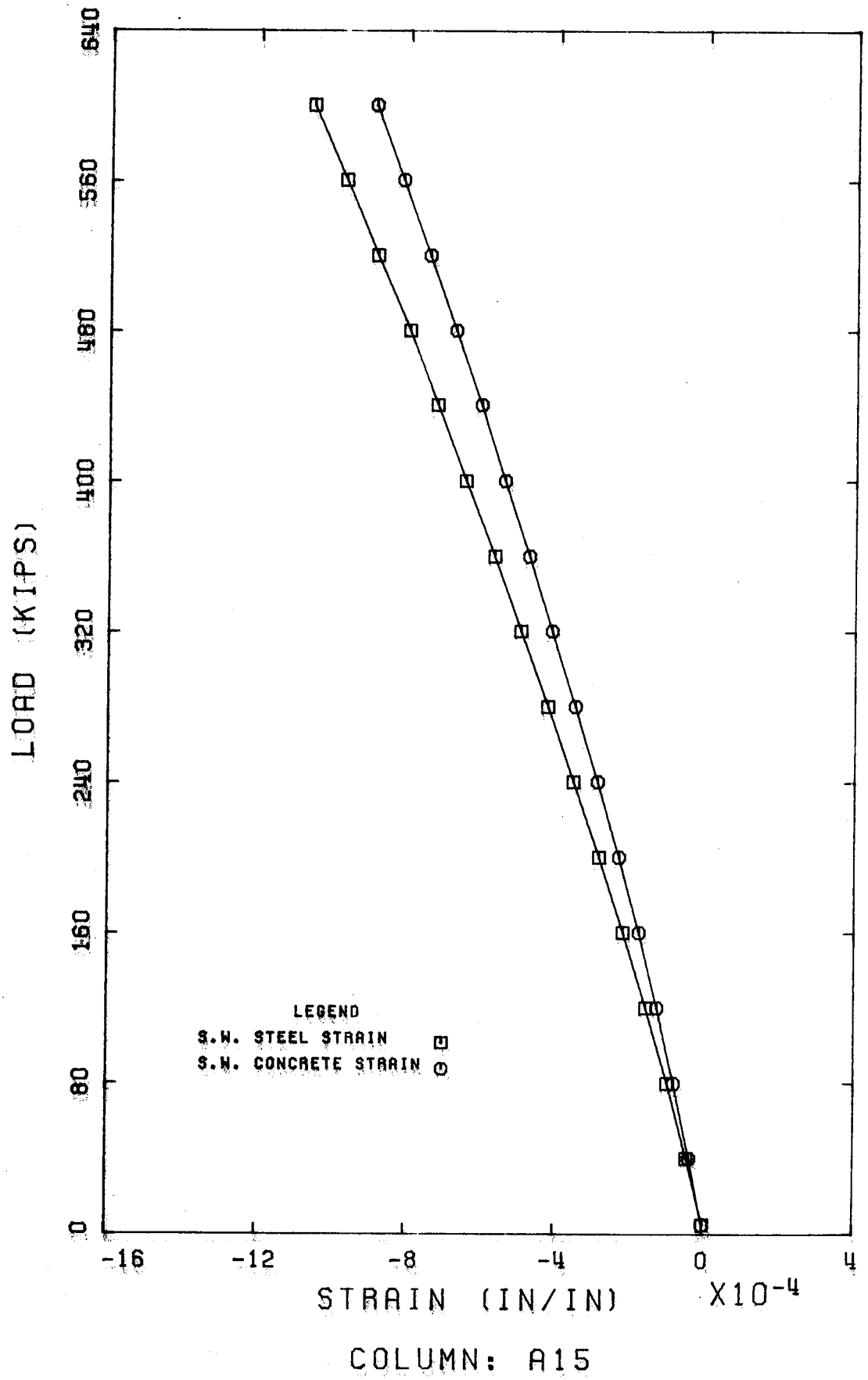
LOAD (KIPS)
640
560
480
400
320
240
160
80
0
-16
-12
-8
-4
0
4
STRAIN (IN/IN) X10-4
LEGEND
S.W. STEEL STRAIN
S.W. CONCRETE STRAIN
COLUMN: A15

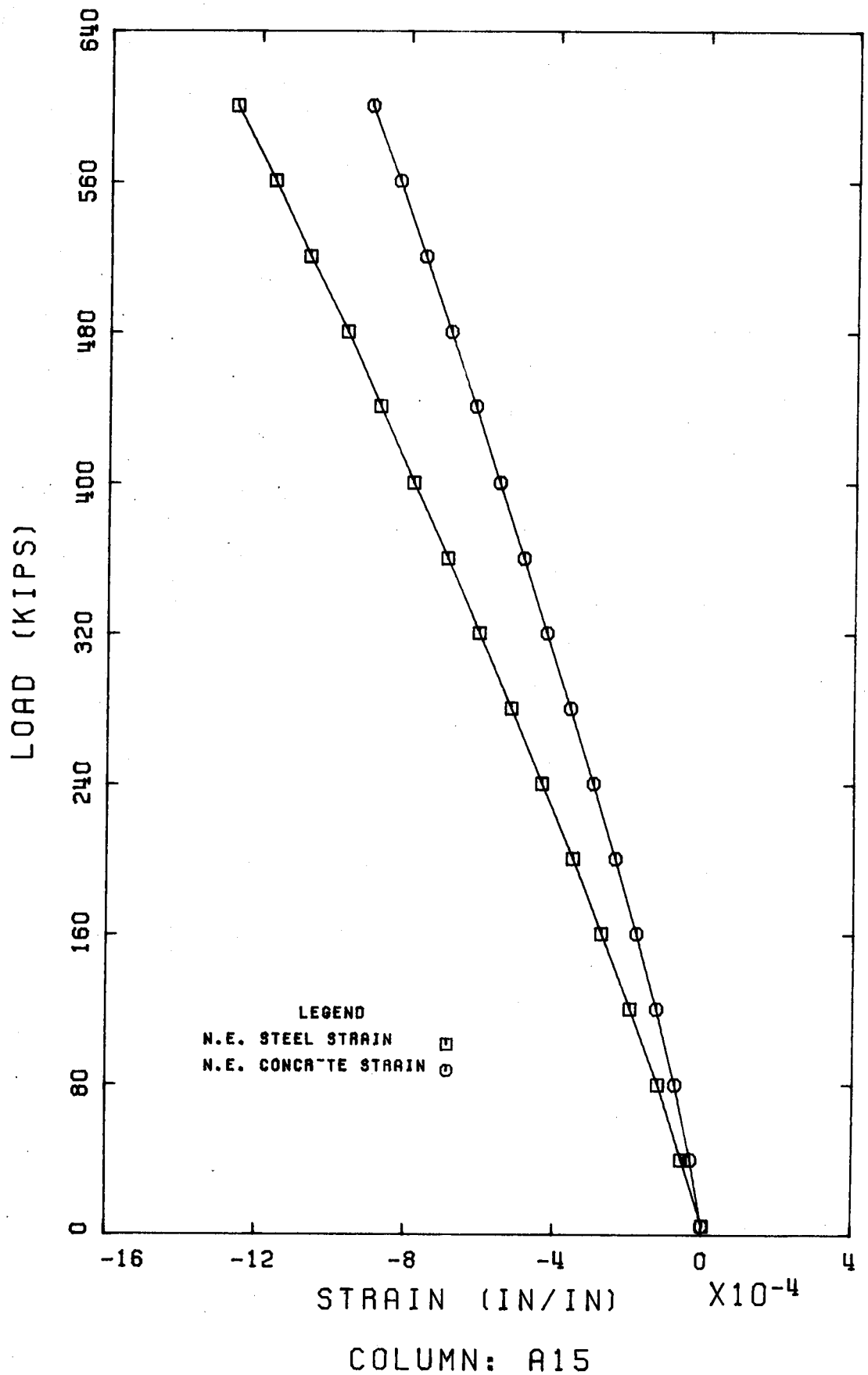
LOAD (KIPS)
0
80
160
240
320
400
480
560
640
-16
-12
-8
-4
0
4
STRAIN (IN/IN)
X10-4
LEGEND
N.E. STEEL STRAIN
N.E. CONCRETE STRAIN

COLUMN: A15

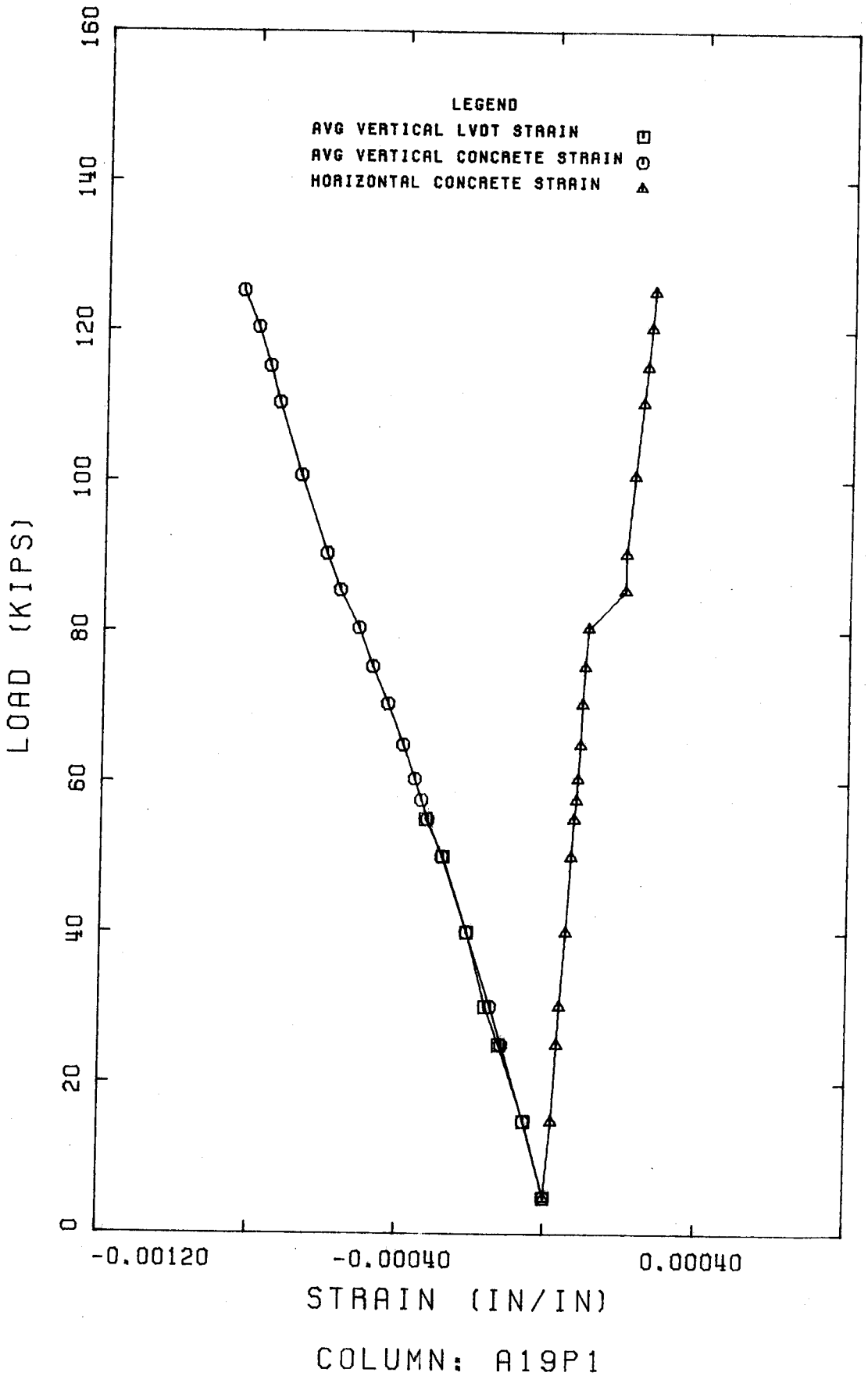
LEGEND
AVG VERTICAL LVDT STRAIN
AVG VERTICAL CONCRETE STRAIN
HORIZONTAL CONCRETE STRAIN
LOAD (KIPS)
0
20
40
60
80
100
120
140
160
-0.00120
-0.00040
0.00040
STRAIN (IN/IN)
COLUMN: A19P1

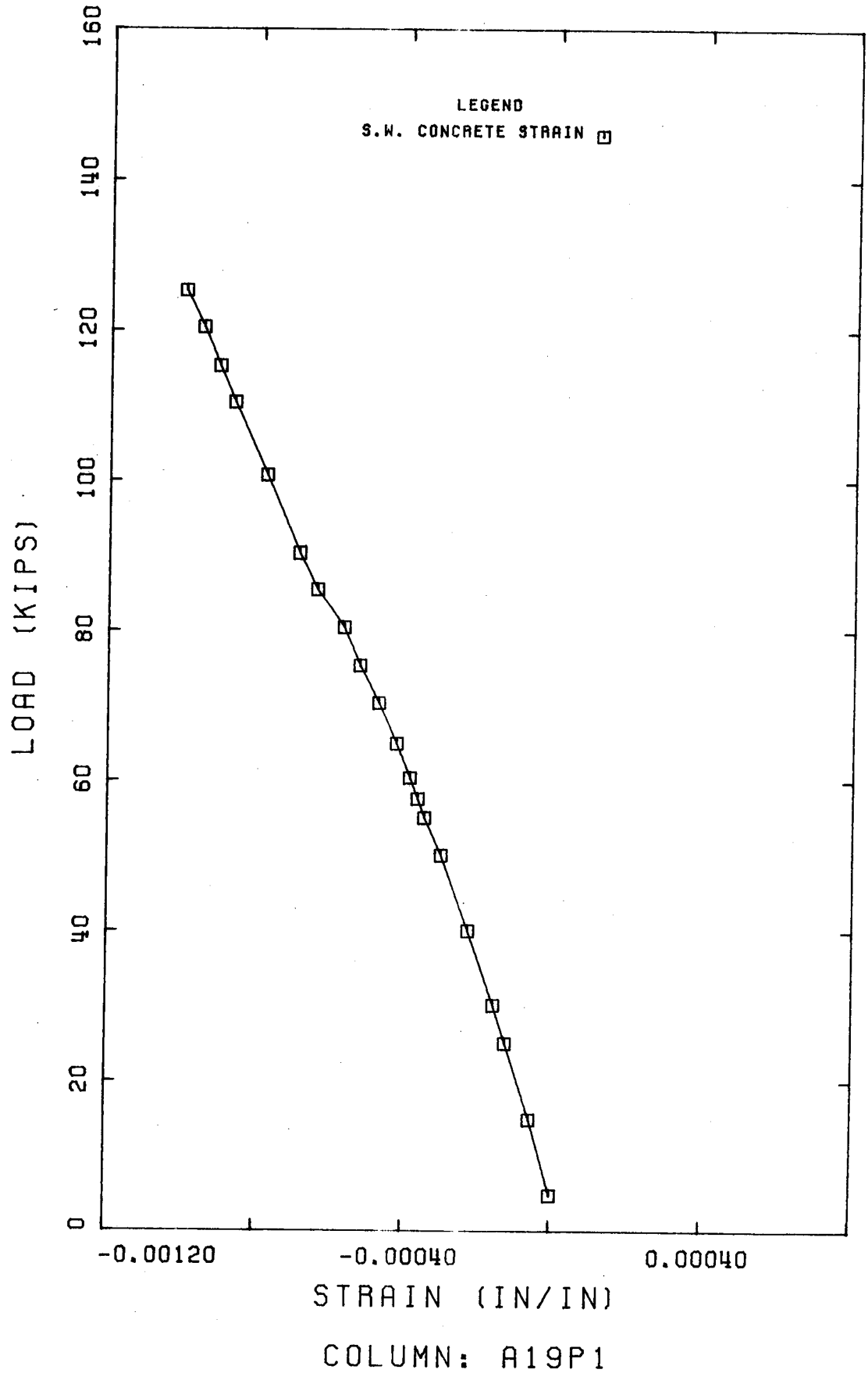

COLUMN: A19P1

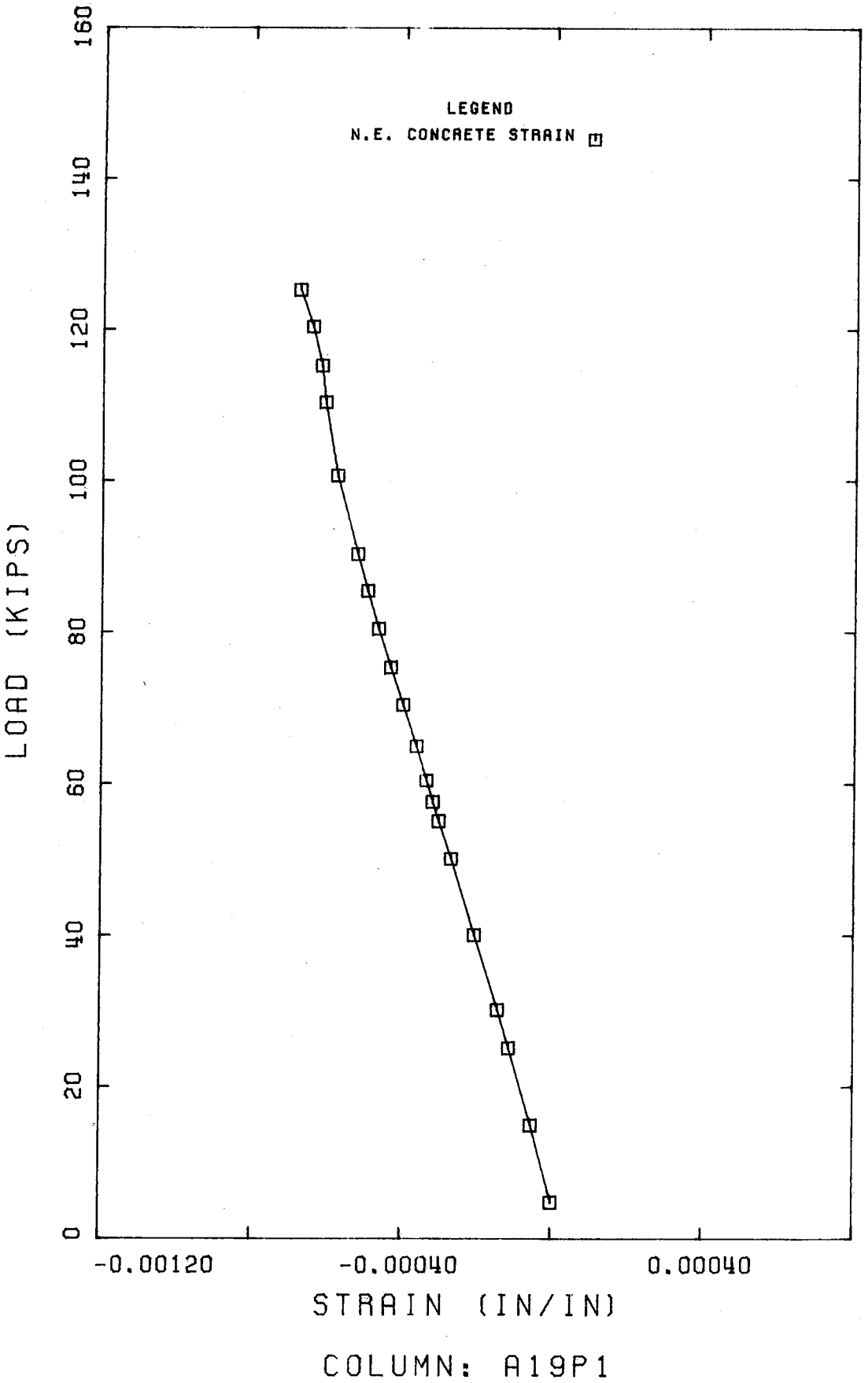

COLUMN: A19P1

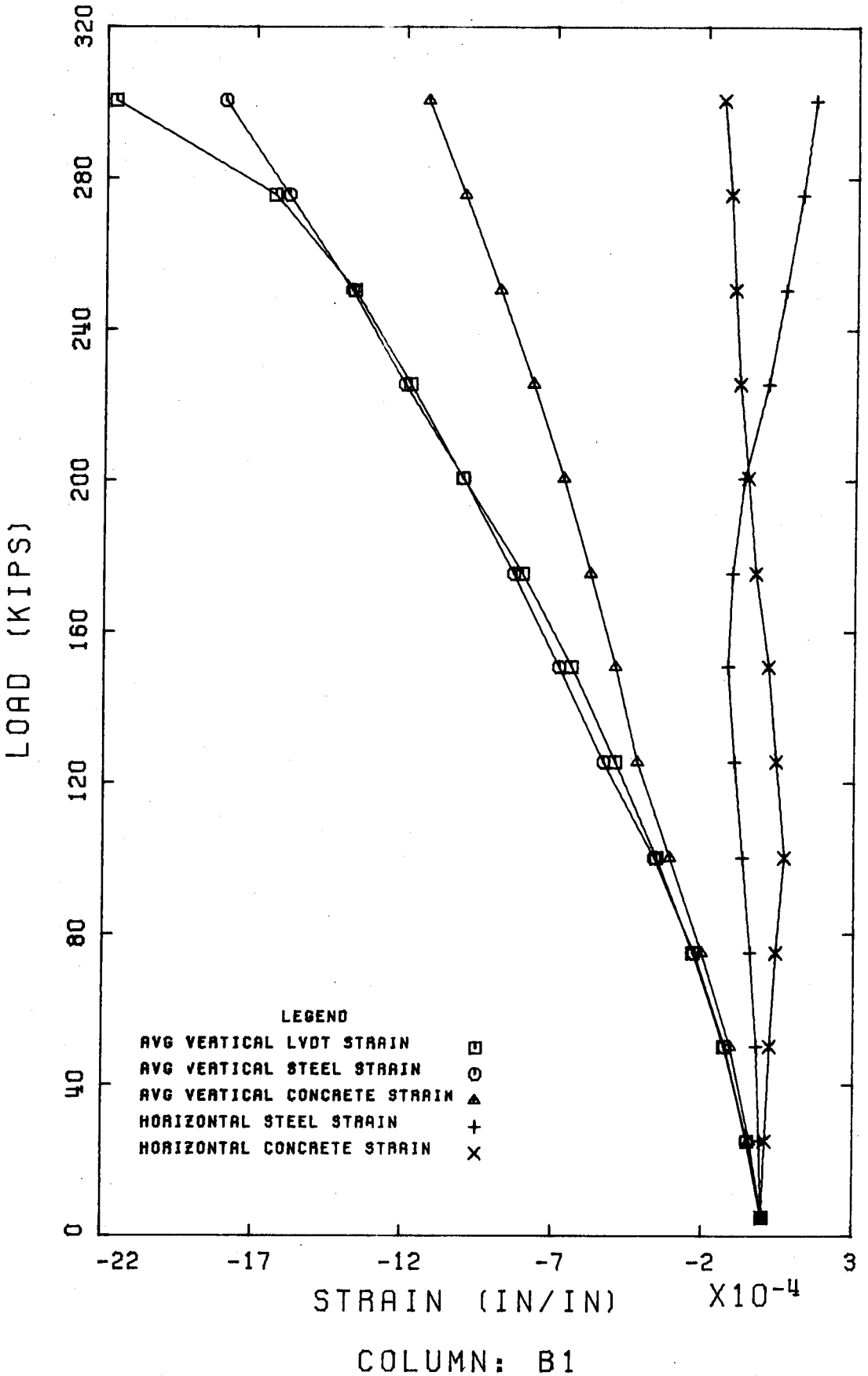
LOAD (KIPS)
0
40
80
120
160
200
240
280
320
-22
-17
-12
-7
-2
3
STRAIN (IN/IN)
X10-4
LEGEND
AVG VERTICAL LVDT STRAIN
AVG VERTICAL STEEL STRAIN
AVG VERTICAL CONCRETE STRAIN
HORIZONTAL STEEL STRAIN
HORIZONTAL CONCRETE STRAIN

COLUMN: B1

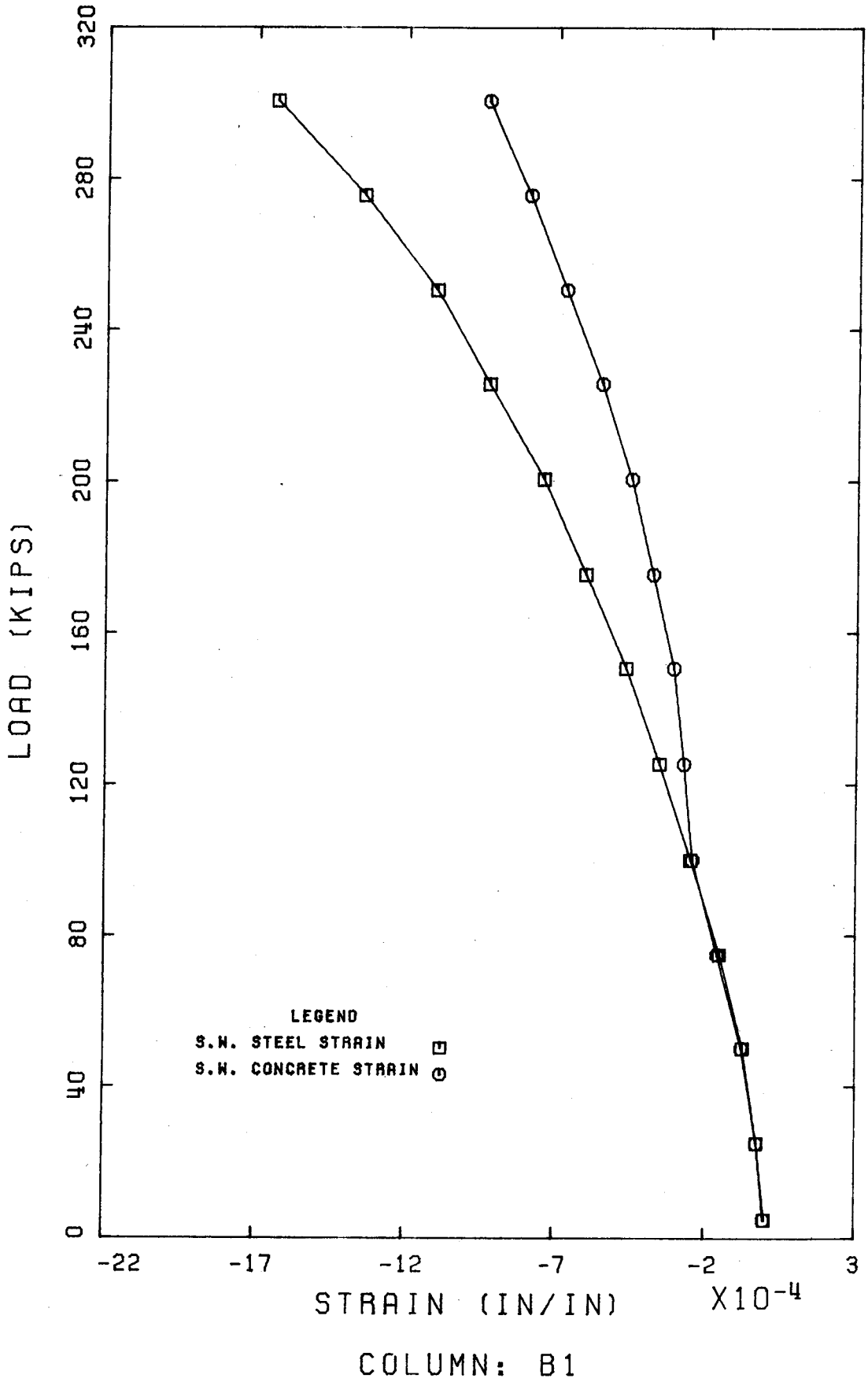
LOAD (KIPS)
320
280
240
200
160
120
80
40
0
-22
-17
-12
-7
-2
3
STRAIN (IN/IN) X10-4
LEGEND
S.W. STEEL STRAIN
S.W. CONCRETE STRAIN
COLUMN: B1

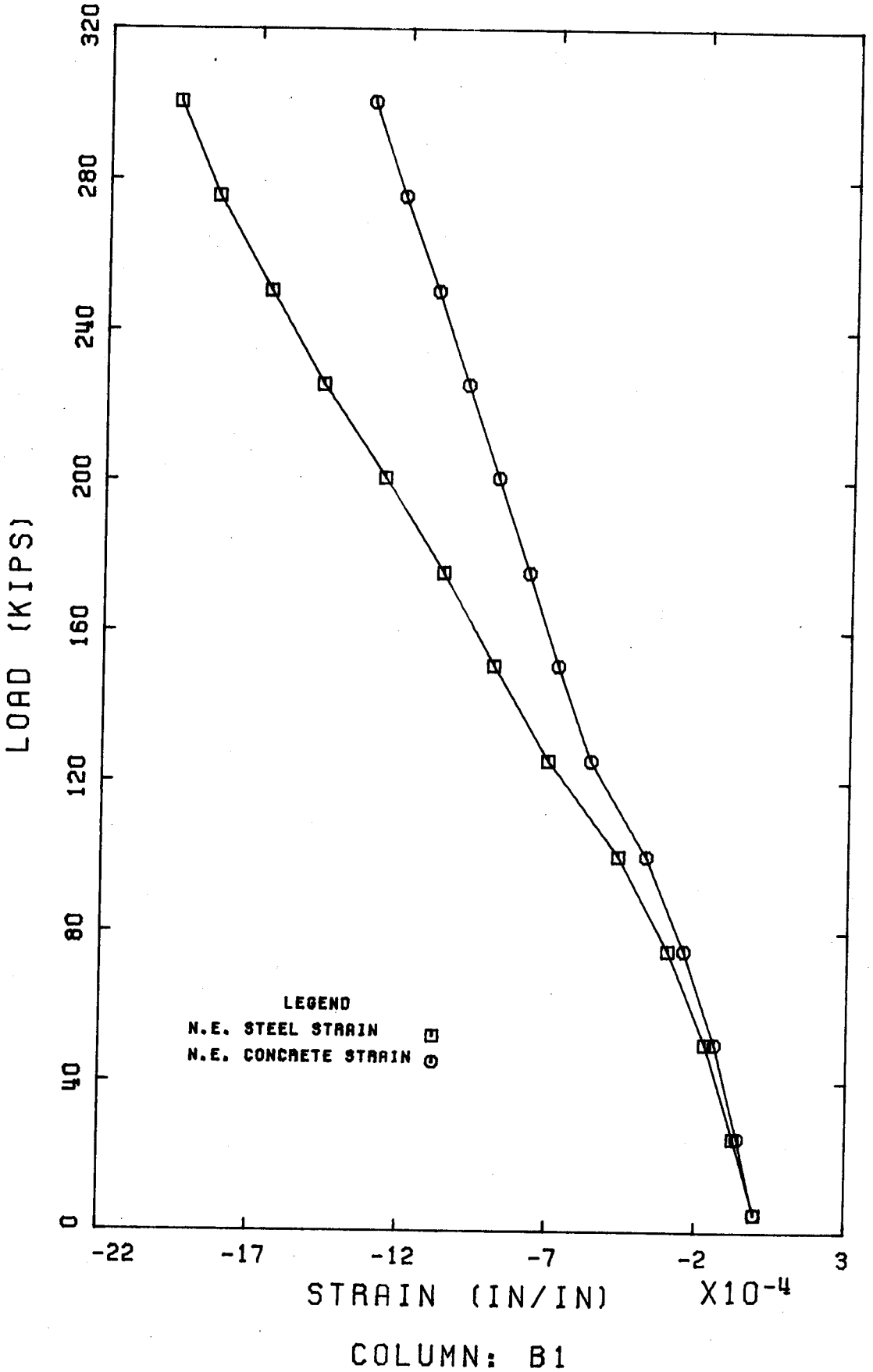
LOAD (KIPS)
0
40
80
120
160
200
240
280
320
-22
-17
-12
-7
-2
3
STRAIN (IN/IN) X10-4
LEGEND
N.E. STEEL STRAIN
N.E. CONCRETE STRAIN

COLUMN: B1

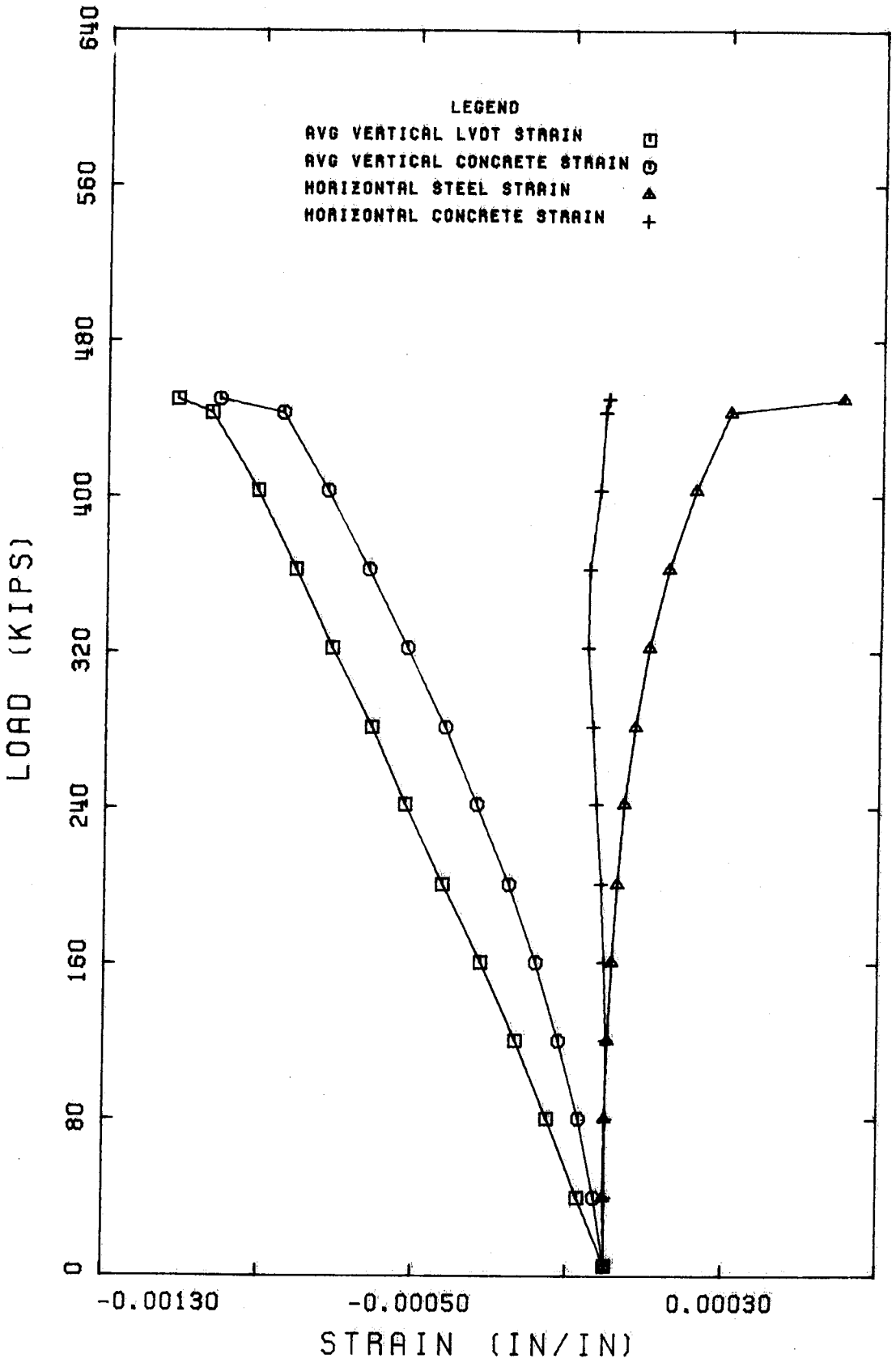
LEGEND
AVG VERTICAL LVDT STRAIN
AVG VERTICAL CONCRETE STRAIN
HORIZONTAL STEEL STRAIN
HORIZONTAL CONCRETE STRAIN
LOAD (KIPS)
0
80
160
240
320
400
480
560
640
-0.00130
-0.00050
0.00030
STRAIN (IN/IN)

COLUMN: C4

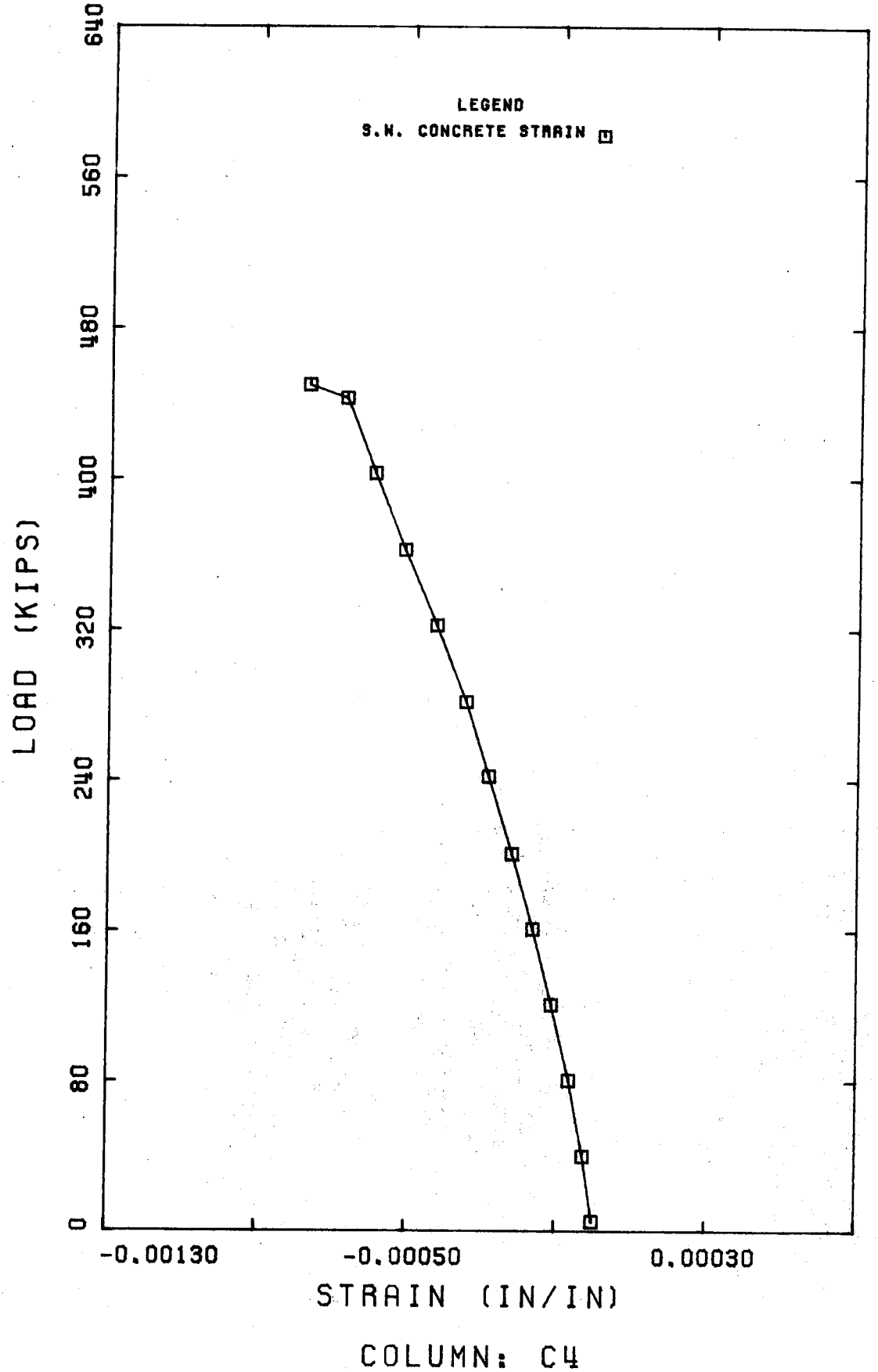
LEGEND
S.W. CONCRETE STRAIN
LOAD (KIPS)
640
560
480
400
320
240
160
80
0
-0.00130
-0.00050
0.00030
STRAIN (IN/IN)

COLUMN: C4

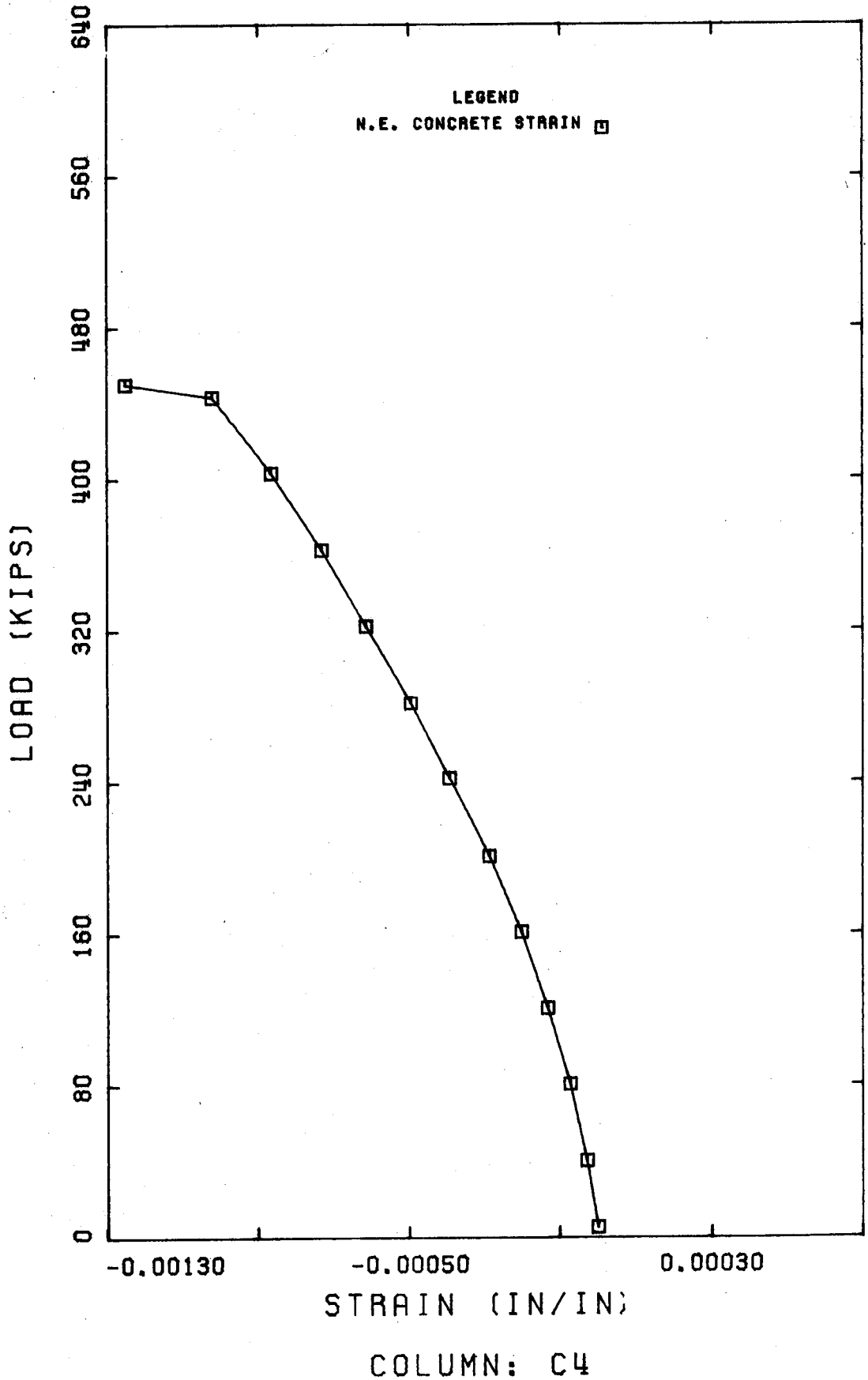
LEGEND
N.E. CONCRETE STRAIN
LOAD (KIPS)
640
560
480
400
320
240
160
80
0
-0.00130
-0.00050
0.00030
STRAIN (IN/IN)

COLUMN: C4

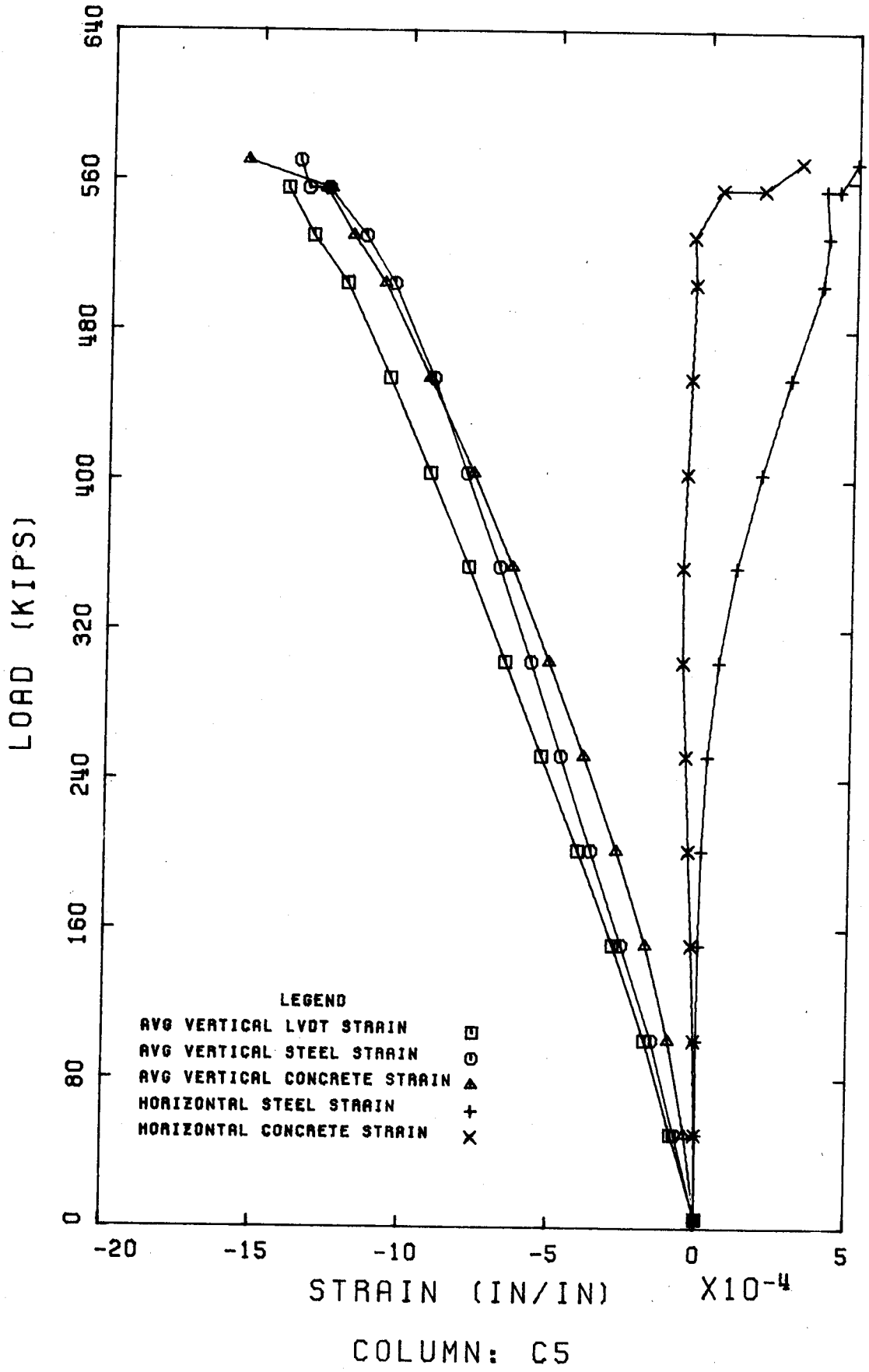
LOAD (KIPS)
640
560
480
400
320
240
160
80
0
-20
-15
-10
-5
0
5
STRAIN (IN/IN) X10-4
LEGEND
AVG VERTICAL LVDT STRAIN
AVG VERTICAL STEEL STRAIN
AVG VERTICAL CONCRETE STRAIN
HORIZONTAL STEEL STRAIN
HORIZONTAL CONCRETE STRAIN

COLUMN: C5

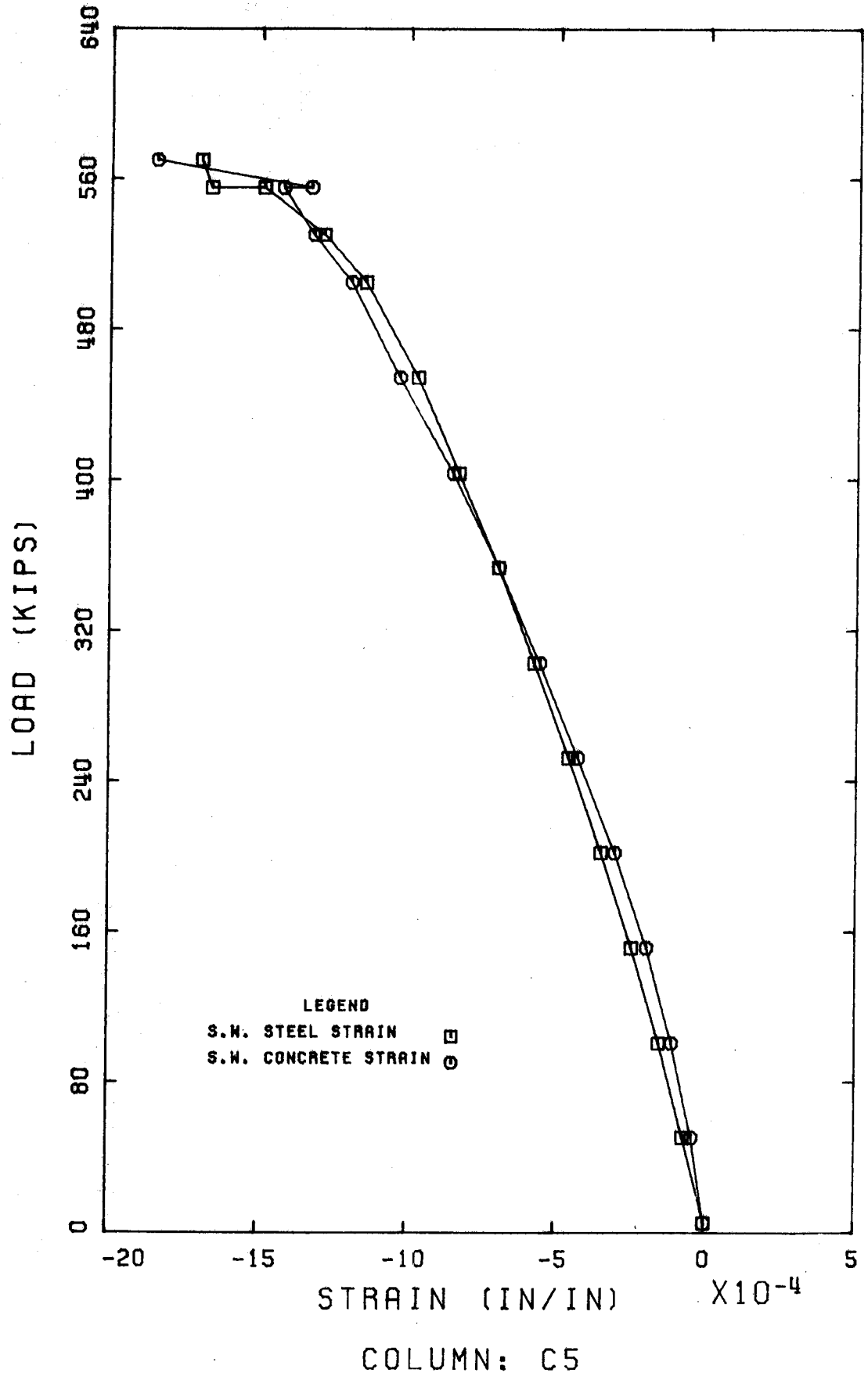
LOAD (KIPS)
640
560
480
400
320
240
160
80
0
-20
-15
-10
-5
0
5
STRAIN (IN/IN) X10-4
LEGEND
S.W. STEEL STRAIN
S.W. CONCRETE STRAIN
COLUMN: C5

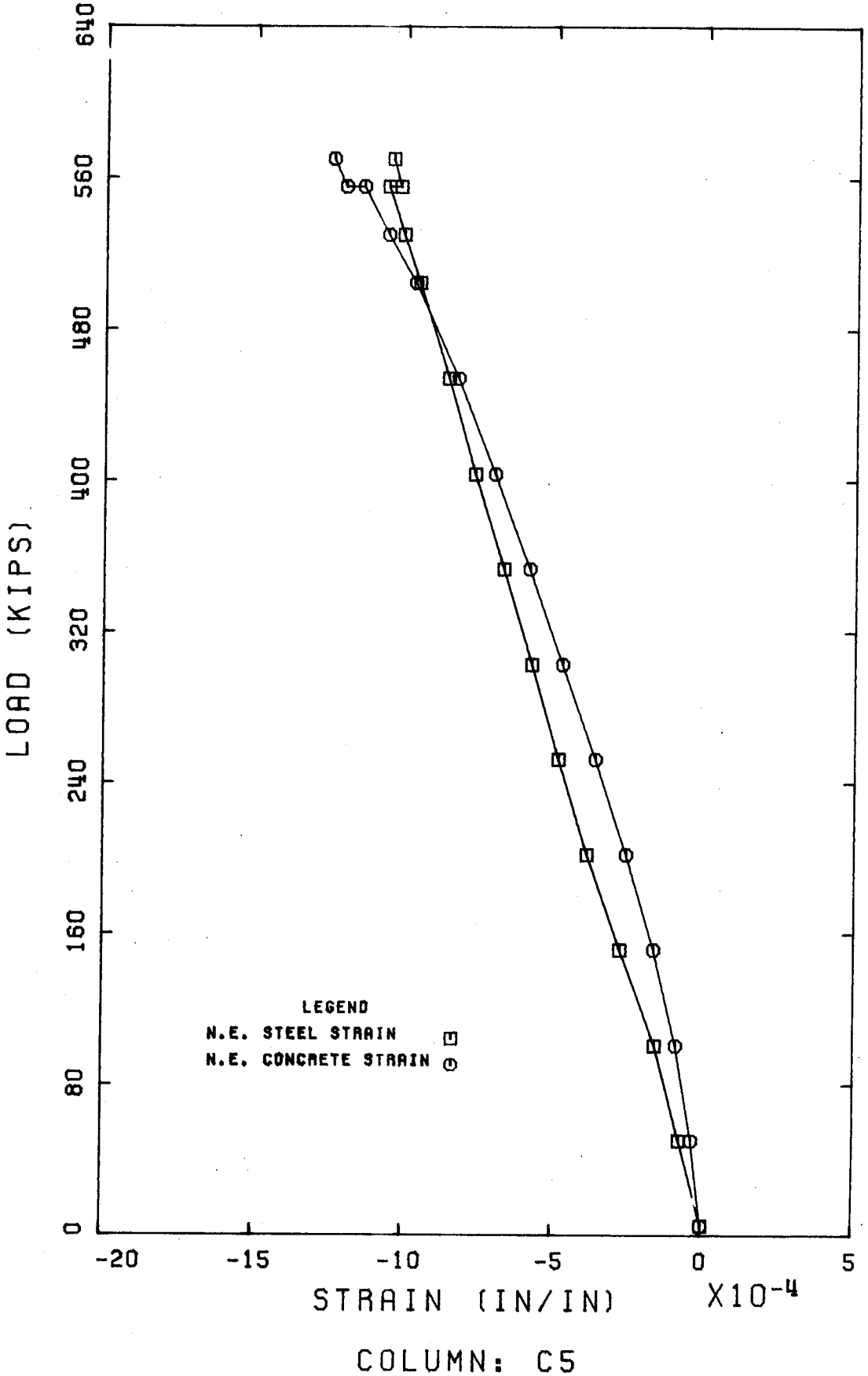
640
560
480
400
320
240
160
80
0
LOAD (KIPS)
-20
-15
-10
-5
0
5
STRAIN (IN/IN)
X10-4
LEGEND
N.E. STEEL STRAIN
N.E. CONCRETE STRAIN

COLUMN: C5

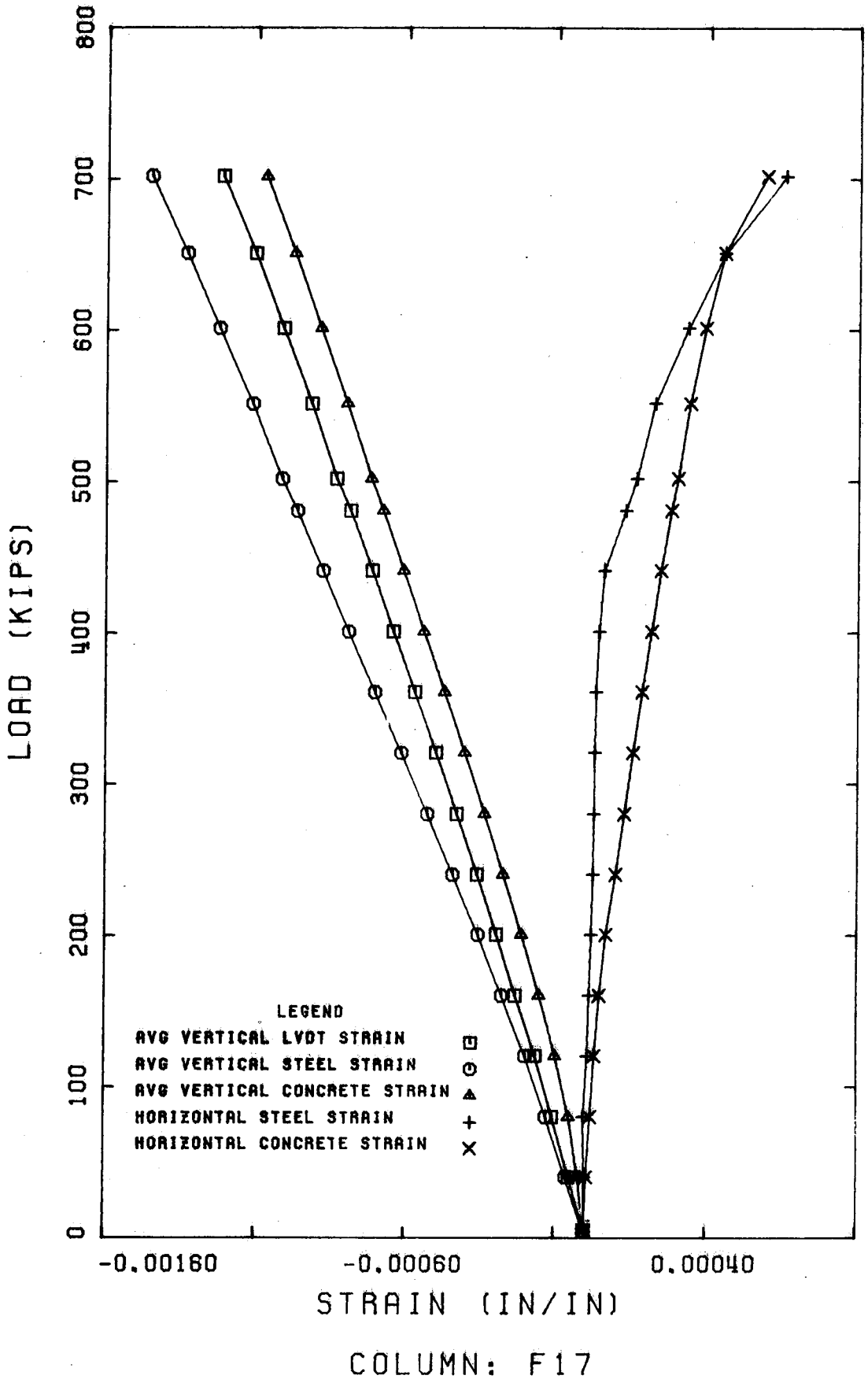
LOAD (KIPS)
0
100
200
300
400
500
600
700
800
-0.00160
-0.00060
0.00040
STRAIN (IN/IN)
LEGEND
AVG VERTICAL LVDT STRAIN
AVG VERTICAL STEEL STRAIN
AVG VERTICAL CONCRETE STRAIN
HORIZONTAL STEEL STRAIN
HORIZONTAL CONCRETE STRAIN

COLUMN: F17

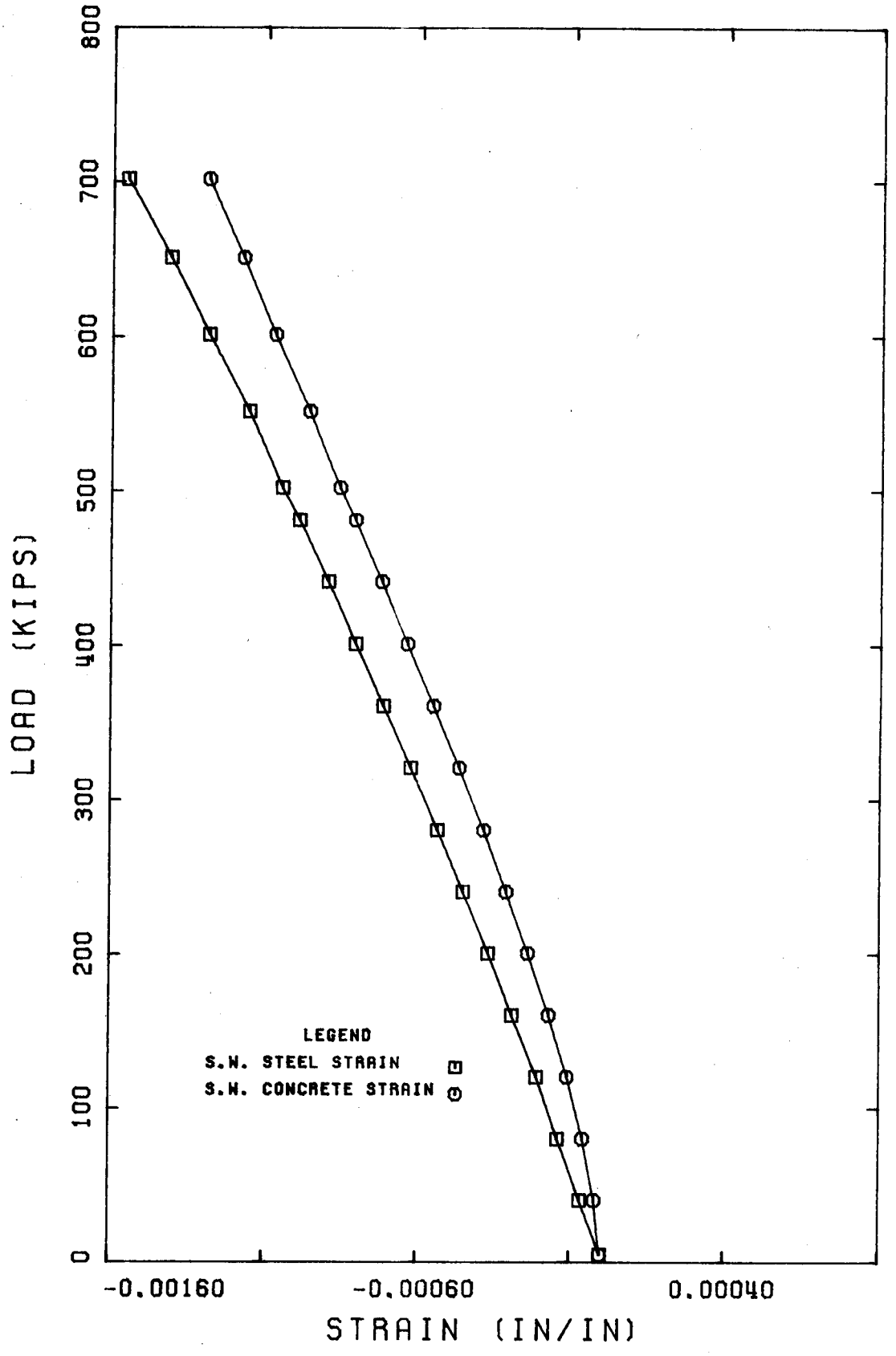
800
700
600
500
400
300
200
100
0
LOAD (KIPS)
LEGEND
S.N. STEEL STRAIN
S.N. CONCRETE STRAIN
-0.00160
-0.00060
0.00040
STRAIN (IN/IN)

COLUMN: F17

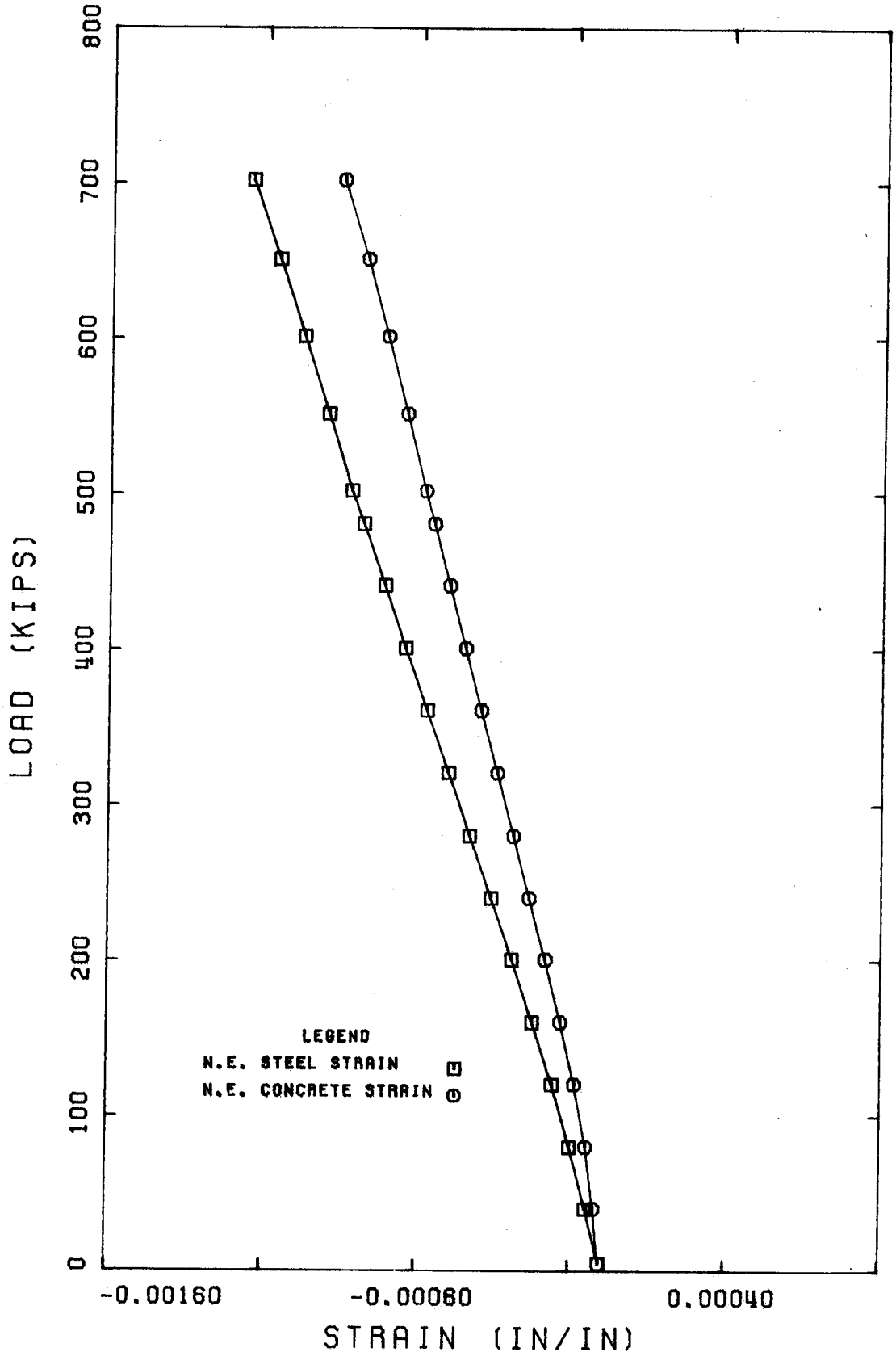
800
700
600
500
400
300
200
100
0
LOAD (KIPS)
LEGEND
N.E. STEEL STRAIN
N.E. CONCRETE STRAIN
-0.00160
-0.00060
0.00040
STRAIN (IN/IN)

COLUMN: F17

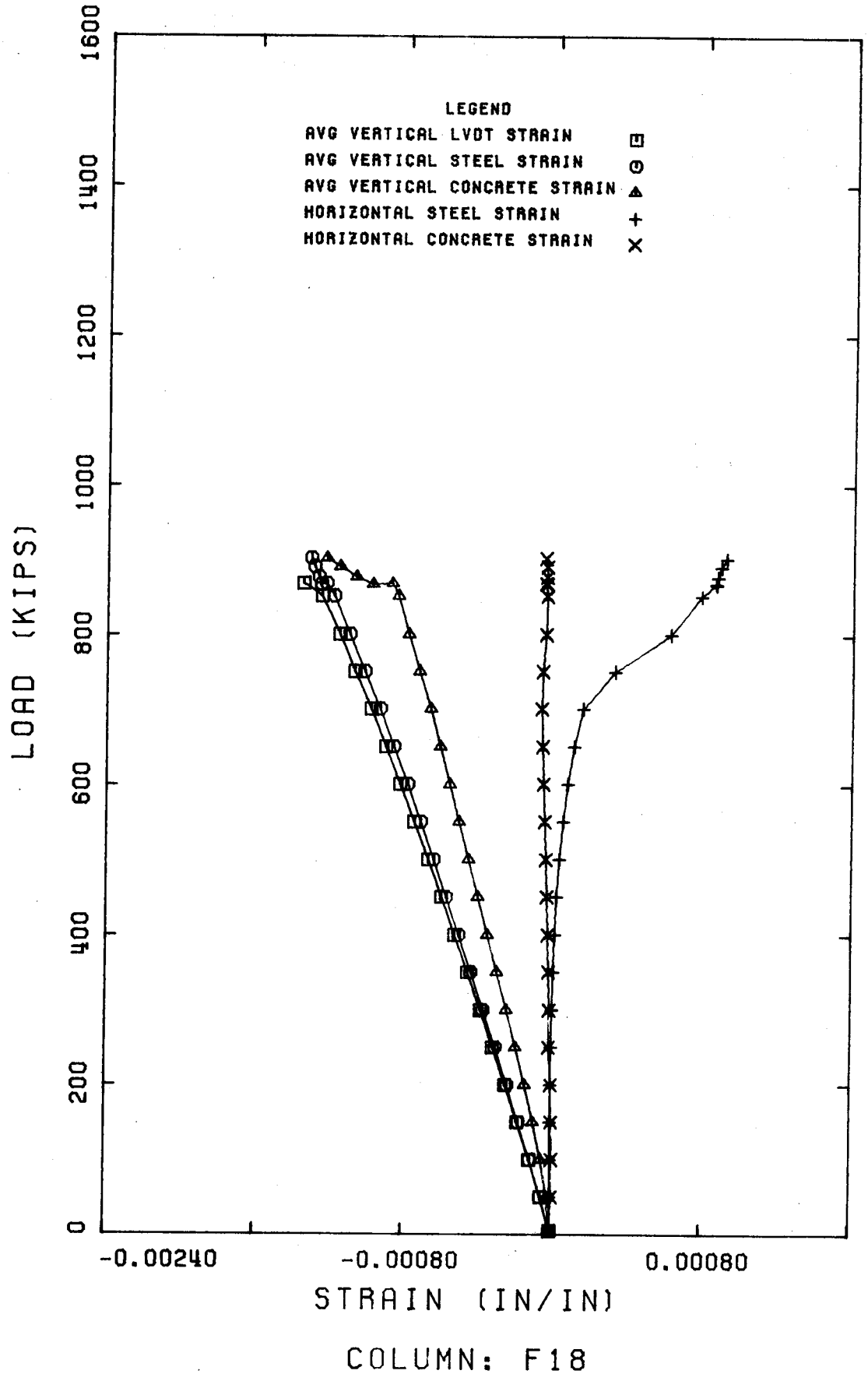
LEGEND
AVG VERTICAL LVDT STRAIN
AVG VERTICAL STEEL STRAIN
AVG VERTICAL CONCRETE STRAIN
HORIZONTAL STEEL STRAIN
HORIZONTAL CONCRETE STRAIN
LOAD (KIPS)
0
200
400
600
800
1000
1200
1400
1600
-0.00240
-0.00080
0.00080
STRAIN (IN/IN)

COLUMN: F18

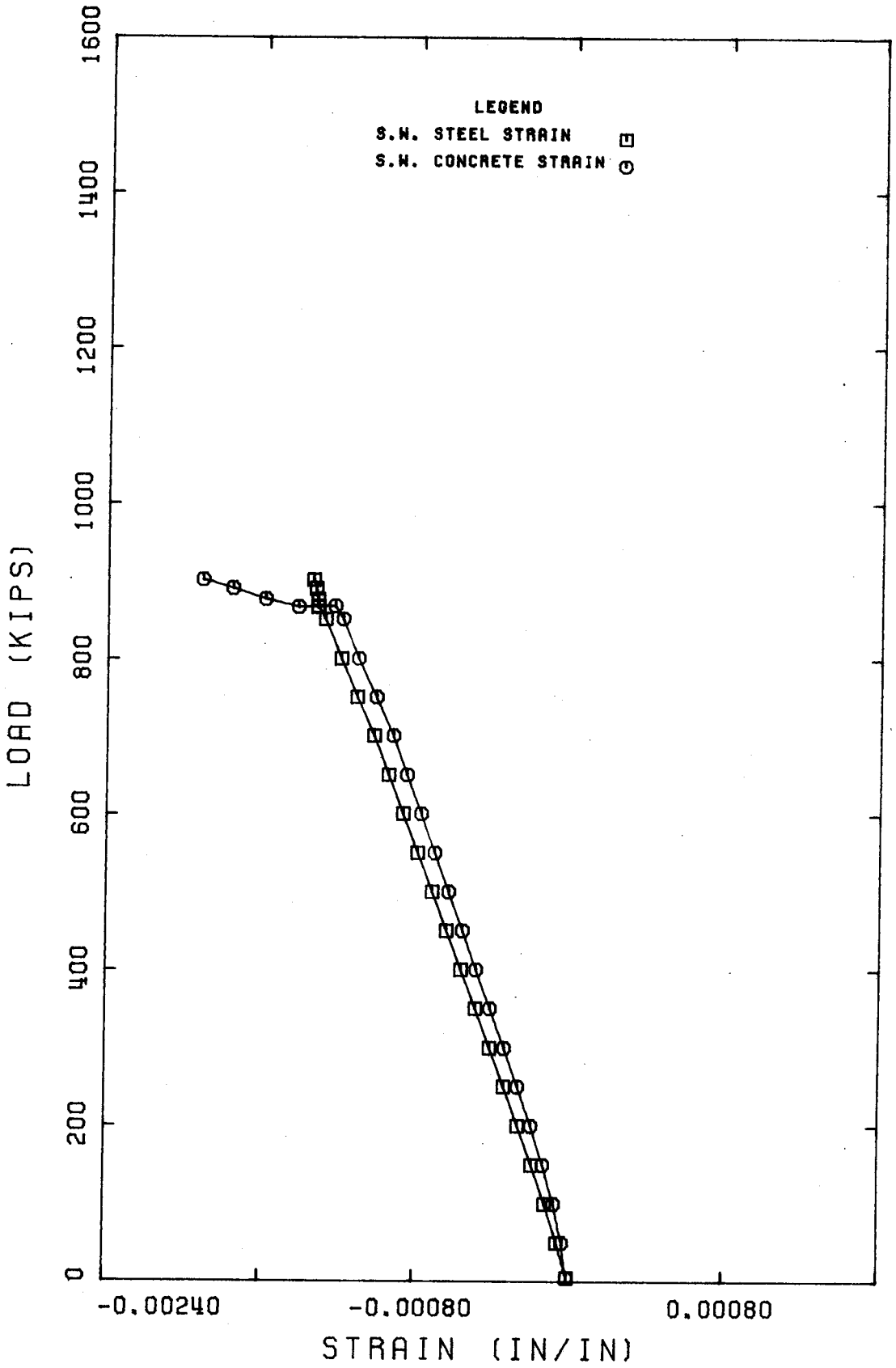
LEGEND
S.W. STEEL STRAIN
S.W. CONCRETE STRAIN
LOAD (KIPS)
0
200
400
600
800
1000
1200
1400
1600
-0.00240
-0.00080
0.00080
STRAIN (IN/IN)

COLUMN: F18

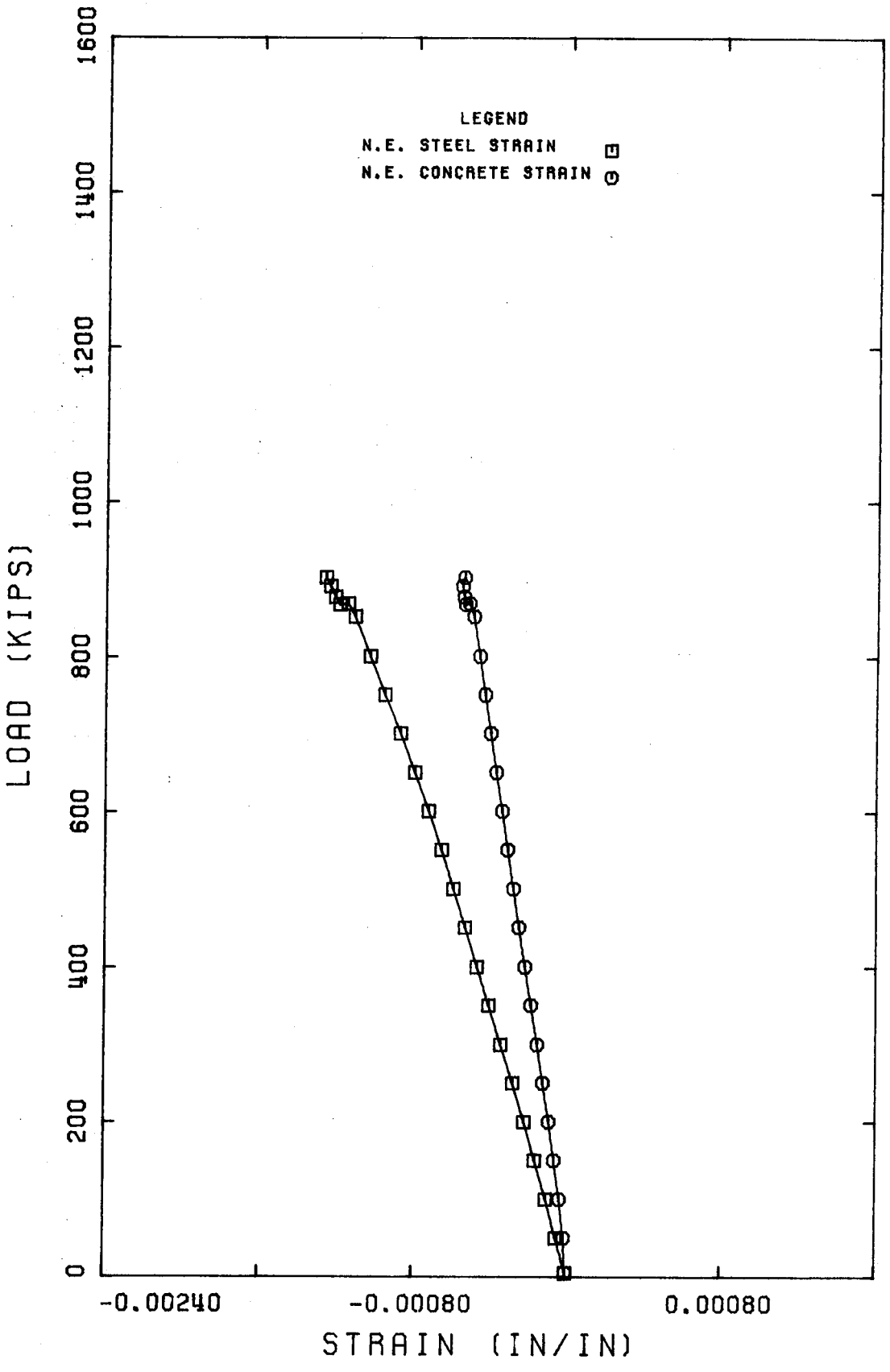
LEGEND
N.E. STEEL STRAIN
N.E. CONCRETE STRAIN
LOAD (KIPS)
0
200
400
600
800
1000
1200
1400
1600
-0.00240
-0.00080
0.00080
STRAIN (IN/IN)

COLUMN: F18

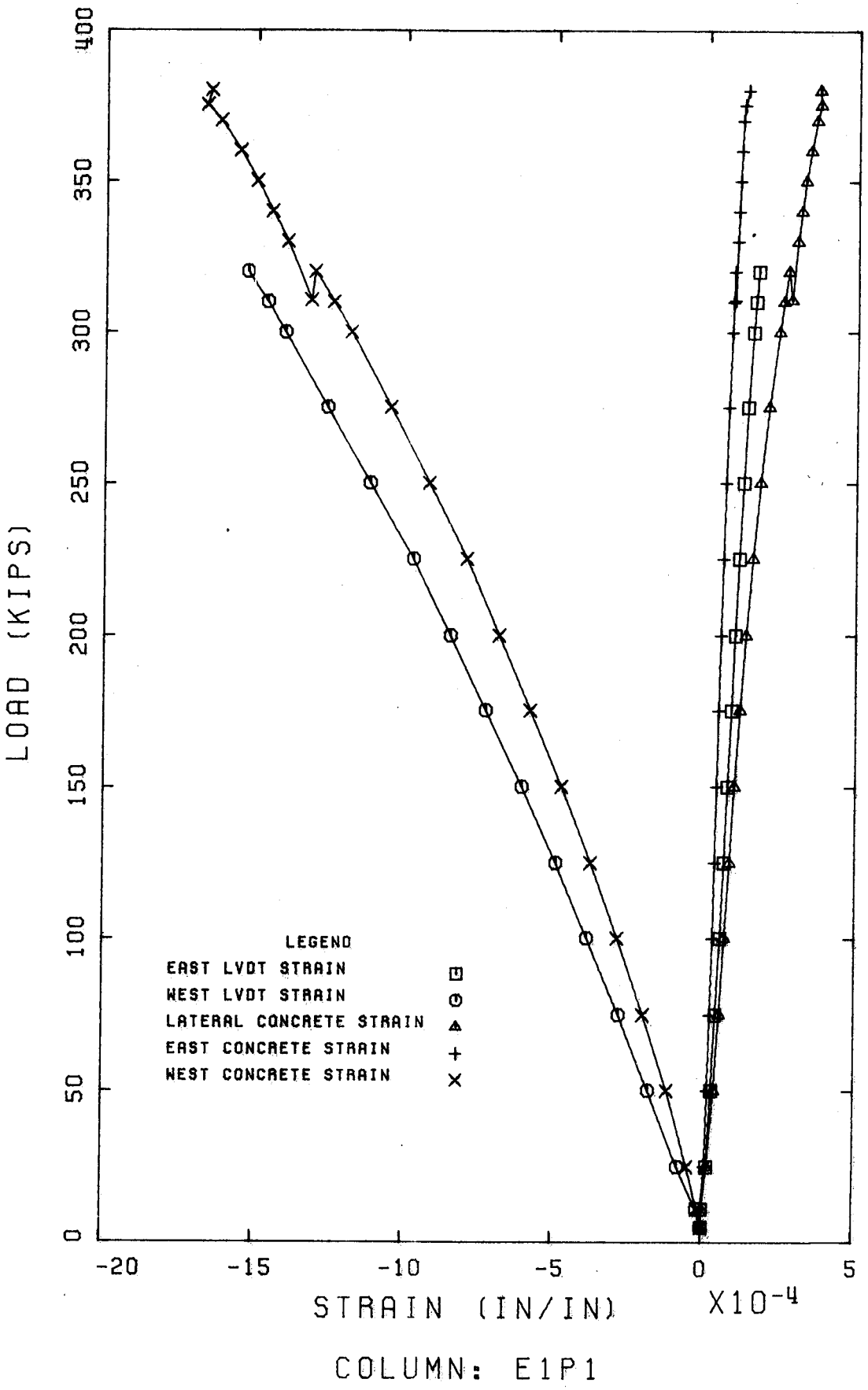
LOAD (KIPS)
400
350
300
250
200
150
100
50
0
-20
-15
-10
-5
0
5
STRAIN (IN/IN) X10-4
LEGEND
EAST LVDT STRAIN
WEST LVDT STRAIN
LATERAL CONCRETE STRAIN
EAST CONCRETE STRAIN
WEST CONCRETE STRAIN

COLUMN: E1P1

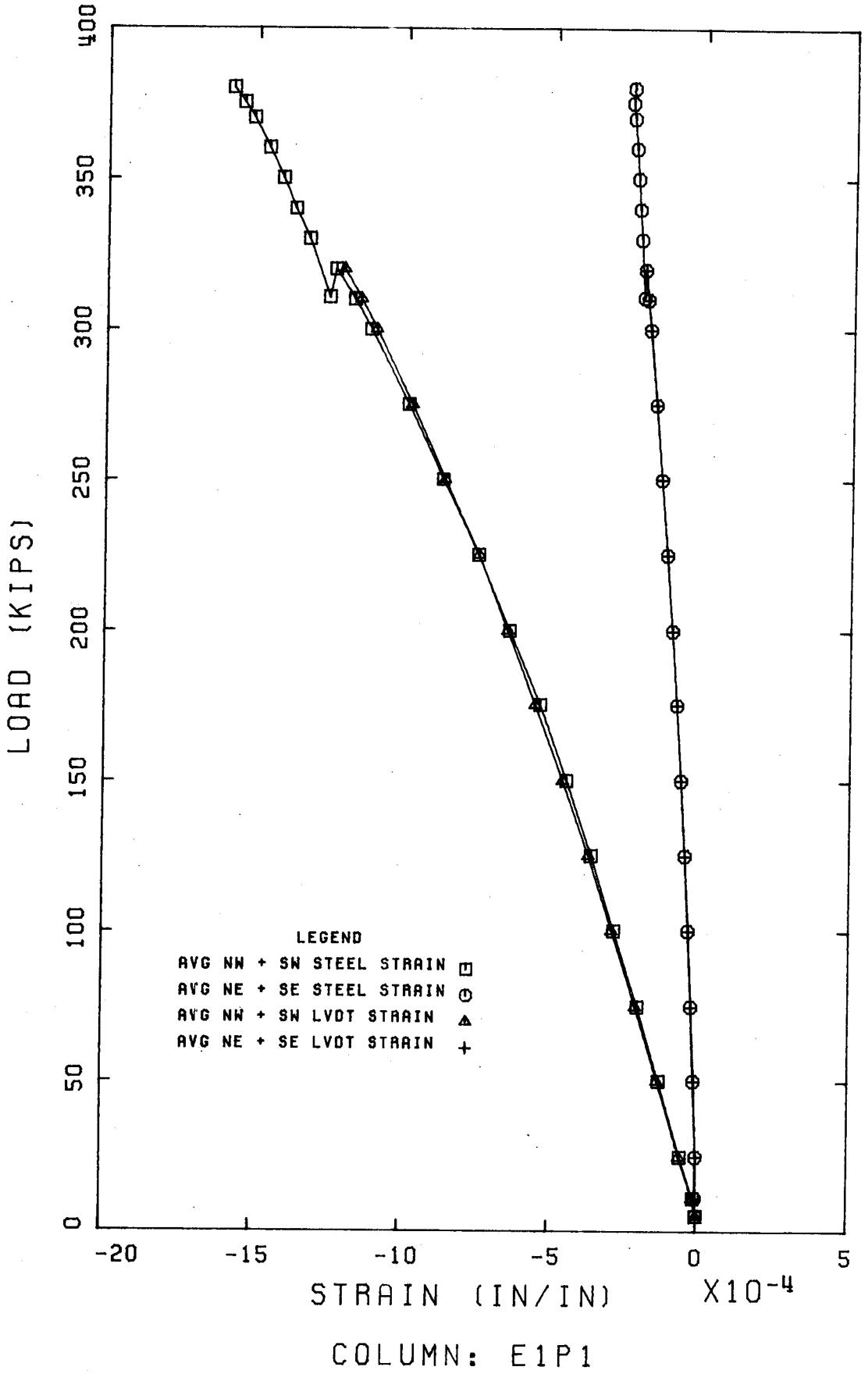
LOAD (KIPS)
400
350
300
250
200
150
100
50
0
-20
-15
-10
-5
0
5
STRAIN (IN/IN) X10-4
LEGEND
AVG NW + SW STEEL STRAIN
AVG NE + SE STEEL STRAIN
AVG NW + SW LVDT STRAIN
AVG NE + SE LVDT STRAIN

COLUMN: E1P1

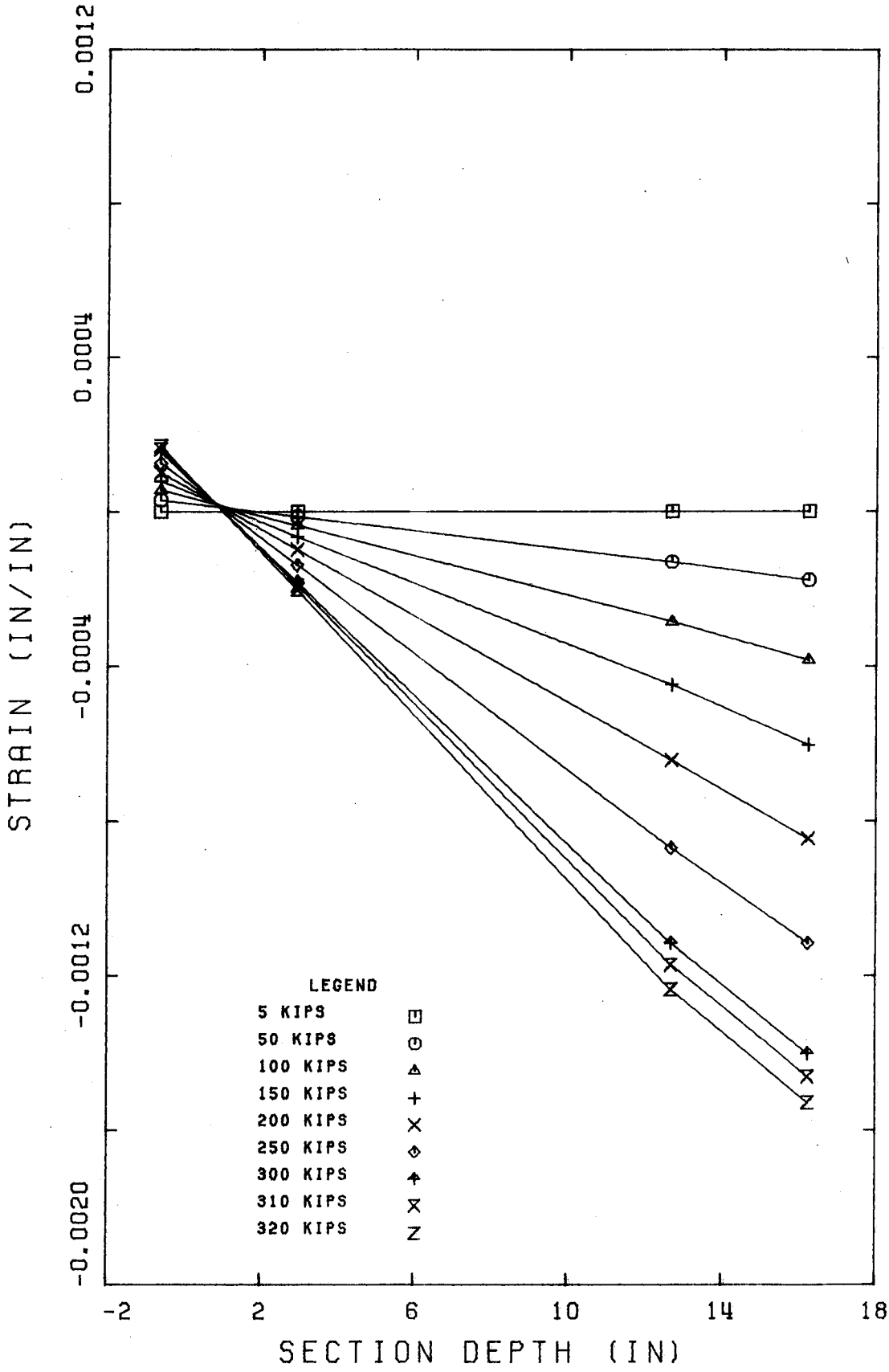
0.0012
0.0004
-0.0004
-0.0012
-0.0020
STRAIN (IN/IN)
-2
2
6
10
14
18
SECTION DEPTH (IN)
LEGEND
5 KIPS
50 KIPS
100 KIPS
150 KIPS
200 KIPS
250 KIPS
300 KIPS
310 KIPS
320 KIPS

COLUMN: E1P1

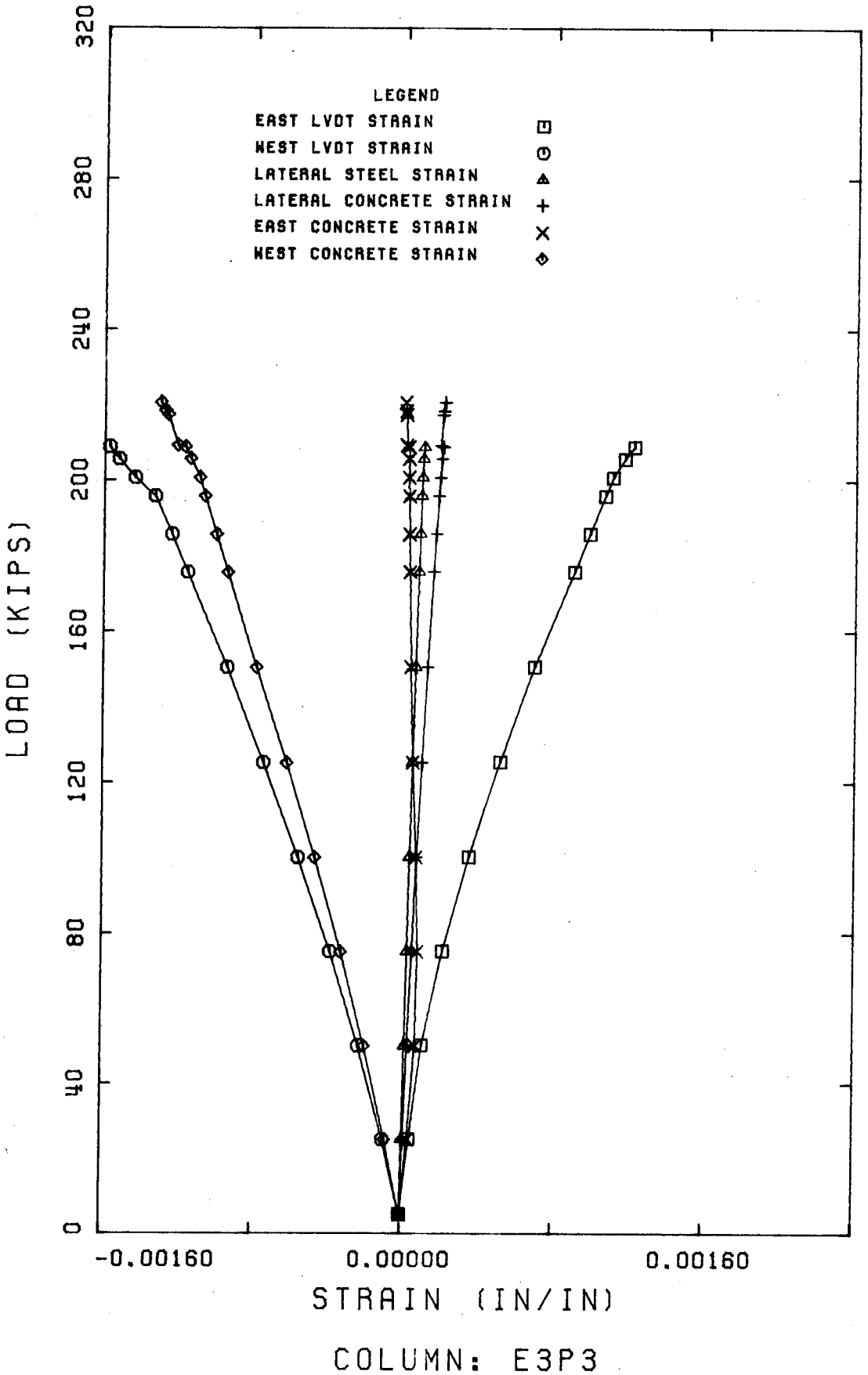
LEGEND
EAST LVDT STRAIN
WEST LVDT STRAIN
LATERAL STEEL STRAIN
LATERAL CONCRETE STRAIN
EAST CONCRETE STRAIN
WEST CONCRETE STRAIN
LOAD (KIPS)
0
40
80
120
160
200
240
280
320
-0.00160
0.00000
0.00160
STRAIN (IN/IN)

COLUMN: E3P3

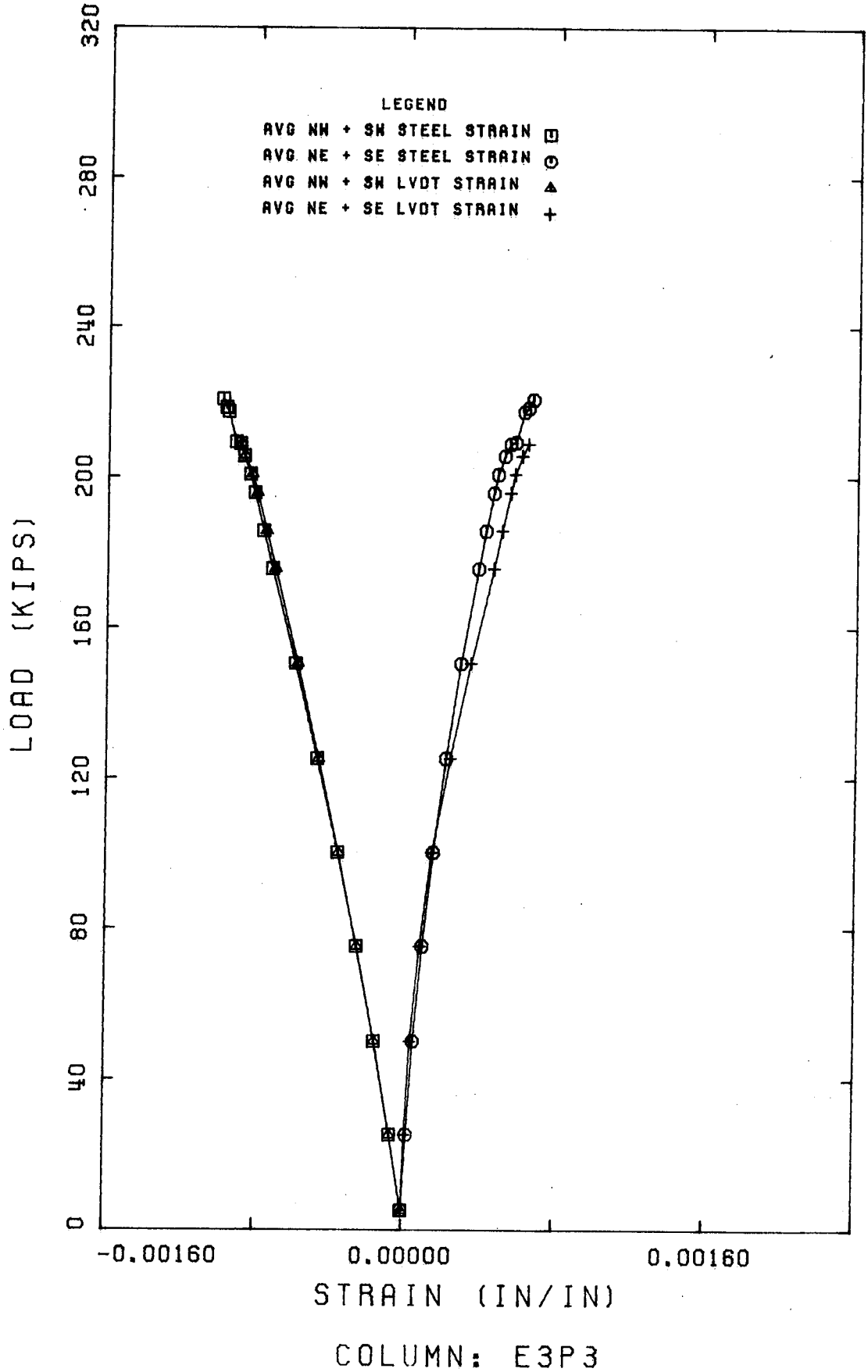
LEGEND
AVG NW + SW STEEL STRAIN
AVG NE + SE STEEL STRAIN
AVG NW + SW LVDT STRAIN
AVG NE + SE LVDT STRAIN
LOAD (KIPS)
0
40
80
120
160
200
240
280
320
-0.00160
0.00000
0.00160
STRAIN (IN/IN)

COLUMN: E3P3

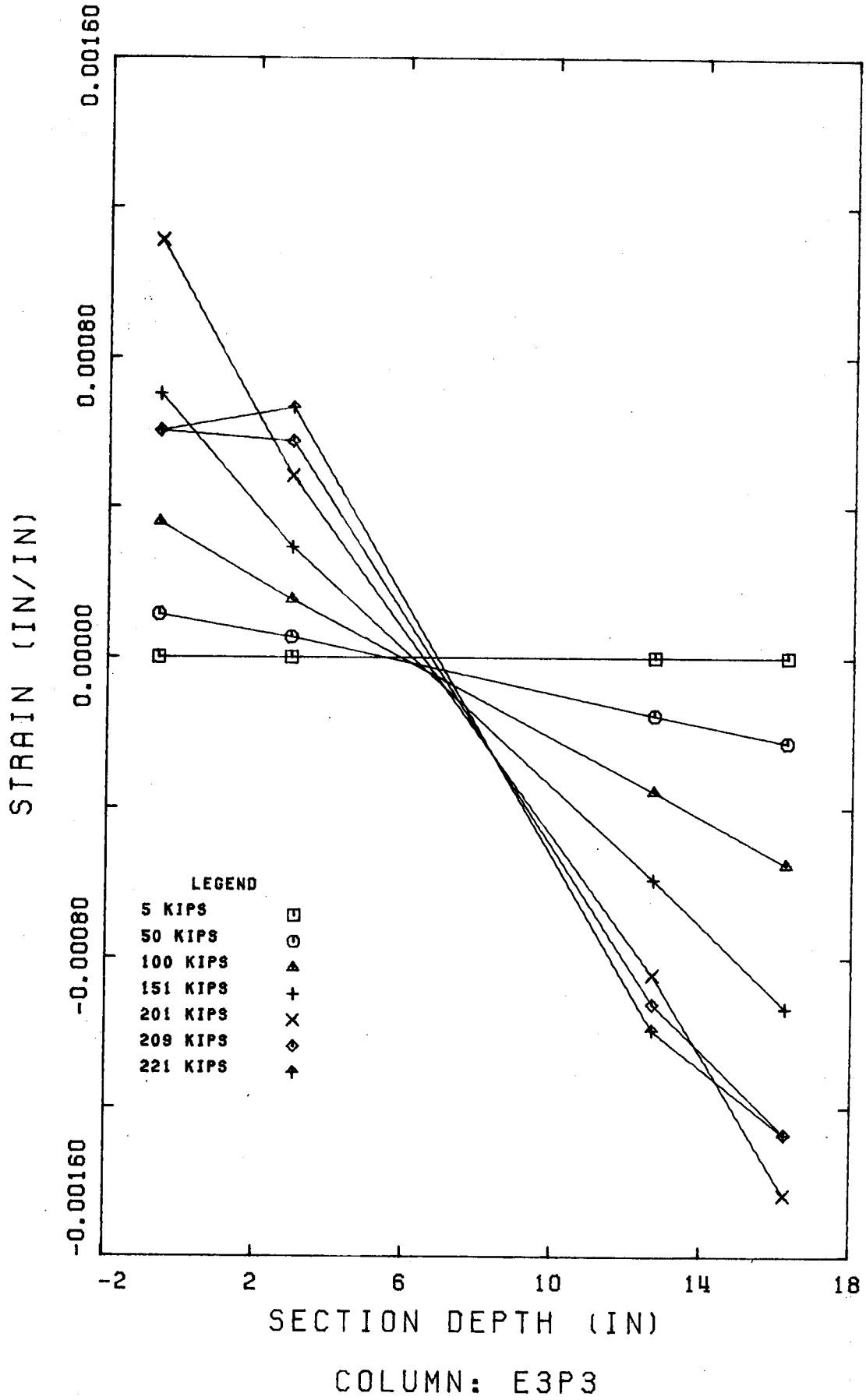
0.00160
0.00080
0.00000
-0.00080
-0.00160
STRAIN (IN/IN)
LEGEND
5 KIPS
50 KIPS
100 KIPS
151 KIPS
201 KIPS
209 KIPS
221 KIPS
-2
2
6
10
14
18
SECTION DEPTH (IN)
COLUMN: E3P3

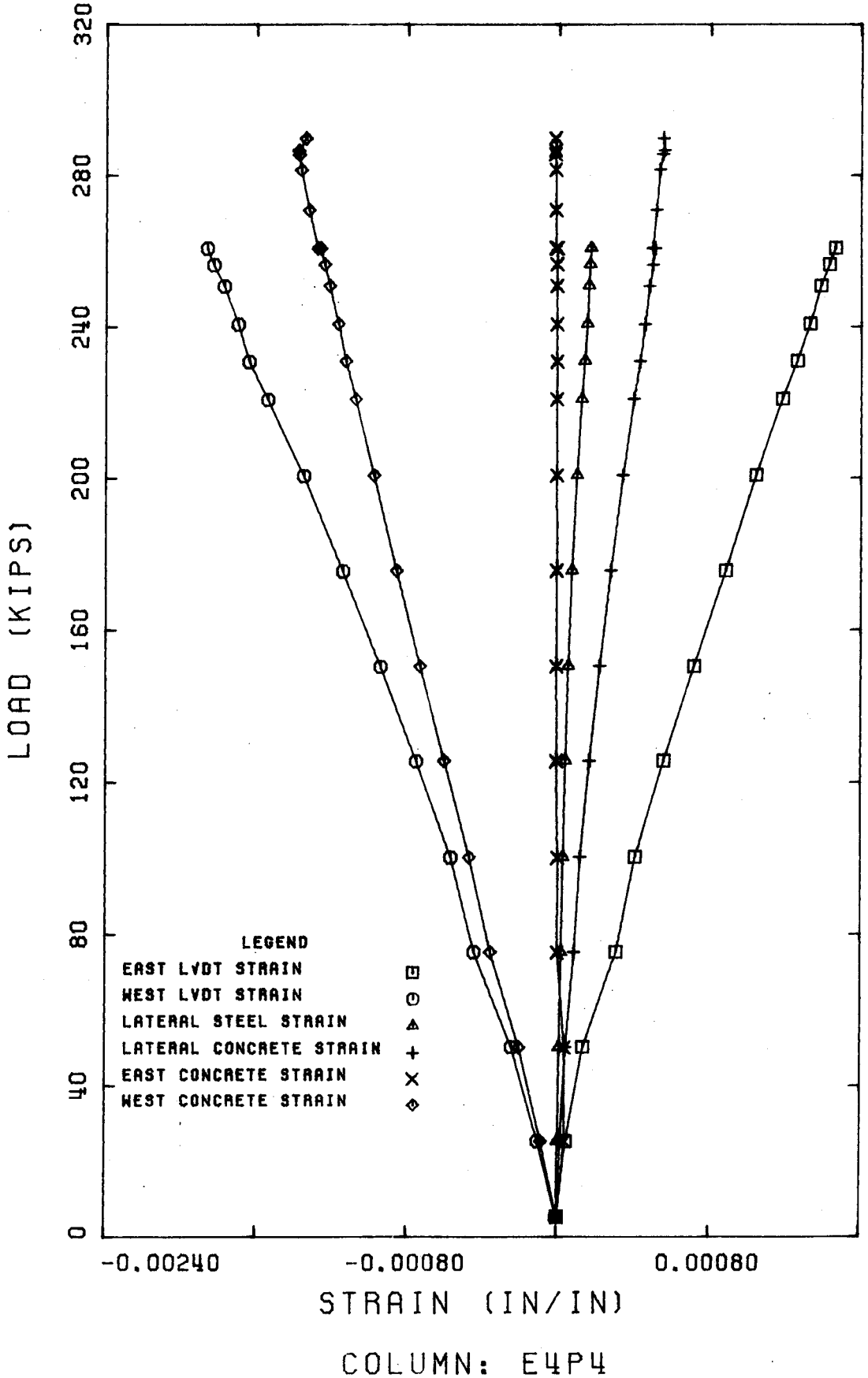
LOAD (KIPS)
320
280
240
200
160
120
80
40
0
-0.00240
-0.00080
0.00080
STRAIN (IN/IN)
LEGEND
EAST LVDT STRAIN
WEST LVDT STRAIN
LATERAL STEEL STRAIN
LATERAL CONCRETE STRAIN
EAST CONCRETE STRAIN
WEST CONCRETE STRAIN

COLUMN: E4P4

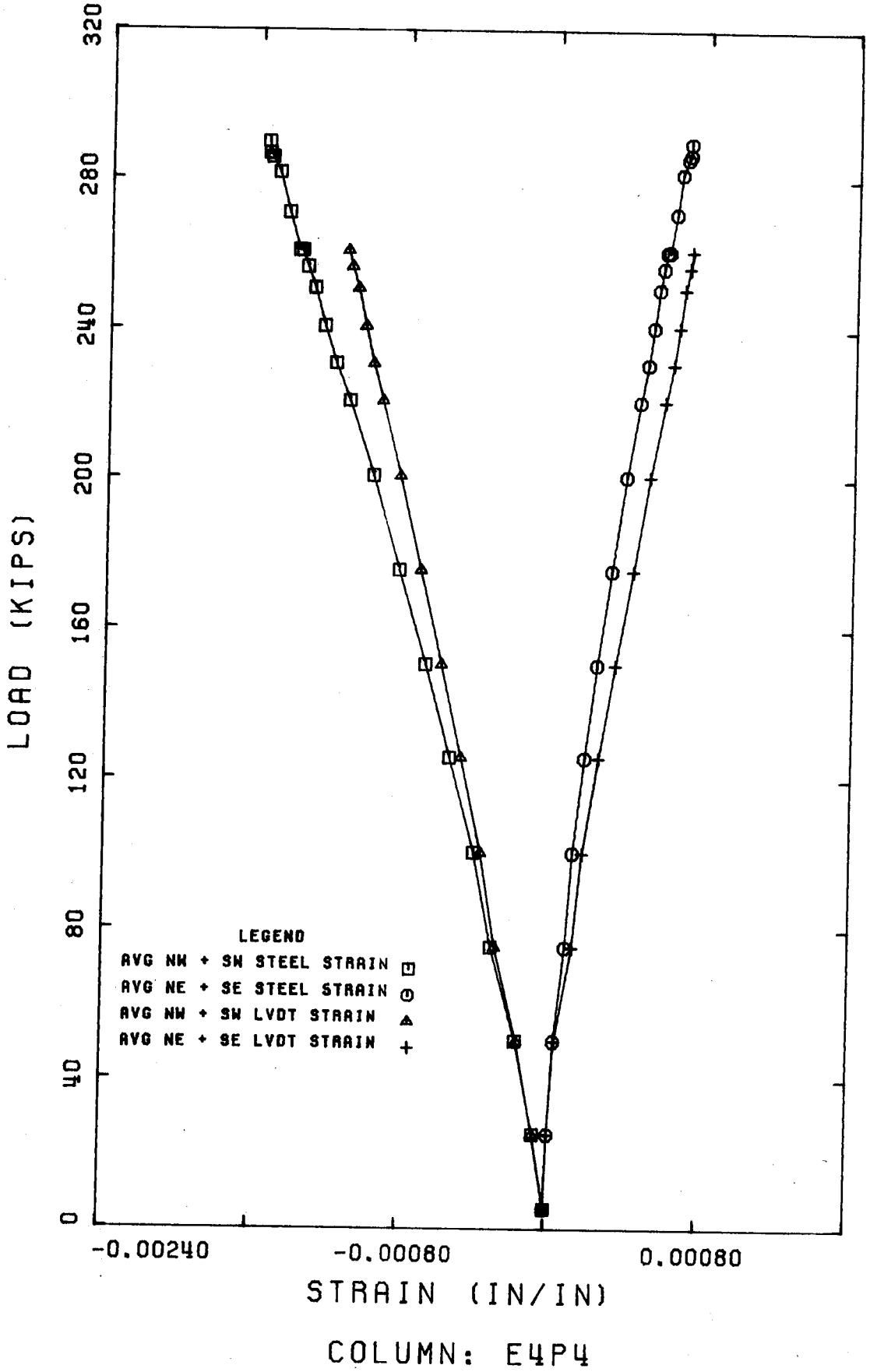
LOAD (KIPS)
320
280
240
200
160
120
80
40
0
-0.00240
-0.00080
0.00080
STRAIN (IN/IN)
LEGEND
AVG NW + SW STEEL STRAIN
AVG NE + SE STEEL STRAIN
AVG NW + SW LVDT STRAIN
AVG NE + SE LVDT STRAIN

COLUMN: E4P4

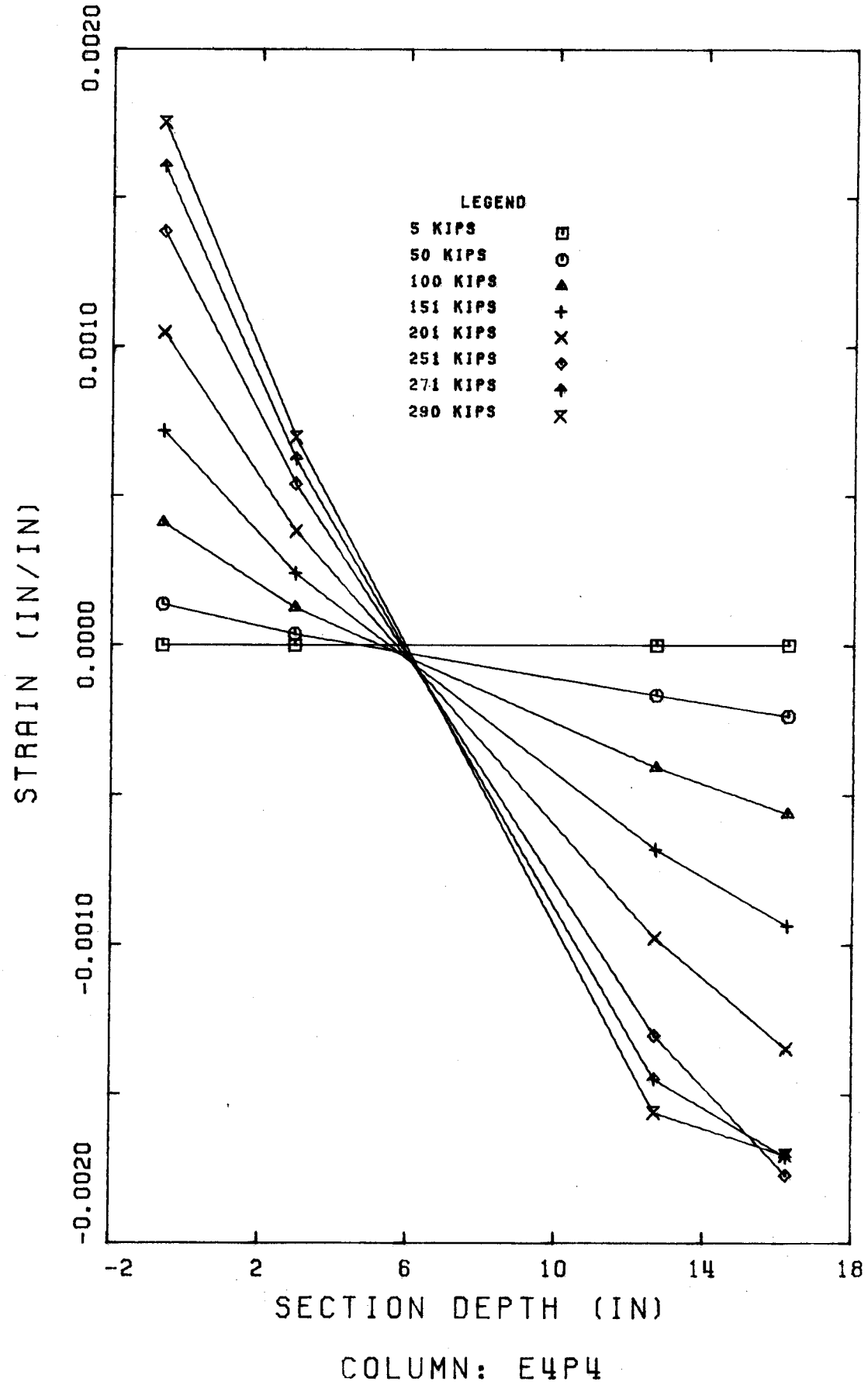
0.0020
0.0010
0.0000
-0.0010
-0.0020
STRAIN (IN/IN)
LEGEND
5 KIPS
50 KIPS
100 KIPS
151 KIPS
201 KIPS
251 KIPS
271 KIPS
290 KIPS
-2
2
6
10
14
18
SECTION DEPTH (IN)
COLUMN: E4P4

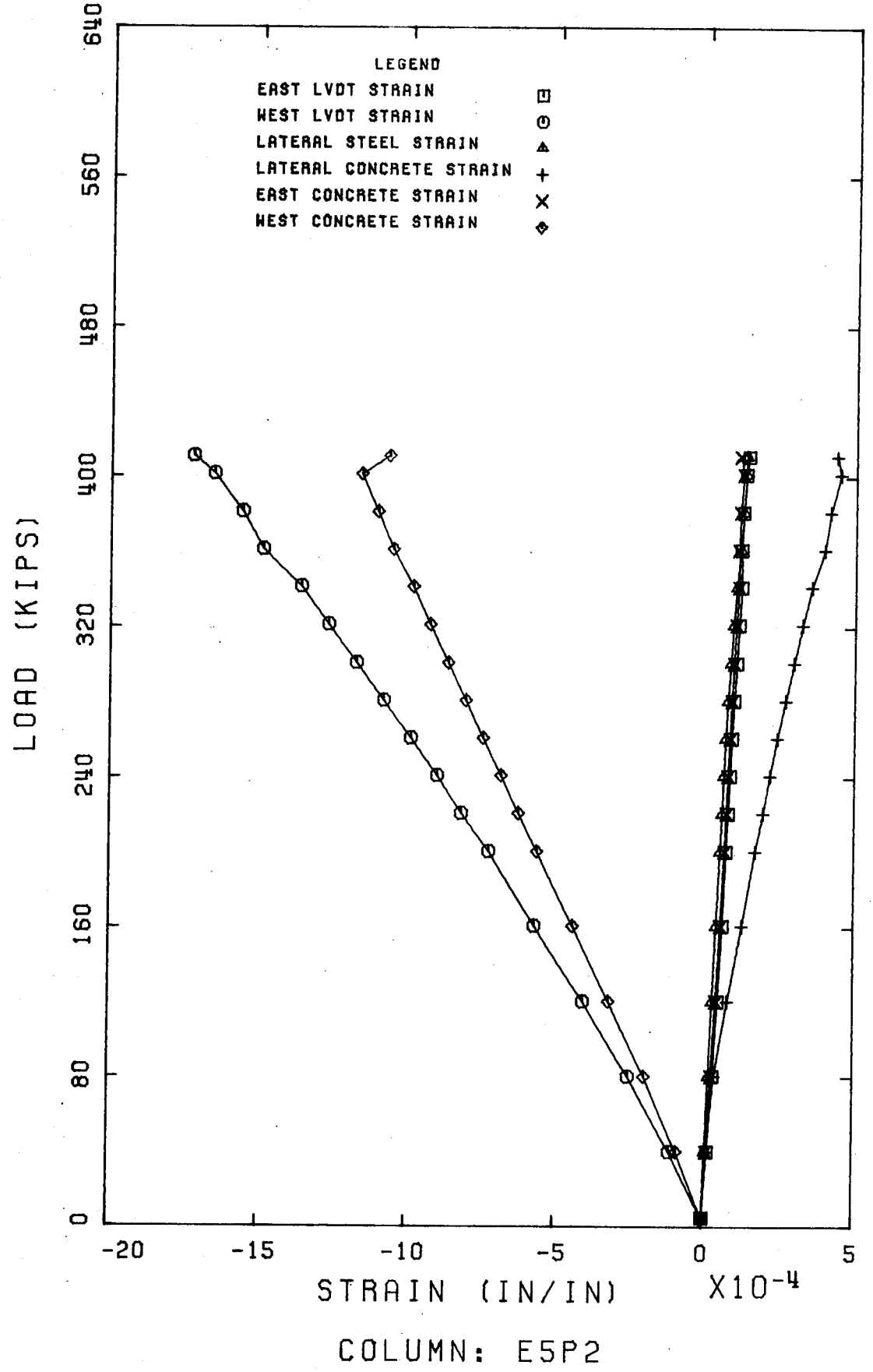
LEGEND
EAST LVDT STRAIN
WEST LVDT STRAIN
LATERAL STEEL STRAIN
LATERAL CONCRETE STRAIN
EAST CONCRETE STRAIN
WEST CONCRETE STRAIN
LOAD (KIPS)
0
80
160
240
320
400
480
560
640
-20
-15
-10
-5
0
5
STRAIN (IN/IN)
X10-4

COLUMN: E5P2

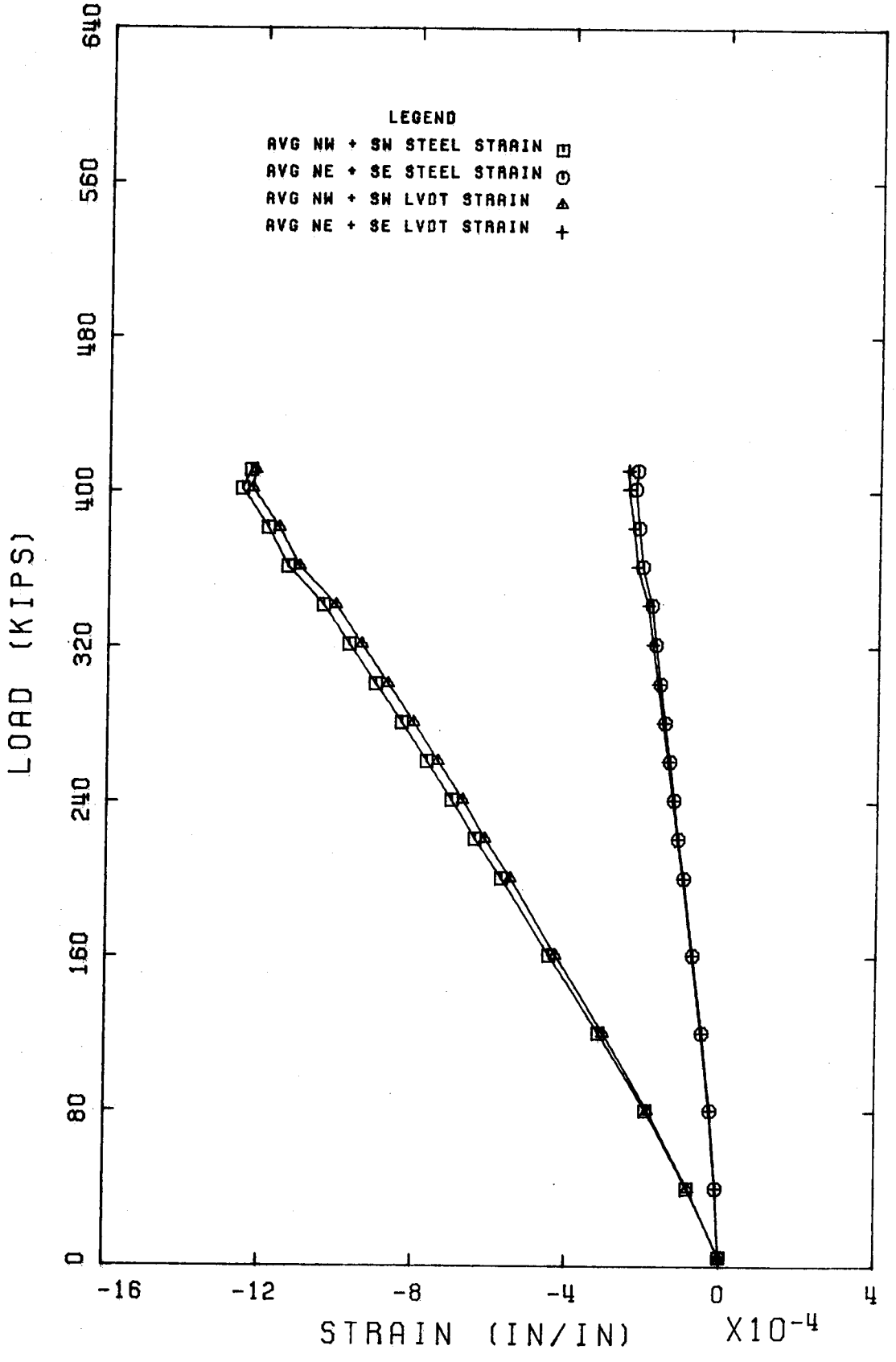
LEGEND
AVG NW + SW STEEL STRAIN
AVG NE + SE STEEL STRAIN
AVG NW + SW LVDT STRAIN
AVG NE + SE LVDT STRAIN
LOAD (KIPS)
0
80
160
240
320
400
480
560
640
-16
-12
-8
-4
0
4
STRAIN (IN/IN)
X10-4

COLUMN: E5P2

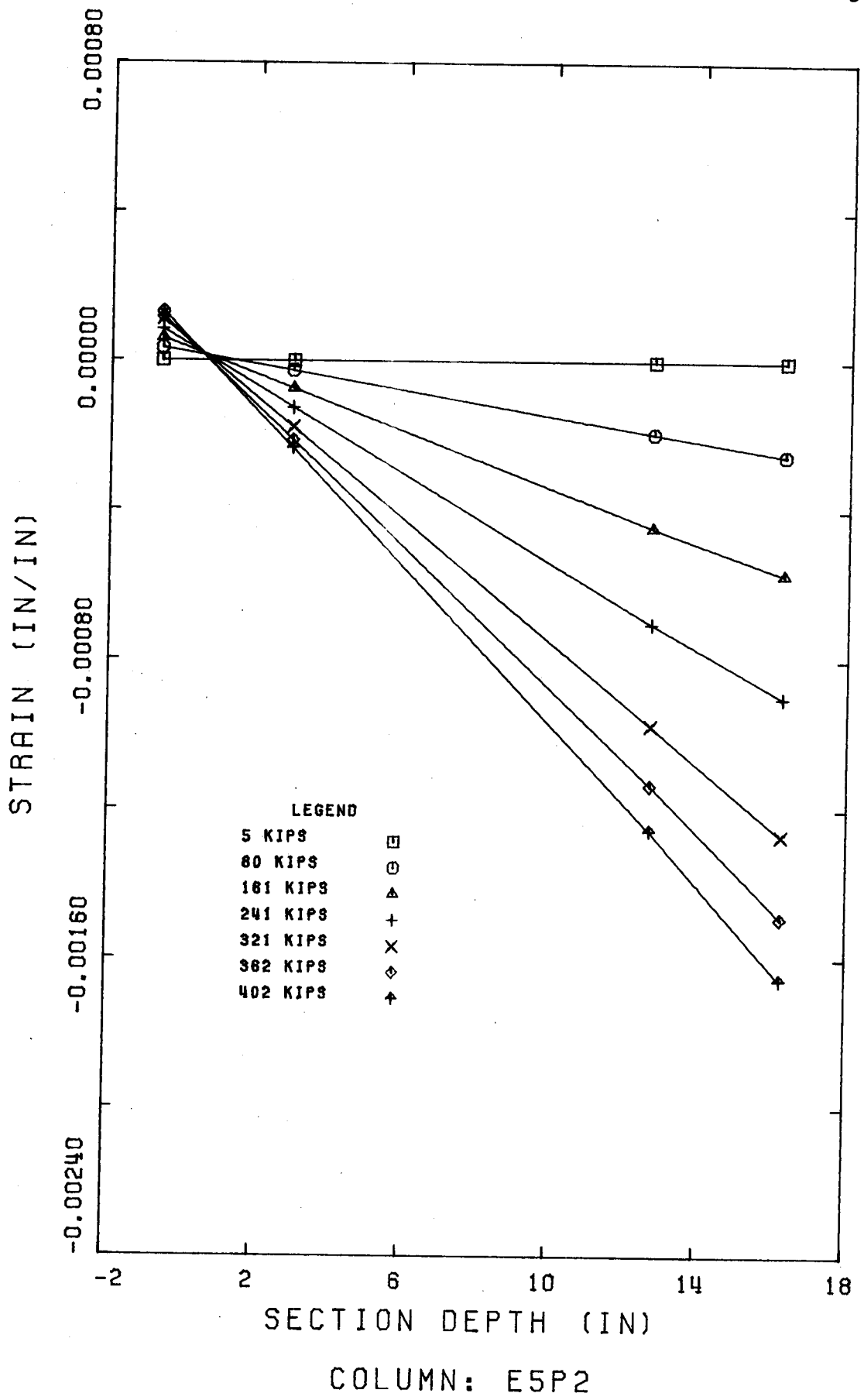
0.00080
0.00000
-0.00080
-0.00160
-0.00240
STRAIN (IN/IN)
-2
2
6
10
14
18
SECTION DEPTH (IN)
LEGEND
5 KIPS
80 KIPS
161 KIPS
241 KIPS
321 KIPS
362 KIPS
402 KIPS

COLUMN: E5P2

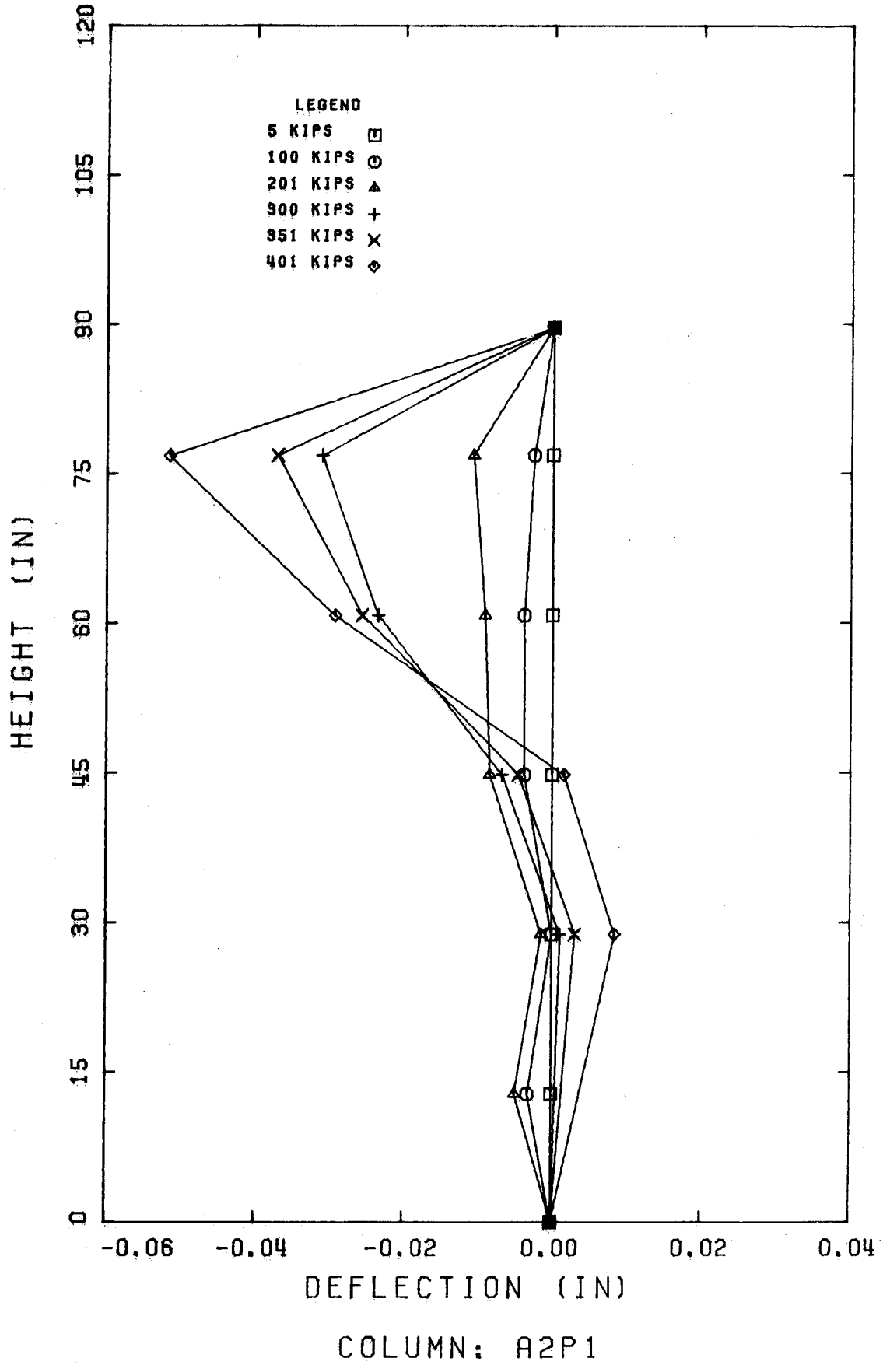
LEGEND
5 KIPS
100 KIPS
201 KIPS
300 KIPS
351 KIPS
401 KIPS
HEIGHT (IN)
0
15
30
45
60
75
90
105
120
-0.06
-0.04
-0.02
0.00
0.02
0.04
DEFLECTION (IN)
COLUMN: A2P1

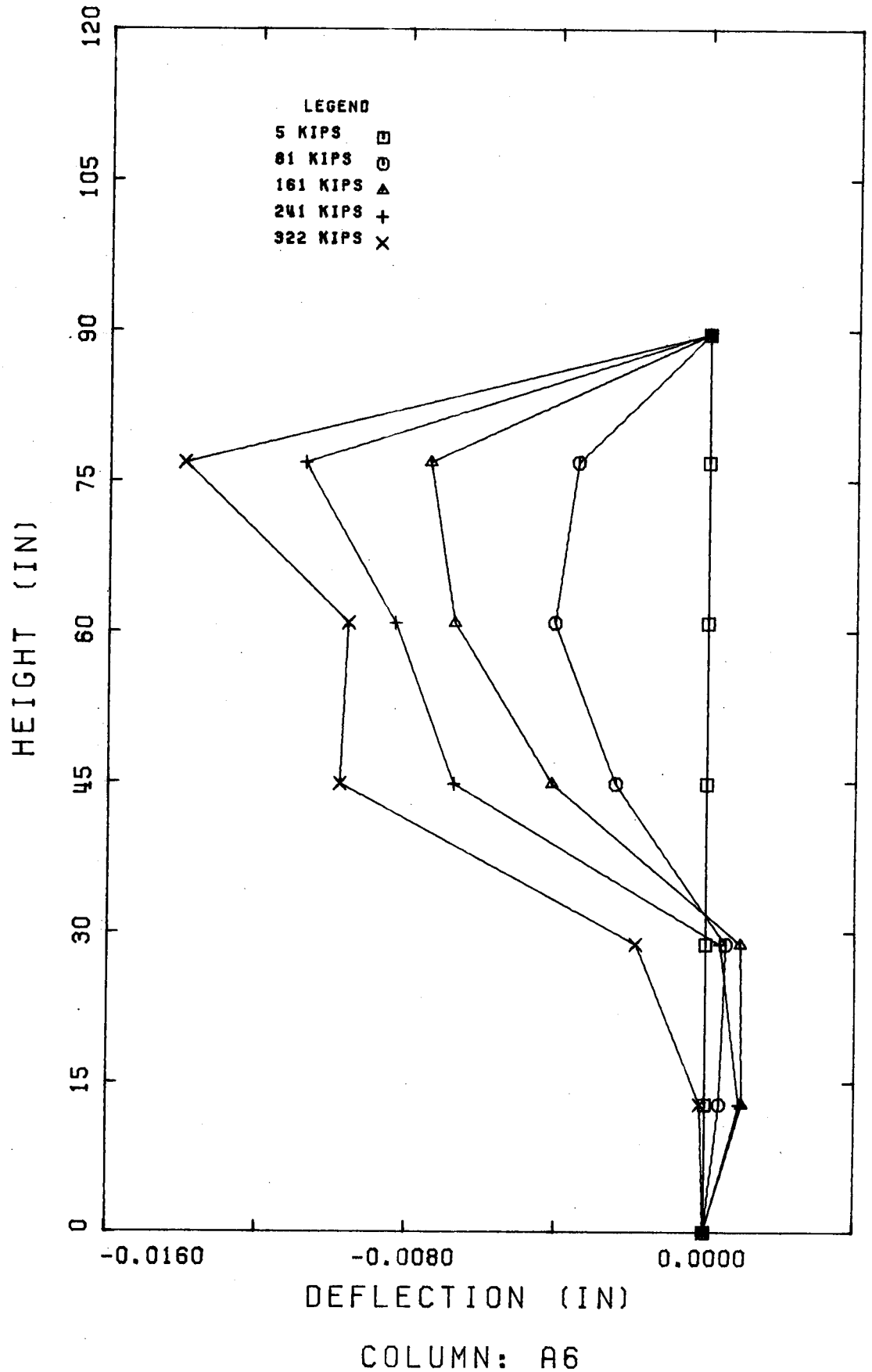
LEGEND
5 KIPS
81 KIPS
161 KIPS
241 KIPS
322 KIPS
HEIGHT (IN)
0
15
30
45
60
75
90
105
120
-0.0160
-0.0080
0.0000
DEFLECTION (IN)

COLUMN: A6

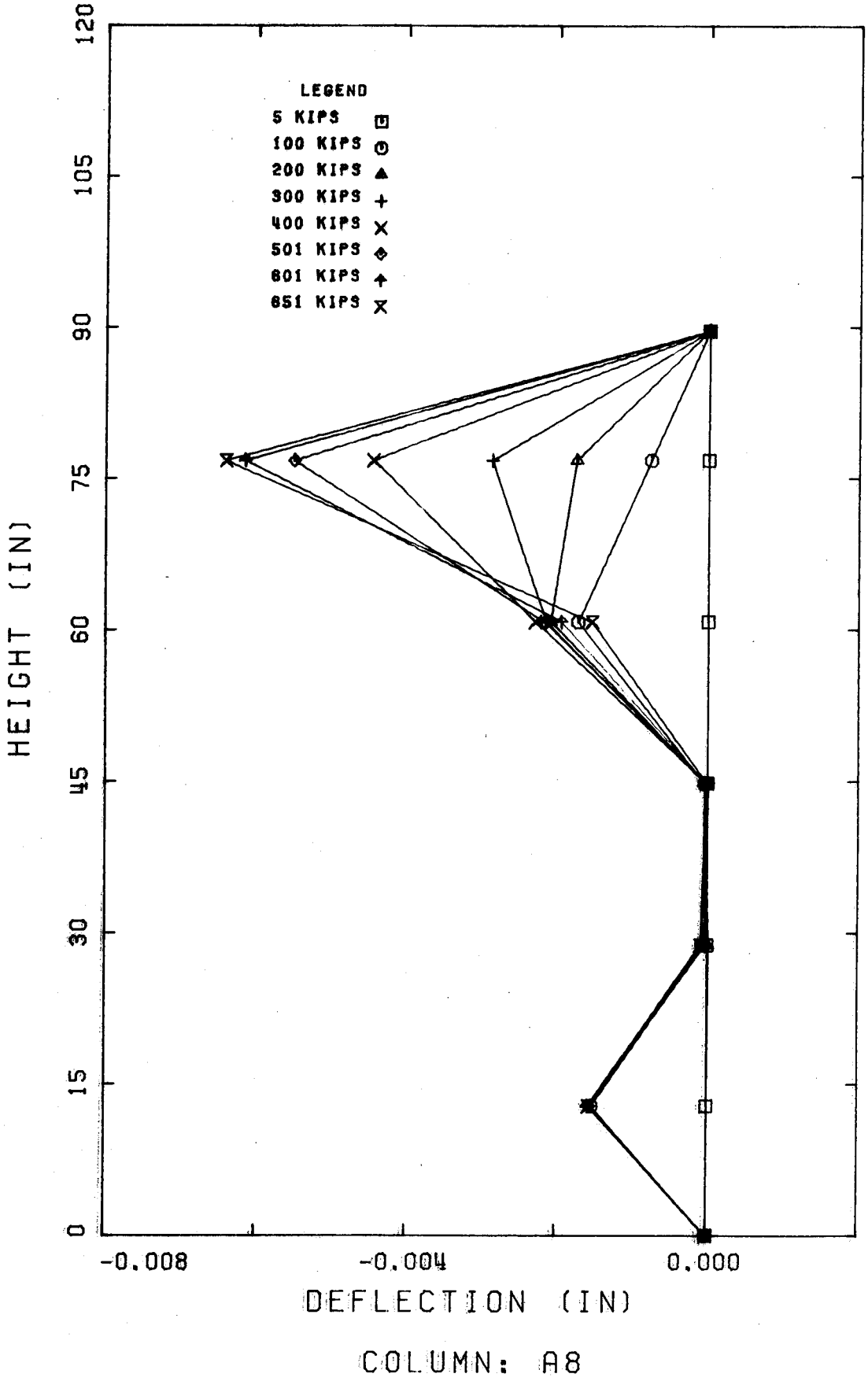
LEGEND
5 KIPS
100 KIPS
200 KIPS
300 KIPS
400 KIPS
501 KIPS
601 KIPS
651 KIPS
HEIGHT (IN)
0
15
30
45
60
75
90
105
120
-0.008
-0.004
0.000
DEFLECTION (IN)

COLUMN: A8

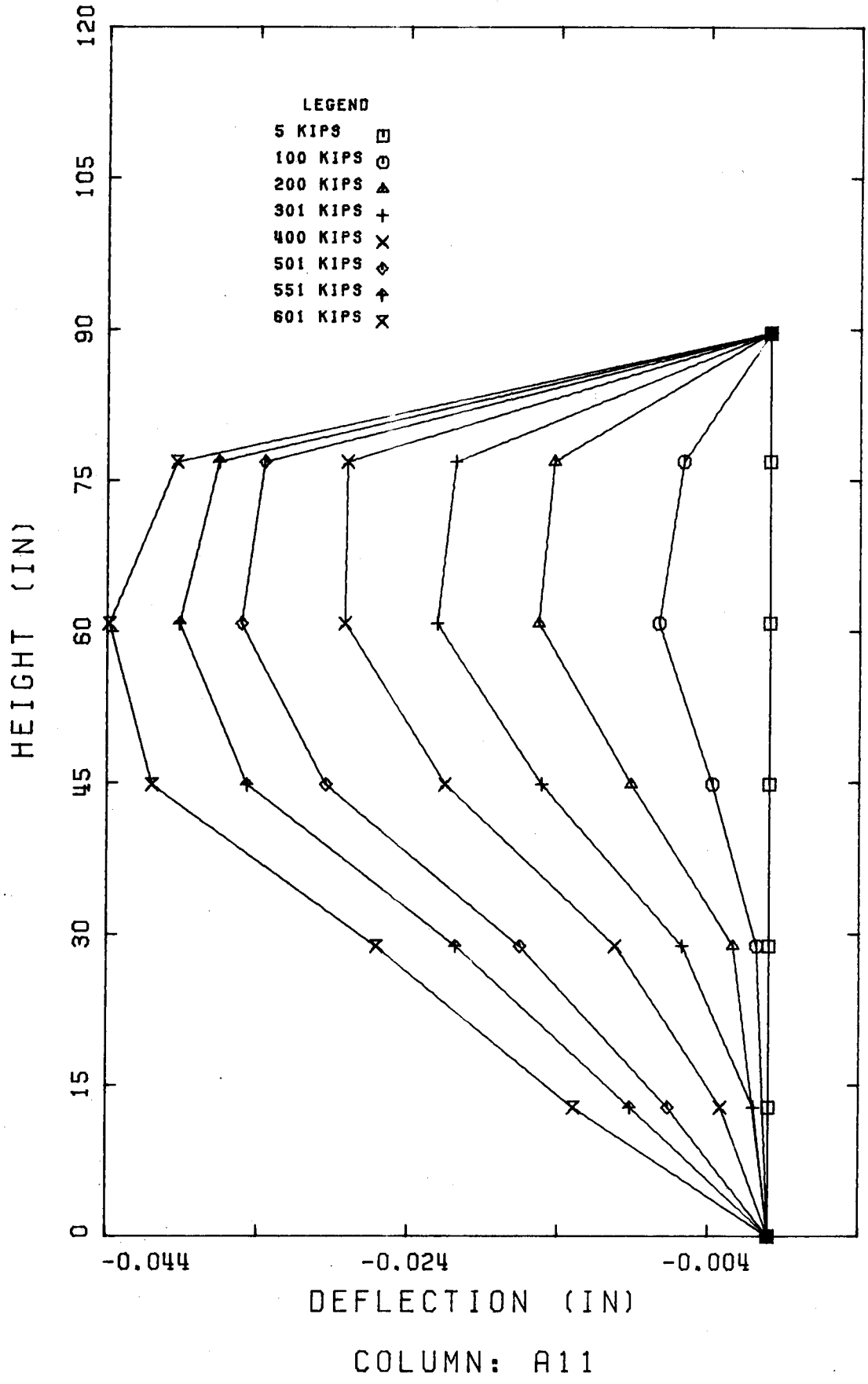
LEGEND
5 KIPS
100 KIPS
200 KIPS
301 KIPS
400 KIPS
501 KIPS
551 KIPS
601 KIPS
HEIGHT (IN)
0
15
30
45
60
75
90
105
120
-0.044
-0.024
-0.004
DEFLECTION (IN)

COLUMN: A11

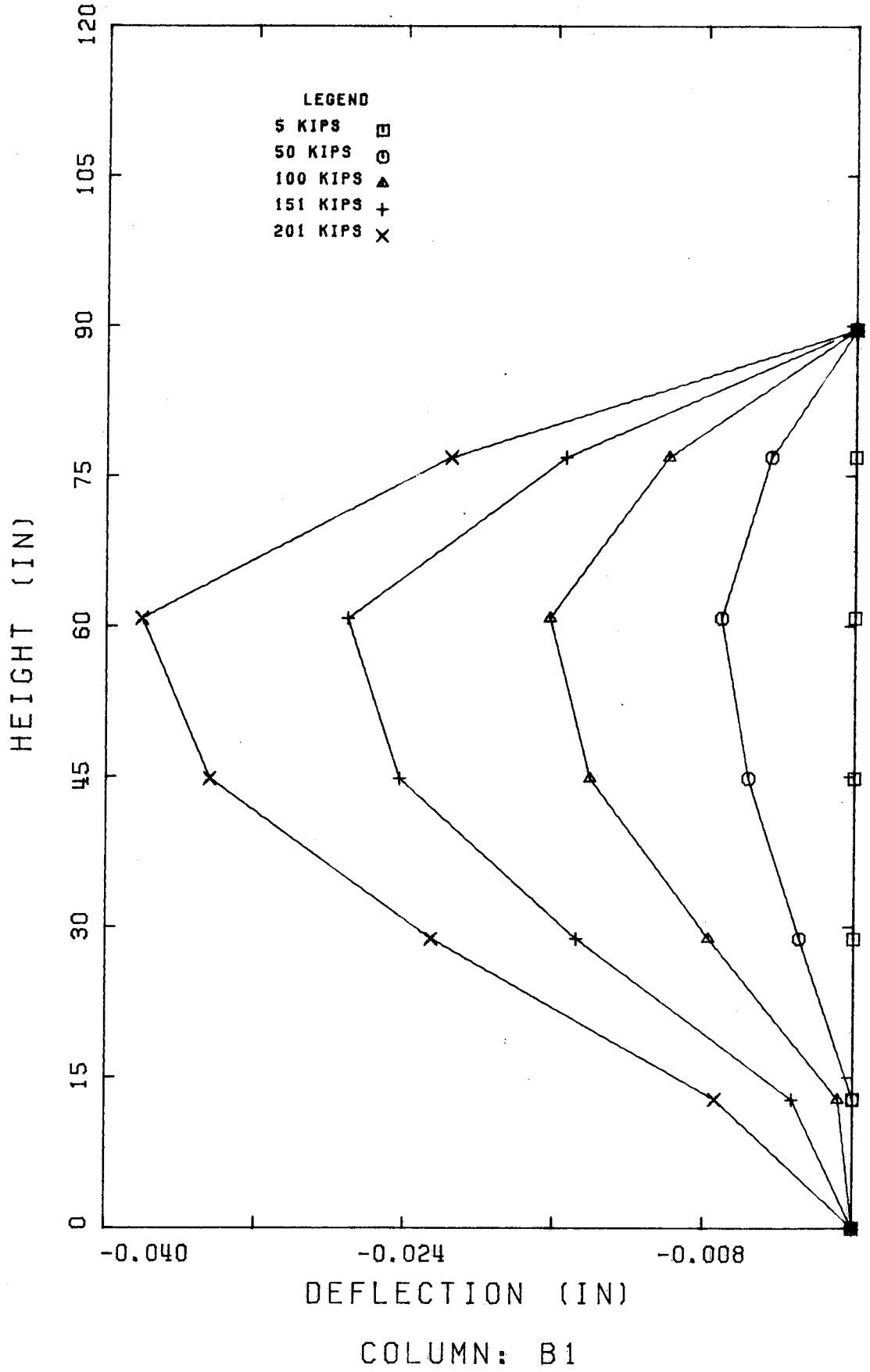
LEGEND
5 KIPS
50 KIPS
100 KIPS
151 KIPS
201 KIPS
HEIGHT (IN)
0
15
30
45
60
75
90
105
120
-0.040
-0.024
-0.008
DEFLECTION (IN)

COLUMN: B1

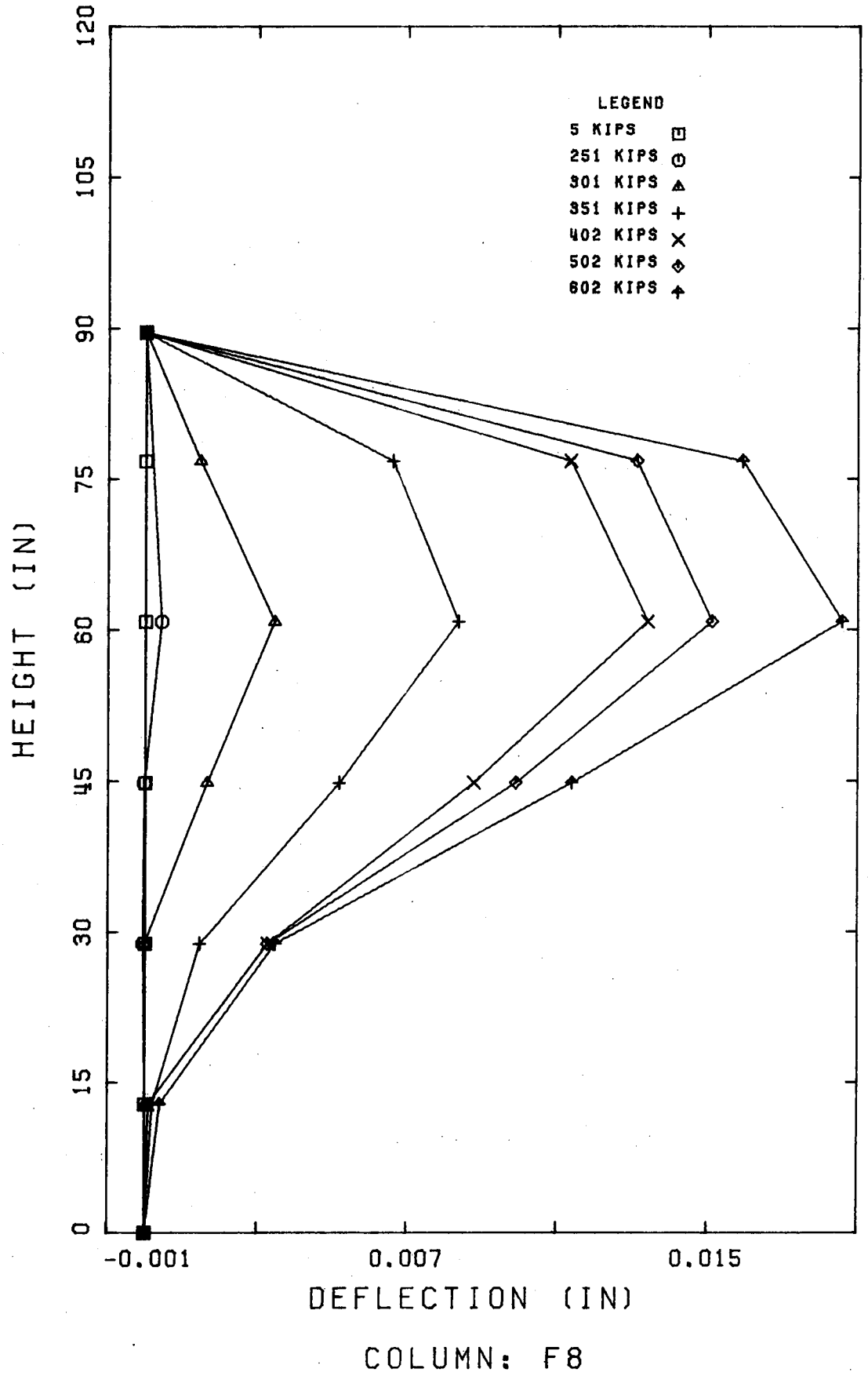
LEGEND
5 KIPS
251 KIPS
301 KIPS
351 KIPS
402 KIPS
502 KIPS
602 KIPS
HEIGHT (IN)
0
15
30
45
60
75
90
105
120
-0.001
0.007
0.015
DEFLECTION (IN)

COLUMN: F8

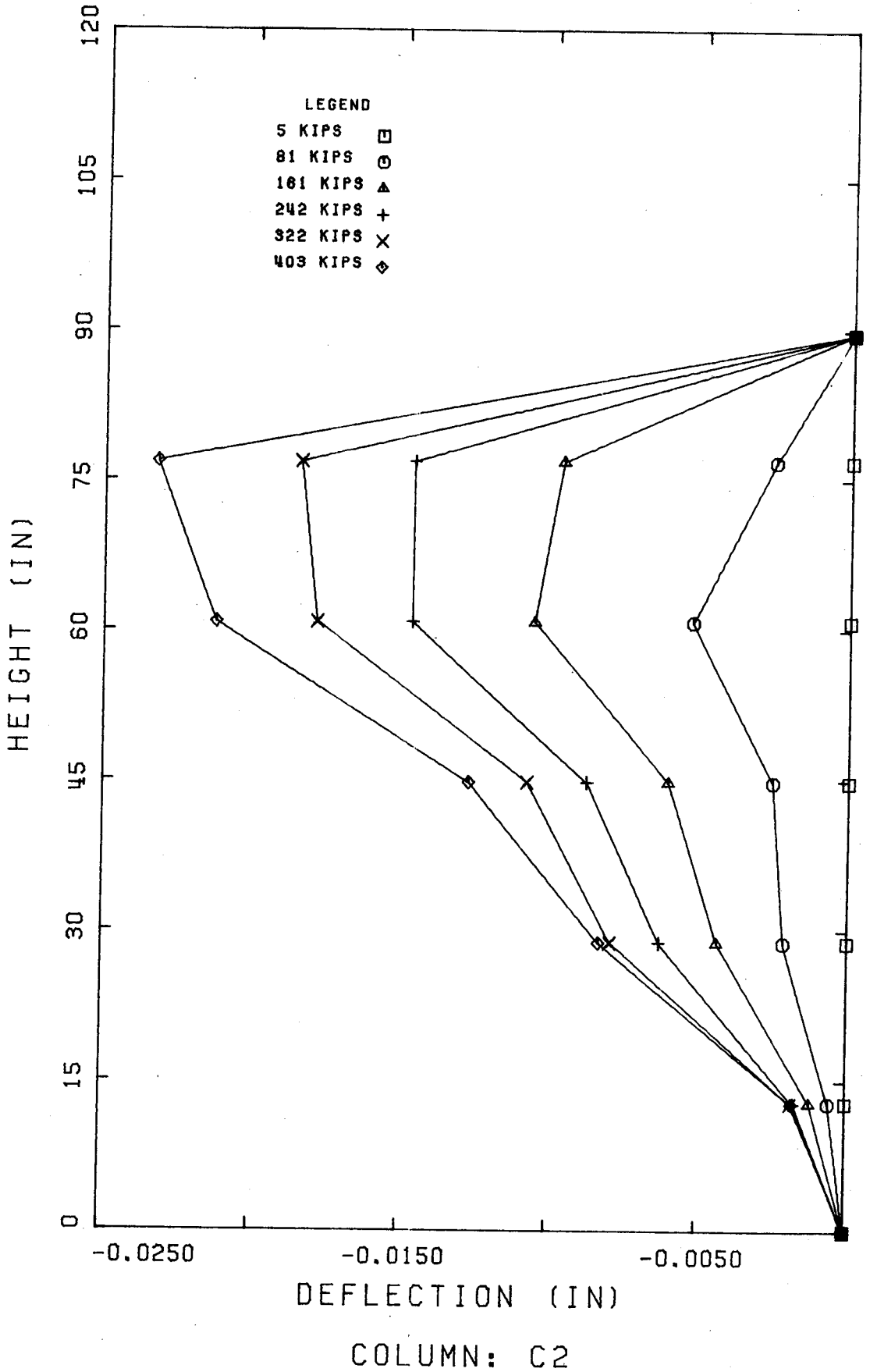
LEGEND
5 KIPS
81 KIPS
161 KIPS
242 KIPS
322 KIPS
403 KIPS
HEIGHT (IN)
0
15
30
45
60
75
90
105
120
-0.0250
-0.0150
-0.0050
DEFLECTION (IN)

COLUMN: C2

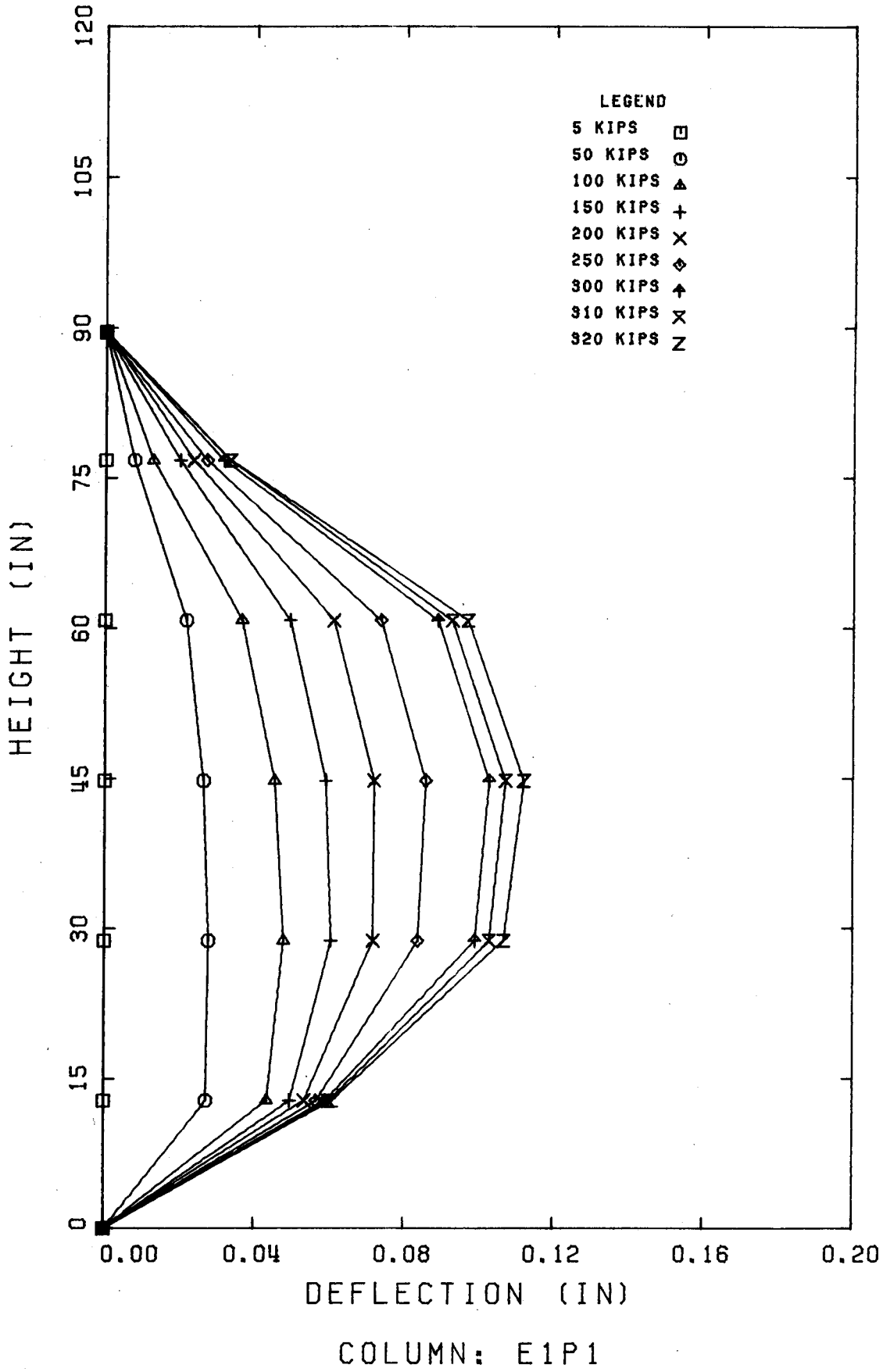
LEGEND
5 KIPS
50 KIPS
100 KIPS
150 KIPS
200 KIPS
250 KIPS
300 KIPS
310 KIPS
320 KIPS
HEIGHT (IN)
0
15
30
45
60
75
90
105
120
0.00
0.04
0.08
0.12
0.16
0.20
DEFLECTION (IN)

COLUMN: E1P1

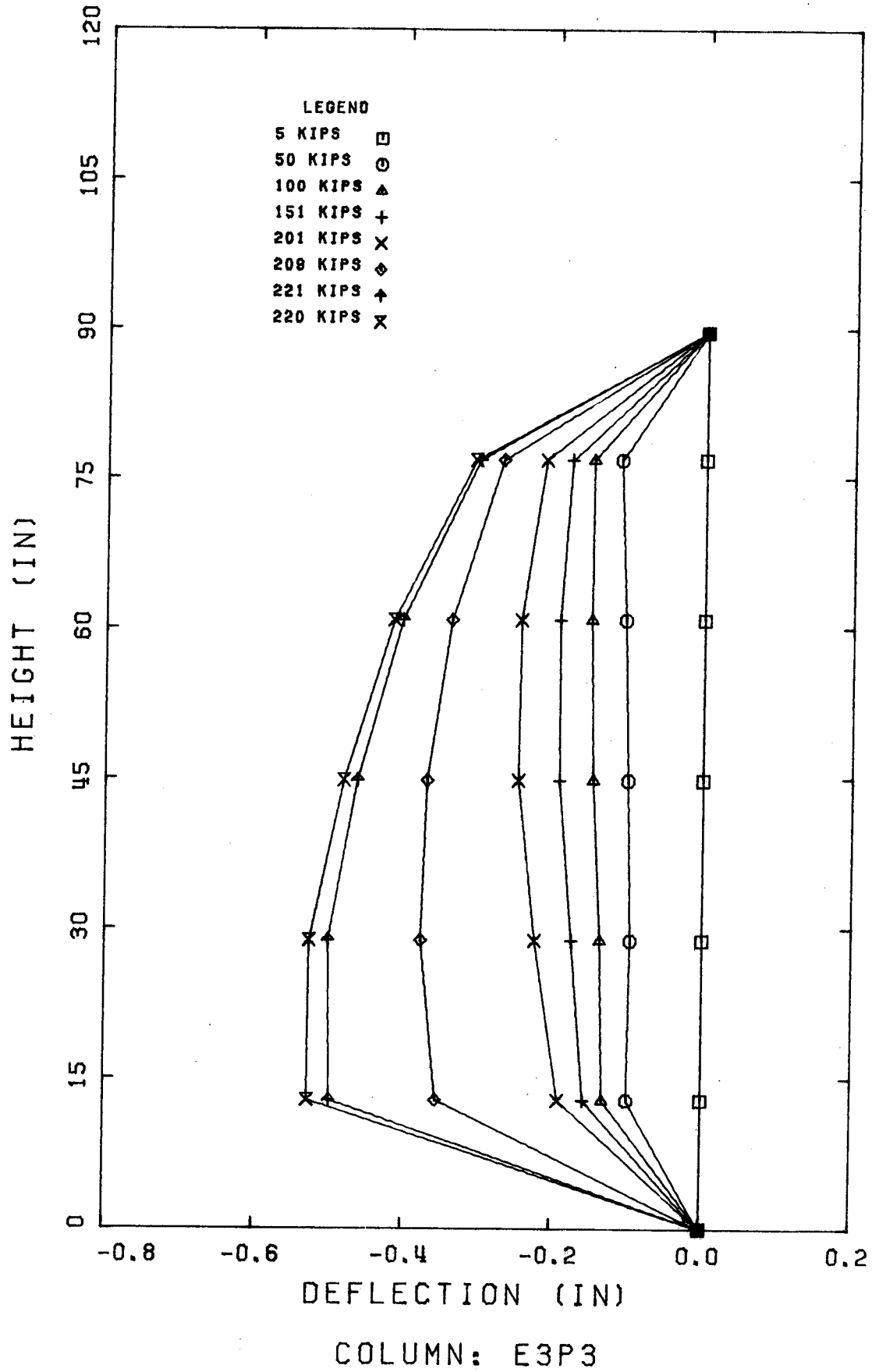
LEGEND
5 KIPS
50 KIPS
100 KIPS
151 KIPS
201 KIPS
209 KIPS
221 KIPS
220 KIPS
HEIGHT (IN)
0
15
30
45
60
75
90
105
120
-0.8
-0.6
-0.4
-0.2
0.0
0.2
DEFLECTION (IN)

COLUMN: E3P3

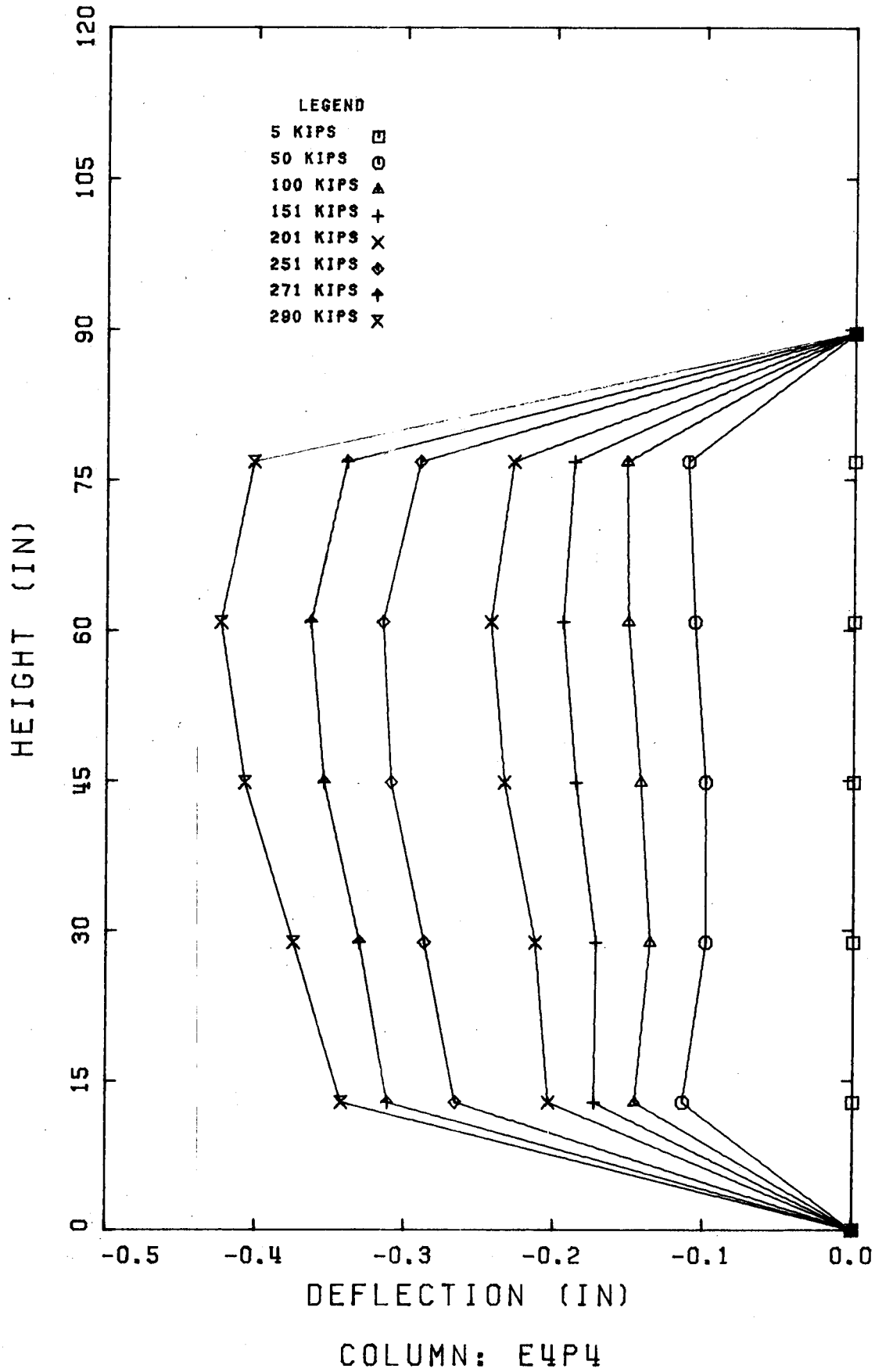
LEGEND
5 KIPS
50 KIPS
100 KIPS
151 KIPS
201 KIPS
251 KIPS
271 KIPS
290 KIPS
HEIGHT (IN)
0
15
30
45
60
75
90
105
120
-0.5
-0.4
-0.3
-0.2
-0.1
0.0
DEFLECTION (IN)

COLUMN: E4P4

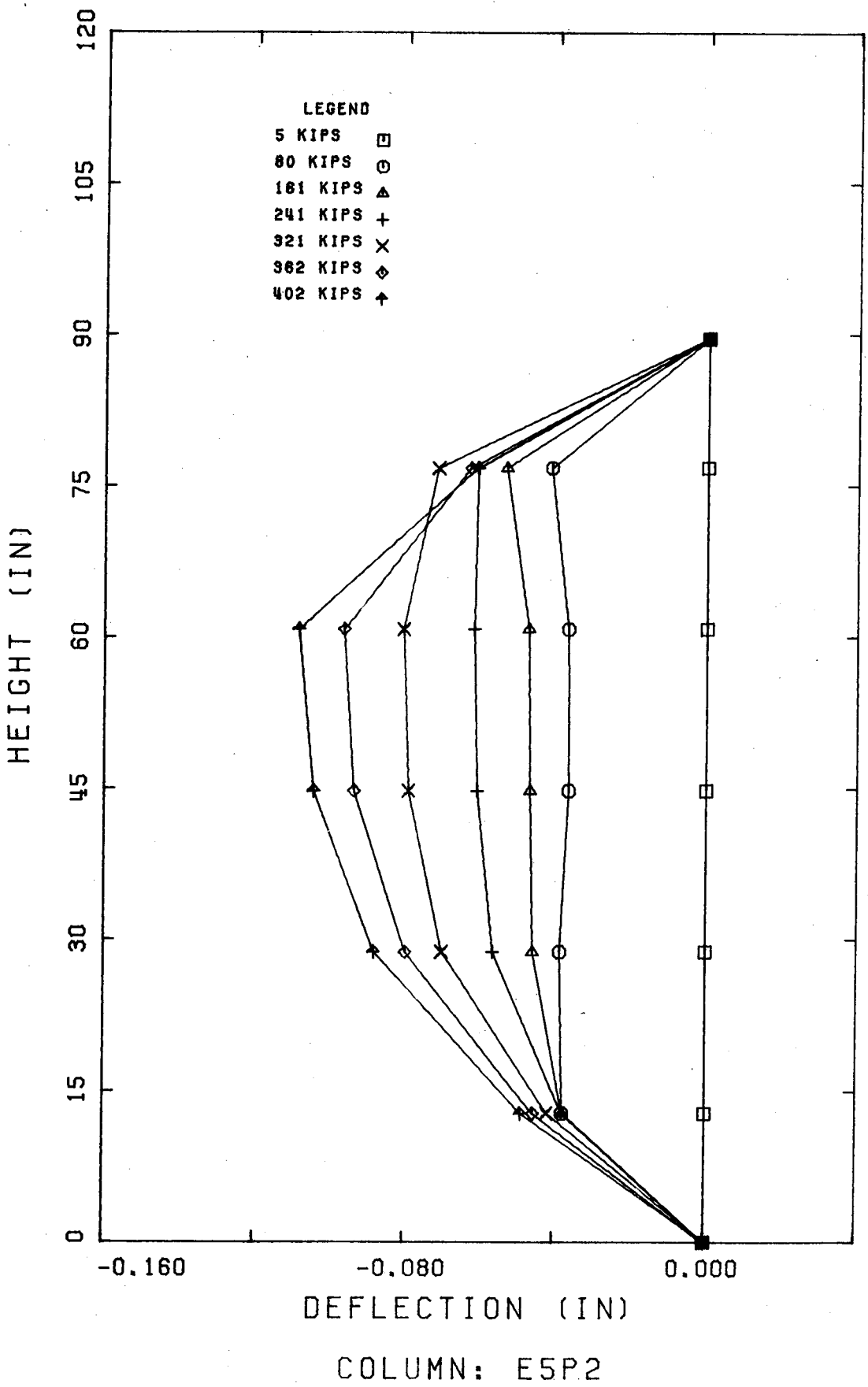
LEGEND
5 KIPS
80 KIPS
161 KIPS
241 KIPS
321 KIPS
362 KIPS
402 KIPS
HEIGHT (IN)
0
15
30
45
60
75
90
105
120
-0.160
-0.080
0.000
DEFLECTION (IN)

COLUMN: E5P2

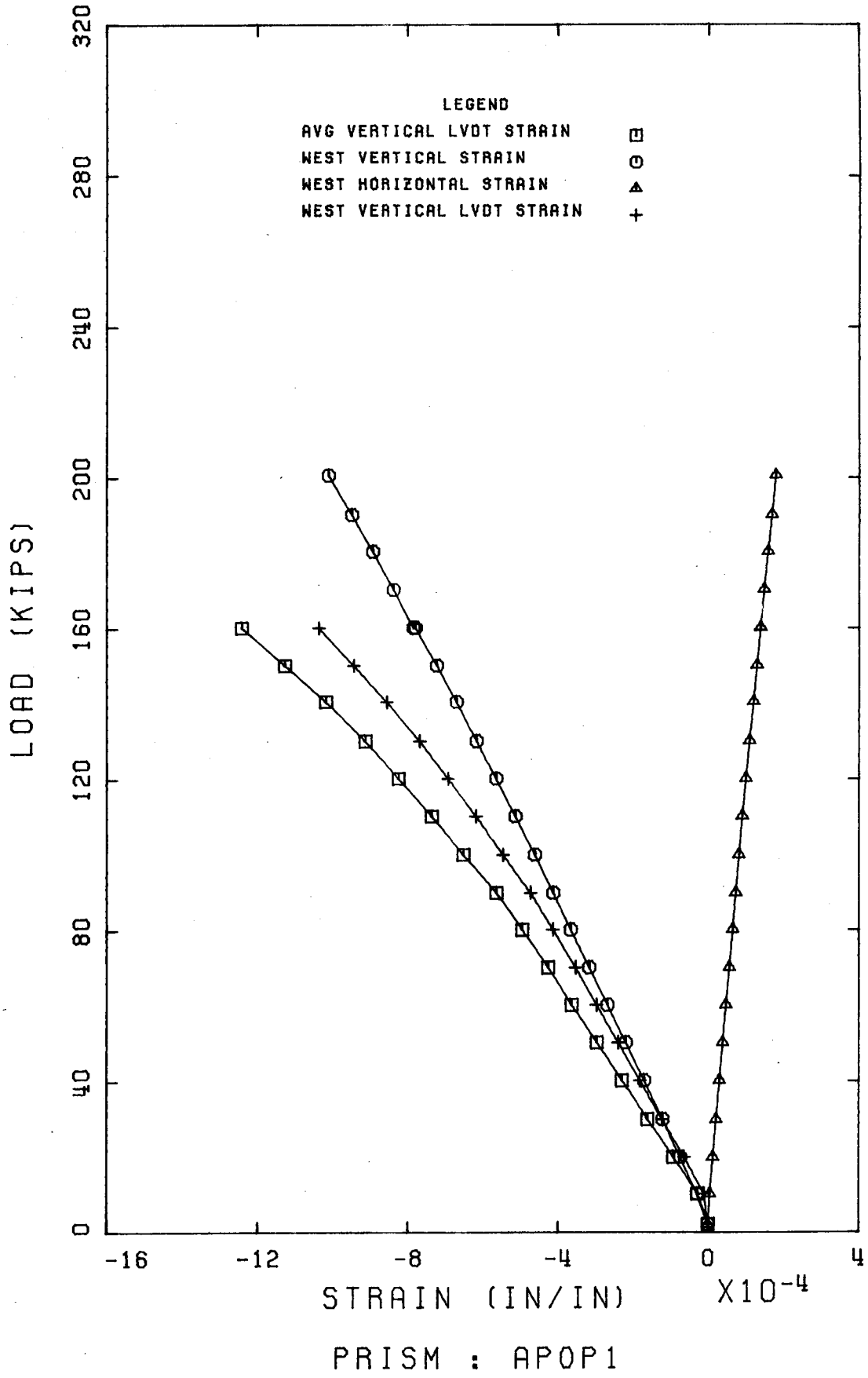
LEGEND
AVG VERTICAL LVDT STRAIN
WEST VERTICAL STRAIN
WEST HORIZONTAL STRAIN
WEST VERTICAL LVDT STRAIN
LOAD (KIPS)
0
40
80
120
160
200
240
280
320
-16
-12
-8
-4
0
4
STRAIN (IN/IN)
X10-4
PRISM : APOP1

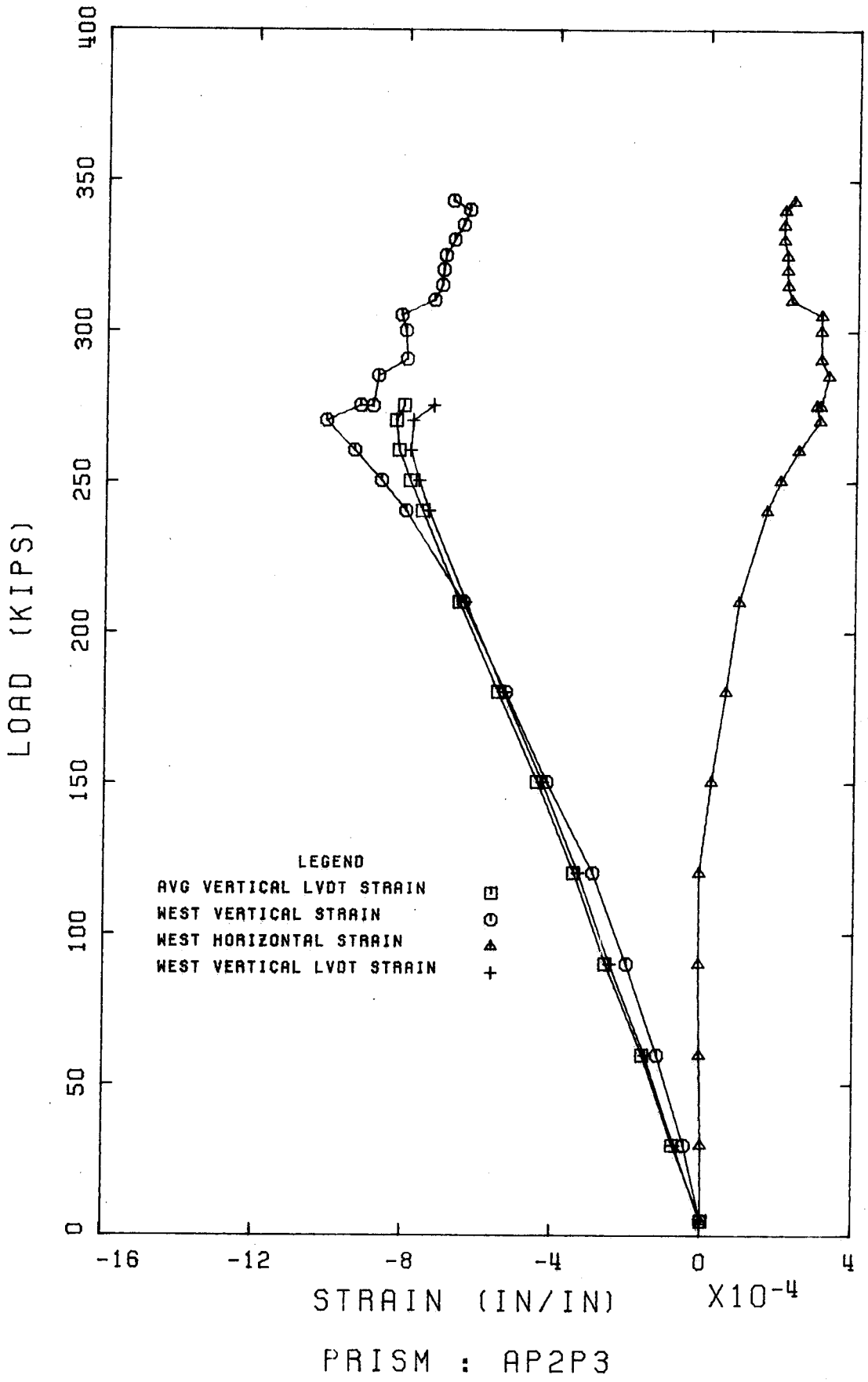
LOAD (KIPS)
0
50
100
150
200
250
300
350
400
-16
-12
-8
-4
0
4
STRAIN (IN/IN) X10-4
LEGEND
AVG VERTICAL LVDT STRAIN
WEST VERTICAL STRAIN
WEST HORIZONTAL STRAIN
WEST VERTICAL LVDT STRAIN

PRISM : AP2P3

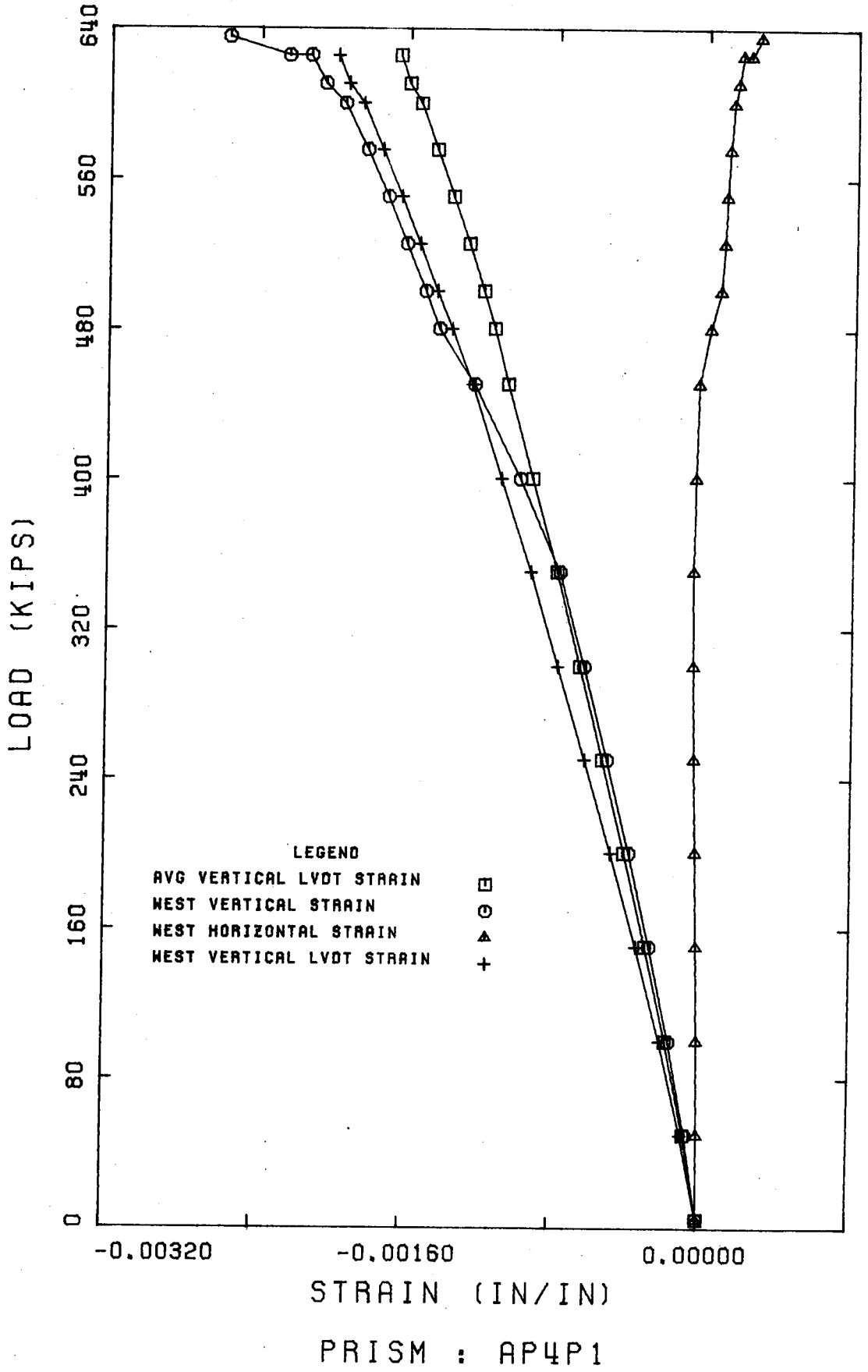
LOAD (KIPS)
640
560
480
400
320
240
160
80
0
-0.00320
-0.00160
0.00000
STRAIN (IN/IN)
LEGEND
AVG VERTICAL LVDT STRAIN
WEST VERTICAL STRAIN
WEST HORIZONTAL STRAIN
WEST VERTICAL LVDT STRAIN
PRISM : AP4P1

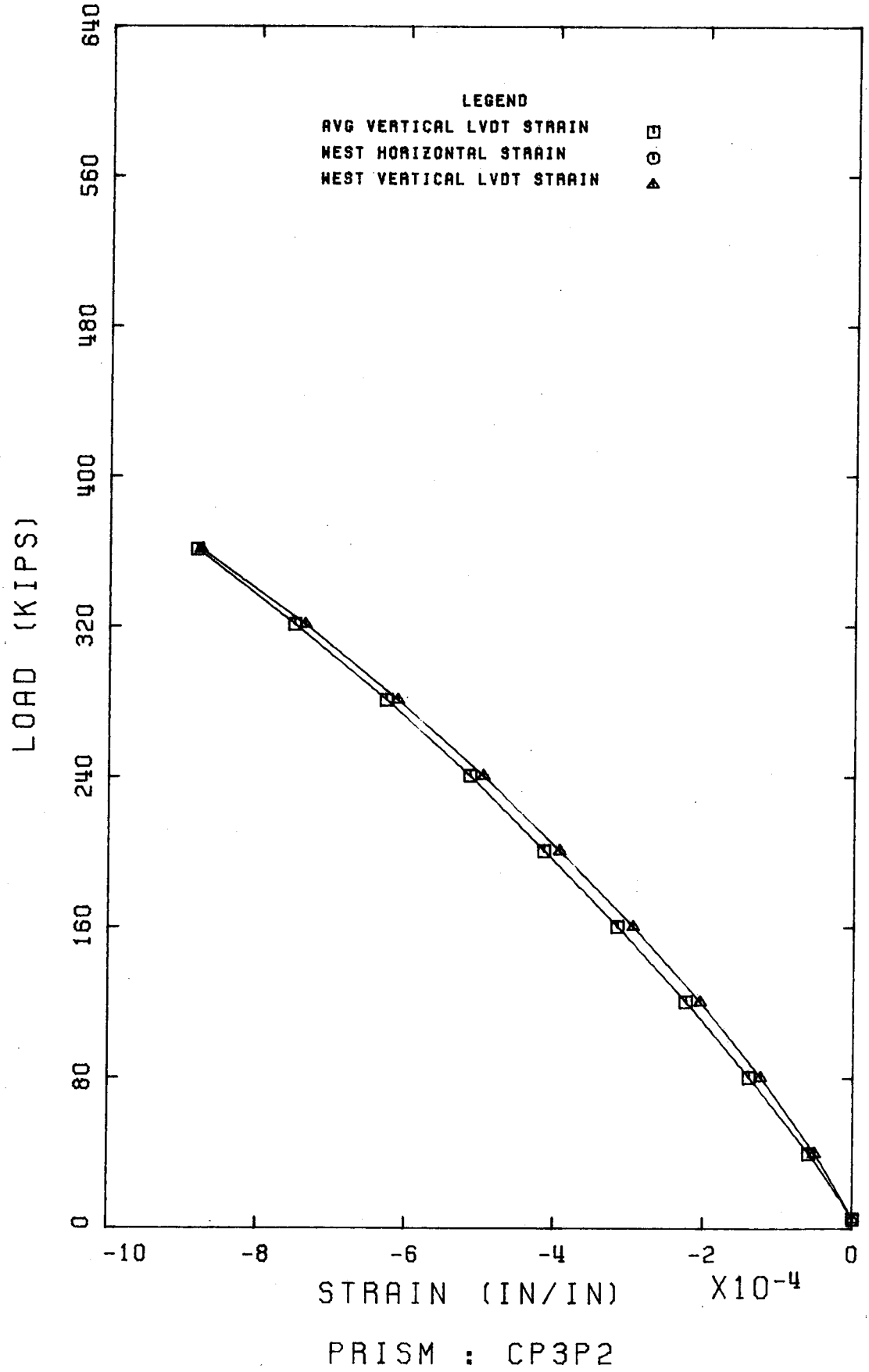
LEGEND
AVG VERTICAL LVDT STRAIN
WEST HORIZONTAL STRAIN
WEST VERTICAL LVDT STRAIN
LOAD (KIPS)
0
80
160
240
320
400
480
560
640
-10
-8
-6
-4
-2
0
STRAIN (IN/IN) X10-4
PRISM : CP3P2

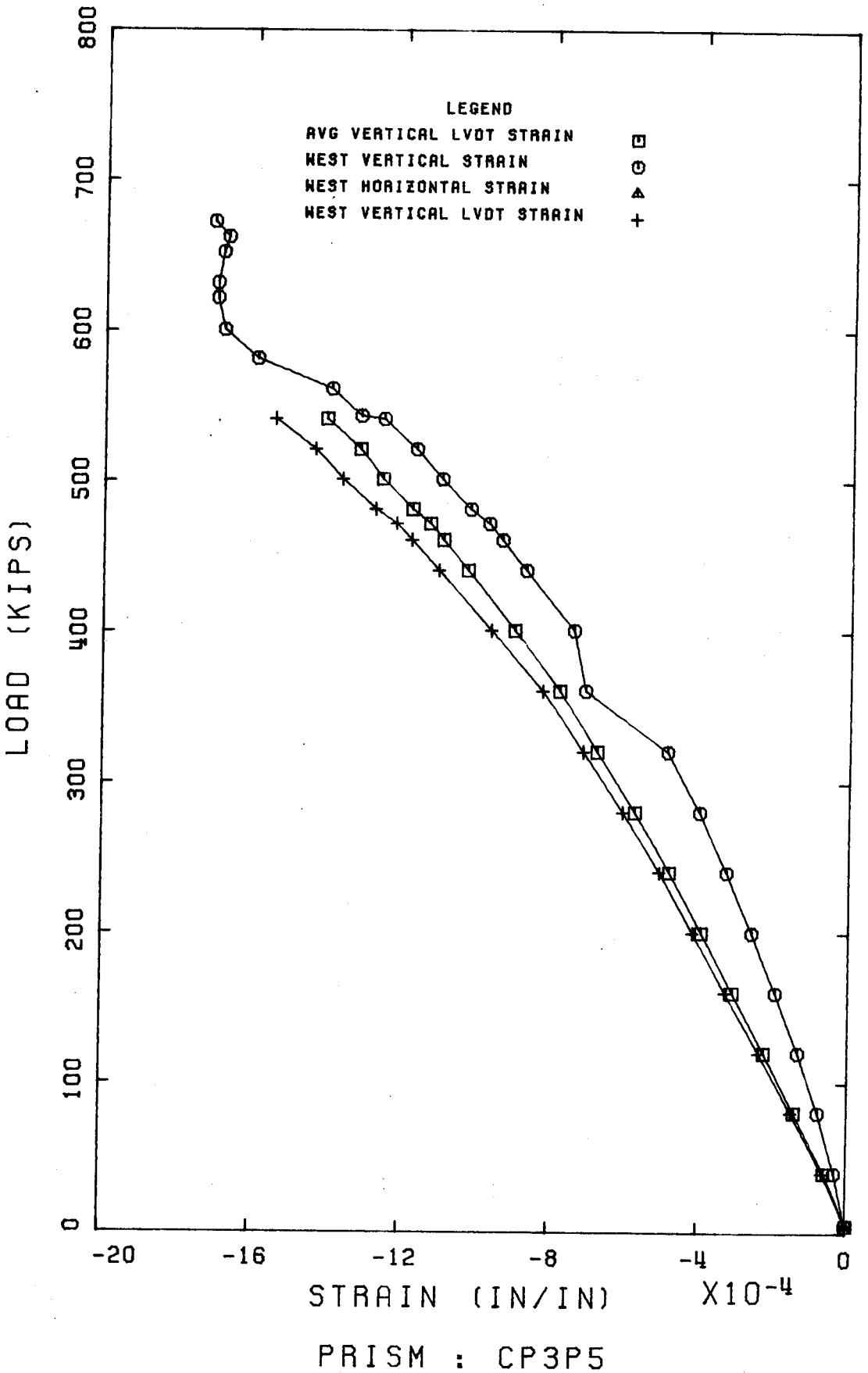
LEGEND
AVG VERTICAL LVDT STRAIN
WEST VERTICAL STRAIN
WEST HORIZONTAL STRAIN
WEST VERTICAL LVDT STRAIN
LOAD (KIPS)
0
100
200
300
400
500
600
700
800
-20
-16
-12
-8
-4
0
STRAIN (IN/IN) X10-4

PRISM : CP3P5

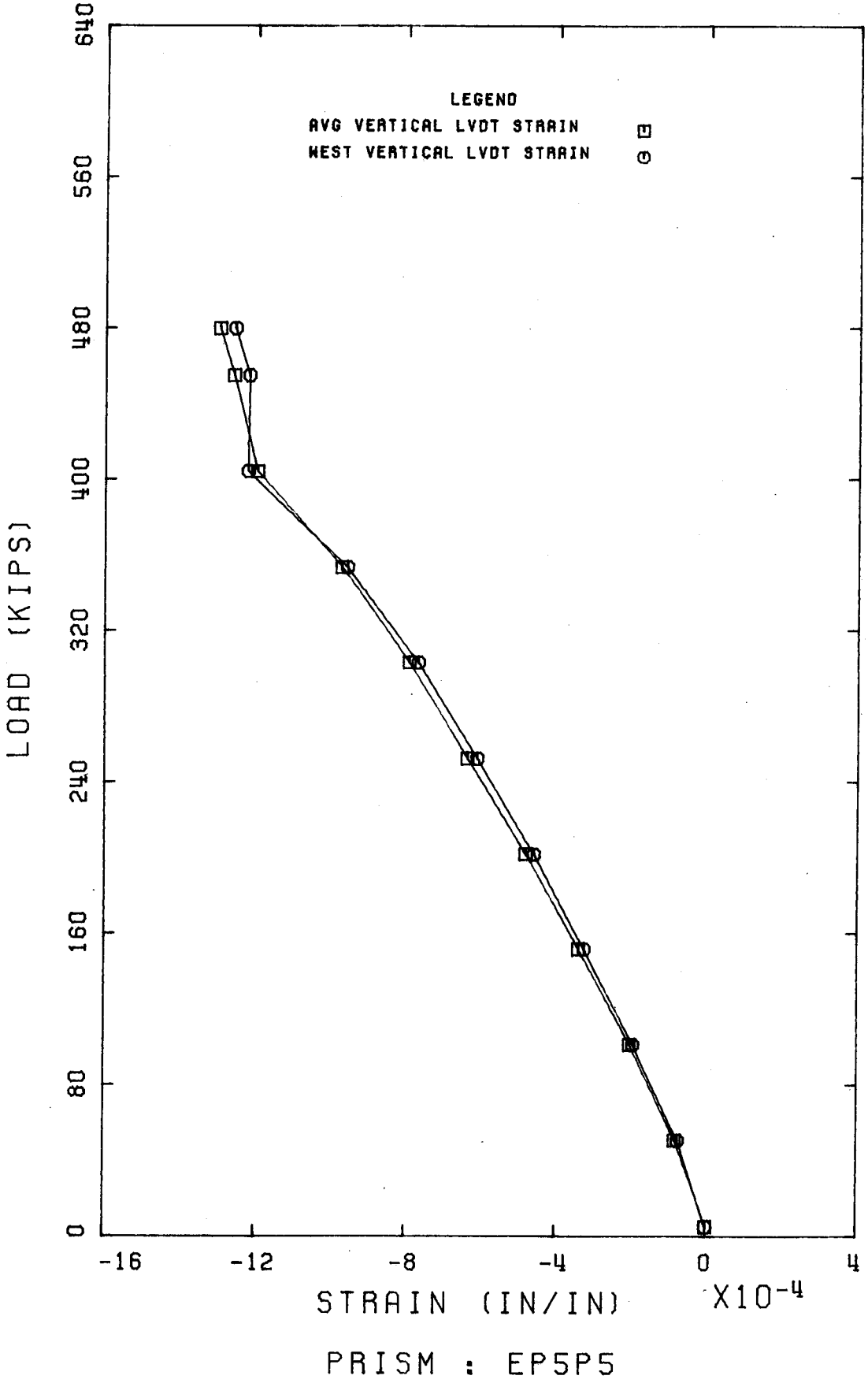
LEGEND
AVG VERTICAL LVDT STRAIN
WEST VERTICAL LVDT STRAIN
LOAD (KIPS)
0
80
160
240
320
400
480
560
640
-16
-12
-8
-4
0
4
STRAIN (IN/IN)
X10-4
PRISM : EP5P5

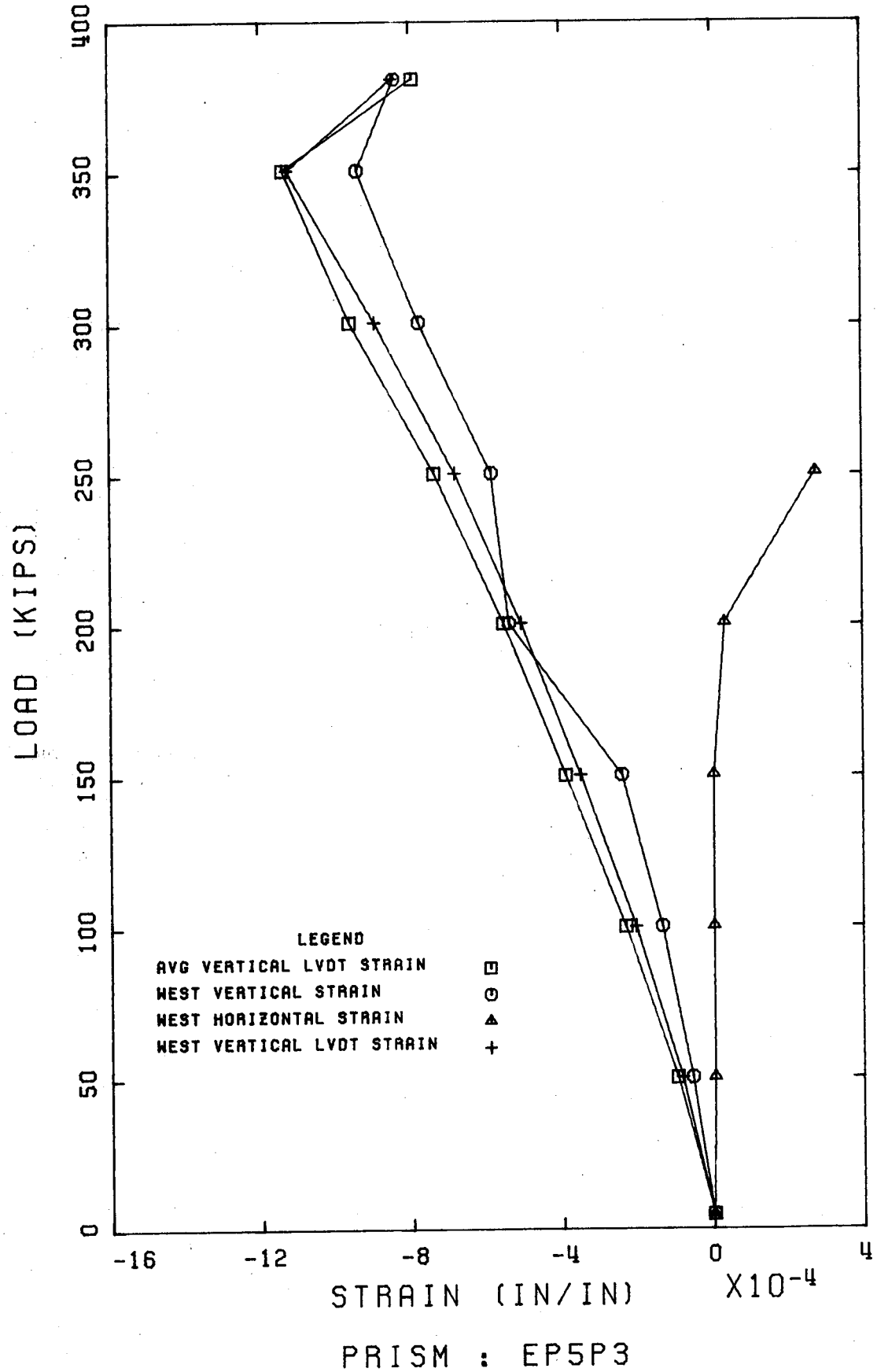
LOAD (KIPS)
0
50
100
150
200
250
300
350
400
-16
-12
-8
-4
0
4
STRAIN (IN/IN)
X10-4
LEGEND
AVG VERTICAL LVDT STRAIN
WEST VERTICAL STRAIN
WEST HORIZONTAL STRAIN
WEST VERTICAL LVDT STRAIN
PRISM : EP5P3

RECENT STRUCTURAL ENGINEERING REPORTS

Department of Civil Engineering

University of Alberta

62. *Behaviour of Open Web Steel Joists* by R.A. Kaliandasani, S.H. Simmonds and D.W. Murray, July 1977.

63. *A Classical Flexibility Analysis for Gentilly Type Containment Structures* by D.W. Murray, A.M. Rohardt, and S.H. Simmonds, June 1977.

64. *Substructure Analysis of Plane Frames* by A.A. Elwi and D.W. Murray, June 1977.

65. *Strength and Behavior of Cold-Formed HSS Columns* by Reidar Bjorhovde, December 1977.

66. *Some Elementary Mechanics of Explosive and Brittle Failure Modes in Prestressed Containments* by D.W. Murray, June 1978.

67. *Inelastic Analysis of Prestressed Concrete Secondary Containments* by D.W. Murray, L. Chitnuyanondh, C. Wong and K.Y. Rijub-Agha, July 1978.

68. *Strength of Variability of Bonded Prestressed Concrete Beams* by D.K. Kikuchi, S.A. Mirza and J.G. MacGregor, August 1978.

69. *Numerical Analysis of General Shells of Revolution Subjected to Arbitrary Loading* by A.M. Shazly, S.H. Simmonds and D.W. Murray, September 1978.

70. *Concrete Masonry Walls* by M. Hatzinikolas, J. Longworth and J. Warwaruk, September 1978.

71. *Experimental Data for Concrete Masonry Walls* by M. Hatzinikolas, J. Longworth and J. Warwaruk, September 1978.

72. *Fatigue Behaviour of Steel Beams with Welded Details* by G.R. Bardell and G.L. Kulak, September 1978.

73. *Double Angle Beam-Column Connections* by R.M. Lasby and Reidar Bjorhovde, April 1979.

74. *An Effective Uniaxial Tensile Stress-Strain Relationship for Prestressed Concrete* by L. Chitnuyanondh, S. Rizkalla, D.W. Murray and J.G. MacGregor, February 1979.

75. *Interaction Diagrams for Reinforced Masonry* by C. Feeg and J. Warwaruk, April 1979.

76. *Effects of Reinforcement Detailing for Concrete Masonry Columns* by C. Feeg, J. Longworth, and J. Warwaruk, May 1979.

77. *Interaction of Concrete Masonry Bearing Walls and Concrete Floor Slabs* by N. Ferguson, J. Longworth and J. Warwaruk, May 1979.

78. *Analysis of Prestressed Concrete Wall Segments* by B.D.P. Koziak and D.W. Murray, June 1979.

79. *Fatigue Strength of Welded Steel Elements* by M.P. Comeau and G.L. Kulak, October 1979.

80. *Leakage Tests of Wall Segments of Reactor Containments* by S.K. Rizkalla, S.H. Simmonds and J.G. MacGregor, October 1979.

81. *Tests of Wall Segments from Reactor Containments* by S.H. Simmonds, S.H. Rizkalla and J.G. MacGregor, October 1979.

82. *Cracking of Reinforced and Prestressed Concrete Wall Segments* by J.G. MacGregor, S.H. Rizkalla and S.H. Simmonds, October 1979.

83. *Inelastic Behavior of Multistory Steel Frames* by M. El Zanaty, D.W. Murray and R. Bjorhovde, April 1980.

84. *Finite Element Programs for Frame Analysis* by M. El Zanaty and D.W. Murray, April 1980.

85. *Test of a Prestressed Concrete Secondary Containment Structure* by J.G. MacGregor, S.H. Simmonds and S.H. Rizkalla, April 1980.

86. *An Inelastic Analysis of the Gentilly-2 Secondary Containment Structure* by D.W. Murray, C. Wong, S.H. Simmonds and J.G. MacGregor, April 1980.

87. *Nonlinear Analysis of Axisymmetric Reinforced Concrete Structures* by A.A. Elwi and D.W. Murray, May 1980.

88. *Behavior of Prestressed Concrete Containment Structures - A Summary of Findings* by J.G. MacGregor, D.W. Murray, S.H. Simmonds, April 1980.

89. *Deflection of Composite Beams at Service Load* by L. Samantaraya and J. Longworth, June 1980.

90. *Analysis and Design of Stub-Girders* by T.J.E. Zimmerman and R. Bjorhovde, August 1980.

91. *An Investigation of Reinforced Concrete Block Masonry Columns* by G.R. Sturgeon, J. Longworth and J. Warwaruk, September 1980.